

# Table of Contents

ABSTRACT.....	i
ACKNOWLEDGEMENTS.....	iii
LIST OF FIGURES.....	ix
LIST OF SCHEMES.....	xviii
LIST OF TABLES.....	xix
LIST OF ABBREVIATIONS.....	xx
CHAPTER ONE: Introduction.....	1
1.1. Abstract.....	1
1.2. General background.....	1
1.3. Current antifouling coatings system.....	3
1.3.1. Insoluble matrix paints.....	3
1.3.2. Soluble matrix paints.....	3
1.4. Conducting polymers.....	6
1.4.1. Introduction to polyaniline and polyaminobenzoic acid.....	6
1.4.2. Mechanisms of conduction for conducting polymers.....	8
1.4.3. Synthesis of conducting polymers.....	9
1.4.3.1. Chemical polymerisation.....	14
1.4.3.2. Electrochemical polymerisation.....	18
1.4.3.3. Other polymerisation techniques.....	20
1.5. Aluminium substrates.....	20
1.5.1. Aluminium Anodising.....	24
1.5.2. Electrochemical polymerisation of aniline on aluminium alloys.....	27
1.5.3. Galvanostatic polymerisation method.....	33
1.5.4. Potentiostatic polymerisation method.....	33
1.5.5. Corrosion resistance studies.....	34
1.5.6. Radical scavenging assay.....	37
1.5.7. Antibacterial properties of polyaniline.....	38
1.6. Aims and objectives of this work.....	40
CHAPTER TWO: Experimental methods.....	43
2.1. Abstract.....	43
2.2. Materials.....	43

2.3.	Chemical synthesis .....	44
2.4.	Electrochemical instrumentation and cells .....	45
2.5.	Electrochemical synthesis.....	46
2.6.	Characterisation Methods .....	49
2.6.1.	Morphology.....	49
2.6.2.	Cyclic voltammograms (CVs) .....	51
2.6.3.	Fourier Transform Infrared (FTIR) spectroscopy.....	52
2.6.4.	Raman spectroscopy .....	53
2.6.5.	Ultraviolet-Visible (UV-Vis) spectroscopy .....	61
2.6.6.	Solid-state Nuclear Magnetic Resonance (SSNMR) .....	64
2.6.7.	Gel permeation chromatograph.....	65
2.7.	Performance properties.....	66
2.7.1.	Adhesion properties .....	66
2.7.2.	Anticorrosive properties.....	66
2.7.3.	Anti-moulding properties.....	67
2.7.4.	Minimum bactericidal concentration (MBC) Protocol.....	69
2.7.5.	Antifouling properties .....	69
2.7.6.	Free Radical scavenging activity .....	69
CHAPTER THREE: Characterisation of chemical and electrochemical synthesis of polyaniline.....		71
3.1.	Abstract.....	71
3.2.	Results and Discussions.....	71
3.2.1.	FTIR spectroscopy .....	71
3.2.2.	Cyclic voltammetry.....	73
3.2.3.	Raman spectroscopy .....	78
3.2.4.	UV-Vis and <i>in-situ</i> UV-Vis spectroscopy .....	81
3.2.5.	SSNMR spectroscopy of polyaniline .....	87
3.3.	Conclusions .....	92
CHAPTER FOUR: Characterisation of polyaminobenzoic acid and aniline-aminobenzoic acid copolymer.....		93
4.1.	Abstract.....	93
4.2.	Results and Discussions.....	93
4.2.1.	(Gel permeation chromatography) GPC.....	93
4.2.2.	FTIR spectroscopy.....	96

4.2.3.	Morphology .....	99
4.2.4.	Antimicrobial properties .....	107
4.2.5.	Anti-moulding performance .....	108
4.2.6.	UV-Vis spectroscopy.....	108
4.2.7.	Cyclic voltammetry of polymers .....	115
4.2.7.1.	Polyaminobenzoic acid .....	115
4.2.7.2.	Polyaniline-co-aminobenzoic acid.....	129
4.2.8.	Raman spectroscopy .....	132
4.3.	Conclusions .....	135
CHAPTER FIVE: Structural studies of polyaniline and aniline-aminobenzoic acid copolymers..... 137		
5.1.	Abstract.....	137
5.2.	Results and Discussions.....	137
5.2.1.	<i>in-situ</i> Raman.....	137
5.2.1.1.	Polyaniline and aniline-aminobenzoic acid copolymers at 1:1 ratio .....	138
5.2.1.2.	Copolymers prepared with two different dopants.....	147
5.2.1.3.	Copolymers at different monomer concentrations.....	152
5.2.2.	SSNMR.....	160
5.3.	Conclusions .....	164
CHAPTER SIX: Electrodeposition of polyaniline on aluminium..... 165		
6.1.	Abstract.....	165
6.2.	Results and Discussions.....	166
6.2.1.	Electrochemical synthesis of polyaniline at a fixed applied potential.....	166
6.2.1.1.	Two-Step process .....	166
6.2.1.2.	One-Step process .....	168
6.2.2.	Electrochemical synthesis using cyclic voltammetry .....	171
6.2.3.	Morphology .....	175
6.2.4.	FTIR spectroscopy.....	184
6.2.5.	Raman spectroscopy .....	185
6.2.6.	Reflectance UV-Vis spectroscopy .....	191
6.2.7.	<i>in situ</i> UV-Vis spectroscopy in 0.5 M oxalic acid solution .....	193
6.2.8.	Corrosion resistance studies .....	196
6.2.9.	Free radical DPPH scavenging evaluation .....	217
6.3.	Conclusions .....	223

CHAPTER SEVEN: Fouling resistance studies .....	224
7.1. Abstract.....	224
7.2. Experimental Procedure .....	225
7.2.1. Materials .....	225
7.2.2. Testing procedure .....	226
7.2.2.1. <i>Escherichia coli</i> strains.....	226
7.2.2.2. <i>Vibrio</i> strains.....	227
7.3. Results and Discussions.....	227
7.3.1. <i>Escherichia coli</i> strains fouling resistance studies .....	227
7.3.1.1. <i>Escherichia coli</i> ATCC 25922 <i>lux</i> .....	230
7.3.1.2. <i>Escherichia coli</i> 536 <i>lux</i> .....	232
7.3.2. <i>Vibrio fischeri</i> and <i>Vibrio harveyi</i> strains fouling resistance studies .....	232
7.4. Conclusions .....	234
CHAPTER EIGHT: Conclusions .....	236
8.1. General Conclusions.....	236
8.2. Future work.....	238
APPENDIX.....	240
REFERENCES .....	244



## LIST OF FIGURES

Figure 1.1. Working scheme and biocide release rates of traditional insoluble matrix paints. “Minimum biocide release” indicates the limit for efficient protection against fouling, dependent on the fouling conditions (adapted from [7]) .....	3
Figure 1.2. Working scheme and biocide release rates of traditional soluble matrix paints. “Minimum biocide release” indicates the limit for efficient protection against fouling, dependent on the fouling conditions (adapted from [7]) .....	4
Figure 1.3. Cleaning and pretreatment of aluminium alloys. ....	23
Figure 1.4. Schematic representation of ordered anodised aluminium oxide (AAO) formation via double-anodisation: (a) first anodisation, (b) removal of the first (disordered) oxide, and (c) second anodisation.....	25
Figure 1.5. Equivalent electrical circuit for impedance measurements (adapted from [25]).	34
Figure 1.6. Ecosystem of biofilm formation (adapted from [166]).	39
Figure 1.7. Surface molecular structures of catecholate inner-sphere complexes on aluminium (A) surface: (a) monodentate, and bidentate (b) mononuclear and (c) binuclear complexes (adapted from [168]).	40
Figure 2.1. Electrochemical cell for growing conducting polymer films on electrode.	45
Figure 2.2. Method two for electrochemically synthesising poly-ABA.....	47
Figure 2.3. The two-step process of electrochemical deposition of PANI on aluminium.....	48
Figure 2.4. Cross-sections of aluminium compounds mounted in epoxy resin. ....	51
Figure 2.5. Oligomers of aniline [199]. ....	56
Figure 2.6. An example of a Nyquist plot with key features labelled. ....	67
Figure 2.7. Chemically synthesised PANI and poly-ABA doped with different dopant was applied on GIB board for anti-moulding evaluation.....	68
Figure 3.1. FTIR spectra of chemically synthesised PANI prepared in (a) 0.5 M H <sub>2</sub> SO <sub>4</sub> with APS, (b) 1.5 M H <sub>2</sub> SO <sub>4</sub> with APS, and (c) 1.5 M H <sub>2</sub> SO <sub>4</sub> with KIO <sub>3</sub> .....	72
Figure 3.2. FTIR spectrum of (a) chemically synthesised PANI, and (b) electrochemically synthesised PANI on Pt electrode both doped with 0.5 M H <sub>2</sub> SO <sub>4</sub> .....	73
Figure 3.3. Chemically synthesised PANI cast on a glassy carbon electrode and cycled in 0.5 M oxalic acid between -0.1 to 0.85 V at a scan rate of 50 mV s <sup>-1</sup> .....	74
Figure 3.4. (a) The first 5 cycles of electrochemically synthesised PANI on Pt at a scan rate of 50 mV s <sup>-1</sup> in 0.5 M H <sub>2</sub> SO <sub>4</sub> , and (b) at cycle 10.....	75
Figure 3.5. Characterisation using cyclic voltammetry for electrochemically synthesised PANI in aniline-free 0.5 M H <sub>2</sub> SO <sub>4</sub> at a Pt electrode. 5 cycles were run between -0.1 to 0.8 V at a scan rate of 50 mV s <sup>-1</sup> , after electropolymerisation for a total of 90 additional cycles to 0.9 V after the scans presented in Figure 3.4(b). ....	76
Figure 3.6. Raman spectra of (a) PANI chemically synthesised in 0.5 M H <sub>2</sub> SO <sub>4</sub> , and (b) PANI electrochemically synthesised in 0.5 M H <sub>2</sub> SO <sub>4</sub> on Pt sheet on blue laser excitation line (λ = 488 nm).....	78
Figure 3.7. Raman spectra of (a) PANI chemically synthesised in 0.5 M oxalic acid, and (b) PANI electrochemically synthesised in 0.5 M oxalic acid on Pt electrode.....	79

Figure 3.8. (a) UV-Vis spectra on an ITO electrode, obtained in a 0.5 M oxalic acid electrolyte after running 10 cycles in 0.5 M oxalic acid + 0.1 M aniline between -0.1 and 1 V at 50 mV s <sup>-1</sup> at 0 to 0.5 V applied potential .....	81
Figure 3.8. (b) UV-Vis spectra on an ITO electrode, obtained in a 0.5 M oxalic acid electrolyte after running 10 cycles in 0.5 M oxalic acid + 0.1 M aniline between -0.1 and 1 V at 50 mV s <sup>-1</sup> at 0.6 to 1.0 V applied potential .....	82
Figure 3.9. (a) UV-Vis spectra on an ITO electrode, obtained in a 0.5 M oxalic acid electrolyte after running 10 cycles in 0.5 M oxalic acid + 0.1 M aniline between -1 and 2.4 V at 50 mV s <sup>-1</sup> .....	83
Figure 3.9. (b) UV-Vis spectra on an ITO electrode, obtained in a 0.5 M oxalic acid electrolyte after running 10 cycles in 0.5 M oxalic acid + 0.1 M aniline between -1 and 2.4 V at 50 mV s <sup>-1</sup> .....	84
Figure 3.10. UV-Vis spectra of PANI synthesised by oxidation with APS doped in (i) 0.5 M H <sub>2</sub> SO <sub>4</sub> (ii) 1.5 M H <sub>2</sub> SO <sub>4</sub> both (a) chemically, and (b) electrochemically prepared.....	85
Figure 3.11. PANI prepared chemically synthesised doped with 1.5 M H <sub>2</sub> SO <sub>4</sub> (i) oxidised with KIO <sub>3</sub> , and (ii) oxidised with APS .....	87
Figure 3.12. <sup>13</sup> C CPMAS spectra of chemically synthesised PANI prepared with KIO <sub>3</sub> dopant (a), and APS dopant (c); NQS spectra of PANI prepared with KIO <sub>3</sub> dopant (b), and APS dopant (d). .....	88
Figure 3.13. NQS spectra of PANI prepared chemically under different dopant concentration (a) 1.5 M H <sub>2</sub> SO <sub>4</sub> , and (b) 0.5 M H <sub>2</sub> SO <sub>4</sub> in APS oxidant.....	89
Figure 3.14. NQS spectra of PANI prepared chemically with 1.5 M H <sub>2</sub> SO <sub>4</sub> dopant under different oxidants, (a) with KIO <sub>3</sub> , and (b) with APS. ....	90
Figure 3.15. <sup>13</sup> C CPMAS spectra of PANI (a) chemically synthesised with KIO <sub>3</sub> in 1.5 M H <sub>2</sub> SO <sub>4</sub> , (b) chemically synthesised with APS in 1.5 M H <sub>2</sub> SO <sub>4</sub> , (c) chemically synthesised with APS in 0.5 M H <sub>2</sub> SO <sub>4</sub> , (d) electrochemically synthesised in 1.5 M H <sub>2</sub> SO <sub>4</sub> , and (e) electrochemically synthesised in 0.5 M H <sub>2</sub> SO <sub>4</sub> . ....	91
Figure 4.1. Auto scale chromatogram of poly-2-ABA doped with 1 M H <sub>2</sub> SO <sub>4</sub> .....	95
Figure 4.2. Auto scale chromatogram of poly-3-ABA doped with 1.5 M H <sub>2</sub> SO <sub>4</sub> .....	95
Figure 4.3. Auto scale chromatogram of poly-3-ABA doped with 1 M HCl.....	96
Figure 4.4. FTIR spectra of ABA monomers (a) 2-ABA and (b) 3-ABA. ....	98
Figure 4.5. FTIR spectra of chemically prepared poly-ABA and oxidised with APS (a) poly-2-ABA doped with 1 M H <sub>2</sub> SO <sub>4</sub> , (b) poly-2-ABA doped with 1 M HCl, (c) poly-3-ABA doped with 1 M HCl, and (d) poly-3-ABA doped with 1.5 M H <sub>2</sub> SO <sub>4</sub> . ....	99
Figure 4.6. SEM images of chemically prepared poly-2-ABA doped with 1 M HCl appears with grape global structure.....	100
Figure 4.7. SEM images of chemically prepared poly-2-ABA doped with 1 M H <sub>2</sub> SO <sub>4</sub> with grape global structure.....	101
Figure 4.8. SEM images of chemically prepared poly-3-ABA doped with 1 M HCl forms sponge like structures.....	102
Figure 4.9. SEM images of chemically prepared poly-3-ABA doped with 1.5 M H <sub>2</sub> SO <sub>4</sub> forming flat sheet appearance .....	103
Figure 4.10. SEM images of chemically prepared PANI-co-3-ABA at 0.5 M H <sub>2</sub> SO <sub>4</sub> with APS as the oxidant formed rod-like structure. ....	104

Figure 4.11. SEM images of chemically prepared PANI-co-3-ABA at 1.5 M H <sub>2</sub> SO <sub>4</sub> with APS as the oxidant formed rod-like structure. ....	105
Figure 4.12. SEM images of chemically prepared PANI-co-3-ABA at 1.5 M H <sub>2</sub> SO <sub>4</sub> with KIO <sub>3</sub> as the oxidant formed random structure. ....	106
Figure 4.13. UV-Vis spectra of 2-ABA monomer and homopolymers in NMP. ....	109
Figure 4.14. UV-Vis spectra of 3-ABA monomer and homopolymers in NMP. ....	109
Figure 4.15. Chemically synthesised polymers doped with 1.5 M H <sub>2</sub> SO <sub>4</sub> (i) poly-3-ABA oxidised with APS, (ii) PANI oxidised with KIO <sub>3</sub> , (iii) PANI-co-3-ABA oxidised with APS, (iv) PANI oxidised with APS, and (v) 3-ABA monomer. ....	110
Figure 4.16. Chemically synthesised polymers doped with H <sub>2</sub> SO <sub>4</sub> and oxidised with APS (i) PANI-co-3-ABA 0.5 M H <sub>2</sub> SO <sub>4</sub> , (ii) PANI-co-3-ABA 1.5 M H <sub>2</sub> SO <sub>4</sub> , (iii) PANI 0.5 M H <sub>2</sub> SO <sub>4</sub> , and (iv) PANI 1.5 M H <sub>2</sub> SO <sub>4</sub> . ....	111
Figure 4.17. Comparison of UV-Vis spectra of chemically and electrochemically synthesised polymers and copolymers using H <sub>2</sub> SO <sub>4</sub> as the dopant (i) chemically prepared poly-3-ABA doped with 1.5 M H <sub>2</sub> SO <sub>4</sub> and APS as oxidant, (ii) electrochemically prepared PANI-co-3-ABA doped with 0.5 M H <sub>2</sub> SO <sub>4</sub> , (iii) chemically prepared PANI-co-3-ABA doped with 1.5 M H <sub>2</sub> SO <sub>4</sub> and APS as oxidant, and (iv) chemically prepared PANI doped with 1.5 M H <sub>2</sub> SO <sub>4</sub> and APS as oxidant. ....	113
Figure 4.18. CVs of the first two cycles for a Pt electrode in 0.1 M 2-ABA, run at 50 mV s <sup>-1</sup> in 1 M HCl. ....	117
Figure 4.19. CVs of a poly-2-ABA film run at 50 mV s <sup>-1</sup> in 1 M HCl of the first 50 cycle for a Pt electrode in 0.1 M 2-ABA, run at 50 mV s <sup>-1</sup> in 1 M HCl. ....	117
Figure 4.20. CVs of the first two cycles for a Pt electrode in 0.1 M 2-ABA, run at 50 mV s <sup>-1</sup> in 0.5 M H <sub>2</sub> SO <sub>4</sub> . ....	118
Figure 4.21. CVs of poly-2-ABA film run at 50 mV s <sup>-1</sup> in 0.5 M H <sub>2</sub> SO <sub>4</sub> of the first 50 cycle on a Pt electrode. ....	118
Figure 4.22. CVs of the first two cycles for a Pt electrode in 0.1 M 3-ABA, run at 50 mV s <sup>-1</sup> in 0.5 M HCl. ....	119
Figure 4.23. CVs of poly-3-ABA film run at 50 mV s <sup>-1</sup> in 1 M HCl of the first 50 cycle on a Pt electrode. ....	119
Figure 4.24. CVs of the first two cycles for a Pt electrode in 0.1 M 3-ABA, run at 50 mV s <sup>-1</sup> in 1.5 M H <sub>2</sub> SO <sub>4</sub> . ....	120
Figure 4.25. CVs of poly-3-ABA film run at 50 mV s <sup>-1</sup> in 1.5 M H <sub>2</sub> SO <sub>4</sub> of the first 50 cycle on a Pt electrode. ....	120
Figure 4.26. CVs of an electrochemically prepared poly-2-ABA film run at 50 mV s <sup>-1</sup> in 1 M HCl, after forming on a Pt electrode. ....	121
Figure 4.27. CVs of a chemically prepared poly-2-ABA film run at 50 mV s <sup>-1</sup> in 1 M HCl, after casting on a glassy carbon electrode. ....	121
Figure 4.28. CVs of an electrochemically prepared poly-2-ABA film run at 50 mV s <sup>-1</sup> in 0.5 M H <sub>2</sub> SO <sub>4</sub> , after forming on a Pt electrode. ....	122
Figure 4.29. CVs of a chemically prepared poly-2-ABA film run at 50 mV s <sup>-1</sup> in 1 M H <sub>2</sub> SO <sub>4</sub> , after casting on a glassy carbon electrode. ....	122
Figure 4.30. CVs of an electrochemically prepared poly-2-ABA film run at 50 mV s <sup>-1</sup> in 0.5 M H <sub>2</sub> SO <sub>4</sub> , after forming on a PANI-Pt electrode. ....	123

Figure 4.31. CVs of electrochemically prepared poly-3-ABA film run at 50 mV s <sup>-1</sup> in 1 M HCl, after forming on a Pt electrode. ....	124
Figure 4.32. CVs of chemically prepared poly-3-ABA films run at 50 mV s <sup>-1</sup> in 1 M HCl, after casting on a glassy carbon electrode.....	125
Figure 4.33. CVs of electrochemically prepared poly-3-ABA film run at 50 mV s <sup>-1</sup> in 1.5 M H <sub>2</sub> SO <sub>4</sub> , after forming on a Pt electrode. ....	125
Figure 4.34. CVs of chemically prepared poly-3-ABA film run at 50 mV s <sup>-1</sup> in 1.5 M H <sub>2</sub> SO <sub>4</sub> , after casting on a glassy carbon electrode.....	126
Figure 4.35. The CVs for the electrolysis of a solution consisting of 0.05 M ABA, 0.05 M aniline and 1 M HCl after 50 cycles cycling between -0.1 to 1.0 V at a scan rate of 50 mV s <sup>-1</sup> at different aniline to 2-ABA concentrations (represented as 9:1 correspond to aniline: 2-ABA monomer). ....	130
Figure 4.36. Cycle 10 – 50 for the electrochemical synthesis of copolymers of doped in 1 M HCl solution, (a) 1:9 (aniline: 2-ABA monomer), and (b) 9:1.....	131
Figure 4.37. Microscopy images of visual appearance of poly-2-ABA grown on a Pt electrode surfaces. ....	133
Figure 4.38. Raman spectra of (a) 2-ABA monomer, (b) chemically synthesised poly-2-ABA doped with 1 M HCl, (c) chemically synthesised poly-2-ABA doped with 1 M H <sub>2</sub> SO <sub>4</sub> , and (d) electrochemically synthesised poly-2-ABA polymerised on Pt electrode with 1 M H <sub>2</sub> SO <sub>4</sub> . ....	133
Figure 4.39. Raman spectra of (a) 3-ABA monomer, (b) chemically synthesised poly-3-ABA doped with 1.5 M H <sub>2</sub> SO <sub>4</sub> , (c) chemically synthesised poly-3-ABA doped with 1 M HCl, and (d) electrochemically synthesised poly-3-ABA polymerised on Pt electrode with 1 M HCl. ....	134
Figure 5.1. <i>in situ</i> Raman spectra of electrochemically synthesised (a) PANI and (b) PANI-co-2-ABA (1:1) copolymer at different applied potentials for 25 mins in 1 M HCl solution obtained with $\lambda = 488$ nm. The PANI film was prepared by cycling the potential between -0.10 and 1.0 V at a scan rate of 50 mV s <sup>-1</sup> in a solution containing 0.1 M aniline and 1 M HCl solution. The copolymer was prepared in the presence of 1:1 of 0.05 M aniline:0.05 M 2-ABA in 1 M HCl electrolyte solution. ....	139
Figure 5.2. 2D synchronous correlation map of PANI in 1 M HCl electrolyte with combined spectra at different applied potentials. ....	140
Figure 5.3. 2D synchronous correlation map of PANI in 1 M HCl electrolyte with combined spectra at different applied potentials. ....	140
Figure 5.4. 2D asynchronous correlation map of PANI in 1 M HCl electrolyte with combined spectra at different applied potentials. ....	141
Figure 5.5. 2D asynchronous correlation map of PANI-co-2-ABA (1:1) in 1 M HCl electrolyte with combined spectra at different applied potentials. ....	141
Figure 5.6. 2D synchronous correlation map of PANI-co-2-ABA (1:1) in 1 M HCl electrolyte with combined spectra at different applied potentials. ....	142
Figure 5.7. Oxidised unit of PANI.....	142
Figure 5.8. PANI-co-2-ABA (7:3, aniline: 2-ABA) on a Pt electrode in 0.5 M H <sub>2</sub> SO <sub>4</sub> electrolyte.....	148
Figure 5.9. 2D synchronous correlation map of PANI-co-2-ABA (7:3, aniline: 2-ABA) in 0.5 M H <sub>2</sub> SO <sub>4</sub> electrolyte with combined spectra at different applied potentials. ....	149

Figure 5.10. 2D asynchronous correlation map of PANI-co-2-ABA (7:3, aniline: 2-ABA) in 0.5 M H <sub>2</sub> SO <sub>4</sub> electrolyte with combined spectra at different applied potentials. ....	149
Figure 5.11. PANI-co-2-ABA (7:3, aniline: 2-ABA) on a Pt electrode in 1 M HCl electrolyte.....	150
Figure 5.12. 2D synchronous correlation map of PANI-co-2-ABA (7:3, aniline: 2-ABA) in 1 M HCl electrolyte with combined spectra at different applied potentials. ....	150
Figure 5.13. 2D asynchronous correlation map of PANI-co-2-ABA (7:3, aniline: 2-ABA) in 1 M HCl electrolyte with combined spectra at different applied potentials. ....	151
Figure 5.14. <i>in situ</i> Raman spectra of electrochemically synthesised PANI-co-2-ABA at 9:1 (aniline: 2-ABA) 1 M HCl electrolyte. ....	152
Figure 5.15. 2D synchronous correlation map of PANI-co-2-ABA at 9:1 in 1 M HCl electrolyte with combined spectra at different applied potentials. ....	152
Figure 5.16. 2D asynchronous correlation map of PANI-co-2-ABA at 9:1 in 1 M HCl electrolyte with combined spectra at different applied potentials. ....	153
Figure 5.17. <i>in situ</i> Raman spectra of electrochemically synthesised PANI-co-2-ABA at 6:4 (aniline: 2-ABA) 1 M HCl electrolyte. ....	154
Figure 5.18. 2D synchronous correlation map of PANI-co-2-ABA at 6:4 in 1 M HCl electrolyte with combined spectra at different applied potentials. ....	154
Figure 5.19. 2D asynchronous correlation map of PANI-co-2-ABA at 6:4 in 1 M HCl electrolyte with combined spectra at different applied potentials. ....	155
Figure 5.20. <i>in situ</i> Raman spectra of electrochemically synthesised PANI-co-2-ABA at 4:6 (aniline: 2-ABA) 1 M HCl electrolyte. ....	155
Figure 5.21. 2D synchronous correlation map of PANI-co-2-ABA at 4:6 in 1 M HCl electrolyte with combined spectra at different applied potentials. ....	156
Figure 5.22. 2D asynchronous correlation map of PANI-co-2-ABA at 4:6 in 1 M HCl electrolyte with combined spectra at different applied potentials. ....	156
Figure 5.23. <i>in situ</i> Raman spectra of electrochemically synthesised PANI-co-2-ABA at 3:7 (aniline: 2-ABA) 1 M HCl electrolyte. ....	157
Figure 5.24. 2D synchronous correlation map of PANI-co-2-ABA at 3:7 in 1 M HCl electrolyte with combined spectra at different applied potentials. ....	157
Figure 5.25. 2D asynchronous correlation map of PANI-co-2-ABA at 3:7 in 1 M HCl electrolyte with combined spectra at different applied potentials. ....	158
Figure 5.26. <i>in situ</i> Raman spectra of electrochemically synthesised PANI-co-2-ABA at 1:9 (aniline: 2-ABA) 1 M HCl electrolyte. ....	159
Figure 5.27. 2D synchronous correlation map of PANI-co-2-ABA at 1:9 in 1 M HCl electrolyte with combined spectra at different applied potentials. ....	159
Figure 5.28. 2D asynchronous correlation map of PANI-co-2-ABA at 1:9 in 1 M HCl electrolyte with combined spectra at different applied potentials. ....	160
Figure 5.29. Cross-polarisation spectra of copolymer (a) chemical 1.5 M H <sub>2</sub> SO <sub>4</sub> with KIO <sub>3</sub> , (b) chemical 1.5 M H <sub>2</sub> SO <sub>4</sub> with APS, (c) chemical 0.5 M H <sub>2</sub> SO <sub>4</sub> with APS, (d) electrochemical 1.5 M H <sub>2</sub> SO <sub>4</sub> , and (e) electrochemical 0.5 M H <sub>2</sub> SO <sub>4</sub> .....	162
Figure 5.30. (a) chemical 1.5 M H <sub>2</sub> SO <sub>4</sub> 1:1 PANI: 2-ABA with APS, (b) chemical 0.5 M H <sub>2</sub> SO <sub>4</sub> 1:1 PANI: 2-ABA with APS. ....	163

Figure 5.31. Chemically synthesised copolymer doped with 1.5 M H <sub>2</sub> SO <sub>4</sub> with different oxidants: (a) with KIO <sub>3</sub> , (b) with APS.....	163
Figure 6.1. (a) Step 1 in 0.5 M oxalic acid, and (b) Step 2 in the presence of 0.1 M aniline monomer and 0.5 M oxalic acid; <i>I-t</i> transient of potentiostatic polarisation of anodising on marine grade aluminium 5083 alloy at 2 V (Ag/AgCl). .....	167
Figure 6.2. Potentiostatic current-time plots recorded for aluminium alloy 1100 in 0.5 M oxalic acid + 0.1 M aniline solution at different applied potentials. ....	168
Figure 6.3. Potentiostatic current-time plots recorded for aluminium alloy 4043 in 0.5 M oxalic acid + 0.1 M aniline solution at different applied potentials. ....	169
Figure 6.4. Potentiostatic current-time plots recorded for aluminium alloy 5083 in 0.5 M oxalic acid + 0.1 M aniline solution at different applied potentials. ....	169
Figure 6.5. Characterisation of the formed polymer on alloy 5083 in aniline-free 0.5 M oxalic acid electrolyte by cycling the potential from -0.1 to 0.9 V at a scan rate of 50 mV s <sup>-1</sup> .....	170
Figure 6.6. (a) Cycle 1 and 40, (b) One step electrodeposition of PANI by CV at cycle 50, 90, 130 and 170 recorded on marine grade aluminium 5083 from a solution containing 0.5 M oxalic acid in the presence of 0.1 M aniline monomer at a scan rate of 50 mV s <sup>-1</sup> .....	172
Figure 6.7. Oxidation and reduction peaks for cycling growth of PANI on marine grade aluminium 5083: (a) charge, and (b) current .....	173
Figure 6.8. (a) Cycle 125 of a one step aniline polymerisation on marine grade aluminium 5083 with 0.5 M oxalic acid in the presence of 0.1 M aniline from -0.2 to 0.9 V at 50 mV s <sup>-1</sup> , (b) cycle 3 of characterisation on alloy 5083 with an aniline-free electrolyte of 0.5 M oxalic acid.....	174
Figure 6.9. SEM images of aluminium alloy surfaces after Alkaline treatment – left column and Desmut – right column with 1100 alloy from the top row to 4043 in the middle while 5083 alloy is on the bottom row. ....	177
Figure 6.10. (a) aluminium as supplied, (b) chemically cleaned and pretreated aluminium, (c) anodised aluminium (Al <sub>2</sub> O <sub>3</sub> ) after being potentiostatically treated at 2 V for 30 mins in 0.5 M oxalic acid, and (d) potentiostatically grown PANI on top of the formed Al <sub>2</sub> O <sub>3</sub> with 0.5 M oxalic acid in the presence of 0.1 M aniline monomer at 2 V for 3 h.....	178
Figure 6.11. Mechanism of PANI growth on aluminium oxide electrode. The polymerisation growth of PANI was followed with time and illustrated that the growth of the CP starts from the metal upwards through the oxide layer and onto the surface of the electrode.....	179
Figure 6.12. (a) SEM images of one step process of step 2 of Figure 6.10(d), anodised and aniline polymerised marine grade aluminium 5083, SEM/EDS of marine grade aluminium 5083 of (b) treated aluminium (from image Figure 6.10(b) above), and (c) anodised aluminium oxide (from image Figure 6.10(d) above). ....	180
Figure 6.13. Atomic force microscope image of two-step electropolymerised PANI on 5083 alloy with step 1 being anodisation for an hour, followed by step 2 of oxidation for 3 h at 2 V. The scan size was (a) and (b) 80 μm, (c) and (d) 20 μm, (e) and (f) 1 μm; three-dimensional AFM pictures with the scan rate 6.1 Hz, with 256 sample points taken on each of the 256 lines to make up the image.....	181

Figure 6.14. Thickness of film formed at different applied voltage with one-step electrochemical polymerisation of aniline. ....	182
Figure 6.15. A cross sectional SEM image of two-step (Step 1; 1 h and Step 2; 0.5 h) electropolymerisation of PANI on marine grade aluminium alloy.....	183
Figure 6.16. FTIR spectra of PANI on marine grade aluminium potentiostatically grown at 2 V for 2 h. ....	184
Figure 6.17. Raman spectra of PANI with 0.5 M oxalic acid in the presence of 0.1 M aniline under potentiostatic method at 2 V for 2 h (a) 1100, (b) 4043, and (c) 5083 aluminium alloy.....	185
Figure 6.18. PANI in different oxidation state: (a) LEB, (b) ES, and (c) EB on 5083 alloy.	186
Figure 6.19. Region of 1600 – 1100 $\text{cm}^{-1}$ of PANI on 5083 in different oxidation state: (a) LEB, (b) ES, and (c) EB.....	186
Figure 6.20. Raman spectra (a) of the 3000 to 500 $\text{cm}^{-1}$ region, and (b) of the 1680 – 400 $\text{cm}^{-1}$ region of anodised electrode in red and anodised with PANI films grown on top in orange on an aluminium electrode. Raman shows characteristic absorption bands for PANI at 1604, 1464, 1226, 1170, 812, 750, 532 and 422 $\text{cm}^{-1}$ . [280].....	189
Figure 6.21. Raman mapping of the 1200 – 1100 $\text{cm}^{-1}$ region for PANI distribution along the anodised and PANI polymerised cross-section.....	190
Figure 6.22. (a) most stable form, (b) fully reduced form, and (c) fully oxidised form. ....	191
Figure 6.23. (a) Absorbance up to a value of 1.6, and (b) up to a value of 0.5, for 300 – 900 nm for <i>in-situ</i> UV-Vis in a 0.5 M oxalic acid electrolyte after running 10 cycles with 0.5 M oxalic acid in the presence of 0.1 M aniline monomer between -0.1 and 2.4 V at 50 $\text{mV s}^{-1}$ with (i) -0.4 V to 0.4 V (max), and (ii) 0.4 V to 1.2 V.....	193
Figure 6.24. (a) Absorbance up to a value of 0.8, and (b) to 0.15, for 300 – 900 nm of <i>in-situ</i> UV-Vis in 0.5 M oxalic acid electrolyte after running 10 cycles in 0.5 M oxalic acid + 0.1 M aniline between -0.1 and 1 V at 50 $\text{mV s}^{-1}$ (i) -0.1 V to 0.5 V (max), and (ii) 0.5 V to 1 V..	194
Figure 6.25. The absorbance on electrode potential for the absorbance band at $\lambda = 720$ nm in red, $\lambda = 445$ nm in blue and at $\lambda = 360$ nm in yellow with the PANI prepared in 0.5 M oxalic acid electrolyte in the presence of 0.1 M aniline monomer after running 10 cycles between (a) -0.1 and 1 V at 50 $\text{mV s}^{-1}$ , and (b) -0.1 and 2.4 V at 50 $\text{mV s}^{-1}$ scan from -0.4 V to 1.2 V.....	195
Figure 6.26. Bode plots of impedance modulus ( $ Z $ ) vs frequency as a function of immersion time in 3.5 wt% NaCl solution for: (a) pure 1100, (b) pure 4043, and (c) pure 5083 alloys.	198
Figure 6.27. Bode plots of impedance modulus ( $ Z $ ) vs frequency as a function of immersion time in 3.5 wt% NaCl solution for (a) PANI grown on 1100 at 1 V, (b) PANI grown on 4043 at 1 V, and (c) PANI grown on 5083 at 1V. ....	199
Figure 6.28. Bode plots of impedance modulus ( $ Z $ ) vs frequency as a function of immersion time in 3.5 wt% NaCl solution for (a) PANI grown on 1100 at 2 V, (b) PANI grown on 4043 at 2 V, and (c) PANI grown on 5083 at 2V. ....	201
Figure 6.29. Bode plots of impedance modulus ( $ Z $ ) vs frequency as a function of immersion time in 3.5 wt% NaCl solution for (a) PANI grown on 1100 at 3 V, (b) PANI grown on 4043 at 3 V, and (c) PANI grown on 5083 at 3 V. ....	202

Figure 6.30. Bode plots of impedance modulus ( $ Z $ ) vs frequency as a function of immersion time in 3.5 wt% NaCl solution for (a) PANI grown on 1100 at 4 V, (b) PANI grown on 4043 at 4 V, and (c) PANI grown on 5083 at 4 V. ....	204
Figure 6.31. Nyquist plot of impedance data for coated and uncoated aluminium alloy at day 3 on (a) and (b) 1100 alloy (c) and (d) 4043 alloy and (e) and (f) 5083 marine grade alloy • pure alloy ○ anodised 1 V ▼ PANI 1 V △ PANI 2 V ■ PANI 3 V □ PANI 4 V. ....	205
Figure 6.32. Nyquist plot of impedance data for coated and uncoated aluminium alloy at day 15 on (a) and (b) 1100 alloy (c) and (d) 4043 alloy and (e) and (f) 5083 marine grade alloy • pure alloy ○ anodised 1 V ▼ PANI 1 V △ PANI 2 V ■ PANI 3 V □ PANI 4 V. ....	206
Figure 6.33. Nyquist plot of impedance data for coated and uncoated aluminium alloy at day 50 on (a) and (b) 1100 alloy (c) and (d) 4043 alloy and (e) and (f) 5083 marine grade alloy • pure alloy ○ anodised 1 V ▼ PANI 1 V △ PANI 2 V ■ PANI 3 V □ PANI 4 V. ....	207
Figure 6.34. Nyquist plot of the imaginary component ( $Z_{imag}$ ) vs the real component ( $Z_{real}$ ) of the impedance for (a) pure marine grade aluminum alloy, (b) chemically pretreated pure marine grade aluminium alloy, ● initial, ▼ Day 15 ■ Day 30, ◇ Day 50. ....	210
Figure 6.35. Nyquist plot of impedance data for (a) anodised marine grade aluminum alloy, (b) PANI coated 5083 at 1 V as a function of immersion time in 3.5 wt% NaCl solution ● initial ▼ Day 15 ■ Day 30 ◇ Day 50. ....	211
Figure 6.36. Nyquist plot of impedance data for PANI coated 5083 at 2 V as a function of immersion time in 3.5 wt% NaCl solution, ● initial ▼ Day 15 ■ Day 30 ◇ Day 50. ....	212
Figure 6.37. Nyquist plot of impedance data for PANI coated 5083 at 3 V as a function of immersion time in 3.5 wt% NaCl solution, ● initial ▼ Day 15 ■ Day 30 ◇ Day 50. ....	212
Figure 6.38. Nyquist plot of impedance data for PANI coated 5083 at 4 V as a function of immersion time in 3.5 wt% NaCl solution, ● initial ○ Day 15 ■ Day 30 ◇ Day 50. ....	214
Figure 6.39. Nyquist plot of impedance data on day 15 for marine grade aluminium as a function of different surface in 3.5 wt% NaCl solutions. ....	215
Figure 6.40. Bode plots ( $\log$ frequency vs. $\log  Z $ ) for impedance spectra at various immersion times for bare aluminium 5083, (a) PANI coated aluminium 5083 grown at 3 V, and (b) on anodised aluminium in 3.5 wt% saline solution at room temperature. ....	216
Figure 6.41. DPPH• scavenging capacity of electrochemically synthesised PANI samples on 5083 alloy; these were grown on alloy for 20 mins. ....	218
Figure 6.42. Complete set of % inhibition of 1100 alloy – 20 mins. ....	218
Figure 6.43. Complete set of % inhibition of 4043 alloy – 20 mins. ....	220
Figure 6.44. Complete set of % inhibition of 5083 alloy – 20 mins. ....	220
Figure 6.45. % inhibition of aluminium alloys electropolymerised at 1 V for 20 mins. ....	221
Figure 6.46. % inhibition of aluminium alloys electropolymerised at 2 V for 20 mins. ....	221
Figure 6.47. % inhibition of aluminium alloys electropolymerised at 3 V for 20 mins. ....	222
Figure 6.48. % inhibition of aluminium alloys electropolymerised at 4 V for 20 mins. ....	222
Figure 7.1. Image of coupon coated PANI by holding the potential at 2 V for 2 h on the bottom ½ while the bare aluminium top ½ act as an internal control. ....	225
Figure 7.2. Observation of coupons upon time. ....	228
Figure 7.3. IVIS image surfaces with quantified area challenged with bioluminescent <i>E. coli</i> ATCC 25922 <i>lux</i> strains taken after 4 days of bacterial fouling, with the top half of each	



aluminium being the control labelled A; while the coated half is labelled B. The pseudocolour bar indicates bioluminescence intensity.....	228
Figure 7.4. Bioluminescence images for coated and control samples. Both PANI and aluminium control samples have their own internal control, as only the bottom half of these were coated. ....	229
Figure 7.5. Mean average radiance values collected from three samples at different time intervals, showing the antifouling performance against <i>E. coli</i> ATCC 25922 <i>lux</i> bacteria. PANI films were grown electrochemically at a fixed potential of 2 V (Ag/AgCl) for 1 h. ..	230
Figure 7.6. Mean average radiance values collected from three samples at different time intervals, showing the antifouling performance against <i>E. coli</i> ATCC 25922 <i>lux</i> bacteria. PANI films were grown electrochemically at a fixed potential of 2 V (Ag/AgCl) for 2 h. ..	231
Figure 7.7. Mean average radiance values collected from three samples at different time intervals, showing the antifouling performance against <i>E. coli</i> 536 <i>lux</i> , a sticker version of <i>E. coli</i> ATCC 25922 <i>lux</i> .....	232
Figure 7.8. <i>Vibrio fischeri</i> for (a) PANI, (b) Control, and (c) commercial. Both PANI and aluminium control samples have their own internal control, as only the top half of these were coated while the bottom half was covered with masking tape in the preparation process and later removed before testing.....	233
Figure 7.9. <i>Vibrio harveyi</i> for (a) control, (b) PANI, and (c) commercial. Both PANI and aluminium control samples have their own internal control, as only the top half of these were coated. ....	233

## LIST OF SCHEMES

Scheme 1.1. The redox and acid-base forms of PANI [42, 43] .....	8
Scheme 1.2. PANI-EB doped with HCl (adapted from [48]) .....	9
Scheme 1.3. Initiation and formation of the aniline radical cation .....	9
Scheme 1.4. Resonance forms of the aniline radical cation .....	9
Scheme 1.5. Subsequently attacks aniline by electrophilic substitution.....	10
Scheme 1.6. Propagation proceeds by oxidation of the primary amine end of a growing polymer chain.....	10
Scheme 1.7. Electrophilic substitution.....	10
Scheme 1.8. Poly-3-ABA in its polaron and bipolaron states .....	12
Scheme 1.9. Synthetic steps during polymerisation .....	13
Scheme 1.10. Reaction of DPPH radical with P being a polymer chain. ....	37
Scheme 1.11. Reaction of DPPH radical with PANI (adapted from [159]). .....	38
Scheme 2.1. 2-ABA oxidation and polymerisation of poly-2-ABA.....	58
Scheme 2.2. Homopolymerisation of 2-ABA (adapted from [210]) .....	59
Scheme 2.3. Copolymerisation of aniline and 2-ABA (adapted from [202]). .....	60
Scheme 2.4. Dimer formation and its absorption values (adapted from [193]).....	64
Scheme 3.1. PANI structure.....	87
Scheme 5.1. Poly-co-2-ABA structure. ....	160

## LIST OF TABLES

Table 2.1. The metal composition of the three grade of aluminium alloys used .....	43
Table 2.2. The assignments for FTIR bands observed in copolymer, PANI-co-3-ABA [44, 48] .....	53
Table 2.3. The assignment of Raman characteristic bands for PANI-co-2-ABA [48] .....	57
Table 3.1. Band assignments for the Raman spectra of PANI obtained with an excitation wavelength of $\lambda = 488$ nm .....	80
Table 3.2. Principal bands – seen in the UV-Vis spectra of the PANIs. ....	86
Table 4.1. Molecular weights of the four poly-ABAs formed prepared via chemical synthesis .....	94
Table 4.2. Minimum bacterial concentration for <i>S. aureus</i> 6838. ....	107
Table 4.3. Minimum bacterial concentration for <i>E. coli</i> 25922 .....	107
Table 5.1. Band assignments of Raman spectra of PANI obtained with $\lambda = 488$ nm.....	146
Table 5.2. Band assignments of Raman spectra of 1 M HCl copolymer at 1:1 obtained with $\lambda = 488$ nm. ....	147
Table 5.3. Assignments of bands from Figure 5.8. ....	148
Table 6.1. Composition of Al, Si and O detected using SEM/EDS of 1100 alloy surfaces ..	176
Table 6.2. Composition of Al, Mg, Si and O detected using SEM/EDS of 4043 alloy surfaces .....	176
Table 6.3. Composition of Al, Mg and Si detected using SEM/EDS of 5083 marine grade aluminium alloy surfaces. ....	176
Table 6.4. Raman spectroscopy assignment for PANI in their different oxidation states.....	186

## LIST OF ABBREVIATIONS

ABA	Aminobenzoic acid
AFM	Atomic Force Microscopy
APS	Ammonium persulfate
$C_{dl}$	double layer capacitance
CFU	Colony forming unit
CP	Conducting polymer
CPMAS	Cross Polarisation Magic Angle Spinning
CV	Cyclic voltammogram
DI	deionised water
DPPH	1, 1-diphenyl-2-picrylhydrazyl
EB	Emeraldine base
$E_{corr}$	corrosion potential
EIS	Electrochemical Impedance Spectroscopy
ES	Emeraldine salt
FTIR	Fourier Transform Infrared (Spectroscopy)
GPC	Gel permeation chromatography
HCl	Hydrochloric acid
$i_{corr}$	corrosion current density
ITO	Indium-doped tin oxide on glass substrate
$KIO_3$	Potassium iodide
LEB	reduced leucoemeraldine base
NMP	N-methyl-2-pyrrolidone

NQS	Non-Quaternary Suppressed
PANI-co-2-ABA	Copolymer PANI and 2-ABA
PANI-co-3-ABA	Copolymer PANI and 3-ABA
Poly-2-ABA	Poly-2-aminobenzoic acid
Poly-3-ABA	Poly-3-aminobenzoic acid
PANI	Polyaniline
PNB	pernigraniline
Pt	platinum
$R_{ct}$	charge transfer resistance
SCE	Saturated Calmoel Electrode
SEM	Scanning electron microscope
SSNMR	Solid-state Nuclear Magnetic Resonance
TBT	Tributyltin
TMS	Tetramethylsilane
UV	Ultraviolet

The following papers and conference presentations have emanated from this thesis:

Publications:

1. To T., Swift S., Kilmartin P. (2013) Evaluation of electrodeposited polyaniline on marine grade aluminium for antifouling properties, *International Conference on Marine Coatings*, Rina HQ, London, UK, 18<sup>th</sup> April 2013. In press.
2. To T., Kilmartin P. (2013) Polyaniline deposition on aluminium alloys – synthesis, characterisation and applications. *Trends in Polyaniline*. Nova Science Publisher, NY, In press.
3. To T., Kilmartin P. (2013) Electrochemically synthesised polyaniline on marine grade aluminium, *Sixth International Conference on Advanced Materials and Nanotechnology*, Auckland, New Zealand, 11-15<sup>th</sup> February, 2013. In press.
4. To T. (2010) Anti-fouling Coatings, *Brush Strokes - SCANZ Magazine*, April, pp. 20-21, 2010.

Conference Presentations:

1. To T., Swift S., Kilmartin P. (2013) Electrodeposited polyaniline on aluminium for antifouling, 2013 Research Showcase, Auckland, New Zealand, 12<sup>th</sup> June, 2013.
2. To T., Swift S., Kilmartin P. (2013) Evaluation of electrodeposited polyaniline on marine grade aluminium for antifouling properties, *International Conference on Marine Coatings*, Rina HQ, London, UK, 18<sup>th</sup> April 2013.
3. To T., Swift S., Kilmartin P. (2012) Electrodeposited polyaniline on marine grade aluminium, *6<sup>th</sup> PERC/3<sup>rd</sup> HP Symposium*, Auckland, New Zealand, 6-7 December, 2012.

4. To T., Kilmartin P., Edmonds N., Conney R., Eastal A. (2011) Polyaniline on aluminium surfaces, *7<sup>th</sup> PERC/2<sup>nd</sup> HP Symposium*, Auckland, New Zealand, 5-7 November, 2011.
5. To T., Wu J., Anderson K., Bennett J., Stevenson D., Edmonds N., Cooney R., Eastal A. (2009) Anti-Microbial Surfaces - nano structured surfaces, *5<sup>th</sup> PERC/2<sup>nd</sup> HP Symposium*, Auckland, New Zealand, 3-4 December, 2009.

Conference Proceedings:

1. To T., Swift S., Kilmartin P. (2013) Electrodeposited polyaniline on aluminium for antifouling, *2013 Research Showcase*, Auckland, New Zealand, 12<sup>th</sup> June, 2013.
2. To T. Edmonds N., Cooney R., Jin J., Gizdavic-Nikolaidis M., Ray S., Kilmartin P. (2012) Evaluation of Polyaniline and aminobenzoic acid copolymer formation by chemical and electrochemical methods, *2012 Chemistry Showcase*, Auckland, New Zealand, 6<sup>th</sup> June, 2012.
3. To T., Edmonds N., Ray S., Cooney R., Gizdavic-Nikolaidis M., Eastal A. (2011) Electrodeposition of polyaniline on aluminium alloy, *2011 Chemistry Showcase*, Auckland, New Zealand, 8<sup>th</sup> June, 2011.



## Co-Authorship Form

This form is to accompany the submission of any PhD that contains research reported in published or unpublished co-authored work. **Please include one copy of this form for each co-authored work.** Completed forms should be included in all copies of your thesis submitted for examination and library deposit (including digital deposit), following your thesis Abstract.

Please indicate the chapter/section/pages of this thesis that are extracted from a co-authored work and give the title and publication details or details of submission of the co-authored work.

Chapter 1. This Chapter was presented as:  
 T. To and P. Kilmartin (2013) Polyaniline deposition on aluminium alloys - synthesis, characterisation and applications. *Trend in Polyaniline*. Nova Science Publisher, NY, In press.

Nature of contribution by PhD candidate	Introduction
Extent of contribution by PhD candidate (%)	90

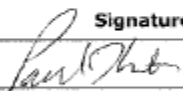
### CO-AUTHORS

Name	Nature of Contribution
Paul Kilmartin	Scientific advice, discussion

### Certification by Co-Authors

The undersigned hereby certify that:

- ❖ the above statement correctly reflects the nature and extent of the PhD candidate's contribution to this work, and the nature of the contribution of each of the co-authors; and
- ❖ in cases where the PhD candidate was the lead author of the work that the candidate wrote the text.

Name	Signature	Date
Paul Kilmartin		1/7/2013



## Co-Authorship Form

This form is to accompany the submission of any PhD that contains research reported in published or unpublished co-authored work. **Please include one copy of this form for each co-authored work.** Completed forms should be included in all copies of your thesis submitted for examination and library deposit (including digital deposit), following your thesis Abstract.

Please indicate the chapter/section/pages of this thesis that are extracted from a co-authored work and give the title and publication details or details of submission of the co-authored work.

Chapter 2 & 6. This Chapter was presented as:  
 T. To and P. Kilmartin (2013) Electrochemically synthesised polyaniline on marine grade aluminium, Sixth International Conference on Advanced Materials and Nanotechnology, Auckland, New Zealand, 11-15<sup>th</sup> February, 2013. In press.

Nature of contribution by PhD candidate	Experimental section
Extent of contribution by PhD candidate (%)	90

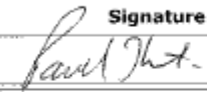
### CO-AUTHORS

Name	Nature of Contribution
Paul Kilmartin	Scientific advice, discussion

### Certification by Co-Authors

The undersigned hereby certify that:

- ❖ the above statement correctly reflects the nature and extent of the PhD candidate's contribution to this work, and the nature of the contribution of each of the co-authors; and
- ❖ in cases where the PhD candidate was the lead author of the work that the candidate wrote the text.

Name	Signature	Date
Paul Kilmartin		1/7/2013

## Co-Authorship Form

This form is to accompany the submission of any PhD that contains research reported in published or unpublished co-authored work. **Please include one copy of this form for each co-authored work.** Completed forms should be included in all copies of your thesis submitted for examination and library deposit (including digital deposit), following your thesis Abstract.

Please indicate the chapter/section/pages of this thesis that are extracted from a co-authored work and give the title and publication details or details of submission of the co-authored work.

Chapter 6 & 7. This Chapter was presented as:

T. To, S. Swift, P. Kilmartin. Evaluation of electrodeposited polyaniline on marine grade aluminium for antifouling properties, International Conference on Marine Coatings, Rina HQ, London, UK, 18th April 2013. In press.

Nature of contribution by PhD candidate

Experimental design, sample preparation procedure, novel testing procedure, Results

Extent of contribution by PhD candidate (%)

90

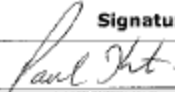
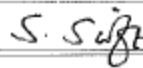
### CO-AUTHORS

Name	Nature of Contribution
Paul Kilmartin	Scientific advice, discussion
Simon Swift	Scientific advice, discussion, antifouling experimental design

### Certification by Co-Authors

The undersigned hereby certify that:

- ❖ the above statement correctly reflects the nature and extent of the PhD candidate's contribution to this work, and the nature of the contribution of each of the co-authors; and
- ❖ in cases where the PhD candidate was the lead author of the work that the candidate wrote the text.

Name	Signature	Date
Paul Kilmartin		1/7/2013
Simon Swift		1 JULY 2013

## CHAPTER ONE: Introduction

This chapter has been partially published as:

1. To. T., Kilmartin P. (2013) Polyaniline deposition on aluminium alloys – synthesis, characterisation and applications. *Trends in Polyaniline*. Nova Science Publisher, NY, in press.
2. To. T. (2010) Anti-fouling Coatings, *Brush Strokes - SCANZ Magazine*, April, 20-21.

### 1.1. Abstract

In this chapter a general introduction will be provided to the problem of marine fouling, aluminium as the material of choice to use in marine applications, along with aniline and substituted aniline polymers. The properties of PANI, in particular, will be introduced, with emphasis on the techniques used in the present study. This includes the reported literature on the understanding of the mechanisms of charge transport in PANI, polyaminobenzoic acid (poly-ABA) and its copolymers, along with relevant spectroscopic studies which have been undertaken to characterise the polymers.

### 1.2. General background

Fouling can occur in both marine and non-marine environments (e.g. pipelines). Antifouling systems are generally defined as coatings that can prevent the settling of marine microorganisms on ship hulls through controlled release of antifouling agents. Unfortunately, the released agents often also exhibit environmental toxicity; hence there is considerable interest in the development of non-toxic coatings. The growth of marine organisms on submerged man-made structures are a major problem, examples of which include: (1) fouling of the hull of ships resulting in high frictional resistance and increased weight due to fouling, requiring greater fuel consumption, reduced speed and increased docking times and maintenance costs [1-3], (2) fouling of ropes, buoys, cages and pontoons used in aquaculture, (3) interference with defective sensor responses.

The problem of marine biofouling has been recognised in aquaculture [4] and combated for more than 2000 years. A variety of coatings were developed in the mid-1800s based on the

idea of dispersing a toxicant in a polymeric vehicle. This fouling is generally controlled by coating the underwater parts of ships with an antifouling treatment, in the form of a chemical biocide. In the early days of sailing ships, lime and later arsenic were used to coat ship hulls, until the modern chemical industry replaced these with metallic compounds in the development of effective antifouling paints. Tributyltin (TBT) was one of the best performing antifouling coating systems, but this has been effectively banned and replaced by other compounds such as cuprous oxides or alternative solutions, as will be discussed in more detail below in Section 1.3. These compounds work in a manner whereby the active agents slowly leach into the sea water killing barnacles and other marine life that have attached to the ship. However, studies have shown that these compounds persist in the water, killing sea-life, harming the marine environment and potentially entering the food chain. For example, the use of organotin TBT [4] has been proven to cause deformation in oysters and sex changes in whelks.

Chemical reactions and diffusion phenomena are key mechanisms in the performance of biocide-based antifouling paints; these mechanisms are affected by sea water conditions. Seawater often has to penetrate into the paint, dissolve the biocides, which then diffuse out into the bulk phase. The organic matrix is designed for the slow release of antifouling actives into seawater from within the paint pores. The chemical characteristics of the binder are a further consideration, and are defined by their water solubility, antifouling being classified into insoluble matrix types and soluble matrix types.

Over the years there have been numerous methods developed to simulate and replicate the ocean environment in a lab to provide accelerated antifouling testing methods [5, 6]. Most research focuses on a) duplicating the marine environment, i.e. setting up a tank at a controlled pH, salinity and temperature, and b) monitoring the test panels over time. Rather than generating and replicating the marine environment in-house, the aim is to develop an antifouling testing method with the use of microorganisms to produce a biofilm and to evaluate the performance at the micro-molecular level, which would ideally reduce the time required to obtaining the necessary information. This is one of the ultimate goals of this project and the ability to use such tests will be beneficial for the coatings industry.

### 1.3. Current antifouling coatings system

#### 1.3.1. Insoluble matrix paints

Insoluble polymer matrices, also known as contact leaching or continuous contact matrices, do not polish or erode after immersion in water. Vinyl, epoxy, acrylic or chlorinated rubber polymers are common commercial polymers in use. Seawater penetrates into the film and dissolves soluble species, (shaded circles in Figure 1.1), through interconnecting pores. After a certain time in service, dissolved actives travel further through the thick leached layer and the rate of release rate falls below the minimum value required for preventing fouling, as illustrated in Figure 1.1. These coatings are mechanically strong and generally resistant to oxidation and photo degradation when in dry docks. However, the main drawback with these coatings is the comparatively short lifetime of the product, typically 12 – 18 months.

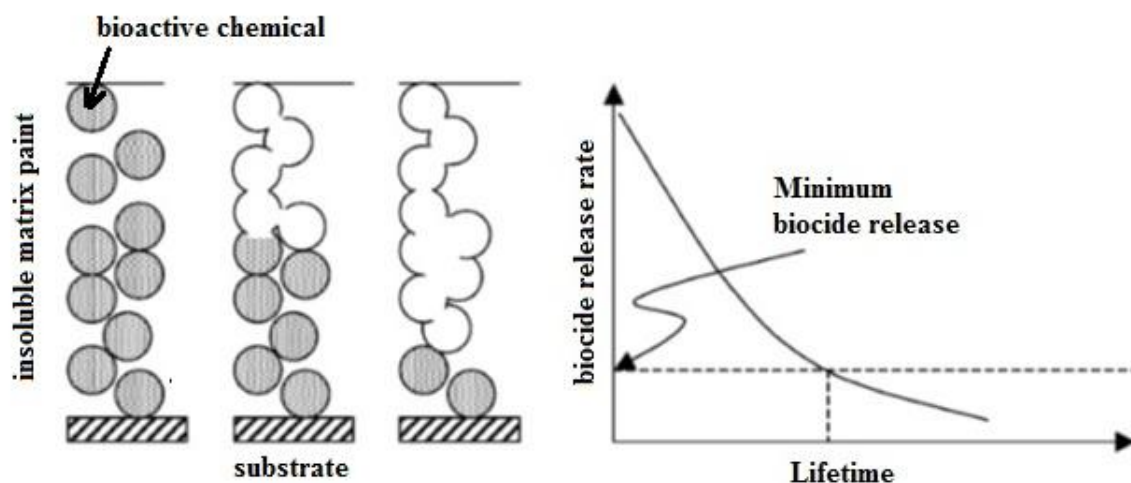


Figure 1.1. Working scheme and biocide release rates of traditional insoluble matrix paints. “Minimum biocide release” indicates the limit for efficient protection against fouling, dependent on the fouling conditions (adapted from [7]).

#### 1.3.2. Soluble matrix paints

Soluble coatings were developed to avoid the loss of antifouling efficiency with time by using a soluble binder (Figure 1.2). Rosin, the classical film-forming material used in such systems, is a natural resin obtained from the exudation of pine and fir trees. One disadvantage of this system is that the erosion rate increases exponentially with increasing vessel speed

when the rosin content exceeds a certain value. However, this invention did not work because of the inability to control the solubilisation rate.

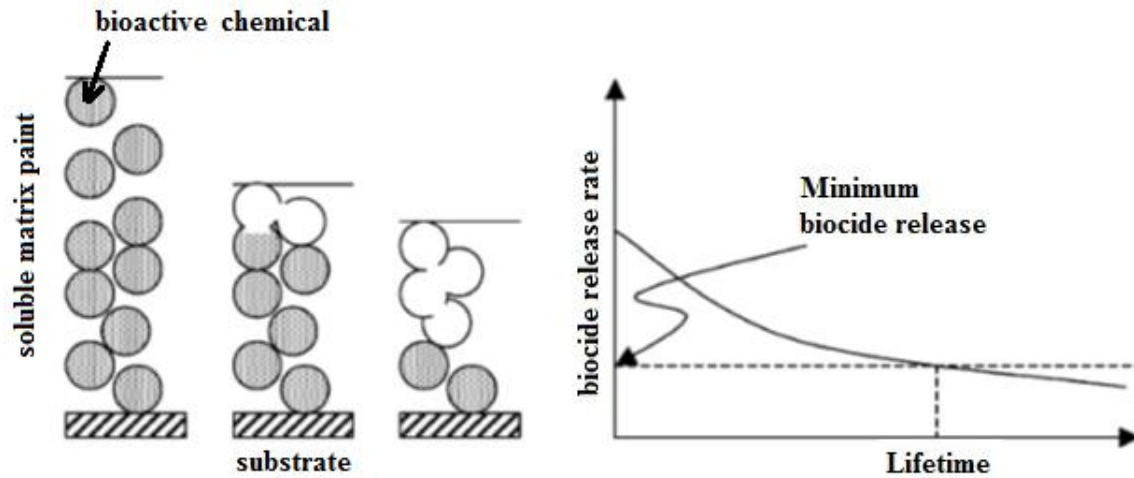


Figure 1.2. Working scheme and biocide release rates of traditional soluble matrix paints. “Minimum biocide release” indicates the limit for efficient protection against fouling, dependent on the fouling conditions (adapted from [7]).

Van de Kerk and his co-workers were first to report the antifouling possibilities of the broad spectrum high toxicity TBT-containing compounds. Soluble matrix paints containing TBT were discovered and commercialised in the early 1960s, and have become the most successful antifouling product to date. Tributyltin self-polishing copolymer paints (TBT-SPC paints) were invented in 1958, the TBT being grafted to a polyacrylic backbone via an ester group. A hydrolysis reaction allows the release of toxic molecules and the erosion of the coating.

However, TBT and its derivatives were found to have a harmful effect on marine ecosystems. As a consequence, the use of TBT-based antifouling paints was banned in New Zealand from 2003, and the presence of such paints on the surface of vessels in New Zealand waters was banned from 2008. The short notice for the removal of TBT-based paints has forced researchers to invent new technologies. The substitution of TBT-paints began at the end of the 1990s by blending polyacrylic resins and rosin with two types of bioactive molecules: organic and mineral biocides. The major drawback for this type of coating is the uncontrolled release of a large quantity of toxic compounds in the early stages of use. The ban of harmful

substances in antifouling paints requires the development of new antifouling coatings with negligible side effects and no potential accumulation in the aquatic environment.

The marine industry is at a critical stage of development and is effectively starved of new technology to replace TBT-based products that would yield the same economic benefits, but would have fewer harmful effects on the environment. While conventional antifouling and slow release antibacterial coatings are still used, most are of limited effectiveness. The importance of this area is further highlighted by current legislation which prohibits the use of tin-based antifouling agents and restricts the use of copper based analogues. However such legal requirements cannot be applied to international shipping, where tin-based antifouling systems are still commonly used. This situation is clearly untenable; however, effective alternative antifouling technologies are not available. With the fear of a complete ban on the use of copper compounds, numerous antifoulants have been introduced in recent years. However, there are concerns that organic booster biocides in the antifouling paints which will replace TBT-based coatings could cause serious environmental damage. Some have described this as moving “out of the frying pan into the fire” [8].

Apart from introducing new antifoulants, there are a number of further approaches being considered, including silyl and copper acrylate chemistry. An additional method is electrochemical plating, where the surface to be protected is electrically charged to prevent attachment of organisms, and which thereby replaces depleting-type rosin based formulations. However, some relatively new non-biodegradable antifoulant compounds in use have showed up in very high levels in water samples in Europe, and concern is again growing about the potential risk to aquatic organisms [9].

If a suitable compound is not found before the complete ban of cuprous compounds, the result will be fouled ships hulls and, therefore, an increase in the burning of fossil fuels resulting in even greater environmental damage. To prevent this, the objective with respect to marine fouling is to prevent or delay significantly the onset of the first stages of microfouling [10]. In nature, some organisms may be heavily fouled over much of their surfaces, retaining fouling resistance for vital processes, whereas others (e.g. echinoderms) can be totally fouling-free, to the extent that it is difficult to even find bacteria on their outer surfaces [9]. The formation of a 10 µm biofilm layer on the hull can cause a 1% decrease in fuel efficiency [9], and macrofouling can cause this layer to increase to several centimetres in thickness thereby greatly reducing fuel efficiency. In addition, these biofilms encourage corrosion [9].

The key to solving this problem lies with new nanotechnology with novel surface functionalities, including chemical and topographical modifications. Such surfaces will provide novel properties including super-hydrophobic behaviour (to impart water repellence and self-cleaning action), antibacterial properties and antifouling performance. Other modifications will provide surfaces with thermo-responsive behaviour, utilising nanodispersed conducting polymers (CPs) as the antibacterial/antifungal components (possibly in combination with other antibacterials).

Marine algae play the most important role in the colonisation of all types of test panels. They are the most dominant fouling group, with animals playing only a secondary role in the fouling community [11]. A number of animal foulers were nevertheless identified and some of the common ones are Tubularia laryx, Bryozoans, Barnacles and Jassa sulcata. Tubularia laryx are colonial animals formed as small white tufts scattered on the panel surface. These reach up to 15% cover on most panels, although exceptionally these can reach 70% coverage on some surfaces. Bryozoans form occasional colonies on panel surfaces. Jassa sulcata are mobile amphipods that form homes amongst the fouling and are not uncommon on panel surfaces.

## **1.4. Conducting polymers**

### **1.4.1. Introduction to polyaniline and polyaminobenzoic acid**

Polyaniline (PANI) was the first CP to show antifouling properties [12]. Studies from Wang et al. suggested that conductive PANI has a special synergetic antifouling effect on other antifouling agents like cuprous oxide [12]. This group has tested the antifouling behaviour of various PANI coatings, the main focus being epoxy-amine and PU coating systems. They have developed antifouling coatings based on PANI that are effective for at least two months, as well as synergetic antifouling using DBSA doped PANI with cuprous oxide or dichlorodiphenyltrichloroethane (DDT).

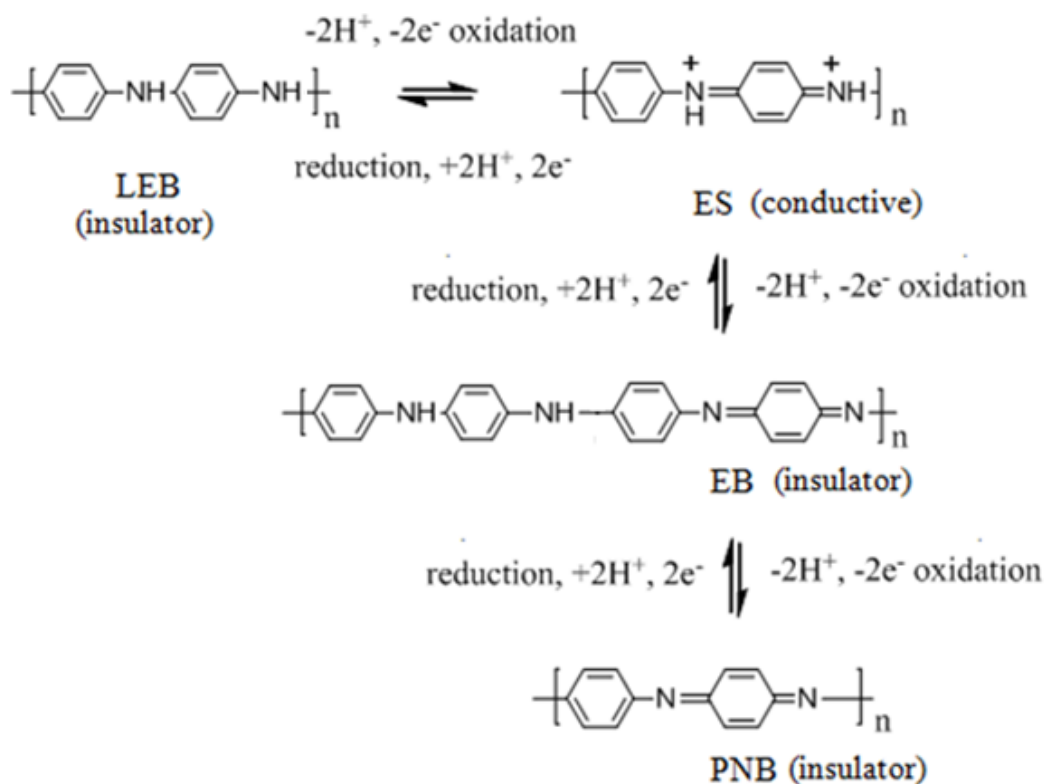
PANI is one of the most promising CPs, which was first known as aniline black in 1835 [13]. It has been intensively studied since the 1980s as a member of the family of CPs recognised at that time [14]. Owing to its well behaved electrochemistry and easy protonation reversibility, excellent redox recyclability, and variable electrical conductivity that can be tuned by varying the pH, PANI is unique in the family of CPs [15-18]. PANI has attracted the attention of scientists due to its numerous advantages over other polymers, i.e. low cost, non-



toxic nature [19], ease of synthesis [19, 20], antifouling and anticorrosive properties [12, 16-19, 21-22], environmental stability and unique chemical, optical and electronic properties [19, 23, 24]. It is these characteristics that enable researchers to extend these properties and use them in applications such as sensors, antioxidant agents, antifouling and anticorrosive protection [12, 16-17, 21-22, 25-26, 27-29].

PANI is a phenylene based polymer with alternating phenylene ring and  $-NH-$  groups that undergoes oxidation, allowing PANI to exist in three different oxidation states: leucoemeraldine, LEB (fully reduced form); emeraldine, EB (partially oxidised form) and pernigraniline, PNB (fully oxidised form), through the loss or gain of electrons and protons, as shown below in Scheme 1.1. However, only one form is conducting, namely the emeraldine salt (ES), which also relies on acid-doping for high conductivity and electroactivity. PANI in intermediate oxidation states thus contains two principle units: (i) the fully reduced form of repeat unit containing two benzenoid (B) rings, and (ii) the fully oxidised form of a repeat unit containing one quinoid (Q) ring and one B ring. In both cases the nitrogen atoms on the polymer backbone may be protonated depending on the dopant used and the pH of the solution. Among the different oxidation states of PANI, LEB and PNB have been found to be insulators [20]. The ability of the polymer to easily adjust conducting oxidation states creates great interest for industry [15]. Given its versatility and the various forms available, PANI is suitable for many applications, including the following: secondary batteries, biosensors [30], corrosion protection [16-17, 21-22], conducting coatings [16-18, 21-22, 25-26, 31-32], films [33-36], composites [37-38] and antistatic packing materials [39]. On the other hand, PANI has drawbacks due to its intractable nature in certain solvents [40].

PANI can be prepared by various methods, mainly electrochemical polymerisation through the anodic oxidation of aniline on an inert electrode [41], and chemical polymerisation via the direction oxidation of aniline by chemical oxidants [19]. Further approaches include photochemical initiated polymerisation, enzyme-catalysed polymerisation and polymerisation employing electron acceptors.



Scheme 1.1. The redox and acid-base forms of PANI [42, 43].

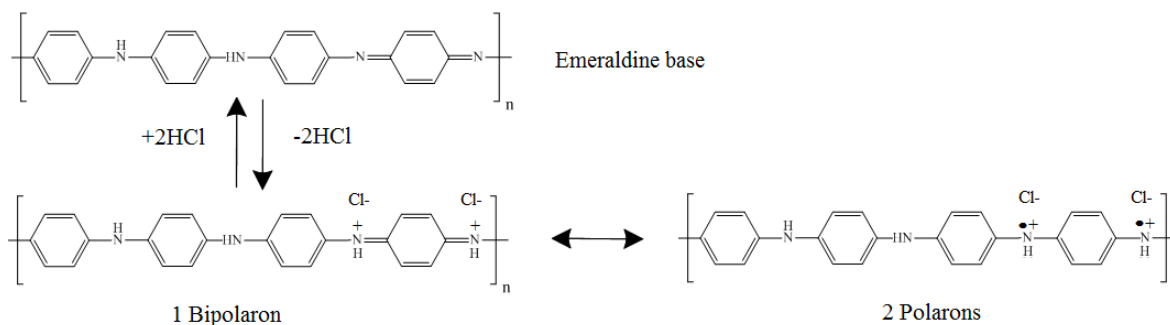
However, there exist limitations with this polymer due to poor processability, owing to stiffness of the backbone along with incompatibility in many solvents. The solubility can be improved by the use of substituted anilines, many of which have been studied. This shortcoming has also been overcome by the synthesis of aniline copolymers, as well as using substituted aniline derivatives [44-46].

The easily synthesised and air-stable PANI, coated on metal substrates, has been considered for a range of applications, for example, corrosion prevention, which has been studied widely, and more recently for surface protection in antibacterial and antifouling coatings. In this thesis, the focus is placed upon chemical and electrochemical oxidative polymerisation of aniline monomers in acidic solutions, for their application to the coating of aluminium surfaces.

#### 1.4.2. Mechanisms of conduction for conducting polymers

Intrinsically CPs exhibit minimal electrical conductivity in the neutral or uncharged forms. However, conductivity can be elevated by doping, which involves addition (*n*-doping) or removal (*p*-doping) of electrons from the polymer backbone to induce localised charges in

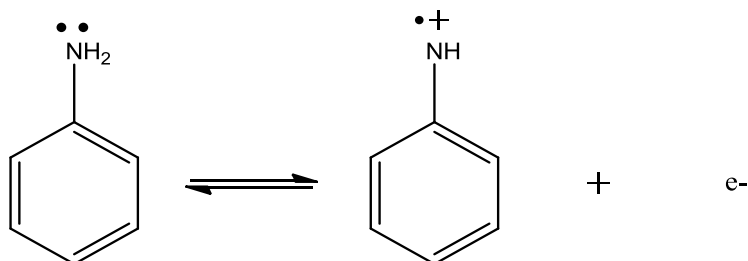
the form of polarons [47]. The formation of a polaron involves the removal of one electron locally from a carbon or nitrogen atom, while the removal of a second electron from an oxidised site forms a bipolaron. These polarons and bipolarons are believed to be the principal charge carriers in conjugated CPs, see Scheme 1.2.



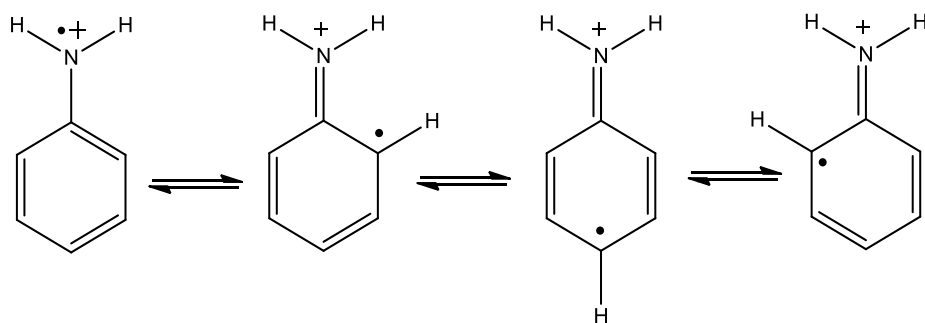
Scheme 1.2. PANI-EB doped with HCl (adapted from [48]).

### 1.4.3. Synthesis of conducting polymers

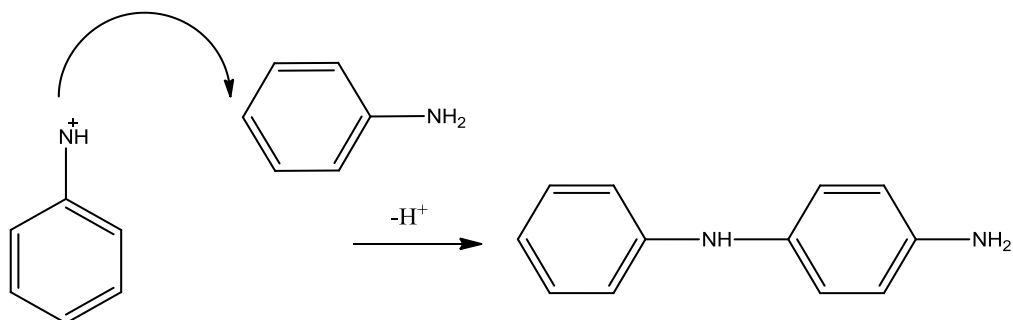
PANI can be synthesised by the use of chemical and electrochemical methods through oxidation of aniline in aqueous or non-aqueous solutions. Oxidative polymerisation of aniline, for instance, proceeds firstly with the formation of the radical cation of the monomer (Scheme 1.3), which is resonance stabilised (Scheme 1.4). The radical cation then reacts with a second radical cation to give a dimer with the elimination of protons (Scheme 1.5) [49]. The dimer or oligomer then further oxidises and reacts with additional monomer and dimer radical cation blocks to build up the aniline chain, and hence polymerisation proceeds (Schemes 1.6 and 1.7) [49].



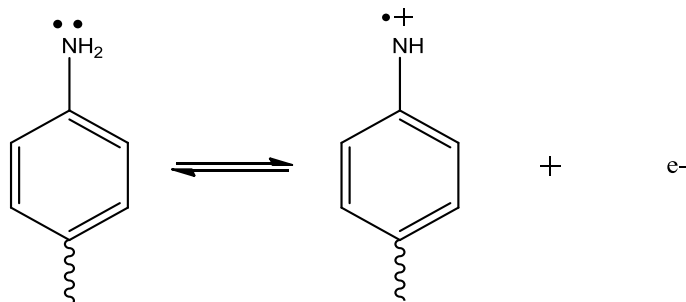
Scheme 1.3. Initiation and formation of the aniline radical cation.



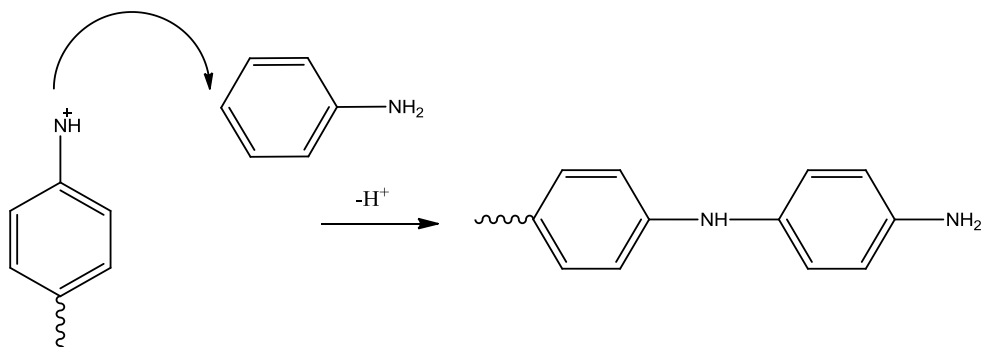
Scheme 1.4. Resonance forms of the aniline radical cation.



Scheme 1.5. Subsequently attacks aniline by electrophilic substitution.



Scheme 1.6. Propagation proceeds by oxidation of the primary amine end of a growing polymer chain.



Scheme 1.7. Electrophilic substitution.

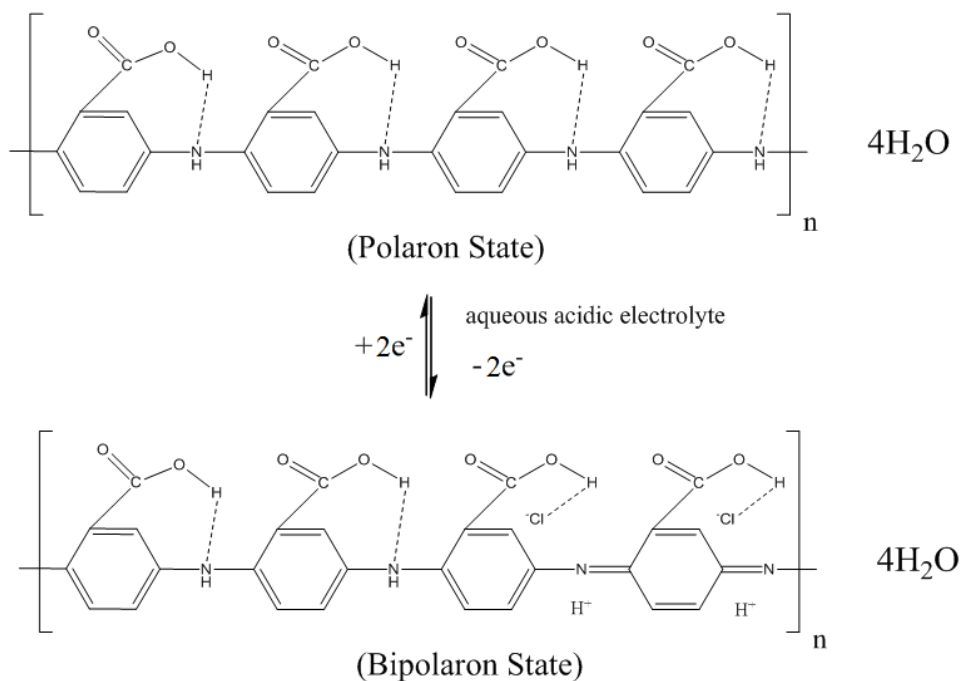
The process has been referred to as reactivation chain polymerisation to highlight the fact that the terminal ends of each chain formed after the addition of aniline must be reactivated to the nitrenium ion by oxidation and proton loss [49]. The product formed is the doped form of PANI.

The presence of incipient cation of the monomer has a great influence on the reactivity of the polymerisation rate as the electrophilic groups such as ABA hinder the reaction in the polymerisation mechanism [44-45]. The aromatic system of ABA is deactivated with respect to an electrophilic substitution reaction due to the electron-withdrawing effect of the carboxyl group [45]. Because of that, the growth rate of the polymer from an ABA should be slower than that from aniline. This electronic effect is responsible for the higher potential needed to oxidise the ABA monomers, compared to aniline [46]. Groups with negative inductive and mesomeric effects direct any new substituent to the ortho-position for 2-ABA that implies coupling in the para-position of the aromatic system relative to the amino group. This suggests that the 1,4-coupling, as it occurs for PANI, is possible with a substituted aniline. Apart from this electronic effect, steric effects also have to be taken into consideration. However, with 3-ABA at the meta position, the polymerisation, which in theory occurs via 1,5-coupling, is sterically hindered and it has been reported that only a coloured oligomeric product but no polymer was found [45]. Furthermore, 4-ABA should couple in the meta-position to the acidic group, i.e. in the ortho-position relative to the amino-group, yielding a polymer in which the monomers are connected via their 2- and 6- positions. However, this thesis will only focus on 2- and 3-ABA as starting monomers for the substituted aniline used in this research project.

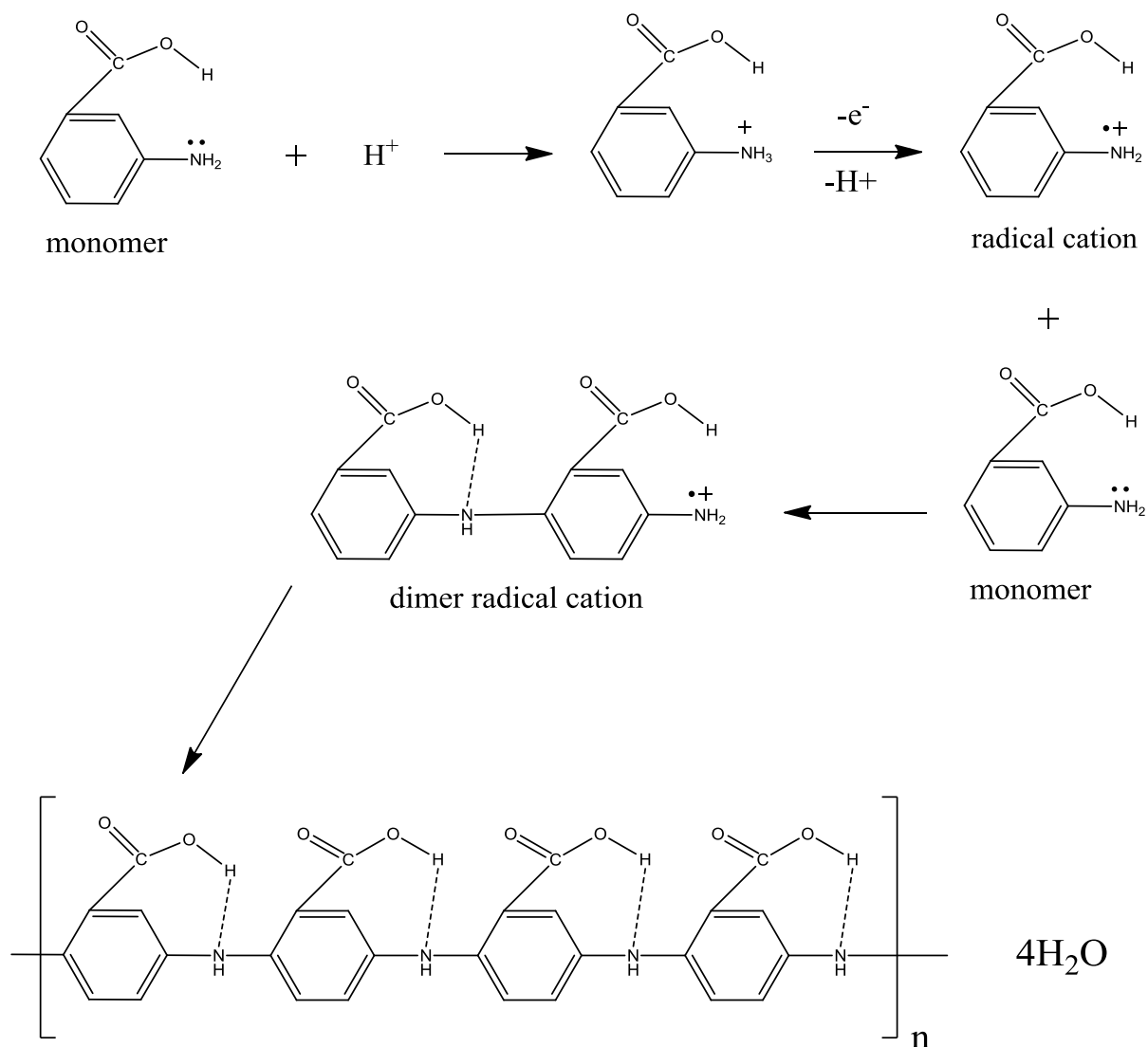
Strong intra- and intermolecular hydrogen bonding in both the doped state of poly-ABA and the aniline-ABA copolymers has been observed, as illustrated in Scheme 1.8. Due to the electropositive effect, the H-bonding is particularly pronounced in the doped form because of the hydrogen attached to the protonated amine and imine nitrogen atoms. At elevated temperature and after expulsion of the HCl dopant, the strong inter-chain interactions due to H-bonding are greatly reduced and no longer exert a stabilising influence on the decomposition of the polymer. A self-doping mechanism of the carboxylic acid group is also possible in homopolymers [50], but is less effective than external doping [51-54].

As shown below in the electrochemical synthesis section, Scheme 1.9, a direct relationship between the content of ABA and the rate of reaction can be established. This is consistent

with the earlier proposed mechanism with ABA acting as electrophilic substitute in the growth of polymer chains. Electron-withdrawing carboxylic acidic groups decrease the reactivity of ABA, as do steric effects [55]. Some of the many reasons for using a substituted aniline over aniline are that it improves solubility [55], the introduction of carboxylic acidic groups as ring substituents influences the acidity constants of the amine groups and appears to offer advantages at less acidic pH values, with evidence of not showing a drop in conductivity with an increase in pH as happens with PANI [55]. The pH range broadens with substituted anilines compared to aniline alone, including improvements of certain properties such as solubility, as well as redox activity [55]. Apart from these improvements, there are also disadvantages with poly-ABA and/or ABA copolymers compared to PANI, as they have low reactivity levels [55]. This could be explained by the localisation of polarons through the interaction between the carboxylic acid groups and the nitrogen in the polymer chains. The increase in the torsional angles between the aromatic rings in order to relieve steric strain exerted by the bulky  $-\text{COOH}$  groups lower the degree of conjugation. UV-Vis spectra of polymers show a hypsochromic shift of the  $\pi-\pi^*$  transition band, which supports this suggestion [55].



Scheme 1.8. Poly-3-ABA in its polaron and bipolaron states.



Scheme 1.9. Synthetic steps during polymerisation.

As an attempt to improve the polymer solubility in most common organic solvents and its reactivity rate, the copolymerisation of aniline [55-58] with aniline derivatives was proposed [59-60]. The interaction between the solvents and the presence of the carboxylic acid group sterically increases the inter-chain distance, weakening inter-chain hydrogen bonds [52-54]. The reactivity of aniline is 7000 times higher than ABA, hence there should be a direct relationship between the content of aniline and the rate of copolymerisation reaction in the polymerisation process [61].

Self-doping in the copolymer suggests that the copolymer films prepared electrochemically are partially self-doped, which indicates that PANI is more rigid [44]. High populations of

bipolarons can be expected due to attractive coulombic interactions between main chain cations and immobile carboxylate counter anions linked directly to main chain B rings for self-doped polymers. The mobility of cations decreases, which makes the dissociation of bipolarons to two independent polarons more difficult [45]. This suggests that the conductivity of copolymers depends on the aniline fraction in the polymer composition.

#### **1.4.3.1. Chemical polymerisation**

Chemical synthesis of PANI is simply a reaction which involves the oxidation of the aniline monomer with the assistance of an oxidising agent under acidic conditions [19-20, 40]. During this process a precipitate, PANI, is formed. Chemical polymerisation of aniline can be carried out under different synthesis conditions [19]. These include a variety of oxidising agents, preparation steps, dopant concentrations, temperature of medium, duration of the reaction, all of which result in variations in the chemical and redox states of the PANI produced [49]. An example of a conventional method of preparation is the use of ammonium persulfate (APS) as an oxidant in an acidic medium, such as HCl or H<sub>2</sub>SO<sub>4</sub>, where a precipitate is formed that can be washed and dried [62]. The chemical polymerisation of aniline is the classical approach by which the aniline monomer is converted directly to a conjugated polymer via a condensation process [49]. The PANI powders can be dispersed in a coating system for application on surfaces of interest, as discussed in Chapter Three. An advantage of chemical polymerisation is that this is a simple process capable of producing bulk quantities of PANI, and is thus well suited for commercial purposes.

The chemically synthesised PANI, either doped (ES form of PANI) or undoped (EB form of PANI), can be incorporated into coatings for use as a primer or top coat for the protection of active metals against corrosion and fouling. Wang et al. reported the use of chemically synthesised PANI as a marine antifouling and corrosion-prevention agent [12]. In their studies, the coatings consisted of different forms of conducting PANI that were cast on to mild steel and then immersed into the sea to evaluate their antifouling effect. Both the base and doped form of PANI were tested and, after the first week, the conductive PANI of an epoxy coating system and p-dodecylbenzenesulfonic acid doped PANI of a polyurethane coating system displayed good antifouling properties, while the base form of PANI in an epoxy system displayed no antifouling behaviour. The antifouling effect of HCl-doped PANI was not as good as DBSA-doped PANI in an epoxy coating system after two weeks. This could be explained by the change of electrical conductivity of the doped PANI. Due to the



alkaline nature of seawater at pH 8, an ideal pH value for organism growth, the conductivity of the PANI decreases with immersion time. The electrical conductivity of HCl-doped PANI dropped sharply from 5 to  $10^{-6}$  S  $\text{cm}^{-1}$  after 8 weeks, while DBSA-doped PANI remained stable along with its antifouling properties. It was reported that the DBSA-doped PANI polyurethane coating was effective as an antifouling coating for at least two months. Although this period is not long enough for real applications, the synergetic antifouling effect between the doped PANI and a biocide, such as cuprous oxide or dichlorodiphenyltrichloroethane (DDT), are an encouraging step forward. DDT epoxy coating was effective for only 1 month, while with the addition of 5 wt% of DBSA-doped PANI, an extra 5 month period of protection was achieved. Similar observations were made with cuprous oxide-epoxy coating systems, as the cuprous oxide alone showed only 2-3 months of antifouling protection, while with the addition of doped PANI this was extended to 9-12 months. This behaviour was explained by the special electron transfer occurring between cuprous (I)-cupric (II) ion and the conducting PANI, which has two redox processes at around 0.10 – 0.15 V (saturated calomel electrode, SCE) and 0.6 – 0.7 V (SCE). Another proposal was that the conducting coating surface had a pH value range from 4 to 5, which may provide a weak acidic micro-environment beneficial to the enhancement of the redox process of the cuprous (I)-cupric (II) ion couple and to improvement of the antifouling behaviour.

PANI can be used as a primer alone, by adding a relatively small concentration (~10 wt%) of chemically synthesised PANI in a coating system [63]. The PANI primer coating can also be followed by a conventional epoxy and polyurethane resin topcoat. In relation to obtaining a good epoxy formulation with the incorporated PANI, it needs to be noted that PANI prepared under normal conditions renders the epoxy powder less electrically charged, and due to the amine terminal groups in PANI the curing of the epoxy becomes more rapid [21, 36]. However, this can be overcome by the use of an appropriate PANI chemical synthesis procedure to produce a successful epoxy coating formulation [21]. PANI can also be used as an additive in paint formulations [64], and can replace commonly used inorganic anticorrosive inhibitors. Modification with a low concentration of CP of less than 1 wt% usually shows better corrosion resistance than unmodified paints [31]. However, for long term protection, a higher pigmented level is required to allow slow release over time of the corrosion inhibitors, particularly in a marine environment [64].

Although a topcoat is the final line of protection, the primer is also very important for antifouling properties. For example, an excellent antifouling effect was observed when the primer was zinc-rich coated [12]. Wang et al. evaluated DBSA doped polyurethane coatings as a primer for corrosion protection and found that it provided a useful antifouling effect [12]. The presence of unknown electron transfer processes between the conducting coating and the primer are expected. PANI used as a pigment in a coating system has provided a non-toxic coating that has attracted attention in the coatings field as a step towards the ideal marine antifouling and corrosion prevention system [65].

The addition of chemically synthesised PANI to epoxy coatings should increase the degree of crosslinking over and above the usual epoxy + hardener system, and provide better barrier properties and corrosion resistance for the epoxy-PANI system, particularly compared to an epoxy alone [23, 66]. In addition, PANI has also shown a self-healing effect with intentionally damaged samples, and this is due to redox characteristics of PANI scavenging ions that provide the ability to additionally crosslink, giving rise to improved barrier properties and self-healing in prevent corrosion of the underlying substrate as reported by Radhakrishnan et al [66]. In many cases, the CP liberates dopant ions near the metal or alloy surface, which creates a passivating layer and limits further corrosion [22]. It must be emphasised that the PANI used in a number of these coatings was not fully doped, so could also capture ions, including the corrosion promoter  $\text{Cl}^-$  [67].

One method of PANI preparation for coatings without altering the polymer is to simply create a blend [68]. Such a blend would combine the properties of the two components without chemical interactions, and add value to the overall coating, i.e. the electrical conductivity of PANI can be provided along with the physical and mechanical properties of the polymeric matrix [34, 37]. Blends of PANI [68] with conventional resins afford corrosion and fouling protection, and the presence of PANI in polyurethane or alkyl resins has been shown to improve the corrosion protection of iron and steel [31, 32]. Research was undertaken by Chen et al. using water-based polyurethane dispersions as the polymer matrix with DBSA-doped PANI [68]. The purpose of the study was to combine the electrical conductivity of DBSA-doped PANI with the physical and mechanical properties of water-based polyurethane and to make a superior coating that could replace current coatings. Polyurethane was chosen due to its versatility and a wide range of excellent properties, which include abrasion resistance, safety in handling, impact strength, low temperature flexibility and an ability to be applied to numerous substrates [68]. DBSA was selected due to the ability of the dopant to

provide a proton acid and to act as a surfactant [68]. Additionally, DBSA-doped PANI has many H-donors and H-acceptors on the backbone structure, which can create various H-bonding types with polyurethane [68-70]. This coating was then casted on polyethylene terephthalate substrates to form water-based polyurethane-DBSA PANI blend films [68].

EB-PANI coatings have been shown to facilitate the extraction of copper from the surface of aluminium AA 2024-T3, leading to a lowering of the galvanic couple between aluminium and copper which accelerates the rate of corrosion on aluminium alloys [71]. The coating was spin coated, drop-cast and immersed in 0.1 M NaCl solution, and kept at room temperature for 10 to 66 hours [71]. The corrosion current density for uncoated metal to coated metal was tenfold more, indicating the importance of the coated surface [71].

The results from Epstein et al. [71] suggests that EB and sulfonated PANI can play an important role in dissolving away the copper containing corrosion products [71]. This explains how the corrosion rate could be decreased as it eliminates the presence of galvanic coupling between the aluminium and copper [71].

There are many reports concerning dispersing PANI in both the doped and undoped form in a coating that displayed corrosion-prevention behaviour [71]. However, the selection of solvent has been challenging in this area, as PANI in the doped or undoped form is insoluble in most solvents commonly used with coatings. Methods of incorporating PANI into a coating system involve dissolving it in xylene [72], *N*-methylpyrrolidinone (NMP) [73-77], DMSO [78], THF [78] or using an alkyl phenol as co-solvent and blending with an epoxy resin [78]. Commercially formulated versions have appeared on the market at times, including VERSICON [79-81], PANDA [32], CORREPAIR [67] or CORRPASSIV [82], which were reported to lower rates of corrosion on various steels [83].

There have also been reports on using an overcoat, often an epoxy top-coat on top of a PANI-coated surface, mainly for the purpose of protecting the PANI-coating and to provide an additional barrier against corrosion. There are many examples of concentrated PANI solutions being applied onto iron or steel [84]. When designing the PANI pigment for coating systems as an antifouling and anticorrosion agent, well-dispersed nanoparticles of uniform size need to be achieved with minimum agglomeration of the intrinsic CPs, which results in superior adhesion [38].

PANI has been dispersed in numerous types of binders, e.g. polyvinyl butyral-co-vinylalcohol-co-vinylacetate, prepared by dispersion with various volume fractions doped with paratoluene sulphonic acid (PANI-pTS) and applied on aerospace aluminium alloy AA 2024-T3 for corrosion protection [85]. The process of initiation and propagation of chlorine-induced filiform corrosion was monitored using an *in-situ* scanning Kelvin probe technique as a quantitative measure of the influence of the PANI-pTS and PANI EB coatings on the AA 2024-T3.

#### 1.4.3.2. Electrochemical polymerisation

Electrochemical synthesis of PANI can involve galvanostatic (constant current), potentiostatic (constant potential) or potentiodynamic (potential scanning or cyclic voltammetric) methods, most often on inert metal and carbon-based electrodes, to produce films directly adherent to the electrode surface. More active metals can also be employed for the deposition of CPs, including aluminium and its alloys. A standard electrochemical set-up involves a three-electrode cell which contains a working electrode (WE), a reference electrode (RE) and a counter electrode (CE). Commonly used WEs are chromium, gold, nickel, copper, palladium, titanium, platinum (Pt), indium tin oxide (ITO) and aluminium [22, 86-92]. The reference electrode is typically a SCE or Ag/AgCl electrode. The CE is usually made of gold or Pt wire.

Electrochemical polymerisation offers the advantage of simultaneous formation and deposition of polymer coatings on the substrate from a controlled environment, along with fine control of the initiation and termination steps [49]. The cleaner reaction guarantees reproducibility of a uniform growth of polymer in chemical and physical properties, which can be altered simply by changing the electrochemical parameters (e.g. the applied potential) [93]. Electrochemical polymerisation has advantages over chemical polymerisation, as it yields purer polymers as no additional chemicals such as oxidants or surfactants are used [67, 84, 94]. Highly controlled thicknesses of the deposited polymer films have been achieved using both cycling and potentiostatic regimes, as mentioned in Chapters Three and Four. On the other hand, scale-up to larger quantities is more difficult. The electrochemical synthesis of PANI on aluminium alloys has proven to be much more difficult than on inert electrodes such as gold and Pt. For many years it was thought that electropolymerisation of PANI could only be achieved on inert metals, but over the past two decades it has been shown that more active substrates can be employed [82], including the likes of Ti, Cr, Al, Zn, brass, stainless

steel [95], iron [18] and mild steels [96-97]. It is important to note that during electropolymerisation of CPs on active electrodes, the dissolved ions of the substrate may be inserted into the polymer, as nickel ions have been reported in the film formation on a Ni substrate electrode when electropolymerising a poly(3-methylthiophene) film [98].

In general, the use of CPs on active metals by electrochemical means requires high positive potentials to form the polymers. At the same time, for potentials greater than 1 V, many of these metals begin to corrode rapidly, which limits the formation of many CPs on their surfaces. During a typical electrochemical polymerisation, an acidic aqueous solution of aniline is kept at a low pH to solubilise the aniline to generate a conducting ES form of PANI in the reaction. The proposed mechanism for electrochemical polymerisation of aniline initiates with the formation of the radical cation of aniline by electrode surface oxidation, followed by the elimination of two protons via a radical coupling, after which the formed dimer or oligomer undergoes further oxidation with aniline on the electrode surface [99].

A model has been proposed by Liu et al. [100] for the formation of aligned PANI nanofibers during stepwise electrochemical polymerisation. There are two possible nucleation sites, the bulk solution and solid substrates, for the growth of PANI in chemical oxidative polymerisation. These two sites compete with each other. It is known that in the polymerisation of aniline the induction time is strongly dependent on the concentration of reagents (aniline, oxidant and acids).

Concentrated aniline (or oxidant) induces PANI to form in bulk solution at a similar or faster rate than it can deposit on solid substrates. By contrast, when very dilute aniline (or oxidant) is used, heterogeneous nucleation occurs first on solid substrates. Consequently, the most active nucleation centres are generated on the solid substrates at a relatively faster rate in the beginning of polymerisation. These active sites would minimise the interfacial energy barrier for the subsequent growth of PANI on solid substrates. However, after induction, PANI nanofibers also form simultaneously in the bulk solution, resulting in the precipitation of PANI. This consumes some reactive aniline cation-radicals and oligomeric intermediates, resulting in the suppression of the growth rate of PANI to grow only vertically from the active nucleation centres generated in the initial stage of polymerisation [101].

The height of the first anodic peak during cyclic voltammograms (CVs) of PANI can be used to provide an estimate of the thickness of the polymer film, and this has been reported by many authors as a way of calculating PANI thickness on a metal surfaces. For example, a

film formed by 55 scans to 1.1 V on a Pt electrode, which showed an anodic peak current, starting from the fully reduced film of  $4.7 \text{ mA cm}^{-2}$ , would have a film thickness of  $\sim 160 \text{ nm}$  [84, 102]. However, this method does not account for polymer porosity and the counter-ion volume, therefore the values calculated only give an estimated thickness for the purpose of comparisons [103].

CPs electrochemically deposited on various metal substrates, such as iron and steel, have shown some effectiveness against corrosion with a doped PANI layer [95, 102, 104-107]. In 1985, DeBerry [95] showed that PANI could be grown on 410 and 430 stainless steels. Wessling [104] reported that PANI has the oxidation capability to passivate mild steel [104], copper [104] and stainless steel [73]. A classical method of electrochemical PANI film formation on active metals is to use an oxalic acid solution to provide both the acidity and also passivation to the active metal. This allows the CP to grow on the electrode before electrode dissolution occurs [108]. Apart from anilines there have also been several studies on ring substituted anilines such as *o*-toluidine, *m*-toluidine, *o*-anisidine and *o*-chloroaniline electrodeposited on passive surfaces [108].

#### **1.4.3.3. Other polymerisation techniques**

Polymerisation of aniline has also been successful via other techniques, such as plasma polymerisation [27, 109]. Plasma polymerisation is a technique that involves fragmented monomer molecules by the action of plasma to form smaller fragments and radicals. Continued radical formation and recombination leads to the formation of plasma polymers [109]. The photopolymerisation technique is a less common method of aniline synthesis. This technique involves addition of aniline in nitric acid to a silver nitrate solution and illuminating it at 365 nm with a 20 W germicide mercury lamp [28]. The aniline radicals formed from the interaction of the photons with solution would then polymerise through head-to-tail coupling [28]. Microwave polymerisation is a promising alternative for chemical polymerisation which has been introduced in the last 2-3 years [29].

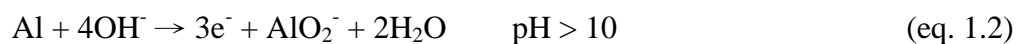
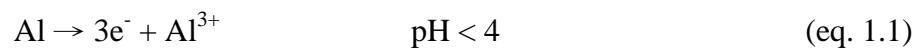
### **1.5. Aluminium substrates**

Aluminium is an abundant metal in nature in its oxide forms. Once processed from its ores, aluminium is easy to handle, and is widely used due to its high technological value in industrial applications, ranging from household industries to aerospace [25]. It is attractive due to its low price, high electrical capacity and high energy density [25], but is prone to

corrosion in seawater [25, 110]. Aluminium is protected from the environment by the formation, on the metal surface, of a thin, but highly stable oxide layer which blocks electron transfer. Aluminium is available in different alloy compositions to provide different grades for various applications. However, the alloying elements are believed to play a role in the corrosion of aluminium [71].

A protective oxide layer on aluminium alloys forms naturally, but a thicker layer can be produced in the process of anodising [111-114], and is well-known to exhibit excellent resistance to general corrosion [22]. The aluminium oxide film growth on the aluminium-coating interface [115] can be followed using a combination of secondary ion mass spectrometry and atomic force microscopy [116]. The anodisation process is often followed by a sealing process, and can involve different methods such as boiling water sealing, dichromate sealing and nickel fluoride sealing. Sealing treatments enhance the protective and mechanical properties of the aluminium alloy [117-123]. Although aluminium forms a protective aluminium oxide layer on the surface, this coating can be breached in aggressive environments causing corrosion [117]. In a marine environment, with the presence of NaCl, the formation of aluminium chlorides can occur, which in turn lowers the effectiveness of the oxide layer in preventing corrosion [110]. Certain grades of aluminium corrode faster than others due to the content of the alloy. For example, aluminium 2024-T3 alloy contains 4-5% copper, and the copper introduces a galvanic couple with the aluminium, thereby accelerating the rate of corrosion [71]. However, it is important to develop a coating for this grade of aluminium as this is an alloy used in aircraft applications where its increased strength adds value to the aluminium structures [71].

Aluminium, shown as Al in the following equations, with a protective oxide layer is quite stable in the pH range from 4-10 [93]. On the other hand, dissolution reactions can occur at higher (eq. 1.2) and lower pH (eq. 1.1.) extremes:



These reactions are limited by the presence of the protective oxide layer. The ionic conductor properties of the aluminium oxide film then feature in the electrochemistry of the surface in solution, which involves aluminium and oxygen vacancies acting as charge carriers within the film [124-125]. Moreover, the movement of point defects through the anodic oxide film

on the aluminium electrode contributes to the film formation (eq. 1.9 – 1.11) [93, 111-113, 125-127].

Aluminum is a suitable substrate electrode for the deposition of a variety of electroactive films, including CPs. The electron transfer processes between CP films and electrode surfaces are accompanied by the movement of ions within the polymer film. This movement of ions is needed to maintain electroneutrality in the film and depends on the electron transfer reaction on the electrode. In turn, this movement of ions and redox state change of the polymer may be accompanied by the movement of solvent into or out of the film caused by a change in the configuration of the polymer chain [128]. As a result of these changes, the physical characteristics of the CP film can be modified significantly by the electrochemical reaction [129-131]. For the case of electropolymerisation on active substrates, it has been reported that the electrodeposition of CPs is usually not easy. This is due to the dissolution of the metallic substrate before the electropolymerisation potential of the monomer is reached. Therefore, an active substrate can be used for electropolymerisation only with certain media, which are able to passivate the electrode surface for protection against more rapid dissolution.

PANI coated on aluminium and its alloys has been the subject of a significant number of studies over the past 15 years. One important procedure prior to coating or electropolymerising of the aluminium alloy is cleaning and pretreatment. The surface must be pretreated in a similar manner to that indicated below (Figure 1.3) to remove residues and to provide a clean surface for good adhesion of the CP. This starts with the pretreatment step prior to electrochemical synthesis, which affects the state the surface and the extent and nature of the oxide layer present on the aluminium surface [93, 132]. It is uncertain whether an acid used in the desmutt treatment process serves to activate the metal surface in some way, or whether it simply adds to the thickening of the aluminium oxide layer due to the passivating character of the acid [93, 132]. By contrast, in marine environments, the aluminium can form aluminium chlorides, which in turn lessen the effectiveness of the oxide layer in preventing corrosion [71].



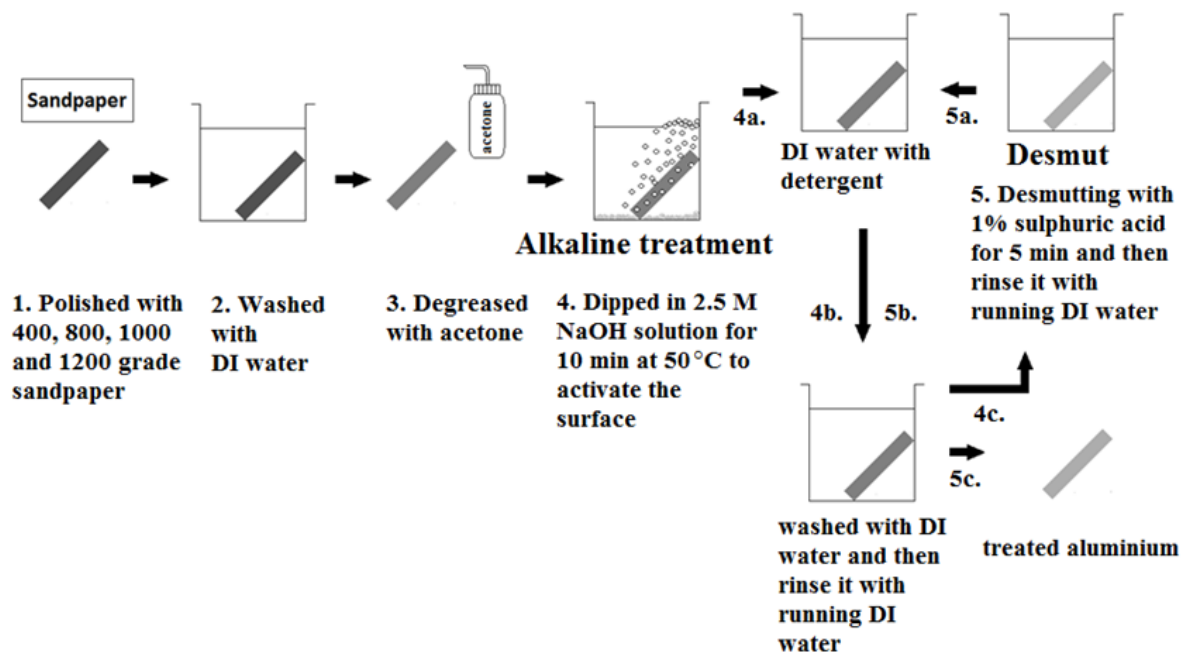


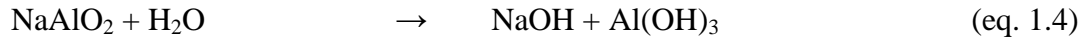
Figure 1.3. Cleaning and pretreatment of aluminium alloys.

The aluminium surface is typically polished with different grades of sand paper (400, 800, 1000 and 1200), prior to rinsing and degreasing with acetone [18]. To activate the surface, aluminium strips can also be alkaline-treated in a strong solution of sodium hydroxide for several minutes at elevated temperatures (eq. 1.3). After this stage, the samples are rinsed with pure water and ultrasonicated for 5 minutes (eq. 1.4). As a final pretreatment stage, the aluminium can go through desmutting in 1%  $\text{H}_2\text{SO}_4$ , an etching process, for a few minutes at room temperature before rinsing (eq. 1.5). It is then dried under nitrogen flow and used for electropolymerisation, as shown in Figure 1.3. Such a cleaning process is important to achieve good adhesion of the CP, while being aware that dissolving precipitated impurities can potentially limit the growth of a CP on an aluminium substrate [93]. With aluminium, pretreatments prior to electrochemical synthesis of a CP can also include anodic [126] or cathodic steps [133]. Some authors have used anodic activation of aluminium in 0.1 M  $\text{HNO}_3$  aniline-containing solution as a pretreatment of the electrode prior to electrodepositing of PANI from a solution of aniline and  $\text{H}_2\text{SO}_4$  [132].

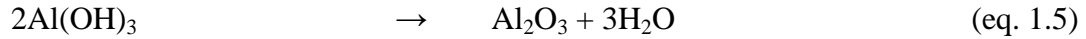
The etching reaction: [134]



Dissolution of the aluminate:



Dehydration of the solid hydroxide:



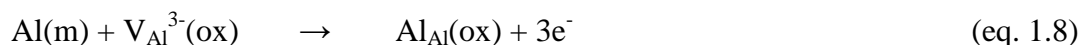
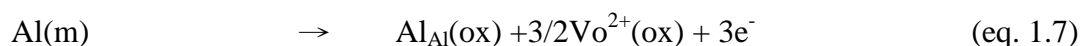
### 1.5.1. Aluminium Anodising

Anodising is a process for producing decorative and protective films on articles made from aluminium and its alloys. It is essentially a process which involves electrochemical formation of a protective anodic film of aluminium oxide layer built up on the surface of the aluminium through the use of a direct current electrical supply [135]. This anodised layer is a suitable substrate for CP growth.

Untreated aluminium often has an oxide layer of around  $10^{-8}$  m in thickness, hence the lack of reactivity with the aluminium surface. Invented in 1923, the anodising process is used commercially to thicken this layer to  $10^{-5}$  m to improve metal corrosion resistance. When the current is flowing in the cell, the following sequence of events is believed to occur. Acid begins to decompose, the hydrogen ions move to the cathode where they are reduced to hydrogen (eq. 1.6): [136]



If a passive oxide layer is formed on the electrode surface, it will protect the aluminium electrode from dissolution and further progress of the aforementioned reactions. The aluminium electrode covered by the aluminium oxide film has interesting electrochemical properties, as the aluminium oxide formed is an ionic conductor in various electrolytic solutions [93, 124]. In this case, aluminium vacancies and oxygen vacancies act as the charge carriers within the film (eq. 1.7 – 1.8.). According to the point defect model, the electrochemical reactions at the aluminium/oxide film interface can be written as follows [93]:



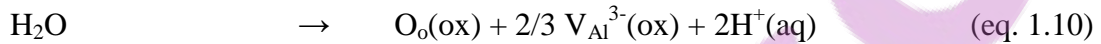
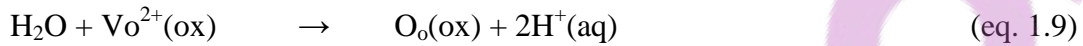
$\text{Al(m)}$  = normal aluminum metal atom in the regular site

$\text{Al}_{\text{Al}}(\text{ox})$  = normal aluminium atom in the regular site of the oxide film

$\text{Vo}^{2+}(\text{ox})$  = positively charged oxygen vacancy in the oxide film

$\text{V}_{\text{Al}}^{3-}(\text{ox})$  = negatively charged aluminium vacancy in the oxide film

The reactions at the film/solution interface can also be written as [15]:



$\text{O}_\text{o}(\text{ox})$  = normal oxygen ion in the regular site of the oxide film

Random porous aluminium oxide films are often formed in the first oxidation, also known as anodisation, and in order to achieve an ordered porous aluminium oxide film double anodisation is normally required. Double anodisation involves the formation of a random porous oxide film followed by the removal of this oxide layer and then repeating the anodisation process under similar conditions (Figure 1.7). The theory is that the pores reaching the aluminium surface have tube-end-like shapes; removal of the first oxide film leaves the aluminium surface with highly ordered semi-spherical pits, which act as seeds for ordered oxide film via omissions second stage of anodisation [136].

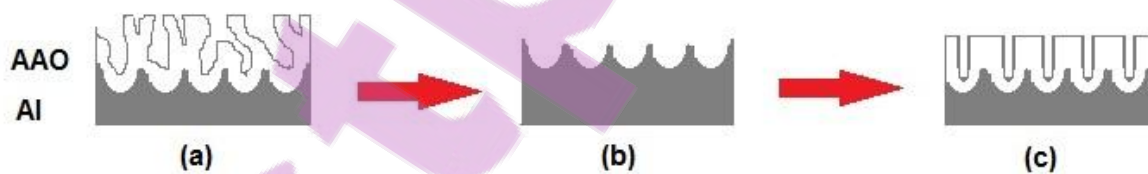


Figure 1.4. Schematic representation of ordered anodised aluminium oxide (AAO) formation via double-anodisation: (a) first anodisation, (b) removal of the first (disordered) oxide, and (c) second anodisation.

During cleaning of aluminium, the process in eq. 1.12 occurs and at the same time negatively charged anions, for example hydroxide, sulfate and possibly oxide ions, also move to the anode. The electrical charge in the circuit causes positively charged aluminium ions ( $\text{Al}^{3+}$ ) (eq. 1.14) to be generated at the anode and in turn move towards the cathode. At the anode

surface they react with oxide and hydroxide ions to form aluminium oxide (in the case of the hydroxide ion, hydrogen ions are released into the solution) [136]

Cleaning:



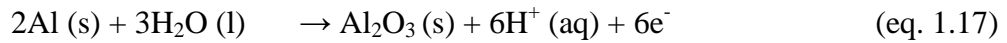
Once the oxide is removed:



Equations for reactions occurring at the anode:



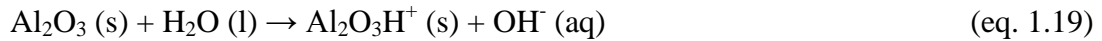
Electrolysis at the anode:



Electrolysis at the cathode:



The oxide coating develops a positive charge by the reaction:



Aluminium electrodes are easily oxidised to form  $\text{Al}^{3+}$  species, leading to a spontaneous reaction producing a non-conducting dielectric ( $\text{Al}_2\text{O}_3$ ) film on the electrode (eq. 1.15) [137].  $\text{Al}^{3+}$  species can continue to be generated at the metal/oxide interface and then migrate through the growing  $\text{Al}_2\text{O}_3$  towards the solution; here oxide ions ( $\text{O}^{2-}$ ) migrate toward the aluminium electrode (eq. 1.16). The  $\text{Al}^{3+}$  encounters water species at the  $\text{Al}_2\text{O}_3$  interface to keep forming the  $\text{Al}_2\text{O}_3$  film (eq. 1.17). During this anodisation process, the electrolyte anion plays a key role in determining the type of oxide porous film formed (eq.1.18) [137]. Surfactant electrolytes are thought to play three important roles which include acting as supporting electrolytes for the formation of the  $\text{Al}_2\text{O}_3$  film. The anodic film (eq. 1.19) formed strongly depends on the electrolyte used, for porous type films, a soluble electrolyte is required, such as sulfuric, phosphoric, chromic or oxalic acid [138].

The anodising thickness formed per volt is strongly influenced by the type of metal anodised [138]. Low temperatures ( $0^\circ\text{C} < T < 5^\circ\text{C}$ ), and hard anodising conditions create thick,

compact and hard porous films, whereas at higher temperatures ( $60^{\circ}\text{C} < T < 75^{\circ}\text{C}$ ) and softer anodising conditions, thin, soft and non-protective films are produced. As the temperature increases, the corresponding current also increases. This does not mean that the higher current density increases film thickness, since the rate of complex dissolution at the electrolyte/oxide interface increases as well. If the temperature is high enough that the rate of dissolution is faster than that of oxide formed, the resulting film will eventually vanish, resulting in electropolished aluminium [138].

Post-treatment of anodised and coated surfaces is as important as pretreatment. Dipping samples in 5%  $\text{H}_3\text{PO}_4$  solution, held at  $30^{\circ}\text{C}$ , has been reported to accomplish the expansion of alumina pores, and these are generally necessary to facilitate an expanded alumina morphology [132]. However, there are also other methods of pretreatment, such as hot and cold sealing, which involve pre-neutralising or multi-stage rinsing.

### 1.5.2. Electrochemical polymerisation of aniline on aluminium alloys

Aqueous electrochemical polymerisation has been found to be an attractive process for the production of primer coatings on metals, particularly for the replacement of existing chromate metal treatments [103]. The advantages of aqueous electropolymerisation are:

- (1) the aqueous solutions used are environmentally favourable
- (2) the technique combines the formation of a polymer and the deposition of the coating in one process, and this process can be easily automated
- (3) the production cost is relatively low
- (4) the properties of the coatings can be controlled by varying the electrochemical parameters

This very reactive metal forms a thin solid protective film of oxide upon oxidation that limits further corrosion of the material. A successful electropolymerisation requires the formation of a passive layer, which might be able to inhibit the dissolution of the oxidisable metal without blocking access of the monomer and its further oxidative polymerisation [93, 103].

The incorporation of CPs onto the metal is a good way of taking advantage of the mechanical properties of the metal, while providing additional protective and functional properties [93, 139]. During the electrochemical polymerisation of PANI on aluminium, two oxidation processes occur: oxidation of the metal, with the formation of aluminium oxides, as occurs

throughout the entire potential range, and aniline monomer oxidation, with the formation of PANI [92, 93,140].

One of the applications considered in the 1990s was the use of PANI to provide corrosion inhibition on active metals [12], including steels and aluminium. While the extent of protection against corrosion in the longer term has been questioned, a number of mechanisms have been proposed for the corrosion protection observed for PANI films, and these include barrier and electrochemical protection effects. The electrochemical protection is caused by the increase of the corrosion potential ( $E_{\text{corr}}$ ) and the formation of a protective passive layer on the metal surface due to redox catalytic properties [17].

Electropolymerisation of PANI offers the advantage of control over the chemical and physical properties of the coating formed on the substrate by changing the electrochemical parameters (e.g. voltage and current) [93]. The nucleation and growth of PANI during the electrochemical oxidation of aniline and polymerisation follows a two electron-transfer process, as shown in scheme in the Section 1.4.3 [141].

During potential cycling there are several factors that can be influential, such as the concentration of the electrolyte, the potential range, the scan rate and also the electrode material. The electrochemical deposition of PANI on an aluminium electrode surface also involves oxidation of the substrate electrode prior to electropolymerisation, including the formation of a passive layer on the electrode surface [93]. The passive film plays two important roles: protection of the electrode against dissolution, and the establishment of a suitable surface for the deposition of the CP [93]. However, aluminium often suffers from localised corrosion when exposed to an environment containing aggressive chloride ions. The deposition of PANI onto aluminium provides the opportunity for protection of aluminium alloys in more aggressive environments. Camelet et al. [96] reported that passivation of oxidisable metals prior to electropolymerisation is necessary to obtain adequate adhesion of a PANI film.

During electropolymerisation of PANI, the formation of aluminium oxides will in fact continue throughout the entire potential range employed. This will have the effect of lowering the current density at the electrode as a passive oxide layer is produced. Studies undertaken by Eftekhari showed that a very stable PANI film was formed on an oxidised aluminium electrode, and even more so than for a comparable electrochemical synthesis of PANI on a Pt electrode [93]. This could be explained by the good connection of the PANI to the electrode

surface with an oxide film present [142]. The presence of the oxide film on aluminium also provides protection against dissolution of the metallic substrate [93]. A smooth and adherent film can be formed on the electrode surface in an acidic medium. The good adhesion of the conductive coating and improvement of corrosion resistance to the metal surface has attracted much attention from industry. A galvanic interaction can occur between aluminium and coatings containing the oxidised and conducting forms of PANI. Cathodic reactions such as oxygen reduction can also be suppressed by the presence of PANI [70].

CPs, such as PANI, are easily electrosynthesised at inert electrodes such as gold and Pt. PANI can be easily formed on conductive oxide films of iron group metals without additional pre-treatment. On the other hand, polymerisation on insulating oxides results in either non-deposition of the CP or the formation of a few conglomerated centers [93]. It is also difficult to generate these polymers at aluminium electrodes. This is connected with the thin, but highly stable protective oxide-hydroxide layer consisting mainly of  $\text{Al}_2\text{O}_3$  that forms on aluminium, which blocks electron transfer and impedes polymer formation and deposition [143], consisting mainly of  $\text{Al}_2\text{O}_3$ . Furthermore, the oxide layer continues to grow throughout the anodisation process in the acidic solutions normally employed in the electrosynthesis of CPs [93]. In the presence of further electrolytes such as oxalic acid, the passive anodic film on the metal can include aluminium oxalate salts. Another advantage of oxalic acid is its relatively high acidity, which favors the electropolymerisation of aniline [89]. It has been shown that the electrodeposition of conductive PANI films on metals needs a very low pH, in contrast to polypyrrole, which can be deposited from aqueous solution at a near neutral pH.

The type of substrate electrode and the electrolyte solution selected are two critical parameters for the successful growth of CPs on active metals. The growth of the  $\text{Al}_2\text{O}_3$  anodic film acts as an excellent barrier for electron transfer and, thus, inhibits electrochemical formation of CP [105]. The induction time before the passive layer on aluminium is built up decreases with increasing the applied current density. At higher applied current densities, shorter induction times result, as more  $\text{Al}^{3+}$  is produced per unit time with the higher currents with concomitant precipitation of more Al oxalate crystals on the substrate [93]. Thus, the substrate can be covered by the passive Al oxalate layer in a shorter time. This passive layer inhibits the further dissolution of  $\text{Al}^{3+}$  without affecting other electrochemical processes [93]. During the electropolymerisation of anilines on aluminium, the current values are observed to decrease with the passage of time and then reach a near constant value. It has been proposed that changes occur on the surface of the electrode after the formation of the initial polymer

layers, and it results in a decrease of the electrical conductance value of the electrode film [93]. In other words, the ability of electron transfer on the electrode surface decreases due to polymer formation [93]. The general definition of “oxidation/reduction” is the donation of electrons by one molecule or atom to another. The species that donates the electron is said to be “oxidised”, and the species receiving the electron is said to be “reduced”. Oxidation and reduction always occur together, oxidation is always accompanied by something being reduced, and reduction is always accompanied by something being oxidised. A porous aluminium oxide film is produced by anodising, an electrolysis process. The metal to be treated becomes the anode in an electrolytic cell and its surface is electrochemically oxidised. Anodisation can improve certain surface properties, such as corrosion resistance, abrasion resistance, hardness, appearance, etc. Furthermore, since the surface film is porous, the aluminium metal can even be coloured by the application of pigments or dyes in the pores [144-146].

Bare aluminium is not suitable for use in highly acidic or basic environments, therefore it is important to oxidise it first prior to use. The aluminium metal oxidation reaction will compete with the oxidation of aniline during electropolymerisation of aniline, providing a challenge to the current research project. An insulating oxide film impedes the current directed for PANI deposition [93]; therefore a high potential and longer duration are required. Moreover, successful electropolymerisation of aniline on aluminium and its alloys has been reported [22, 93, 86-92]. Pretreatments are essential for a successful formation of films [133]. Studies of the electropolymerisation of pyrrole by Martins et al. support the importance of the anodic alumina layer, as it plays a role in providing nucleation centres in the polymerisation process [91]. Electropolymerisation of aniline on aluminium using oxalic acid [86] and tosylic acid [22] solutions have been carried out and the galvanostatic interaction between the polymer and aluminium was observed to give rise to oxidation of the aluminium substrate and reduction of the polymer [22]. The PANI deposit has then been observed to provide increased corrosion resistance for the aluminium substrate [22]. PANI has been grown on numerous aluminium alloys: Tallman et al. studied the corrosion protection of aerospace industry AA 2024-T3 [85, 88, 90, 92, 123], AA 6061 – T6 [20] and AA 7075 grades of aluminium with electrochemically synthesised PANI [135]. The electrochemical polymerisation of aniline on aluminium alloys can be undertaken either on top of the outer oxide layer ( $\text{Al}_2\text{O}_3$ ), or immediately following an intermediate step whereby the initial oxide layer is stripped off the surface under acidic conditions. This later approach allows more ordered pore formation and



greater adhesion between the coating and the substrate. Different grades of aluminium alloys show that etching the aluminium in a pretreatment process dissolves out silicon and magnesium precipitates, which otherwise play an important role in PANI growth. Previous research [12, 22, 92] has shown that there can be a strong influence from the pretreatment, it was found that conducting polymers such as polypyrrole coatings could not be formed on AA 6061-T6 substrates after a chemical etching treatment [12, 22, 92], as will be further investigated in Chapter Six. Some authors weigh the aluminium strips before and after polymerisation and rinsing with propanone to determine the amount of PANI coated on the aluminium alloy strip. This was not undertaken in the present study, as the difference in weight measurements was not large enough to justify using this method.

One major benefit of the use of an electrochemical method for coating aluminium alloys is the ability to coat hard-to-reach corners and it allows a reproducible uniform coating, which is otherwise difficult to achieve with spray applications. Although the electrochemical method provides many advantages, there could be practical limitations when applying this approach to large objects. The effectiveness of a PANI coating formed electrochemically has been shown to be sensitive to the preparation conditions, as discussed in Chapter Three.

A non-uniform PANI coating can also accelerate the rate of corrosion on aluminium substrates and the galvanic action between the substrate and PANI decreases with time upon exposure to an electrolyte. Upon aging in air, the PANI coated aluminium would thicken due to the formation of an oxide with atmospheric oxygen [85, 147]. However, PANI in its doped form would not change due to exposure to atmospheric oxygen, because the electropolymerised PANI is already in an oxidised state [74, 85].

Electrochemically synthesised PANI coated on an aluminium surface has great potential for replacing the currently used toxic chromate-based treatments [92], as chromate has been listed as hazardous to the environment and to human health [92]. For antifouling applications, there is the potential for CPs to replace the toxic and/or carcinogenic inhibitors currently used in several protective coating systems [148].

In a further study, aluminium was subjected to anodic galvanostatic pretreatment in a 0.1 M HNO<sub>3</sub> aniline-containing solution, prior to electrodeposition of PANI from a solution of aniline and sulfuric acid [132]. Corrosion tests in 0.1 M NaCl showed the importance of this pretreatment for resistance to corrosion [132]. However, the reason for the improved

protection was not clear, as it could be due to surface activation or from the formation of a thicker aluminium oxide film due to the passivating character of nitric acid [132].

Wang et al. [22] electropolymerised PANI on 1100 wire beam aluminium with 1 M tosylic acid solution using a potentiostatic method [22]. This was the first published article with PANI electropolymerised on wire beam electrode to study the electrodeposition process [22]. The electrode was cathodically pretreated at a potential of -0.90 V prior to electrodeposition [22]. This pretreatment prevented localised corrosion of AA 1100 and ennobled the pitting potential by about 0.13 V [22].

There are other approaches to electrochemically depositing PANI on aluminium. Huerta-Vilca et al. used alizarin as a chelating agent in the electrosynthesis of PANI films on aluminium, and found that the film formation induction time was lower and growth rates were increased compared to the absence of a chelating agent, although the stability of the films was weak [87]. Pournaghi-Azar et al. pretreated their aluminium in an  $\text{H}_2\text{PtCl}_6$  solution prior to electrodeposition of PANI [149]. The pretreatment provided the opportunity to lower the monomer concentration and induction time needed to initiate the polymerisation process, and at the same time it increased the polymer growth rate and the stability of the PANI film on the electrode [149].

The process of electropolymerisation of aniline on oxidisable metal surfaces presents several advantages, including achieving a thicker physical barrier towards corrosive agents in a shorter time owing to the conductive properties of the material used. These polymers carry molecular groups or can be doped with specific anions, they may act as inhibitors and shift the potential of coated material to a value where the rate of corrosion of the underlying metal may be reduced significantly [150]. For example, Racicot et al. [142] studied a double strand form of PANI, and the polyanion composition provided corrosion protection for the aluminium AA 7075 alloy.

PANI has been electrochemically synthesised on numerous grades of aluminium but never on essentially pure aluminium (grade 1100), alloy 4043 and marine grade aluminium (5083), for antifouling properties, which is the focus of Chapter Six. The presence of high levels of additives in alloy 4043 made the electrochemical synthesis process challenging. However, the success of this work in particular with the marine grade aluminium, 5083, will be of interest to the marine industry, given that this grade of aluminium is the most commonly used grade for items near coastlines. *In situ* UV-Vis spectroscopy appears to be an effective and

useful tool for studying the early stages of electropolymerisation as well as the tool to detect short-lived intermediates formed during electrooxidation of aniline [94]. The concentration of monomer present in the reaction has been reported [94] to be an important factor in the position of the absorption bands of PANI, with lower concentration of aniline showing a lower wavelength in the UV-Vis spectrum than higher concentration [94].

### **1.5.3. Galvanostatic polymerisation method**

Galvanostatic polymerisation methods for the deposition of PANI have been reported. This approach provided more uniform CP film deposition under specific conditions compared to other methods of electrochemical deposition. PANI prepared galvanostatically at current densities of 0.5, 1.5, 5 and 15 mA cm<sup>-2</sup> on AA 3004 aluminium alloy was studied by Shabani-Nooshabadi et al. [89]. During the polymerisation, the potential values increased over a period of 30 to 900 s to reach a plateau value of around 15 V on the AA 3004 electrode. The combined metal oxide and CP layer eventually restricted electron transfer and resulted in a decrease in the electrical conductivity [89].

### **1.5.4. Potentiostatic polymerisation method**

Martins et al [92] reported the electropolymerisation of 0.5 M aniline on a 6061-T6 aluminium alloy at different constant potentials, in an attempt to optimise the conditions of growth at this particular substrate [92]. The anodic current was found to generally increase due to the nucleation and growth of the polymer, and the induction time involved in this increase depended upon the applied potential. At the same time, for a low applied potential from 0.7 to 0.8 V, an increase in the maximum current was seen, indicative of a higher polymerisation rate [92]. However, for potentials above 0.8 V, a dramatic decrease was seen in the maximum current values produced. This suggests that an increase to a more positive potential is observed in over-oxidised polymers showing signs of degradation [87]. The presence of Si and Mg precipitates were shown to play an important role in the aniline electropolymerisation process [92]. During etching these species dissolve away and this affects the polymer growth rate, indicating that they are involved in conduction pathways. It is commonly agreed on that there is a galvanic interaction between aluminium and a coating containing the oxidised and CP forms [92]. As a result, the ES form of PANI can polarise the underlying aluminium to potentials where cathodic reactions such as oxygen reduction are greatly suppressed [92]. Without a topcoat the protection of PANI is temporary [145], and

coating failure is commonly related to the polymer changing from the doped state to the undoped state [92].

### 1.5.5. Corrosion resistance studies

Electrochemical impedance spectroscopy (EIS) is commonly used in studies involving CPs and corrosion projects, as a way to evaluate the corrosion properties of a surface. The EIS output enables the coating capacitances and films resistances to be determined. This can be monitored as a function of their exposure time to various aqueous environments, including seawater for marine applications [25]. In the case of aluminium, the oxidation of aluminium is expected to take place with a PANI-coated aluminium surface, where the PANI redox reactions also take place [86].

A typical electrical equivalent circuit used for fitting EIS data is given in Figure 1.5 below [25], and contains a number of circuit elements that can be related to physical properties of the electrochemical cell involving a PANI-coated aluminium surface. EIS studies are commonly carried out at open circuit potential from high to low frequencies ranging from  $10^4$  to  $10^{-2}$  Hz, with the amplitude of the superimposed AC signal being around 10 mV [25].

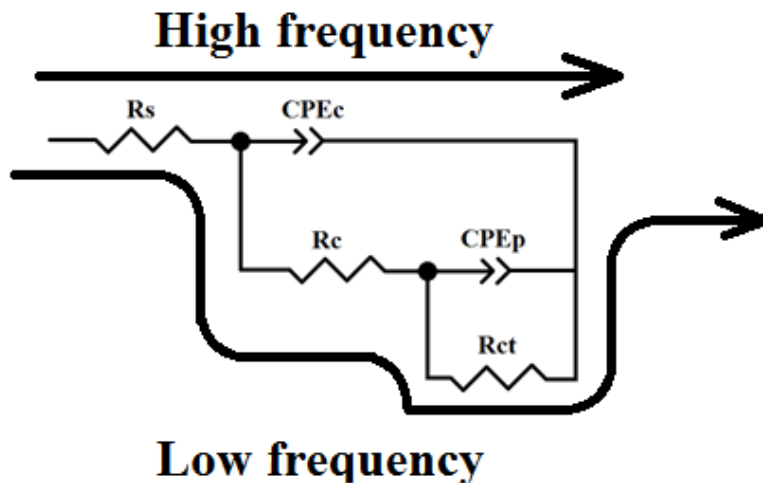


Figure 1.5. Equivalent electrical circuit for impedance measurements (adapted from [25]).

$R_s$  = electrolyte resistance

$R_{ct}$  = charge transfer resistance

$R_c$  = coating resistance

$CPE_c$  = constant phase elements connected with a coating capacitance

$CPE_p$  = electrochemical phenomena (double layer capacitance –  $C_{dl}$  and possible diffusion processes) in the coating pores

Corrosion of metals is a serious problem throughout the world [25], with implications for many chemical and manufacturing industries [15]. Pigments based on lead oxides and chromates are most commonly used, and replacing them with CP would be a breakthrough for this area. Many studies have been undertaken in this area using CPs, which are promising coatings for the corrosion protection of iron, steel, zinc, aluminium and other oxidisable metallic materials [104, 78]. DeBerry [95] and Wessling [104] emphasised the important role the passivation of the metal surface plays in the protective activity of PANI when used as an anticorrosive coating.

The unique ability of CPs to store and transport charge, to anodically protect metals against rapid rates of corrosion, is one of their most attractive features [84]. The mechanisms by which PANI exerts corrosion control over aluminium and its alloys have been explained by the galvanic interaction that can occur between aluminium and coatings containing the oxidised and conducting forms of PANI, namely the ES form, often doped with acids such as HCl, H<sub>2</sub>SO<sub>4</sub> or oxalic acid [85]. When the CP coating is used as a primer alone under immersion conditions, the protective nature of the PANI coating can be temporary [88]. Coating failure is attributed to the reduction of conducting PANI ES form to non-conducting (non-oxidising) LE form [85]. However, it has been claimed by others [71, 84, 151] that the non-conductive form of PANI is also an effective corrosion inhibitor. The ability to moderate proton activity and changes in local acidification can contribute to the efficiency of undoped PANI coatings [83]. Cecchetto et al. [152] proposed that it is at the aluminium-coating interface, via an acid-base interaction with a hydrated surface oxide, that the conversion of undoped PANI to doped PANI takes place, leading to ennoblement of the substrate, which in turn is thought to improve the prevention of corrosion.

The nature of the dopant anion and its interaction with the conducting coating is also important in determining the level of corrosion protection afforded to aluminium alloys, such as AA 2024 [153]. The dopant anions arising from the doped PANI can act as inhibitors in their own right. Corrosion reactions that occur at a coating defect drive the release of inhibitor anions, which in turn stifle cathodic oxygen reduction on the likes of copper-rich inter-metallic particles [85].

Improvements in the anticorrosion properties of epoxy coatings can be made on treated aluminium during anodising as investigated by Hosseini et al. with the use of PANI-polymer matrix with clay [25], which exhibits better coating resistance than an epoxy incorporated PANI and an epoxy alone without any clay. Chemically synthesising PANI in camphorsulfonic acid with ammonium peroxydisulfate as surfactant in the presence of montmorillonite nanocomposite materials has been reported by Hosseini [25]. The method used was *in-situ* emulsion polymerisation in the presence of inorganic nanolayers of clay on aluminium Al 5000 [25]. The initial coating resistance value for the PANI-polymer matrix with clay coating on anodised aluminium was calculated to be  $1.32 \times 10^5 \Omega \cdot \text{cm}^2$ , while PANI in an epoxy coating without clay under the same conditions led to a lower resistance value of  $15,520 \Omega \cdot \text{cm}^2$ , whereas the epoxy coating alone had a resistance of only  $1400 \Omega \cdot \text{cm}^2$ . The electrolyte diffusion process was influenced by increasing the clay loading and hence an increase in the coating resistance [25]. The first sign of electrolyte diffusion took place after 8 to 23 hours of immersion with clay loadings of 0.5 to 1%. However, the first step of diffusion for 5% of clay loading was not observed, and this could be explained by greater agglomeration of the clay in the polymer matrix with an increase in clay content [25].

Studies by Armelin et al. showed that epoxy with PANI in the base form showed better corrosion resistance than the conducting form when used as a system pigment [64]. The authors suggested that the protection was based on the fact that the base form of PANI has the ability to store charge, acting as a molecular condenser, and that the mechanism was based on the electroactivity of partially oxidised polymers more so than direct conductive properties [64]. Epstein et al studied the corrosion protection properties of PANI in both the undoped and doped forms, when cast-deposited on aluminium AA 3003 and AA 2024-T3 alloys. When exposed to chloride environments, the coatings were effective in lessening corrosion. It was suggested that the PANI coating facilitated the extraction of copper from the surface of the AA 2024-T3 alloy, which lessened the galvanic coupling between aluminium and copper, and thereby lowered the corrosion rate [71]. Ceccetto et al. [83] suggested that an EB coating promotes proton activity and delays local acidification and its contribution to corrosion [85]. The conversion between EB and the PANI ES is believed to occur on the aluminium-coating interface via an acid-base interaction with a hydrated surface oxide, leading to substrate ennoblement, which in turn is thought to improve corrosion protection [152]. The dopant anions associated with PANI can also play an important role in determining the level of corrosion protection afforded to aluminium alloys, as these can act as

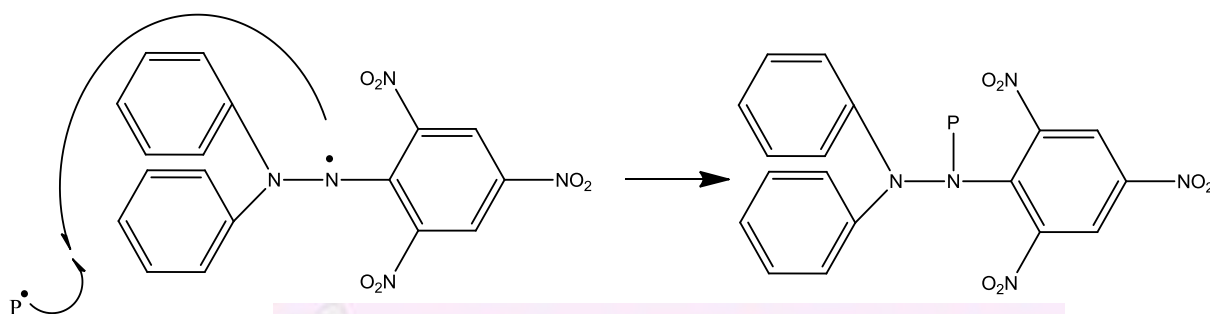
inhibitors in their own right. In this sense, the PANI layer can operate as a “smart-release” coating, where corrosion reactions occurring at a coating defect drive the release of inhibitor anions, which in turn can stifle cathodic oxygen reduction on copper-rich inter-metallic particles [85].

### 1.5.6. Radical scavenging assay

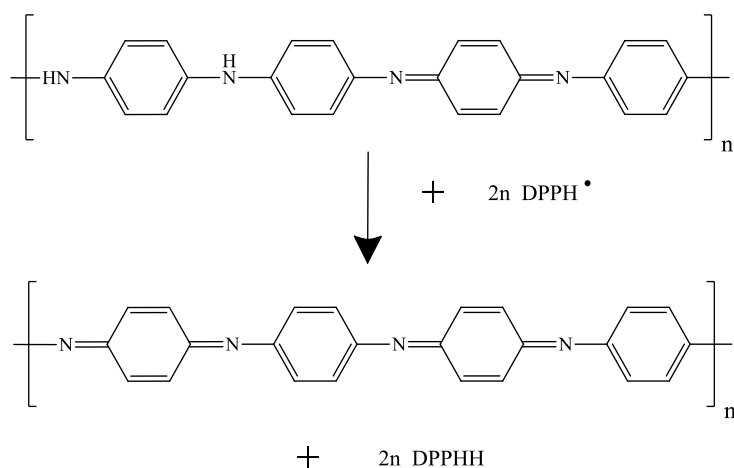
The evaluation of antioxidant activity by the 1, 1-diphenyl-2-picrylhydrazyl (DPPH) assay was a method developed by Brand-Williams, Cuvelier and Berset in 1995 [153]. It was later modified by Sanchez-Moreno, Larrauri, and Saura-Calixto in 1998 [154]. For the purpose of CPs studies, it can be used to assess the antioxidant potential of the polymers considered as solid antioxidant materials, and also to evaluate the extent of surface availability of redox-active CP segments. The DPPH radical is one of the most commonly used antioxidant assay for plant samples, and the assay is based on the measurement of the scavenging ability of antioxidant test substances towards the stable DPPH radical [155, 156].

As the first oxidation process for PANI occurs at around 0.10 to 0.20 V (Ag/AgCl) in aqueous solutions, this is comparable to antioxidant polyphenols containing catechol-groups, which are also able to be oxidised by the DPPH radical, itself a weak oxidising agent. At the same time, potentials beyond 0.80 V are required to fully oxidise PANI under acidic conditions [157], which means that the DPPH radical, with an intermediate oxidation potential, is not expected to be able to fully oxidise PANI on its own.

The DPPH• [155-158] scavenging activities can be monitored by UV-Vis spectrophotometer, based on the absorption of the radical at 517 nm [155]. The hydrogen atom (Scheme 1.10) or electron-donating ability (Scheme 1.11) is measured by the bleaching of the purple-coloured methanol solution of DPPH•. The DPPH• radicals are decolourised upon reduction, which react with intrinsic CPs are introduced into solutions containing the free radicals.



Scheme 1.10. Reaction of DPPH radical with P being a polymer chain.



Scheme 1.11. Reaction of DPPH radical with PANI (adapted from [159]).

### 1.5.7. Antibacterial properties of polyaniline

PANI and poly-ABA have been examined for applications in biomedicine, and their antibacterial performance with gram-positive *Staphyococcus aureus* (*S.aureus* 6838) and gram-negative bacteria *Escherichia coli* (*E. coli* 25922) [160]. In one fundamental study, PANI was synthesised with oxidative persulfate at 0 – 4°C in the presence of p-toluene sulfonic acid as the dopant, and was casted with polyvinylalcohol on optically transparent, ultrasonically cleaned glass substrates [161-162]. Antibacterial tests were performed by film attachment method, according to the FITI Testing & Research Institute – Antibacterial of Polymeric Materials (FC-TM-20) [163]. The agar plates containing test samples and control were incubated at 37°C for 18 h. The reductions of bacteria were calculated using the formula,  $\text{Reduction (\%)} = \frac{B_{bt} - B_{at}}{B_{bt}} \times 100$ , where  $B_{bt}$  is the bacteria number before the test and  $B_{at}$  is the bacteria number after the test [162]. Acidic dopants on the molecular chains of PANI may react with the bacteria resulting in bacterial death. On the other hand, the electrostatic adherence between PANI molecules and the bacteria carry charges of different polarity leading to the destruction of bacterial walls, exposure of bacterial contents or leakage resulting in bacterial death [162]. The presence of PANI, in general, reduces the effect of charge-carrier delocalisation and suggests that electrostatic adherence between the PANI molecules and bacteria may play a very important role in antibacterial protection. PANI on its own has shown good antibacterial activity due to its interaction with bacterial cell walls [160]. The mechanism of inhibition of PANI and metal nanoparticles on gram-positive and gram-negative bacteria has been reported by many researchers [164-165]. Biofouling, i.e. bacterial growth, on surfaces is one of the processes that contribute to marine fouling and



the prevention of this film formation would interrupt the formation of the fouling ecosystem hence preventing antifouling, see Figure 1.6.

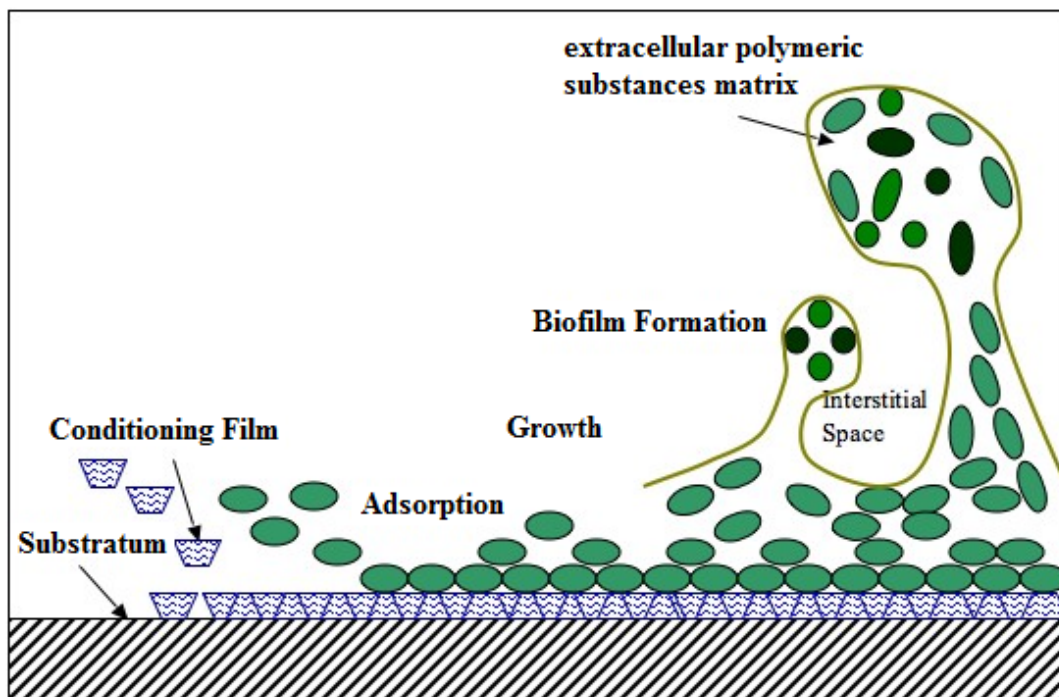


Figure 1.6. Ecosystem of biofilm formation (adapted from [166]).

Marine fouling is rather complex but can be generalised into four basic stages [4, 166-167]: deposition of conditioning film, microbial (planktonic) attachment to the conditioning film [168], growth and bacterial colonisation and, finally, biofilm formation. Conditioning films is a process which alters the surface properties allowing microorganisms to adhere to the surface that occurs within the first minute of immersion caused by van der Waals interaction. In the next 24 hours, this modified surface then invites microorganisms of interest to adhere to form an initial microbial attachment. By the end of the first week, bacteria that anchor the surface would then be allowed to grow their colonies, and that leads to the final step of biofilm formation. Within 2 to 3 weeks, an extracellular polymeric substances matrix and vertical structure separated by interstitial spaces biofilm are fully developed.

Some bacteria are able to synthesise catecholate siderophore compounds and these are found in the adhesives secreted by a variety of aquatic organisms, such as mussels [169]. Spectroscopic studies by Petrone [168] proposed catecholate siderophores as possibly involved during the initial stage of biofilm formation on metal oxide surfaces such as

aluminium. The surface molecular structures of catecholate inner-sphere complexes on aluminium are presented in Figure 1.7.

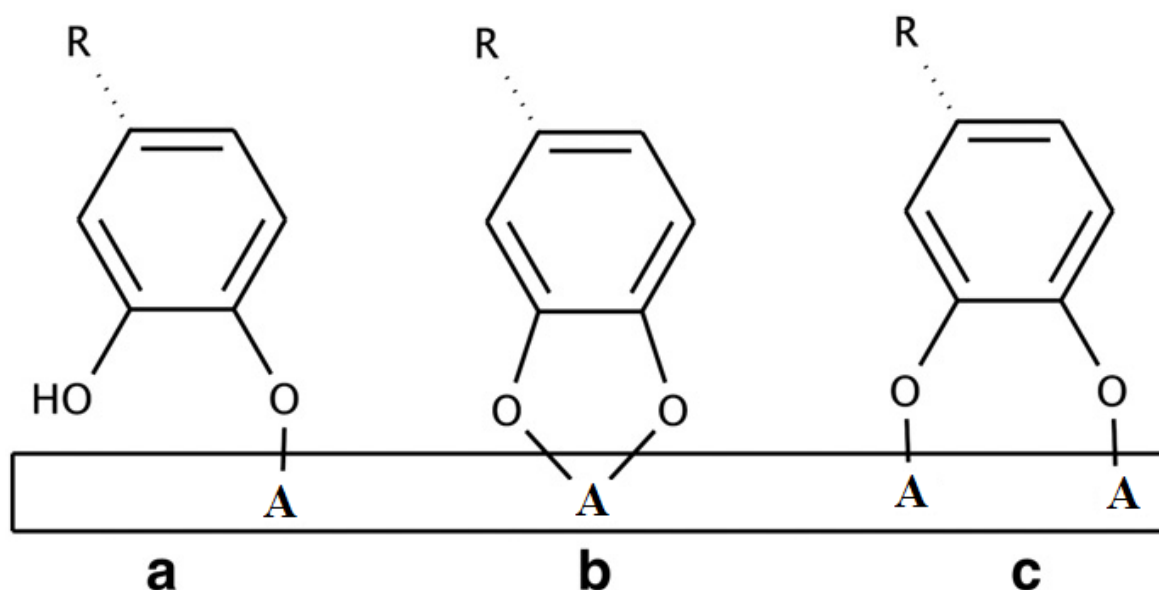


Figure 1.7. Surface molecular structures of catecholate inner-sphere complexes on aluminium (A) surface: (a) monodentate, and bidentate (b) mononuclear and (c) binuclear complexes (adapted from [168]).

## 1.6. Aims and objectives of this work

This study focuses on developing novel antifouling coatings, potentially replacing the copper-based and other environmentally hazardous materials currently in use. More particularly, the focus is on producing a system to inhibit biofilm formation using an antimicrobial polymer on the surface of metal substrates for numerous applications. These include powerboats, yachts and cruises, off shore constructions, pulp and paper mills, water treatment plants, power plants and fish farming nets (liquid impregnator).

The incorporation of CPs such as PANI as a pigment or filler for the coating system has great potential. However, intractable CPs compounds are not easily incorporated into coatings, and this is the greatest challenge for the project. The development of the antifouling coatings requires optimisation of the application method to a range of materials, including steel, aluminium, concrete, polymer composites and timber. All of these materials are currently used for boat hulls, and the aim is to provide ease of use, adhesion, efficacy and acceptable durability on all substrates. The study will also develop technologies such as antibacterial

coatings with significant commercial potential in a wide range of applications. Such technologies will also have applications in other industries, for example, in the dairy industry, which has an urgent need for technologies to maintain stainless steel pipes free from the build-up of deposits and thereby reduce the need for aggressive cleaning regimes. This may be achievable using a nanolayering or nanopatterning technology, thereby avoiding the need for chemical modification of food-contact surfaces and the consequent requirements for FDA approvals.

Growth of marine organisms on the hulls of ships is usually controlled by painting the underwater parts of ships with antifouling coatings. The best performing solution is an antifouling paint based on TBT, but this has been effectively banned and replaced by other solutions [170-173]. Most of the present tin-free and solvent-based coating systems rely on the action of cuprous oxide and organic biocides. Although this is considered to be friendlier to the environment than TBT, there is a need to develop better solutions. In this project an attempt to develop new types of antifouling coatings based on PANI CPs and aim to achieve a finished product that provides promising antibacterial, anticorrosive and antifouling properties, in a system that does not release toxic chemicals into the environment. The project will consist of:

1. Chemically and electrochemically synthesising the PANI and substituted aniline
2. Electrodeposition of PANI on marine grade aluminium
3. Test and evaluation of novel coatings
4. Examination of the underlying chemical mechanisms of the new coatings

This novel antifouling coating could also be used as a pretreatment, as well as a direct antifouling and antibacterial coating. Industrial treatment of metals before being subjected to painting uses conversion steps such as phosphation and chromation, mainly to protect the surfaces from corrosion. Alternatives are now being sought as international anti-pollution regulations strongly restrict the use of these chemical treatments due to their adverse environmental impact.

The electrodeposition of CPs on oxidisable metals can be a more environmentally-friendly treatment method as it utilises the electrodeposition baths, which would be a cheap alternative treatment and also lower the overall pollution. The advantage of these coatings is that they do not contain toxic substances that are harmful to the environment. Their production process is

simple and economical, with the added advantage that the CPs act as physical and electronic barriers, improving the protection afforded by other materials that simply act as physical barriers alone. While CPs, in particular PANI, have been widely studied over the last 30 years, their antifouling properties and performance have not been thoroughly explored, which is the main focus of this thesis.

The physical and chemical properties of the polymer are influenced by the preparation method [11, 16, 151, 153], dopant, doping levels [31, 63, 174] and oxidation state [32, 33] all of which are examined in this thesis. The preparation via both chemical and electrochemical methods of the polymerisation of aniline are examined in Chapter Three, followed by an investigation of poly-ABA and its copolymers in Chapter Four. The change in properties and understanding how the different oxidation states are formed and are influenced by the external environment are presented in Chapter Five. The ability to electrochemically synthesise PANI on aluminium surfaces, and the composition of aluminium alloy, have been reported to play important roles in the polymerisation rate, as investigated in Chapter Six. An accelerated testing method for antifouling testing, along with the overall performance of the coatings on marine grade aluminium, is presented in Chapter Seven. Future lines of investigation are discussed in Chapter Eight.

## CHAPTER TWO: Experimental methods

### 2.1. Abstract

In this chapter the details of the various experimental and data analysis procedures used in this thesis are outlined. The equipment and experimental settings are supplied below.

This chapter has been partially published as:

To T., Kilmartin P. (2013) Electrochemically synthesised polyaniline on marine grade aluminium, *Sixth International Conference on Advanced Materials and Nanotechnology*, Auckland, New Zealand, in press.

### 2.2. Materials

Aniline, obtained from Sigma-Aldrich, was distilled under reduced pressure before use and stored in a refrigerator. Aminobenzoic acid (ABA), sulfuric acid (H<sub>2</sub>SO<sub>4</sub>), ammonium persulfate (APS), potassium iodide (KIO<sub>3</sub>) and sodium hydroxide (NaOH) were purchased from Sigma-Aldrich, while solid oxalic acid was provided by Ajax Finechem and used as supplied. The solutions for the electrochemical polymerisation of PANI were kept at 0.1 M of monomer in 0.5 M oxalic acid (C<sub>2</sub>H<sub>2</sub>O<sub>4</sub>.2H<sub>2</sub>O), HCl and H<sub>2</sub>SO<sub>4</sub> supporting electrolytes. All solutions were prepared using pure water and used as supplied.

Three types of aluminium alloy were used as working electrodes of PANI desposition, namely 1100 aluminium alloy (high purity Aluminium), 4043 alloy (high Si, ~5% Si content) and 5083 alloy (marine grade aluminium, with a thickness of 3 mm, from Austral Bronze Crane Copper Limited). The composition of the alloys is believed to have an affect on the rate and performance of electropolymerisation, therefore three different aluminium alloys were selected for testing. These three alloys were selected due to their high content level of Si (4043), Mg (5083) and aluminium (1100).

Aluminium grade	elemental composition/%								
	Si	Fe	Cu	Mn	Mg	Cr	Zn	Ti	Al
5083	0.4	0.4	0.1	0.4-1.0	4.0-4.9	0.05-0.25	0.25	0.15	92.55-94.25
1100	0.95		0.05-0.20	0.05			0.1		99
4043	4.5-6	0.8	0.3	0.05	0.05		0.1	0.2	92.5-94

Table 2.1. The metal composition of the three grade of aluminium alloys used.

A new piece of aluminium was used for each experiment, and was pretreated prior to use, see Figure 1.3. The pretreated alloys were masked with insulating tape to get an effective working area of  $1\text{ cm}^2$  before being used for electropolymerisation of PANI. A Pt wire was used as the counter electrode along with an Ag/AgCl reference electrode (0.207 V versus SHE), from BASi. To prepare electropolymerised samples for Raman spectroscopy a  $1\text{ cm}^2$  Pt sheet was used as the working electrode. To clean each working Pt electrode between experiments, the electrode was cycled to 2 V in  $\text{H}_2\text{SO}_4$  solutions until the breakdown of the polymer film was observed. The electrode was further cleaned by cycling between -0.1 to 1.3 V in 0.5 M  $\text{H}_2\text{SO}_4$  until a typical CV of Pt in  $\text{H}_2\text{SO}_4$  was obtained [175]. All potentials reported here are relative to the Ag/AgCl electrode scale.

### 2.3. Chemical synthesis

For aniline polymerisation, aniline (50 mmol) was dissolved in 300 mL acidic aqueous solution in beaker A. Beaker B contained 3.5 mmol (APS) in 200 mL acidic aqueous solution. The solution from beaker B was slowly added dropwise into beaker A with vigorous stirring. After adding, the mixture was stirred overnight for complete polymerisation. Polymers were then filtered and washed with deionised (DI) water, followed by acetone to obtain green powder samples which were then dedoped with diluted ammonia solution. PANI was obtained by chemical oxidation of aniline in different acids, oxalic acid and  $\text{H}_2\text{SO}_4$ . Different dopant concentrations (0.5 M and 1.5 M) were used, along with two different oxidants (APS or  $\text{KIO}_3$ ).

The chemical synthesis of poly-ABA was carried out in the manner reported earlier by Rivas et al [63]. The synthesis of poly-ABA (poly-2-ABA and poly-3-ABA) in two solutions was performed. Solution A contained 6 g (21.9 mmol) of monomer (ABA) dissolved in an acidic medium (HCl or  $\text{H}_2\text{SO}_4$ ), for example 190 mL of 1 M HCl, pH = 0.8 (a clear solution). Solution B contained 9.9 g (21.9 mmol) of APS dissolved in 28.8 mL of 1.5 M HCl. Each solution was heated to  $50^\circ\text{C}$  to dissolve the reactants prior to the reaction. The reaction was carried out in a 500 mL round-bottomed flask at  $50^\circ\text{C}$ . The solution of APS (solution B) was added dropwise with stirring into solution A. After 8 hours, the solution was filtered and washed with hot HCl followed by warm water. The filtered product was then dried in a vacuum oven for 2 days at  $60^\circ\text{C}$  [45]. The same chemical procedures were followed for 1:1 copolymers of 21.9 mmol of monomer dissolved in 190 mL of acidic solution.

## 2.4. Electrochemical instrumentation and cells

The electrochemical cell used for electropolymerisation consisted of a glass container and Teflon cap, with inlet sites to insert electrodes, and nitrogen supply for deaerating the solution, see Figure 2.1. The solutions used for the electrochemical polymerisation were 0.1 M of aniline, 0.1 M ABA or 0.05 M aniline + 0.05 M aniline monomer with the total monomer concentration kept at 0.1 M in 0.5 M oxalic acid ( $C_2H_2O_4 \cdot 2H_2O$ ), 0.5 M/1.0 M/1.5 M  $H_2SO_4$  or 1 M HCl supporting electrolyte. A Pt wire was used as the counter electrode, along with an Ag/AgCl reference electrode in 3 M NaCl from BASi. Five types of working electrodes were used, including a Pt electrode coated with a Teflon holder from BASi for the electropolymerisation of PANI. A glassy carbon working electrode also from BASi was used for characterisation of chemically synthesised polymers. Moreover, three grades of aluminium alloy were used as working electrodes for PANI growth: 1100 aluminium alloy (high purity Aluminium), 4043 alloy (high Si, ~5% Si content) and 5083 alloy (marine grade aluminium) as presented in Chapter Six. To prepare electropolymerised samples for SSNMR and Raman a  $1\text{ cm}^2$  Pt sheet was used as the working electrode. Three instruments were used in this thesis, a CH Instruments electrochemical workstation (model 650C, CH Instruments, USA), VersaSTAT and EDAQ potentiostat with E-corder 410, with most of the electrochemically synthesised PANI carried out on the EDAQ potentiostat.

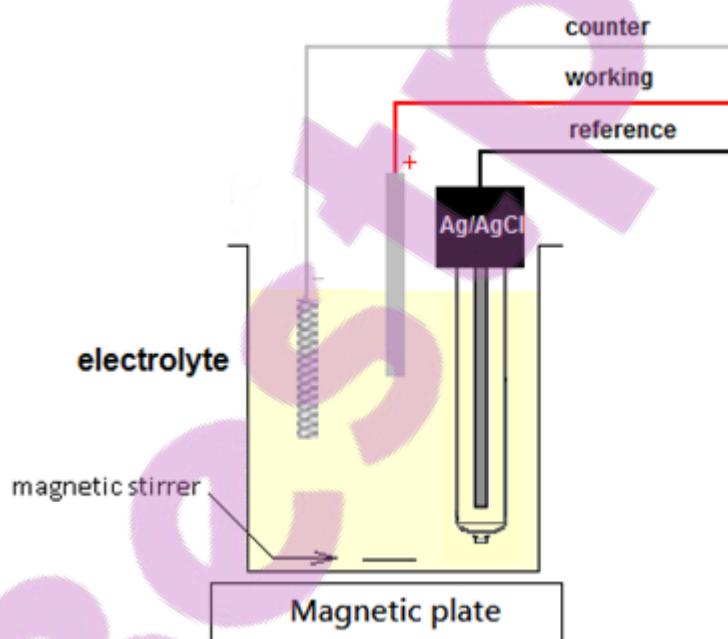


Figure 2.1. Electrochemical cell for growing conducting polymer films on electrode.

## 2.5. Electrochemical synthesis

A three electrode cell setup, see Figure 2.1, was used for the voltammetric preparation of PANI films. The solutions for the electrochemical polymerisation were 0.1 M of aniline monomer in 0.5 M oxalic acid ( $C_2H_2O_4 \cdot 2H_2O$ ) or  $H_2SO_4$  supporting electrolyte. All electropolymerisation solutions were deaerated with oxygen-free nitrogen for at least 15 min prior to use.

The polymers were formed using cycling from -0.1 to 0.9 – 1.1 V at a scan rate of  $50 \text{ mV s}^{-1}$  and a film was formed on the surface of the electrode during polymerisation. The film was washed with electrolyte used in the polymerisation without monomer present for characterisation.

Poly-ABA polymer and its copolymers with aniline were all grown on a BASi Pt working electrode with a working area of  $1 \text{ cm}^2$  in  $H_2SO_4$  and HCl electrolyte solution. All electrochemically synthesised polymers mentioned in this chapter were prepared using an EDAQ potentiostat with E-corder 410.

Electrochemical synthesis of a homopolymer of poly-ABA was prepared using two different methods:

1. Polymers were prepared directly on a Pt electrode in either 1 M HCl or 0.5 M  $H_2SO_4$ . All poly-ABA electrochemically synthesised polymers were polymerised in the potential range between -0.1 to 1.2 V for the first two cycles, except for poly-2-ABA doped with 1 M HCl where the upper potential limited was lowered (-0.1 to 1.1 V) followed by another 2 cycles between -0.1 to 1 V, see Chapter Four for more details. To build thicker films, the polymers were cycled for 100 more cycles between -0.1 to 1 V at a scan rate of  $50 \text{ mV s}^{-1}$ .
2. Poly-ABA was grown on a PANI surface, which had been prepared already under the conditions mentioned above, on a Pt electrode in 0.5 M  $H_2SO_4$  electrolyte, see Figure 2.2.



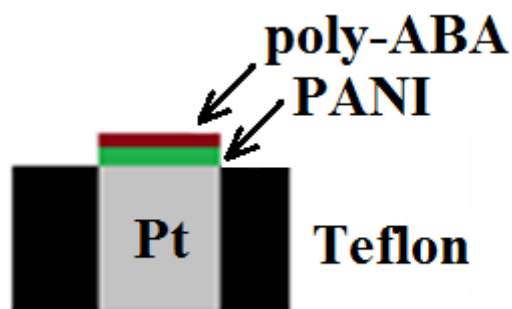


Figure 2.2. Method two for electrochemically synthesising poly-ABA.

Electrochemical polymerisation was carried out by cycling the potential in 0.5 M  $\text{H}_2\text{SO}_4$  containing 0.05 M of ABA and 0.05 M of aniline. The solutions used for the copolymerisation experiments had a total concentration of 0.1 M, i.e. 9:1 (ABA: aniline), and were prepared at a scan rate of  $50 \text{ mV s}^{-1}$  for 100 cycles -0.1 to 1.0 V.

The coated electrodes were transferred to a solution of pure electrolyte for electrochemical characterisation. Cyclic voltammetry was undertaken using the same potentiostat; three cycles were necessary to establish steady-state conditions.

Prior to electrosynthesis the aluminium was cleaned as mentioned in Chapter One. Electrochemically synthesised PANI on marine grade aluminium was studied using different methods. The formation of a PANI coating on a marine aluminium electrode was undertaken using both one-step and two-step processes at a fixed potential of 2 V (Ag/AgCl). Step 1 was an anodisation step with the formation of an oxide layer,  $\text{Al}_2\text{O}_3$ , by electrolysis carried out for an hour in the absence of the aniline monomer, which allowed the oxidation of metal to occur first (Figure 2.3). This was followed by an electropolymerisation of aniline for 3 hours (step 2). The experimental conditions are shown below in Figure 2.3.

A one-step process, involving only step 2 from Figure 2.3, was also applied. In this case both oxidation reactions will occur simultaneously, the oxidation of the metal with the formation of aluminium oxide and aniline monomer oxidation with the formation of PANI.

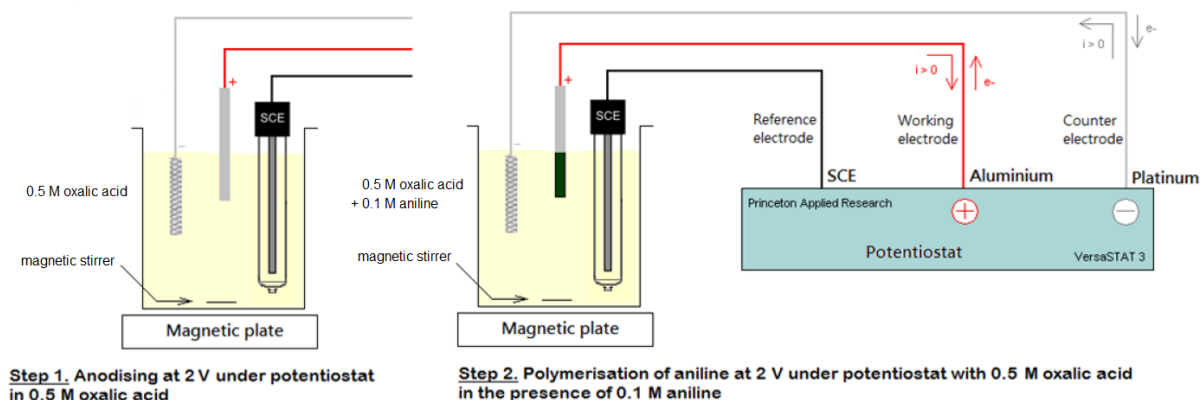


Figure 2.3. The two-step process of electrochemical deposition of PANI on aluminium.

Electropolymerisation of aniline on marine grade aluminium was carried out by cycling from between  $-0.4$  to  $-1$  V for the lower potential, and an upper potential ( $E_{\lambda a}$ ) that varied from  $1.5$  to  $2.4$  V. The films were grown at a scan rate of  $50 \text{ mV s}^{-1}$  cycled for 170 cycles using a VersaSTAT 3 potentiostat.

The formation of PANI using potentiostatic polarisation of  $2$  V was undertaken in a one-step process with an Ag/AgCl reference and Pt counter electrode from an  $0.5$  M oxalic acid solution containing  $0.1$  M aniline monomer.

PANI films were successfully grown under potentiostatic condition on all three grades of aluminium, with the process carried out at a fixed potential of  $1$  V,  $2$  V,  $3$  V and  $4$  V in  $0.5$  M oxalic acid and the presence of  $0.1$  M aniline monomer. Moreover, anodised samples were prepared at a fixed potential of  $1$  V only and in the absence of monomer. The choice of oxalic acid over other acids was based on the fact that when using preparing a conducting polymer at potentials greater than  $1$  V, the high positive potential can corrode the metal surface before it gets a chance to oxidise aniline to PANI, as discussed earlier in Chapter One [96, 108].

The morphology and oxidation state of PANI grown on the aluminium alloys has also been characterised. Tapping mode Atomic Force Microscopy (AFM) was used to provide information about surface features of the polymer films. The relationships between the growth conditions, anticorrosion, antifouling and the scavenging of DPPH radicals (antioxidant), have been used to measure the activity of the PANI coating, see Chapter Six for details.

## 2.6. Characterisation Methods

CP layers are commonly characterised by both electrochemical techniques, such as CV and AC impedance, and the use of spectroscopic techniques that allow the identification of structural changes in the polymer during redox processes. The spectroscopic techniques used in spectroelectrochemistry include UV-Vis absorption spectroscopy, Raman spectroscopy and infrared spectroscopy [72]. These methods provide structural information about the CP that has been deposited, including oxidation state, the presence of dopants and degradation characteristics.

### 2.6.1. Morphology

The morphology of the polymer is strongly dependent on and controlled by three major steps, the generation of nucleates, their assembly, and the growth of PANI chains from nucleates [48]. This can be controlled by the type of nucleate organisation and synthesis conditions. The morphology of the resulting polymers can be monitored through the use of AFM and Scanning Electron Microscopy (SEM).

The surface morphology of the PANI samples was characterised using AFM, SEM and Raman spectroscopy. AFM imaging is a non-destructive and convenient process that does not require any specific sample preparation. Electrochemically synthesised PANI on marine grade aluminium alloy, 5083, was used to obtain the three-dimensional AFM pictures with the scan rate 6.1 Hz, with 256 sample points taken on each of the 256 lines to make up the image. AFM has been applied to CPs such as PANI for many years [176-177]. The main features obtained, and the particular equipment used to record images of electrochemically synthesised samples, will be presented in Chapter Six. The physical operation of AFM involves scanning the surface of the sample with a sharp tip which is extremely sensitive to small forces. An image is produced as the tip and cantilever move up and down over the surface in response to the extremely small repulsive forces ( $10^{-9}$  to  $10^{-8}$  N).

AFM was used to study the morphology of PANI in its doped form with different anionic surfactants and functionalised organic anions, such as camphorsulphonate, methanosulphonate and trifluorosulphonate, as reported in an article in 2000 [182]. AFM was used to identify changes in the morphology of electronic conductive polymers. It was shown through the incorporation of an anionic surfactant that the use of dopants changes the observed surface morphology.

AFM was used to study the morphology of PANI films grown by self-organization on a silicon substrate, modified initially with a self-assembled monolayer [179]. Highly oriented crystalline PANI films were obtained by tapping mode AFM. Both micro and nano scale features could be detected with AFM studies. [183] presented the electrochemical synthesis of PANI films on fluorine tin oxide and ITO in acid media [183]. The roughness and morphology of the polymer coatings was determined with the use of AFM. In addition to SEM images, AFM provides 2D and 3D topography images.

The electropolymerisation process on ITO has been followed by AFM in 0.5 M H<sub>2</sub>SO<sub>4</sub> [184]. This was superior to SEM, as SEM does not have sufficient resolution to show hemispherical nuclei of the deposited species, especially in the early stages of electrocrystallisation of metals and polymers. It was suggested that the overlay of hemispherical nuclei of Ni and Co on an Au substrate, with a mean diameter of approximately 20 nm, was detectable [184]. The AFM analysis of PANI deposited on ITO surfaces showed a strong influence of the substrate on the film morphology. It was shown that globular aspects of the ITO surface were still present during the early stages of polymer deposition, and for less anodic potential values, the roughness values of the film morphology increased. At high magnification neighbouring globular deposits under these experimental conditions showed similar aspects to those observed in metal electrocrystallisation. As more positive potentials were applied this globular morphology was changed to a flat-like surface.

The morphology and surface component of coatings has been observed by means of SEM. The EDX spectrum can also be obtained and used to indicate the presence of PANI features on the samples [62]. The samples for SEM imaging were coated with Pt using a Polaron SC7640 Sputter Coater for 300 s at 5 – 10 mA and 1.1 kV prior to analysis. SEM Philips XL30S FEG SEM provides high magnification images for a detailed study of surface structures, and uses electrons for imaging. Secondary electrons or Energy Dispersive X-ray Spectroscopy (EDS) provide a powerful tool for matching microstructures to elemental composition. Cross sectional samples were also examined both under Raman and SEM for use in determining the film thickness as well as PANI distribution formed after different deposition times. Aluminium coupons of 0.5 cm<sup>2</sup> cubes were mounted in 2-pack epoxy resin and allowed to set overnight to dry. The set epoxy block was then sanded and ground in a perpendicular direction and held in spot. The first grind is the critical stage, and it is necessary to polish the resin until it reaches the metal. Polishing aluminium can be done in three stages of grinding with 80, 240, 500 and 1200 grit paper followed by three stages of

diamond polishing with 6  $\mu\text{m}$ , 3  $\mu\text{m}$  and 1  $\mu\text{m}$ . After each stage the specimen surface was washed with detergent, rinsed with water and ethanol, blow dried before continuing the next polishing stage. A microscope was used after each stage to check on the finish of the polished surface, as shown in Figure 2.4.

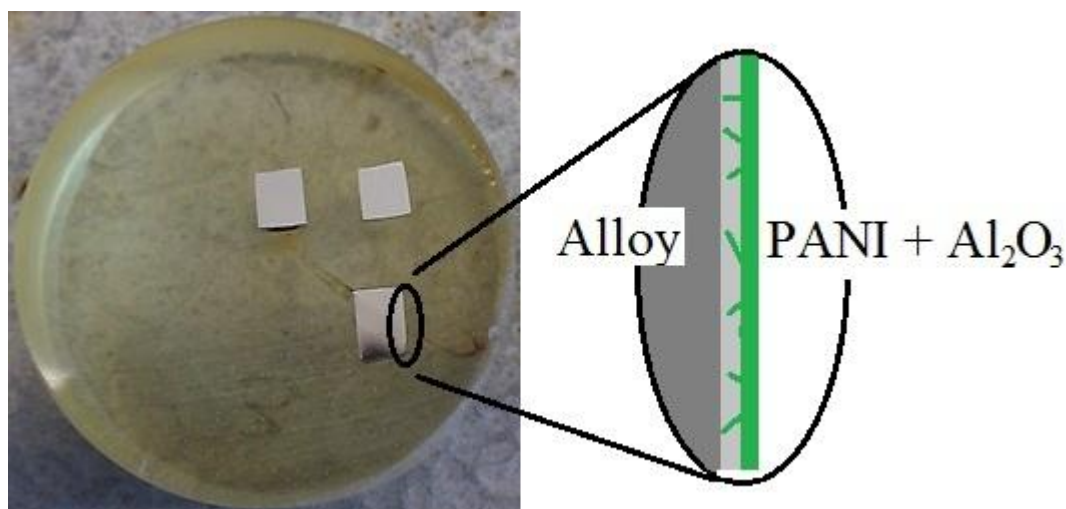


Figure 2.4. Cross-sections of aluminium mounted in epoxy resin.

Samples prepared with one step polymerisation at different applied potentials of 1 V, 2 V, 3 V, 4 V, 5 V and 6.5 V are shown in Chapter Six.

### 2.6.2. Cyclic voltammograms (CVs)

CVs of chemically prepared PANI were collected with an EDAQ potentiostat using a solution dispersed in methanol. The samples were prepared by casting on the working electrode and were measured by cycling between -0.1 to 0.9 V at a scan rate of 50  $\text{mV s}^{-1}$ . The characterisation of the films was carried out by cyclic voltammetry, in a monomer-free aqueous electrolyte solution of oxalic acid,  $\text{H}_2\text{SO}_4$  or  $\text{HCl}$ . A bare glassy-carbon electrodes (GCE), also supplied by BASi, was used as the working electrode to characterise polymers that were chemically prepared for electrochemical analysis. The electrode was first polished with 1700 diamond paper, followed by  $\text{Al}_2\text{O}_3$  slurry (0.05  $\mu\text{m}$  alumina supplied by BAS) on emery paper prior to use. Then it was rinsed with pure water and sonicated in 1:1 nitric acid: acetone, and pure water for 10 minutes. Following these steps, the electrode was held at a potential of +1.5 V versus  $\text{Ag}/\text{AgCl}$  in sulfuric acid electrolyte for 5 minutes and then cycled in the potential range -0.5 to +1.5 V at a scan rate of 50  $\text{mV s}^{-1}$  for 15 minutes prior to the collection of characteristic polymer voltammogram.

### 2.6.3. Fourier Transform Infrared (FTIR) spectroscopy

FTIR spectra were obtained using a Thermo Electron Nicolet 8700 FTIR spectrometer with the accessory of Smart Orbit Diamond Attenuated Total Reflection (ATR) Single Reflection, specular reflectance or KBr pellet. Electrochemically synthesised polymers were obtained by carefully scraping the product from the electrode surface. Before scraping, adhering monomers were removed by cycling the coated electrode five times in the working electrolyte in the potential range of -0.1 to 0.9 V at a scan rate of 50 mV s<sup>-1</sup> followed by washing with ethanol to remove any oligomers and electrolyte present on surface. An average of 64 scans with a resolution of 4 cm<sup>-1</sup> was taken. The spectra were ATR corrected using the OMNIC spectroscopic software program.

FTIR is a fast and effective analysis measurement for detecting the presence of polymers. For PANI characterisation by FTIR, the following features are typically seen. A doublet at 3200 cm<sup>-1</sup> and 3260 cm<sup>-1</sup> represents the secondary amine N-H stretching band [40], while 1500 cm<sup>-1</sup> and 1580 cm<sup>-1</sup> bands represent the C=C stretching vibrations of benzenoid and quinoid rings of PANI [25]. These peaks are often used as indicators for the ratio of quinoid to benzenoid aniline units [25] and a larger 1580 to 1590 cm<sup>-1</sup> peak suggests that the polymer is oxidised [25]. Peaks appearing at 2900 to 2950 cm<sup>-1</sup> and 3267 cm<sup>-1</sup> are due to the stretching vibration modes of the -C-H (-CH<sub>3</sub> or -CH<sub>2</sub>-) and -N-H bonds [68]. The bands at 1310 and 1247 cm<sup>-1</sup> are due to the C-N stretching of secondary aromatic amine modes [25], for the proton conducting state of the benzenoid ring, while a peak at 1113 cm<sup>-1</sup> is due to the plane bending vibration of C-H which is formed during protonation [185]. The doped PANI oxidation or protonation states are associated with the aromatic amine nitrogen of the C-N stretching vibration region at 1240 – 1200 cm<sup>-1</sup> [25]. During deprotonation of PANI, this 1130 – 1140 cm<sup>-1</sup> band shifts to ~1162 cm<sup>-1</sup>, assigned to a vibrational mode of the -NH<sup>+</sup>- structure of a partially oxidised polymer [25, 186, 187].

The reduced polymer would be responsible for the band at 1191 cm<sup>-1</sup> for the CH in-plane bend of benzenoid rings [25]. The existence of this band indicates the degree of doping of the polymer backbone [188]. A characteristic feature of the B-NH-Q bond or the B-NH-B bond is the out-of-plane bending vibrations of the benzenoid and quinonoid -C-H and -N-H bonds [68], which give rise to peaks in the 800 to 700 cm<sup>-1</sup> range. The 1,4-disubstituted aromatic rings are associated with the 830 cm<sup>-1</sup> band [25]. Upon oxidation, the benzenoid band at 1500

– 1490  $\text{cm}^{-1}$  is decreased while the intensity of band due to quinoid rings increases at 1595 – 1585  $\text{cm}^{-1}$  [187, 191-191].

Table 2.2. The assignments for FTIR bands observed in copolymer, PANI-co-3-ABA [44, 48].

Bond	Vibration Mode	FTIR band ( $\text{cm}^{-1}$ )
C=O	Stretching of carboxylic group	1670
C=N	Stretching vibration of quinonimine rings	1578
C-C	Stretching vibration of aromatic rings	1490
C-H	Stretching vibration	1298
C-N	Stretching vibration	1234
C-H	Aromatic bending in-plane	1122
C-H	Aromatic bending out-plane	794

The C=O bonds stretching in carboxylic groups at 1670  $\text{cm}^{-1}$  confirms the incorporation of ABA units on the copolymers. This band also appears to be smaller in the PANI-co-2-ABA than in PANI-co-3-ABA [44]. This suggests that the quantities of ABA units are present in smaller quantities than that of 3-ABA, which is in agreement with the findings reported in [44]. The intensity of this band decreased as the amount of aniline increased, and at high aniline levels, the band at 1670  $\text{cm}^{-1}$  is not even detectable as it could possibly be so weak that it would be covered up by the conduction band and the spectra produced resembled that of a doped form of PANI [44].

#### 2.6.4. Raman spectroscopy

Surface analysis from Raman spectra was obtained with a Renishaw 1000 Raman spectrophotometer employing a 488 nm laser beam. A low laser power of 0.26 mW was used for pure PANI to avoid sample decomposition. Raman can be used to characterise CPs as both a powder and as electrode films. Raman spectroscopy is an excellent tool for identification and characterisation of polymers: the electrochemical features [192] can be observed based on the excitation line wavelength, hence *in situ* Raman of PANI and copolymers were studied. Raman analysis of conducting polymers requires the registration of

the different oxidation states of the polymer and a better understanding of the ability control the oxidation state of the polymer. These samples were prepared by cycling the potential between -0.1 to 0.9 V/1.0 V at a scan rate of 50 mV s<sup>-1</sup> for 100 cycles on a Pt electrode prior to analysis, immersed in an electrolyte and at a fixed potential. Copolymers of varying monomer ratios were prepared by cycling the potential between -0.1 to 0.9 V/1.0 V at a scan rate of 50 mV s<sup>-1</sup> for 100 cycles. The Raman spectra collected were slightly smoothed and baseline corrected.

The Raman effect is particularly important to CPs. In Raman scattering, usually a laser source in the visible spectrum is used as an incident photon of energy  $h\omega_1$  which collides with a molecule at an energy level  $E_1$ . The release of a scattered photon from the molecule of energy  $h\omega_2$  at a second energy level  $E_2$  would follow, and is often referred to as the vibrationally excited state, as in Stokes Raman scattering). The emitted photon has a lower energy level, hence  $E_2 - E_1 = h(\omega_1 - \omega_2)$ . Therefore, with the initial state of the molecule being a vibrationally excited state and the final one as the ground state, anti-Stokes Raman scattering can be observed, a less intense phenomenon [185, 191-196]. As the molecule shifts by an amount from the centre of negative charge (the electrons) to the centre of positive charge (the nuclei) the incident photon with its associated electric field  $E$  induces a dipole  $\mu$  in the molecule:  $\mu = \alpha E$ , with  $\alpha$  as the polarisability tensor. It is when the molecular vibration produces a change in the polarisability that the Raman Effect is seen, and the molecular vibration is described as ‘Raman active’. This differs from the ‘infra-red active’ criteria, in which case a change in the dipole moment is required for vibration. Therefore, complementary vibrational mode information can be obtained by Raman and infra-red spectroscopy, and if the molecule has a centre of symmetry, all infra-red inactive modes will be Raman active and vice versa.

With CPs in particular, higher intensities are usually obtained in what is known as resonance Raman scattering, which happens when an absorption of the photon reaches a real molecular state. This virtual state of the molecule, corresponding to the absorption of the laser photon in ordinary Raman scattering, is not the ‘real’ state of the molecule. In order to avoid this, one needs to tune the laser light to an electronic transition of the molecule of interest during the analysis. In addition, if a fluorescent upper limit is reached, background fluorescence can obstruct the Raman signals, which creates difficulties in obtaining vibrational modes using Raman spectroscopy.



In the case of using a roughened metal electrode, a surface-enhanced Raman scattering can develop. The incident photon used in resonance with conduction band electrodes in the metal surface enhances the vibrational modes of species adsorbed on its surface.

Raman bands corresponding to vibrations of the molecule(s) were being studied against wavenumbers in the 200 to 2000  $\text{cm}^{-1}$  region. *In situ* Raman spectroscopy was performed in a solution transparent glass cell, so laser light can be emitted past glass as it is transparent and Raman photons are emitted under controlled potential. The intense band given by the C=C stretching mode at about 1650  $\text{cm}^{-1}$  in Raman spectroscopy has proven to be particularly effective for unsaturated species, with substituted benzene rings also giving a sharp band near 1600  $\text{cm}^{-1}$  [193, 194, 197-198]. This is in contrast to infra-red measurement which tends to be dominated by bands arising from certain highly polar groups [194].

The raman spectrum of doped PANI is more defined than the undoped form with band at 1626  $\text{cm}^{-1}$  and 1193  $\text{cm}^{-1}$  [190]. For the reduced form of PANI, a stronger band at 1624  $\text{cm}^{-1}$  was observed and reported by Sariciftci and Kuzmany [199]. C=N stretching of the EB at 1491  $\text{cm}^{-1}$  and the C-N stretching at 1220  $\text{cm}^{-1}$  disappear upon protonation of the polymer. A band at 1336  $\text{cm}^{-1}$  is assigned to the C-N stretching of the cation radical species. The presence of these bands confirms the doping of the PANI sample and the existence of a bipolaronic structure in the polymer. A displacement band correlated to C-N stretching mode from 1220  $\text{cm}^{-1}$  to 1260  $\text{cm}^{-1}$  was observed in this doped PANI. A benzenoid ring band at 883  $\text{cm}^{-1}$  and the quinoid ring at 835  $\text{cm}^{-1}$  were also detectable [190].

Raman spectroscopy is a useful tool for qualitative discrimination of different PANI forms [190]. During PANI formation many aniline oxidation products are expected, the following oligomers of polyaniline might also be expected to form at some point, Figure 2.5 [200].

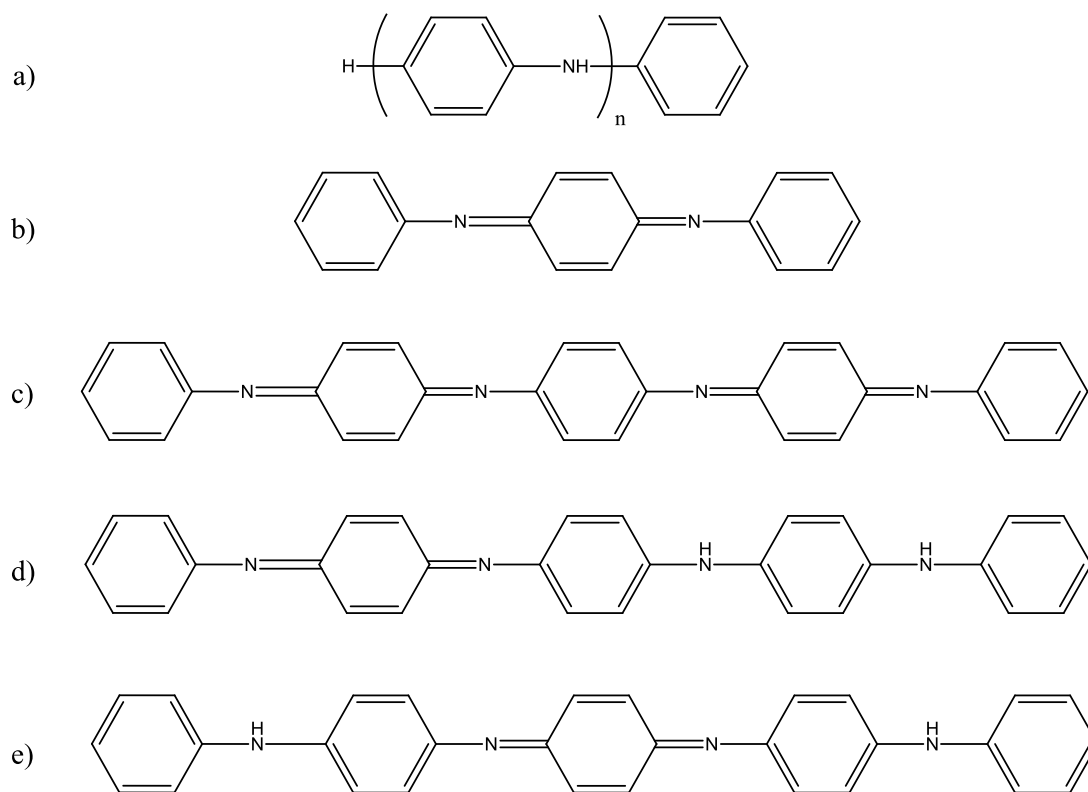


Figure 2.5. Oligomers of polyaniline [199].

The blue excitation line (488 nm) is expected to lead to a localised polaron excitation, the red line to the exciton excitation, and the near-IR line to an intrachain excitation. The band in the  $1626 - 1221 \text{ cm}^{-1}$  region corresponds to the aromatic C-C stretching, and a C-H in-plane band is seen at  $1197 - 1181 \text{ cm}^{-1}$  and is used to characterise the para-substituted benzenoid form [190]. The presence of a band at  $1485 - 1471 \text{ cm}^{-1}$  corresponds to C=N stretching of quinone diimine structures (for the oxidised PANI EB form). This band decreases from  $1491$  to  $1479 \text{ cm}^{-1}$ , indicating that electrons on quinone diimine parts of the polymer are much more localised than those in the EB form of PANI [201]. As the polymer is oxidised the in-plane C-H bends moves to  $1166 - 1157 \text{ cm}^{-1}$  [190]. The band for C-N stretching of the cation radical species appears at  $1344 - 1312 \text{ cm}^{-1}$  and the C-N band of the benzenoid units at  $1220 \text{ cm}^{-1}$ , which is consistent with the delocalised polaron form of the radical cation [190]. Aniline vibrates at  $993$  and  $1031 \text{ cm}^{-1}$  for monosubstituted benzene rings which would be absent in PANI [185].

Table 2.3. The assignment of Raman characteristic bands for PANI-co-2-ABA [48].

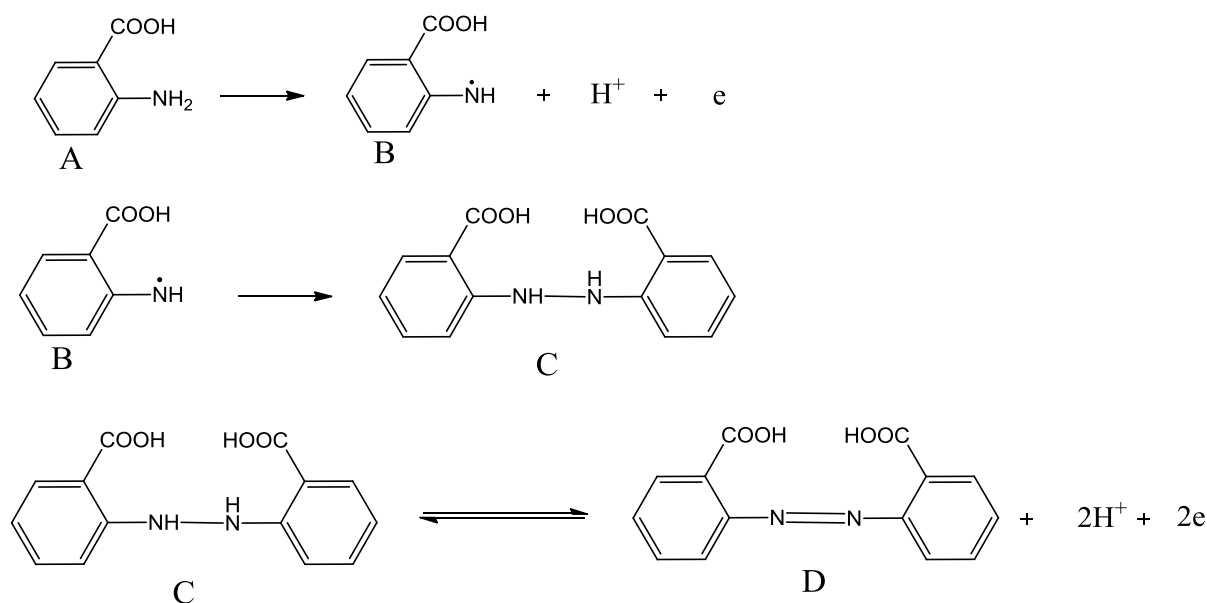
Bond	Vibration Mode	Raman band (cm <sup>-1</sup> )
>C=C<	Q stretching	1578
>C=N-	Q stretching	1456
C-C	Q stretching	1396
>C-N <sup>*+</sup>	SQ stretching	1326
>C-N-	B stretching	1207
C-H	Q bending in plane	1155
	B Symmetric ring stretching	804
	Q Ring deformation	762
	Q imine deformation	734

Which oxidation states the CPs will take on strongly depends on the surrounding environment, as well as the method of preparation. For a better understanding of the structure and mechanism of the polymers (PANI, poly-2-ABA and copolymer with ABA) formed on a Pt electrode, polymers were prepared and the samples were then exposed to different applied potentials measured using *in-situ* Raman spectroscopy. The aim of the model studies was to understand the growth of band intensity during a positive potential shift up to a maximum, located around  $E$  (V, Ag/AgCl) = 0.9/1.0 V. After this its decrease was examined with a further potential shift indicating the existence of intermediate species during the redox transformation of the polymer; for further details see Chapter Five.

PANI is characterised by the arrangement of repeat units containing four rings separated by nitrogens and differentiated by the ratio of benzenoid rings B (amine N) and quinoid rings Q (imine N) in the polymer. The most oxidised polymer is the purple pernigraniline (2Q + 2B), while the leucoemeraldine (4B) is the most reduced form. Intermediate forms such as emeraldine base EB (Q + 3B) can easily be protonated to give the salt [202, 203] and polymer formed by the incorporation of counter-ion and radical cation can present a metallic character [202, 203]. In theory, only a half-filled conduction band is observed with a metallic state [204], while the conducting properties of ES [205] are due to the electrons localised on the imine sites, leading to electron delocalisation or formation of bipolarons resulting in a large ‘polaron lattice’ [206]. Protonated and fully oxidised PANI has been described a polymer

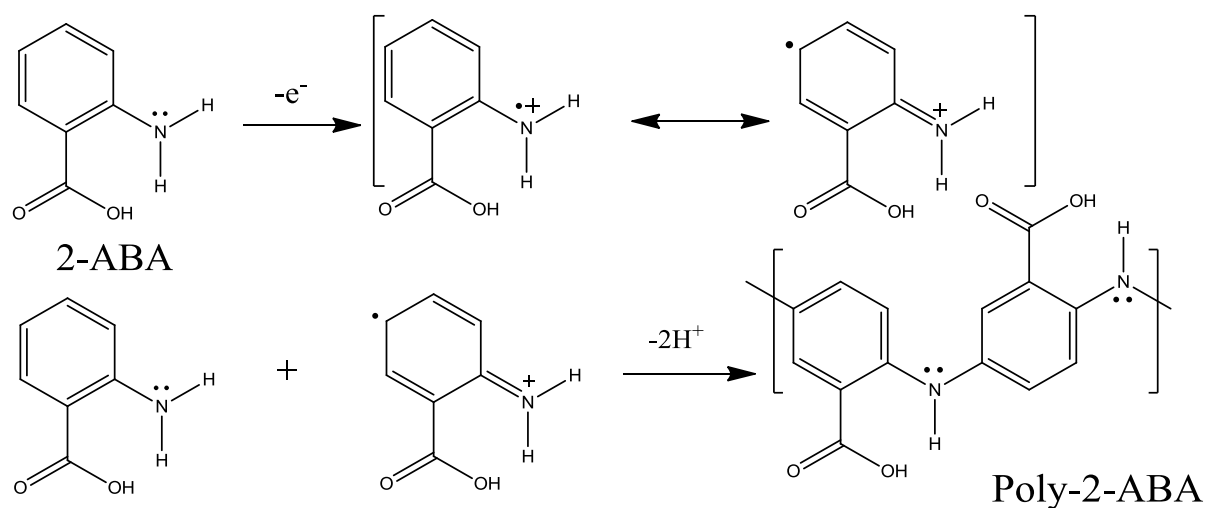
form having a polaron lattice character; moreover, both leucoemeraldine and PNB can be protonated which does not lead to conduction properties [207, 208]. The many possibilities of protonation and oxidation reactions that allow the formation of different transition states add to the complexities of PANI research [202, 203]. Films are protonated in acid medium and the level increases with potential, which allows electrochemical oxidation a good control of protonation phenomena [202, 203].

Head-to-tail coupling at N and C<sub>4</sub> positions is predominant in the aniline polymerisation, the insulating alkali-treated PANI consists of structures in which one quinone diimine is sandwiched by one or consecutive p-disubstituted benzenes on both ends [202]. The quinone diimine parts are much more delocalised at  $\pi$ -electrons and such a quinone-diimine structure is transformed into a p-disubstituted benzene-type structure upon reduction resulting in a decrease in electrical conductivity. The delocalisation of  $\pi$ -electrons is essential to its high electrical conductivity [202].



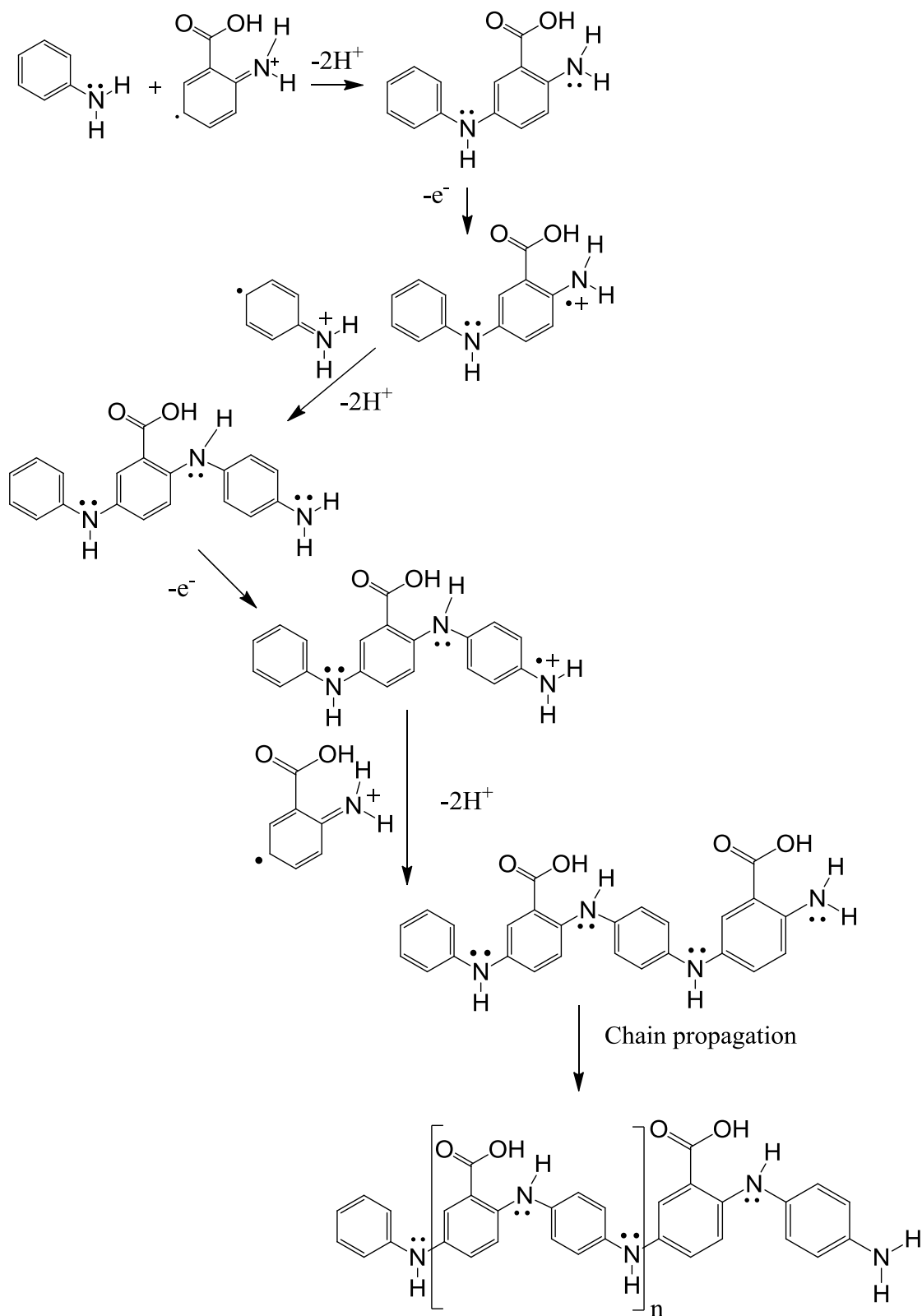
Scheme 2.1. 2-ABA oxidation and polymerisation of poly-2-ABA.

2-ABA was firstly oxidised to free radical (B) peak 1; the free radical (B) combined together rapidly to hydrazobenzoic acid. C was oxidised to azobenzoic acid (D) peak 3, and azobenzoic acid (D) reduced to hydrazobenzoic acid (C) peak 2. The 2-ABA electrochemical behaviour at glassy carbon electrode was consistent with the reference reported [209].



Scheme 2.2. Homopolymerisation of 2-ABA (adapted from [210]).

The competing mechanism of 2-ABA oxidation and polymerisation is shown in Scheme 2.1. Electrochemical polymerisation of the monomer is believed to proceed via a radical cation which would then react with a second radical cation resulting in a dimer. This polymerises further as the radical cation of monomer builds up the backbone of the polymer chain.



Scheme 2.3. Copolymerisation of aniline and 2-ABA (adapted from [202]).

In the copolymerisation reaction, the chain could be built by formation through conjugation of radicals of two different monomers followed by propagation, as shown in scheme 2.3 [202].

Mažeikienė [193, 194] reported chemically synthesised polymer studied with *in-situ* Raman with blue laser ( $\lambda = 476.5$  nm) excitation. During *in-situ* Raman, as the film was taken from being fully reduced to being fully oxidised at 0.40 V, when a new band started to grow at around  $1169\text{ cm}^{-1}$ . This feature almost masked the band around  $1192\text{ cm}^{-1}$  in the later stages of oxidation, and was assigned to the C-H stretching of the quinoid rings in the polymer matrix [193, 194, 197-198]. As the potential continued to increase, up to 0.60 V, the band at around  $1354\text{ cm}^{-1}$ , assigned to C-N stretching of semiquinone radical state, grew in intensity and then gradually decreased afterwards with a further potential shift. New bands of quinoid structure modes were present at around  $1510$  and  $1579\text{ cm}^{-1}$  [194, 197-198]. The charge of amine nitrogens transfers from LEB to radical cations, which is a transformation of sites to a random isolated polaronic one. The disappearance of isolated or delocalised polarons promotes the benzenoid segments due to a breakage in the resonance conditions resulting in the formation of the oxidised form [202, 203]. At low potentials, two bands at  $1197$  and  $1626\text{ cm}^{-1}$  strongly enhanced phenyl signature and hindered other spectral features [202, 203]. The band at  $1341\text{ cm}^{-1}$  can be assigned to the formation of isolated polarons to the amine sites [203, 203].

Aniline copolymerised with 3-ABA caused two important effects. First, intensity of some of the PANI-co-3-ABA bands diminishes or disappears. This suggests the breakage of carboxylic acidic groups or symmetry planes on the polymer molecules backbone in the amount of polarisable bonds [44-46]. The attributed  $>\text{C-N}^{\bullet+}$  stretching would increase in intensity in the area of  $\sim 1326\text{ cm}^{-1}$ . This behaviour implies that the increased in 3-ABA groups also increases the concentration of the cation radical [44-46].

### 2.6.5. Ultraviolet-Visible (UV-Vis) spectroscopy

The UV-Vis spectra of PANI in the doped form were obtained by dissolving the polymer in NMP solution, and recording the spectra using a Shimadzu UV-2102PC spectrophotometer or Shimadzu UV-1700 spectrophotometer at room temperature.

The basic electronic structure of CPs can be explained with optical property changes as these changes are associated with changes in the chain conformation, oxidation states and the

extent of protonation of PANI-EB. Hence, UV-Vis is commonly used to characterise the structure of PANI molecules present. The two characteristic peaks [211] in the UV-Vis spectrum of EB of PANI dissolved in NMP solution are ~330 nm (often referred as the B peak) corresponding to the  $\pi \rightarrow \pi^*$  transition in the B ring [188] and the second peak at ~630 nm (often referred as the Q peak), which is assigned to the highest occupied molecular orbital (HOMO,  $\pi_b$ ) transition of an electron of the B part of EB to the lowest unoccupied molecular orbital (LUMO,  $\pi_b$ ) of the Q ring [212]. The intensity ratio of these two peaks is often referred to as the Q/B ratio, which correlates to the proportional ratio of the quinoid units to benzenoid units along the emeraldine backbone.

PANI-co-3-ABA copolymer has three absorption bands. The first shoulder occurs at ~280 nm and is attributed to the  $n \rightarrow \pi^*$  transition because of the presence of nonbonding electrons on the carboxylic acid groups [44, 45]. The extended conjugation between adjacent rings in the polymeric chain contributes to the  $\pi \rightarrow \pi^*$  band between 320 and 338 nm [44, 45]. Copolymers are less conjugated than PANI, therefore, this peak appears at a lower wavelength than in PANI [213-214]. As the concentration of 3-ABA increases in the copolymer component, this band shifts to a greater wavelength, blue shifted when compared to PANI, indicating a decrease in the extent of conjugation and an increase in the transition energy [215]. The third band at 555 – 643 nm is assigned to the transition of the exciton of the quinone and is related to the hopping electronic intra- and inter-chain [213-215], while the  $\lambda_{\max}$  of this band depends on the oxidation of the copolymer [213-215]. The Q band is not present in UV-Vis spectra of PANI in the ES form, but instead new bands occur in the region from 400 to 450 nm and from ca. 700 nm in the near NIR region.

Solid state UV-vis of PANI was measured using USB2000 miniature fiber optic UV-Vis absorption spectrometer (Ocean Optics) in the region of 300 – 880 nm, to determine the oxidation state. Measurements involved a boxcar smoothing of 5, a 20 ms integrating time, with 50 spectra averaged. The dc conductivity of a PANI film on aluminium was measured using a Jandel four-point probe with a current of 100  $\mu$ A passed through the films while the voltage was measured.

*In situ* UV-Vis spectroelectrochemical measurements were made in a quartz cuvette of 1 cm path length by inserting an indium-doped *Tin Oxide* (ITO)-coated glass substrate CG-411N-S107 (4-8  $\Omega$ , 25 mm x 75 mm x 0.7 mm) obtained from Delta Technologies and cut to size with a diamond cutter. ITO acted as the working electrode with PANI grown on it prior to

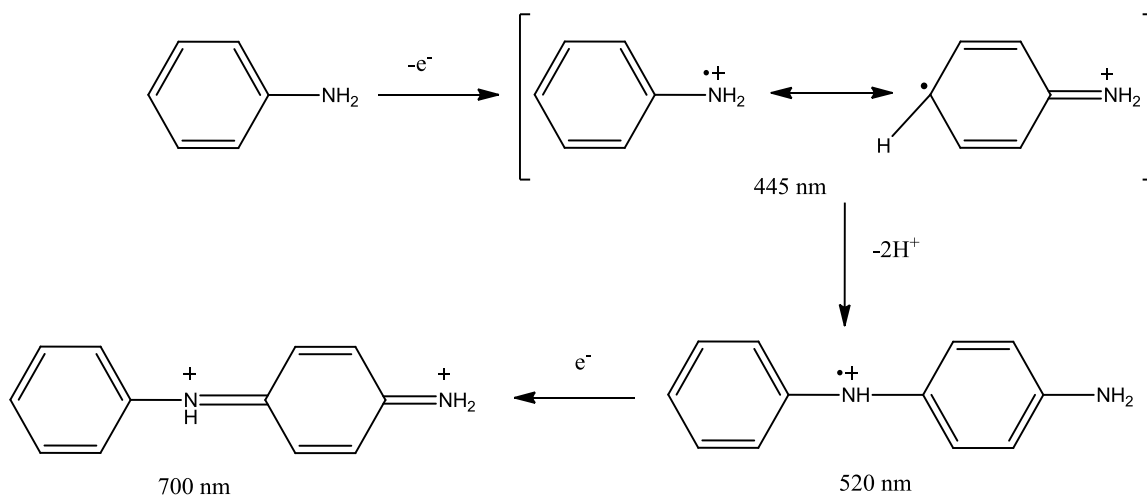


being held at varying applied potentials. Oxalic acid (0.5 M) electrolyte was used. The study was carried out for better understanding of the chemical structure formed by observing the absorption peak detected in wavelength region of 300 – 900 nm for spectral feature. Once it was shown that reproducible films of PANI on aluminium electrodes could be generated successfully by cycling the potential between -1 to 2.4 V at a scan rate of  $50 \text{ mV s}^{-1}$ , this procedure was extended to ITO electrodes. In order to compare and better understand the polymer formed, PANI films were grown on ITO substrates under different reduced potential by 10 cycles scanning between -0.1 to 1 V at a scan rate of  $50 \text{ mV s}^{-1}$  in a 0.5 M oxalic acid aqueous solution containing 0.1 M aniline monomer. The course of homopolymerisation of aniline at constant potential was followed with *in situ* UV-Vis spectroelectrochemical measurement by cyclic voltammetry method under two growth conditions on ITO-coated glass electrodes (in aqueous solution of 0.5 M oxalic acid and 0.1 M aniline) at -0.1 to 2.4 V and -0.1 to 1 V, at a scan rate of  $50 \text{ mV s}^{-1}$  for 10 cycles. The aim was to identify conceivable stages of the subsequent polymer formation while a second set of studies was performed to characterise and study potential variations. Before each experiment, a new piece of ITO-coated glass was degreased with acetone and ultrasonically cleaned and rinsed with pure water. All spectra recorded are background-corrected with the reference channel containing an ITO-coated glass electrode without polymer coating.

The synthesis of aniline is simple, but to obtain a high quality PANI is not easy and it is essential to achieve precise control of the polymer oxidation state and the level of proton doping. The oxidation state of as-prepared PANI ranges from emeraldine to PNB form, and UV-Vis spectroscopy of PANI solutions in NMP has proven to be a suitable and accurate method for determination of the oxidation state of PANI samples.

Under UV-visible spectroscopy the following PANI bands can be observed [216]:

- 300 and 450 nm show the  $\pi \rightarrow \pi^*$  transition of B rings and is characteristic of the LEB form of PANI [188], see Figure 3.8.
- 356 – 391 nm;  $\pi \rightarrow \pi^*$  electronic transition of neutral species [188, 216]
- 471 – 489 nm; indicative of polymerisation (more obvious with *in-situ* UV-visible spectroelectrochemical studies) [188, 216], see Figure 3.9.
- 650 – 895 nm; exciton transition from the B to the Q segments [188, 216-217], see Figure 3.8.



Scheme 2.4. Dimer formation and its absorbance values (adapted from [193]).

$\pi$ - $\pi^*$  electronic absorptions are seen with neutral conjugated polymers in the ultraviolet to visible region. Upon doping, new absorptions corresponding to charged excitations (polarons and bipolarons) created by doping appears in the visible to infrared regions. Charged excitations arising from vibrational spectra can be obtained by the use of resonance Raman spectroscopy with a wide range of excitation wavelengths from visible to the infrared.

#### 2.6.6. Solid-state Nuclear Magnetic Resonance (SSNMR)

All SSNMR experiments were carried out on dry, dedoped powder samples using a Bruker AVANCE 300 spectrometer operating at 300.13 MHz proton frequency. Spectra were obtained by using the CPMAS (Cross-Polarization Magic Angle Spinning) and NQS (Non-Quaternary Suppressed) techniques. The experiments were carried out using a 7 mm Bruker spinning probe with zirconia rotors. The magic angle was adjusted by maximizing the sidebands of the  $^{79}\text{Br}$  signal of a KBr sample. The proton  $90^\circ$  pulse duration was  $4.2 \mu\text{s}$  (the  $180^\circ$  pulse was  $8.4 \mu\text{s}$ ) and the frequency of the decoupling field was 62.5 kHz. The contact time was 1.5 ms, the recycle delay was 1 s and spectral width was 40 kHz. CP and NQS experiments were carried out with 5000-10000 scans at ambient temperature using samples enclosed in the rotors. The  $^{13}\text{C}$  chemical shift scale is referenced to TMS. Samples were rotated at  $7000 \pm 1 \text{ Hz}$ .

SSNMR, especially CPMAS and related techniques, has been used very effectively to study PANI [163, 186, 215-224]. These techniques can sensitively detect mutual interactions of the spins and their interactions with the external magnetic field [163, 186, 216-223], which

makes them useful in structural investigations of insoluble solid materials such as PANI and other CPs. However, there are some limitations of solid SSNMR techniques with respect to the structural analysis of CPs. The presence of paramagnetic polarons can broaden signals beyond their detection limits. Also, local fluctuations in conformation and configurational geometries and a distribution in chain packing contribute to line broadening. This produces inhomogeneously broadened resonances (linewidth  $\approx 10$  pm), which consist of superposed overlapping narrow peaks.

The chemical structure of the polymer could be determined from the chemical shifts data derived from  $^{13}\text{C}$  SSNMR spectroscopy. The localised B and Q ring structures in PANI could be shown from the  $^{13}\text{C}$  cross polarisation magic angle spinning nuclear magnetic resonance (CPMAS NMR) [221, 225].

Nevertheless, the chemical shift data derived from solid-state  $^{13}\text{C}$  NMR spectroscopy of polymers provides valuable information on the chemical structure of the polymer.  $^{13}\text{C}$  cross polarization magic angle spinning nuclear magnetic resonance (CPMAS NMR) spectra, in particular, show signals due to localised B and Q ring structures in PANI [221, 225].

#### **2.6.7. Gel permeation chromatography (GPC)**

The polymer molecular weight measurement was carried using the Gel permeation chromatography (GPC) system consisted of a Waters 515 HPLC pump, a Degasex DG-4400 on-line degasser connected to a TSK Gel Super AWM-H column (9  $\mu\text{m}$ , 6 x 150 mm) with guard, and 0.5  $\mu\text{m}$  in-line filters, a Rheodyne manual injector, and a Waters column oven. The flow rate was 0.12 mL and the eluent was NMP. The injection volume was 200  $\mu\text{L}$ . The sample solution concentrations were 10 mg/mL and filtered through 0.45  $\mu\text{m}$  syringe PTFE filters before injection. Agilent Easical GPC/SEC calibration standards of polystyrene standards were used. The detector was a Shimadzu RID-10A Differential Refractive Index detector (Wyatt Technologies Inc.). The columns and RI detector were maintained at 35  $^{\circ}\text{C}$ . Data acquisition and processing were performed using the ASTRA 4 software (Wyatt Technologies Corporation).

## 2.7. Performance properties

### 2.7.1. Adhesion properties

Coatings adhesion was tested with ASTM adhesion tape test using an Elcometer cross hatch cutter, which has a number of blades at equal spacing of 1 mm, which is used to score through the coating down to the substrate. Two cuts are made at right angles to each other resulting in a grid of small squares. Debris was removed from the surface of the sample and then adhesive tape was applied over the grid. After removal of the tape, the coating adhesion was assessed by reference to charts shown in the table of ASTM D 3359-09 standard test methods for measuring adhesion by tape test.

### 2.7.2. Anticorrosive properties

The assembly was connected to either an EG&G potentiostat/galvanostatic (Princeton Applied Research, model 280) coupled to an EG&G 1025 Frequency Response Analyser, or a Bio-Logic potentiostat (VSP-300) system. Impedance measurements for corrosion performance studies were carried out using the Powersine software for a frequency range of 100 kHz with an open circuit at different exposure time in 3.5 wt% NaCl solution at room temperature ( $\sim 21 - 22^\circ\text{C}$ ), which served as electrolyte for the impedance measurements using a standard three-electrode test method, see Figure 2.1. A Pt wire and Ag/AgCl were used as the counter and reference electrodes, respectively. Tafel extrapolation method was determined by the corrosion potential ( $E_{\text{corr}}$ ) and corrosion current density ( $i_{\text{corr}}$ ). The charge transfer resistance ( $R_{\text{ct}}$ ) and double layer capacitance ( $C_{\text{dl}}$ ) were determined from the Nyquist plot by fitting the data using Boukamp software. All measurements, at least four replicates were run for each sample type to ensure reproducibility. All potentials were reported with respect to the Ag/AgCl reference electrode.

Electrical Impedance Spectroscopy (EIS) is a non-destructive measurement of the surface properties. A classic way to present EIS data uses a Nyquist plot with  $Z_{\text{re}}$  on the x-axis, versus  $-Z_{\text{im}}$  on the y-axis, see Figure 2.6. The semi-circular arc observed is influenced by  $R_{\text{ct}}$  of electrons across an interface. A  $45^\circ$  angle straight line may follow the semi-circular arc, indicating the low frequencies dominated by diffusion-controlled processes.

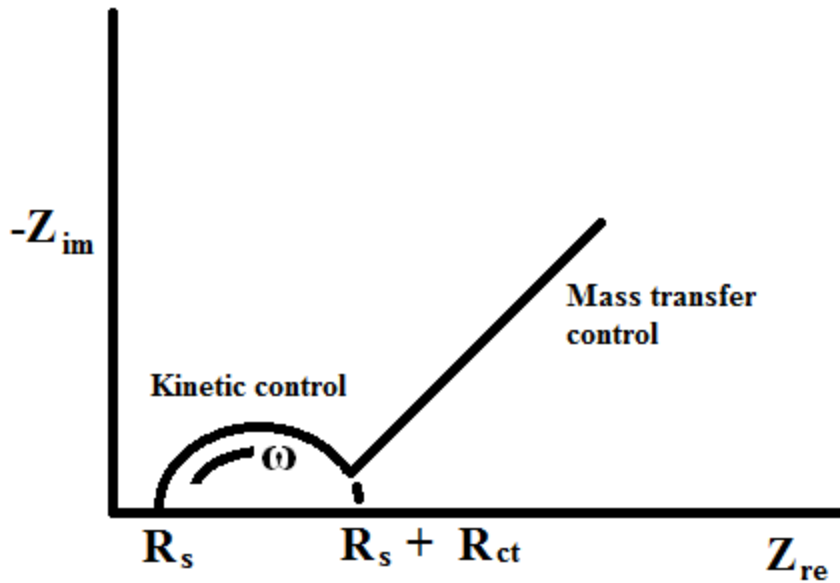


Figure 2.6. An example of a Nyquist plot with key features labelled.

### 2.7.3. Anti-moulding properties

Chemically synthesised of PANI and poly-ABA at their two different positions, 2-ABA and 3-ABA, doped with HCl and H<sub>2</sub>SO<sub>4</sub> were mixed into commercially available bathroom and ceiling paint and then applied onto weatherboard for field trial evaluation. The following samples were prepared with 1 wt% of polymers dispersed in coatings prior coated with a prepcoat (acrylic sealer undercoat) used as primer coat.

1. One coat ceiling – control without antimould properties, white.
2. Wash & Wesar 101 barrier technology – control with antimould properties, white.
3. 1 wt% PANI 1 M HCl in one coat ceiling, white.
4. 1 wt% PANI 0.5 M H<sub>2</sub>SO<sub>4</sub> in one coat ceiling white, off white with greyish undissolved particles shown on surface of coatings.
5. 1 wt% PANI 0.5 M oxalic acid in one coat ceiling white, off white with very fine PANI bits.
6. 1 wt% poly-2-ABA 1 M HCl in one coat ceiling white, greyish purple with undissolved particles shown on surface of coatings.
7. 1 wt% poly-3-ABA 1 M HCl in one coat ceiling white, beige in colour.
8. 1 wt% poly-2-ABA 1 M H<sub>2</sub>SO<sub>4</sub> in one coat ceiling white, greyish with dark brown/black powder undissolved shown on surface of coatings.

9. 1 wt% poly-3-ABA 1.5 M H<sub>2</sub>SO<sub>4</sub> in one coat ceiling white, off white.

The coated GIB board was placed on top of the heat and humidity chamber running 8 hours a day at ~60 – 70°C with the remaining time allowed to cool off to replicate a bathroom ceiling condition.



One coat ceiling	PANI HCl	1% PANI 0.5M H <sub>2</sub> SO <sub>4</sub>	PANI 0.5 M oxalic acid	Poly-3-ABA 1M HCl
Wash & Wear 101 barrier technology	Wash & Wear 101 barrier technology	Poly-2-ABA 1M HCl	Poly-2-ABA 1M H <sub>2</sub> SO <sub>4</sub>	Poly-3-ABA 1.5M H <sub>2</sub> SO <sub>4</sub>

Figure 2.7. Chemically synthesised PANI and poly-ABA doped with different dopant was applied on GIB board for anti-moulding evaluation.

#### 2.7.4. Minimum bactericidal concentration (MBC) Protocol

The test determines the lowest amount of polymer which will kill all bacteria in suspension. The amount of bacteria used was  $1 \times 10^6$  colony forming unit (CFU)/mL. The polymer was suspended at 4% w/v (40 mg/mL) in Brain-Heart Infusion (BHI) broth. The polymer-broth suspension was sonicated until homogenous solution was formed. The first row of wells in a 96 well microtitre plate in triplicate for each microorganism was tested with 100  $\mu$ L of homogenised polymer suspension. The remaining rows of wells (B-H) were filled with 50  $\mu$ L with BHI broth. Double dilutions were performed by the transfer of 50 $\mu$ L from the first row of wells (A) to the next (B). A new pipette tip was used each time. The remaining rows of wells were filled in the same manner. The last 50  $\mu$ L of row G was discarded as row H were the positive control wells with no polymer. The concentrations obtained from this process would be 4%, 2%, 1%, 0.5%, 0.25%, 0.125% and 0.06% w/v. All wells received 50  $\mu$ L BHI broth containing  $1 \times 10^6$  CFU/mL of the microorganism, *S.aureus* 6838, *E. coli* 25922, to be tested. The plates were covered and incubated at 37°C with shaking at 200 rpm for 24 hours. Shaking enabled the polymer to be kept in suspension over the incubation period. Lines were drawn on agar plates for 8 segment concentration division of polymer (2%, 1%, 0.5%, 0.25%, 0.125%, 0.06%, 0.03% and 0%). 20 $\mu$ L of the eight different treatments from the microtitre plate were dispensed onto the BHI agar plate after incubation. The plates were allowed to air-dry in laminar flow hood, inverted and incubated at 37°C/5% CO<sub>2</sub> overnight. The MBC was determined as the lowest concentration which killed 99.9% of the microorganism. If the segment did not show confluent colony growth then it was still the MBC.

#### 2.7.5. Antifouling properties

Aluminium coupons were used to test for biofouling against four strains of bacteria, *E. coli* ATCC 25922 *lux* [226], *E. coli* 536 *lux* [227], *Vibrio fischeri* [228] and *Vibrio harveyi* [229]. These four bacteria are selected due to the reason that they are the most common type in the environment. An IVIS kinetic (Perkin Elmer) was used in this novel accelerated antifouling evaluation test. This instrument provides quantitative fluorescence images using a sensitive EMCCD camera, as is discussed in detail in Chapter Seven.

#### 2.7.6. Free Radical scavenging activity

DPPH free radical method is a widely used to provide an estimate of antioxidant activity. The % inhibition capacity of PANI was evaluated using the

1, 1-diphenyl-2-picrylhydrazyl (DPPH) assay, as determined by free radical scavenging activity. 20 mL of an 83.7  $\mu\text{M}$  methanolic DPPH solution was added to  $1.00 \pm 0.02 \text{ cm}^2$  of test samples measured using an electronic LCD Caliper Digit Ruler Micrometer. The samples were left to react at room temperature for different time intervals (0.5, 1, 2, 3, 5, 7 and 24 hours), after which the absorption of the supernatant at 516 nm was measured using a Shimadzu UV-1700 UV-visible spectrophotometer. Three trials of each sample were undertaken. Control samples of DPPH solution without any test sample, a pure aluminium strip and an aluminium oxidised strip were also set up. The amount of DPPH• which reacted over 24 h period was then calculated after subtracting away the background loss of a DPPH• solution added to test sample, using an adaptation of the DPPH assay for use with polymeric samples [230-231].

#### Calculation:

DPPH radical scavenging activity

$$\text{Percent scavenging effect (\%)} = (A_0 - A_1) / A_0 \times 100$$

$A_0$  = absorbance of the control

$A_1$  = absorbance in the presence of the sample

DPPH radicals do react with light and some radicals, which can compete with their reaction with the sample in question therefore it is important to keep the DPPH solution in the dark.

The percentage of the DPPH remaining is calculated as

$$\% \text{ DPPH}_{\text{rem}} = 100 \times [\text{DPPH}]_{\text{rem}} / [\text{DPPH}]_{T=0}$$

This calculated  $\% \text{ DPPH}_{\text{rem}}$  is proportional to the antioxidant concentration, and the concentration that causes a decrease in the initial DPPH concentration by 50% is defined as  $\text{EC}_{50}$  concentration and is calculated from the kinetic curve and defined as  $T_{\text{EC}50}$ .



## CHAPTER THREE: Characterisation of chemical and electrochemical synthesis of polyaniline

### 3.1. Abstract

The aim of this chapter is to compare the chemical and electrochemical synthesis of PANI and better understanding of structures formed. The synthesis of PANI was carried out as indicated in Chapter Two, Sections 2.3 – 2.5. PANI obtained from these two methods was characterised by FTIR, Raman spectroscopy, *in-situ* UV-Vis spectroscopy, cyclic voltammetry, and SEM. The difference in the efficiency of oxidation or polymerisation, and the properties and arrangement of the polymer chains, shown by SSNMR spectroscopy as a result of the different synthesis methods, were also examined. PANI can be chemically and electrochemically synthesised in many different ways. Apart from the comparison of the preparation methods used in this study, the following chapter also examines the use of two different oxidants, APS and KIO<sub>3</sub>, as well as two dopant concentrations for the chemically synthesised PANI in H<sub>2</sub>SO<sub>4</sub>. In addition to the direct comparison between the polymers formed under different preparation methods, the chemically synthesised PANI can also be used as a pigment through dispersing it in paint for anti-moulding and antibacterial evaluation.

### 3.2. Results and Discussions

#### 3.2.1. FTIR spectroscopy

FTIR is a quick and effective method to detect the formation of PANI; therefore, the chemically synthesised PANI was first examined with FTIR for the presence of PANI in the sample. The FTIR spectra of three chemically synthesised PANIs under different conditions are shown below in Figure 3.1. These peaks can be assigned as follows, in agreement with those reported in literature [25] mentioned in Chapter Two, Section 2.6.3.

The presence of para-disubstituted benzene rings is shown by the strong bands at 1167 – 1191 cm<sup>-1</sup> and 1580 – 1626 cm<sup>-1</sup>. The position of these bands depends upon the oxidation state of the polymer, with a higher wavenumber for the reduced form, with both C-C stretching and C-H in-plane bending modes. Bands for the partially oxidised polymer appear in the region from 1515 – 1590 cm<sup>-1</sup> and 1339 cm<sup>-1</sup> for the CNC stretch. The intensity ratio of

the bands for the Q and B ring stretching has been shown to provide an estimate of the degree of PANI oxidation [25].

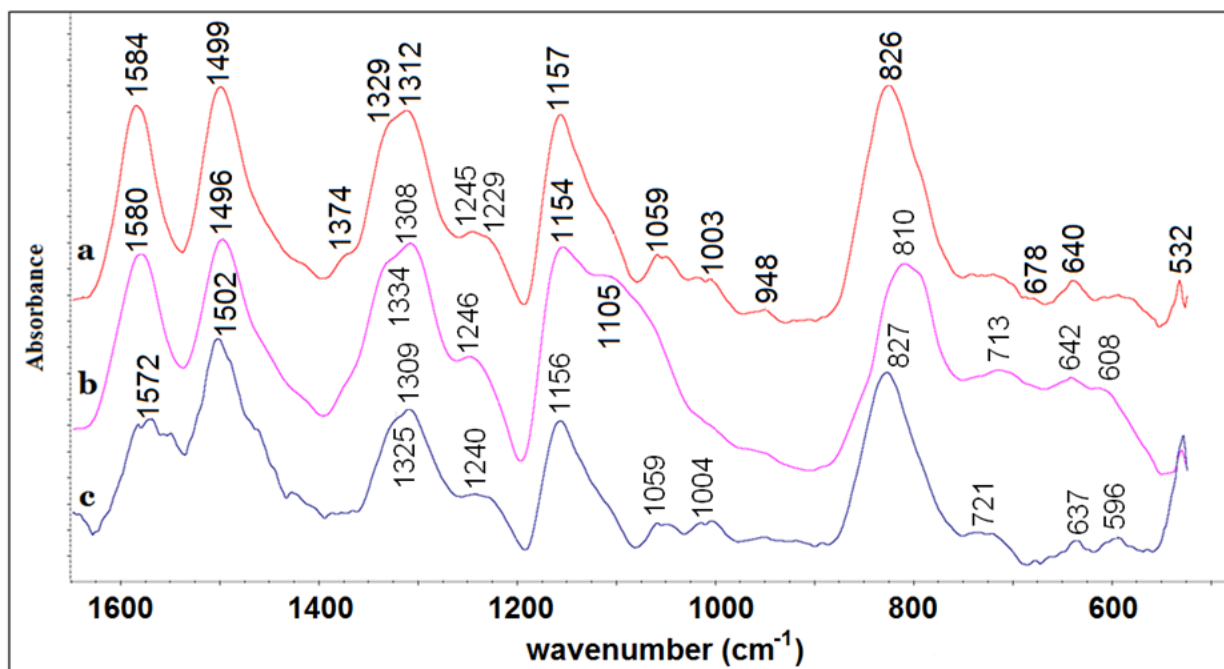


Figure 3.1. FTIR spectra of chemically synthesised PANI prepared in (a) 0.5 M H<sub>2</sub>SO<sub>4</sub> with APS, (b) 1.5 M H<sub>2</sub>SO<sub>4</sub> with APS, and (c) 1.5 M H<sub>2</sub>SO<sub>4</sub> with KIO<sub>3</sub>.

Increasing the APS dopant concentration shifted the C-C stretching vibration of the phenyl ring to a lower wavenumber, and the absorbance ratio of the two bands was noticeably different depending on the oxidant used to prepare the polymer. When using APS, the Q and B ring ratio was close to unity, however, when KIO<sub>3</sub> was used, the C=C ring stretching of the B diamine unit showed only half the intensity of the C=C stretching vibration of the Q diimine unit, suggesting that the use of different oxidant has an effect on the overall polymeric structure formed. There was a shoulder feature at 1374 cm<sup>-1</sup> which was more noticeable in H<sub>2</sub>SO<sub>4</sub> doped PANI compared to the KIO<sub>3</sub> doped form. A higher H<sub>2</sub>SO<sub>4</sub> concentration led to slight differences, more broadening and overlapping in the bands of C-H in-plane bending absorption of the aromatic ring, with broad and overlapping bands around the 1160 and 830 cm<sup>-1</sup> peak.

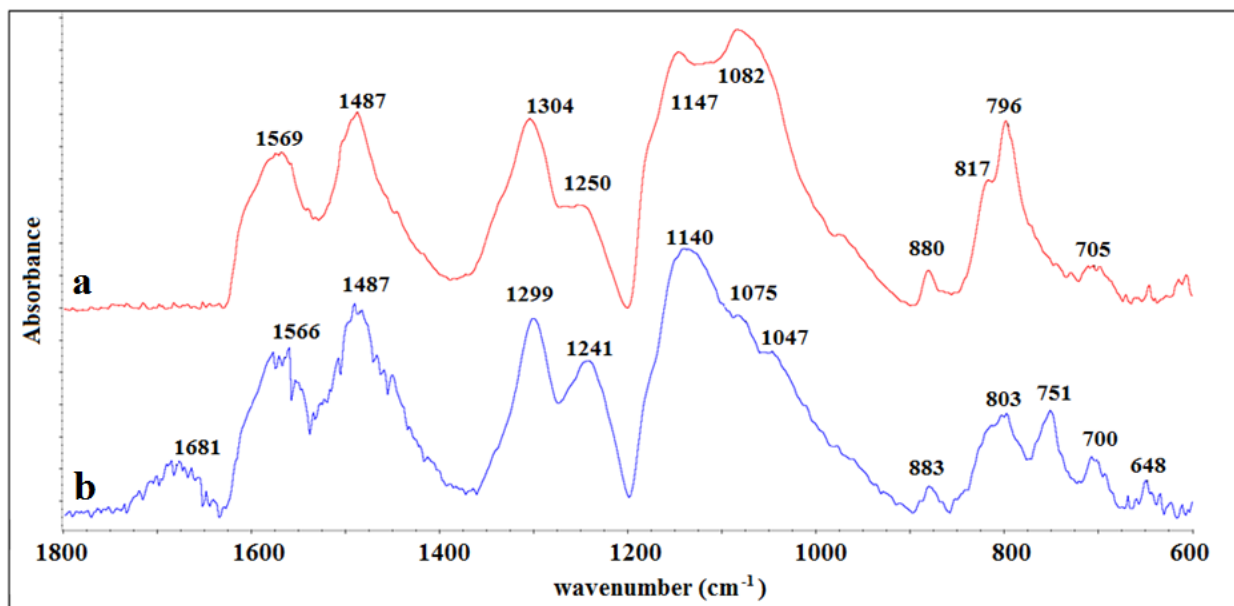


Figure 3.2. FTIR spectrum of (a) chemically synthesised PANI, and (b) electrochemically synthesised PANI on Pt electrode both doped with 0.5 M H<sub>2</sub>SO<sub>4</sub>.

FTIR spectra prepared by the two different methods, chemically and electrochemically both showed characteristic bands for PANI (Figure 3.2). However, the two spectra are quite different in the para-disubstituted benzene ring regions with the electrochemically synthesised PANI showing slightly lower wavenumber.

### 3.2.2. Cyclic voltammetry

Chemically prepared PANI was characterised electrochemically using cyclic voltammetry on a glassy carbon electrode in either 0.5 M H<sub>2</sub>SO<sub>4</sub> or 0.5 M oxalic acid for 5 cycles. The use of a different dopant had no major effect on the peaks observed in the voltammograms. The voltammograms shown below were obtained firstly after repeated cycling of chemically synthesised PANI cast on a glassy carbon electrode (Figure 3.3), and then compared to electrochemical synthesis of PANI on Pt in 0.5 M H<sub>2</sub>SO<sub>4</sub> (Figure 3.4). The CV in Figure 3.3 clearly demonstrates that an active PANI was synthesised as it shows the two characteristic redox peaks for the polymer.

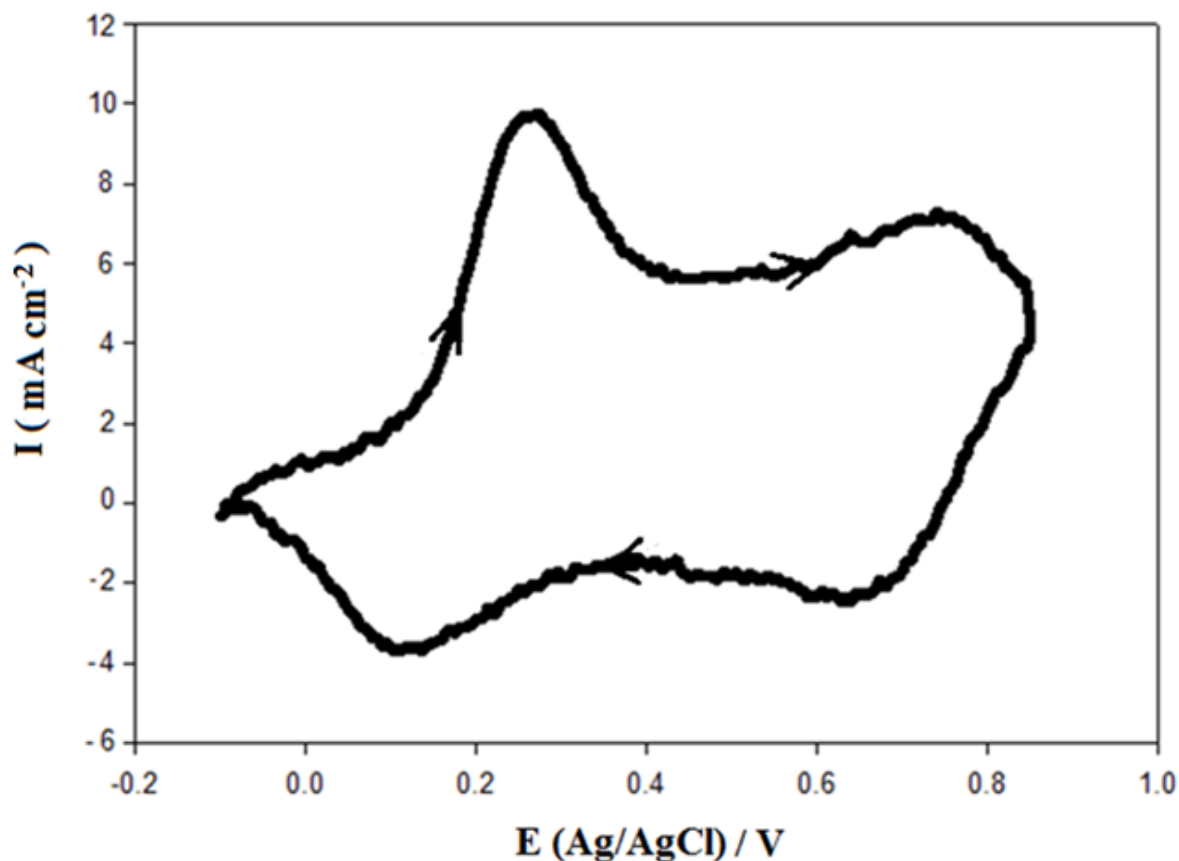
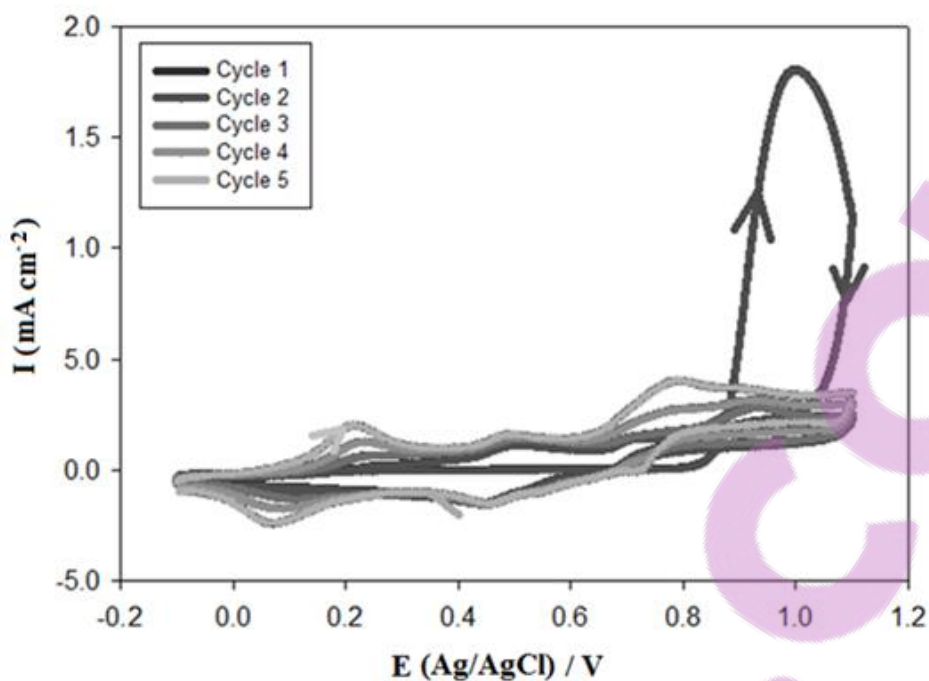
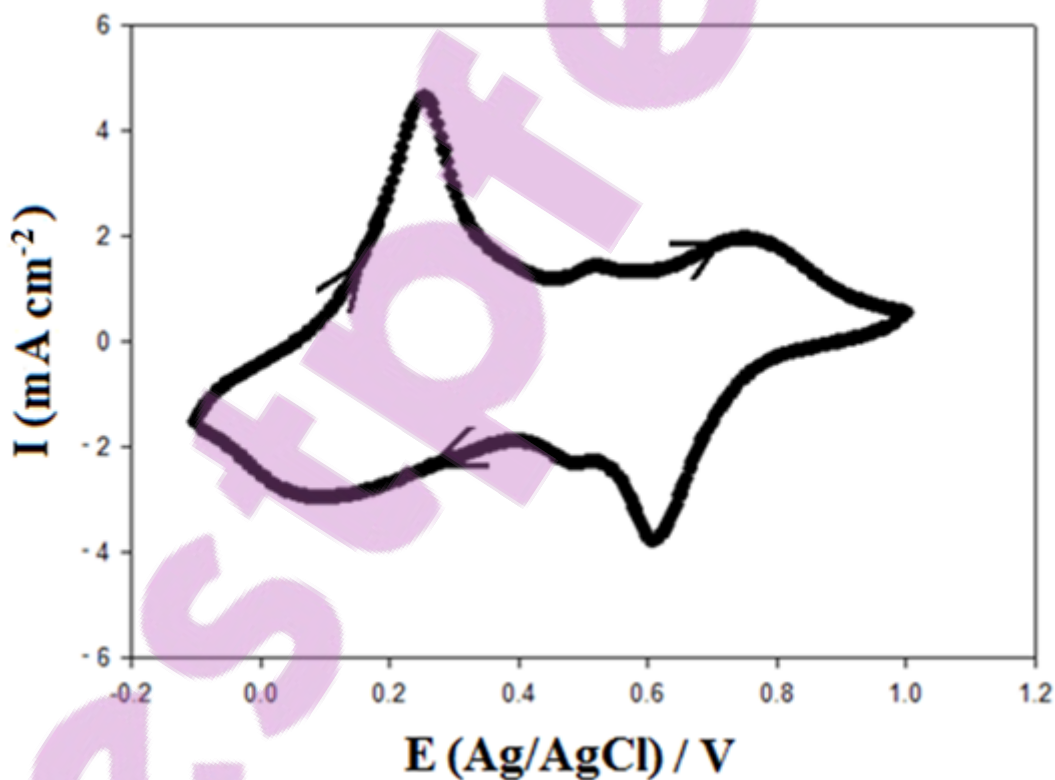


Figure 3.3. Chemically synthesised PANI cast on a glassy carbon electrode and cycled in 0.5 M oxalic acid between -0.1 to 0.85 V at a scan rate of 50 mV s<sup>-1</sup>.

During the electrochemical polymerisation (Figure 3.4), the strong peak at around 1.1 V in the first cycle is a characteristic aniline monomer oxidation peak which decreases with cycling. On subsequent cycling, three anodic and three cathodic peaks appeared due to the conducting polymer. The peak currents increased with the number of cycles, indicative of continued PANI growth on the electrode.



(a)



(b)

Figure 3.4. (a) The first 5 cycles of electrochemically synthesised PANI on Pt at a scan rate of  $50 \text{ mV s}^{-1}$  in  $0.5 \text{ M H}_2\text{SO}_4$ , and (b) at cycle 10.

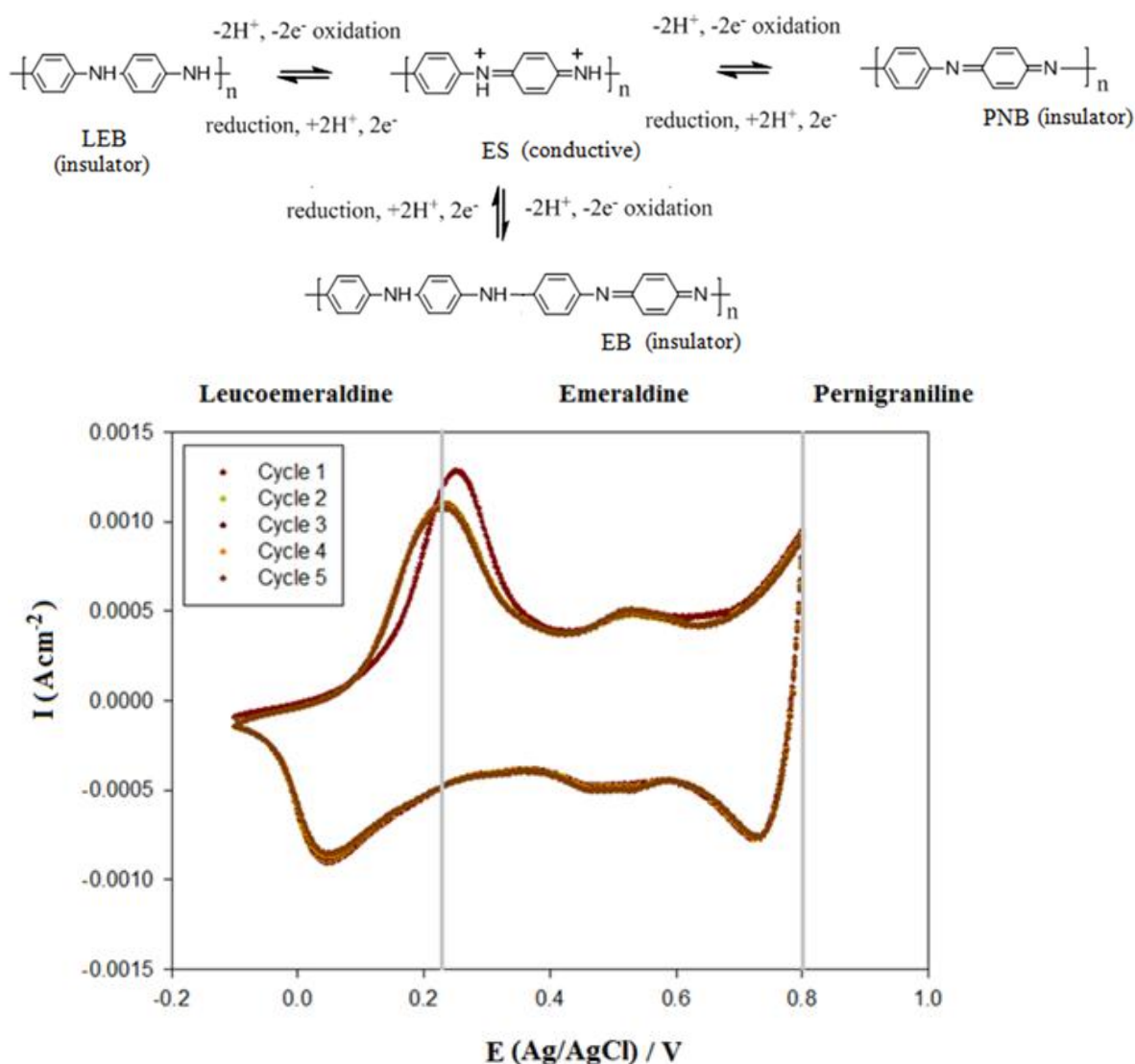


Figure 3.5. Characterisation using cyclic voltammetry for electrochemically synthesised PANI in aniline-free 0.5 M  $\text{H}_2\text{SO}_4$  at a Pt electrode. 5 cycles were run between -0.1 to 0.8 V at a scan rate of  $50 \text{ mV s}^{-1}$ , after electropolymerisation for a total of 90 additional cycles to 0.9 V after the scans presented in Figure 3.4(b).

During cycling the polymer goes through different oxidation stages and this could be clearly seen with the different colour changes at different applied potentials. At a potential of around 0.15 V versus Ag/AgCl, a proton and electron addition/elimination reaction occurred indicated visually by colour change from yellowish green to dark green [232]. The height of the first anodic peak after a prolonged reduction of the polymer can provide an indication of the thickness of the polymer film. The height of this peak is often lower on subsequent cycles

due to the incomplete reduction of the polymer during the course of a short reverse scan [232]. The middle peak indicates the presence of over-oxidised by-products during the cross-linking of PANI caused by the reaction of nitrenium species [233, 234]. Increasing the upper potential increases the rate of growth for PANI. However, increasing the upper potential also increases the middle peak producing more over-oxidised products. Therefore, the ideal cycling potential condition is to cycle the potential to a high upper potential for the first two to five cycles and then decrease it once the growth has been initiated. Starting the growth of PANI on surfaces is the most difficult part of the synthesis and once a thin film has grown, further polymer growth is easier to maintain. Other reactions that take place during the redox cycling are insertion/elimination of electrolyte anions into/from the polymer film [235]. Since this involves anion exchange, the observed colour change can be assigned to the oxidation change of PANI and is achievable via different preparation conditions [232].

CVs of PANI grown electrochemically (Figure 3.5) show three redox pairs [15, 235, 232-234], while chemically synthesised polymer (Figure 3.3) polymer only consisted of the two outer sets of redox peaks. The intermediate peak observed for the electrochemically prepared PANI is likely to have been caused by the degradation due to the higher scan rate during polymer formation resulting from overoxidation. The purpose of growing PANI at an upper potential of 1.1 V was also to align with the growing conditions for ABAs shown in Chapter Four. However, it has demonstrated that growing PANI at such high potential is not necessary and would only degrade the polymer formed. The redox reaction between the reduced LEB and EB forms generates the first set of redox peaks ( $E = 0.2$  V (Ag/AgCl)), while oxidised quinone or quinoneiminie type degradation products can contribute to redox activity at intermediate potentials. The third set of redox peaks corresponds to the EB and PNB transition is indicated with the peak at 0.80 V [232]. The overoxidised products formed during polymerisation would also be present, but most of these would have been removed during the washing process. The electrochemically synthesised PANI was prepared by cycling between -0.1 to 0.9 V – 1.1 V at a scan rate of  $50 \text{ mV s}^{-1}$ , as shown in Figure 3.4. The upper potential of 1.1 V in the electrochemical synthesis of PANI has proven to be too high and led to the accentuated degradation products as seen in Figures 3.4(b) and 3.5, hence, in order to avoid the formation of degradation and intermediate products, a lower upper potential would be more favourable.

### 3.2.3. Raman spectroscopy

The surface analytical Raman spectroscopy technique was employed to study the films of chemically and electrochemically synthesised PANI. The spectra provided valuable information about the redox reactions involved and the oxidation state at each applied potential.

The Raman spectra of some PANIs prepared both chemically and electrochemically are shown below in Figures 3.6 and 3.7. The electrochemical preparations were made on various substrates in either 0.5 M H<sub>2</sub>SO<sub>4</sub> or 0.5 M oxalic acid, by cycling between -0.1 to 0.85/0.9 V at a 50 mV s<sup>-1</sup> scan rate. The Raman spectra of the chemically synthesised PANI had the least overlapping bands and looked visually much simpler than those for the electrochemically synthesised PANIs. However, the bands position for the samples prepared via the two different synthesis methods lie in similar positions indicating that the same CP had formed.

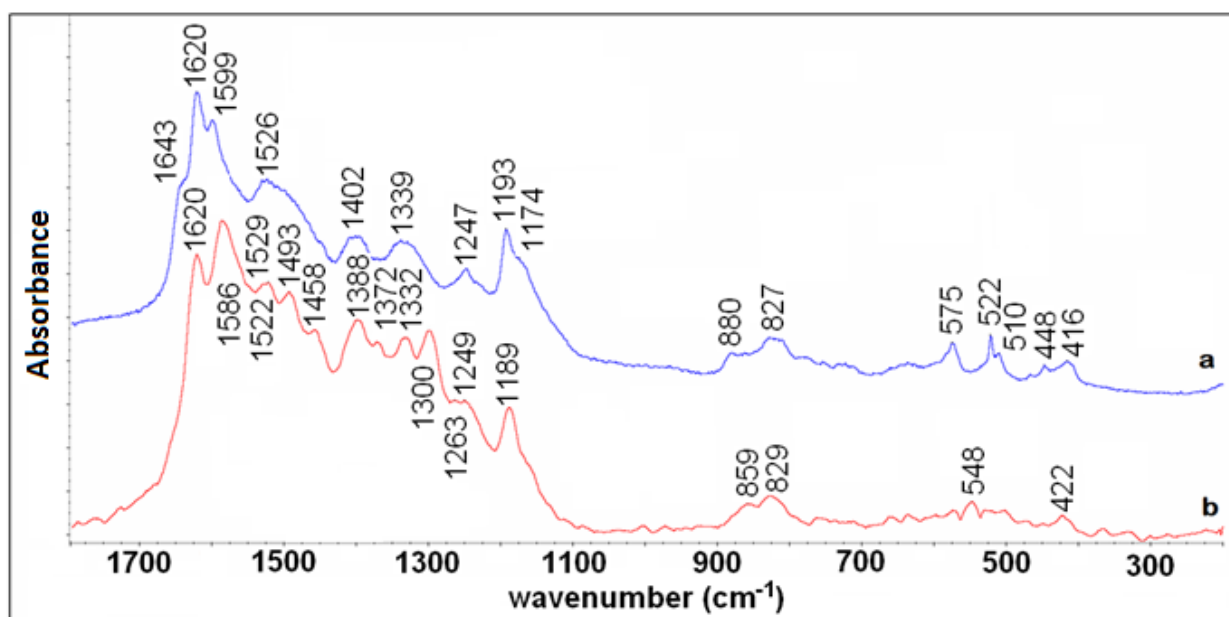


Figure 3.6. Raman spectra of (a) PANI chemically synthesised in 0.5 M H<sub>2</sub>SO<sub>4</sub>, and (b) PANI electrochemically synthesised in 0.5 M H<sub>2</sub>SO<sub>4</sub> on Pt sheet on blue laser excitation line ( $\lambda = 488$  nm).



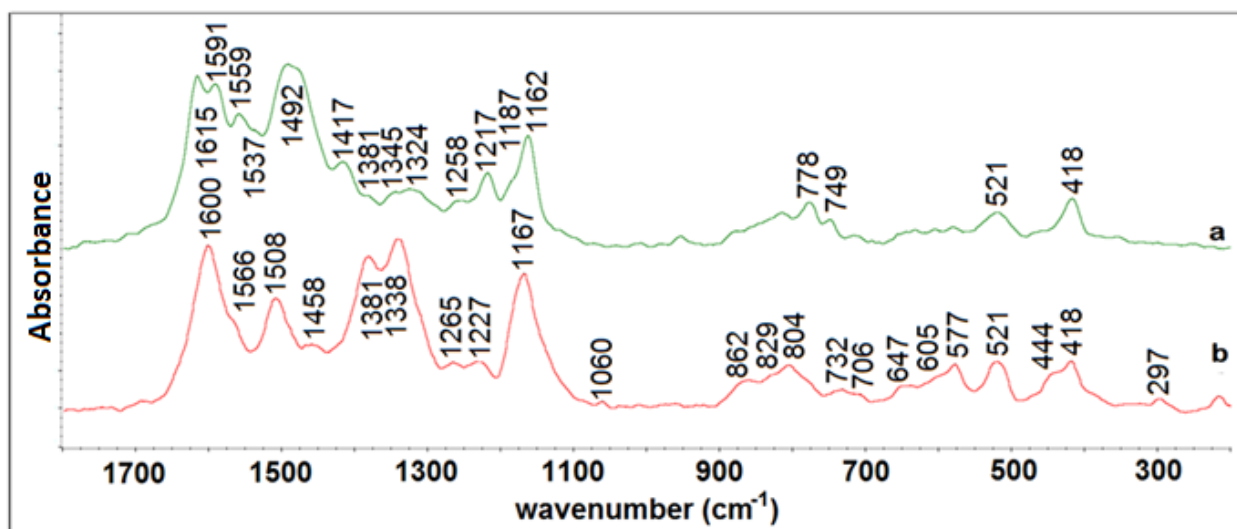


Figure 3.7. Raman spectra of (a) PANI chemically synthesised in 0.5 M oxalic acid, and (b) PANI electrochemically synthesised in 0.5 M oxalic acid on a Pt electrode.

The major bands along with their assignments are given in Table 3.1. All of the PANIs, regardless of the preparation method or dopants used, showed similar major characteristic bands. These included C-C deformation bands assigned to the B structure at around  $1620\text{ cm}^{-1}$  [187, 109, 200]. The C-C and C-H benzene deformation modes, indicating the presence of Q rings, appeared at  $1580$  and  $1150\text{ cm}^{-1}$ . The  $1514\text{ cm}^{-1}$  band ascribed to N-H bending deformation band of protonated amine, was also detected [147, 236-237]. The  $\text{C}=\text{N}^{\bullet+}$  stretching mode of Q units can be seen at around  $1460\text{ cm}^{-1}$ , while the band at  $1260\text{ cm}^{-1}$  can be assigned to the C-N stretching mode of the polaronic unit. The  $1263\text{ cm}^{-1}$  band is due to a mixed mode of C-N and ring C-C stretching vibrations, because it can shift down by 4 and  $26\text{ cm}^{-1}$  with 15N- and 2H- substitution [237-238]. The electronic absorption of free charge carriers, and the conducting nature of the polymeric compound are indicated by the band at  $1338\text{ cm}^{-1}$ . This corresponds to the  $\text{C}-\text{N}^{\bullet+}$  stretching mode of the delocalised polaronic charge carrier at  $1380\text{ cm}^{-1}$  [236-238] and  $1300\text{ cm}^{-1}$  [236-238]. The position of the benzene C-H bending deformation band characteristic of the reduced and semiquinone structures is seen at around  $1171\text{ cm}^{-1}$  in the polymer matrix [236-237].

Table 3.1. Band assignments for the Raman spectra of PANI obtained with an excitation wavelength of  $\lambda = 488$  nm.

Modes	Chemically Prepared (wavenumber/cm <sup>-1</sup> )		Electrochemically Prepared on Pt (wavenumber/cm <sup>-1</sup> )	
	0.5 M H <sub>2</sub> SO <sub>4</sub>	0.5 M oxalic acid	0.5 M H <sub>2</sub> SO <sub>4</sub>	0.5 M oxalic acid
$\nu_{CC}$ (B)	1625	1615 [185]		1600
	1620s		1620	
$\nu_{CC}$ (Q, SQ)*	1600	1591	1586	
		1599		1566
$\nu_{C=C}$ (SQ)	1526	1537	1529, 1522 doublet	
		1496		1508
$\nu_{C=N}/\nu_{C=C}$ (Q)		1482 [185]	1493	1458
	1458			1466
		1417 1427		
	1402	1381	1398	
		1372	1372	1381
$\nu_{CNC}$ (SQ)	1339	1345, 1332	1330	1338
$\nu_{CN}$	1247	1260 [185]	1263	1265
		1256	1249	
		1215		
$\delta_{CH}$ (B)	1193		1189	
$\delta_{CH}$ (Q, SQ)	1174	1164		1167
		952		
		822		
		774 760		
		753		
		712		
		579 596		
		524 511		
		418 446		

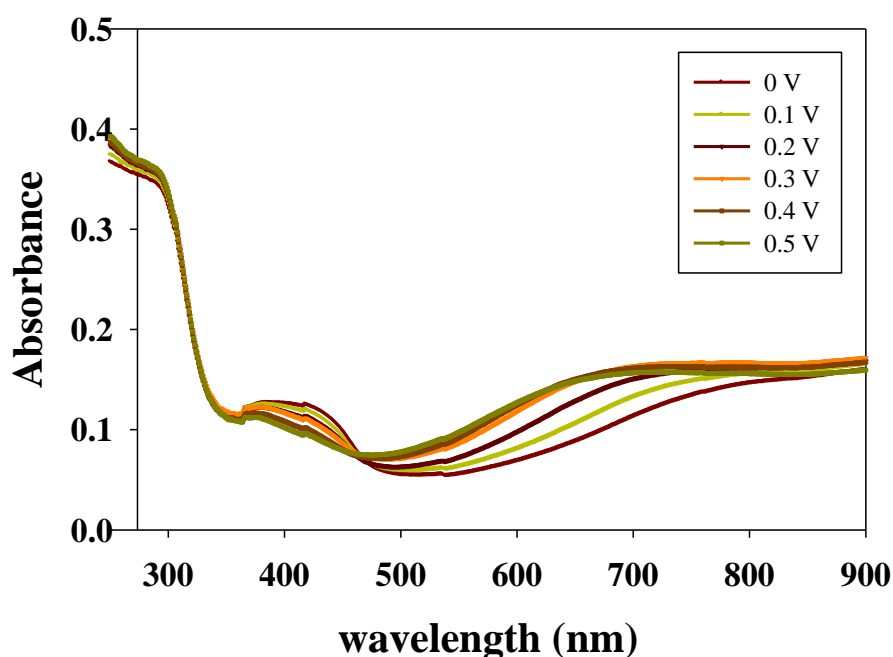
\*deformation modes [185, 187, 190, 200]

Although all of the characteristic peaks were present under different preparation methods and surfaces, the structures of the PANIs formed were slightly different. The differences in ratio of the stretching vibrations of B and Q rings, as indicated in the region of  $\sim 1620$  and  $1580$  cm<sup>-1</sup>, point to differences in the oxidation state. In particular, there was a significant blue shift for the electrochemically synthesised PANI grown on Pt, such as the C-C and C-H

benzene deformation mode shifts. The chemically synthesised PANI was stored for a week after synthesis prior to infrared measurement. Bands shown with these polymers were relatively broad, and the stretching vibrations of the B and Q rings in the  $1580 - 1626 \text{ cm}^{-1}$  regions overlapped with C=N and C=C vibration bands at  $\sim 1450 - 1300 \text{ cm}^{-1}$ .

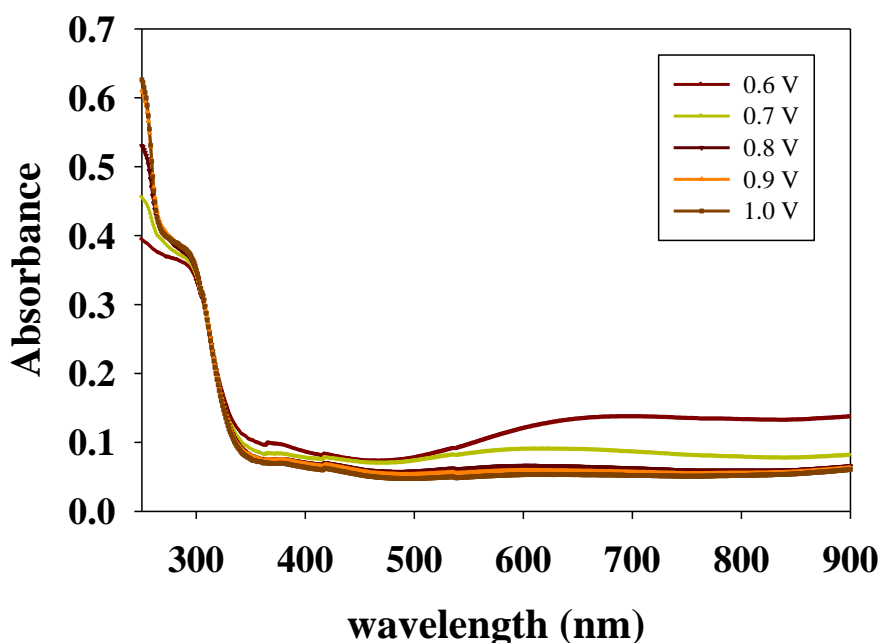
### 3.2.4. UV-Vis and *in-situ* UV-Vis spectroscopy

Electrooxidation of aniline was undertaken on an indium tin oxide (ITO) electrode, Figure 3.8.



(a)

Figure 3.8. (a) UV-Vis spectra on an ITO electrode, obtained in a 0.5 M oxalic acid electrolyte after running 10 cycles in 0.5 M oxalic acid + 0.1 M aniline between -0.1 and 1 V at  $50 \text{ mV s}^{-1}$  at 0 to 0.5 V applied potential.



(b)

Figure 3.8. (b) UV-Vis spectra on an ITO electrode, obtained in a 0.5 M oxalic acid electrolyte after running 10 cycles in 0.5 M oxalic acid + 0.1 M aniline between -0.1 and 1 V at  $50 \text{ mV s}^{-1}$  at 0.6 to 1.0 V applied potential.

The electrode potential of the ITO glass electrode in a solution of aniline was first shifted to  $E_{\text{Ag}/\text{AgCl}} = 1.0 \text{ V}$ . *In-situ* UV-Vis spectroscopy on the ITO coated glass electrode revealed the initial and intermediate stages of polymerisation involving the cross-reaction of cation radicals resulting in a head-to-tail dimer or oligomer formation. Bands reported previously for PANI at  $\lambda = 360, 440$  and  $700 \text{ nm}$  were all observed in the oxidised state of the polymer in the UV-Vis spectra [239]. The absorption at  $\lambda = 440 \text{ nm}$  was assigned to the aniline cation radical or oxidised benzidine dimer, the localised polarons that are characteristic of the protonated PANI. The band at  $\lambda = 360 \text{ nm}$  was assigned to the  $\pi \rightarrow \pi^*$  electronic transition of neutral species. The broader band at  $\lambda = 700 \text{ nm}$  could correspond to *N*-phenyl-paraphenylenediamine (PPD) dimer and its dication. An extended absorption that appears at around  $\sim 845 \text{ nm}$  represents the conducting ES phase of the polymer [240].

In the reduced state an absorption band was found in the UV-Vis spectra in the region of  $\lambda \sim 350 - 450 \text{ nm}$ , which decreased as the film was oxidised. The absorption band at

$\lambda \sim 300$  nm has been assigned to the  $\pi \rightarrow \pi^*$  transition in the aromatic benzene unit and is characteristic of the LEB form of PANI.

The absorption peak at  $\sim 360$  nm is due to the  $\pi \rightarrow \pi^*$  transition of B rings in PANI. The absorption peak shifts from 414 to 430 nm and another shift  $\sim 880$  to 670 nm with the change in colour from yellow to blue. This band at 670 nm is attributed to the  $\pi \rightarrow \pi^*$  transition of the Q rings on PANI chains. The band absorption has greatly lowered for a potential of 0.8 V to 1.0 V. The main absorption band in the red region of  $\sim 620$  to 740 nm of the spectra corresponds to the conducting emeraldine state of PANI. The growth of intensity of this band at 306 nm shows a progressive oxidation of PANI film from its LEB form into the EB form. The incorporation of  $\text{SO}_4^{2-}$  ions to the formation of the polymer structure is indicated by a blue shift of the 306 nm band [241].

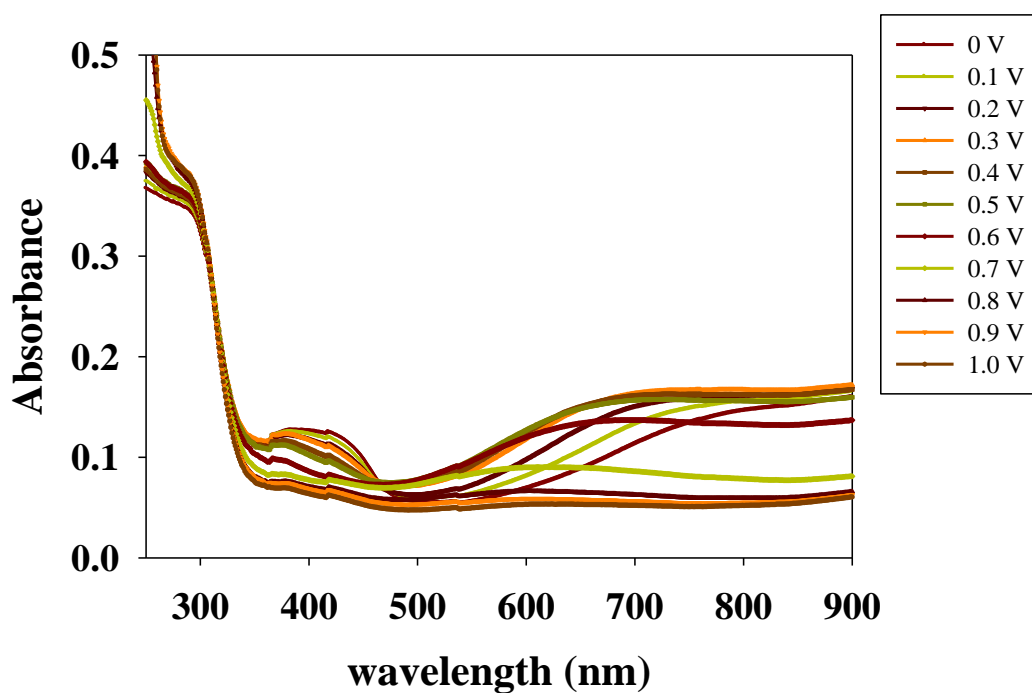
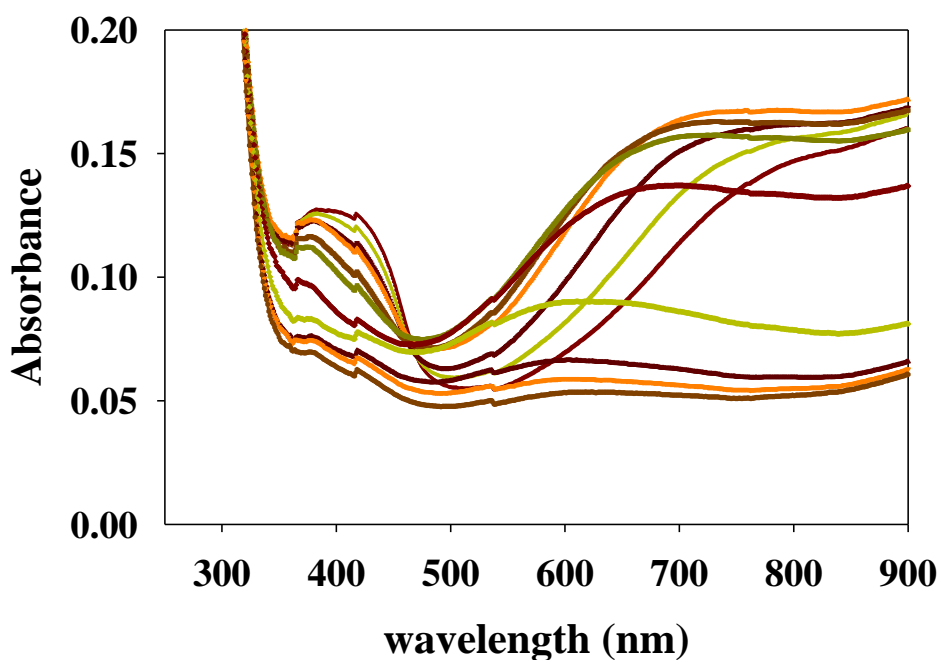


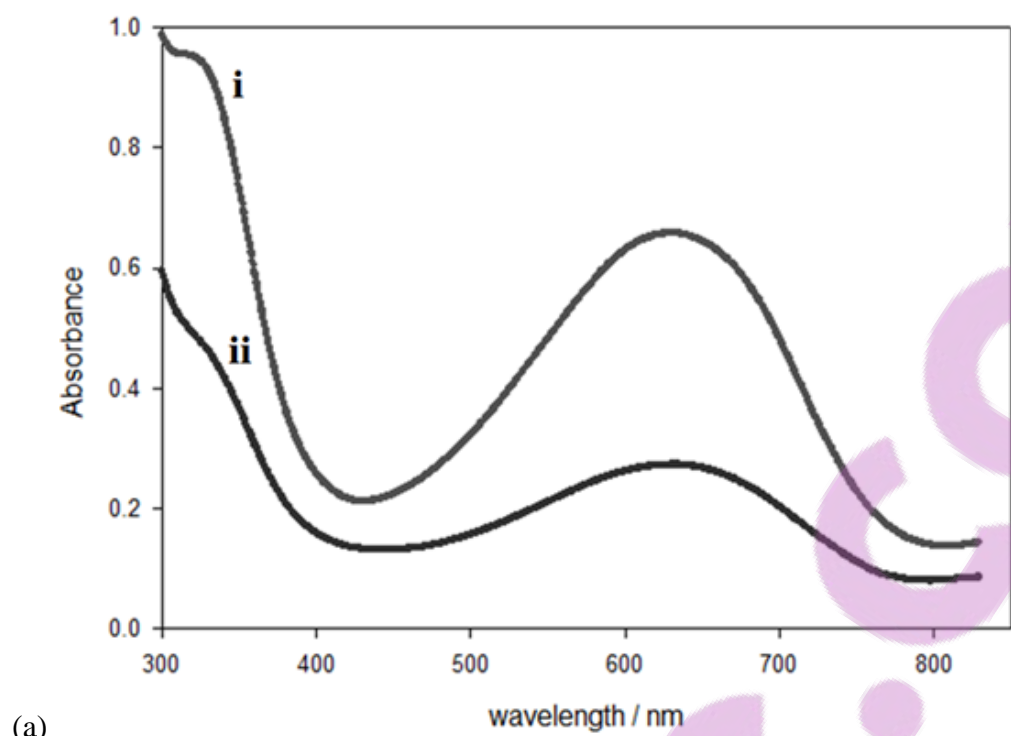
Figure 3.9. (a) UV-Vis spectra on an ITO electrode, obtained in a 0.5 M oxalic acid electrolyte after running 10 cycles in 0.5 M oxalic acid + 0.1 M aniline between -1 and 2.4 V at  $50 \text{ mV s}^{-1}$ .



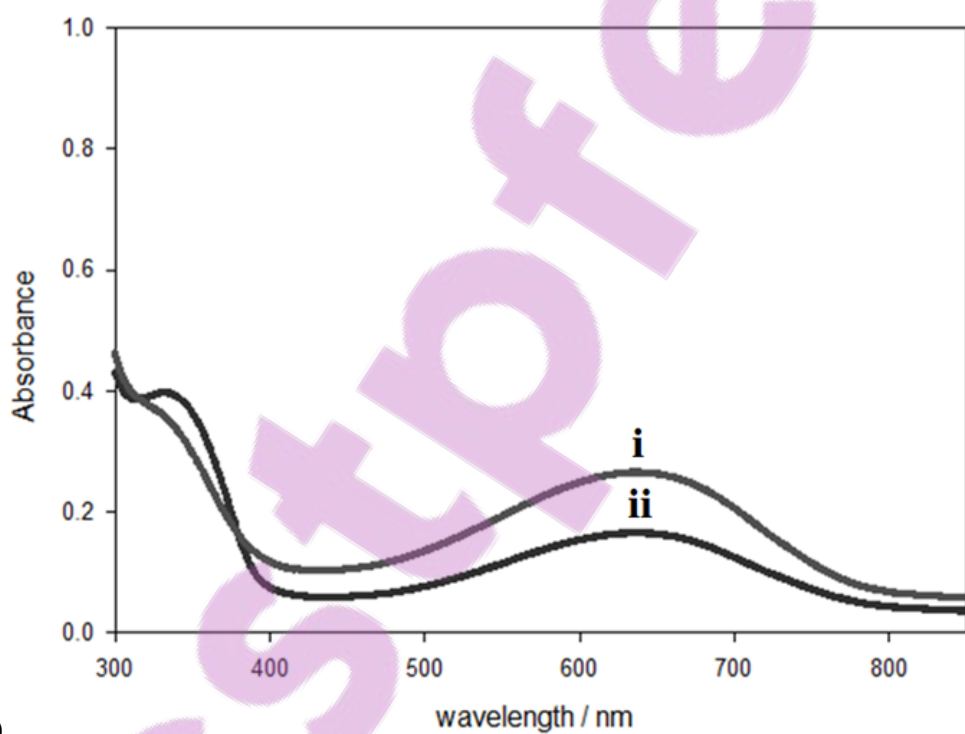
(b)

Figure 3.9. (b) UV-Vis spectra on an ITO electrode, obtained in a 0.5 M oxalic acid electrolyte after running 10 cycles in 0.5 M oxalic acid + 0.1 M aniline between -1 and 2.4 V at  $50 \text{ mV s}^{-1}$ .

Spectra for PANI prepared under different conditions and dissolved in NMP solvent are presented in Figures 3.10 – 3.11. The EB form of PANI usually absorbs in two areas,  $\sim 330$  and  $\sim 640$  nm, as shown in Table 3.2. PANI chemically prepared with the use of different oxidants,  $\text{KIO}_3$  and APS, at a fixed 1.5 M  $\text{H}_2\text{SO}_4$  dopant level are shown in Figure 3.10 and there is not much difference in the excitation of the B and Q segments in the PANI chain. However, the concentration of the polymer is in direct relationship with the absorption. The peak wavelengths of chemically synthesised PANI are close to the 328 nm excitation wavelength, while the peak of the electrochemically synthesised PANI is at 348 nm. This shift suggests that the degree of doping on the excitation of the benzene segments for chemically and electrochemically synthesised PANI are slightly different. This is once again shown with a higher level of dopant used: note the difference in the wavenumbers between the third and second columns in the table.



(a)



(b)

Figure 3.10. UV-Vis spectra of PANI synthesised by oxidation with APS doped in (i) 0.5 M H<sub>2</sub>SO<sub>4</sub> (ii) 1.5 M H<sub>2</sub>SO<sub>4</sub> both (a) chemically, and (b) electrochemically prepared.

Table 3.2. Principal bands - seen in the UV-Vis spectra of the PANIs.

	$\lambda_{\max}$ 0.5M H <sub>2</sub> SO <sub>4</sub> (nm)	$\lambda_{\max}$ 1.5M H <sub>2</sub> SO <sub>4</sub> (nm)
Chemically synthesised PANI	328, 635	337, 636
Electrochemically synthesised PANI	348, 634	353, 636

The first band at ~330 nm is assigned to the  $\pi$ - $\pi^*$  excitation of the para-substituted B segment (-B-NH-B-NH) and its value is a function of intra-chain interactions [242]. The other band at 640 nm is associated with the excitation of the Q segment (-N=Q=N-). The  $\pi$ - $\pi^*$  excitation of the para-substituted B segments for the chemically synthesised and electrochemically synthesised PANI align with each other and show similar band positions. Although the same polymer concentration was used, a different intensity indicating more concentrated acid was observed with polymer at higher dopant level. Neither the concentration nor dopant used (H<sub>2</sub>SO<sub>4</sub> or oxalic acid) had an effect on the wavelength position, as also shown by CV results, see Figures 3.3 and 3.4.

A much higher intensity was observed in Figure 3.11(i) with 1.5 M H<sub>2</sub>SO<sub>4</sub> doped PANI oxidised with KIO<sub>3</sub>, which could possibly be due to the experimental sample collection and the fact that there was more PANI in the pathlength in this particular sampling period. However, the  $\pi$ - $\pi^*$  excitation shifted to a higher wavenumber with electrochemically synthesised PANI compared to the chemically synthesised polymer. UV-Vis spectroscopy studies the changes in electronic energy levels within the molecule and the increase of wavenumber between the two different preparation methods suggest that the  $\pi$ - $\pi^*$  transition band of PANI electron systems of the electrochemically prepared PANI could be more doped than that of the chemical PANI formed. The broad band correlated with the extent of conjugation between the adjacent rings in the polymer chain.



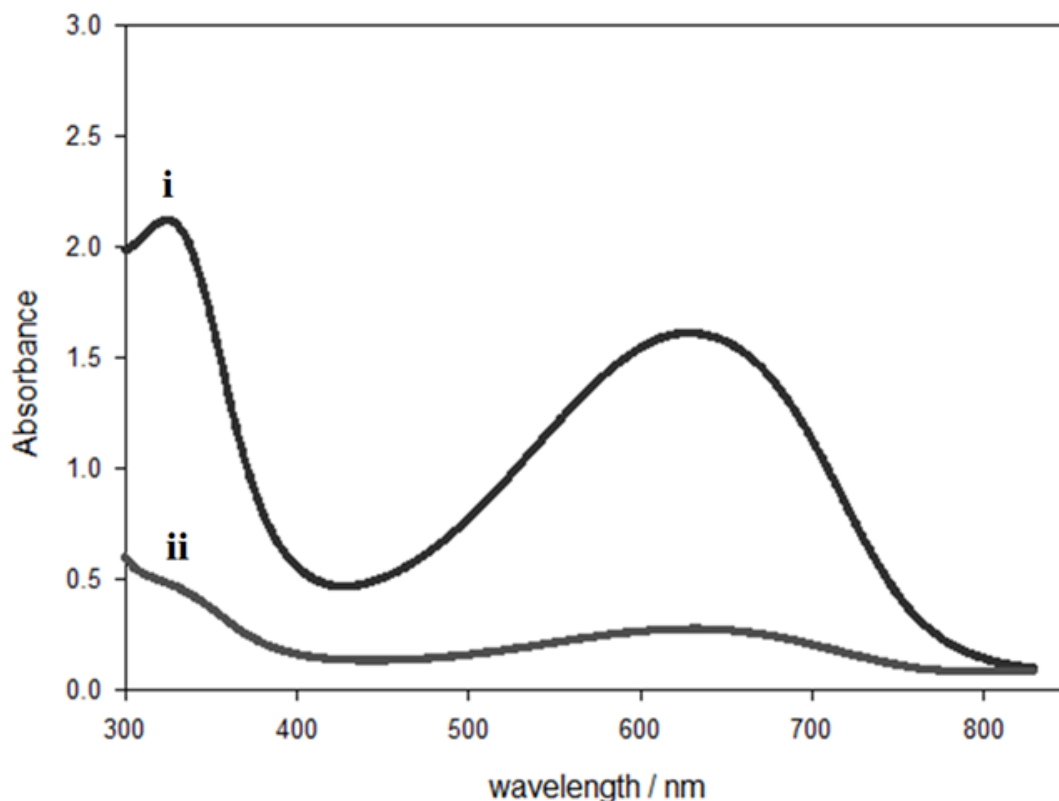
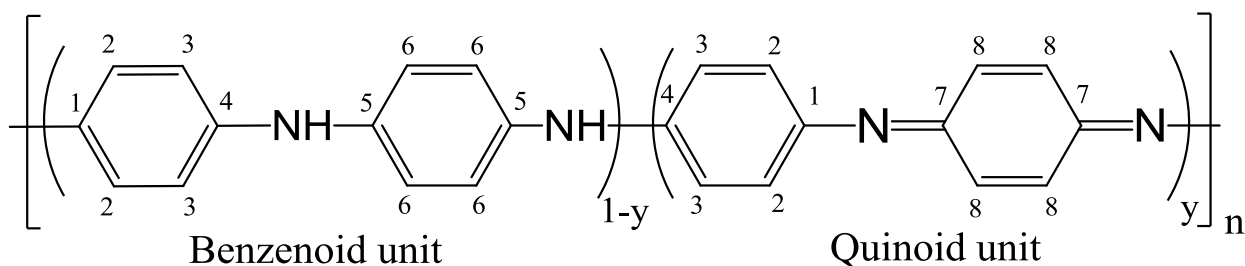


Figure 3.11. PANI prepared chemically synthesised doped with 1.5 M H<sub>2</sub>SO<sub>4</sub> (i) oxidised with KIO<sub>3</sub>, and (ii) oxidised with APS.

### 3.2.5. SSNMR spectroscopy of polyaniline

SSNMR is a useful technique for structural studies of CPs such as PANI. CPMAS reflects the mutual interactions of the spins and the external magnetic field. Nonquaternary suppression (NQS) [243-244] was also obtained for better insight into the molecular structure of PANI prepared either chemically or electrochemically.



Scheme 3.1. PANI structure.

Six overlapping and broad resonances were observed at 114 (shoulder), 123, 136, 141, 147 and 158 ppm (Figure 3.15) [230]. Carbon C-2, 3 and C-6 are responsible for the peak at

123 ppm and 114 ppm, Scheme 3.1. The Q part of PANI structure corresponds to the 136 ppm that originates from the protonated C-8 carbon and so does the non-protonated C-7 peak at 158 ppm [230]. The non-protonated carbons C-4 and C-1 are associated with peaks at 141 and 147 ppm [230].

The resonance at 137 ppm C-8, 147 ppm C-1 and 158 ppm C-7, assigned to the Q part, was relatively increased due to the difference in the oxidant used and possibly caused by the oxidation, Figures 3.15(b) and 3.15(d) [230]. The CPMAS spectrum of PANI prepared in APS dopant also consisted of similar bands but with different intensities and with slight chemical shifts. The carbon environment of the Q segment appeared a little different as shown from C-5, C-2, C-3, C-8 and C-6 with the two oxidants used in the chemical polymerisation of PANI, Figures 3.12(a) and 3.12(c) [230].

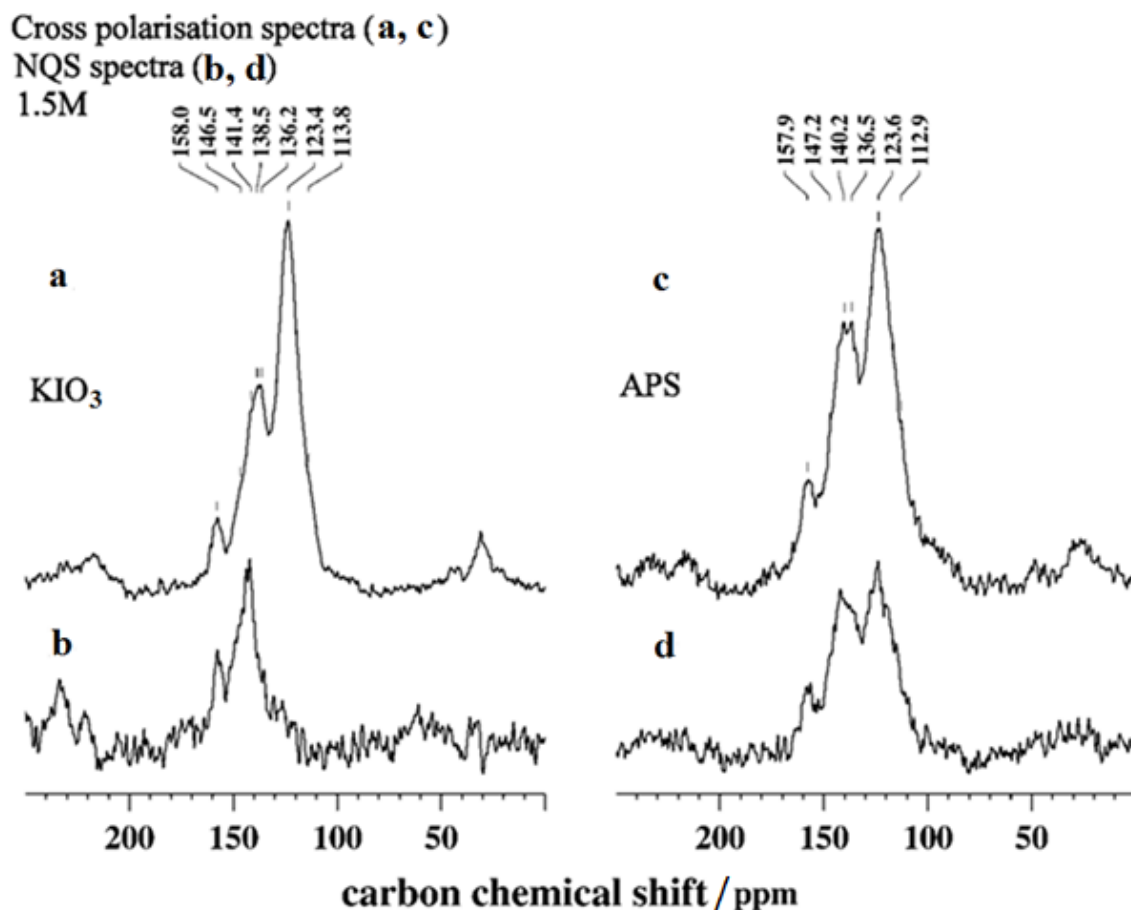


Figure 3.12. <sup>13</sup>C CPMAS spectra of chemically synthesised PANI prepared with KIO<sub>3</sub> dopant (a), and APS dopant (c); NQS spectra of PANI prepared with KIO<sub>3</sub> dopant (b), and APS dopant (d).

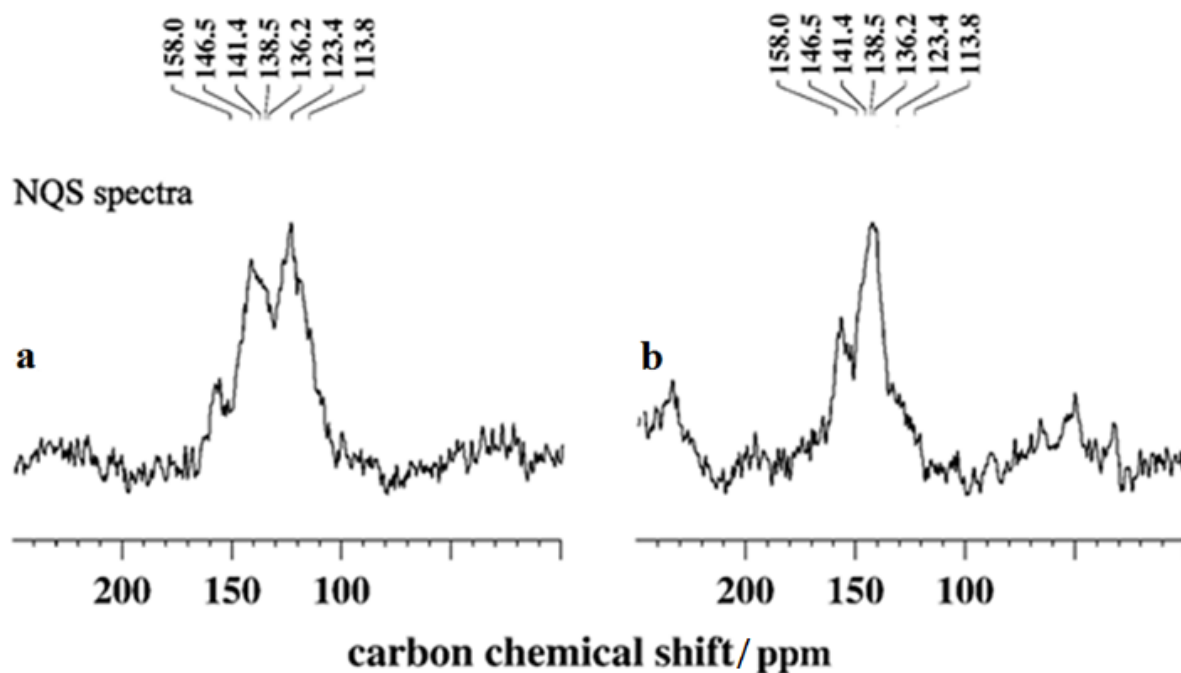


Figure 3.13. NQS spectra of PANI prepared chemically under different dopant concentration (a) 1.5 M H<sub>2</sub>SO<sub>4</sub>, and (b) 0.5 M H<sub>2</sub>SO<sub>4</sub> in APS oxidant.

Due to lower resolution in the <sup>13</sup>C CPMAS spectra, NQS experiments were performed in order to check whether there were differences in the structures of PANI samples obtained under different conditions. The NQS spectra are shown in Figures 3.12(b) and 3.12(d). The NQS experiments separate resonances based on protonation (the direct bonding or physical proximity of hydrogens) and mobility of different structural units. NQS experiments at longer dephasing delays yield a series of spectra in which protonated carbon resonances are gradually suppressed due to a dipolar interaction with protons. Also, carbons in rigid structural units are more prone to dipolar interactions and consequently the resonances from these carbons become efficiently suppressed compared to the ones from mobile molecular groups. In this way the non-protonated and/or mobile units dominate the spectra. The results shown in Figures 3.12(b) and 3.12(d) are in line with the assignments given above. Based on this, it can be concluded that the peaks on the left hand side of the CPMAS spectra originate from non-protonated structural units groups, whereas the ones on the right hand side belong to protonated groups. Also, the <sup>13</sup>C spectra imply that both samples consist of alternating segments of Q and B units. However, getting the exact ratio of Q to B units in <sup>13</sup>C CPMAS spectra would be difficult due to low resolution. However, it is evident (especially noticeable in NQS spectra) that there are differences in the PANI samples obtained with KIO<sub>3</sub> and APS, especially in the Q segment.

The B peaks at 114 ppm (C-6) and at 123 ppm (C-2, 3) were diminished when PANI was prepared under low dopant levels. However, note that SSNMR were measured in their dedoped state. The initial doping level however has an effect on the overall structure formed. The 137 ppm (C-8), 141 ppm (C-4), 147 ppm (C-1) and 158 ppm (C-7) are all of a different intensity.

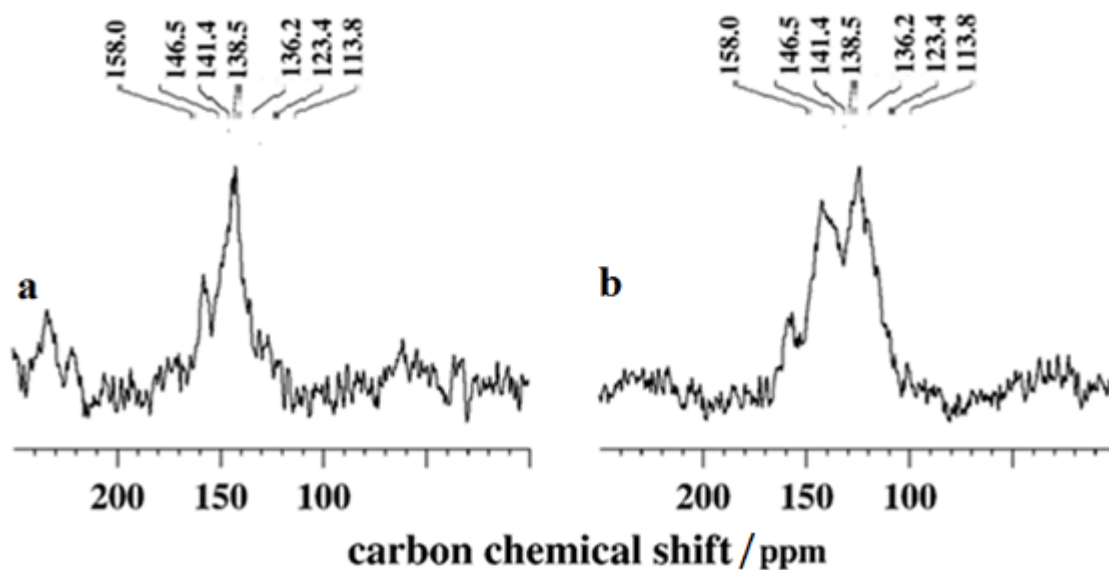


Figure 3.14. NQS spectra of PANI prepared chemically with 1.5 M  $\text{H}_2\text{SO}_4$  dopant under different oxidants, (a) with  $\text{KIO}_3$ , and (b) with APS.

The resonance at 158 ppm (C-7), 147 ppm (C-1) and 137 ppm corresponding to the Q part was relatively broadened going from the  $\text{KIO}_3$  oxidant to the APS oxidant possibly due to the differences in the oxidant used.

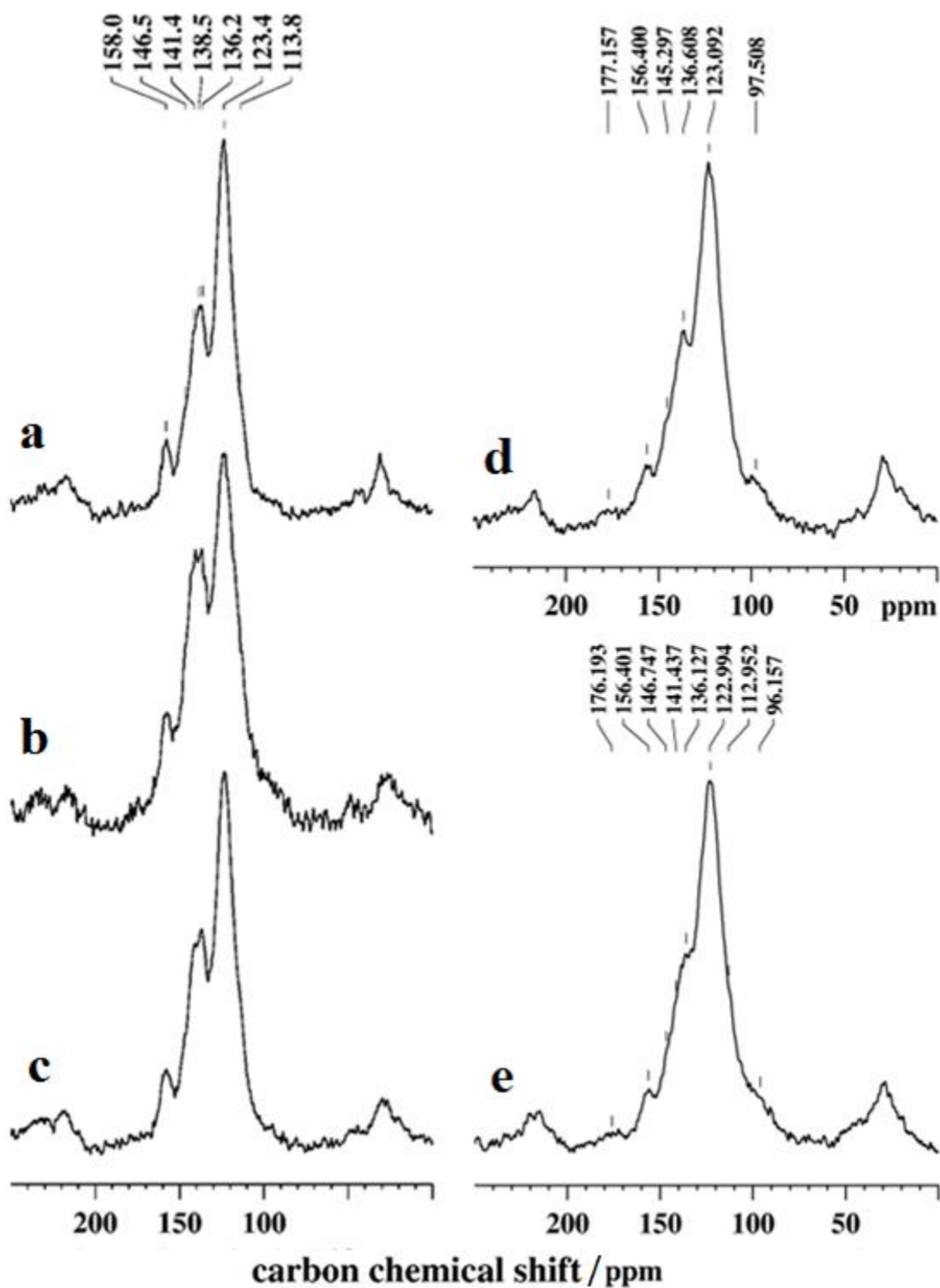


Figure 3.15.  $^{13}\text{C}$  CPMAS spectra of PANI (a) chemically synthesised with  $\text{KIO}_3$  in 1.5 M  $\text{H}_2\text{SO}_4$ , (b) chemically synthesised with APS in 1.5 M  $\text{H}_2\text{SO}_4$ , (c) chemically synthesised with APS in 0.5 M  $\text{H}_2\text{SO}_4$ , (d) electrochemically synthesised in 1.5 M  $\text{H}_2\text{SO}_4$ , and (e) electrochemically synthesised in 0.5 M  $\text{H}_2\text{SO}_4$ .

PANI prepared electrochemically showed more overlapping resonances. Both 158 ppm (C-7) and 147 ppm (C-1) shifted to a lower ppm at 156 ppm and 145 ppm. The peaks at 137 ppm (C-8) and 123 ppm (C-2, 3) remained the same. The observed differences between the two different syntheses methods in SSNMR suggest that the structure were slightly different. More overlapping peaks were observed with electrochemically prepared PANI indicating that the PANI polymers formed under this method experience a different carbon environment, possibly due to the presence PANI segments of different molecular weights.

### **3.3. Conclusions**

PANI samples doped with different dopants, H<sub>2</sub>SO<sub>4</sub> and oxalic acid, were synthesised, characterised and compared. The FTIR and UV-Vis spectroscopy spectra were largely identical, with characteristic peaks observed. An increase in the concentration of H<sub>2</sub>SO<sub>4</sub> shifted the wavenumber for the B rings to a higher value from 328 to 337 nm. The dopant used in the polymerisation had an influence on the PANI properties as indicated by the UV-Vis spectra. The use of a higher H<sub>2</sub>SO<sub>4</sub> concentration shifted the  $\pi$ - $\pi^*$  excitation of the para-substituted B segment (-B-NH-B-NH) to a higher value assigned to the function of intra-chain interactions. Raman spectra of electrochemically synthesised PANI were more complex than that of chemically synthesised polymers. This could possibly suggest that there were more intermediate, branching intermediates formed when PANI was synthesised electrochemically compared to the chemical oxidant preparations, as confirmed with CVs. Both chemically and electrochemically synthesised PANI were characterised using cyclic voltamograms. Two redox pairs are observed with the chemically synthesised polymer, while three redox pairs were observed with electrochemically synthesised polymer, with the third middle set of peaks being ascribed to quinone or quinoneiminie type degradation products. The CV characterisation for PANI grown on inert electrodes also provides valuable comparative information for use when attempting to grow PANI on aluminium and its alloys for antifouling applications in the later chapters of this thesis, as a means of evaluating the PANI formed.

## **CHAPTER FOUR: Characterisation of polyaminobenzoic acid and aniline-aminobenzoic acid copolymer**

### **4.1. Abstract**

PANI has been extensively studied in the earlier chapters. This chapter will focus on the substituted aniline, aminobenzoic acid (ABA), as well as copolymerisation with aniline. Substituted anilines can be both electron donating, i.e. alkylated [245--249] or alkoxy [243, 250-251], and electron withdrawing, e.g. chloro or nitro groups [244, 252]. This, however, comes at the cost of lower conductivity and reactivity compared to PANI itself. For better understanding of the effects of the substituent on the resulting polymer, anilines with a carboxylic acid group have been polymerised both alone and in mixtures with aniline at various ratios shown below. Electrochemical polymerisation of ABAs and of mixtures of aniline and ABAs in various ratios has been carried out by potential sweeps in sulfuric acid and HCl solutions. Copolymers at different amount ratios of ABA and aniline were formed and the rate of polymerisation has been increased by the addition of aniline. In some studies, it has been suggested that the copolymers formed could be used as melamine sensors [55]. The synthesis and characterisation of the polymer has been well documented. The physical and chemical properties of the polymer were influenced by the preparation method and the dopant used. The electroactivity of poly-ABA was examined in acidic solutions, and film morphology was studied by SEM. Poly-ABA and copolymers formed have been characterised voltammetrically and evidence concerning the polymer structure and chemical composition has been obtained from Raman spectroscopy, FTIR spectroscopy, CVs and SSNMR.

### **4.2. Results and Discussions**

#### **4.2.1. Gel permeation chromatography (GPC)**

The chemical synthesis was carried out on 2-ABA and 3-ABA monomers to determine if polymerisation occurs with two different electrolyte solutions, in either HCl or H<sub>2</sub>SO<sub>4</sub>. Four homopolymers of poly-ABA were chemically prepared as mentioned in Chapter Two. Poly-2-ABA and poly-3-ABA samples were doped with either HCl or H<sub>2</sub>SO<sub>4</sub> and oxidised with APS. The molecular weights of these four homopolymers were investigated with GPC. A

very low molecular weight oligomer formed for 2-ABA oxidised in 1 M HCl, hence it eluted out at the solvent level so it could not be detected. The remaining three polymers, poly-2-ABA doped with 1.5 M H<sub>2</sub>SO<sub>4</sub> (Figure 4.1) and poly-3-ABA doped with 1.5 M H<sub>2</sub>SO<sub>4</sub> (Figure 4.2) and 1 M HCl (Figure 4.3), were collected, with the poly-3-ABA polymer doped with 1.5 M H<sub>2</sub>SO<sub>4</sub> showing a low intensity peak at rather high molecular weight. This peak is out of character with moderate molecular weight PANI-type polymers suggesting that it could possibly be an artifact of the system and the materials formed are most likely of low molecular weight, oligomers.

Moreover, it was the only polymer formed that did not turn brown but instead appeared beige. The reason for the use of a higher dopant level for this polymer is that the 3-ABA monomer was insoluble at a lower dopant level of 1 M H<sub>2</sub>SO<sub>4</sub>; therefore, a higher dopant level was used instead. Furthermore, additional testing was carried out to further determine and confirm if a polymer was formed from this chemical synthesis process. Poly-2-ABA doped with 1 M H<sub>2</sub>SO<sub>4</sub> and poly-3-ABA doped with 1 M HCl appeared to show similar molecular weights to what has been reported by others. Ayad et al [57] reported a molecular weight of 1450 for poly-2-ABA doped with 1 M H<sub>2</sub>SO<sub>4</sub> made via another method.

	Poly-2-ABA		Poly-3-ABA	
	1 M H <sub>2</sub> SO <sub>4</sub>	1 M HCl	1.5 M H <sub>2</sub> SO <sub>4</sub>	
<b>Peak 1 - Molecular weight (repeat unit size)</b>	1,634 (17.5)	-	1,787 (19.2)	302,517 (3248)
<b>Peak 2 - Molecular weight (repeat unit size)</b>	577 (6.2)	-	462 (5)	110,020 (1181)

Table 4.1. Molecular weights of the four poly-ABAs formed prepared via chemical synthesis.



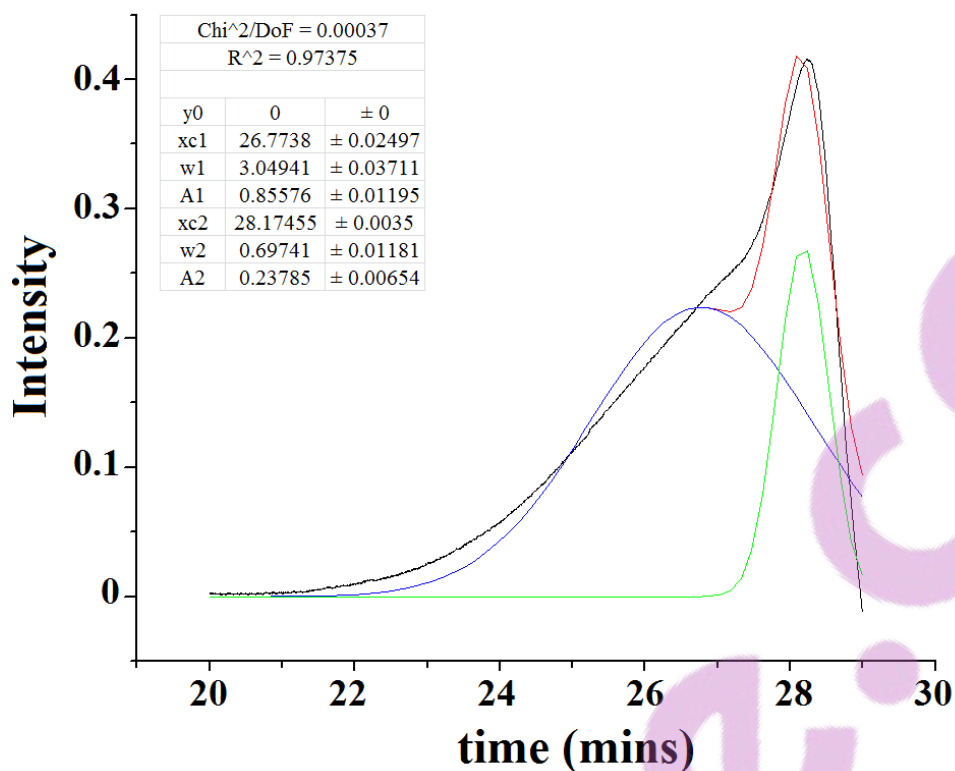


Figure 4.1. Auto scale chromatogram of poly-2-ABA doped with 1 M H<sub>2</sub>SO<sub>4</sub>.

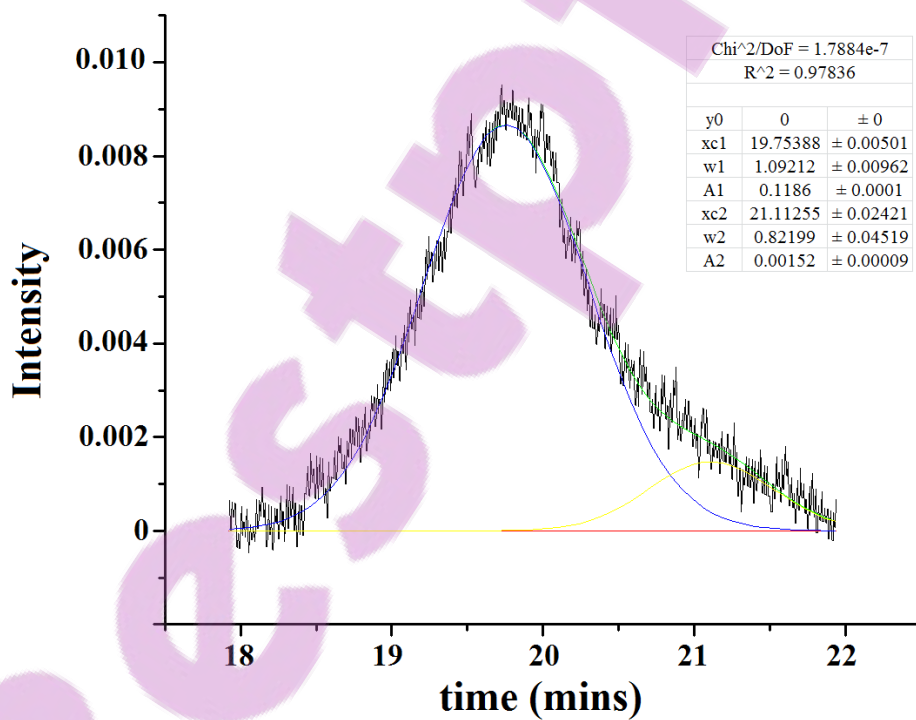


Figure 4.2. Auto scale chromatogram of poly-3-ABA doped with 1.5 M H<sub>2</sub>SO<sub>4</sub>.

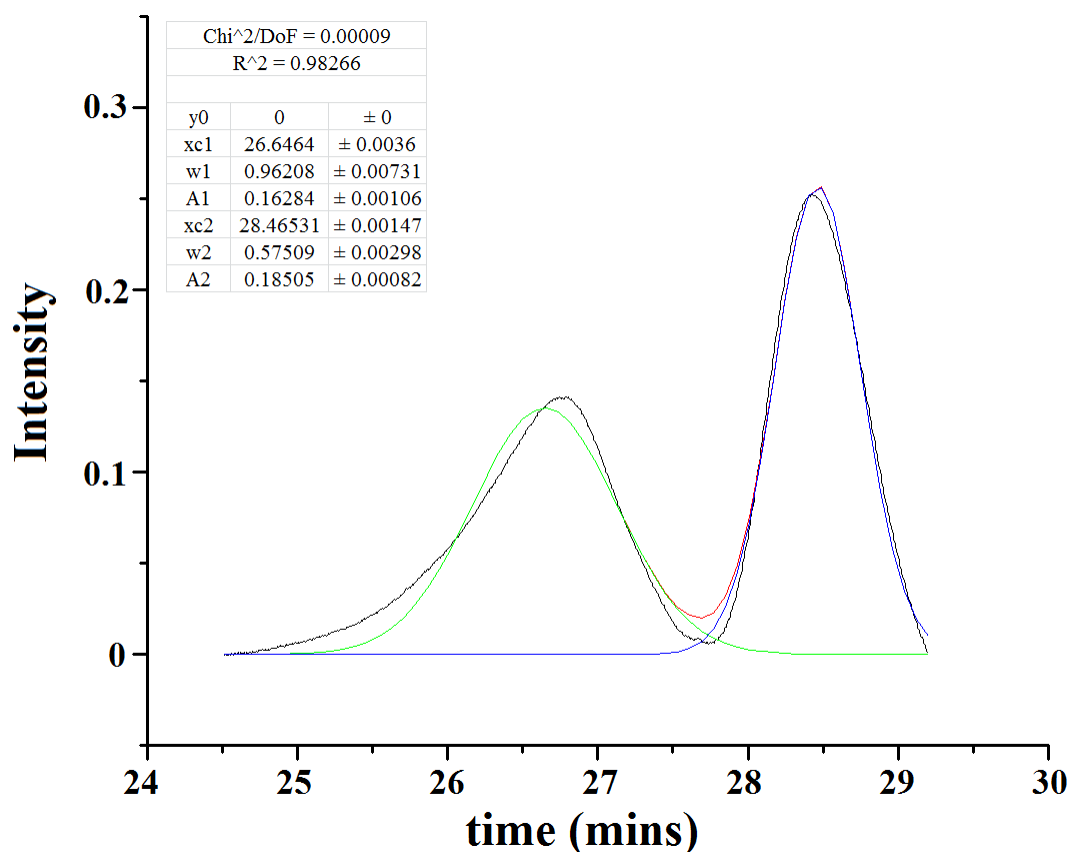


Figure 4.3. Auto scale chromatogram of poly-3-ABA doped with 1 M HCl.

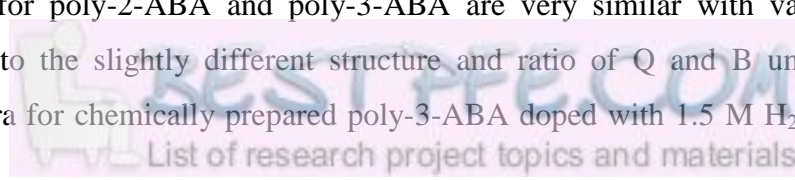
#### 4.2.2. FTIR spectroscopy

Figure 4.5 shows the spectra of the four poly-ABAs prepared by the chemical method of polymerisation. Infrared absorption band for poly-2-ABA appears at  $\sim 700\text{ cm}^{-1}$  in the case of polymer, and there is a strong absorption band at  $692\text{ cm}^{-1}$  in the case of monomer, which can be attributed to NH wagging deformation in aromatic amine [57]. The aromatic C-H out of plane bending vibration band of 1,4-disubstituted benzene ring appears at  $\sim 800\text{ cm}^{-1}$  [202]. Two strong absorption bands appear at  $836\text{ cm}^{-1}$  and  $931\text{ cm}^{-1}$  for 2-ABA monomer, while in the case of poly-2-ABA polymer, a group of absorption bands in the region of  $879\text{ cm}^{-1}$  and  $1078\text{ cm}^{-1}$  are observed, which can be ascribed to C-C stretching vibration in benzene ring [57]. Three medium absorption bands at  $\sim 1160$ ,  $1240$  and  $1300\text{ cm}^{-1}$  [5] observed with monomer appear as one broad band at  $1250\text{ cm}^{-1}$  for the formed polymer, which can be ascribed to C-O stretching vibration in carboxylic acid group. The C-N stretching vibrations of poly-2-ABA shifted from  $1360\text{ cm}^{-1}$  as reported for 2-ABA monomer to  $1370\text{ cm}^{-1}$  for

polymer, shown in the below Figure 4.5. The NH<sub>2</sub> deformation band for 2-ABA monomer with primary aromatic amine appeared at 1581 cm<sup>-1</sup> [57], while a medium absorption band for poly-2-ABA polymer appeared at 1600 cm<sup>-1</sup> which can also attributed to C-N stretching vibration for Q structure.

Peaks in the region of 1690 and 1500 cm<sup>-1</sup> correspond to the deformation of different types of N-H bonds [202]. Strong absorption bands at ca.1690 cm<sup>-1</sup> can be assigned to carboxylic acid groups. These bands are absent in the spectra, which suggests that the incorporation of substituted monomer is small. There are definitely different growth patterns with aniline substituted polymers as the spectra appears quite different with respect to PANI with C=O absorption band appears at 1680 cm<sup>-1</sup> for poly-ABA, a feature which would not be observed in PANI spectra [44]. Absorption above 1600 cm<sup>-1</sup> suggests the existence of carbon-nitrogen double bonds, while weak absorption between 1580 and 1490 cm<sup>-1</sup> are typical for secondary amines. The 1580 and 1510 cm<sup>-1</sup> peaks can be assigned to the C=C stretching vibration of Q and B rings [202, 205-206]. Main absorption bands observed at 1477 cm<sup>-1</sup> and 1565 cm<sup>-1</sup> correspond to the B and Q ring stretching frequency of PANI and similar bands are detected around this region for homopolymer of ABA [205-206, 253-254]. The absorption band at around 1300 cm<sup>-1</sup> is related to the C-N stretching vibration of secondary aromatic amine [206]. Deformation vibration of the carboxylic acid group is observed at 1380 cm<sup>-1</sup> [202]. The characteristic band of the conducting protonated form is observed at 1238 cm<sup>-1</sup> and is ascribed to the C-N<sup>•+</sup> stretching vibration in the polaron structure [202]. The 1113 cm<sup>-1</sup> band can be assigned to the -NH<sup>+</sup> vibration mode structure, which is formed by protonation [202, 204, 254]. The small peaks in the region of 1150 – 1050 cm<sup>-1</sup> correspond to the aromatic C-H in-plane bending vibration [202]. The high degree of electron delocalisation is responsible for the broad nature which was expected because of the greater degree of oxidation [202, 255]. The peaks at 1174 and 613 cm<sup>-1</sup> derived from the presence of sulfate ions in the film could be seen [255], as sulfuric acid was used as electrolyte during the preparation and characterisation of the polymer films [202]. Nevertheless, the spectra do show differences with respect to PANI, so the presence of the substituted monomer in solution clearly alters the growth pattern of the polymer film [202]. The presence of para-disubstituted benzene rings is shown by the strong bands at 1160 – 1191 cm<sup>-1</sup> and 1600 – 1626 cm<sup>-1</sup>.

The FTIR spectra for poly-2-ABA and poly-3-ABA are very similar with varying band intensity ratio due to the slightly different structure and ratio of Q and B units formed. However, the spectra for chemically prepared poly-3-ABA doped with 1.5 M H<sub>2</sub>SO<sub>4</sub> appear



distinctively different to those of the other three polymers formed. There were concerns raised from the GPC results above about justifying if a polymer was formed. Although a high molecular weight was seen in the GPC results in Table 4.1 calculated from Figure 4.2 of the poly-3-ABA chemically synthesised in  $\text{H}_2\text{SO}_4$ , a conclusion could be drawn that the product formed is not a polymer but rather either an oligomer or dimer. Such narrow and sharp peaks would not otherwise be observed for a polymer. The most important absorption characteristic bands are  $1693$  and  $1686\text{ cm}^{-1}$  (C=O stretching),  $1575 - 1567\text{ cm}^{-1}$  (C=C stretching),  $1511 - 1508\text{ cm}^{-1}$  (benzenoid ring C=C stretching), and  $838 - 685\text{ cm}^{-1}$  (C-H out of plane bending modes) [256]. These results suggest the presence of an emeraldine structure for both homopolymers formed.

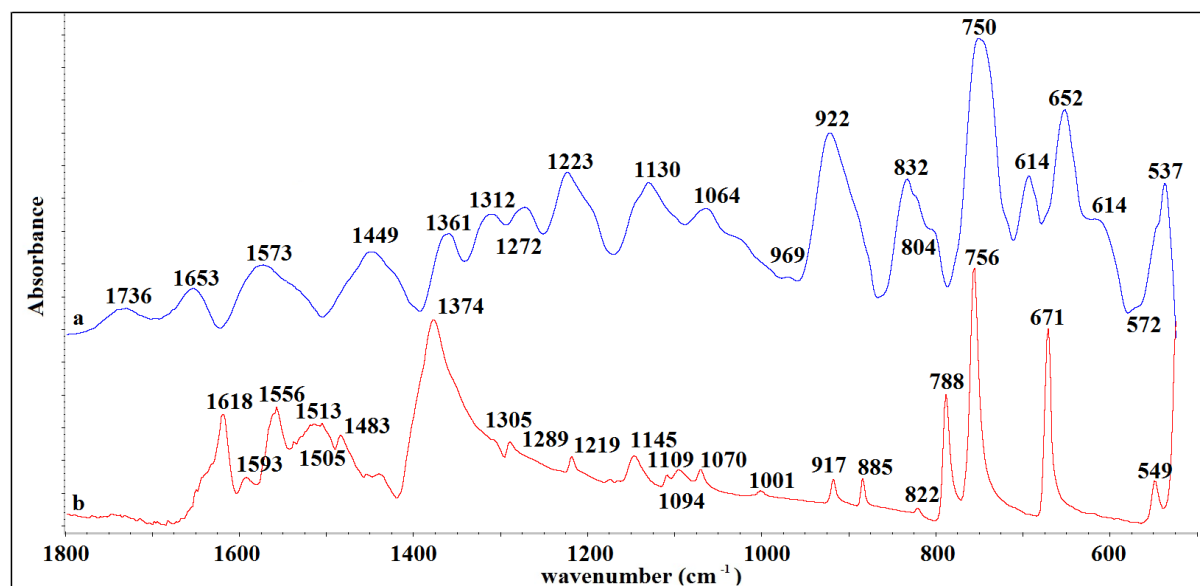


Figure 4.4. FTIR spectra of ABA monomers (a) 2-ABA and (b) 3-ABA.

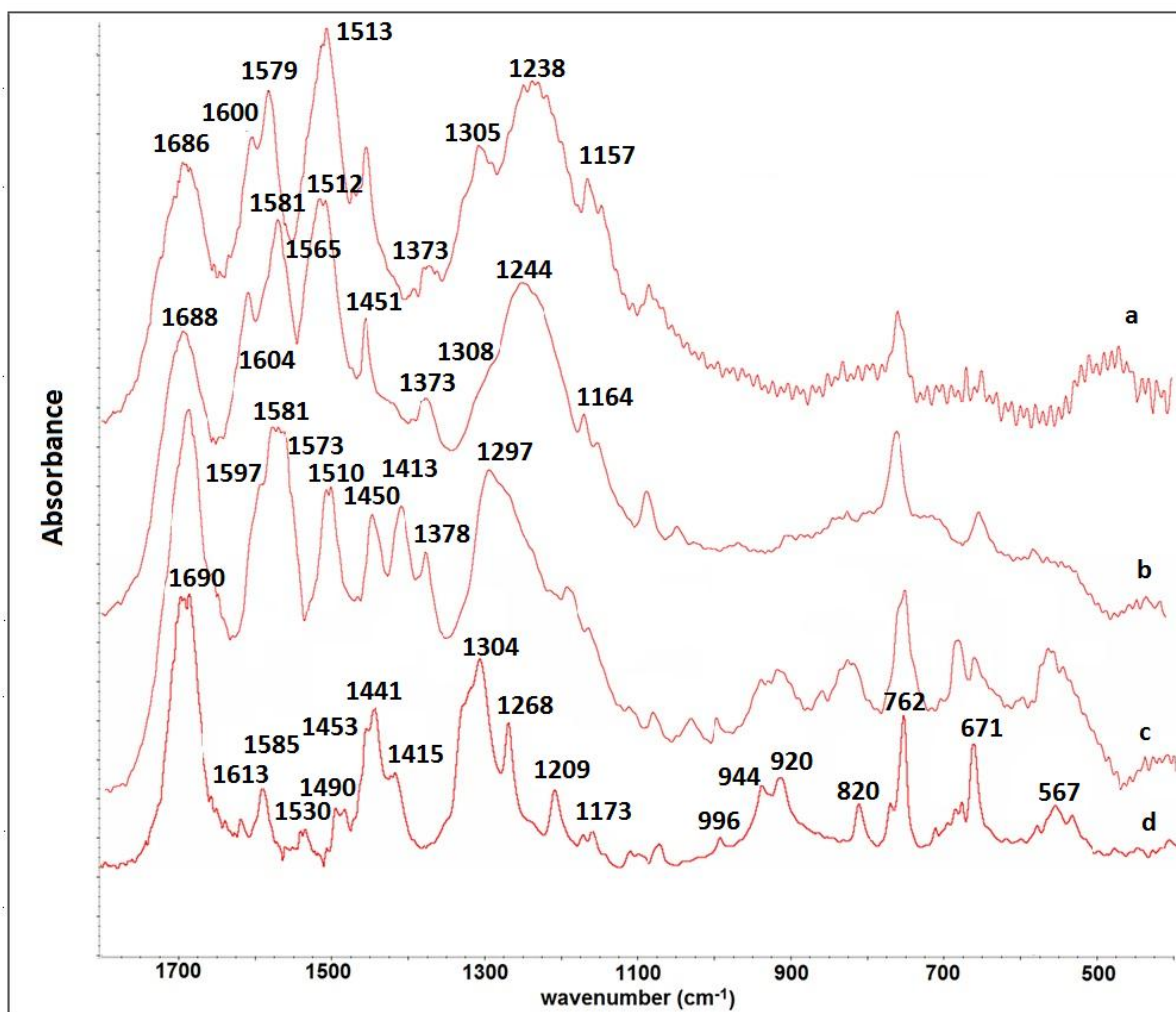


Figure 4.5. FTIR spectra of chemically prepared poly-ABA and oxidised with APS (a) poly-2-ABA doped with 1 M H<sub>2</sub>SO<sub>4</sub>, (b) poly-2-ABA doped with 1 M HCl, (c) poly-3-ABA doped with 1 M HCl, and (d) poly-3-ABA doped with 1.5 M H<sub>2</sub>SO<sub>4</sub>.

#### 4.2.3. Morphology

The dopant used was either HCl or H<sub>2</sub>SO<sub>4</sub> for the polymerisation of 2-ABA, and these formed a global grape structure, with HCl doped polymer more than double the size of that doped with H<sub>2</sub>SO<sub>4</sub>, shown in Figures 4.6 and 4.7, taken with SEM. Severe agglomeration occurred with poly-3-ABA doped with 1M HCl, forming sponge-like structures, while the polymer doped with 1.5 M H<sub>2</sub>SO<sub>4</sub> formed flat sheets, again atypical of a PANI-type polymer. However, the two poly-ABA samples of similar molecular weight (poly-2-ABA doped with 1 M H<sub>2</sub>SO<sub>4</sub> and poly-3-ABA doped with 1 M HCl) with carboxylic acid substitution at different positions and doped with different acids appear significantly different in morphology: poly-3-ABA formed flat sheets, while poly-2-ABA formed sponge-like

structures. Copolymers of aniline and 3-ABA doped with  $H_2SO_4$  formed rod-like structures with ‘fluff’ on the surface: at lower concentration of dopants there seemed to be less ‘fluff’ on the rods, while at higher concentration of dopants the surface of rods appear to be more ‘fluffy’. The fluffy appearance is a characteristic CP morphology which has the advantage of creating surface roughness that ideally would limit bacteria adhesion to such a surface.

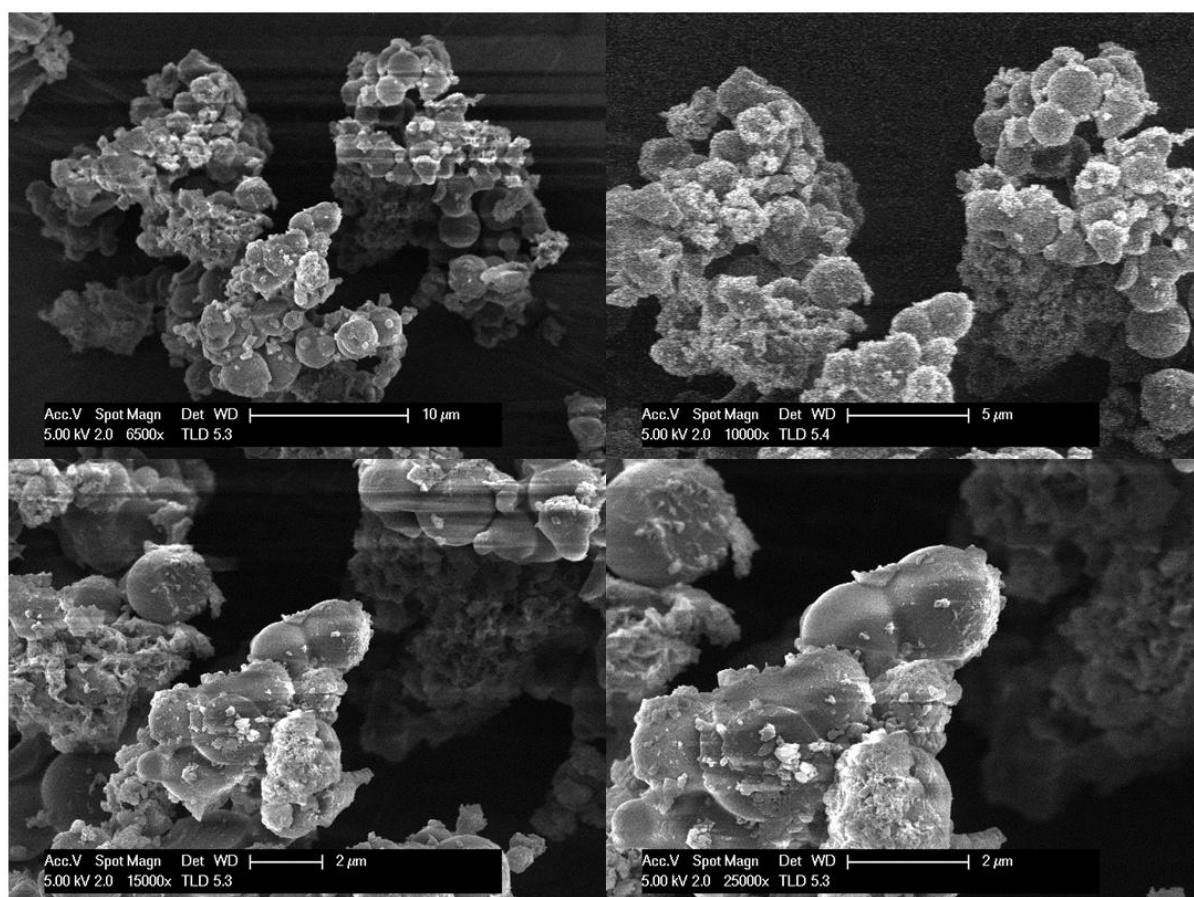


Figure 4.6. SEM images of chemically prepared poly-2-ABA doped with 1 M HCl appears with grape globalstructure.



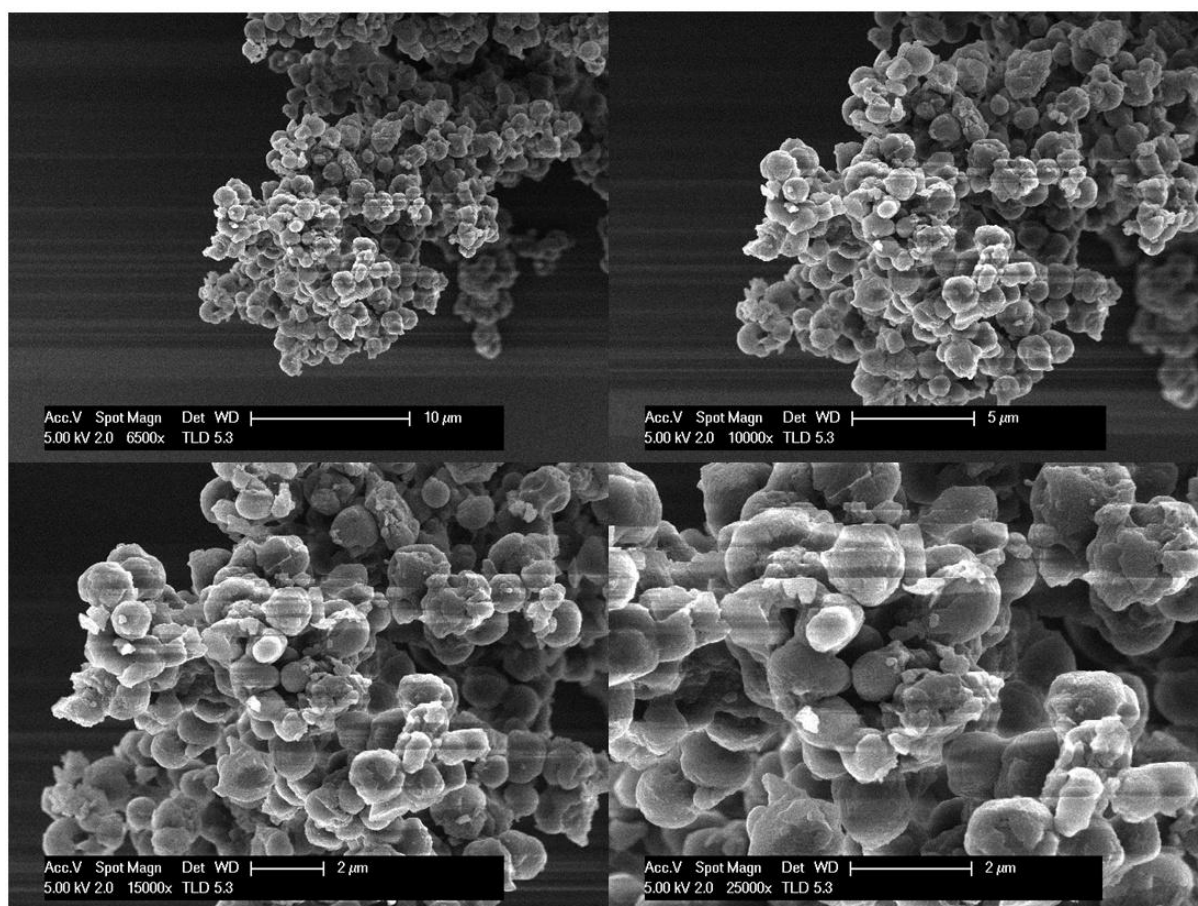


Figure 4.7. SEM images of chemically prepared poly-2-ABA doped with 1 M  $\text{H}_2\text{SO}_4$  with grape global structure.

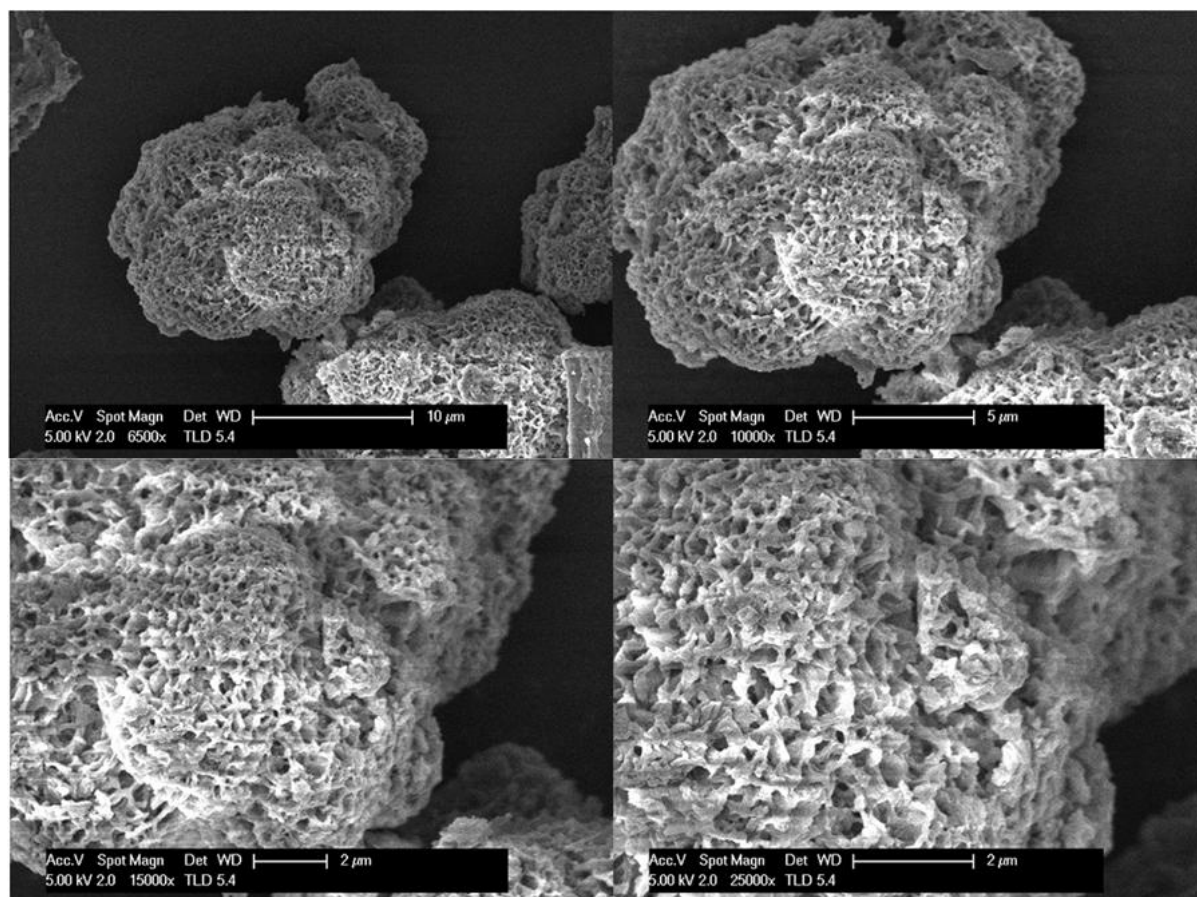


Figure 4.8. SEM images of hemically prepared poly-3-ABA doped with 1 M HCl forms sponge like structures.



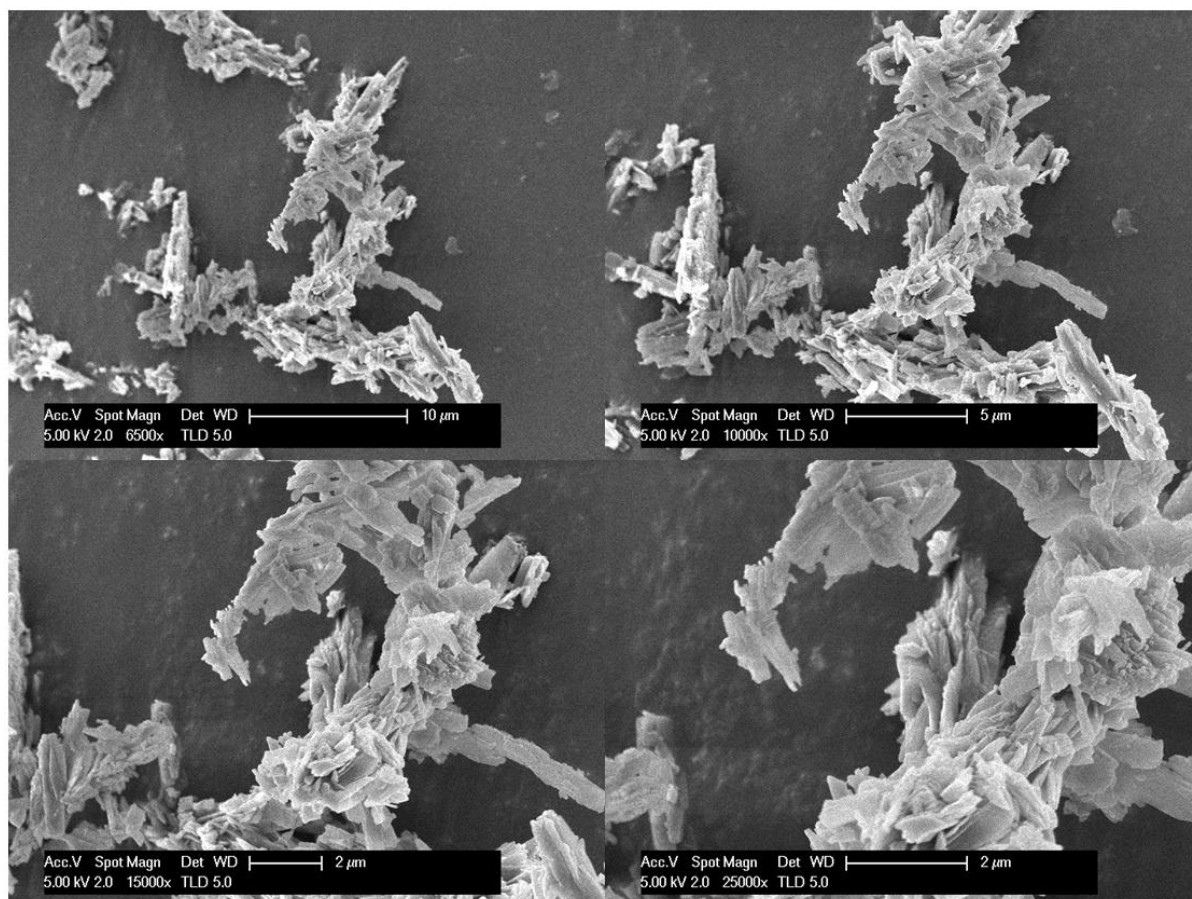


Figure 4.9. SEM images of chemically prepared poly-3-ABA doped with 1.5 M H<sub>2</sub>SO<sub>4</sub> forming flat sheet appearance.

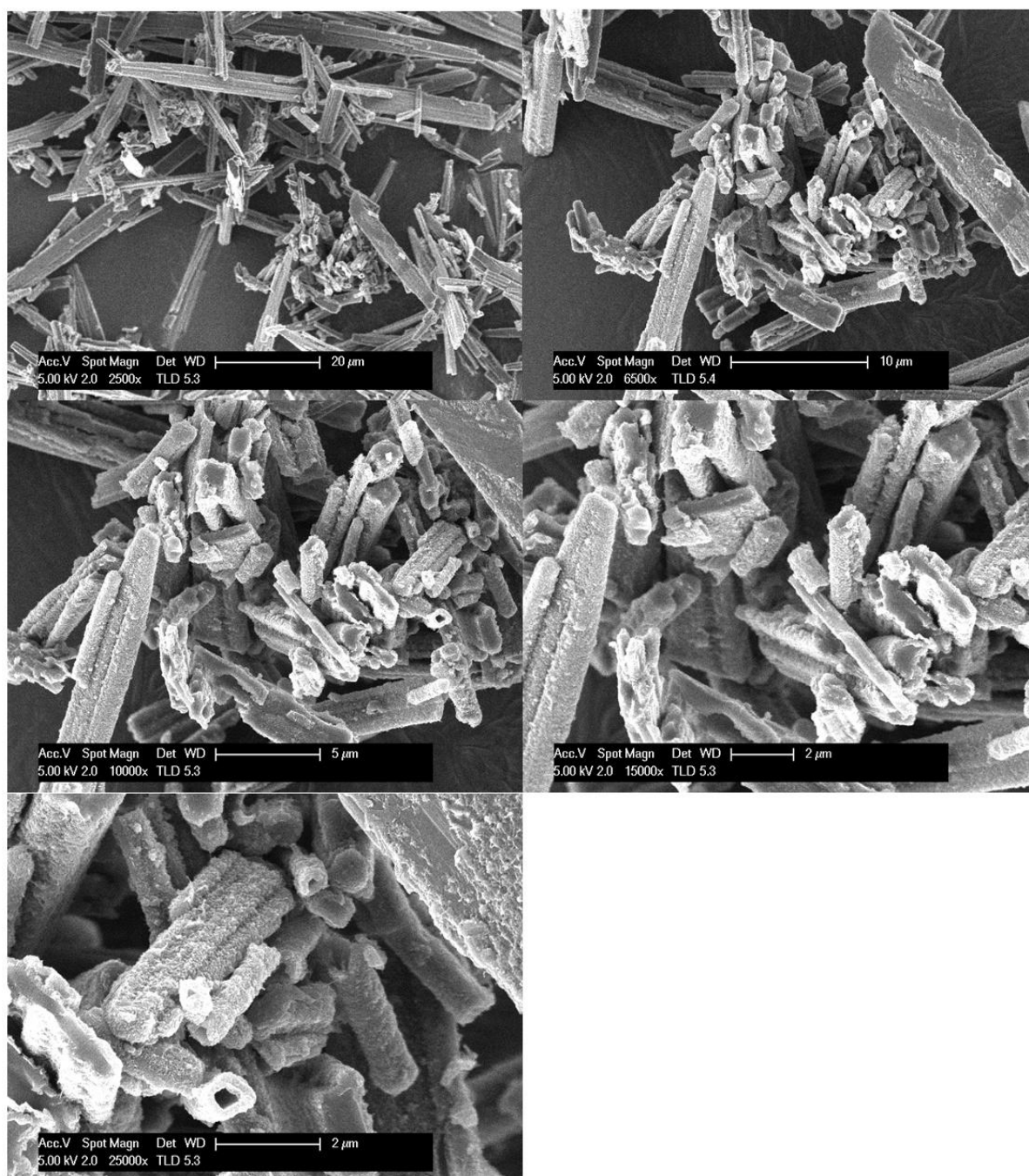


Figure 4.10. SEM images of chemically prepared PANI-co-3-ABA at 0.5 M H<sub>2</sub>SO<sub>4</sub> with APS as the oxidant formed rod-like structure.

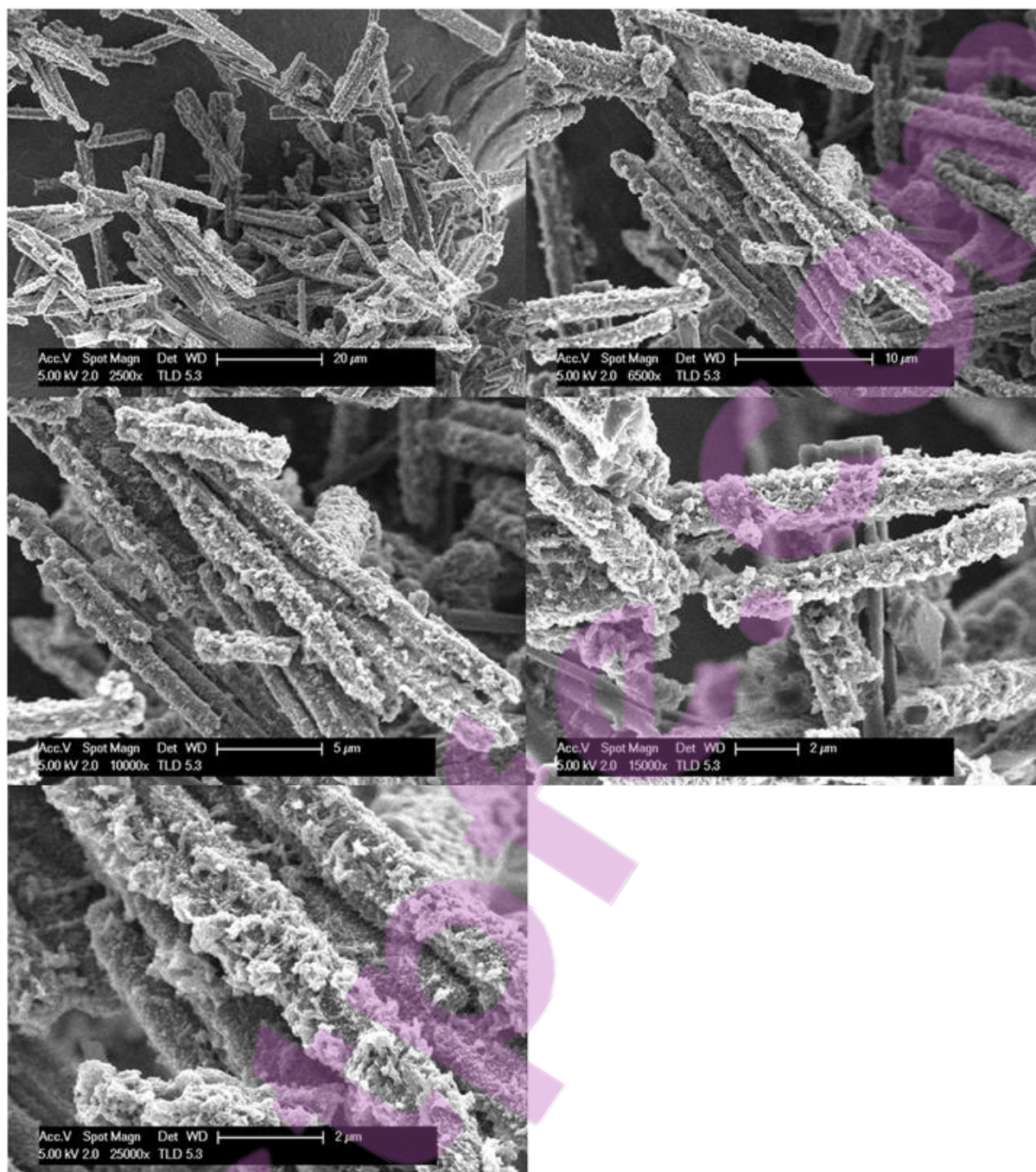


Figure 4.11. SEM images of chemically prepared PANI-co-3-ABA at 1.5 M H<sub>2</sub>SO<sub>4</sub> with APS as the oxidant formed rod-like structure.



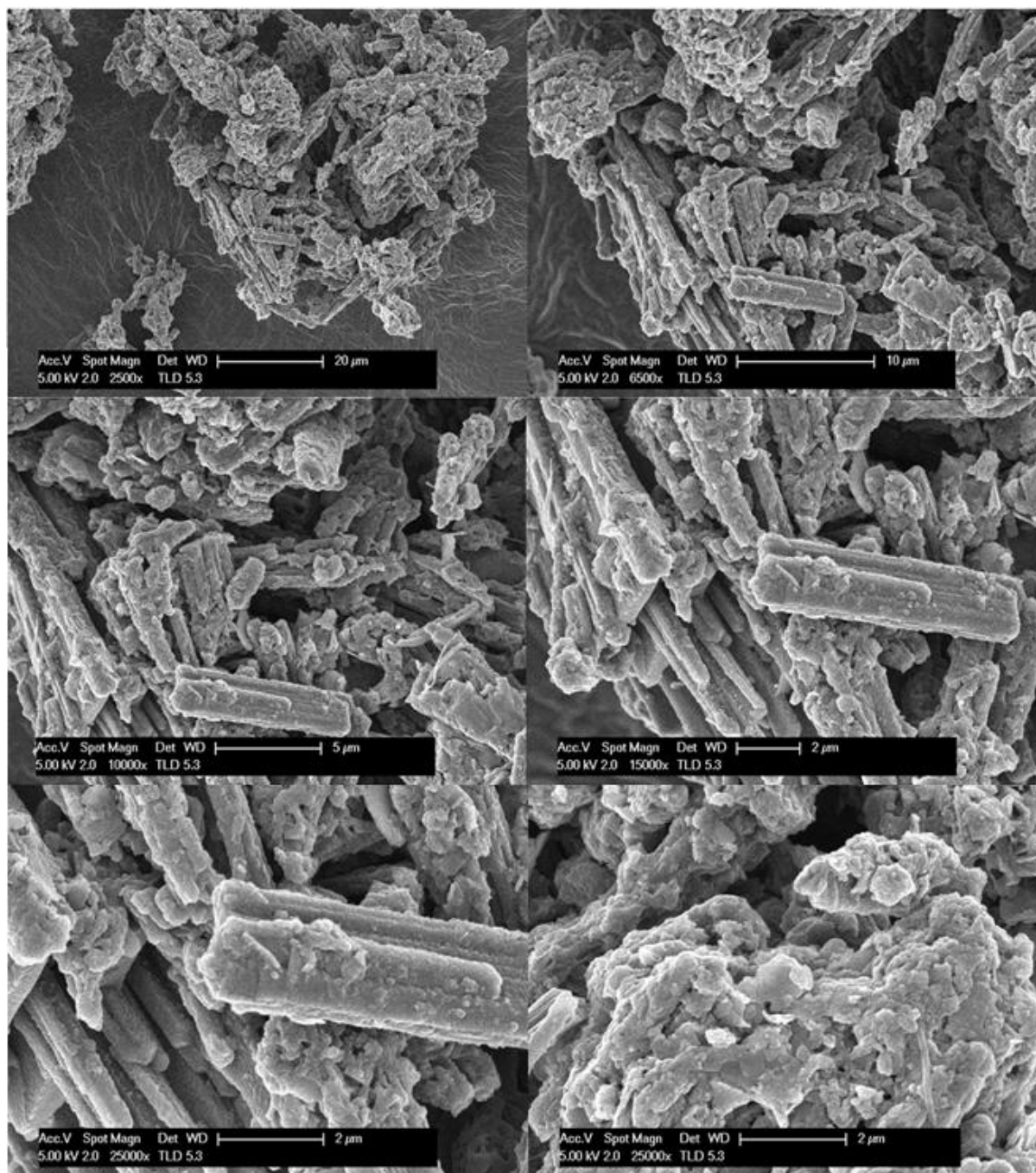


Figure 4.12. SEM images of chemically prepared PANI-co-3-ABA at 1.5 M H<sub>2</sub>SO<sub>4</sub> with KIO<sub>3</sub> as the oxidant formed random structure.

#### 4.2.4. Antimicrobial properties

The antimicrobial properties were evaluated by incubating  $1 \times 10^6$  CFU *S.aureus* 6838 cells for 24 hours on the chemically synthesised poly-ABA polymers doped with different dopants, summarised in Tables 4.2 and 4.3. The minimum bacterial concentration (MBC) for chemically synthesised substituted aniline polymers is shown in Table 4.2.

Compound	MBC 1/%	MBC 2/%	MBC 3/%	Average/%
Poly-2-ABA 1 M H <sub>2</sub> SO <sub>4</sub>	0.12	0.25 <sup>^</sup>	0.25	<b>0.25</b>
Poly-2-ABA 1 M HCl	0.12 – 0.25	0.12 – 0.5 <sup>#</sup>	0.12 – 0.5*	<b>0.25</b>
Poly-3-ABA 1 M HCl	0.5	1	1	<b>1</b>
Poly-3-ABA 1.5 M H <sub>2</sub> SO <sub>4</sub>	2 – >2	2	2	<b>2</b>
Benchmark – Poly-3-ABA 1.25 M HCl	0.5	0.5**	0.5	<b>0.5</b>

Table 4.2. Minimum bacterial concentration for *S. aureus* 6838.

\*\* : 1 colony at 0.5%

<sup>^</sup> : 38 colonies at 0.12%

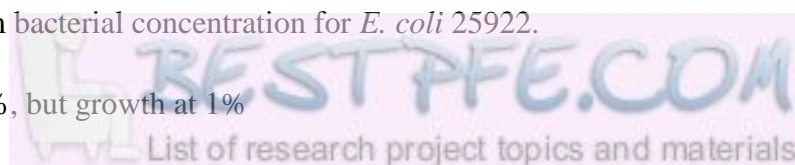
<sup>#</sup> : no growth at 0.12%, but growth at 0.25%

\* : 18 colonies at 0.25%

Compound	MBC 1/%	MBC 2/%	MBC 3/%	Average/%
Poly-2-ABA 1 M H <sub>2</sub> SO <sub>4</sub>	1	1	1	<b>1</b>
Poly-2-ABA 1 M HCl	1	1	2	<b>1</b>
Poly-3-ABA 1 M HCl	>2	>2	>2	<b>&gt;2</b>
Poly-3-ABA 1.5 M H <sub>2</sub> SO	>2	>2	>2	<b>&gt;2</b>
Benchmark – Poly-3-ABA 1.25 M HCl	0.5	0.5*	0.5	<b>0.5</b>

Table 4.3. Minimum bacterial concentration for *E. coli* 25922.

\* : no growth at 0.5%, but growth at 1%



The chemically synthesised poly-2-ABA samples showed good antibacterial efficacy ( $\leq 1$  wt%), and the results demonstrated that poly-2-ABA samples were better antibacterial agents against both *S. aureus* 6838 and *E. coli* 25922 than poly-3-ABA samples. The killing mechanism may be complex, and Gizdavic-Nikolaidis et al. suggested that the mechanism involves metabolic dysregulation and oxidative stress [257].

#### **4.2.5. Anti-moulding performance**

The chemically prepared PANI doped with H<sub>2</sub>SO<sub>4</sub>, HCl and oxalic acid from Chapter Three and chemically synthesised poly-2-ABA and poly-3-ABA, doped with HCl and H<sub>2</sub>SO<sub>4</sub>, were chemically synthesised and were dispersed in one-pack acrylic bathroom ceiling paint as a pigment acting as an antimould agent on weatherboards. Initial testing was carried out with the testing procedure provided in Chapter Two, Section 2.7.3. The samples were prepared with 1 wt% of polymers dispersed in coatings prior coated with a precoat (acrylic sealer undercoat) used as primer coat. Preliminary results suggest promising performance after 2 years of exposure with no sign of mould growth compared to the fungicide-containing control after 1.5 years of exposure.

#### **4.2.6. UV-Vis spectroscopy**

NMP was used as a solvent. The spectra were obtained using as-prepared samples, of whatever oxidation state resulted at the end of the synthesis procedure. The concentration used for each sample solution was  $\sim 0.01$  wt%.

The UV-Vis spectra provide information on the oxidation state and proton doping level of the polymers, as well as an indication on which excitation line to use for Raman analysis. As all of the polymers had a high degree of insolubility, they were dissolved in NMP, but this had the effect of dedoping the polymers. Hence the spectra recorded below are all in their base form rather than the salt form. The spectra were recorded with a Shimadzu UV-2102PC spectrophotometer at room temperature.

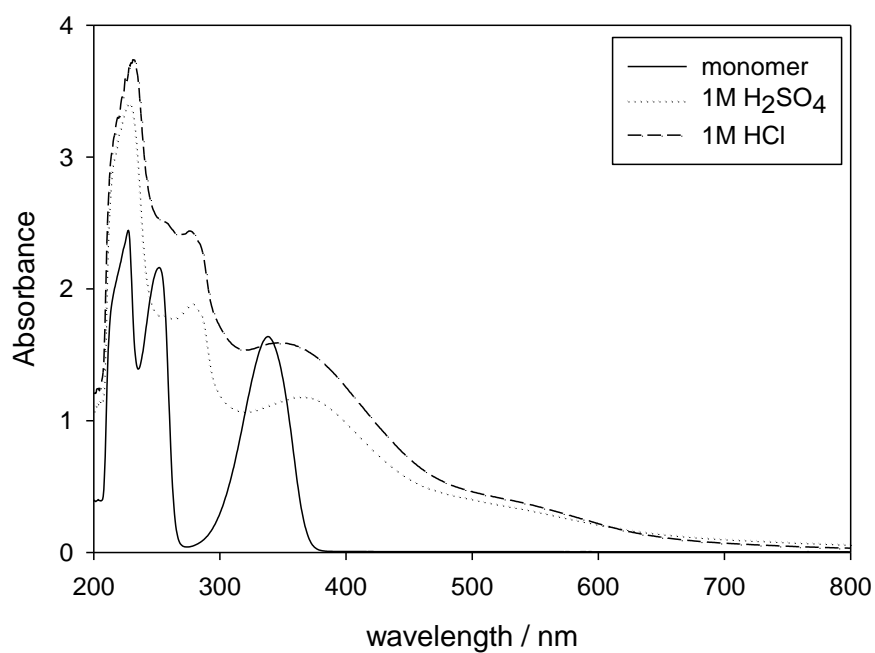


Figure 4.13. UV-Vis spectra of 2-ABA monomer and homopolymers in NMP.

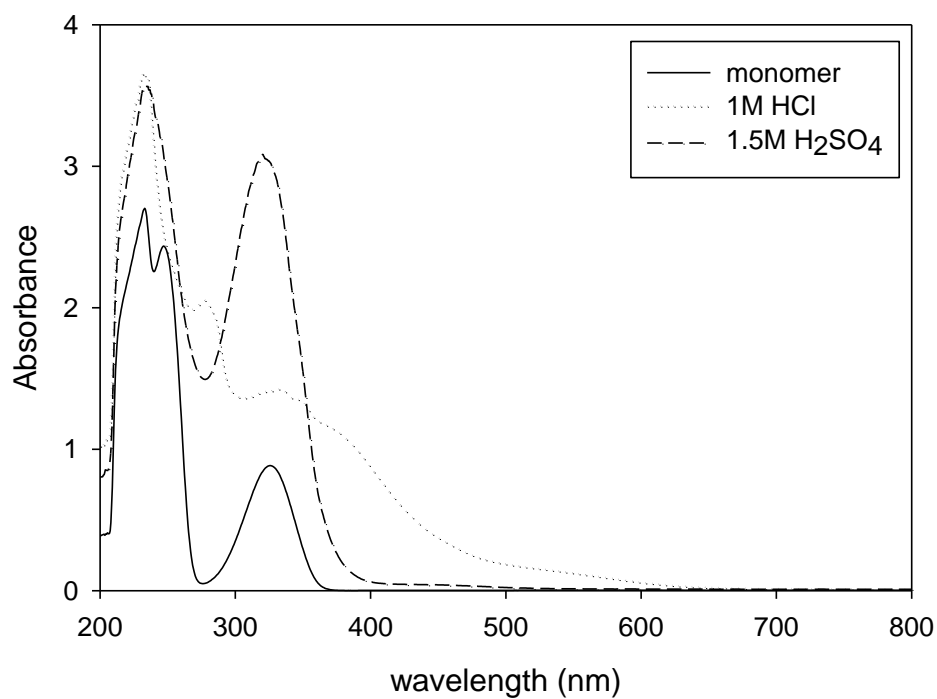


Figure 4.14. UV-Vis spectra of 3-ABA monomer and homopolymers in NMP.

The spectra in Figures 4.13 and 4.14 show three absorption bands observed for the ABA monomers. The spectra for both poly-2-ABA and poly-3-ABA doped with 1 M HCl polymer showed ~4 absorption bands, while the poly-3-ABA doped with 1.5 M H<sub>2</sub>SO<sub>4</sub> showed similar spectra to the monomer. The absorption at 228 nm observed in the monomer was also detected in the formed polymer spectra doped with either dopant, suggesting that there were still some unreacted monomers or short chain oligomers present in the product. The observed 278 nm band is possibly due to the shift of 252 nm or 338 nm peak from the monomer, and it suggests that the steric effect of the carboxylic acid groups in the polymer chain causes perturbation of the coplanarity of the  $\pi$ -system, hence lowering the degree of conjugation as well as hindering charge transfer between chains [217, 254, 258]. The absorption at 338 nm for the monomer is assigned to the  $\pi$ - $\pi^*$  transition and it is related to the extent of conjunction between adjacent phenyl rings in the polymer chain. The broad absorption at 500 – 600 nm is assigned to the exciton transition caused by interchain charge transfer in the B and Q segments [217, 254, 258].

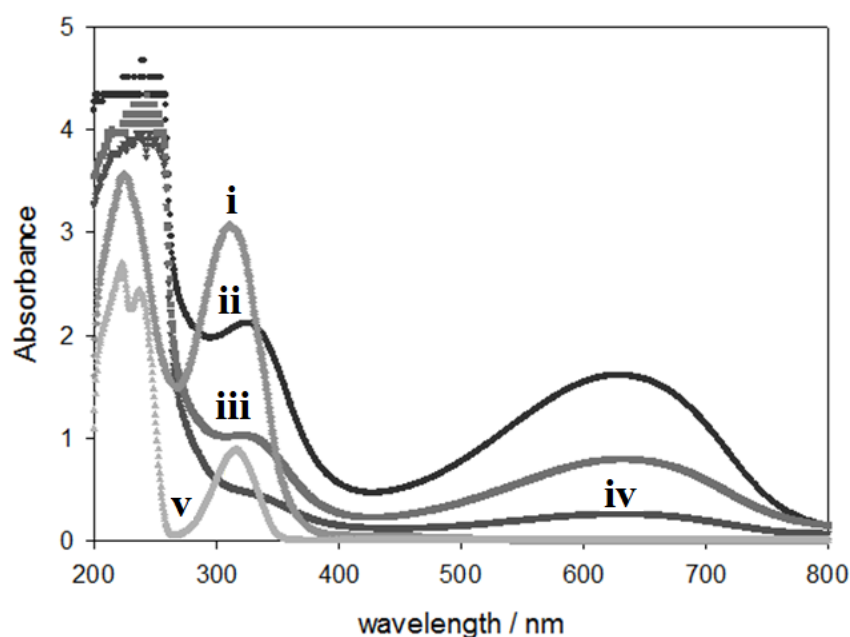


Figure 4.15. Chemically synthesised polymers doped with 1.5 M H<sub>2</sub>SO<sub>4</sub> (i) poly-3-ABA oxidised with APS, (ii) PANI oxidised with KIO<sub>3</sub>, (iii) PANI-co-3-ABA oxidised with APS, (iv) PANI oxidised with APS, and (v) 3-ABA monomer.



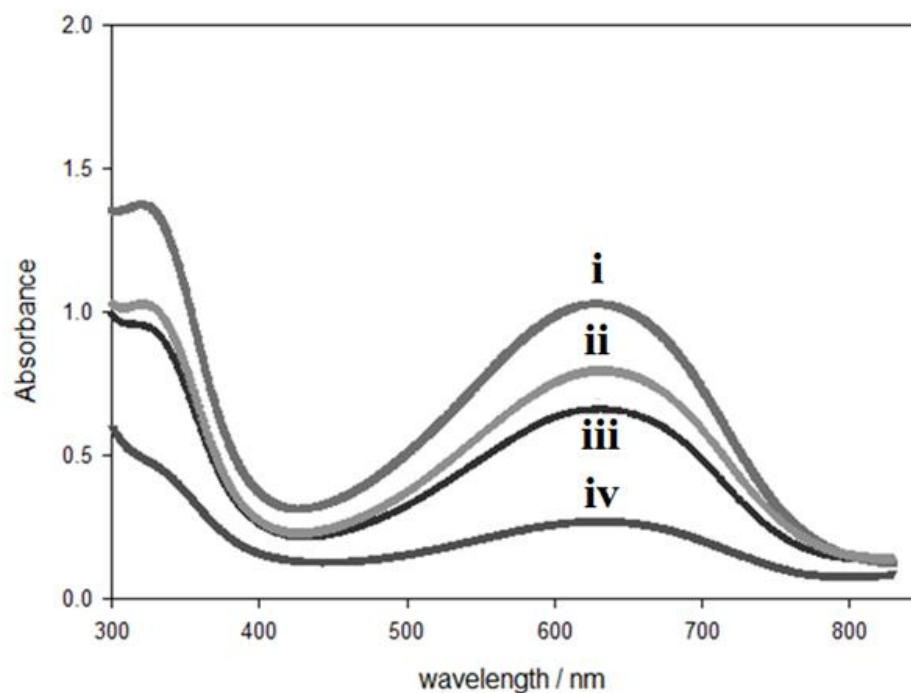


Figure 4.16. Chemically synthesised polymers doped with  $\text{H}_2\text{SO}_4$  and oxidised with APS (i) PANI-co-3-ABA 0.5 M  $\text{H}_2\text{SO}_4$ , (ii) PANI-co-3-ABA 1.5 M  $\text{H}_2\text{SO}_4$ , (iii) PANI 0.5 M  $\text{H}_2\text{SO}_4$ , and (iv) PANI 1.5 M  $\text{H}_2\text{SO}_4$ .

These chemically synthesised polymers of PANI or poly-ABA using either APS or  $\text{KIO}_3$  as oxidant show that there were no significant differences between the influences of the oxidants used. The ratio between the two peaks at ca. 330 and ca. 620 nm could be slightly affected; however, in general, there are no shifts observed between the PANI and copolymer, PANI-co-3-ABA.

No distinct Q band (~630 nm) was observed in the spectra. The spectrum can be described as containing a broad band decreasing in intensity continuously from the region of  $\pi \rightarrow \pi^*$  transitions below 300 nm to ca. 800 nm, on which two shoulders corresponding to maxima at ca. 400 and 500 nm occur [203]. Bands occurring at 400 and 550 nm should be ascribed to transitions in the doped poly-ABA [203]. Compared with the same characteristic absorption peak of EB-PANI, it was shifted ca. 60 nm to longer wavelength, which indicates that the conjugate conjunction of poly-2-ABA decreased compared with EB-PANI [202]. This may be caused by the following reasons [202]:

- (a) Carboxylic acid groups doped into the backbone of the polymer chain are strongly attracting free radicals which greatly decreased the electron cloud density of aromatic rings.
- (b) Due to the special resistance effect of carboxylic acid groups, the planar conjugated conjunction of aromatic rings decreased.

A combination of the above caused the lowering of the conjugate conjunction around the whole polymer chain [202]. In a self-doped polymer, such as poly-ABA, a high population of bipolarons can be expected due to attractive coulombic interactions between main-chain cations and immobile COO<sup>-</sup> counter-anions linked directly to main-chain benzene rings, which makes the dissociation of a bipolaron into two independent polarons difficult. Nevertheless, the question whether the bands observed in poly-ABA spectra are associated with polarons or bipolarons, or both, cannot be answered on the basis of the results available and it needs further experimental and theoretical investigation [203].

However, for doped PANI localised polarons are used for characterisation of the protonated PANI at 410 nm, together with a peak at ~845 nm corresponding to conducting ES phase of the polymer. The 845 nm band decrease in wavelength and increase in frequency, also known as a blue shift, was observed in the PANI spectra as the ratio of ABA increased. This was caused by the decrease in the extension of the conjugation along the macromolecule relating to the steric factor of the carboxylic acid group in the polymer chain.

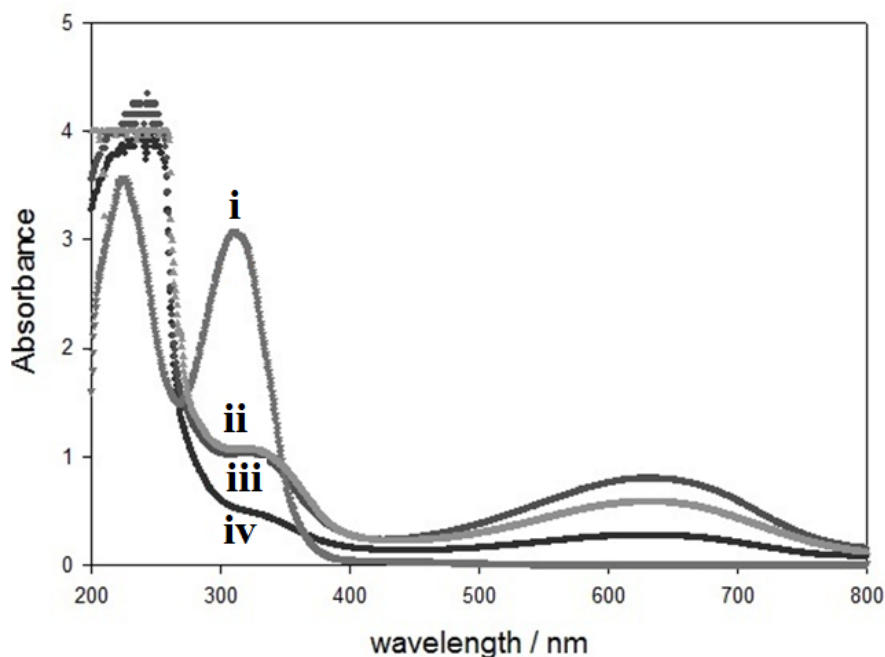


Figure 4.17. Comparison of UV-Vis spectra of chemically and electrochemically synthesised polymers and copolymers using  $\text{H}_2\text{SO}_4$  as the dopant (i) chemically prepared poly-3-ABA doped with 1.5 M  $\text{H}_2\text{SO}_4$  and APS as oxidant, (ii) electrochemically prepared PANI-co-3-ABA doped with 0.5 M  $\text{H}_2\text{SO}_4$ , (iii) chemically prepared PANI-co-3-ABA doped with 1.5 M  $\text{H}_2\text{SO}_4$  and APS as oxidant, and (iv) chemically prepared PANI doped with 1.5 M  $\text{H}_2\text{SO}_4$  and APS as oxidant.

The first indication of the presence of the EB form of PANI would be the blue colour, followed by two peaks appearing at 330 and 620 nm. However, for poly-3-ABA doped with 1.5 M  $\text{H}_2\text{SO}_4$  the solution was beige in colour. This spectrum does not show any characteristic peak expected for a polyaniline, therefore it can be further concluded that it was not a polymer that was obtained from this chemical synthesis. Two peaks were observed with copolymers appearing in the spectrum of Figure 4.17 at  $\sim 330$  and  $\sim 620$  nm. The conjugation extends between adjacent phenyl rings in the polymer chain and is observed at the 330 nm absorption peak, which is attributed to the  $\pi$ - $\pi^*$  transition [247, 258, 259]. The exciton transition from B to Q segments caused by interchain charge transfer is assigned to the second absorption at 620 nm [48, 217, 232]. The conductivity in polymers is believed to be related to the extended conjugation of  $\pi$  orbitals, which requires coplanarity of the atoms involved in the  $\pi$ -cloud delocalization for maximum resonance interaction [254]. The coplanarity of the  $\pi$  system is affected by the steric effect of the carboxylic acid groups, hence lowering the degree of conjugation, and as a result hindering charge transfer between

chains [254]. This second absorption band is found to be dependent on the overall oxidation state of the polymer formed [253, 254]. This  $\pi$ - $\pi^*$  transition is related to the extended conjugation between adjacent rings in the polymeric chains [44, 212, 253, 260]. The band at 330 nm shifted to a lower wavelength of  $\sim$ 280 nm going from copolymer to homopolymer of aniline, implying a decrease in the extent of conjugation and an increase in the transition energy [48, 60]. This also suggests that the steric effect of the carboxylic acid groups in the copolymer chain causes perturbation of the coplanarity of the  $\pi$ -system, hence lowering the degree of conjugation as well as hindering charge transfer between chains [217, 254]. An addition of 2-ABA monomer in the polymer chain exhibits a hypsochromic shift [254], which is observed in UV-Vis results, see Figure 4.13. The third peak at about 270 nm is attributed to the  $n$ - $\pi^*$  transition because of the presence of non-bonding electrons on the  $\text{COO}^-$  groups [261-262] indicating a substantial reduction in the level of conjugation along the polymer backbone [217]. There is no exciton band, suggesting little or no intra- or inter-chain charge transfer [217]. The band between 320 and 338 nm is attributed to the  $\pi \rightarrow \pi^*$  transition and it is related to extended conjugated between adjacent rings in the polymeric chain [44]. This signal appears at a smaller wavelength than in PANI as the poly-ABA polymers are less conjugated than PANI hence showing an increase in transition energy [44]. The third band can be assigned to the transition of the exciton of the quinone and is related to the hopping electronic intra- and inter-chain [211, 260]. A decrease in conductivity has been reported to have lead to a increase in band gap, which is in agreement with sulfonate ring-substituted PANI [212, 263, 264].

For copolymers, a blue shift for the band at around 845 nm was observed with the incorporation of ABA monomer in the polymer chain, which also points to a decrease in conjugations of ABA monomers [254]. Incorporation of ABA monomer has been reported to decrease this band and it would eventually disappear with an increase in monomer concentration [254]. This is believed to be due to the steric effect of the neighboring carboxylic acid group present in the polymer chain [254].

Chemically and electrochemically synthesised PANI-co-3-ABA doped with  $\text{H}_2\text{SO}_4$  from Figure 4.17(ii) and Figure 4.17(iii) showed similar a  $\pi$ - $\pi^*$  transition absorption at 330 nm. However, the ratio between the 330 nm and 620 nm wavelength in UV-Vis spectra was different: the chemically synthesised copolymer had a higher intensity for the 620 nm absorption band. This is ascribed to the exciton transition from B to Q segments caused by interchain charge transfer, indicating that the  $\pi$ - $\pi^*$  transition between adjacent rings in the

polymeric chains is greater for chemically synthesised copolymer than for the electrochemically synthesised one [44, 212, 253, 260]. UV-Vis results of PANI and its copolymer appear to be similar, however, the homopolymer of 3-ABA doped with 1.5 M H<sub>2</sub>SO<sub>4</sub> appears to be uniquely different with two distinct peaks at around 300 nm and 240 nm, which matches closer to the monomer unit. The UV-Vis results seem to show that the polymer, which has a distinct flat-sheet appearance, did not polymerise. Out of the four samples, two 2-ABA polymers and two 3-ABA polymers each doped with different dopant of either H<sub>2</sub>SO<sub>4</sub> or HCl, the poly-3-ABA doped with 1.5 M H<sub>2</sub>SO<sub>4</sub> was the only precipitate that was not brown in colour, but beige.

#### **4.2.7. Cyclic voltammetry of polymers**

##### **4.2.7.1. Polyaminobenzoic acid**

A CV is used to examine how the different chemical structures can be oxidised and reduced within a polymer. For this purpose, chemically synthesised polymers were dispersed in methanol, and a droplet of the dispersed solution was placed on top of a glassy carbon electrode. The solution was then allowed to dry and a CV was run in an acidic aqueous electrolyte to probe the electrochemical behaviour of poly-2-ABA.

Poly-ABA films were also grown electrochemically from solutions containing either H<sub>2</sub>SO<sub>4</sub> or HCl and 0.1 M ABA monomer, by cycling the potential from -0.1 to 0.9 V/1.1 V at a scan rate of 50 mV s<sup>-1</sup> on a Pt electrode. Polymer growth was terminated after 100 complete voltammetric cycles. The films were washed with water and cycled in monomer-free electrolyte to obtain a CV prior to each electrochemical experiment.

Given the low reactivity of ABAs, a higher potential was required to oxidise the ABA than for ordinary aniline [261]. In an earlier chapter PANI was grown at an upper potential of 1.1 V and that has proven to be unnecessary and led to degradation. However, this is not the case for ABAs, suggesting that a higher potential is indeed required for ABA polymerisation. Different positive potential limits were investigated to find the optimum level for film formation and give the optimal results while minimising degradation products. The appearances of new peaks in the CVs and a decrease in observed currents on cycling in monomer-free electrolyte are both indicators of degradation. The first two cycles for the growth of poly-ABA were cycled between -0.1 to 1.2 V, followed by another 2 cycles

between -0.1 to 1.1 V before maximising the positive potential at 1.0 V with the remaining cycles as shown below.

In the Figures 4.18 – 4.25 the voltammograms obtained from the oxidation of 2-ABA and 3-ABA in either an HCl or H<sub>2</sub>SO<sub>4</sub> electrolyte are presented. All of the polymers formed electrochemically on a Pt electrode were visibly brown. This was also true of the chemically oxidised polymers that were characterised voltammetrically.

Electrosynthesis of poly-2-ABA in 1 M HCl and in the presence of 0.1 M 2-ABA monomer was performed by potential cycling between -0.1 to 1.1 V for the first two cycles in Figure 4.18, followed by cycling between -0.1 to 1.0 V for a further 50 cycles versus Ag/AgCl as shown in Figure 4.19. To oxidise ABA a slightly higher potential than aniline was required, hence the upper potential was at 1.1 V. The CVs recorded differ in shape to that of PANI under the same conditions as shown in Chapter Three. The first anodic peak corresponds to the insulating to conducting transition and was shifted to a higher potential than that observed for PANI. The peaks observed were also not as well-defined as for PANI.

Poly-2-ABA was electrosynthesised again, but under slightly different conditions – with the upper potential now at 1.2 V rather than 1.1 V and with a different acidic solution. Instead of using 1 M HCl as the electrolyte in the polymerisation, 0.5 M H<sub>2</sub>SO<sub>4</sub> was used. Despite the increase in the upper potential, the current observed in the first two scans running between -0.1 to 1.2 V at a scan rate of 50 mV s<sup>-1</sup> was lower than the earlier poly-2-ABA doped with 1 M HCl. The subsequent scan shown in Figure 4.21 showed similar peaks to those observed in Figure 4.19. Peak growth was observed, however, the rate of polymerisation was very slow as indicated by the small increase in peak intensities.

The use of two different dopants for the electrosynthesis of poly-3-ABA showed similar CVs in their first two scan, Figures 4.22 and 4.44. With continuous scanning (Figures 4.23 and 4.25) for poly-3-ABA, growth was also observed with the polymer grown in 1.5 M H<sub>2</sub>SO<sub>4</sub>, indicating a greater rate of reaction than in 1 M HCl.

Polymers grown both chemically and electrochemically were characterised by CVs shown below. Performing 5 cycles between the potential of -0.1 to 0.9 V at a scan rate of 50 mV s<sup>-1</sup> enabled a stabilised CV to be collected. The overall observations and results indicate the presence of conductive forms as typical PANI redox properties were shown in CVs below [202, 210].

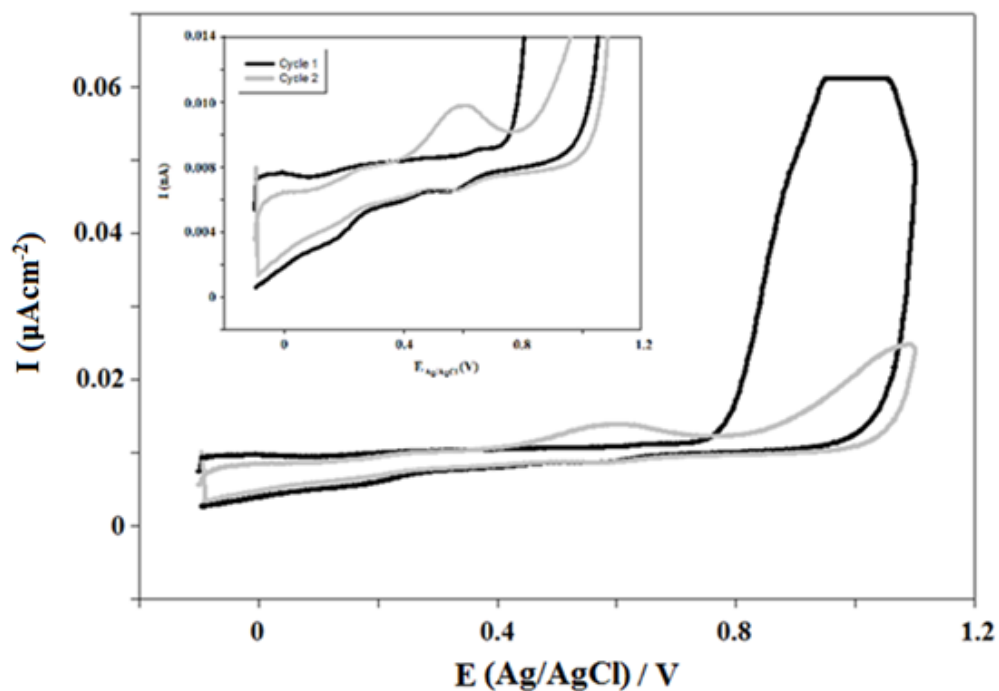


Figure 4.18. CVs of the first two cycles for a Pt electrode in 0.1 M 2-ABA, run at  $50 \text{ mV s}^{-1}$  in 1 M HCl.

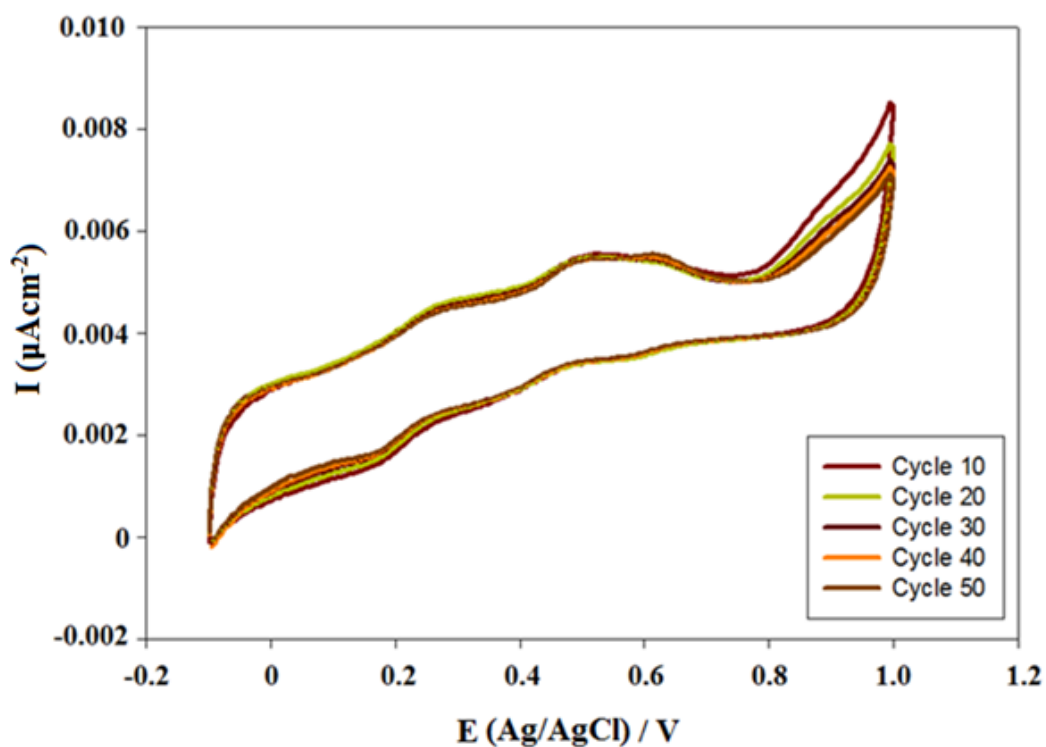


Figure 4.19. CVs of a poly-2-ABA film run at  $50 \text{ mV s}^{-1}$  in 1 M HCl of the first 50 cycle for a Pt electrode in 0.1 M 2-ABA, run at  $50 \text{ mV s}^{-1}$  in 1 M HCl.

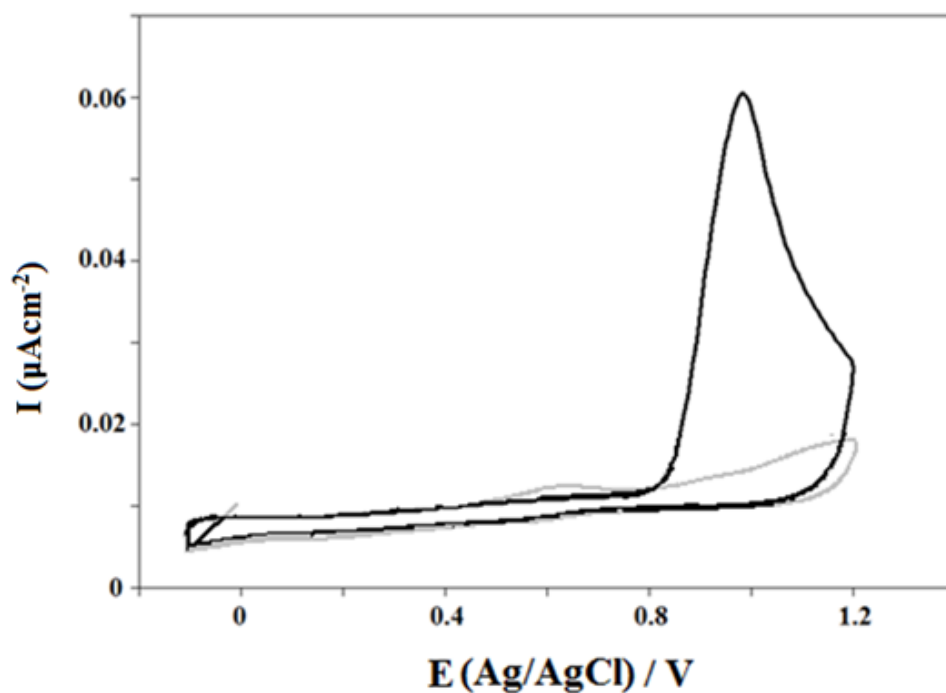


Figure 4.20. CVs of the first two cycles for a Pt electrode in 0.1 M 2-ABA, run at  $50 \text{ mV s}^{-1}$  in  $0.5 \text{ M H}_2\text{SO}_4$ .

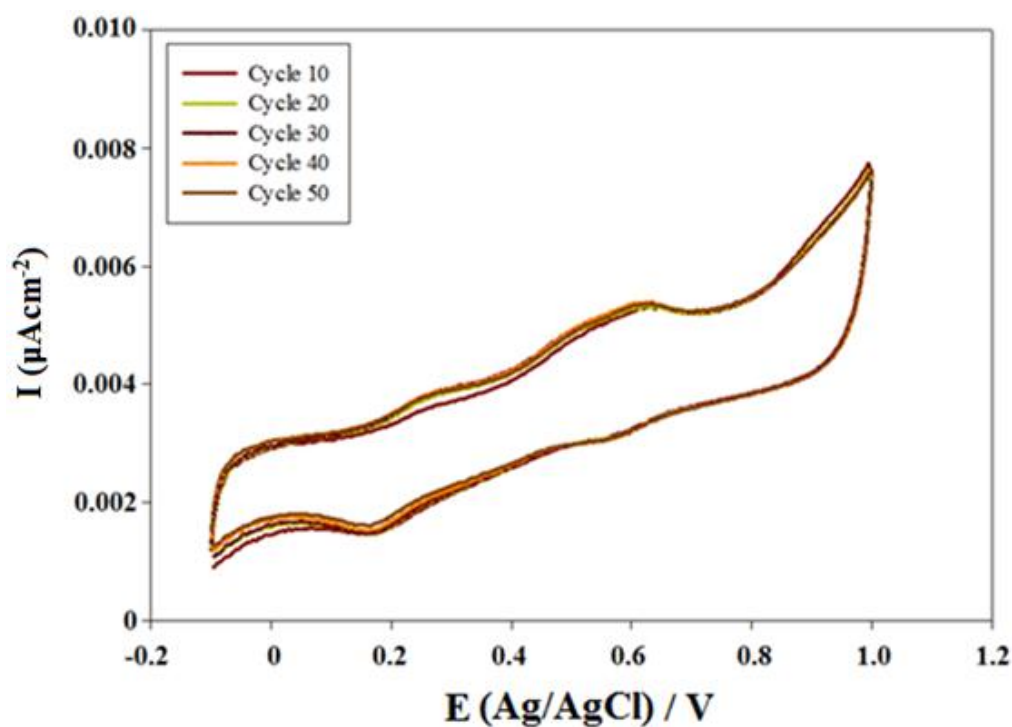


Figure 4.21. CVs of poly-2-ABA film run at  $50 \text{ mV s}^{-1}$  in  $0.5 \text{ M H}_2\text{SO}_4$  of the first 50 cycle on a Pt electrode.



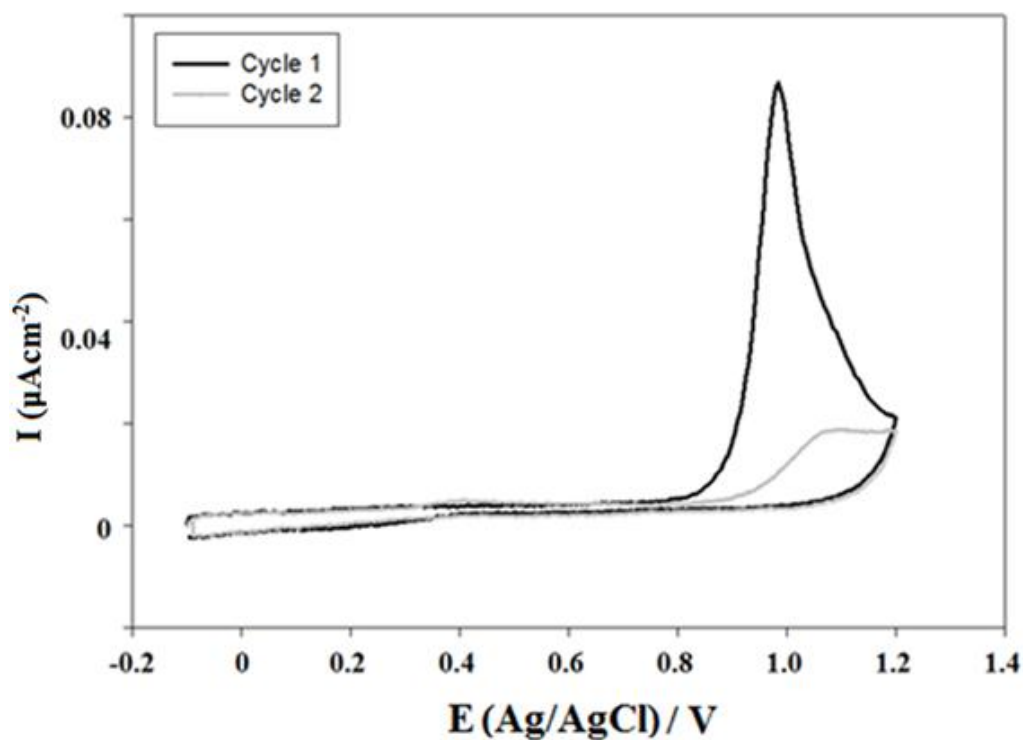


Figure 4.22. CVs of the first two cycles for a Pt electrode in 0.1 M 3-ABA, run at  $50 \text{ mV s}^{-1}$  in 0.5 M HCl.

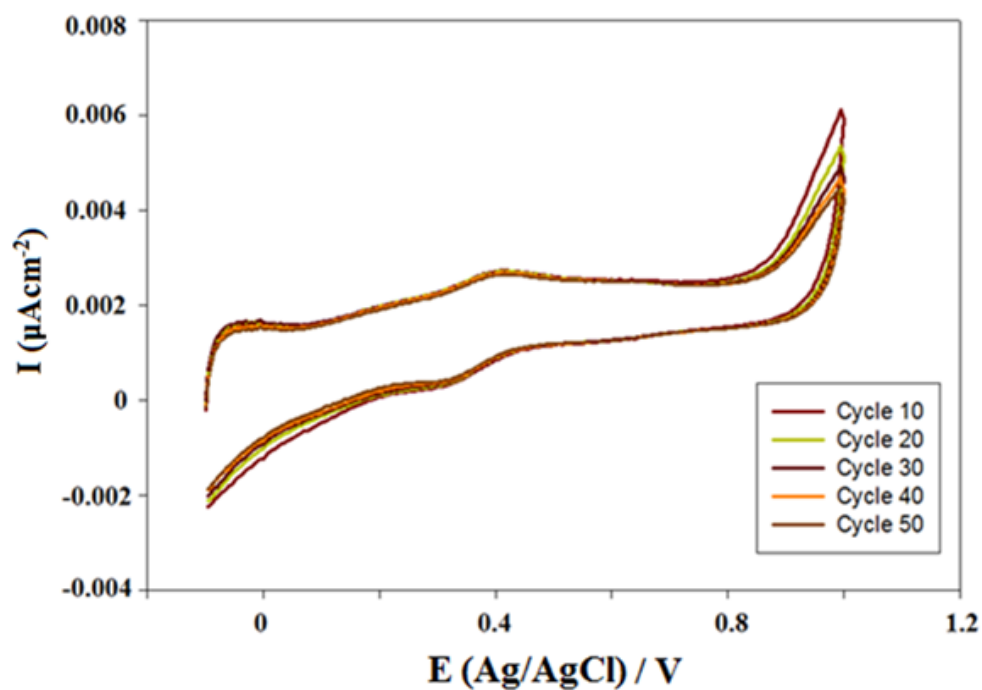


Figure 4.23. CVs of poly-3-ABA film run at  $50 \text{ mV s}^{-1}$  in 1 M HCl of the first 50 cycle on a Pt electrode.

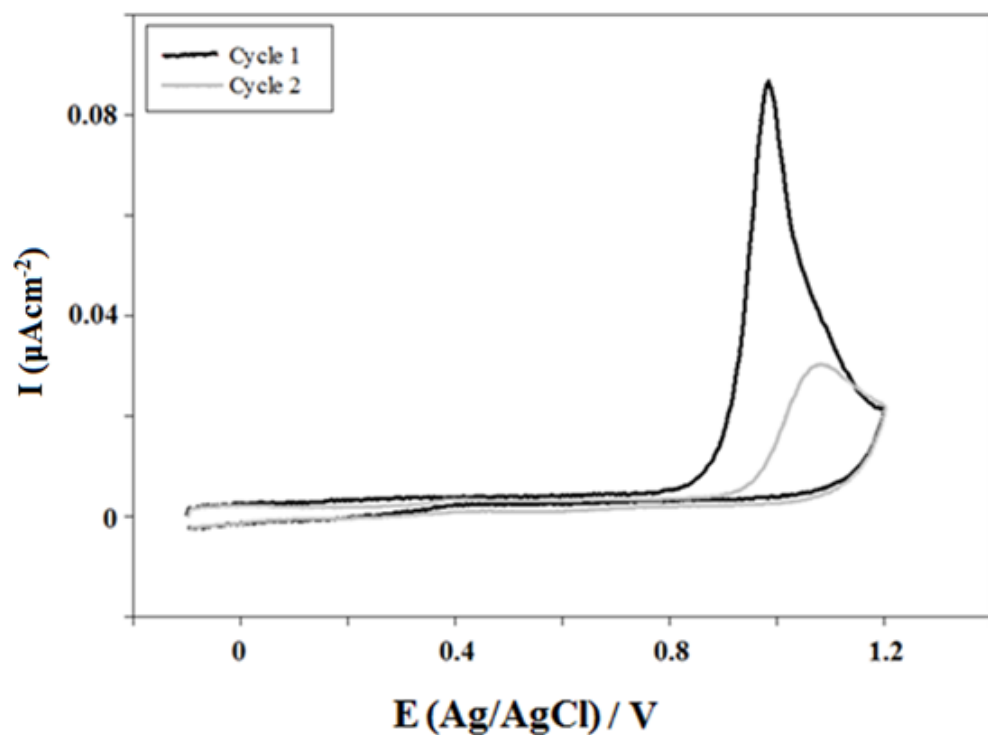


Figure 4.24. CVs of the first two cycles for a Pt electrode in 0.1 M 3-ABA, run at  $50 \text{ mV s}^{-1}$  in  $1.5 \text{ M H}_2\text{SO}_4$ .

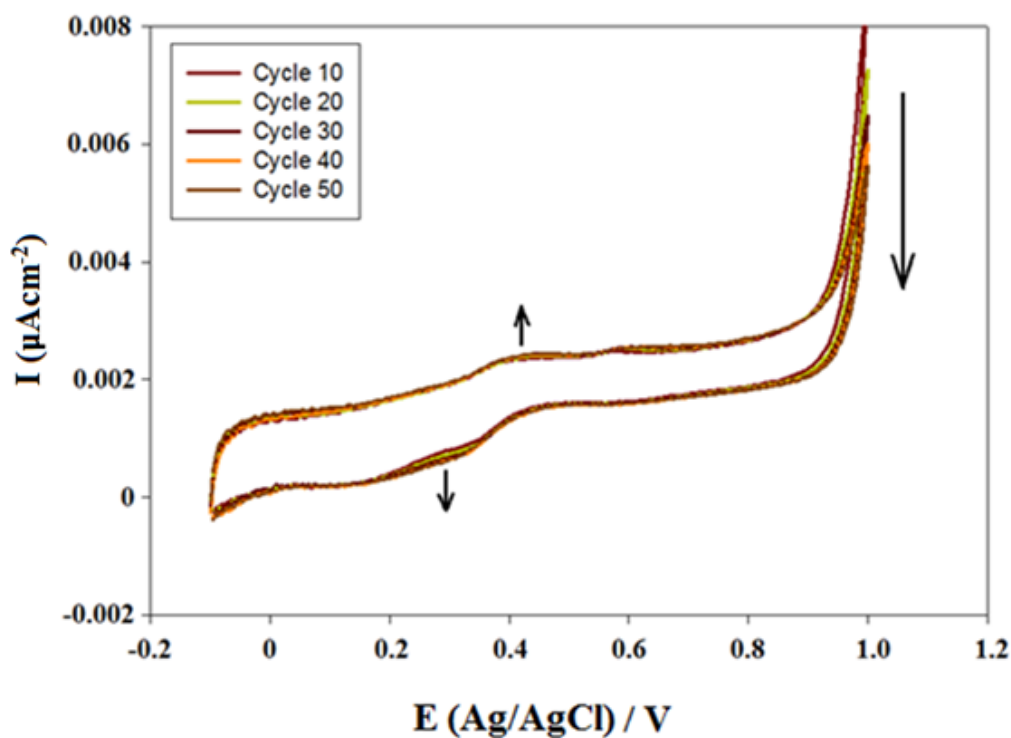


Figure 4.25. CVs of poly-3-ABA film run at  $50 \text{ mV s}^{-1}$  in  $1.5 \text{ M H}_2\text{SO}_4$  of the first 50 cycle on a Pt electrode.

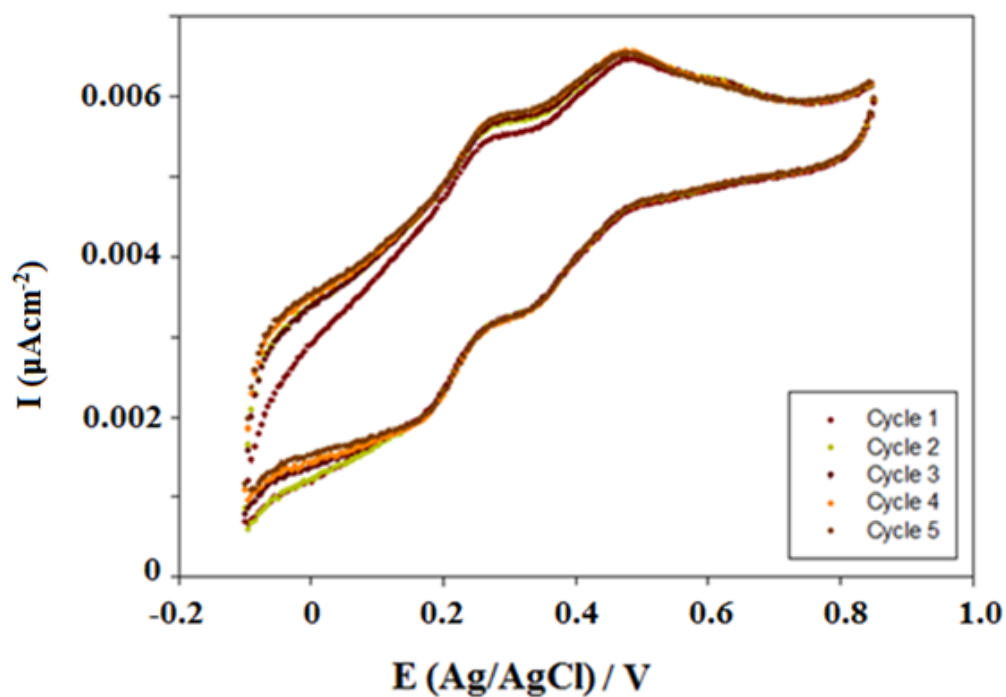


Figure 4.26. CVs of an electrochemically prepared poly-2-ABA film run at  $50 \text{ mV s}^{-1}$  in 1 M HCl, after forming on a Pt electrode.

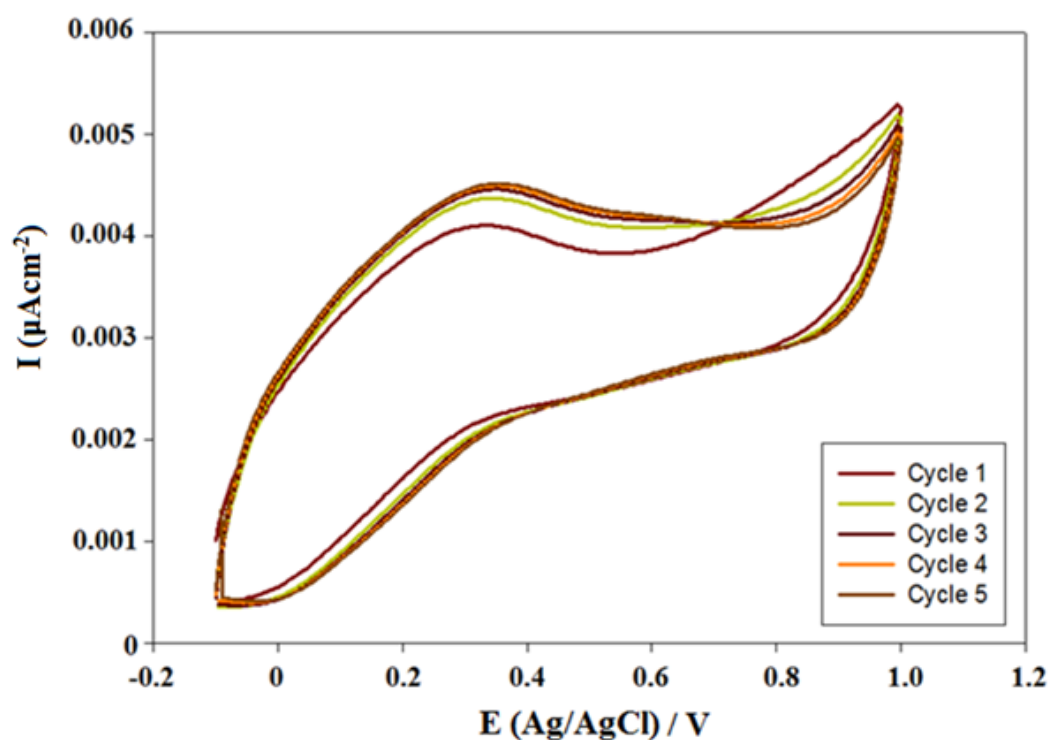


Figure 4.27. CVs of a chemically prepared poly-2-ABA film run at  $50 \text{ mV s}^{-1}$  in 1 M HCl, after casting on a glassy carbon electrode.

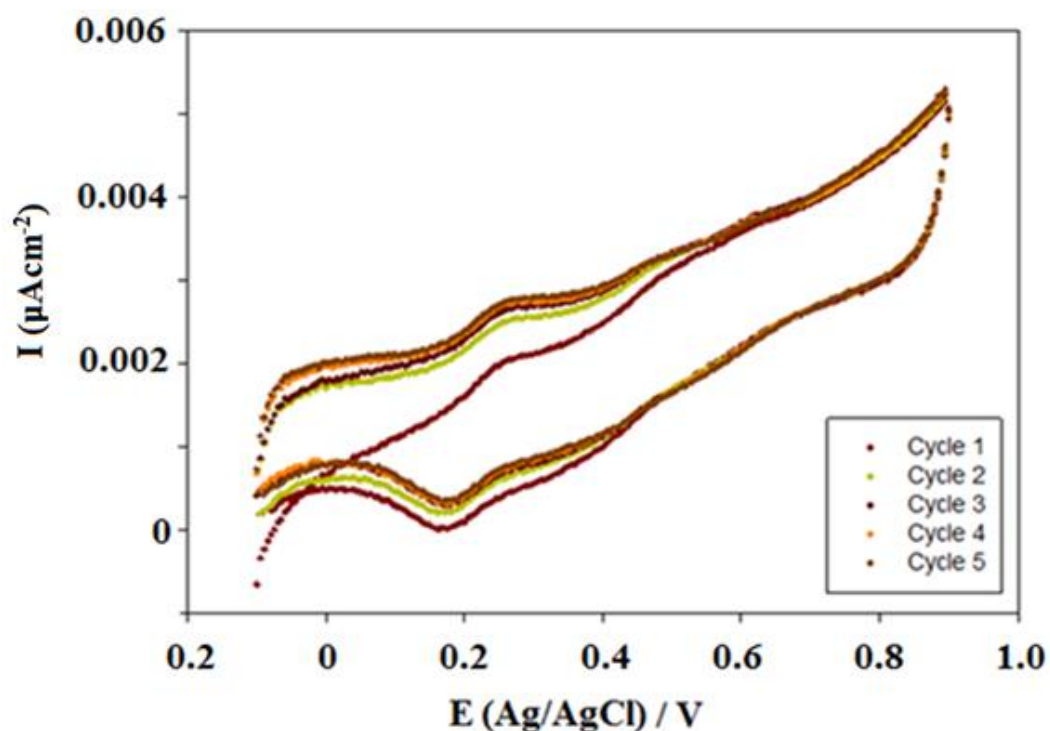


Figure 4.28. CVs of an electrochemically prepared poly-2-ABA film run at  $50 \text{ mV s}^{-1}$  in  $0.5 \text{ M H}_2\text{SO}_4$ , after forming on a Pt electrode.

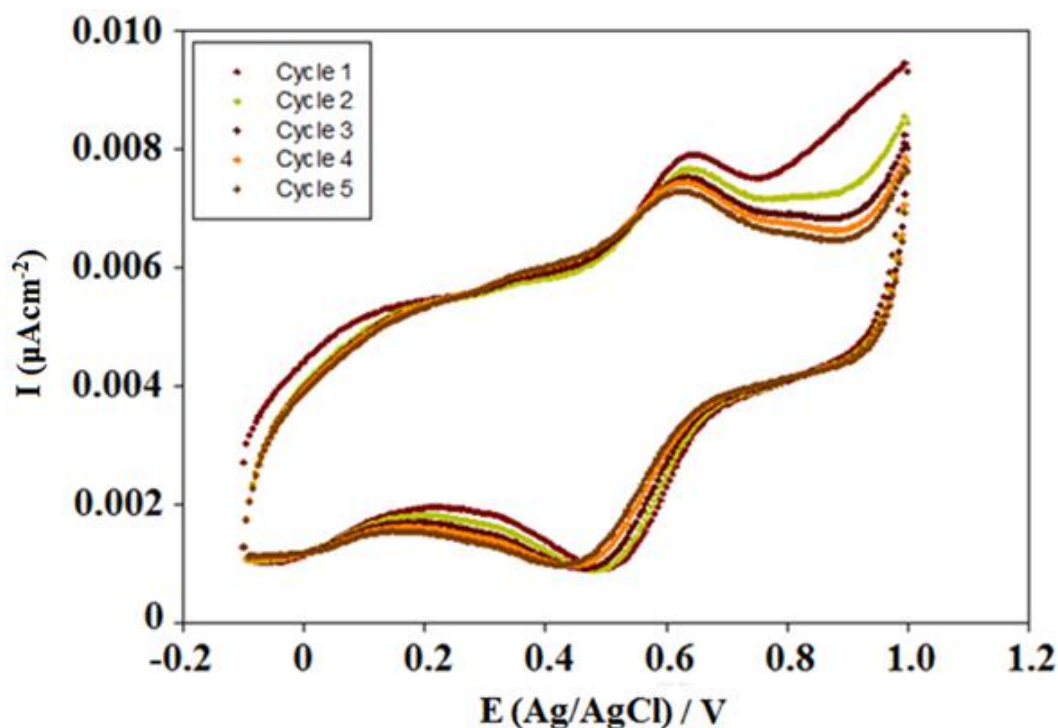


Figure 4.29. CVs of a chemically prepared poly-2-ABA film run at  $50 \text{ mV s}^{-1}$  in  $1 \text{ M H}_2\text{SO}_4$ , after casting on a glassy carbon electrode.

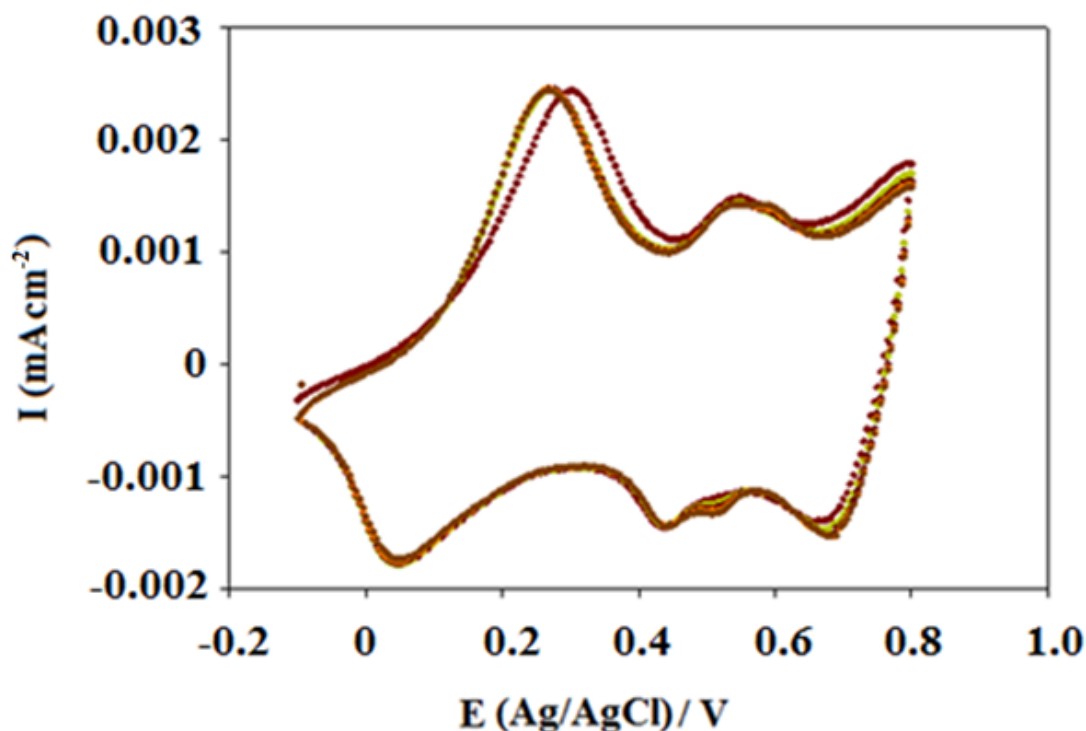


Figure 4.30. CVs of an electrochemically prepared poly-2-ABA film run at  $50 \text{ mV s}^{-1}$  in  $0.5 \text{ M H}_2\text{SO}_4$ , after forming on a PANI-Pt electrode.

The preferred polymerisation mechanism for 2-ABA implies coupling in the C4-position of the aromatic system, i.e. in the para-position relative to the amino group. This is because the groups with negative inductive and mesomeric effects are direct substituents to the meta-position [202]. For 2-ABA, electronic effects during polymerisation have to be taken into consideration, while for 3-ABA, the steric effects matter more, predicting 1,5-coupling. Poly-2-ABA polymer prepared via different methods, see Figures 4.28, 4.29 and 4.30, showed different internal redox properties, suggesting that the polymers formed were slightly different from one another. Poly-2-ABA was also grown on the surface of a Pt electrode previously coated with PANI, and the CV showed that it consisted of characteristic peaks of PANI rather than the poly-2-ABA polymer. Therefore, this sample preparation method was discarded; even though the growth rate was much faster, given that the polymer was grown on a surface that consisted of polymer rather than an inert metal. Poly-2-ABA prefers to grow on a polymerised surface rather than on inert surfaces. The electrochemically synthesised poly-2-ABA exhibits similar voltammetric behaviour as PANI, displaying two redox peaks compared to two for PANI. The redox peaks for poly-2-ABA doped with  $1 \text{ M HCl}$  at the more negative potential are caused by the conversion between EB and LEB states, while the

peaks at more positive potentials are caused by the fully oxidised state [247, 265, 266]. Slightly different ratios of the two least defined peaks were observed on the CVs of the chemically synthesised poly-2-ABA. The other electrochemically prepared poly-2-ABA doped with sulfuric acid showed similar redox peaks, but they were of different current intensity due to the dopant effect. Moreover, the truly interesting CV was that of the poly-2-ABA chemically prepared doped with 1.5 M H<sub>2</sub>SO<sub>4</sub>: the two redox peaks shown shifted to a higher potential in both cases. Chemically and electrochemically synthesised poly-3-ABA with the use of two different dopants were characterised by CVs as shown below in Figures 4.31 to 4.34.

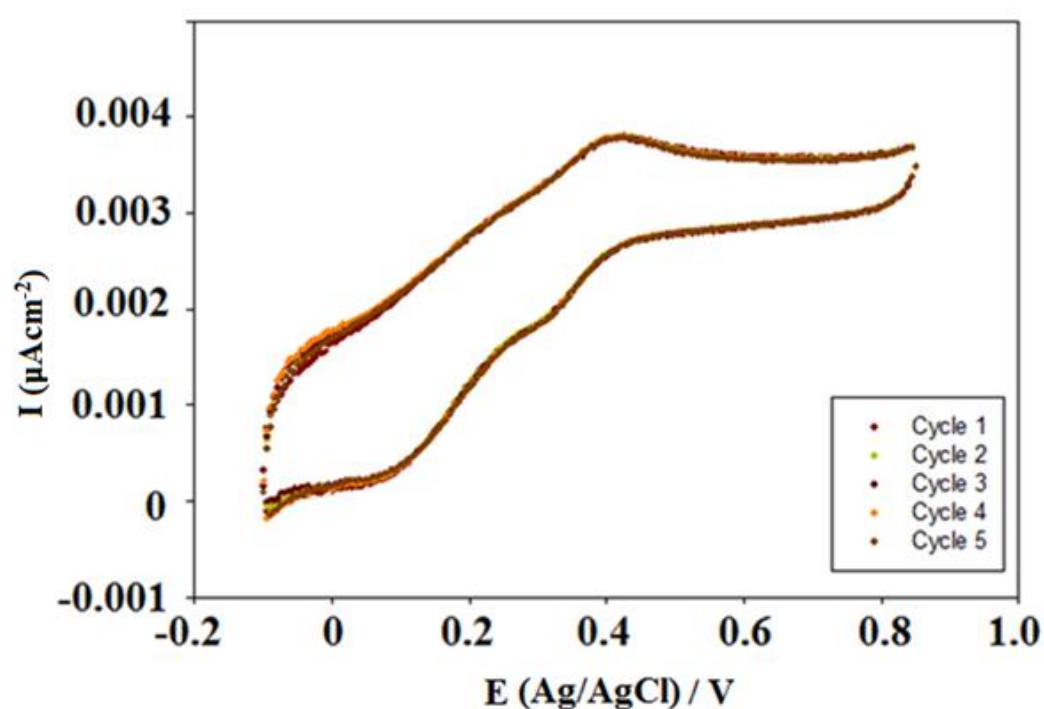


Figure 4.31. CVs of electrochemically prepared poly-3-ABA films run at  $50 \text{ mV s}^{-1}$  in 1 M HCl, after forming on a Pt electrode.

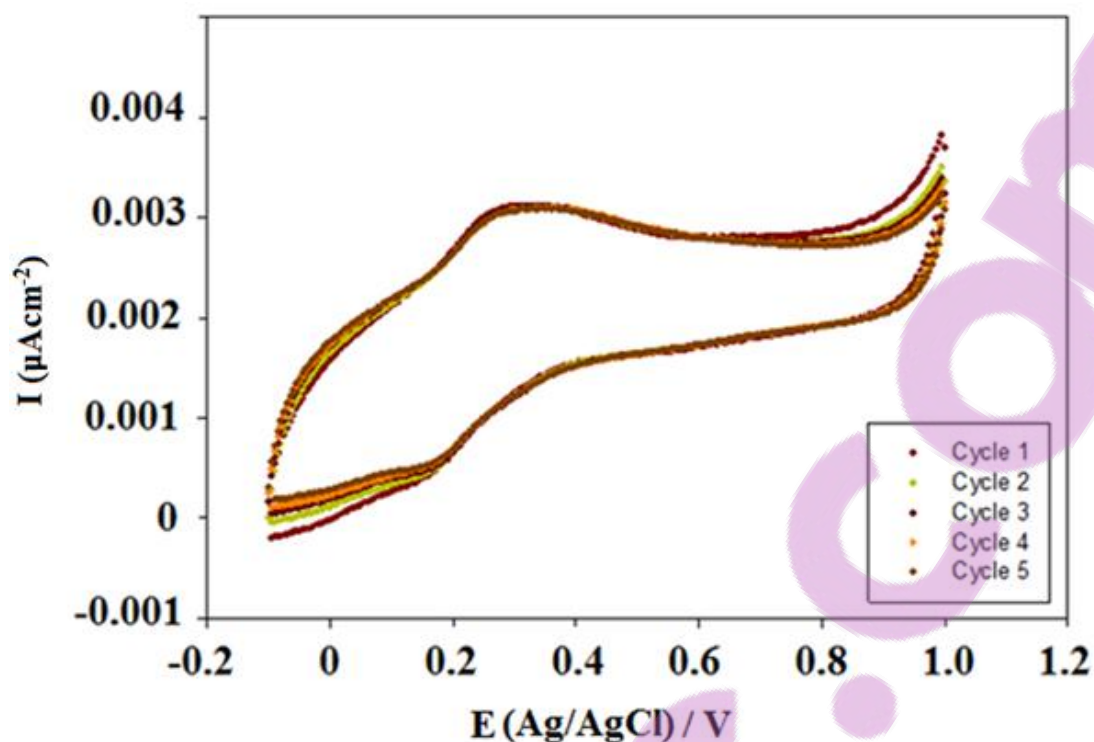


Figure 4.32. CVs of chemically prepared poly-3-ABA films run at  $50 \text{ mV s}^{-1}$  in 1 M HCl, after casting on a glassy carbon electrode.

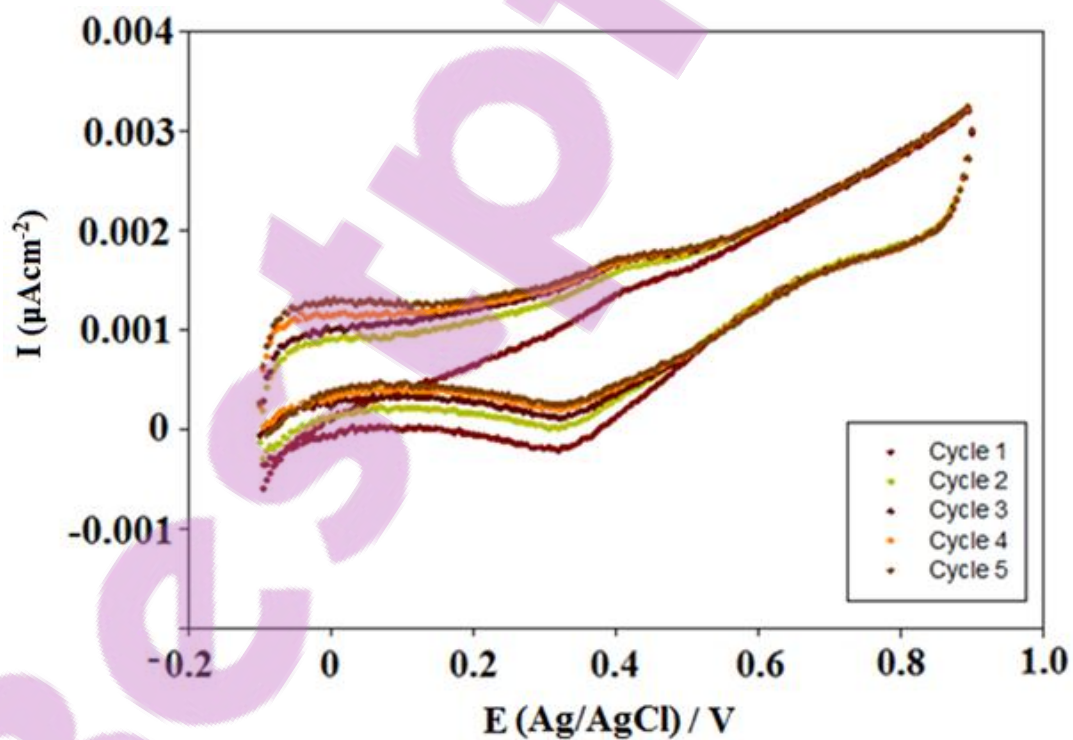


Figure 4.33. CVs of electrochemically prepared poly-3-ABA film run at  $50 \text{ mV s}^{-1}$  in 1.5 M  $\text{H}_2\text{SO}_4$ , after forming on a Pt electrode.



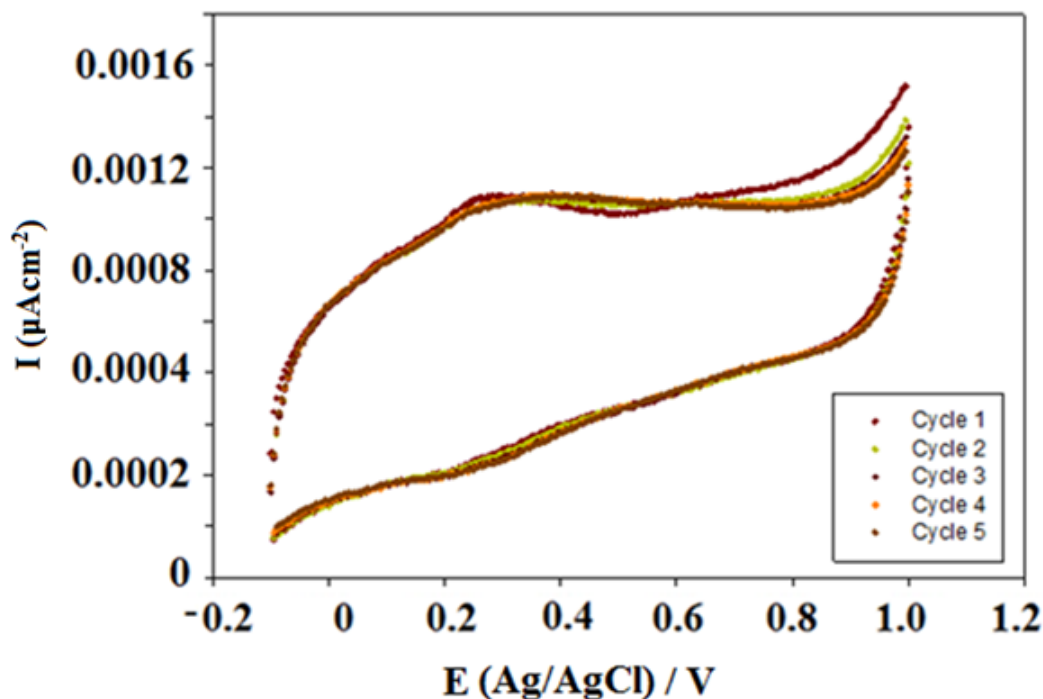


Figure 4.34. CVs of chemically prepared poly-3-ABA film run at  $50 \text{ mV s}^{-1}$  in  $1.5 \text{ M H}_2\text{SO}_4$ , after casting on a glassy carbon electrode.

Poly-3-ABA (Figures 4.31 to 4.34) only showed one broad redox peak in the intermediate potentials of the two redox processes of poly-2-ABA, indicating that its conjugated molecular structure must be different to that of PANI (Figure 3.5 and 4.30) and poly-2-ABA (Figures 4.26 to 4.29). Moreover, the poly-3-ABA doped with  $1.5 \text{ M H}_2\text{SO}_4$  (Figure 4.34) did not show clear internal redox properties, once again suggesting the oligomer formed (if not a polymer) has little or even no conductivity.

In general, the CVs for films prepared from solutions of 2-ABA and 3-ABA presented above during the electropolymerisation of the ABAs differ in shape from those of PANI under the same conditions. Firstly, the anodic peak corresponding to the insulating to conducting transition is shifted towards a higher potential and is less well defined (compare Figure 3.5 with Figures 4.28 and 4.33), which has been reported elsewhere [202]. In Shim et al. [267] it has been suggested that the shoulder at  $\sim 0.28 \text{ V}$  versus Ag/AgCl is due to the oxidation of oligomers in which the chain length is between that of dimers and a full PANI. The rate of reaction is relatively slow when compared to the formation of PANI. Due to the electron-withdrawing effect of the carboxyl group, the aromatic system of an ABA is deactivated with respect to an electrophilic substitution reaction [202]. Hence, the growth rate of

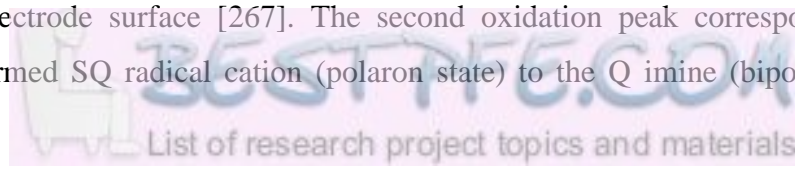


polymerisation for an ABA should be slower than that of aniline. This is another reason why a slightly higher potential is required to oxidise the ABA monomers compared to aniline [202]. It shows that the film formed is not highly conducting, which further suggests that the formation of oligomer species is more likely than the formation of a long-chain polymer [202].

Unlike PANI, poly-ABA did not show well-defined redox peaks in the scanned potential range and the rate of polymer growth was much lower for the polymerisation of substituted anilines than for aniline (compare Figure 3.4 with Figures 4.21 and 4.25). Only two pairs of relatively weak current peaks at  $\sim 0.233$  V/ $0.003$  V and a broad redox pair at  $\sim 0.577/0.450$  V can be observed with the polymers in general (Figures 4.26 to 4.29 and Figures 4.31 to 4.34), caused by LEB/EB and EB/PNB reversible transition [202].

There are two redox peaks that occur at  $0.270/0.170$  V and  $0.475/0.335$  V [12, 202, 210] for poly-2-ABA doped with 1M HCl on a platinum electrode (Figure 4.26). The anodic peak decreases with time, suggesting that the film formed partially blocks the electrode. The first anodic peak corresponds to the insulating to conducting transition which is shifted to a higher potential. The peaks are also less clearly defined [202]. The weak current indicates that the film formed is not highly conductive and the rate of reaction is relatively slow as shown by continuing consecutive scans. Two kinds of reactions could potentially be connected to electrochromism of PANI. One observed at  $0.10$  V versus Ag/AgCl assigned to the addition/elimination reaction of protons and electrons accompanied by a colour change from yellowish green to dark green [202]. Insertion/elimination of electrolyte anions into/from the polymer film correlates to the reaction [202, 267]. Although this latter reaction involves anion exchange, a colour change is expected for oxidised PANI [267].

The oxidation of monomer was seen at  $0.995$  V (Figure 4.29). This band decreased with time with scans as the monomer reacted. The removal of one electron from a nitrogen atom of the amino group to give radical cation corresponds to the first peak. The presence of the carboxylic acid group in the ortho position facilitates the oxidation process forming radical cation at a low potential [267]. The radical cation interacts with other monomers to form dimeric radical cations, which can further react with existing monomers to give trimer radical cations [267]. The polaron state, semiquinone (SQ) radical cation is formed, which is adsorbed on the electrode surface [267]. The second oxidation peak corresponds to the oxidation of the formed SQ radical cation (polaron state) to the Q imine (bipolaron state)



[267] occurring at 0.93 V versus Ag/AgCl [202, 210, 267]. The second redox process is attributed to the conversion of radical cations to the fully oxidised form (quinoidal structure), see Section 1.4.2 [267].

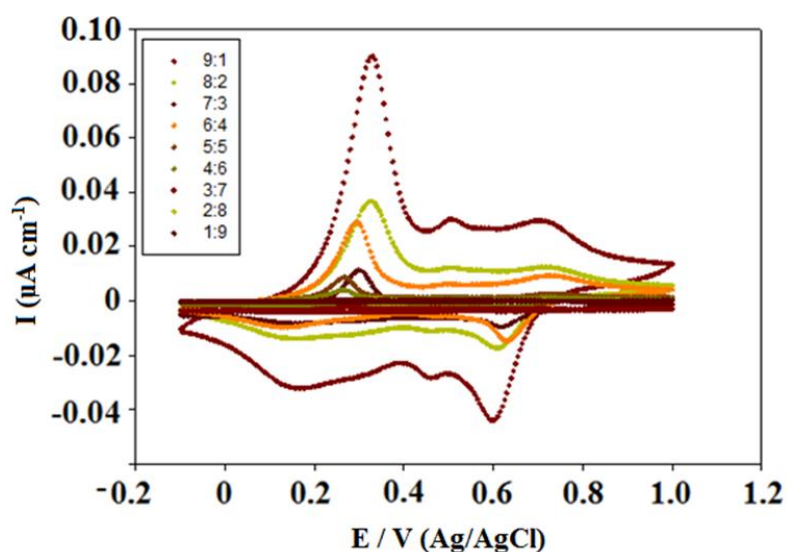
During polymerisation a brown polymer film is rapidly nucleated and deposited on the electrode surface. In the second scan the peak of oxidation occurs at 0.45 V, 0.65 V and 0.84 V (Figure 4.28). The three redox characteristics of polymerisation represent the growth of poly-2-ABA. It has been reported that the potential difference between the first and second oxidation peaks (I and II) is ~1.22 V and the presence of the middle peaks indicates the existence of degradation products, higher regularity, homogeneity and adherence of the deposited film on the electrode surface [267]. On the reverse scan the anodic current is very small, indicating the presence of an adhered layer of the polymer on the electrode surface [267]. The presence of a reactive anodic peak beyond ~0.50 V (III) in the reverse scan of Figure 4.28 indicates the partial removal of the deposited polymer film from the surface as a result of degradation process and consequently radical cation formation at this potential [267]. A decrease in the current with cycling in a pure electrolyte and the appearance of new peaks in the CVs are evidence of the degradation process [267]. Initially, the growth was fast and upon continuous scanning, the current did not increase (Figures 4.19, 4.21, 4.23 and 4.25), which could possibly be due to the polymer reaching its polymerisation saturation [267]. The voltammetric behaviour of poly-2-ABA (Figure 4.30) is similar to that of PANI, displaying two redox peaks resulting from three redox states of PANI, LEB, EB and PNB. The conversion between EB and LEB states and EB to the fully oxidised state of PANI are the redox peaks observed at more negative potential and more positive potential [247, 265, 266]. For poly-3-ABA (Figures 4.31 to 4.34), only one broad redox peak was observed in the intermediate potentials of the two redox processes of PANI and poly-2-ABA (Figures 4.26 to 4.29), indicating that the conjugated molecular structure must differ from that of PANI and poly-2-ABA. Results from these suggest that 2-ABA is a more suitable candidate from the carboxylated PANI range of substituted anilines as it has a higher electroactivity and is subject to easier electropolymerisation. At the same time, the potential position of the redox peaks did not shift with an increasing number of cycles, indicating that the reversibility of the redox reactions was independent of the polymer thickness.

The anodic peak at 1.2 V detected in the first CV cycle decreased in current over time (Figures 4.20, 4.22 and 4.24) [202, 210]. A less positive potential was observed during the first cathodic scan showing three reduction peaks beyond 0.80 V, 0.65 V and 0.51 V that showed their corresponding tips of oxidation in the second positive cycle [202, 210].

CVs of the synthesised poly-2-ABA films show two characteristic pairs of redox peaks (Figures 4.26 to 4.29) [202, 210]. Two redox processes at 0.48/0.42 V and 0.73/0.57 V are observed, with the second pair of redox peaks lower than those of the first redox process for poly-2-ABA (Figures 4.26 to 4.29). The charge of the first peak is higher than that of the second peak indicating that not all formed radical cations interact to give polaron and then bipolaron [267].

#### 4.2.7.2. Polyaniline-co-aminobenzoic acid

To illustrate the effect of the presence of aniline on the overall rate of polymerisation, the following section focuses on the copolymer formation of aniline and 2-ABA at various ratios in 1 M HCl electrolyte. Nine copolymers at different aniline to 2-ABA ratios were prepared and presented in Figure 4.35 which clearly illustrates that aniline plays an important role in determining the kinetic of the polymerisation reaction. The aniline content is in direct relationship to the current intensity with peak positions shifted to more positive potential. The two electrochemically synthesised copolymers with the highest aniline and ABA content are shown in Figure 4.36: this figure clearly demonstrated the differences and similarities of the obtained CV at two extreme monomer levels.



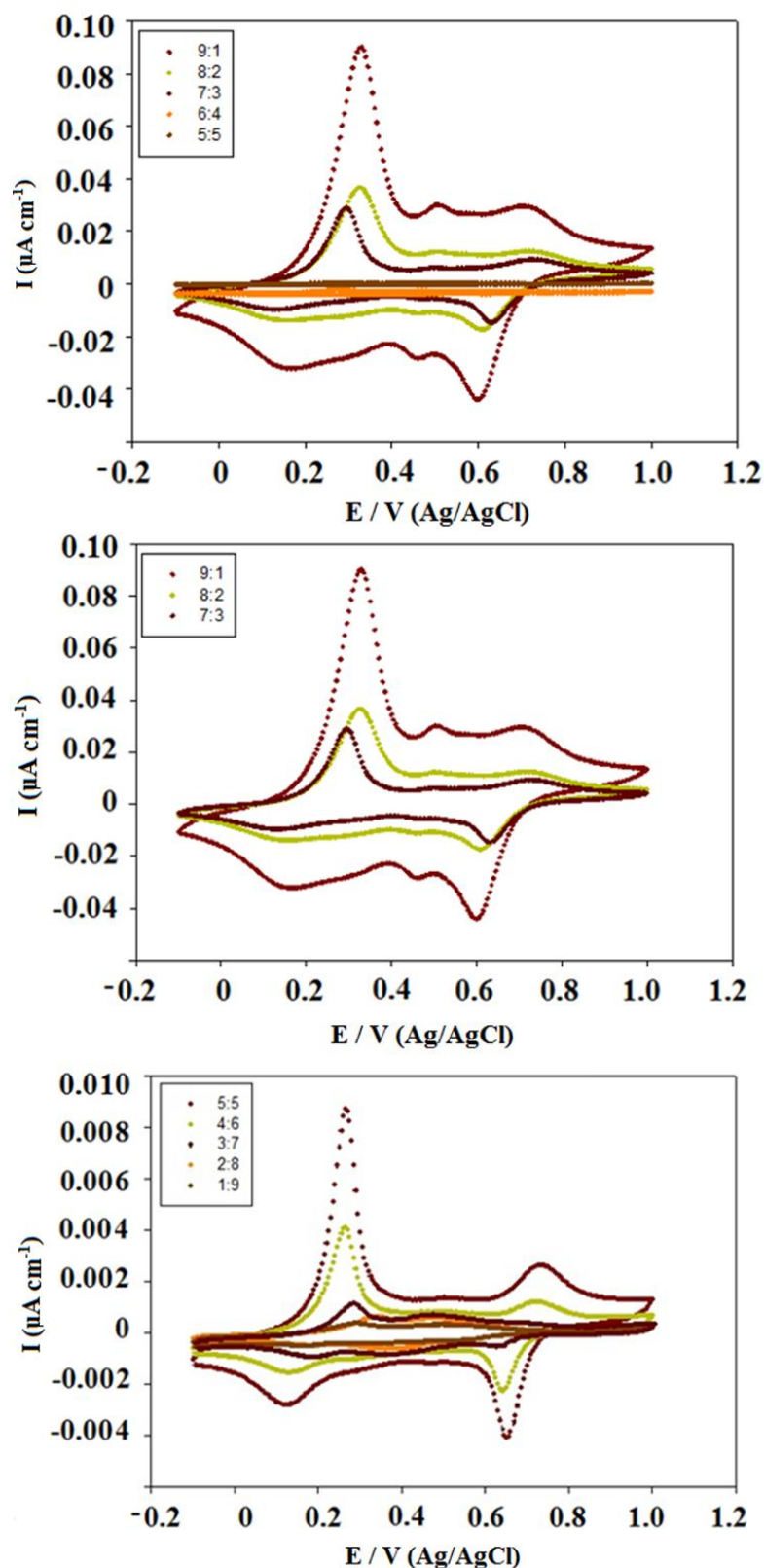
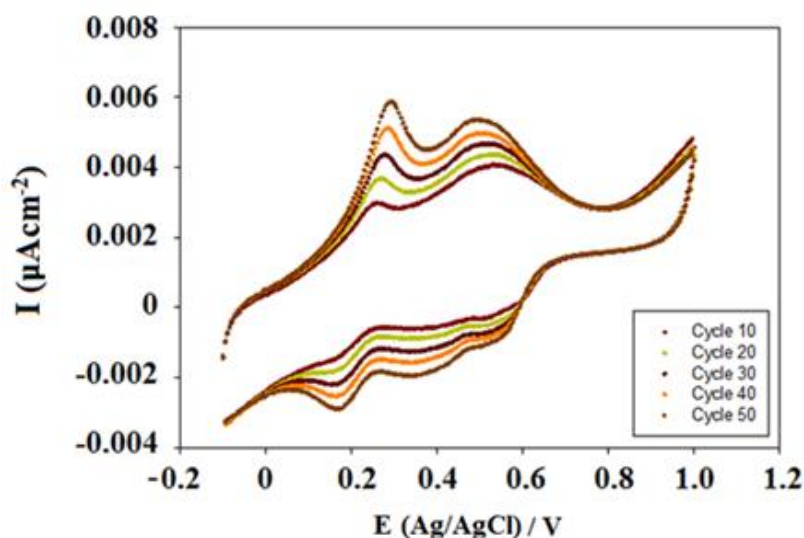
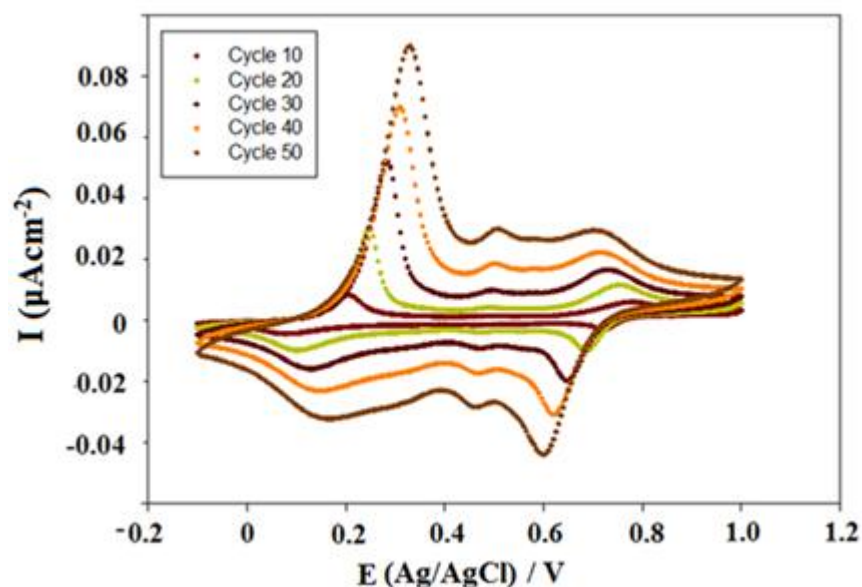


Figure 4.35. The CVs for the electrolysis of a solution consisting of 0.05 M ABA, 0.05 M aniline and 1 M HCl after 50 cycles cycling between -0.1 to 1.0 V at a scan rate of  $50 \text{ mV s}^{-1}$  at different aniline to 2-ABA concentrations (represented as 9:1 correspond to aniline: 2-ABA monomer).

Although the electrochemically synthesised poly-ABA films are brown, the colour of the copolymer films was green, with the intensity of the colour depending on content of ABA monomer present. The anodic peak corresponding to the insulating to conducting transition was shifted towards a higher potential with an increase in aniline concentration in the copolymer.



(a)



(b)

Figure 4.36. Cycle 10 – 50 for the electrochemical synthesis of copolymers of doped in 1 M HCl solution, (a) 1:9 (aniline: 2-ABA monomer), and (b) 9:1.

Two redox processes were observed with substituted PANI, the first redox peak is assigned to the LEB and EB transition, while the second corresponds to the EB and PNB transition [268, 269]. Substituted polyanilines often shows more positive values for the first peak potential compared to PANI [44]. This could possibly be due to the electron withdrawing groups of carboxylic acid group on the aromatic ring, creating difficulty for oxidation of the amine units. The coplanarity of the oxidised units is decreased by the steric effect of any group in the ring making overlap of rings more difficult [44]. This effect leads to a decrease in conductivity and favors the formation of oxidised units [269, 270]. A shift in the peaks to more positive potentials was observed as the amount of ABA units in the copolymer increased [44]. The oxidation of substituted aniline is often at a higher potential than that of the aniline monomer in the first cycle [55]. The oxidation of ABA and aniline in polymerisation is a simultaneous reaction, resulting in two anodic peaks at 0.47 V and 0.77 V, with corresponding reduction counter parts at 0.75 V, 0.66 V and 0.37 V [202]. Three pairs of redox peaks appear on the CV for the electrochemical polymerisation of aniline in acidic solutions [55], while the synthesis of ABA shows two pair of redox peaks. This suggests that the change associated with the second pair of redox peaks in the electrochemical polymerisation of the copolymer is more important than that obtained with poly-ABA, with peaks increasing as the number of potential cycles increased. The increase of current with the copolymer film is a good indication of film growth over time [202].

The peak at ~0.5 V versus SCE (Figure 4.36) [271] was identified as that of the oxidation of the head-to-tail dimer of aniline [202]. Shim et al [267] showed that *p*-aminophenol and *p*-benzoquinone, are the main products with a peak at ~0.5 V, and are oxidative degradation products of PANI and its oligomers. However, Geniès et al [272] suggest that the peak at 0.45 V (versus Cu/CuF<sub>2</sub>) can be attributed to the formation of crosslinked PANI chains.

#### **4.2.8. Raman spectroscopy**

Raman spectra of poly-ABA prepared under two different methods and dopants were collected and are displayed in Figure 4.38. The optical image shown in Figure 4.37 clearly demonstrated that the polymer formed on Pt electrode surface was not a uniform film but instead islands. The spectrum of poly-2-ABA prepared electrochemically on a Pt electrode is similar to that of poly-2-ABA polymerised chemically.



Figure 4.37. Microscopy images of the visual appearance of poly-2-ABA grown on a Pt electrode surfaces.

Although the Raman and CV could be obtained with poly-2-ABA, the polymer film often forms in isolated islands on certain areas of the Pt electrode rather than forming as a consistent uniform film.

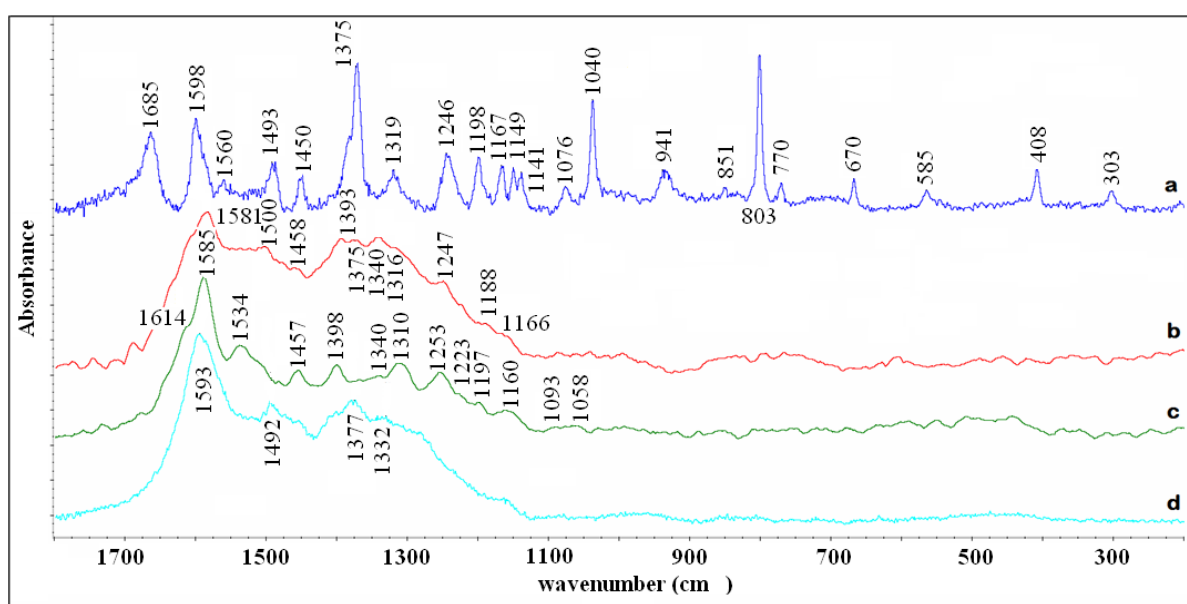


Figure 4.38. Raman spectra of (a) 2-ABA monomer, (b) chemically synthesised poly-2-ABA doped with 1 M HCl, (c) chemically synthesised poly-2-ABA doped with 1 M H<sub>2</sub>SO<sub>4</sub>, and (d) electrochemically synthesised poly-2-ABA polymerised on Pt electrode with 1 M H<sub>2</sub>SO<sub>4</sub>.

The 1600 cm<sup>-1</sup> monomer substituted benzene rings peak observed in 2-ABA ascribed to C=C stretching mode with substituted benzene rings [44, 273-274] shifted to a lower wavenumber upon polymerisation to around 1585 – 1590 cm<sup>-1</sup>. The C-C and C-H benzene deformation



modes, indicating the presence of Q rings, and the ring C=C Q stretching mode could also be assigned in this region. The band at  $1460\text{ cm}^{-1}$  corresponds to the  $\text{C}=\text{N}^{*+}$  stretching mode of the Q units [274]. A very weak C-C stretching mode is detected at  $\sim 1455\text{ cm}^{-1}$  with a SQ radical cation for oxidised protonated PANI salt at  $\sim 1500\text{ cm}^{-1}$  [44]. The presence of the  $1450\text{ cm}^{-1}$  bands correlate to the C-C stretching [44]. Electronic absorption of the free charge carriers is observed with a peak at  $\sim 1380\text{ cm}^{-1}$ , indicating the conducting nature of the polymeric compound. The band at  $1335\text{ cm}^{-1}$  corresponds to the  $\text{C}-\text{N}^{*+}$  stretching modes of the delocalised polaronic charge carriers. The  $1225\text{ cm}^{-1}$  band is ascribed to the C-N stretching mode of the single bond, while the band at  $1260\text{ cm}^{-1}$  can be assigned to the C-N stretching mode of the polaron unit [202, 210]. The symmetrical CNC stretch is present in the  $1312 - 1344\text{ cm}^{-1}$  region along with C-N stretching modes and in-plane CH bend in the oxidised polymer at  $\sim 1150$  and  $1170\text{ cm}^{-1}$ . A weak band at  $1060\text{ cm}^{-1}$  is assigned to the C-COOH stretching band, while the C=O in-plane bend is present at  $1015\text{ cm}^{-1}$ . Out of plane bend for C-H is detected as a very weak peak in the region of  $\sim 810 - 840\text{ cm}^{-1}$ .

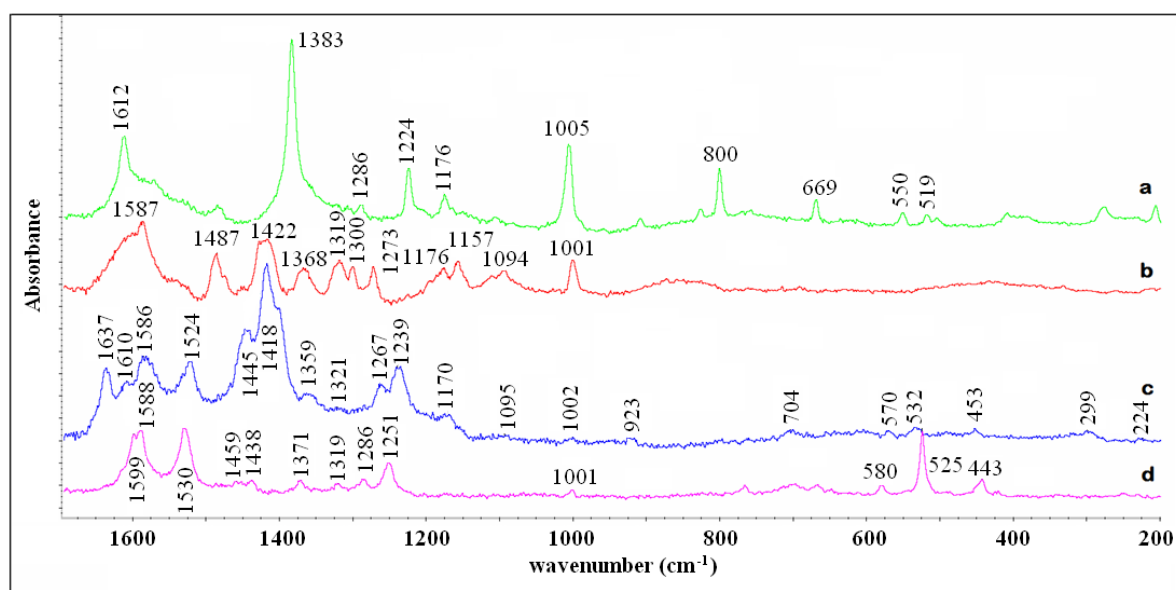


Figure 4.39. Raman spectra of (a) 3-ABA monomer, (b) chemically synthesised poly-3-ABA doped with 1.5 M  $\text{H}_2\text{SO}_4$ , (c) chemically synthesised poly-3-ABA doped with 1 M HCl, and (d) electrochemically synthesised poly-3-ABA polymerised on Pt electrode with 1 M HCl.

There are a few overlapping bands in the broad region of  $1587\text{ cm}^{-1}$  observed for poly-3-ABA doped with 1 M HCl. This region is responsible for the CC deformation bands at the B rings and ring C=C Q stretching mode [192, 274]. The C-N stretching mode is detected at



1525  $\text{cm}^{-1}$  [274]. Q ring vibrational modes of C=N indicated the presence of Q diimine structures are given by a band at  $\sim 1487 - 1471 \text{ cm}^{-1}$ , a mixed mode  $\nu(\text{C=N})^+\text{Q}$  [274]. The band at  $1447 \text{ cm}^{-1}$  corresponds to the  $\text{C=N}^{*\text{+}}$  stretching mode of the Q units [201, 210].

### 4.3. Conclusions

These studies have shown that the synthesis of poly-ABA can be accomplished using either chemical or electrochemical methods. The data shows that chemical methods are suitable for large scale production, while electrochemical synthesis produces small quantities. The CVs of poly-ABA are different to that of pure PANI [232]. The decrease in conductivity observed from CVs are due to two possible reasons, 1) the presence of the strong intramolecular hydrogen bonding between the carboxylic acid groups and the cationic radical nitrogen atoms that gives rise to favourable six-membered chelates [202]. The movement of electrons is more localised in these structures, hence the adverse effect on conductivity [202]. 2) carboxylic acid groups generate steric effects, which are more likely to disrupt the overlapping of orbitals resulting in a lowering of the degree of conjugation, by forcing the aromatic rings out of plane relative to each other [202]. The intramolecular interaction between the carboxylic acid groups and the cationic radical nitrogen atoms are stronger [202].

Polymerisation of poly-ABA and its copolymer with aniline was successful under both chemical and electrochemical preparation methods, with the exception of chemically prepared poly-3-ABA doped with 1.5 M  $\text{H}_2\text{SO}_4$ . Results obtained from both GPC and FTIR suggest that oligomers are more likely to be the products of the polymerisation process for poly-3-ABA doped with 1.5 M  $\text{H}_2\text{SO}_4$ . The molecular weight could not be recorded and the FTIR bands observed appear to be more characteristic of monomer and oligomer rather than polymer. Chemical synthesis of poly-2-ABA prepared with either dopant, 1 M  $\text{H}_2\text{SO}_4$  and 1 M HCl, and poly-3-ABA showed better polymeric structure formation. The global grape morphology of poly-2-ABA prepared via chemical synthesis method showed similar FTIR spectroscopy regardless of the dopant used and GPC results were able to detect the molecular weight of the poly-2-ABA doped with 1 M  $\text{H}_2\text{SO}_4$  to be around 1634 and 557  $\text{g mol}^{-1}$ . Poly-3-ABA doped with 1 M HCl was measured to have similar molecular weight; however, the morphology of that polymer was more sponge-like. These four prepared polymers all showed excellent antimicrobial performance, with poly-2-ABA performing better in general against the two strains of bacteria tested *S. aureus* 6838 and *E. coli* 25922.

Electrochemical synthesis of poly-ABA was also carried out, also with two types of dopant. CVs indicate that all electrosynthesised poly-ABA have internal redox processes, and they tend to differ in shape when compared to that of PANI. The poly-2-ABA doped with 1 M HCl, which could not provide any molecular weight data of the polymer formed, showed redox properties from CV. When compared with electrochemically prepared polymer, the peaks observed were similar but were less well defined. In contrast, the poly-2-ABA polymer doped with H<sub>2</sub>SO<sub>4</sub> presents more intermediates in the polymerisation process and the polymer is degrading with the peak clearly seen at ~0.5 V vs Ag/AgCl. Moreover, similar observations have been made with poly-3-ABA doped with either dopant. In both cases, the electrochemically synthesised polymer showed greater number of intermediates and by-products formed. Due to the slow reaction rate of polymerisation with the carboxylic acid substituted aniline, electrochemical polymerisation was carried out on a platinum electrode. The hypothesis that the incorporation of aniline would increase the reaction rate significantly was proven to be correct. Poly-2-ABA tended to provide a more promising polymerisation; therefore, this process was investigated further using *in situ* Raman spectroelectrochemistry in Chapter Five in order to better understand the structures formed. The ability to grow a poly-ABA film was proven to be difficult therefore an attempt to explore copolymerisation options with the very potential antimicrobial poly-ABAs, with expected superior antifouling properties to pure PANI.

## CHAPTER FIVE: Structural studies of polyaniline and aniline-aminobenzoic acid copolymers

### 5.1. Abstract

PANI and its copolymers can occur in different oxidation states, which are strongly dependent on the surrounding environment as well as the preparation method. Polymers formed electrochemically on a Pt electrode were monitored by holding them at the external applied potential of interest. *In situ* Raman spectroscopy was carried out under a blue laser (488 nm) excitation line in an attempt to identify the structural changes in the polymers during redox processes under different conditions. PANI, along with its copolymers at different concentration ratios, was studied by initially forcing the polymer into its fully reduced state and gradually oxidising it at 0.1 V intervals. The electrochemical features observed are intrinsic properties of these macromolecular systems [192]. This model study offered a better understanding of the structures formed under different copolymer concentration ratios as well as at different applied potentials.

### 5.2. Results and Discussions

#### 5.2.1. *in-situ* Raman

Given the low reactivity rate for poly-2-ABA, it was impossible to carry out *in situ* Raman spectroelectrochemistry studies on this homopolymer. As the film is forced from the fully reduced to the fully oxidised state, the film experiences quite severe conditions, which proved to be too harsh for this fragile electrochemically synthesised polymer. Therefore, the following results are those of copolymers prepared at different monomer concentration ratios. Copolymers of varying monomer ratios were prepared by cycling the potential between -0.1 to 0.9/1.0 V at a scan rate of 50 mV s<sup>-1</sup> for 100 cycles. The whole range of ratios of different concentration was prepared (aniline:2-ABA): 9:1, 8:2, 7:3, 6:4, 5:5, 4:6, 3:7, 2:8 and 1:9. However, only the copolymers with the highest aniline concentration at 9:1 (aniline: 2-ABA), followed by 7:3 (aniline: 2-ABA), 6:4 (aniline: 2-ABA), 4:6 (aniline: 2-ABA), 3:7 (aniline: 2-ABA) and 1:9 (aniline: 2-ABA) are presented here, as the small changes in the ratio of monomers used were not sufficient to display major differences.



### 5.2.1.1. Polyaniline and aniline-aminobenzoic acid copolymers at 1:1 ratio

The *in situ* Raman spectra for electrochemically synthesised PANI and copolymer, Figure 5.1, were prepared by cycling the potential between -0.1 to 0.9 V at a scan rate of 50 mV s<sup>-1</sup> for 100 cycles before this spectroelectrochemical measurement experiment at various applied electrode potentials in the anodic direction. Studies shown in Chapter Three indicate that holding the potential at 1.0 V degrades the polymer and eventually leads to the formation of intermediates; hence a lower upper potential limit was used in this chapter. For this study the blue excitation line at 488 nm was used, which would aid in understanding the first and second oxidation process with changes in spectra, and allow the formation of PNB units to be observed accompanied by deprotonation of the polymer [57-58].

Under a relatively high electrode potential of ca. 1.0 V, PANI is in its fully oxidised form, thus, the Raman spectra contain contributions from PNB forms [193]. In solutions of low pH, a protonated oxidised form of sulfonated PANI should be predominant, whereas for solutions of higher pH studied, the Raman spectra probably contain contributions from the corresponding base forms [115].

Within the wavenumber region ranging from 1520 to 1620 cm<sup>-1</sup>, C-C and C=C stretching vibrations of B and Q rings are most prominent (Figure 5.1). The presence of both types of these rings in an oxidised form of the copolymer is evidenced by two Raman bands located at approx. 1635 and 1595 cm<sup>-1</sup>, corresponding to C-C and C=C stretching vibrations.

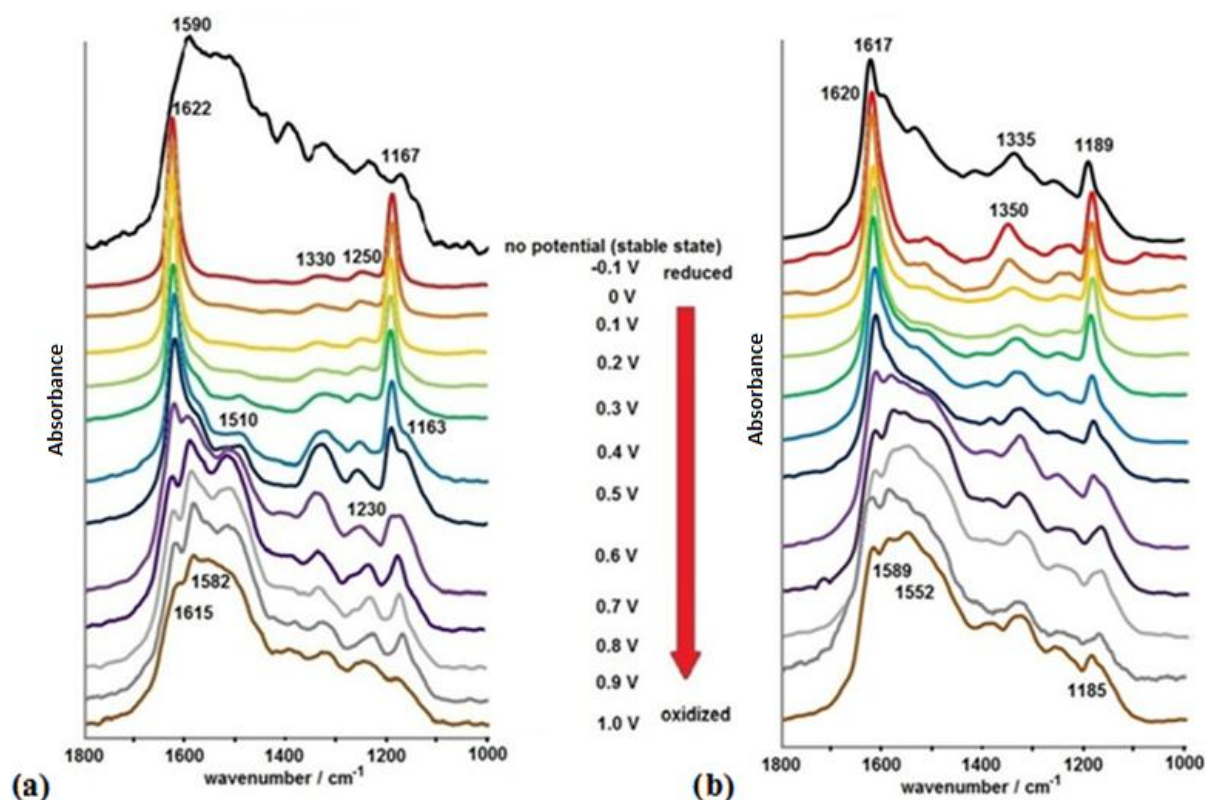


Figure 5.1. *in situ* Raman spectra of electrochemically synthesised (a) PANI and (b) PANI-co-2-ABA (1:1) copolymer at different applied potentials for 25 mins in 1 M HCl solution obtained with  $\lambda = 488$  nm. The PANI film was prepared by cycling the potential between -0.10 and 1.0 V at a scan rate of  $50 \text{ mV s}^{-1}$  in a solution containing 0.1 M aniline and 1 M HCl solution. The copolymer was prepared in the presence of 1:1 of 0.05 M aniline: 0.05 M 2-ABA in 1 M HCl electrolyte solution.

The 2D synchronous correlation map given below in Figure 5.3 is the symmetric in-phase change of bands, and show which bands increased and decreased at the same time, as the electrode potential was varied. The asynchronous correlation map shown in Figure 5.4 is asymmetric out-of-phase where one band increase and the other decreases at a different rate. The spectra from Figure 5.1 were plotted against each other to produce the 2D synchronous correlation map (Figure 5.3), the diagonal red line signifies the point where two spectra cross one another, which means that all bands observed on the red line must be ignored as these are overlapped areas of the spectra. The changes in these peaks are concentrated mostly in the region of  $\sim 1650 - 1100 \text{ cm}^{-1}$ , hence studies are focused on this region despite the fact that the whole region of  $2000 - 200 \text{ cm}^{-1}$  was measured.

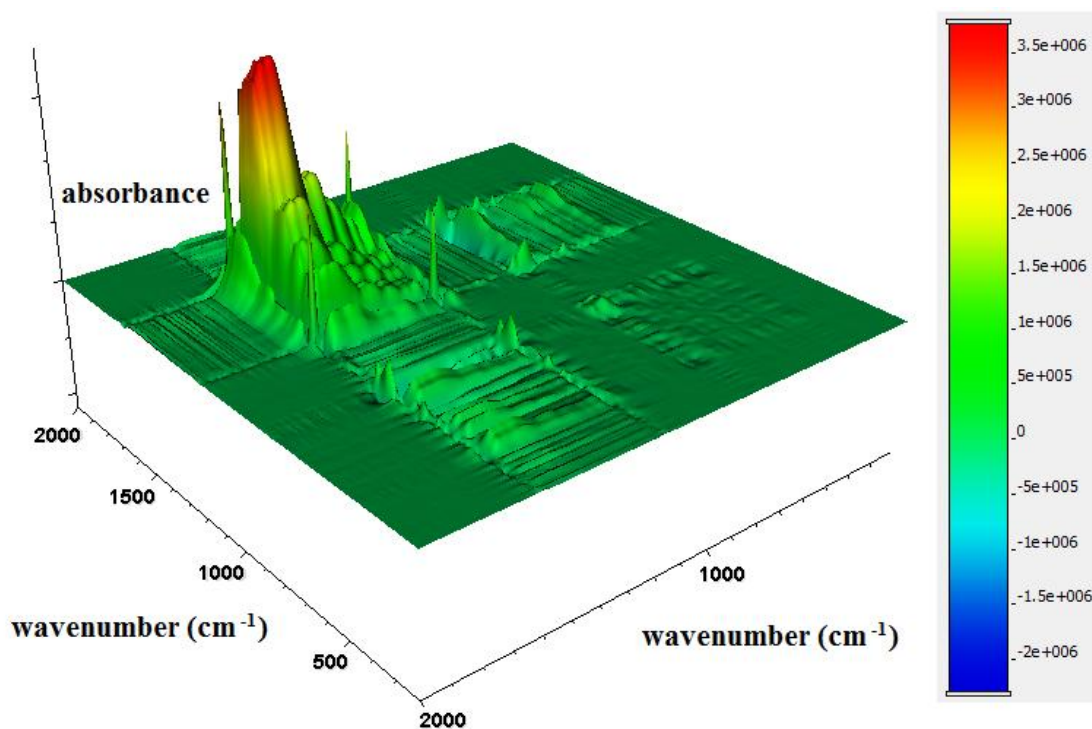


Figure 5.2. 2D synchronous correlation map of PANI in 1 M HCl electrolyte with combined spectra at different applied potentials.

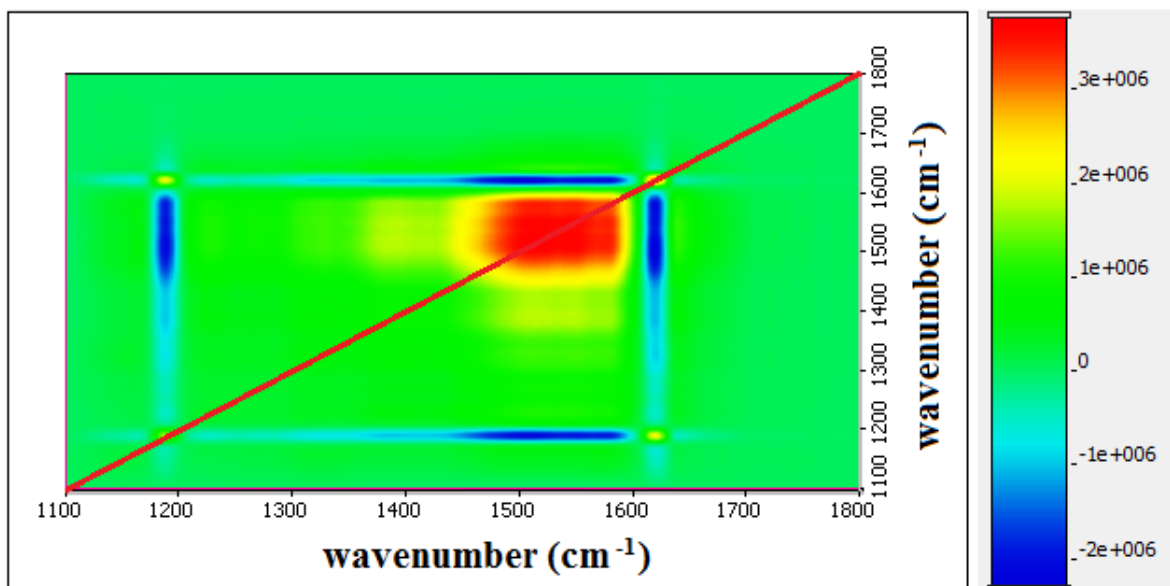


Figure 5.3. 2D synchronous correlation map of PANI in 1 M HCl electrolyte with combined spectra at different applied potentials.

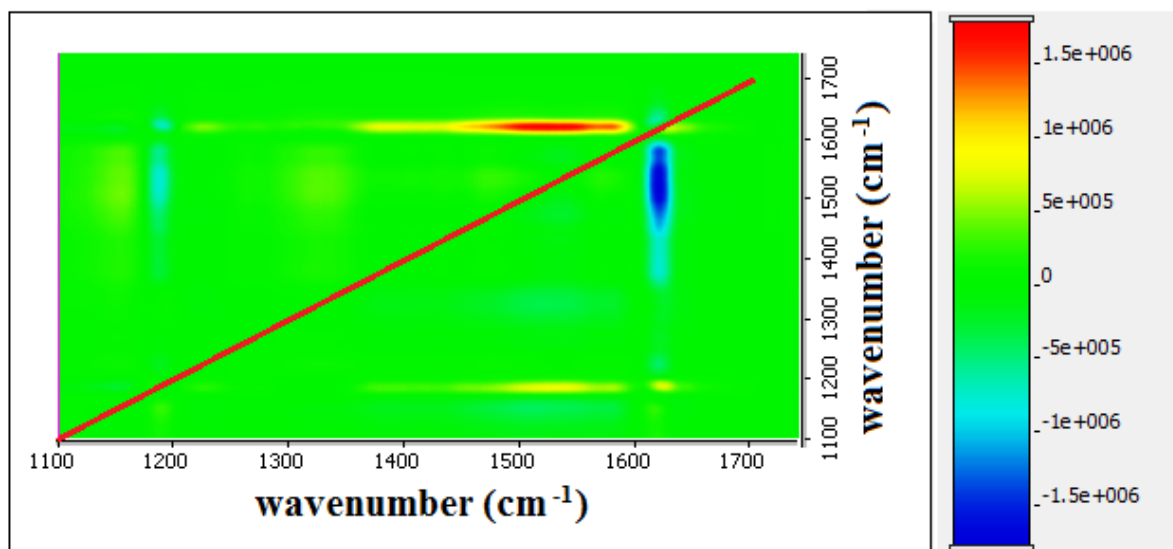


Figure 5.4. 2D asynchronous correlation map of PANI in 1 M HCl electrolyte with combined spectra at different applied potentials.

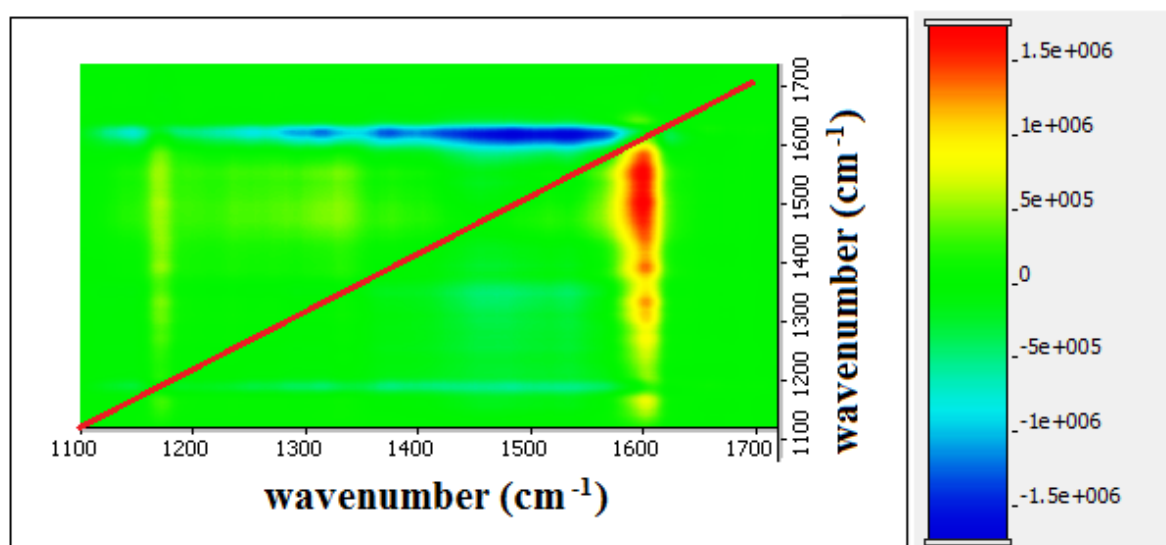


Figure 5.5. 2D asynchronous correlation map of PANI-co-2-ABA (1:1) in 1 M HCl electrolyte with combined spectra at different applied potentials.



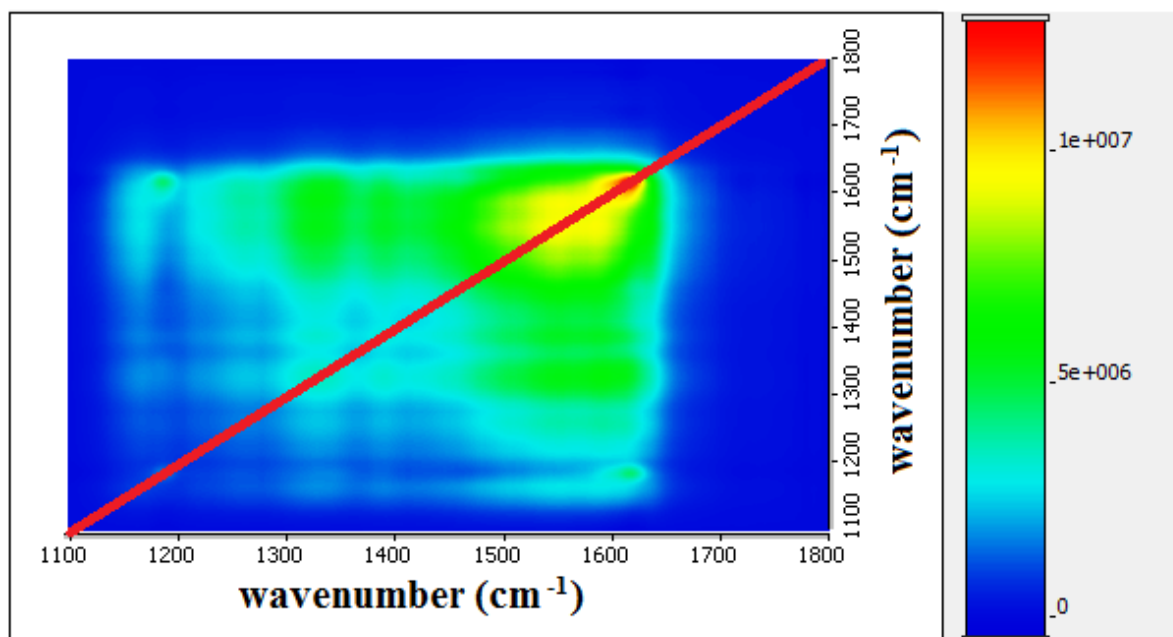


Figure 5.6. 2D synchronous correlation map of PANI-co-2-ABA (1:1) in 1 M HCl electrolyte with combined spectra at different applied potentials.

For PANI at -0.1 V, a potential below the onset of the first oxidation, two peaks at 1190 and 1622  $\text{cm}^{-1}$  were observed and can be assigned to C-H in plane bending and C-C stretching deformations in B-type rings [57-58]. The band at 1622  $\text{cm}^{-1}$  was observed as the reduced form of PANI continued to change, while the band at 1250  $\text{cm}^{-1}$  shifts to lower wavenumber with oxidation. Upon the second oxidation process, SQ radical segments undetectable by Raman spectroscopy became unstable and deprotonated to give oxidised units in this basic form shown in Figure 5.7 [57-58]:

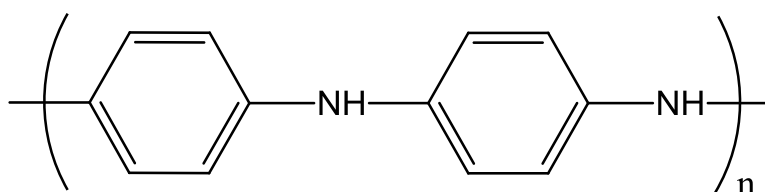


Figure 5.7. Oxidised unit of PANI.

The second oxidation indicated growth of three peaks characteristic of unprotonated Q rings at 1230  $\text{cm}^{-1}$  ( $>\text{C}-\text{N}<$  stretching), at 1470  $\text{cm}^{-1}$  ( $>\text{C}=\text{N}$  stretching) and 1585  $\text{cm}^{-1}$  ( $-\text{C}=\text{C}-$  stretching in the Q ring) [57-58]. The peak at 1510  $\text{cm}^{-1}$  is the characteristic Q-type segments band. The five stretching modes, which must appear for semi-quantitative utilisation of



spectra, are the peak at  $\approx 1612\text{ cm}^{-1}$  ascribed to the stretching vibration of the B rings [202, 203]. The stretching vibrations at  $\approx 1595\text{ cm}^{-1}$  and  $\approx 1490\text{ cm}^{-1}$  are assigned to the C=N groups and the Q rings respectively and indicate the presence of imine groups. During this oxidation, a singlet at  $1622\text{ cm}^{-1}$  corresponding to C-C ring-stretching in Q segments splits into a doublet at  $1585$  and  $1615\text{ cm}^{-1}$  ascribed to C-C stretching deformation in B rings [57-58]. The peak at  $1170\text{ cm}^{-1}$  due to C-H in-plane deformations ascribed to B and Q structures [57-58].

B ring dominant peaks were seen at  $1193\text{ cm}^{-1}$  ascribed to ring C-H bending,  $881\text{ cm}^{-1}$  to ring-breathing,  $675\text{ cm}^{-1}$  for ring-CH-bending, out of plane and  $604.5\text{ cm}^{-1}$  for ring-deformation [193]. Two of the three SQ radical structures in the spectral region of  $1300 - 1400\text{ cm}^{-1}$  showed blue shifts to ca.  $1379$  and  $1408\text{ cm}^{-1}$  [57-58]. The peak at  $\approx 1330\text{ cm}^{-1}$  can be ascribed to the stretching vibration of  $-\text{C}-\text{N}^{*+}$ - groups and corresponds to the presence of polarons. The broad  $1330\text{ cm}^{-1}$  band represents the four different C-N stretching environments, the nitrogen peak deconvolution corresponds to protonated or non-protonated amine and imine sites and another C-N stretching inside a polaron lattice [57-58, 193]. The stability of the sharp  $1341\text{ cm}^{-1}$  polaron band was seen up to  $0.50\text{ V}$ , then this band generally appears broad, extending from  $1310$  to  $1340\text{ cm}^{-1}$  with at least two sub-bands [202, 203]. These bands are used as diagnostic of SQ radical structure and do not appear in other forms of PANI [57-58]. The C=N stretching deformations band ascribed the presence of Q units and is well separated from the  $1500\text{ cm}^{-1}$  band [57-58]. The peak at  $1330\text{ cm}^{-1}$  is characteristic of the protonated SQ radical structure [57-58]. Charge localisation and delocalisation modified the Q ring stretching.

The very complicated spectra of PANI are caused by the presence of excitons, which are the coexistence of B and Q rings stretching, but if the delocalisation was fully occupied it would lead to a polaron lattice [12]. The minor peak at  $1400\text{ cm}^{-1}$  correlating to  $-\text{N}=\text{N}-$  mode, which relates to the formation of head-to-head coupling during voltammetric cycling, indicates damage to the polymerised film [12].

In brief, as PANI was being oxidised from the fully reduced form ( $-0.1\text{ V}$ ) to  $1\text{ V}$ , and the following was observed:

- $\nu(\text{C-C})$  benzene band at  $\sim 1622\text{ cm}^{-1}$  shifted to a lower wavenumber with broadening due to environment change.

- the C-H band at  $\sim 1167\text{ cm}^{-1}$  and C-C band at  $\sim 1622\text{ cm}^{-1}$  changed from a singlet to a doublet with an increase in the applied potential.

The spectra of PANI at 0.1 V associated with the reduced form of polymer suggested the presence of para-disubstituted benzene rings shown by the strong bands at  $1167 - 1191\text{ cm}^{-1}$  and  $1622 - 1626\text{ cm}^{-1}$  (Figure 5.1). A strong band at  $1624\text{ cm}^{-1}$  has been observed as a reduced form of PANI with blue laser excitation (457.9 nm), which ensured a strong pre-resonance for the B structure present in the reduced form of the polymer. The increase in the proportion of partially oxidised radical cations formed in the polymer could be monitored by the intensity of the bands at  $1167\text{ cm}^{-1}$  and  $1580\text{ cm}^{-1}$ . The lack of a strong band in the  $1470 - 1487\text{ cm}^{-1}$  region is consistent with the absence of Q diimine units in the fully oxidised polymer.

At potentials between 0.15 – 0.20 V (pale yellow films), the spectra correspond to LEB; a single polaron is stable at  $1330\text{ cm}^{-1}$  and is present throughout the range of potentials, increasing to a maximum at 500 mV and then decreasing again [202, 203]. From 0.25 to 0.35 V (green films), the increasing oxidation of polymer was followed with the C=N band at  $\approx 1500\text{ cm}^{-1}$  [202, 203]. Between 0.30 and 0.55 V, the polaron peak is still increasing in the ring stretching range leading to broadening and overlapping of bands, i.e. the band at  $1622\text{ cm}^{-1}$  changed from singlet to a doublet [202, 203]. At around 0.60 V the formation of a blue film can be observed, while at 0.75 V a PNB base without a polaron peak and an almost colourless form of LEB stable at a low potential of -0.10 V was obtained [202, 203]. The observed weak broad peak of  $1325\text{ cm}^{-1}$  at 0.80 V corresponds to the protonated SQ radical structure [57-58]. This observation of PNB base is spontaneous deprotonation of PANI occurring during the oxidation of EB to PNB in the experiments. As the polymer is scanned from the reduced to the oxidised form, more peaks were observed and there was more overlapping of bands in the spectra as the polymer was oxidised.

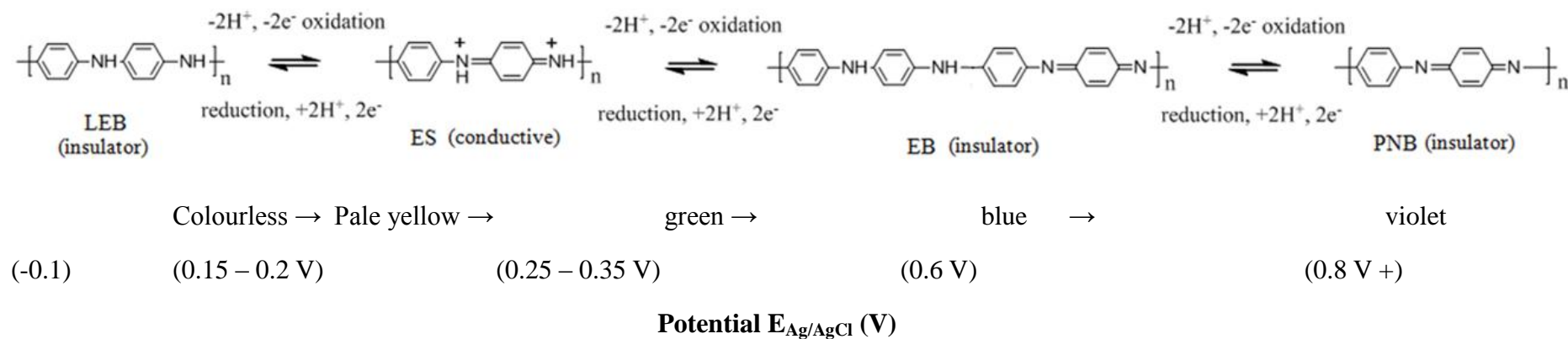
At an applied potential at 0.30 V, the band at  $1620\text{ cm}^{-1}$  to  $1618\text{ cm}^{-1}$  shifted. Under a relatively high electrode potential of ca. 0.8 V, PANI is in its oxidised form, thus, the Raman spectra contain contributions from both EB and PNB forms [193]. In solutions of low pH, a protonated oxidised form of sulfonated PANI should be predominant, whereas for solutions of higher pH studied, the Raman spectra probably contain contributions from the corresponding base forms [193]. The stability of the sharp  $1341\text{ cm}^{-1}$  polaron band was detected up to 0.50 V, with the band generally appearing broad, extending from 1310 to

1340  $\text{cm}^{-1}$  with at least two sub-bands [202, 203]. The band at 1622  $\text{cm}^{-1}$  continued to change, while the band at 1250  $\text{cm}^{-1}$  oxidises and shift to lower energy.

Within the wavenumber region ranging from 1520 to 1620  $\text{cm}^{-1}$ , C-C and C=C stretching vibrations of B and Q rings were most prominent. The presence of both types of these rings in an oxidised form of copolymer is evidenced by two Raman bands located at approx. 1635 and 1595  $\text{cm}^{-1}$ , corresponding to C-C and C=C stretching vibrations. Among all bands,  $\nu_{\text{CC}}$  and  $\beta_{\text{CH}}$  of benzene rings appear to be effective in establishing the type of PANI formed. ES at 1616  $\text{cm}^{-1}$  and 1181  $\text{cm}^{-1}$ , LEB at 1618  $\text{cm}^{-1}$  and 1181  $\text{cm}^{-1}$ . The Raman spectra of EB and of PNB forms of PANI related to Q rings, most representative are  $\nu_{\text{C=N}}$  (ca. 1490  $\text{cm}^{-1}$  for  $\lambda = 632.8 \text{ nm}$ ), and  $\nu_{\text{C=C}}$  (ca. 1600  $\text{cm}^{-1}$  for  $\lambda = 632.8 \text{ nm}$ ) [202, 256]. The band at 1325  $\text{cm}^{-1}$  indicates the conductive form of PANI (ES), assigned to C-N $^{\bullet+}$  stretching of SQ radicals [55].

Electrochemical oxidation of LEB or protonation of EB forms leads to protonated PANI which exhibits a SQ radical and displays conductivity. Protonation of PNB and EB by an internal redox process also generates these radicals.

## PANI in 1M HCl

Table 5.1. Band assignments of Raman spectra of PANI obtained with  $\lambda = 488$  nm.

Initial	-0.1 V	0 V	0.1 V	0.2 V	0.3 V	0.4 V	0.5 V	0.6 V	0.7 V	0.8 V	0.9 V	1.0 V	description of vibrations
1591-1550	1622	1623	1622	1621	1622	1620	1621	1620	1617	1617	1622	1609	C-C stretching [9]
	1540	1542										1584	C-C stretching [9]
1446													C-C stretching Q [9]
1400	1419	1414	1425					1410				1446	C-C stretching Q [9]
1325	1326	1331	1332	1331	1320	1325	1325	1340	1328	1332	1328	1325	protonated structure [9]
1240	1245	1247	1247	1247	1250	1255	1256	1250	1234	1230	1230	1240	C-N stretching (X-sens) [9]
1175	1187	1187	1190	1190	1190	1190	1190	1190	1171	1172	1171	1175	C-H bending [9]

Table 5.2. Band assignments of Raman spectra of 1 M HCl copolymer at 1:1 obtained with  $\lambda = 488$  nm.

Initial	-0.1 V	0 V	0.1 V	0.2 V	0.3 V	0.4 V	0.5 V	description of vibrations
1620	1621	1621	1621	1621				C-C stretching [57, 58]
1588								>C=C< stretching [57]
1532	1533	1536	1540					C-C stretching [57, 58]
1414	1417							C-C stretching Q [57, 58]
1336	1351	1349	1345	1335				protonated structure [57]
1260	1228	1233	1245	1245				C-N stretching [57, 58]
1189	1186	1187	1189	1190				C-H bending [57, 58]

### 5.2.1.2. Copolymers prepared with two different dopants

However, before exploring further the different copolymers at different monomer ratios, the use of electrolyte for the *in situ* Raman spectroelectrochemistry was investigated. Rather than studying this using PANI, the copolymer was of more interest, hence the process was investigated with the copolymers at a 7:3 ratio (aniline: 2-ABA) doped with two different dopants, either HCl or H<sub>2</sub>SO<sub>4</sub>, as shown in Figures 5.8 and 5.13 below. The formed polymer film on Pt electrode was forced to the reduced form at -0.1 V and then, as the voltage being applied was gradually increased, oxidising the polymer at 0.1 V intervals. The stable film was the one with no applied potential and was collected before the start of the *in situ* Raman spectroelectrochemistry study.

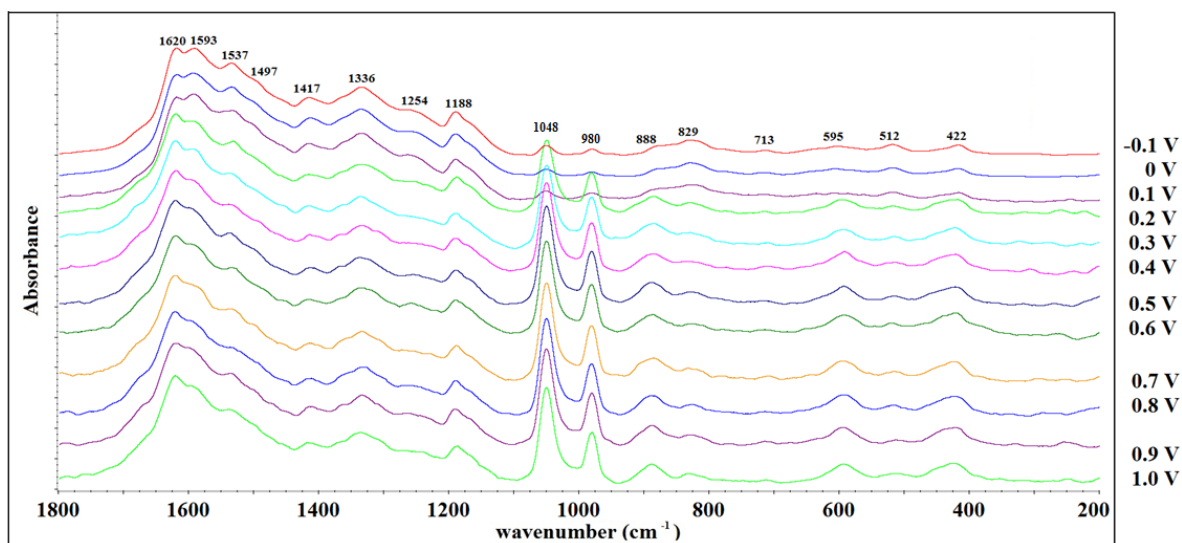


Figure 5.8. PANI-co-2-ABA (7:3, aniline: 2-ABA) on a Pt electrode in 0.5 M H<sub>2</sub>SO<sub>4</sub> electrolyte.

wavenumber	assignment
1619	C-C stretching in B rings
(1619 - 1616)	1650 - 1520 cm <sup>-1</sup> C-C & C=C stretching vibration of B & Q type rings
1592 - 1588	C=C stretching in Q rings
1529	1520-1210, C-N, C=N (1490) & C~N <sup>+</sup> ; ~ intermediate bond between a single and double stretching vibrations
1416	C-C stretching in Q
1330	C~N <sup>+</sup> stretching in polaronic form (polarons), indicating emeraldine salt form of PANI
1260	C-N stretching of Q rings
1251	C-N stretching in EB (amines)
1200-1100	C-H bending vibrations of B or Q type rings
1187	C-H bending in LE salt
1048*	C-H bending in B
980*	B deformation
886	B deformation
829	Amine deformation C-N-C bending
771	ring deformation Q [57]
712	imine deformation [57]
597	Ring deformation B [57]

[55, 57, 58] \*the presence of S=O from the electrolyte

Table 5.3. Assignments of bands from Figure 5.8.

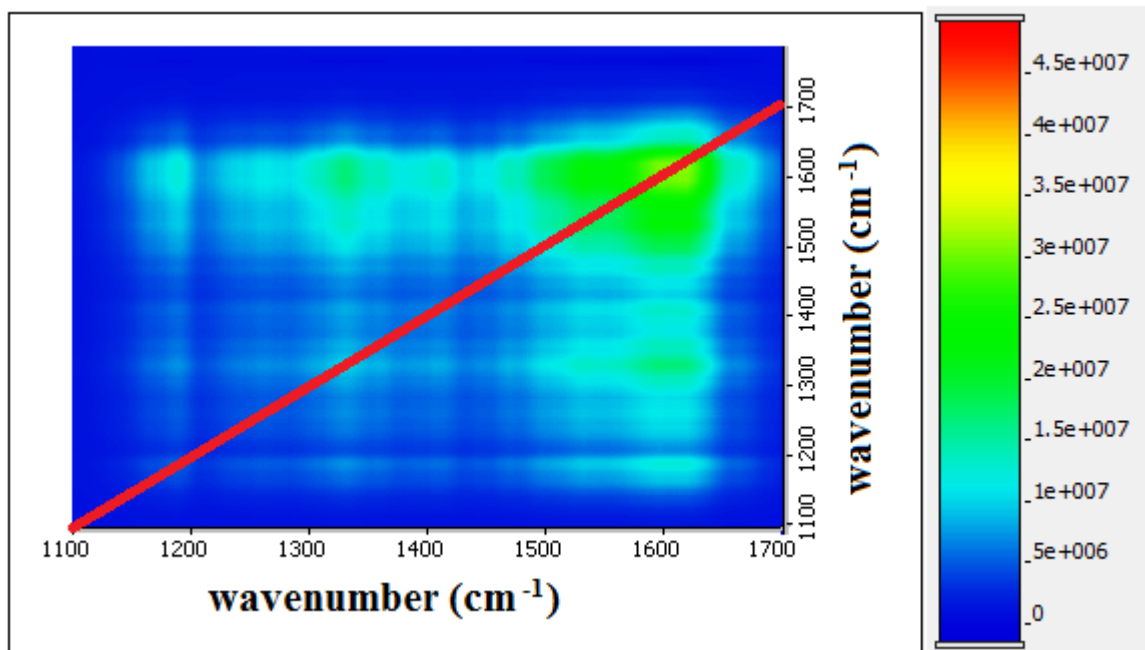


Figure 5.9. 2D synchronous correlation map of PANI-co-2-ABA (7:3, aniline: 2-ABA) in 0.5 M  $\text{H}_2\text{SO}_4$  electrolyte with combined spectra at different applied potentials.

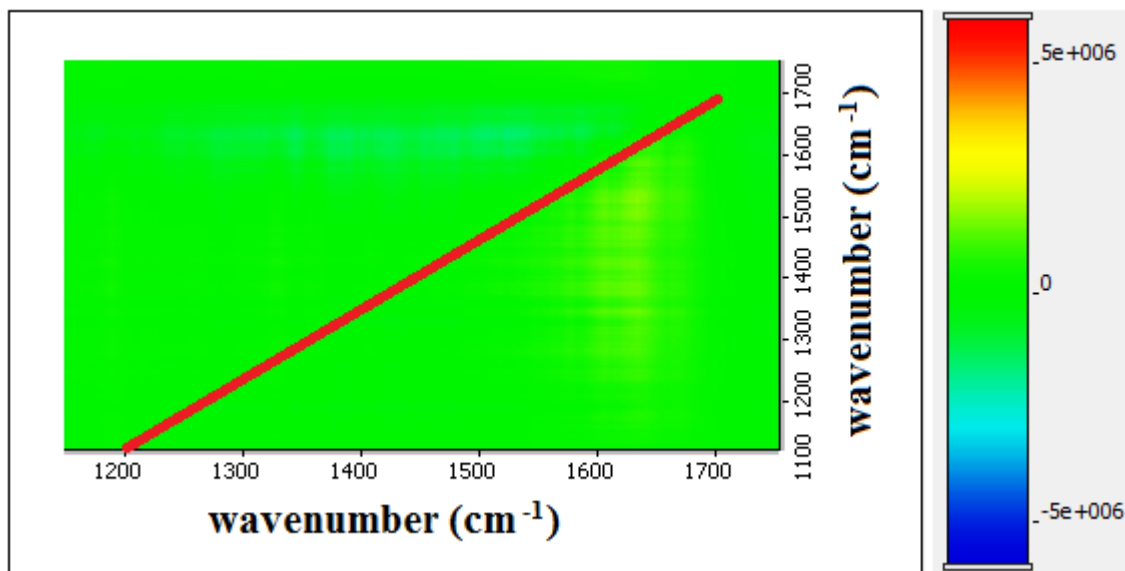


Figure 5.10. 2D asynchronous correlation map of PANI-co-2-ABA (7:3, aniline: 2-ABA) in 0.5 M  $\text{H}_2\text{SO}_4$  electrolyte with combined spectra at different applied potentials.

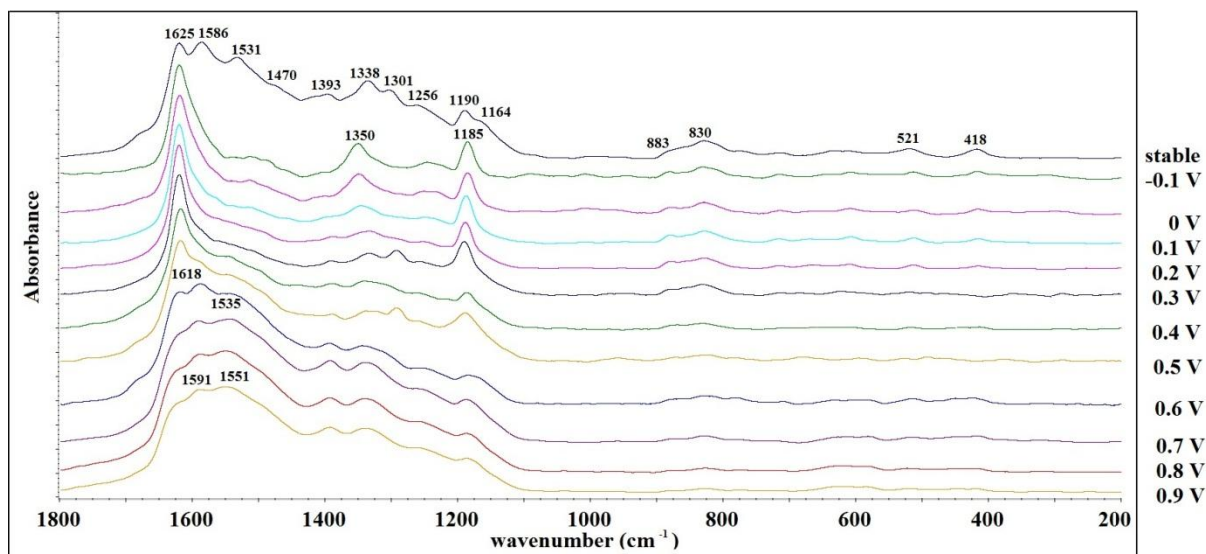


Figure 5.11. PANI-co-2-ABA (7:3, aniline: 2-ABA) on a Pt electrode in 1 M HCl electrolyte.

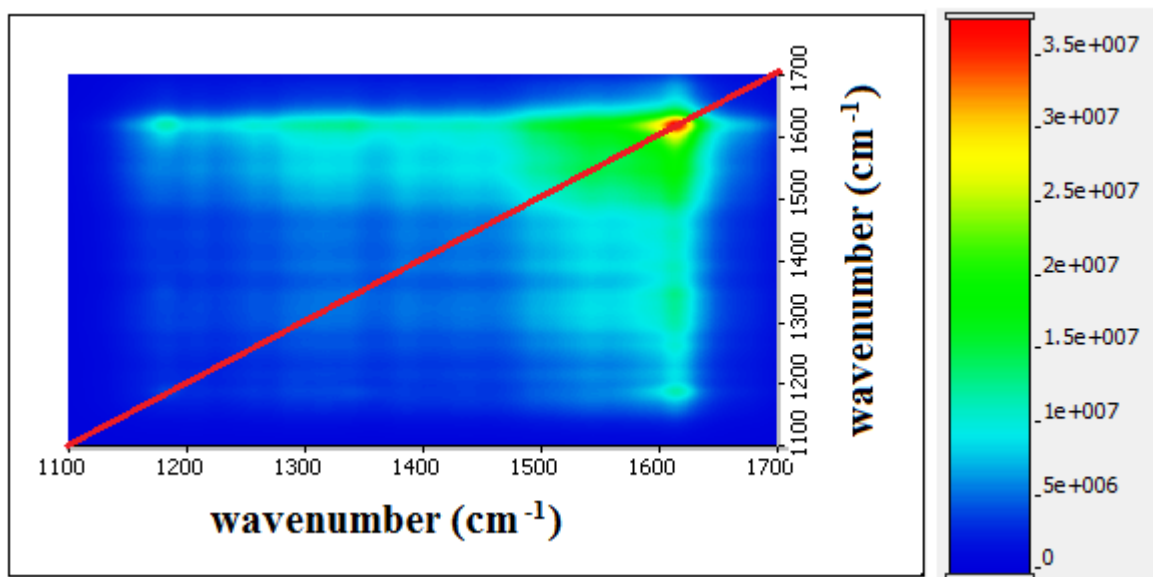


Figure 5.12. 2D synchronous correlation map of PANI-co-2-ABA (7:3, aniline: 2-ABA) in 1 M HCl electrolyte with combined spectra at different applied potentials.



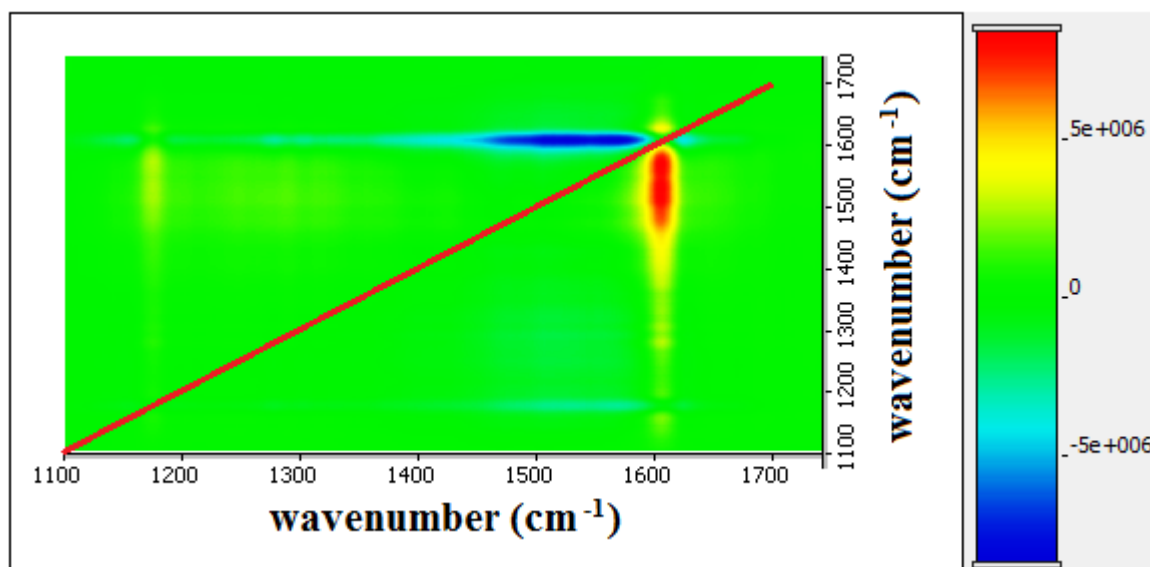


Figure 5.13. 2D asynchronous correlation map of PANI-co-2-ABA (7:3, aniline: 2-ABA) in 1 M HCl electrolyte with combined spectra at different applied potentials.

The peak absorption ratio in the region of  $1650 - 1500 \text{ cm}^{-1}$  is characteristic of the C-C stretching in B and Q rings. Although the same copolymer was used and the only difference was the dopant used, the peaks appear quite different for the two sets of spectra in Figures 5.8 and Figure 5.13 when the film was being oxidised from the fully reduced state of  $-0.1 \text{ V}$  to  $0.9/1.0 \text{ V}$ . Therefore in the remaining study of copolymers prepared at different ratios, all of the analyses were performed using HCl as the electrolyte rather than  $\text{H}_2\text{SO}_4$ . Moreover, there were bands observed at around  $1048$  and  $980 \text{ cm}^{-1}$  ascribed to the S=O [275] which could possibly be from the electrolyte, hence later *in situ* Raman spectroelectrochemistry only HCl was used as the electrolyte.

For the PANI-co-2-ABA at 7:3 ratio in 1 M HCl, the peak at  $1590 \text{ cm}^{-1}$  ascribed to the C-C stretch of PANI salt form began to grow at/after  $0.4 \text{ V}$  and, according to Figure 5.11, as this peak increases the bands around  $1600 - 1450 \text{ cm}^{-1}$  spontaneously decrease at the same time. The characteristic C-C stretch of the Q ring at  $1622 - 1430 \text{ cm}^{-1}$  changed from a singlet to a doublet with broadening due to numerous overlapping bands at  $0.6 \text{ V}$  and beyond (till  $0.8 \text{ V}$ ). The shoulder of the  $\sim 1391 \text{ cm}^{-1}$  band at  $1350 \text{ cm}^{-1}$  assigned to protonated structure began to grow into a peak and became more intense at  $0.6 \text{ V}$  and above. The formation of a singlet to doublet suggests the conversion of C-N<sup>+</sup> stretching polaronic form, to the C-C stretching in Q ring (Figure 5.12, symmetric peak formation). The broadening and eventually decrease of the

1188  $\text{cm}^{-1}$  peak assigned to the C-H bending could be due to the change in environment upon oxidation.

### 5.2.1.3. Copolymers at different monomer concentrations

For the electrochemically synthesised PANI-co-2-ABA at 9:1 (aniline: 2-ABA) doped with 1 M HCl electrolyte the bands begin to change the most at 0.4 V in the *in situ* Raman spectra.

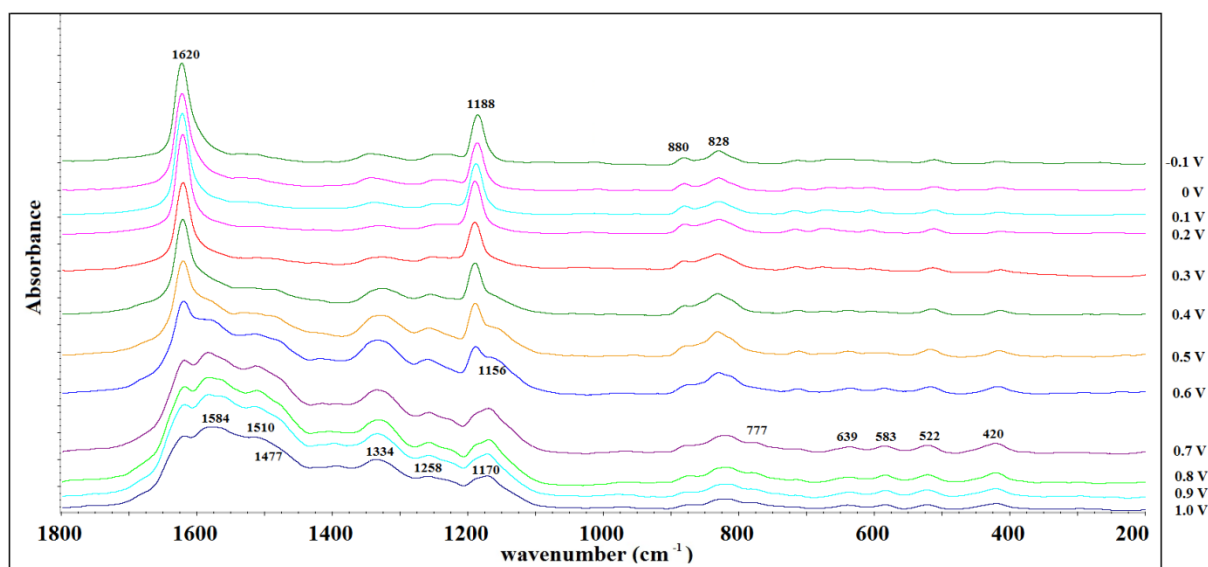


Figure 5.14. *in situ* Raman spectra of electrochemically synthesised PANI-co-2-ABA at 9:1 (aniline: 2-ABA) 1 M HCl electrolyte.

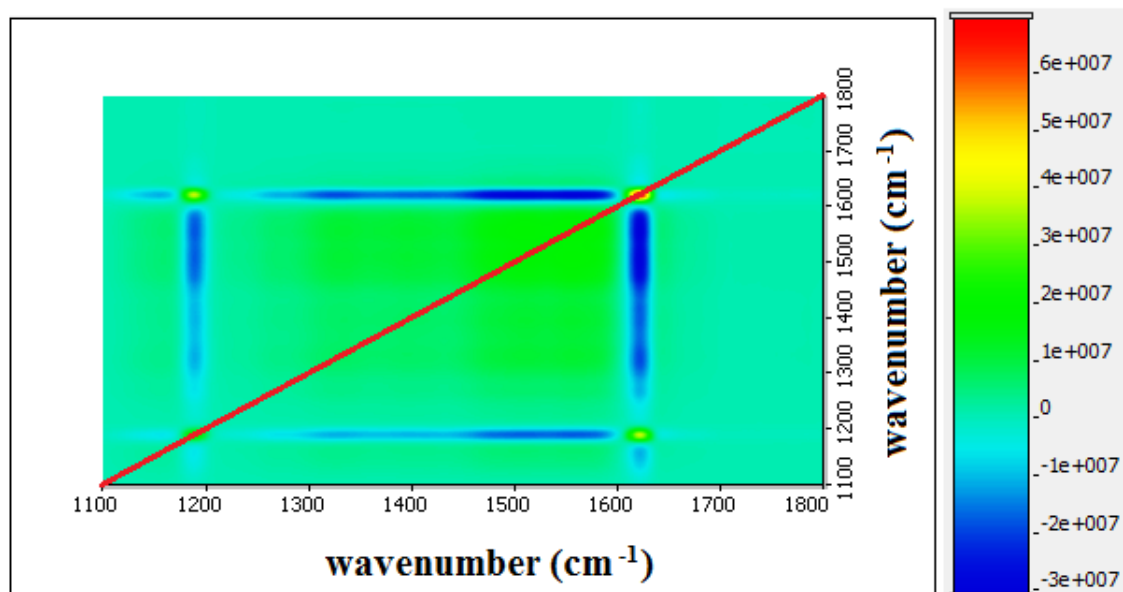


Figure 5.15. 2D synchronous correlation map of PANI-co-2-ABA at 9:1 in 1 M HCl electrolyte with combined spectra at different applied potentials.

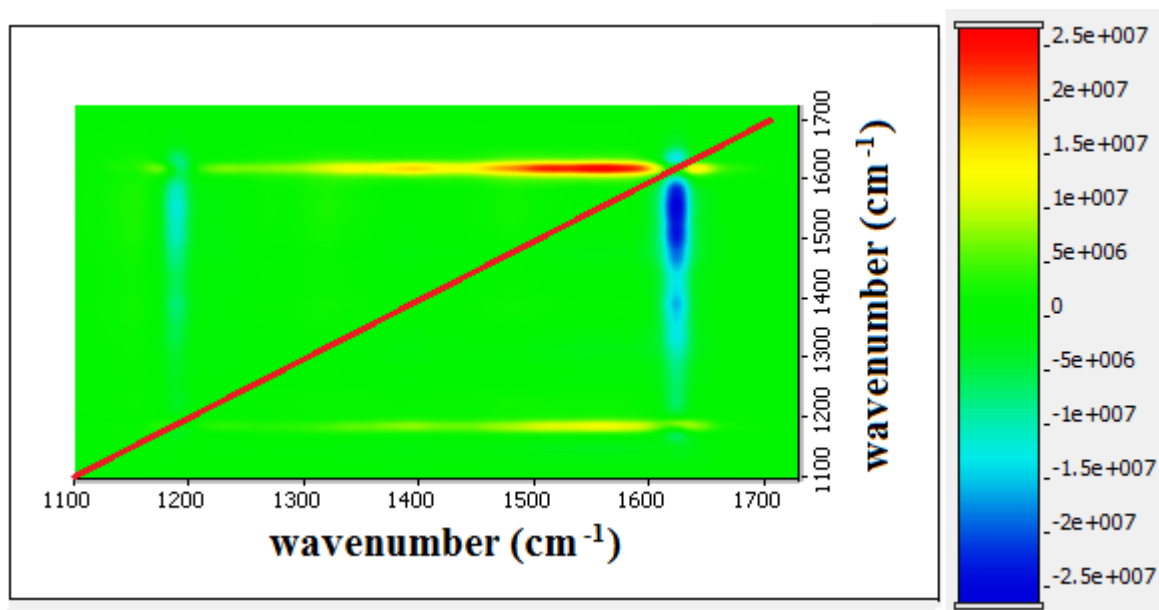


Figure 5.16. 2D asynchronous correlation map of PANI-co-2-ABA at 9:1 in 1 M HCl electrolyte with combined spectra at different applied potentials.

The singlet  $1620\text{ cm}^{-1}$  band assigned to the C-C stretching deformations in benzenoid-type rings [57, 58] overlapped with another newly formed band at  $1584\text{ cm}^{-1}$ , which correlates to the  $\text{-C=C-}$  stretching in the quinoid ring and it occurs for both the symmetric and asymmetric direction according to Figures 5.15 and 5.16. This remained the same at 0.5 V, but at 0.6 V this new band characteristic of the  $\text{-C=C-}$  stretching in quinoid ring showed a greater absorption than that of the C-C stretching deformations, suggesting that more  $\text{-C-C-}$  were converted to  $\text{-C=C-}$ , therefore it could be concluded that the oxidation was occurring. Similar observations were made with the bands at  $1188\text{ cm}^{-1}$  and  $1156\text{ cm}^{-1}$ , due to C-H in-plane deformations ascribed to benzenoid and quinoid structures. The increase in absorption in the  $1620\text{ cm}^{-1}$  band corresponded to C-C ring-stretching in quinoid segments splitting into a doublet at  $1584$  and  $1620\text{ cm}^{-1}$  ascribed to C-C stretching deformation in B rings [57, 58]. In general, the whole region of  $1600$  and  $1420\text{ cm}^{-1}$  consists of many overlapping bands. More overlapping and the formation of new bands was also observed around  $1334 - 1170\text{ cm}^{-1}$ , and those spectra correspond to LEB; a single polaron is stable at  $1334\text{ cm}^{-1}$  and is present throughout the range of potentials. However, this polaron has a maximum increase at  $\sim 0.6\text{ V}$  and then it decreases [202, 203].

Similarly the bands described above for 9:1 ratio copolymers are seen in other copolymers at different ratios, but the changes occur at slightly different applied potential. For copolymers

at the highest aniline concentration of 9:1 ratio, the observable oxidation change can be determined by the peak change at 0.4 V. As the aniline monomer concentration decreases, the applied potential required to oxidise the copolymer increases, i.e. at 6:4, 5:5 and 4:6 ratio it is at 0.6 V, as seen in Figures 5.1, 5.17 and 5.20.

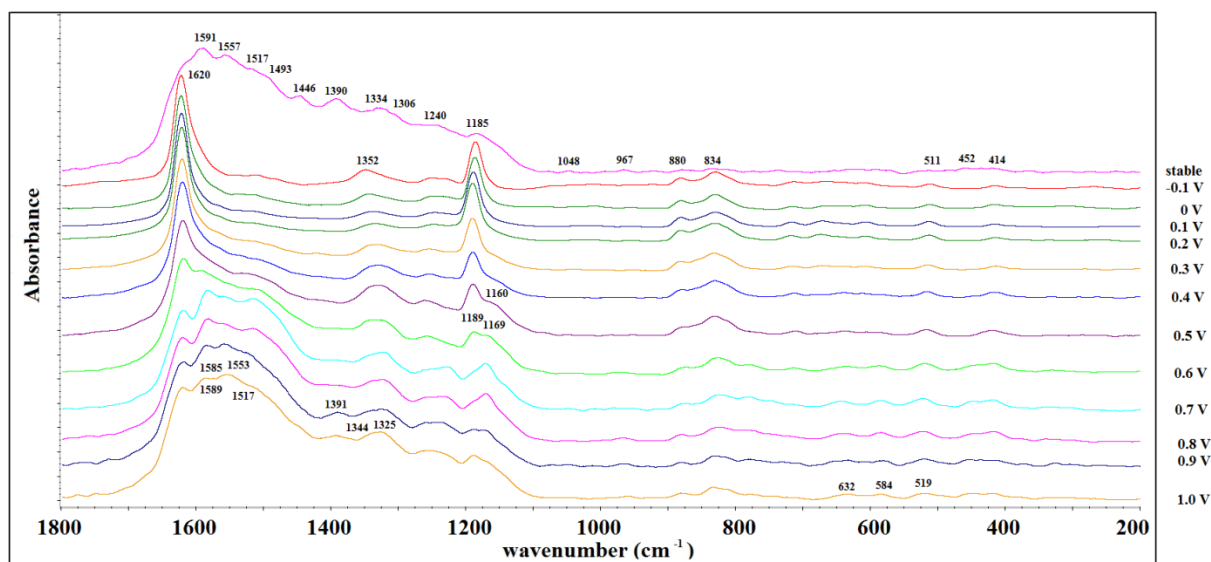


Figure 5.17. *in situ* Raman spectra of electrochemically synthesised PANI-co-2-ABA at 6:4 (aniline: 2-ABA) in 1 M HCl electrolyte.

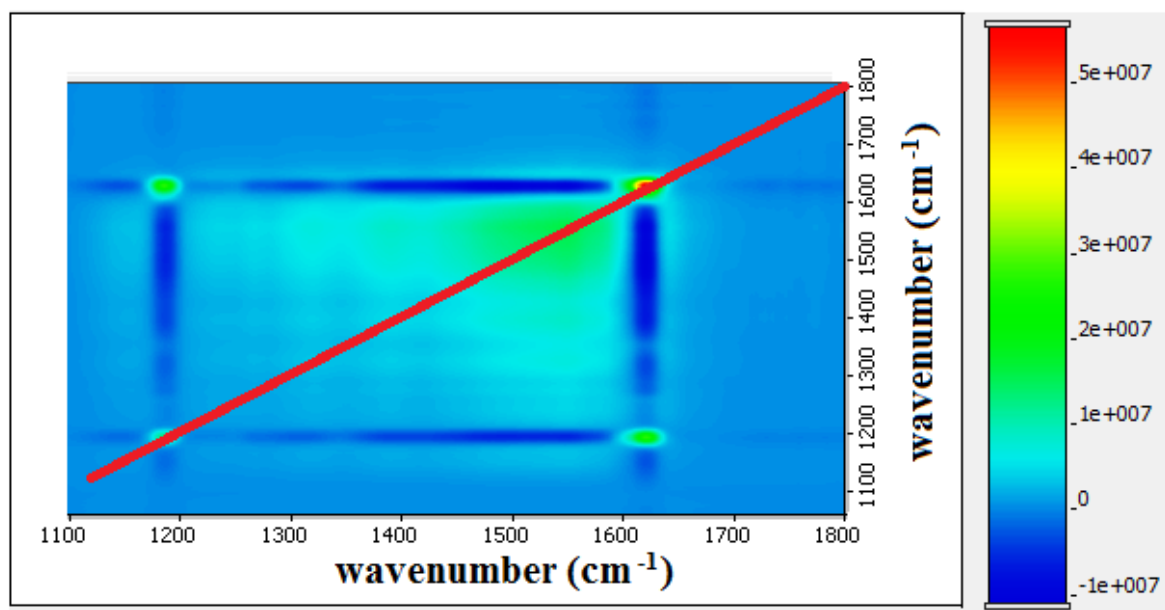


Figure 5.18. 2D synchronous correlation map of PANI-co-2-ABA at 6:4 in 1 M HCl electrolyte with combined spectra at different applied potentials.

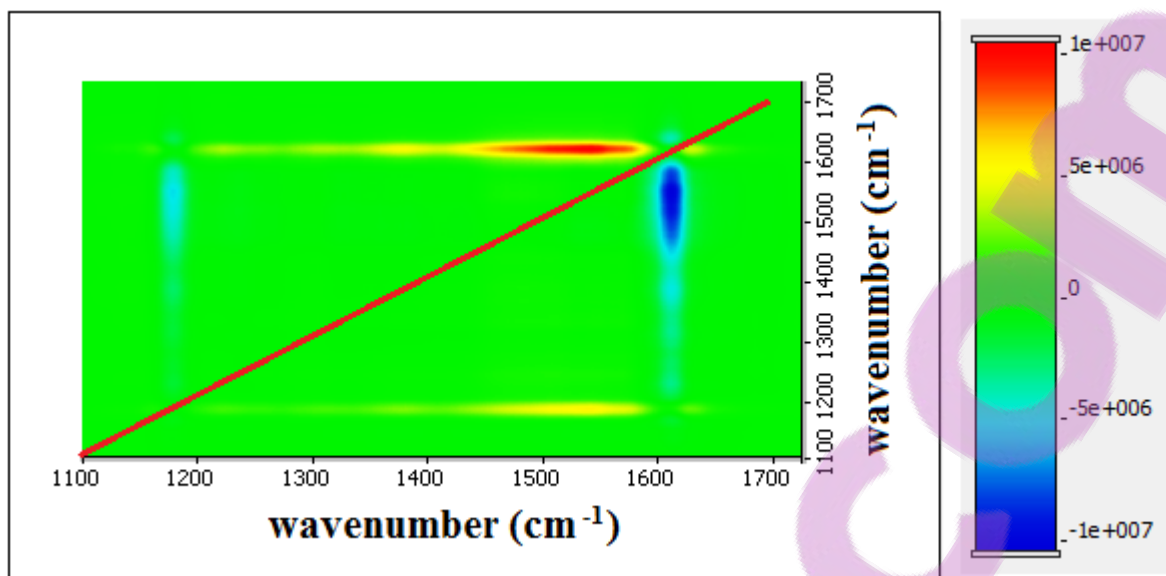


Figure 5.19. 2D asynchronous correlation map of PANI-co-2-ABA at 6:4 in 1 M HCl electrolyte with combined spectra at different applied potentials.

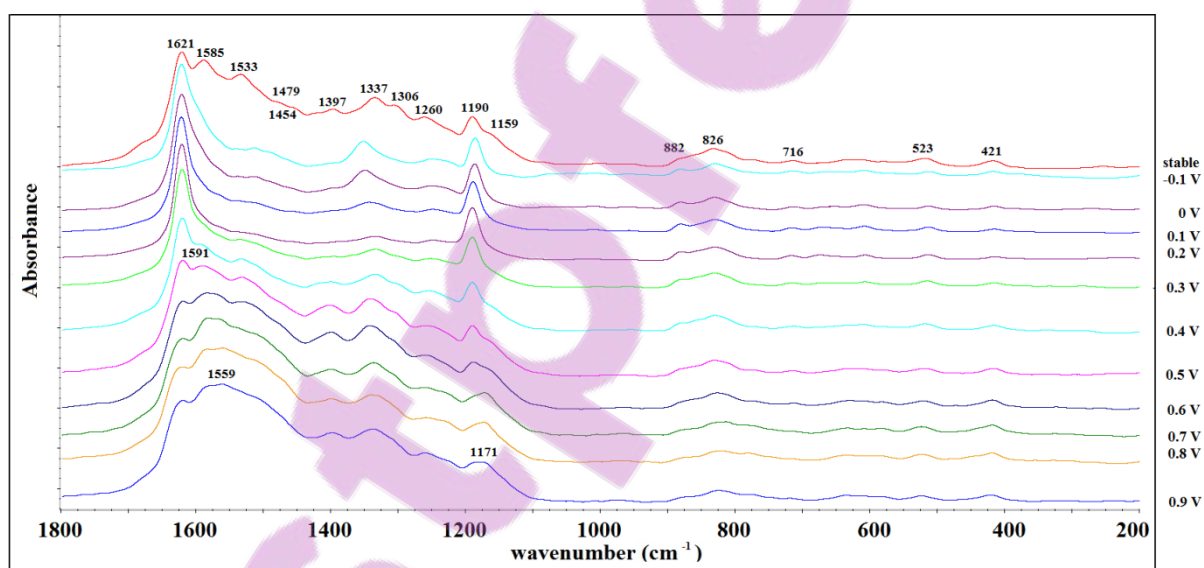


Figure 5.20. *in situ* Raman spectra of electrochemically synthesised PANI-co-2-ABA at 4:6 (aniline: 2-ABA) in 1 M HCl electrolyte.

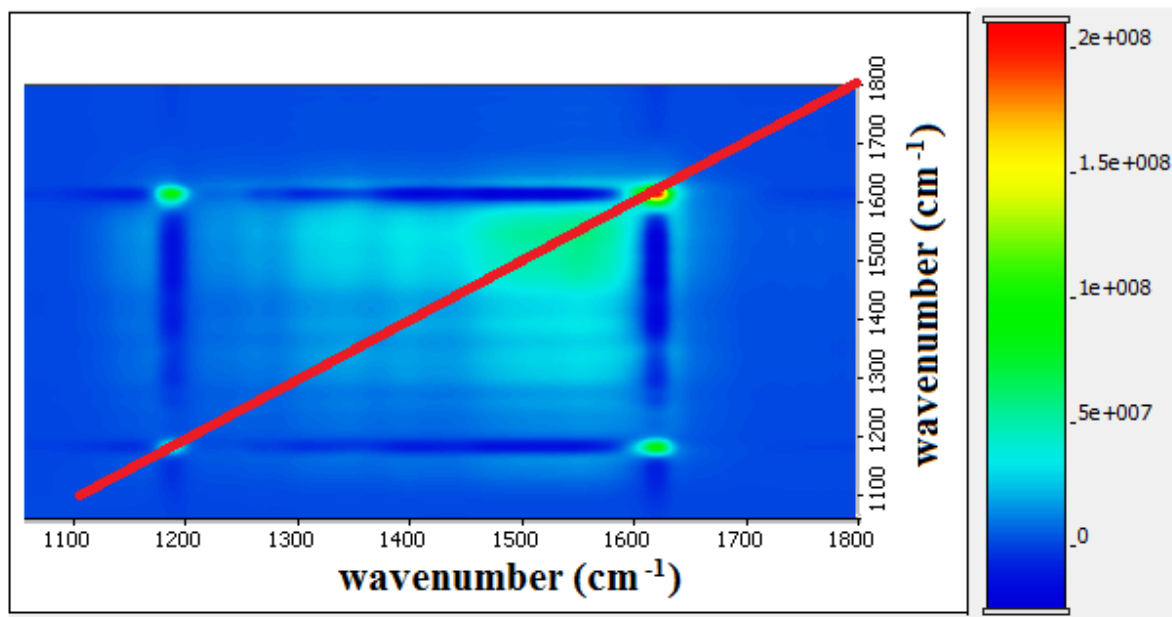


Figure 5.21. 2D synchronous correlation map of PANI-co-2-ABA at 4:6 in 1 M HCl electrolyte with combined spectra at different applied potentials.

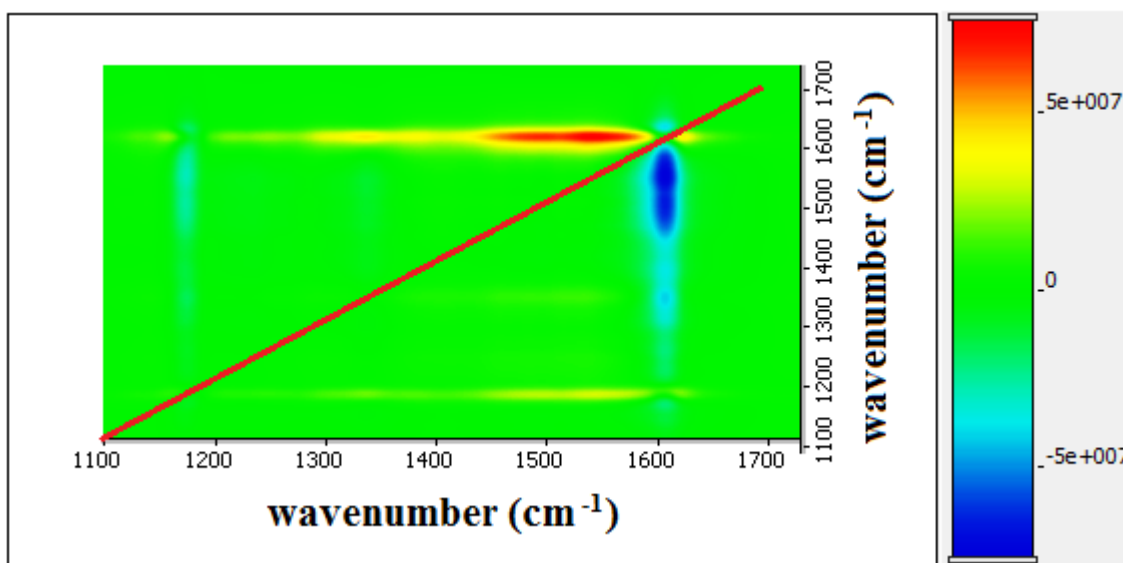


Figure 5.22. 2D asynchronous correlation map of PANI-co-2-ABA at 4:6 in 1 M HCl electrolyte with combined spectra at different applied potentials.

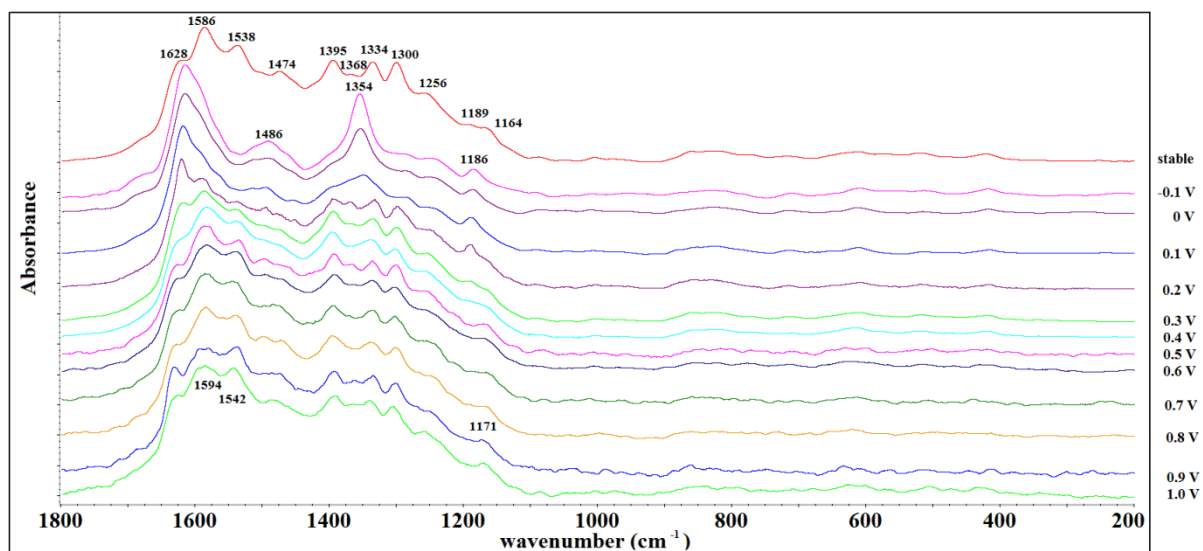


Figure 5.23. *in situ* Raman spectra of electrochemically synthesised PANI-co-2-ABA at 3:7 (aniline: 2-ABA) 1 M HCl electrolyte.

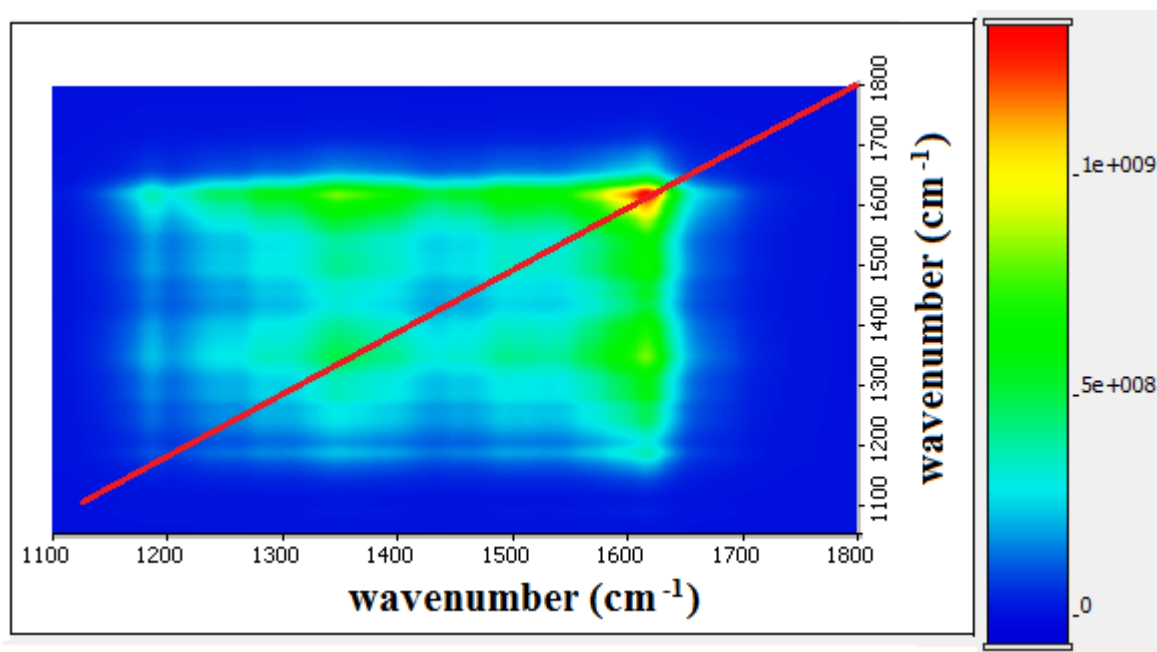


Figure 5.24. 2D synchronous correlation map of PANI-co-2-ABA at 3:7 in 1 M HCl electrolyte with combined spectra at different applied potentials.



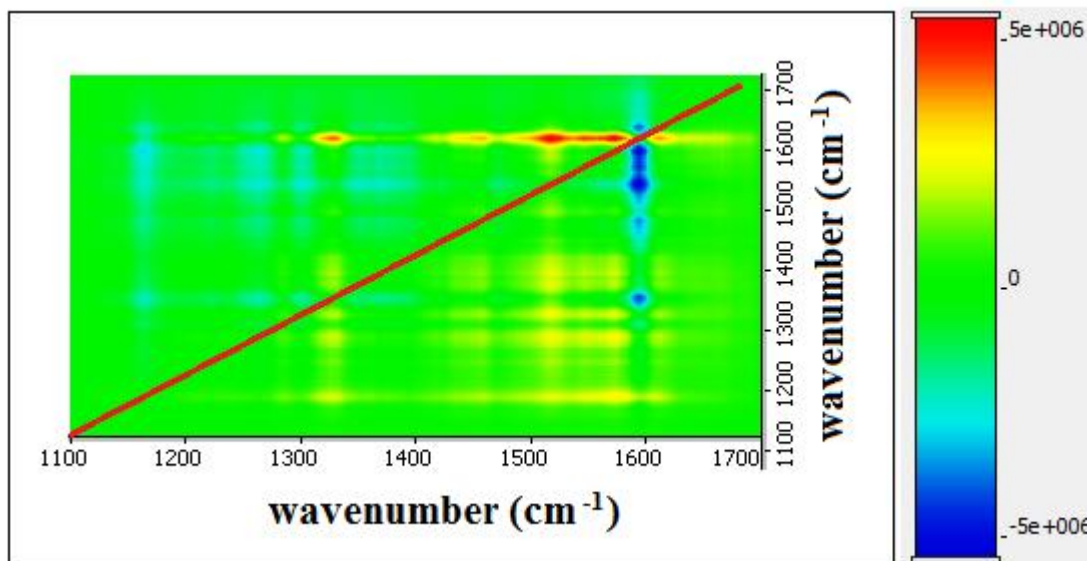


Figure 5.25. 2D asynchronous correlation map of PANI-co-2-ABA at 3:7 in 1 M HCl electrolyte with combined spectra at different applied potentials.

The observations related to changes in bands wavenumber, formation of new peaks and shifts are similar for all 6:4, 4:6, 7:3 and 3:7 ratio copolymers (Figures 5.11 – 5.13 and Figures 5.17 – 5.25), with the only noticeable differences being the absorption values. As the aniline concentration decreased relative to 2-ABA, so did the intensity of the absorption peak, apart from cases when the change of ratio was not significant enough to show dramatic differences between the copolymers formed.

The oxidation reaction had occurred at 0.2 V, as indicated by the growth of the 1588, 1536 and 1490  $\text{cm}^{-1}$  peaks correlating to the  $-\text{C}=\text{C}-$  stretching in the Q ring in the 3:7 ratio copolymer. As the increase in potential continued, the band at 1622  $\text{cm}^{-1}$  ascribed to C-C stretching deformation in B rings decreased in absorption and shifted to a higher wavenumber after 0.3 V. The 1515  $\text{cm}^{-1}$  band ascribed to the C=N stretching deformations indicative of the presence of Q units disappeared after 0.1 V and the singlet at 1491  $\text{cm}^{-1}$  turned into a doublet at 1450 and 1473  $\text{cm}^{-1}$ , which was caused by modes of the Q structure. The C-N stretching of the SQ radical state grew in intensity at 1355  $\text{cm}^{-1}$ , and changed from a singlet at -0.1 V into a doublet of 1386 and 1335  $\text{cm}^{-1}$  at 0 V. The oxidation characteristic peak of C-H stretching of Q rings in the polymer matrix at 1163  $\text{cm}^{-1}$  grew with increased applied potential. This corresponded to C-H in-plane deformations to B and Q structures formed at 0.2 V (1300  $\text{cm}^{-1}$ ) derived from the earlier band of 1283  $\text{cm}^{-1}$ .



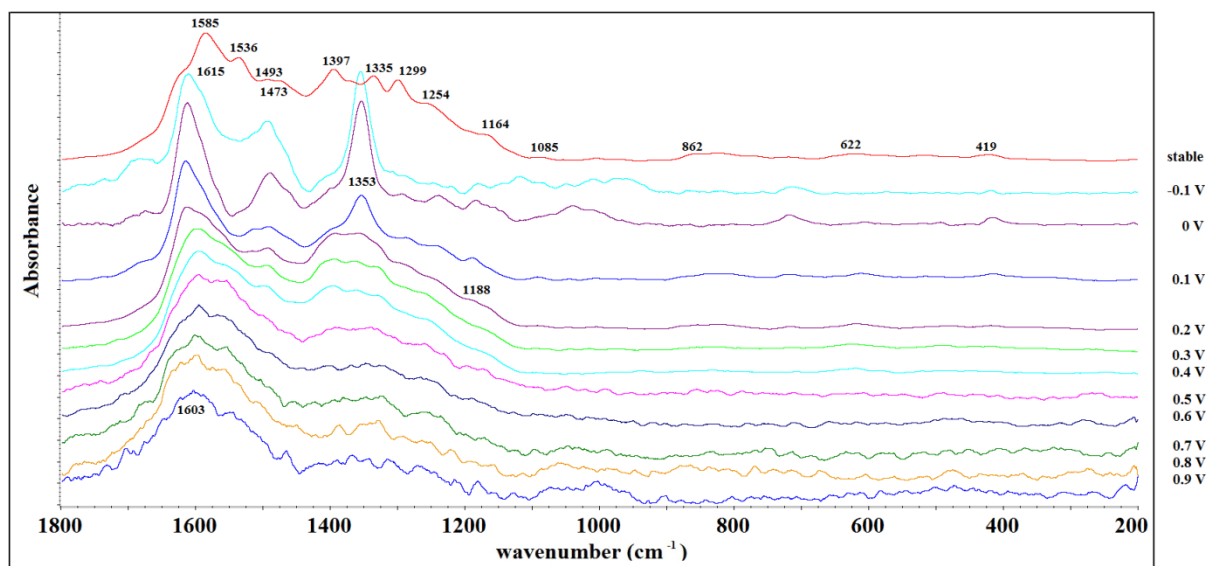


Figure 5.26. *in situ* Raman spectra of electrochemically synthesised PANI-co-2-ABA at 1:9 (aniline: 2-ABA) 1 M HCl electrolyte.

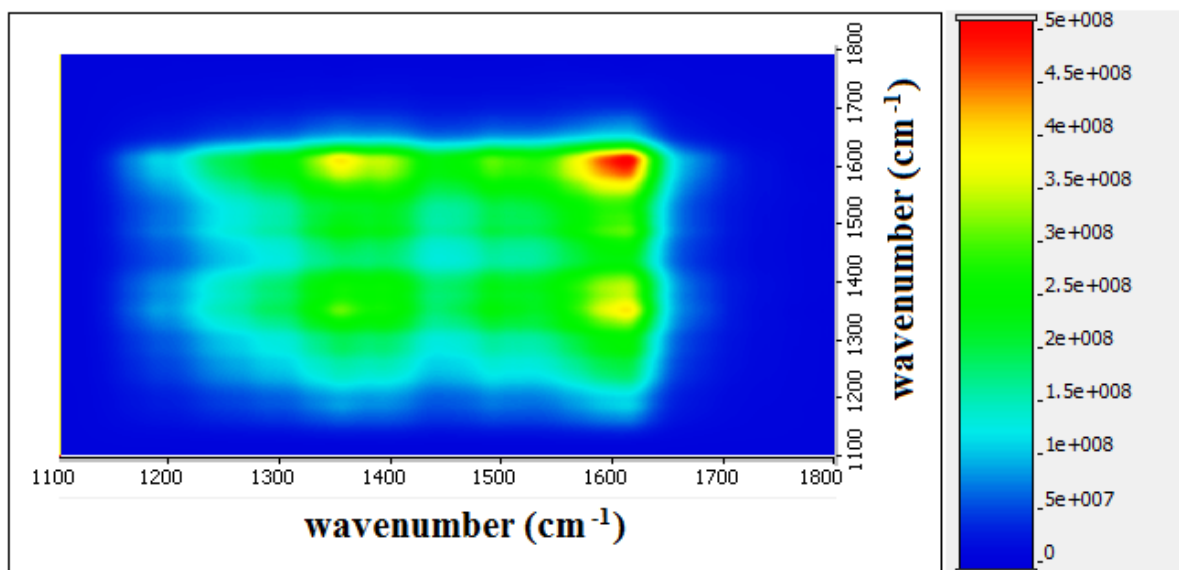


Figure 5.27. 2D synchronous correlation map of PANI-co-2-ABA at 1:9 in 1 M HCl electrolyte with combined spectra at different applied potentials.

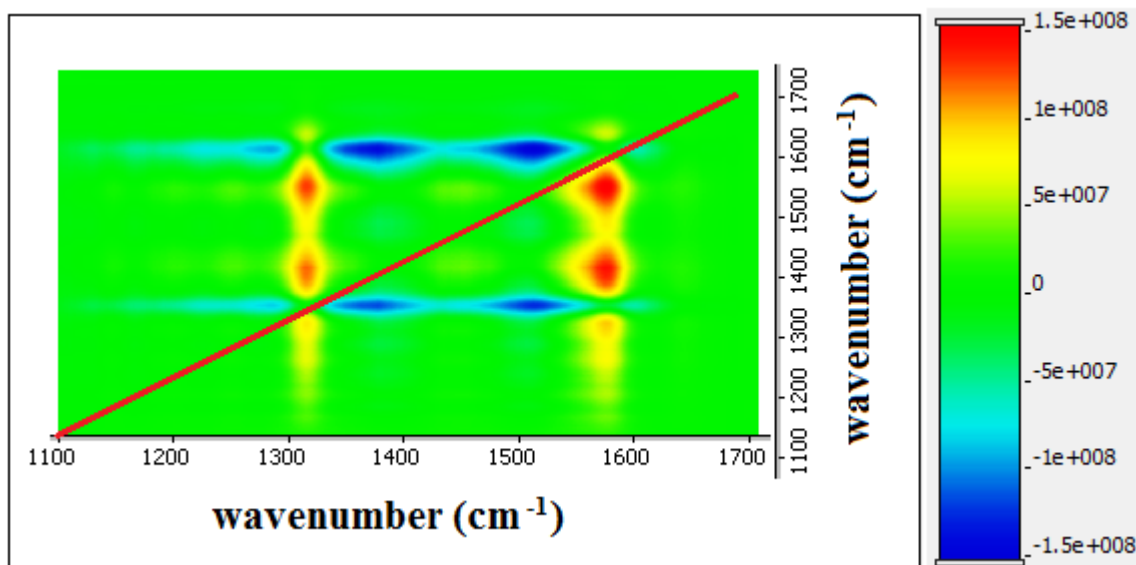
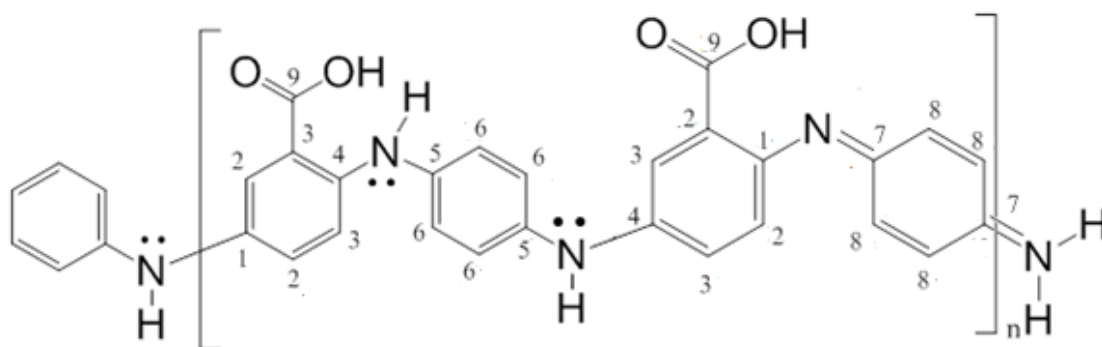


Figure 5.28. 2D asynchronous correlation map of PANI-co-2-ABA at 1:9 in 1 M HCl electrolyte with combined spectra at different applied potentials.

### 5.2.2. SSNMR

It was near impossible to prepare enough samples for SSNMR analysis for the ABA homopolymers due to its very low reactivity rate, hence only the copolymer of aniline and ABA polymer were analysed. Both chemically and electrochemically synthesised copolymers of aniline with 2-ABA were prepared for analysis. The spectra were obtained by using the CPMAS and NQS technique shown below in Figures 5.29 – 5.31.



Scheme 5.1. Poly-co-2-ABA structure.

Seven overlapping and broad resonances that are characteristic for PANI were observed at 115 (shoulder), 122, 125, 137, 140, 148 and 158 ppm [215]. The electrochemically synthesised copolymer peaks observed in Figure 5.29 were broadened significantly compared to the chemically synthesised polymer, which suggests that the chemical environments were quite different, and that more resonances were present with the electrochemically synthesised copolymer. The peak at 122 ppm is broad and consists of several resonances, due to the different chemical environment of C2 and C3 carbons [276]. Peaks at 137 ppm and 158 ppm originate from protonated C-8 and non-protonated C-7 carbons respectively in the Q structure of the copolymer. The peaks at 140 ppm and 147 ppm are associated with C4, 5 and C1 non-protonated carbons respectively. The small peak at around 170 ppm shown in Figure 5.29(c) is a characteristic peak assigned to the carboxylic acid group. This C=O peak was observed at a higher ppm in the electrochemically synthesised copolymer at 175 – 180 ppm. The use of different oxidants and concentrations of dopant, as shown in Figures 5.29(a) – (c), demonstrate that there are slight differences in the position of the resonance, hence the broadening of peaks. However, the overall general characteristic peaks are observed. On the other hand, when comparing chemically and electrochemically synthesised copolymers, Figures 5.29(a) – (c) versus Figures 5.29(d) and 5.29(e), the peaks observed from the copolymer prepared via electrochemistry were not as well-defined as those of the chemically prepared polymer. This suggests that the electrochemically prepared polymer formed a greater polymer variety, which resulted in greater exposure to wider range of chemical environments, hence the observed overlap and broadening of bands. As observed earlier from CVs, this indicates that electrochemical synthesis tends to generate more intermediate and cross-branching products, hence more overlapping of peaks is expected, as shown in Figures 5.29(d) and 5.29(e).

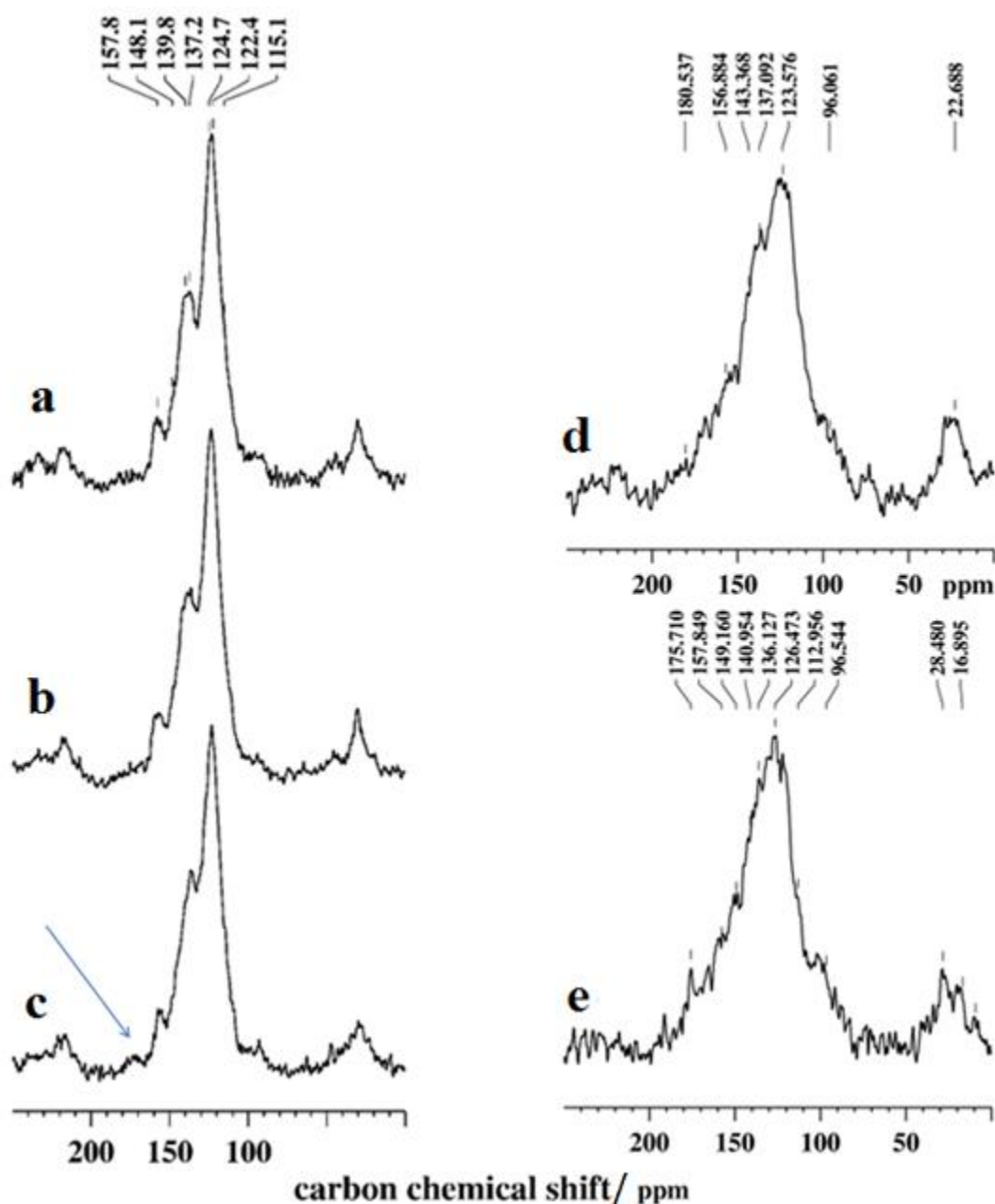


Figure 5.29. Cross-polarisation spectra of copolymer (a) chemical 1.5 M  $\text{H}_2\text{SO}_4$  with  $\text{KIO}_3$ , (b) chemical 1.5 M  $\text{H}_2\text{SO}_4$  with APS, (c) chemical 0.5 M  $\text{H}_2\text{SO}_4$  with APS, (d) electrochemical 1.5 M  $\text{H}_2\text{SO}_4$ , and (e) electrochemical 0.5 M  $\text{H}_2\text{SO}_4$ .

Broadening of peaks could also be brought upon by local fluctuations in conformational and configurational geometries, as well as distributions in chain packing [243--244]. To exclude the possibility of this occurring, an NQS experiment was carried out, which allowed the protonated carbon resonances to be partially suppressed, so that the nonprotonated carbons dominate the spectra.

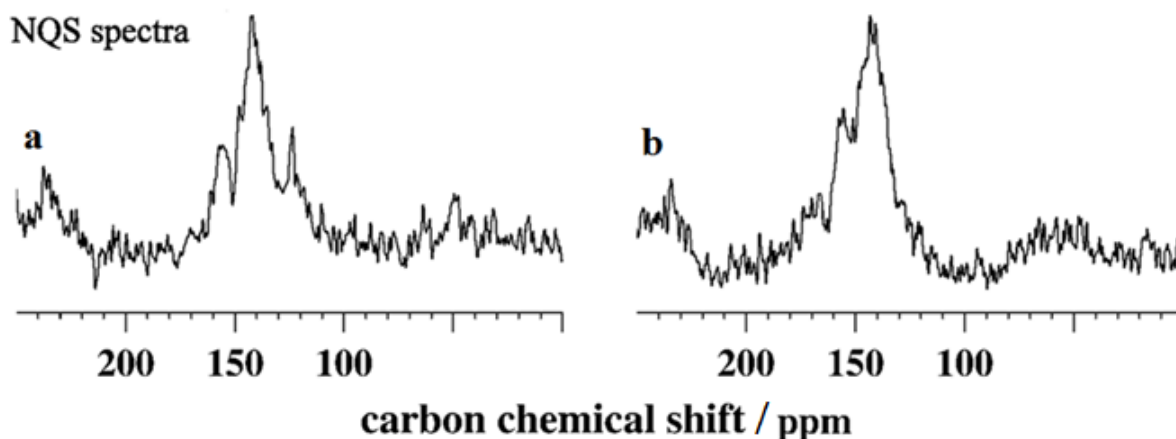


Figure 5.30. (a) chemical 1.5 M H<sub>2</sub>SO<sub>4</sub> 1:1 PANI: 2-ABA with APS, (b) chemical 0.5 M H<sub>2</sub>SO<sub>4</sub> 1:1 PANI: 2-ABA with APS.

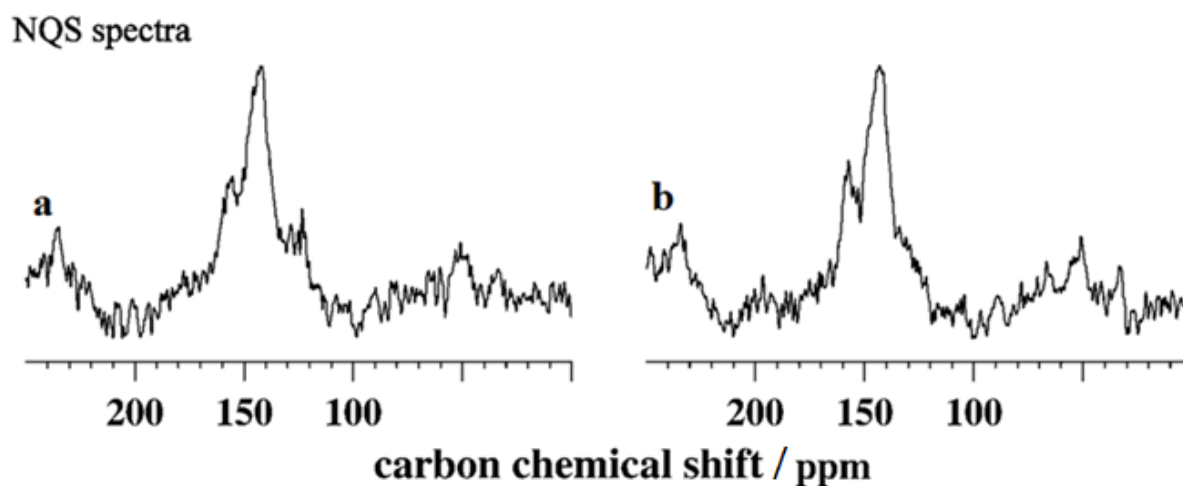


Figure 5.31. Chemically synthesised copolymer doped with 1.5 M H<sub>2</sub>SO<sub>4</sub> with different oxidants: (a) with KIO<sub>3</sub>, (b) with APS.

The peak at nonprotonated C-1 at 148 ppm and the peak at 175-180 ppm ascribed to the carboxylic acid group can be observed and detected in both Figure 5.30 (chemically synthesised copolymer oxidised with the same oxidant and with the same dopant but at different concentrations) and in Figure 5.31 (the NQS spectra for the copolymer oxidised with different oxidant at the same doping level).

### **5.3. Conclusions**

The results from the model study provided information on the chemical structure of the key copolymers at any given applied potential, using in situ Raman spectroscopy. Concentration ratio of the two monomers, aniline and ABA, was studied and with aniline properties dominating the characteristic peaks. Polymerised analysed in H<sub>2</sub>SO<sub>4</sub> was proven to be difficult as the high concentration of sulfuric acid employed showed a strong band in the spectra could potentially overlap with peaks that absorb in that wavenumber hence the study was carried out HCl electrolyte solution. This study allowed a clear identification of the oxidation state and the chemical structure of the polymer formed under different conditions and on different substrates with the use of in situ Raman spectroscopy. The ability to control the chemical structure formed with applied potential would aid in designing the ideal polymer for anticorrosive, antibacterial, anti-moulding and antifouling performance. The added feature from this study is that this could be used as a fast characterisation method of determining the polymer formed on the surface by simply correlating the polymer prepared with this set of reference spectrum.

## CHAPTER SIX: Electrodeposition of polyaniline on aluminium

### 6.1. Abstract

This chapter focuses on the electrochemical synthesis of PANI on three grades of aluminium. Electrosynthesis has attracted interest over other preparation methods due to its reproducibility and ease of control. The composition of the alloys is thought to affect the growth rate as well as the adhesion and performance of coatings, therefore three different aluminium alloys were selected for examination. Marine grade aluminium is of major interest for the marine industry, and contains high levels of magnesium. The 4043 alloy consists of high levels of silicon (~5% Si content). Pure aluminium, 1100 grade (99%+ aluminium), was also selected for testing. More details on the alloys have been provided in Chapter Two. The presence or absence of specific components in the substrate can be an advantage or a disadvantage, as, for example, the presence of Fe affects electroactivity [91]. The morphology of the coatings formed can also be different from one another, which can largely affect the size of pores in the anodised aluminium alloy. All this would enable a better understanding of the growth rate of PANI at aluminium alloys of different compositions. The use of different electrolytes and conditions for anodisation can affect properties, including the thickness and quality of the oxidised layer. This can also affect the overall performance and activity of the coatings.

PANI growth via different methods has been investigated under a variety of experimental conditions (of supporting electrolyte, electrode potential etc.). The results of CV, UV-Vis spectroscopy, Raman spectroscopy, SEM-EDX and AFM studies of PANI are presented and discussed in this chapter.

This chapter has been partially published as:

1. To T., Swift S., Kilmartin P. (2013) Evaluation of electrodeposited polyaniline on marine grade aluminium for antifouling properties, *International Conference on Marine Coatings*, Rina HQ, London, UK, 18<sup>th</sup> April 2013. In press.
2. To T., Kilmartin P. (2013) Kilmartin. Electrochemically synthesised polyaniline on marine grade aluminium, *Sixth International Conference on Advanced Materials and Nanotechnology*, Auckland, New Zealand. In press.

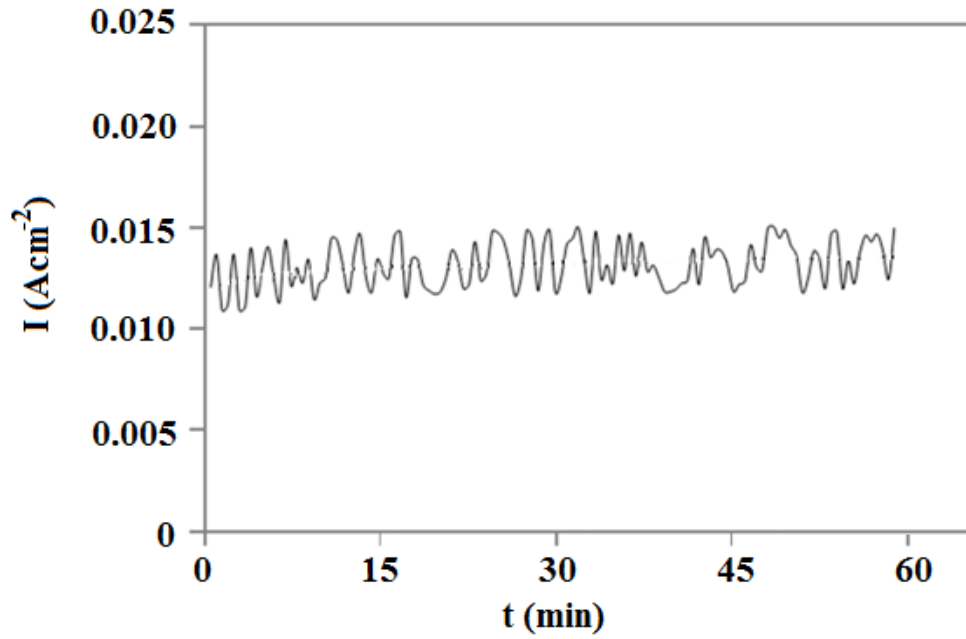
## 6.2. Results and Discussions

### 6.2.1. Electrochemical synthesis of polyaniline at a fixed applied potential

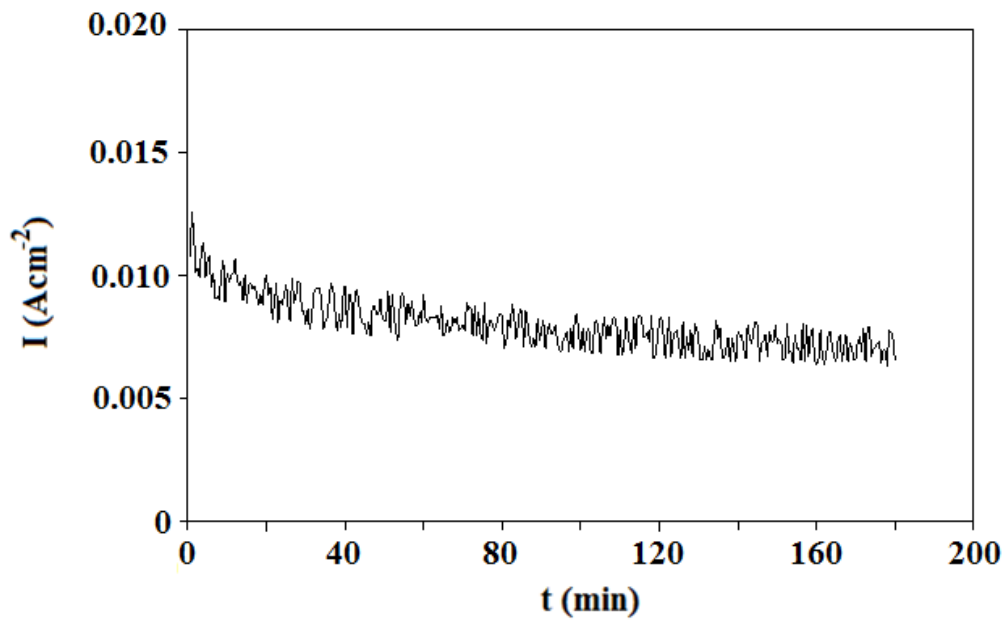
#### 6.2.1.1. Two-Step process

A two-step preparation process was carried out on marine grade aluminium as shown in Figure 6.1 for better understanding of the processes taking place in the anodising reaction. It was also undertaken in order to understand how the formation of the oxide layer prior to electrodeposition of PANI affects the overall current versus time curve. A potentiostatic current density versus time ( $I-t$ ) transient for aniline-free oxalic acid solution is shown first, where an anodised surface was obtained prior to aniline electropolymerisation. This curve in the absence of the aniline monomer, Figure 6.1(a), shows behaviour typical of the formation of aluminium oxide layer in an anodisation process. It is believed that more  $\text{Al}^{3+}$  is produced per unit time at higher applied potential with concomitant precipitation of Al oxalate crystals on the substrate [277]. Thus, in a shorter time at a higher potential, the substrate could be covered with more passive Al oxalate layer. In the initial period of aluminium anodisation at constant voltage the current increases due to the fact that aluminium protected by a thin aluminium oxide film that offers little resistance, and later on, the current drops to a steady state value [277]. This is caused by the results of two competing process: the exponential decrease of barrier film formation and the pore formation current. A steady state value is reached after a certain time and the film thickness grows proportionally to the charge per surface area in the aluminium piece being anodised [277]. Aluminium oxidises to aluminium ions, and the electrolyte oxalic acid dissociates into hydrogen and oxalate ions, contributing to the rise in anodic current seen at 0.8 V. In the case of the presence of an barrier oxide layer with anodising and polymerisation at fixed voltage, the current decreased to a lower values [277]. PANI deposition on the aluminium oxide electrode at an applied potential of 2 V is shown in Figure 6.1(b). In this case, the current gradually declined due to electrodeposition occurring across a growing insulating film of aluminium oxide mixed with PANI. During this second step, two oxidation reactions take place simultaneously: the oxidation of the metal alloy leading to the further formation of aluminium oxide, and aniline monomer oxidation with the formation of PANI.





(a)



(b)

Figure 6.1. (a) Step 1 in 0.5 M oxalic acid, and (b) Step 2 in the presence of 0.1 M aniline monomer and 0.5 M oxalic acid;  $I$ - $t$  transient of potentiostatic polarisation of anodising on marine grade aluminium 5083 alloy at 2 V (Ag/AgCl).

Upon the completion of the reaction, green PANI films were successfully electrosynthesised on marine grade aluminium 5083, using the above two-step process in an 0.5 M oxalic acid solution containing 0.1 M aniline.

### 6.2.1.2. One-Step process

PANI film growth on an aluminium surface in the following section was carried out at four different constant potential values, using an 0.5 M oxalic acid containing 0.1 M aniline, in a one-step process, which involved only step two of the two-step process. The aluminium alloy electrode was anodised and aniline polymerised all in one step straight after the pretreatment stage. The current versus time curves obtained for the potentiostatic synthesis of PANI at different applied potential are shown in Figures 6.2 – 6.4.

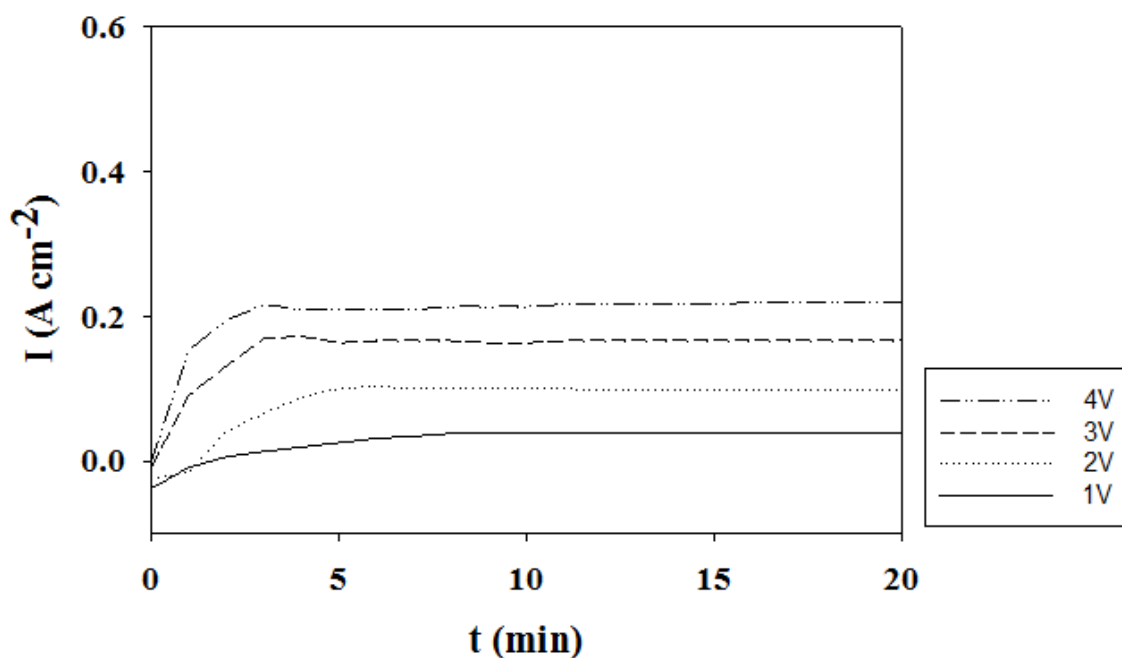


Figure 6.2. Potentiostatic current-time plots recorded for aluminium alloy 1100 in 0.5 M oxalic acid + 0.1 M aniline solution at different applied potentials.

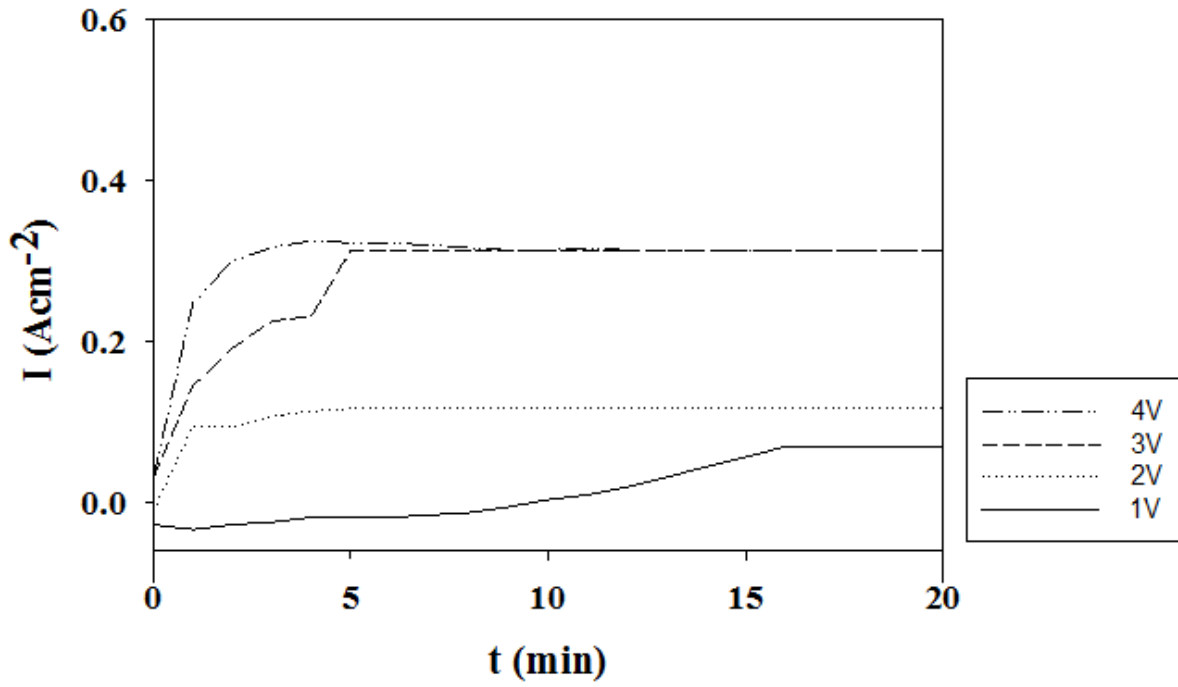


Figure 6.3. Potentiostatic current-time plots recorded for aluminium alloy 4043 in 0.5 M oxalic acid + 0.1 M aniline solution at different applied potentials.

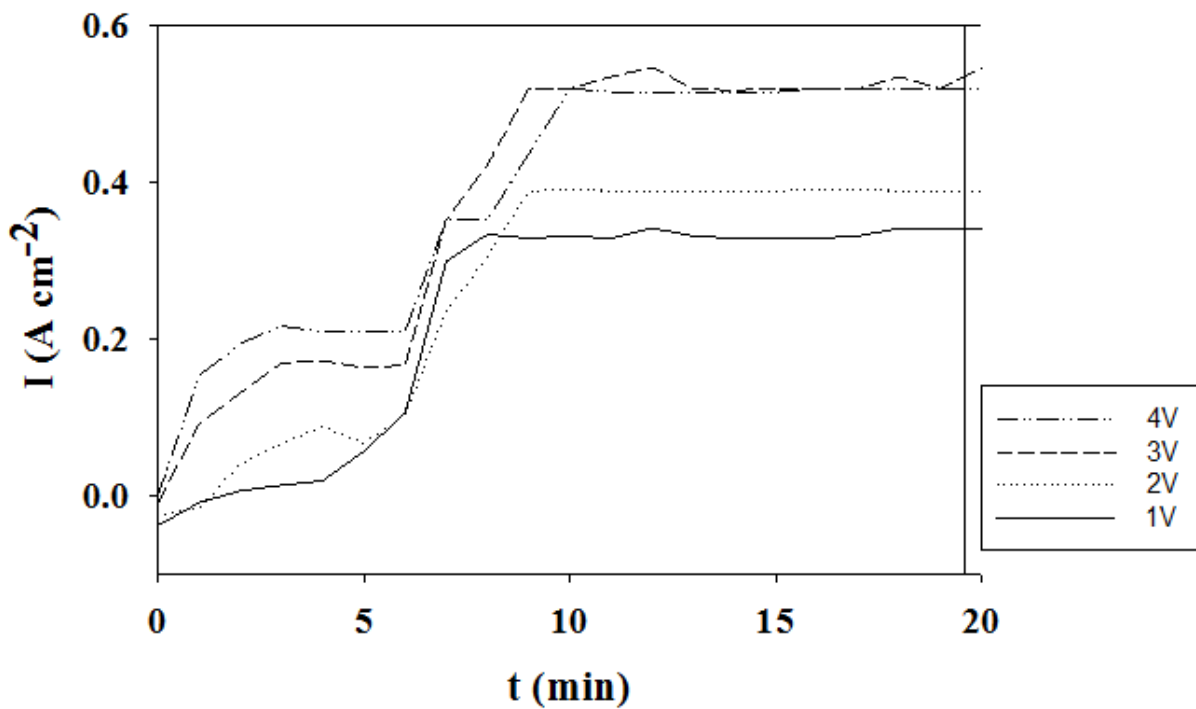


Figure 6.4. Potentiostatic current-time plots recorded for aluminium alloy 5083 in 0.5 M oxalic acid + 0.1 M aniline solution at different applied potentials.

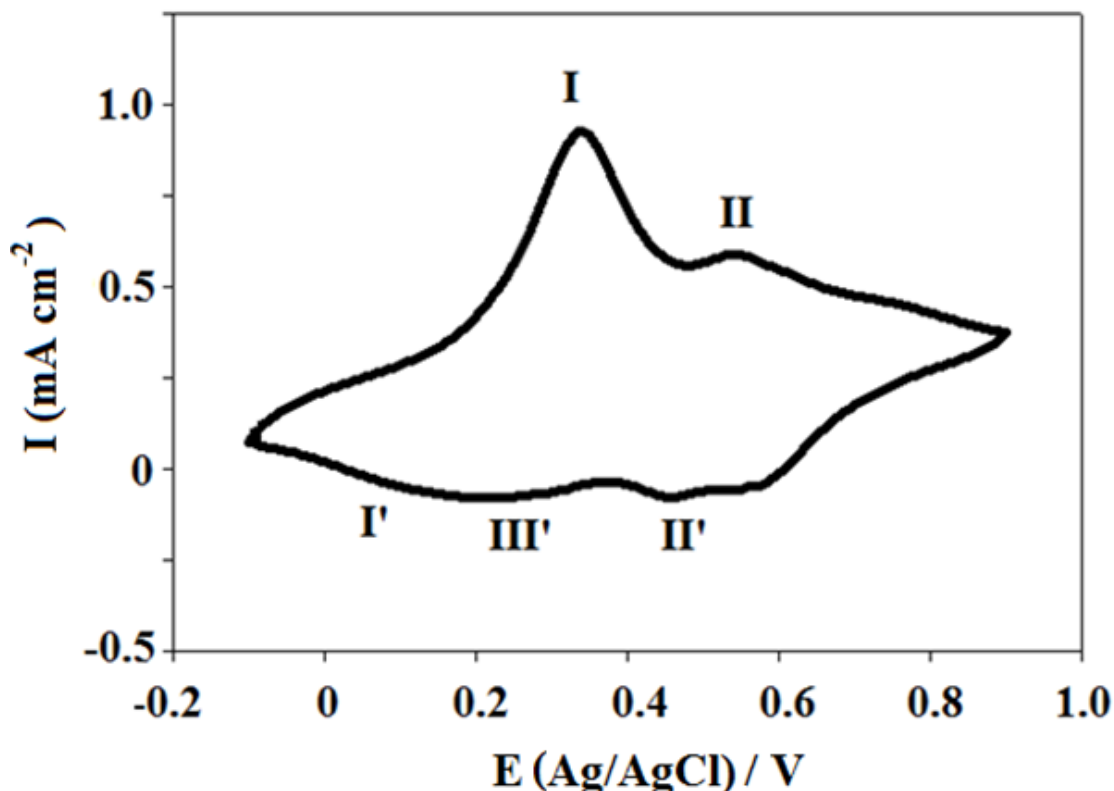


Figure 6.5. Characterisation of the formed polymer on alloy 5083 in aniline-free 0.5 M oxalic acid electrolyte by cycling the potential from -0.1 to 0.9 V at a scan rate of  $50 \text{ mV s}^{-1}$ .

Note that the behaviour of alloy 5083 at 2 V in Figure 6.4 of one-step process and that of Figure 6.1(b) after the surface has been anodised are quite different. The presence of an oxide barrier layer lowers the current before it stabilises during the one-step process, Figure 6.4. The initial observation is similar to what was being observed for anodising. This suggests that anodising dominates the one-step reaction in the first few minutes of the process, while the aniline polymerisation reaction has a delayed induction time of  $\sim 8$  minutes.

Both alloy 1100 and alloy 4043 showed similar behaviour with an increase in current over time, and with a fairly constant value being obtained after a few minutes. Alloy 1100 produced the least current at each voltage set compared to the other two alloys. The trend of longer induction times needed with a higher voltage, to reach a current plateau, was seen with all three of the alloys. However, the marine grade aluminium showed a unique characteristic step change in current that was not seen with the other two alloys, and it also showed the highest current values after 20 minutes of applied voltage. At around 6 – 7 mins a step

increase in current was observed with the marine grade aluminium, which could be due to the formation of the oxide layer on the alloy that required more current than the polymer growth.

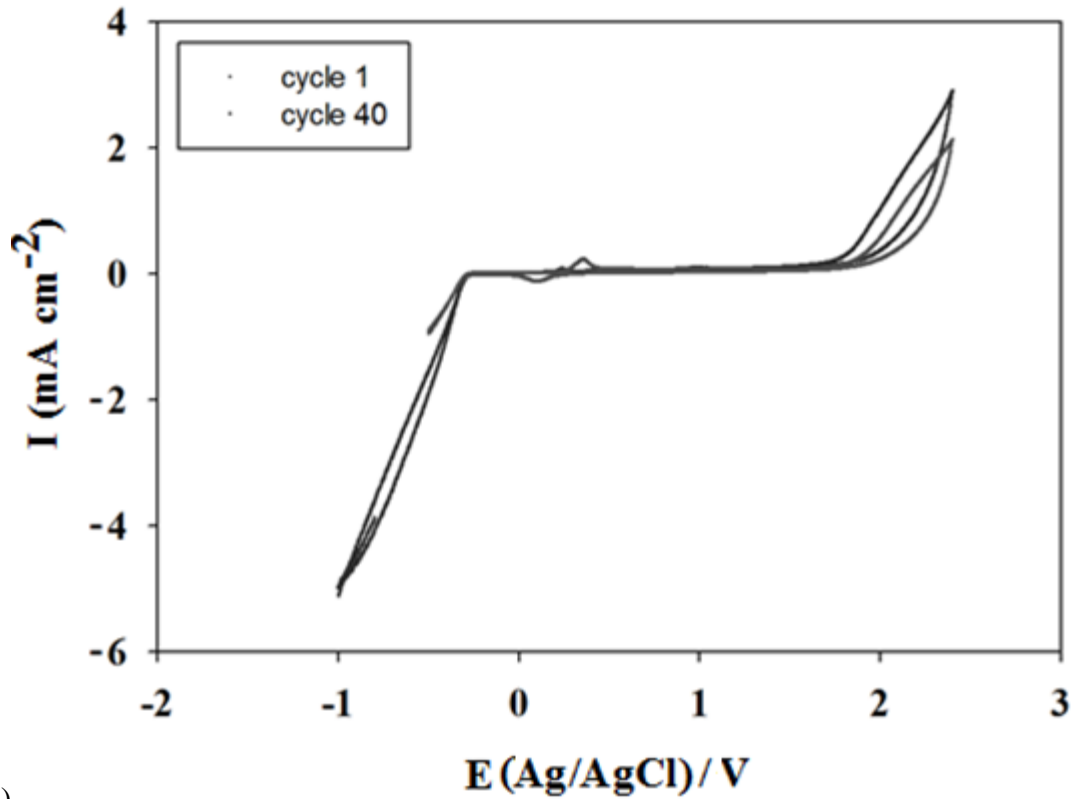
The internal redox process observed in the characterisation of the PANI film formed in Figure 6.5 prepared from constant potential at 2 V appeared to be similar to that prepared with cycling in Figure 6.8: hence the redox process would be discussed later together with cycling results.

### **6.2.2. Electrochemical synthesis using cyclic voltammetry**

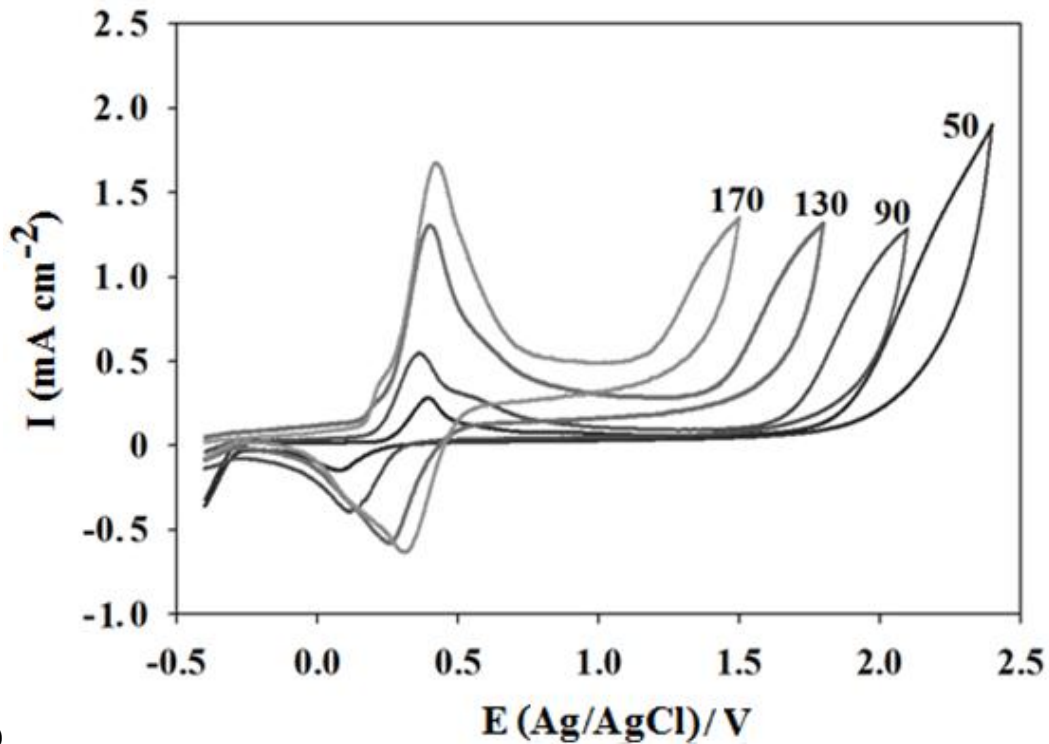
The approach used in section on cyclic voltammetry was only undertaken with the marine grade aluminium all in one-step process. During cycling, a rapid increase in current was observed for potentials higher than 1.8 V, which correlates to green film PANI-co-3-ABA formation on the 5083 electrode. The growing current in the potential region from ~0.2 and ~0.4 V indicates growth of the polymer, and the peaks shown are due to the reversible oxidation of PANI on the electrode.

A similar reaction was observed in the absence of any monomer (only oxalic acid). As the number of cycles increased, the intensity of this current rise decreased, as a layer of PANI was built up upon the electrode surface, as shown in Figure 6.6(b) [90].

CVs obtained in 0.5 M oxalic acid solution containing 0.1 M aniline on marine grade aluminium 5083 showed that internal redox processes for PANI were well established by cycle 40 (Figure 6.6). The typical conducting polymers peaks were detected showing the first set of redox peaks at around 0.40 V, the peak illustrates an increase in peak intensity with cycle time, the internal redox peaks for PANI appearing at around 0.4 V. The potential range was initially from -1 to 2.4 V, as a higher potential was required to initiate polymerisation. The upper potential limit of the electropolymerisation was progressively lowered to 1.5 V over time, in an attempt to minimise oxidative degradation. The addition of aniline into the solution led to a decrease of current values by adsorption of anodic products on polymer surface. The anodic peak potential shifted to positive values and the current at 1 V and above could possibly be due to the oxidation of aniline and/or the oxidation of the formed PANI to its fully oxidised PNB state.



(a)



(b)

Figure 6.6. (a) Cycle 1 and 40, (b) One step electrodeposition of PANI by CV at cycle 50, 90, 130 and 170 recorded on marine grade aluminium 5083 from a solution containing 0.5 M oxalic acid in the presence of 0.1 M aniline monomer at a scan rate of  $50 \text{ mV s}^{-1}$ .

During the one-step electrodeposition of PANI by cycling between -0.4 to -1 V for the lower potential, and an upper potential that varied from 1.5 to 2.4 V, the anodic peak current and charge (see Figure 6.7) passing through the electrode continued to increase indicating that there was on-going PANI growth throughout the entire number of extended cycles.

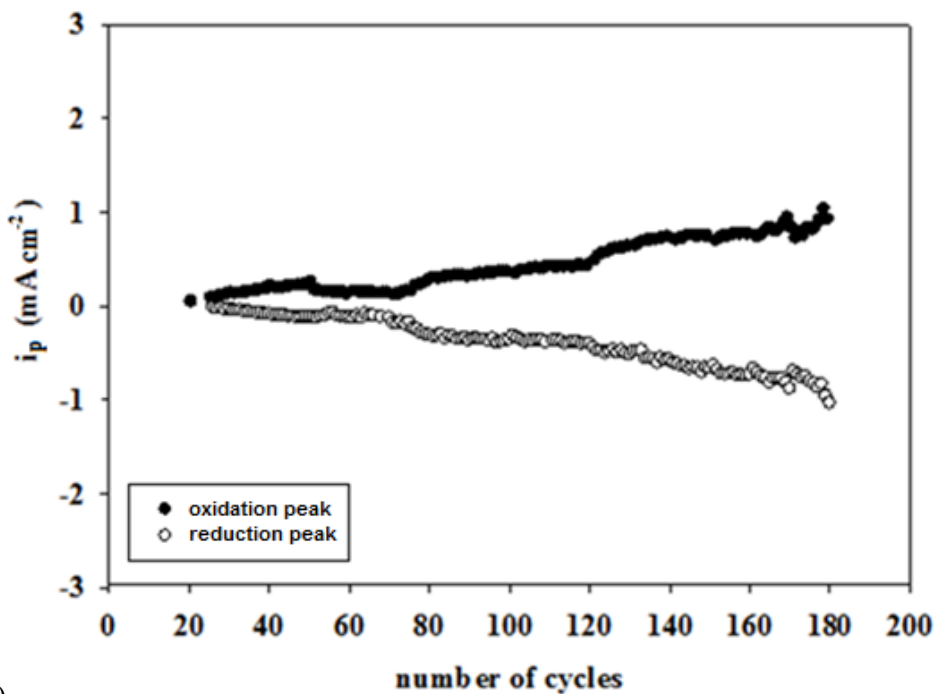
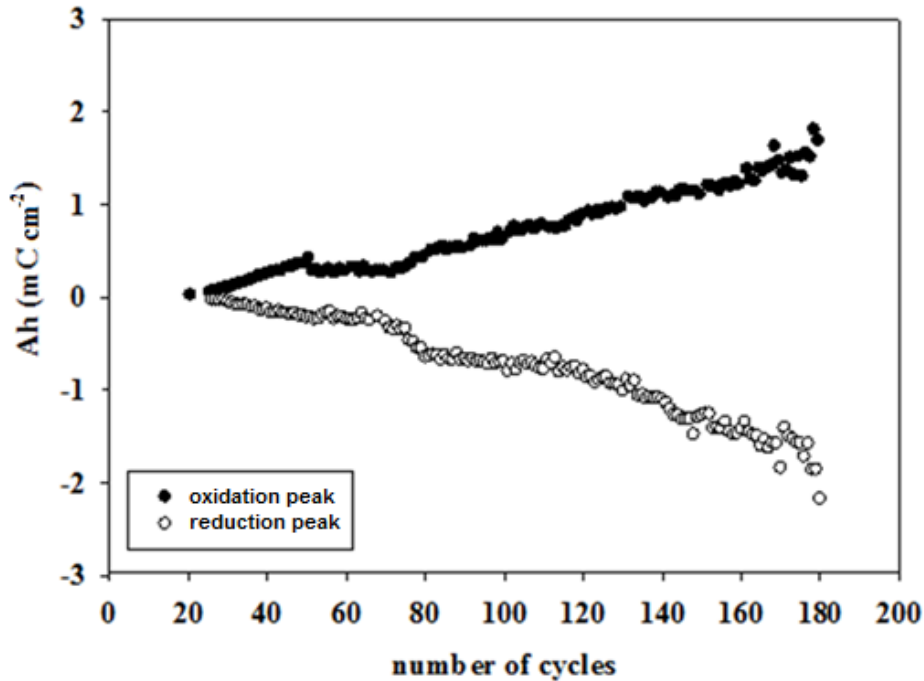
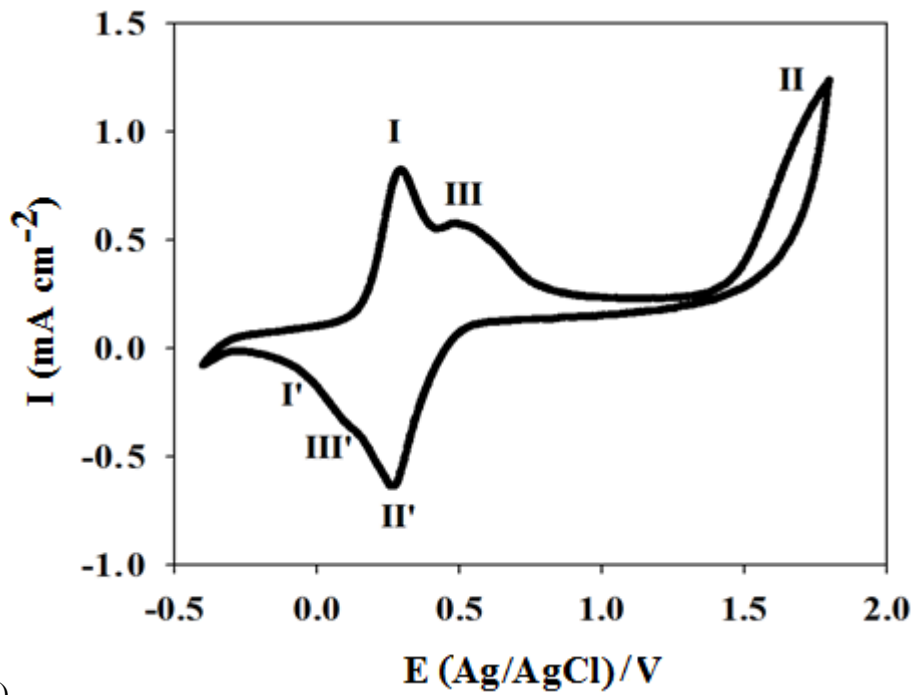
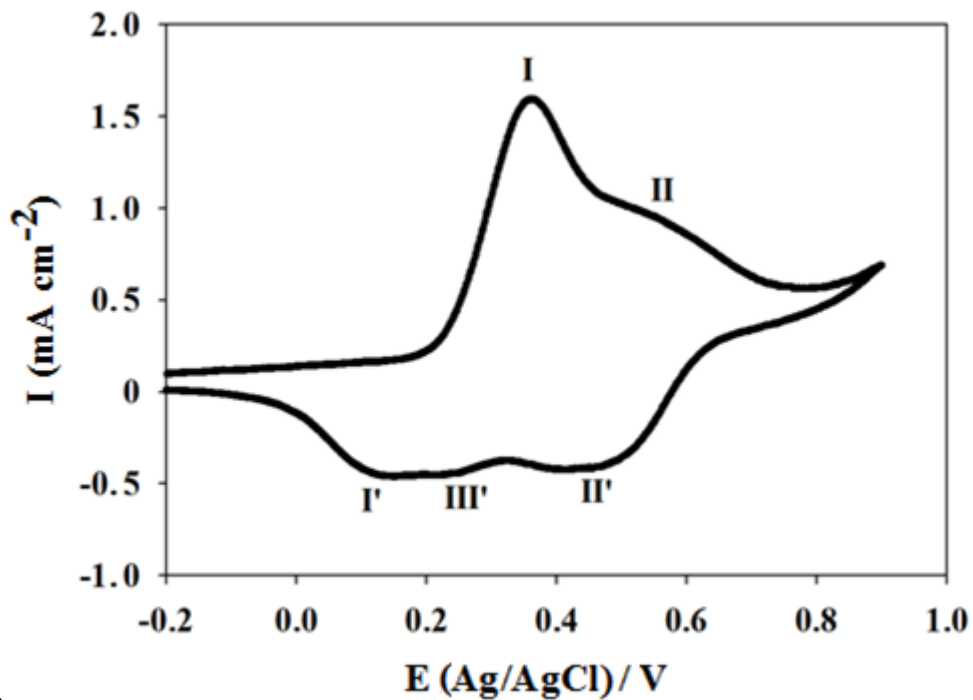


Figure 6.7. Oxidation and reduction peaks for cycling growth of PANI on marine grade aluminium 5083 (1 cm<sup>-2</sup>): (a) charge, and (b) current in 0.5 M oxalic acid.



(a)



(b)

Figure 6.8. (a) Cycle 125 of a one step aniline polymerisation on marine grade aluminium 5083 with 0.5 M oxalic acid in the presence of 0.1 M aniline from -0.2 to 0.9 V at  $50 \text{ mV s}^{-1}$ , (b) cycle 3 of characterisation on alloy 5083 with an aniline-free electrolyte of 0.5 M oxalic acid.



The films produced potentiostatically, Figure 6.6, and cycling, Figure 6.8(b), were electroactive. The characteristic waves are associated with the inter-conversion between LEB and the EB conducting form (I/I') of PANI, and between the EB conducting form and PNB (II/II'), which were also observed during the formation of the polymer [92]. It has been reported that the second oxidation peak changes due to PANI being unstable in aqueous solutions where it undergoes degradation of a hydrolytic nature. Therefore, reliable spectroelectrochemical data can only be obtained for potentials lower than the onset of the second oxidation peak, below 0.7 V vs. Ag/AgCl. The pH of oxalic acid solution is at 1.2 at the start of the experiment and increased to 1.4 after the reaction. The combination of slightly higher pH and aluminium, the potential range is likely more limited than for PANI used in stronger acid such as HCl or H<sub>2</sub>SO<sub>4</sub>. The position of EB to PNB transition could also be affected by the pH of the 0.5 M oxalic acid electrolyte used.

As preparative cycling continued, the colour intensified as a thicker layer of PANI was formed. Continuous potential cycling can also lead to a new wave system appearing between the other two sets of peaks, and a middle reduction peak (III') is suggested in Figure 6.8. This current is a characteristic behaviour of PANI films when submitted to cycling at higher oxidation potentials [92, 103, 194, 200], and has been attributed to redox processes involving reaction intermediates, such as p-benzoquinone, formed during the degradation of PANI films [28, 278]. With the present PANI preparation, the gap between oxidation peaks I and II was not particularly large, and a higher peak separation is seen for electrochemical polymerisation of aniline on inert metals such as platinum and gold and also the influence of pH of the electrolyte used.

### 6.2.3. Morphology

The SEM/EDS results obtained from Tables 6.1 – 6.3 of the three grades of aluminium alloy selected in its pure, sanded and treated form (alkaline treatment followed by desmutting) indicate that alkaline treatments do partially dissolve the silicon precipitates on aluminium alloy, but not magnesium precipitates. As shown, the low level of impurities on 1100 and marine grade aluminium alloys was completely dissolved after the alkaline treatment. However, the higher level of mixed metals on 4043 alloy remained the same. This suggested that it is unlikely that impurities are dissolved completely during the treatment process. Moreover, the presence of other metals might have an effect on the overall properties and growth rate of aniline, which will be investigated in this chapter. Wang et al. [22] suggest that

the presence of magnesium and silicon in the alloy act as the starting pathway for electropolymerisation growth for the flow of current. This is proven to not be the case, as shown in the Figures 6.1 – 6.3: the induction time for the pure aluminium alloy was the lowest, suggesting that the rate of reaction is much faster for this grade of alloy compared to the other two, both of which contained some impurities.

	Al %	Si %	O %
<b>Pure</b>	98	0.6	-
<b>Sanded</b>	98	0.6	0
<b>Alkaline treated</b>	98	0	-
<b>Desmut</b>	98	0	

Table 6.1. Composition of Al, Si and O detected using SEM/EDS on 1100 alloy surfaces.

	Al %	Mg %	Si %	O %
<b>Pure</b>	93	0	3	0
<b>Sanded</b>	93	0	3	0
<b>Alkaline treated</b>	93	0	3	0
<b>Desmut</b>	93	0	3	0

Table 6.2. Composition of Al, Mg, Si and O detected using SEM/EDS on 4043 alloy surfaces.

	Al %	Mg %	Si %
<b>Pure</b>	93	2	0.4
<b>Sanded</b>	93	2	0.4
<b>Alkaline treated</b>	93	2	0
<b>Desmut</b>	93	2	0

Table 6.3. Composition of Al, Mg and Si detected using SEM/EDS on 5083 marine grade aluminium alloy surfaces.

Scanning Electron Microscopy (SEM) is a very effective technique to examine changes in the aluminium surface. The surface morphology of pure aluminium, 1100, showed a honeycomb surface after the alkaline treatment, with features appearing more pronounced after desmut treatment, as shown below in Figure 6.9. However, aluminium alloy 4043, with trace amounts of impurities and a high silicon content, exhibited less of a honeycomb structure on the surface after the alkaline and desmut treatment. Moreover, the marine grade aluminium 5083 seemed to show the smoothest surface of all.

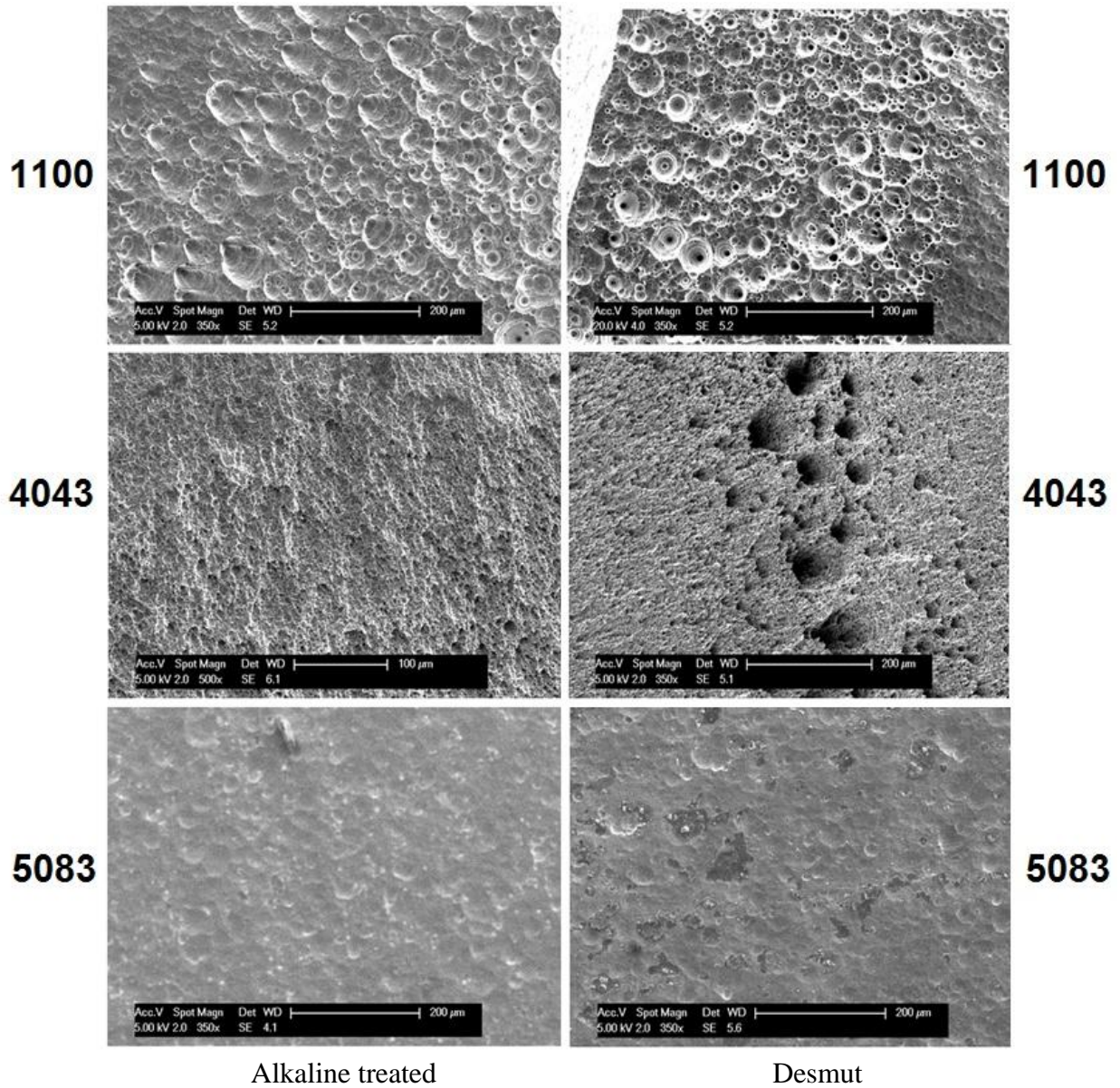


Figure 6.9. SEM images of aluminium alloy surfaces after alkaline treatment – left column and Desmut – right column with 1100 alloy from the top row to 4043 in the middle while 5083 alloy is on the bottom row.



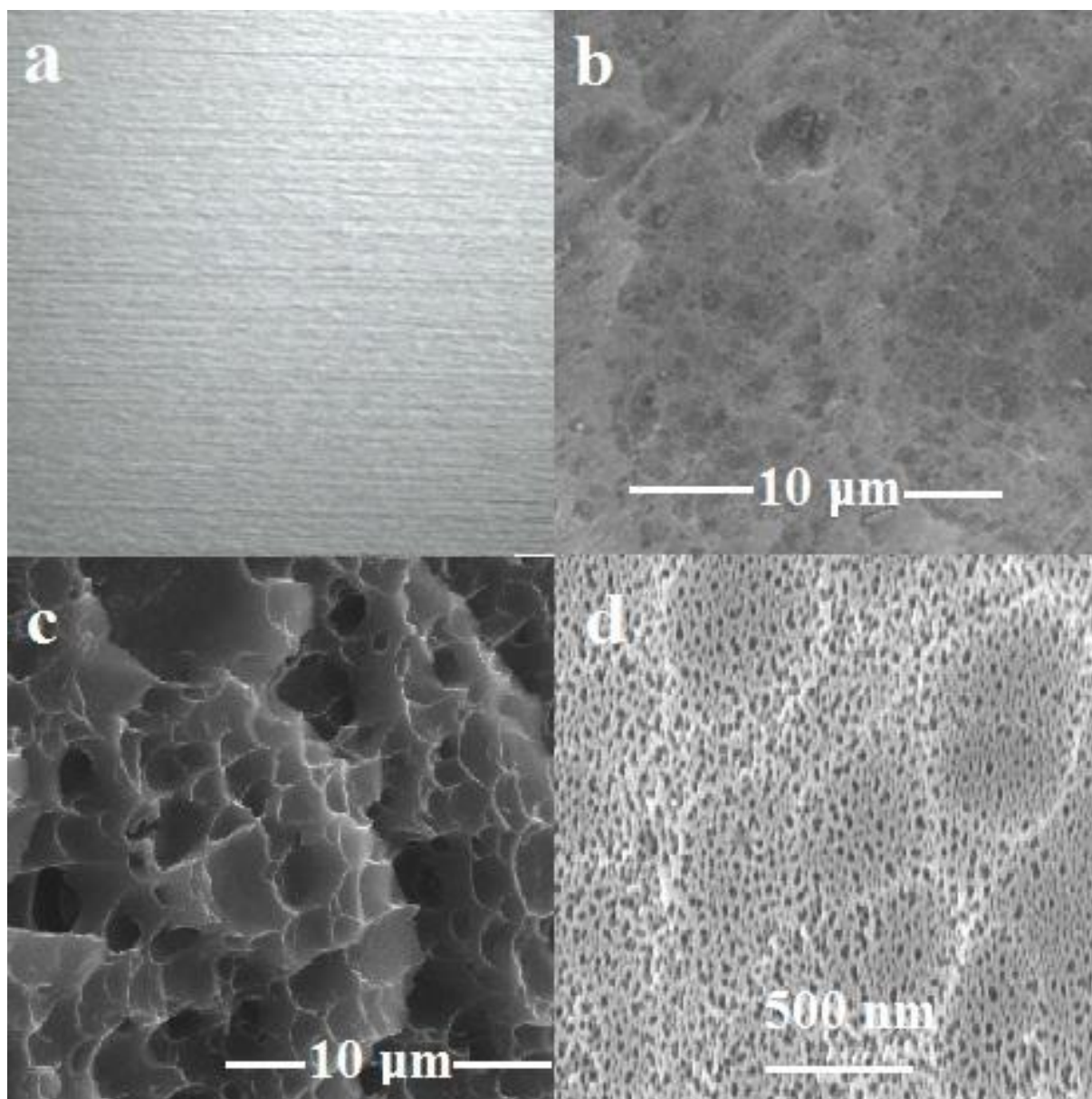


Figure 6.10. (a) aluminium as supplied, (b) chemically cleaned and pretreated aluminium, (c) anodised aluminium ( $\text{Al}_2\text{O}_3$ ) after being potentiostatically treated at 2 V for 30 mins in 0.5 M oxalic acid, and (d) potentiostatically grown PANI on top of the formed  $\text{Al}_2\text{O}_3$  with 0.5 M oxalic acid in the presence of 0.1 M aniline monomer at 2 V for 3 h.

A pure aluminium surface is often smooth in appearance, but after chemical treatment, the surface roughens as seen from Figure 6.10(b). The surface can be modified further to a honeycomb-like structure through anodisation processes (Figure 6.10(c)), while a fluffier porous surface is obtained following the electrochemical deposition of PANI, also dependent upon the electrolyte solution employed, in this case an oxalic acid solution (Figure 6.10(d)).

The honeycomb-like structure enables PANI to grow in the pores which practically benefit adhesion of the CP on the aluminium surface. The anodisation process allows the production of a honeycomb structure on the aluminium alloy surface, creating nanopores and enabling PANI to grow upon them. Dividing the growth into two stages allowed for a better understanding of the growth mechanism. The growth of PANI on aluminium oxide starts from the metal upwards through the oxide layer and finally onto the surface of the electrode, as shown in Figure 6.11 below.

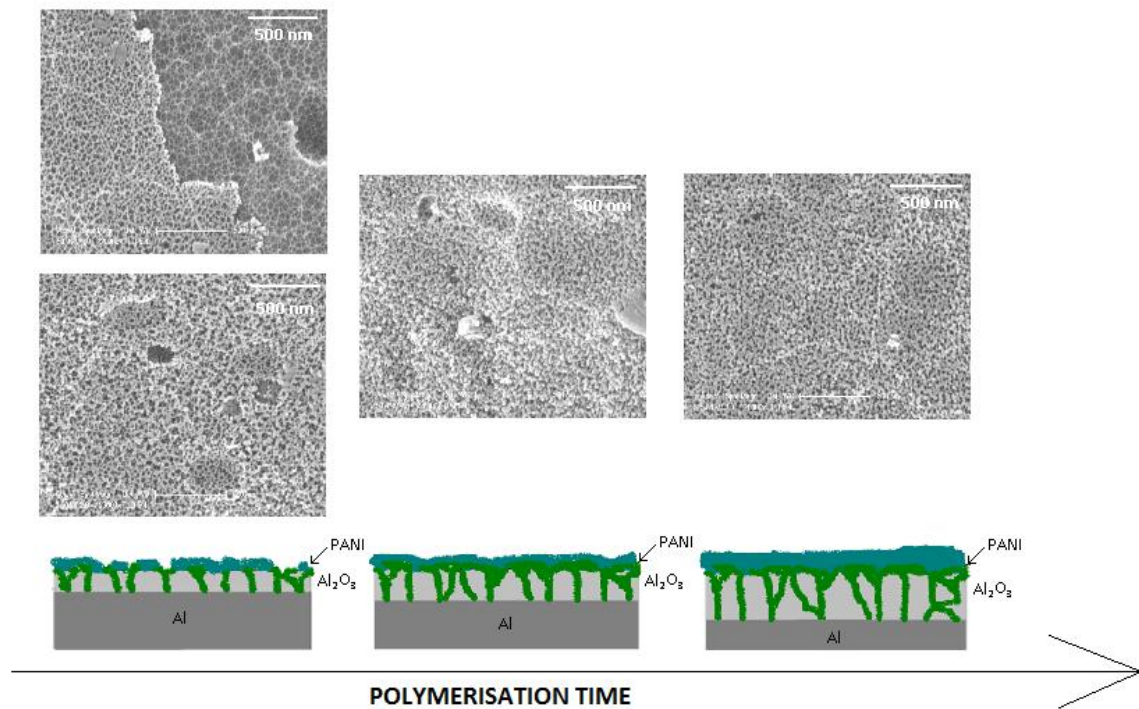


Figure 6.11. Mechanism of PANI growth on aluminium oxide electrode. The polymerisation growth of PANI was followed with time and illustrated that the growth of the CP starts from the metal upwards through the oxide layer and onto the surface of the electrode.

Figure 6.11 is a representative image of the growth mechanism obtained from collective of SEM images growing PANI on aluminium under the same conditions but with different polymerisation durations.

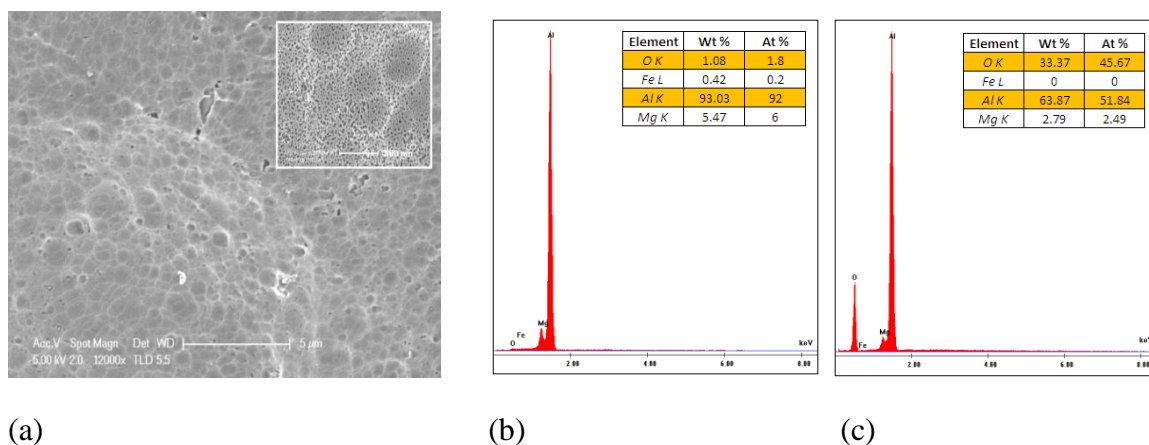


Figure 6.12. (a) SEM images of one step process of step 2 of Figure 6.10(d), anodised and aniline polymerised marine grade aluminium 5083, SEM/EDS of marine grade aluminium 5083 of (b) treated aluminium (from image Figure 6.10(b) above), and (c) anodised aluminium oxide (from image Figure 6.10(d) above).

In addition to the SEM image observed in Figure 6.10(c) for anodised aluminium, the images obtained with SEM/EDS were also very useful (Figure 6.12). As shown, the formation of the aluminium oxide layer increased the oxygen level significantly, providing a fast and quick way to characterise and confirm the formation of this layer using SEM/EDS.

Porter et al studied PANI films on images taken with 2 to 10 μm sides with AFM. Bundles of polymer growth were readily seen, with an average diameter of 100 nm [178-179]. However, there were no crystalline structures seen with AFM. One paper in 1996 reported the use of AFM to investigate the morphologies of ultra-thin PANI films on Si surfaces [180], while another study in 2002 was devoted to the electrochemical growth of PANI and its monitoring using AFM during oxidation and reduction cycles [181].

PANI nanofibres tend to form a bundle, resulting in a large hollow mat (as shown in Figure 6.10(d)); the tips of the individual nanofibers are at the nanometer scale and this is what is observed under AFM. The electrochemically synthesised PANI surface on the marine grade aluminium alloy was rough and the pores ranged from 5 μm to the nanometer scale.

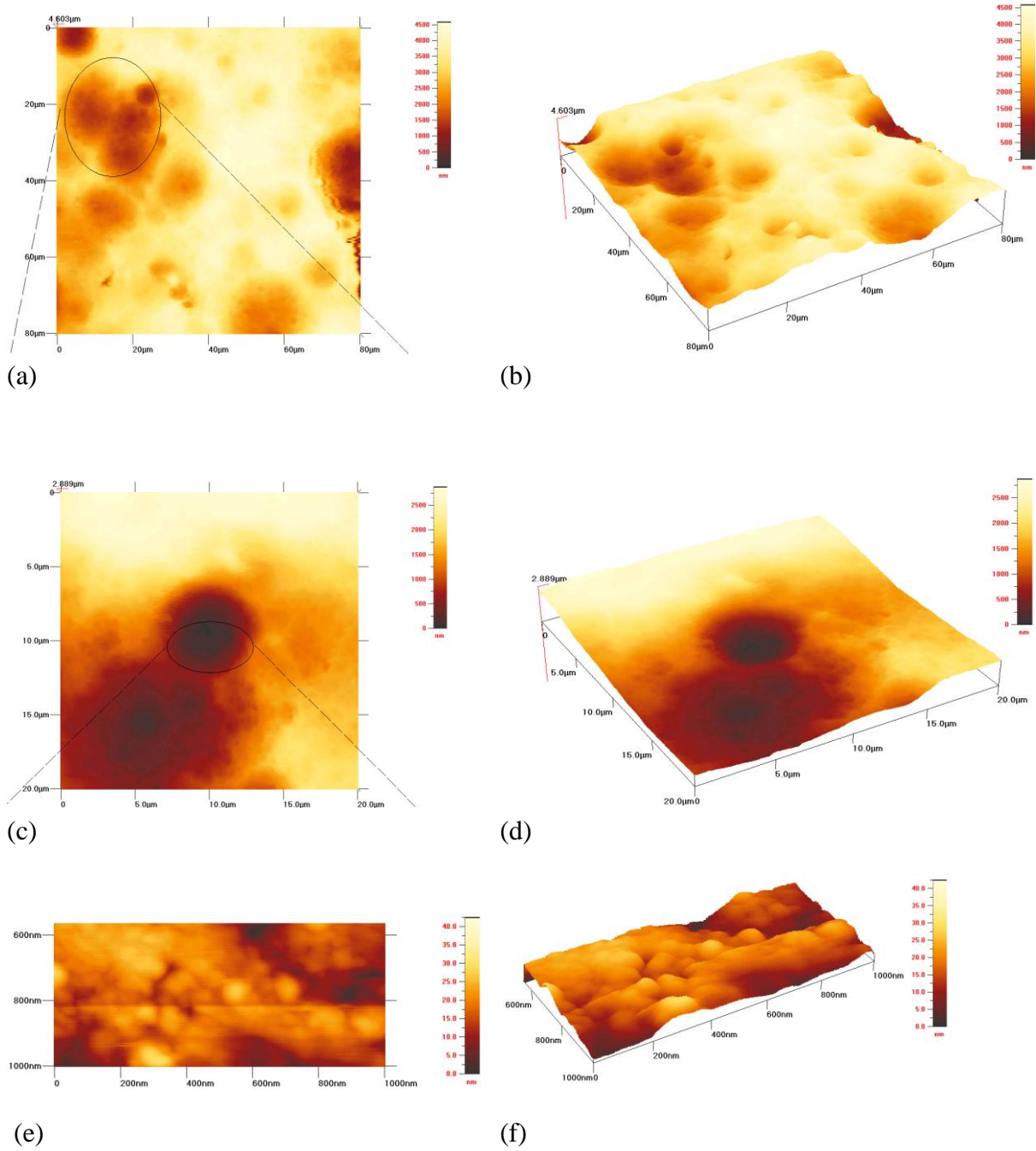


Figure 6.13. Atomic force microscope image of two-step electropolymerised PANI on 5083 alloy with step 1 being anodisation for an hour, followed by step 2 of oxidation for 3 h at 2 V. The scan size was (a) and (b) 80 μm, (c) and (d) 20 μm, (e) and (f) 1 μm; three-dimensional AFM pictures with the scan rate 6.1 Hz, with 256 sample points taken on each of the 256 lines to make up the image.

The overall thickness of film formed could be determined with a cross section SEM image, with the sample preparation method discussed in Chapter Two and in Figure 6.14. To better understand the relationship between the polymerisation time and the film thickness formed under the same conditions, but at different applied potential, a set of samples were prepared. The film thickness was recorded by imaging the cross-section using SEM, an example shown in Figure 6.15. The readings of each sample were recorded and plotted in Figure 6.14.

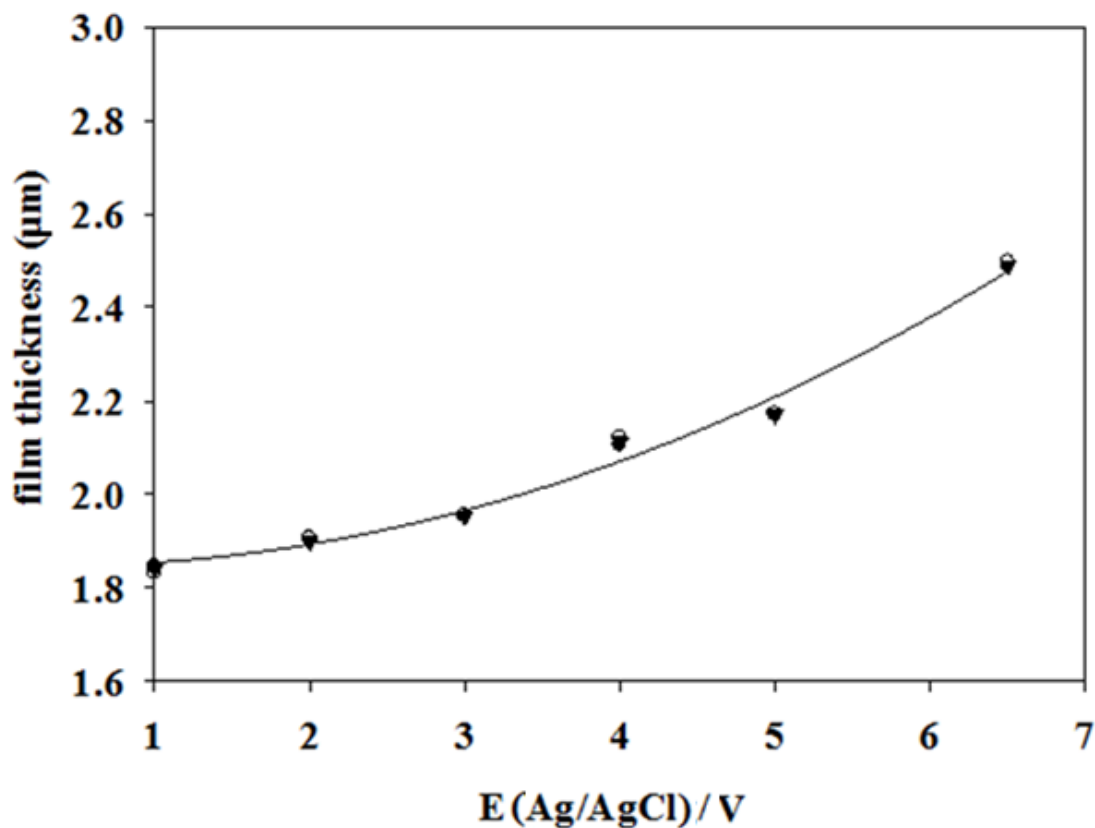


Figure 6.14. Thickness of film formed at different applied voltage with one-step electrochemical polymerisation of aniline.

There was a direct linear relationship between the film thickness formed and the voltage that was applied on the aluminium substrate with the one-step electrochemically synthesised PANI.



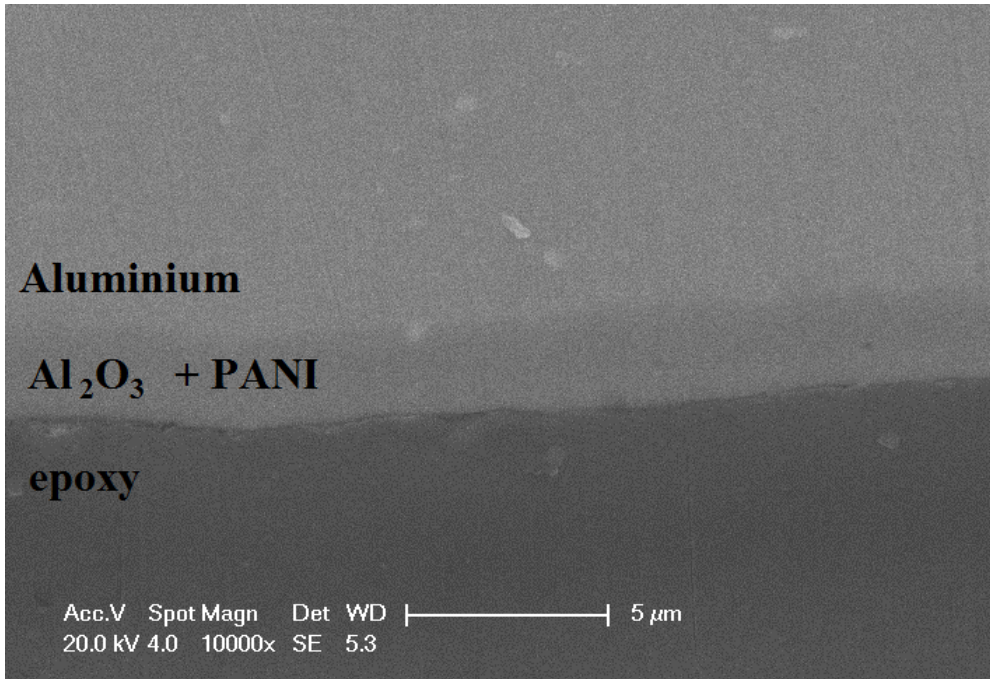


Figure 6.15. A cross sectional SEM image of two-step (Step 1; 1 h and Step 2; 0.5 h) electropolymerisation of PANI on marine grade aluminium alloy.

Adherence of the polymers to the substrate was tested by both tape and cross hatch tape test, commonly used in the coatings industry for testing coating adhesion upon surfaces, see Chapter Two for details. Coatings that were electrochemically synthesised for 3 h at 2 V appear to show the best adhesion with no removal of the coating during the adhesion tests. Although surface coatings of the rest of the electrochemically synthesised systems showed residue on tape upon pulling, there was no visual damage on the substrate surface, suggesting that only the surface of the coating was being removed rather than the bulk. This indicates that the result is due to a cohesion failure rather than an adhesion failure, and this could be improved with post-anodising treatment [117, 119-120, 123].

#### 6.2.4. FTIR spectroscopy

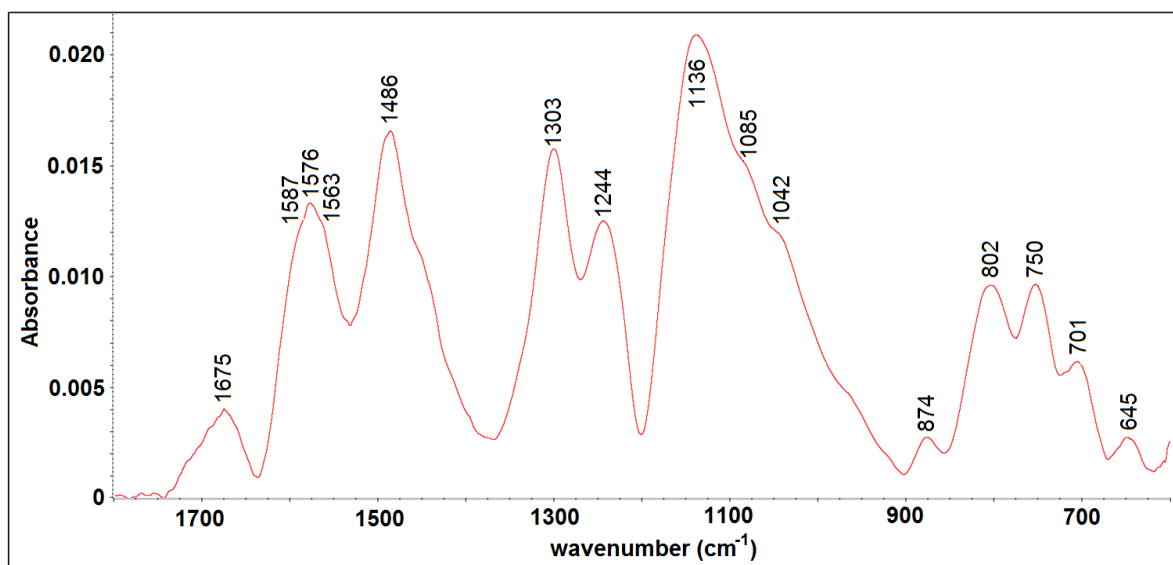


Figure 6.16. FTIR spectra of PANI on marine grade aluminium potentiostatically grown at 2 V for 2 h.

FTIR spectra of the electropolymerised layer of polyaniline on the aluminium alloy by a potentiostatic method are presented in Figure 6.15. The bands around 1675, 1587, and 1486  $\text{cm}^{-1}$  correspond to C=O of oxalates (oxalate of sodium, natroxalate) and to quinoid and benzenoid rings of PANI respectively [72, 279]. The band around 1244  $\text{cm}^{-1}$  is a characteristic band of the conducting protonated form observed at 1238  $\text{cm}^{-1}$  and ascribed to the C-N<sup>+</sup> stretching vibration in the polaron structure of PANI [92]. The spectral peaks at 1576, 1486, 1303, and 1085  $\text{cm}^{-1}$  are due to PANI. The PANI formed under potentiostatic conditions had both Q and B moieties [72]. At the same time, bands due to the aluminium substrate and its oxide layer can also be seen with FTIR. The montmorillonite is observed at ca 800  $\text{cm}^{-1}$  [25].

### 6.2.5. Raman spectroscopy

The surface of each of the aluminium alloys was analysed using Raman spectroscopy. The spectra were collected at a blue laser excitation ( $\lambda = 488 \text{ nm}$ ).

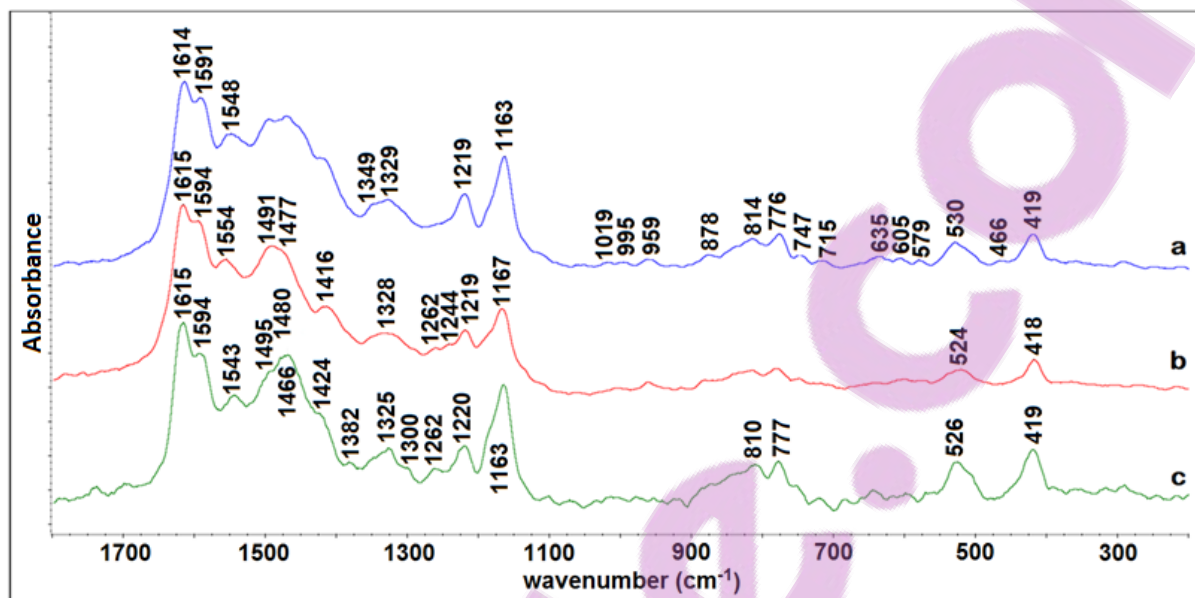


Figure 6.17. Raman spectra of PANI with 0.5 M oxalic acid in the presence of 0.1 M aniline under potentiostatic method at 2 V for 2 h (a) 1100, (b) 4043, and (c) 5083 aluminium alloy.

Characteristic bands for PANI were observed with all three alloys, as seen in Figure 6.17. However, the C-C deformation bands assigned to the B structure at around  $1620 \text{ cm}^{-1}$  and Q rings at  $\sim 1580 \text{ cm}^{-1}$  formed in slightly different ratios, depending on the type of alloy used. PANI grown on marine grade aluminium contained more B structures in the polymer, while the 1100 and 4043 alloys showed similar B and Q rings ratios. This is reflected in the C=C at  $\sim 1543 \text{ cm}^{-1}$  blue shift in the marine grade aluminium compared with the other two alloys. The C=N<sup>•+</sup> stretching mode of quinoid units at around  $1460 \text{ cm}^{-1}$  overlapped in this area with neighboring bands forming a broad peak, which consisted of possibly three or more bands. This indicated the complex neighboring environment arising in this region. The C-N stretching mode of the polaronic unit at  $\sim 1220 \text{ cm}^{-1}$  and C-H bending deformation at  $1163 \text{ cm}^{-1}$  were observed in all three spectra.

Electrochemically prepared PANI on marine grade aluminium 5083 exhibited different colours in 0.5 M oxalic acid, which suggested the existence of different oxidation states. The Raman spectra data confirmed the finding.

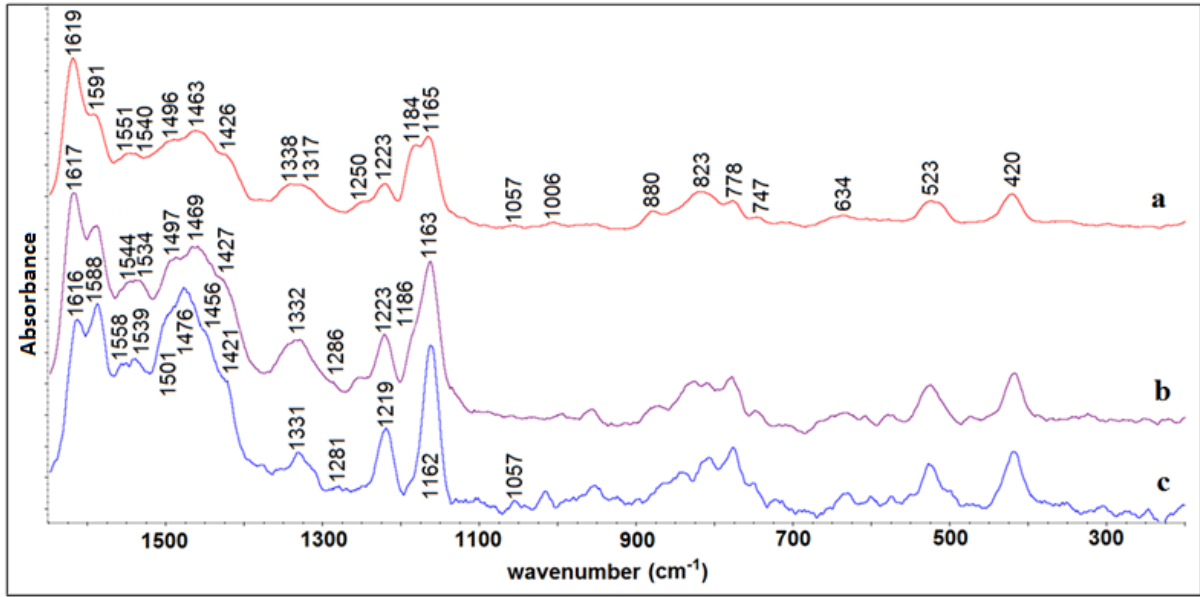


Figure 6.18. PANI in different oxidation state: (a) LEB, (b) ES, and (c) EB on 5083 alloy.

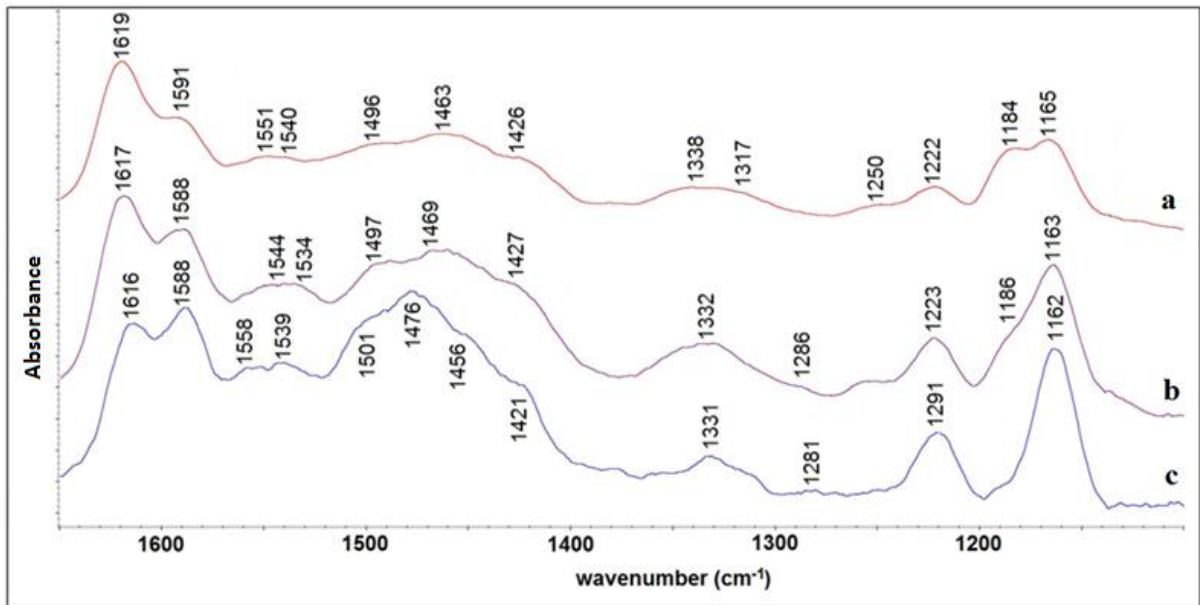


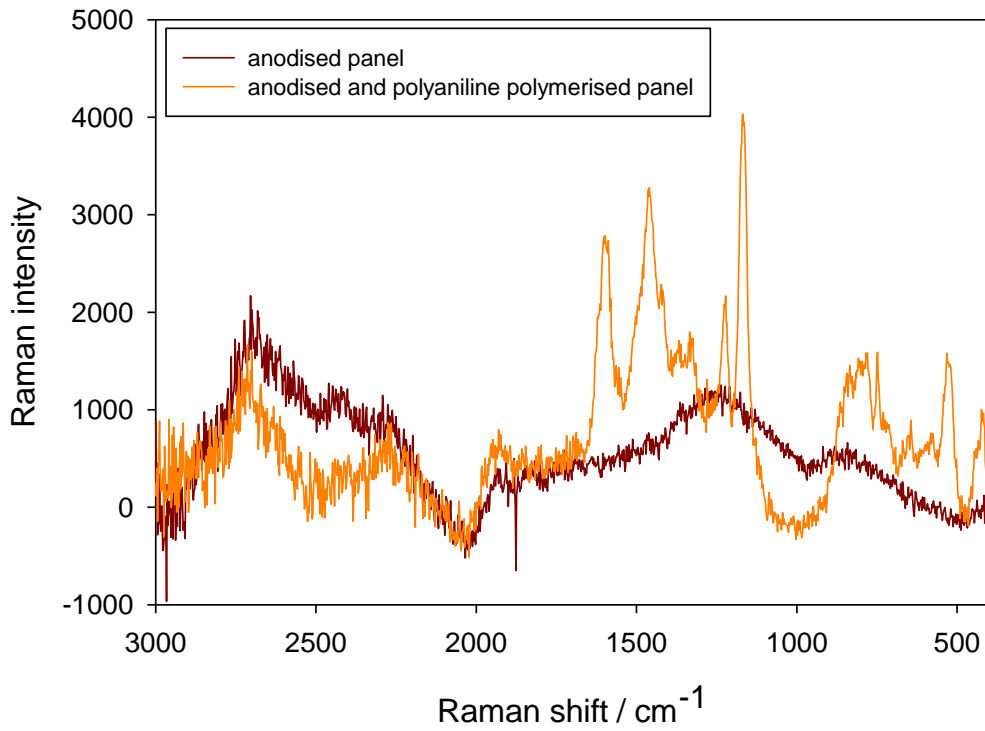
Figure 6.19. Region of 1600 – 1100  $\text{cm}^{-1}$  of PANI on 5083 in different oxidation states: (a) LEB, (b) ES, and (c) EB.

PANI			vibrational assignment
LB	ES	EB	
1619s	1617s	1616m	vC-C B stretch rings
1591	1588	1588m	vC=C Q stretch ring
1551*	1544	1558	vC=C SQ
1540*	1534	1539	1515 to 1590 cm <sup>-1</sup> vCC for the partially oxidised polymer
1496*	1497	1501	vC-C stretch & C-H bend ring
1463*	1469	1476	C-H bend ring + vC-C stretch, vC=N Q ring
1426*	1427	1421	C-N-H bend
1338*	1332s	1331s	C-H bend B, vCNC at 1339 cm <sup>-1</sup> for the partially oxidised polymer
1317*			C-H bend
1286*	1281		C-H bend
1250*	1250		asymm vC-N stretch
1222	1223	1219	symm vC-N, vCN 1220 cm <sup>-1</sup>
1184*	1186		C-H bend, CH in-plane bend 1191 cm <sup>-1</sup> for the B rings of the reduced polymer
1165*	1163s	1162s	C-H bend stretch + vC-C stretch, CH in-plane bend 1167 cm <sup>-1</sup> for the partially oxidised polymer
1006			ring def
880			ring def

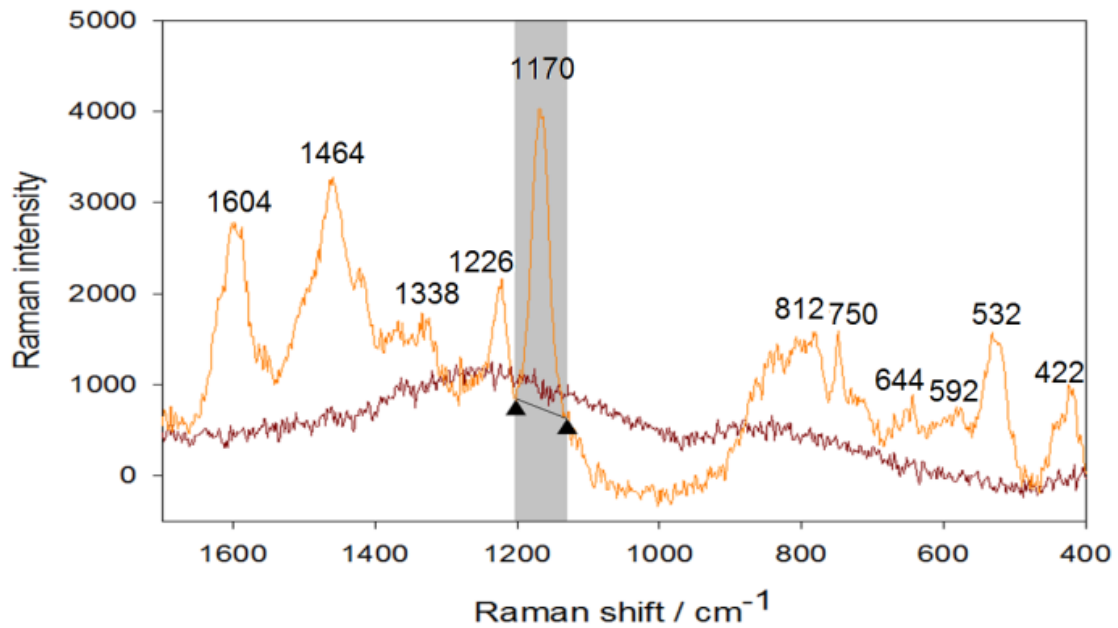
\*peaks that are normally not present in the LEB form, but are nevertheless present indicate that there are also some other forms of PANI present when LEB is being prepared, i.e. mixture of EB and LEB present at the same time.

Table 6.4. Raman spectroscopy assignment for PANI in their different oxidation states from film electrodeposited on 5083 alloy from Figure 6.18 and 6.19.

The typical PANI Raman spectrum includes the following: a strong band at  $1470\text{ cm}^{-1}$  corresponding to the presence of the C=N stretching mode of Q units, and a C-N stretching mode of single bonds at  $1219\text{ cm}^{-1}$ . The C-C and CH benzene deformation modes indicate the presence of Q rings and are observed at  $1595$  and  $1163\text{ cm}^{-1}$ . The presence of these two bands indicates the presence of separated, and thus localised, single and double bonds in the structure. The conducting form of PANI, ES, assigned to C-N<sup>•+</sup> stretching of semiquinone radical at  $1331\text{ cm}^{-1}$  [48]. The  $\nu_{\text{CC}}$  and  $\beta_{\text{CH}}$  bands of benzene rings are the characteristic vibrational assignments of LEB form of PANI [280]. This strong band at  $1619\text{ cm}^{-1}$  points to the B mode structure and indicates that the polymer present here is in a reduced form of PANI [199]. The characteristic peak for Q rings in Raman spectra relates to EB and PNB form at  $1500\text{ cm}^{-1}$  assigned to  $\nu_{\text{C=N}}$ , and  $1590\text{ cm}^{-1}$  assigned to  $\nu_{\text{C=C}}$  [1876], while the mixed mode of C-N and ring C-C stretching vibrations are at  $1250\text{ cm}^{-1}$  band [201]. There were no shifts in the bands at  $\sim 1490\text{ cm}^{-1}$  for  $\nu_{\text{C=N}}$  band and  $\nu_{\text{C-N}}$  at  $1220\text{ cm}^{-1}$  as the polymer was being oxidised, however, the ratio of bands at  $\nu_{\text{C=C}}$  at  $1590\text{ cm}^{-1}$  and  $\nu_{\text{CC}}$  band at  $1618\text{ cm}^{-1}$  differed. As the polymer was being oxidised, the Q rings of CH benzene deformation modes at  $1163\text{ cm}^{-1}$  changed from a doublet to a singlet. In the fully oxidised state the  $1163\text{ cm}^{-1}$  band completely masks the band at around  $1184\text{ cm}^{-1}$  and can be assigned to the C-H stretching of Q rings in the polymer matrix [214]. The band ratio of the B and Q rings at  $1615$  and  $1590\text{ cm}^{-1}$  changed as the film was being oxidised and the overlapping bands of quinoid rings in the  $1500\text{-}1430\text{ cm}^{-1}$  region narrowed. The bands,  $1589$ ,  $1476$  and  $1163\text{ cm}^{-1}$ , indicate the fully oxidised structures of EB form of PANI.



(a)



(b)

Figure 6.20. Raman spectra (a) of the 3000 to 500  $\text{cm}^{-1}$  region, and (b) of the 1680 – 400  $\text{cm}^{-1}$  region of anodised electrode in red and anodised with PANI films grown on top in orange on an aluminium electrode. Raman shows characteristic absorption bands for PANI at 1604, 1464, 1226, 1170, 812, 750, 532 and 422  $\text{cm}^{-1}$  [281].



Figure 6.20 shows PANI on the surface of an alloy and demonstrates that the strong peak at  $\sim 1170\text{ cm}^{-1}$  would be a good indication of the presence of PANI or the oxide layer on the surface of the alloy. Therefore, Raman mapping scan in the region of  $1200 - 1100\text{ cm}^{-1}$  was used to identify the distribution of PANI in the cross section of the aluminium alloy, as shown in Figure 6.21.

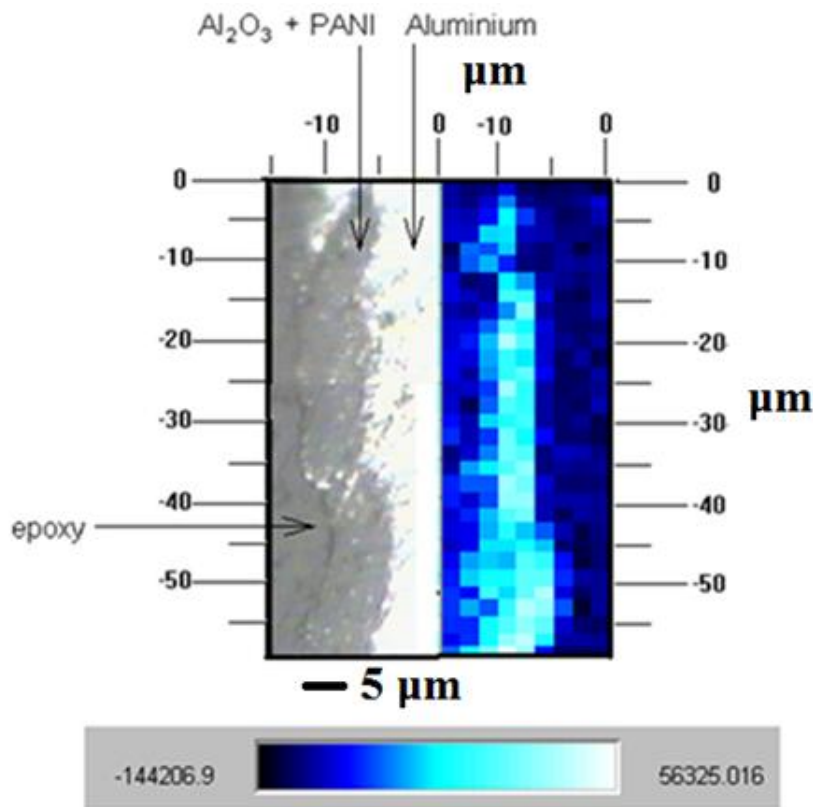


Figure 6.21. Raman mapping of the  $1200 - 1100\text{ cm}^{-1}$  region for PANI distribution along the anodised and PANI polymerised cross-section.

The scale in Figure 6.20 indicates the colour intensity scale of the  $1170\text{ cm}^{-1}$  peak and suggests that the PANI growth is evenly distributed throughout the aluminium oxide layer of the alloy with a higher concentration near the aluminium-aluminium oxide surface compared to the surface of the alloy. This indicates that the growth of the polymer is more likely to be from the alloy up rather than from the surface down, with a proposed mechanism included in the discussion section of this chapter.



### 6.2.6. Reflectance UV-Vis spectroscopy

The most stable state of electrochemically synthesised PANI on marine grade aluminium shows two absorption bands, Figure 6.22(a), from 300 to 450 nm is ascribed to a  $\pi \rightarrow \pi^*$  transition of B rings [29, 282]. The peak at around 660 nm is assigned to the excitation of the Q segment (-N=Q=N-) [29], and corresponds to the conducting ES form of PANI responsible for the molecular excitation associated with the Q diimine structure [283]. This further confirms the presence of PANI on the 5083 aluminium alloy.

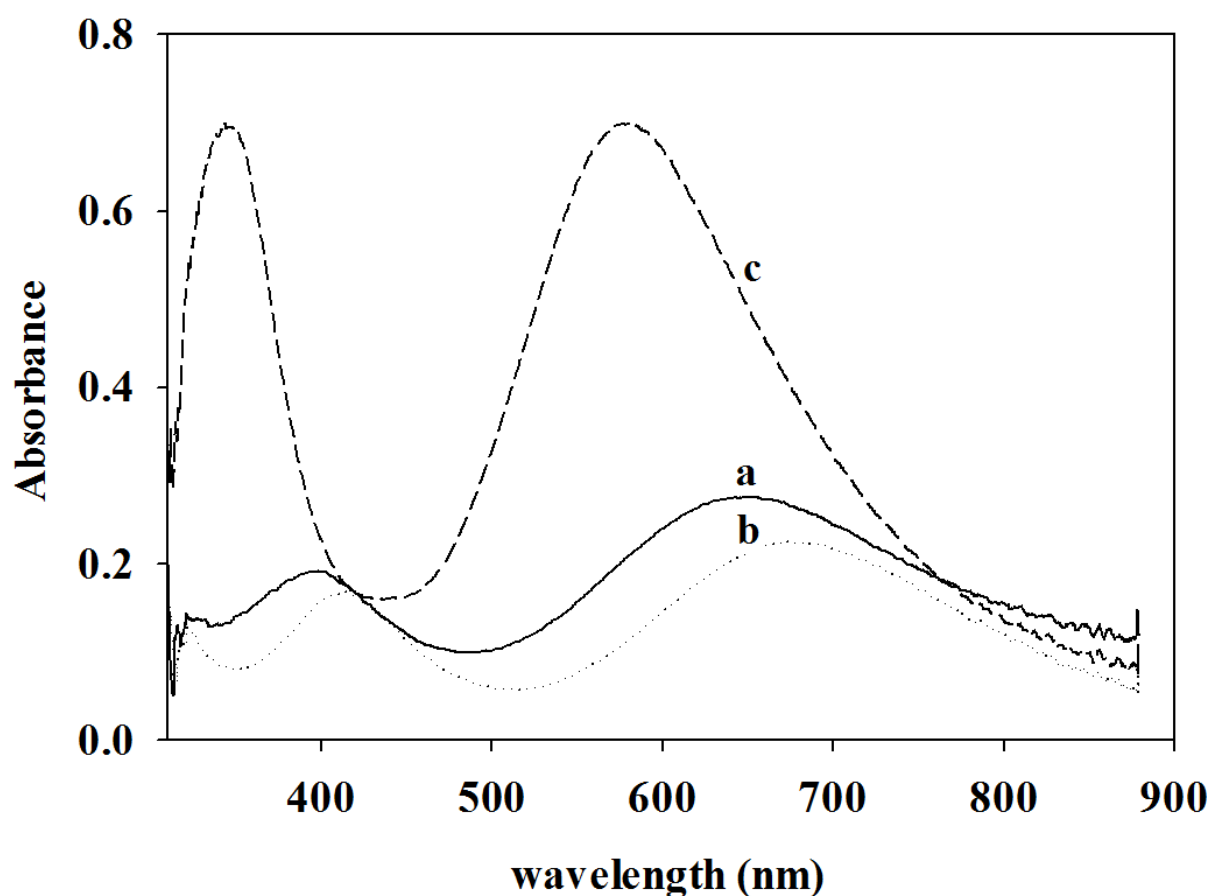


Figure 6.22. (a) most stable form, (b) fully reduced form, and (c) fully oxidised form.

		wavelength		
c	→	a	→	b
		321 nm		321 nm
341 nm	→	395 nm	→	408 nm
577 nm	→	651 nm	→	674 nm

The absorption bands at around 300 and 450 nm show the  $\pi \rightarrow \pi^*$  transition of the B rings and are characteristic of the LEB form of PANI [284], while the absorption at around  $\lambda = 340$  nm is caused by the  $\pi \rightarrow \pi^*$  transition of B rings and is characteristic of the PNB form of PANI [284], with a decrease in intensity as well as a shift to higher values reported by others [29, 283, 284]. The LEB oxidation state shows peaks at 320 nm and 600 – 660 nm [93, 287, 288, 289]. Peaks at around 600 – 660 nm are ascribed to the excitation of the Q segment (-N=Q=N-) [29, 284, 285, 286]. The peak at 550 nm is ascribed to a energy gap transition in the PNB form of PANI and reflects the fully oxidised state of PANI [58, 201]. The main absorption band in the red region of 650 nm, which corresponds to the conducting ES of PANI responsible for molecular excitation associated with the quinone diimine structure, shifts to 674 nm [58]. The growth of intensity of the ca. 600 nm band in the red region simultaneously with a simultaneous decrease in the intensity of the band at  $\lambda = 340$  nm shows a progressive oxidation of the PANI film from the LEB form to the EB form [94, 283]. In oxidised samples, this peak moved in the opposite direction reaching 577 nm, which can be attributed to a energy gap. A similar shift was observed for the peak at around 400 nm: the band at 396 nm for PNB shifted to a higher wavelength (408 nm) for fully reduced samples and shifted again in the opposite direction for fully oxidised samples (to 341 nm) exhibiting a  $\pi$ - $\pi^*$  transition [58]. The band at 340 nm decreased in intensity and shifted to a higher value when the polymer went from a fully oxidised form to the EB form [58].

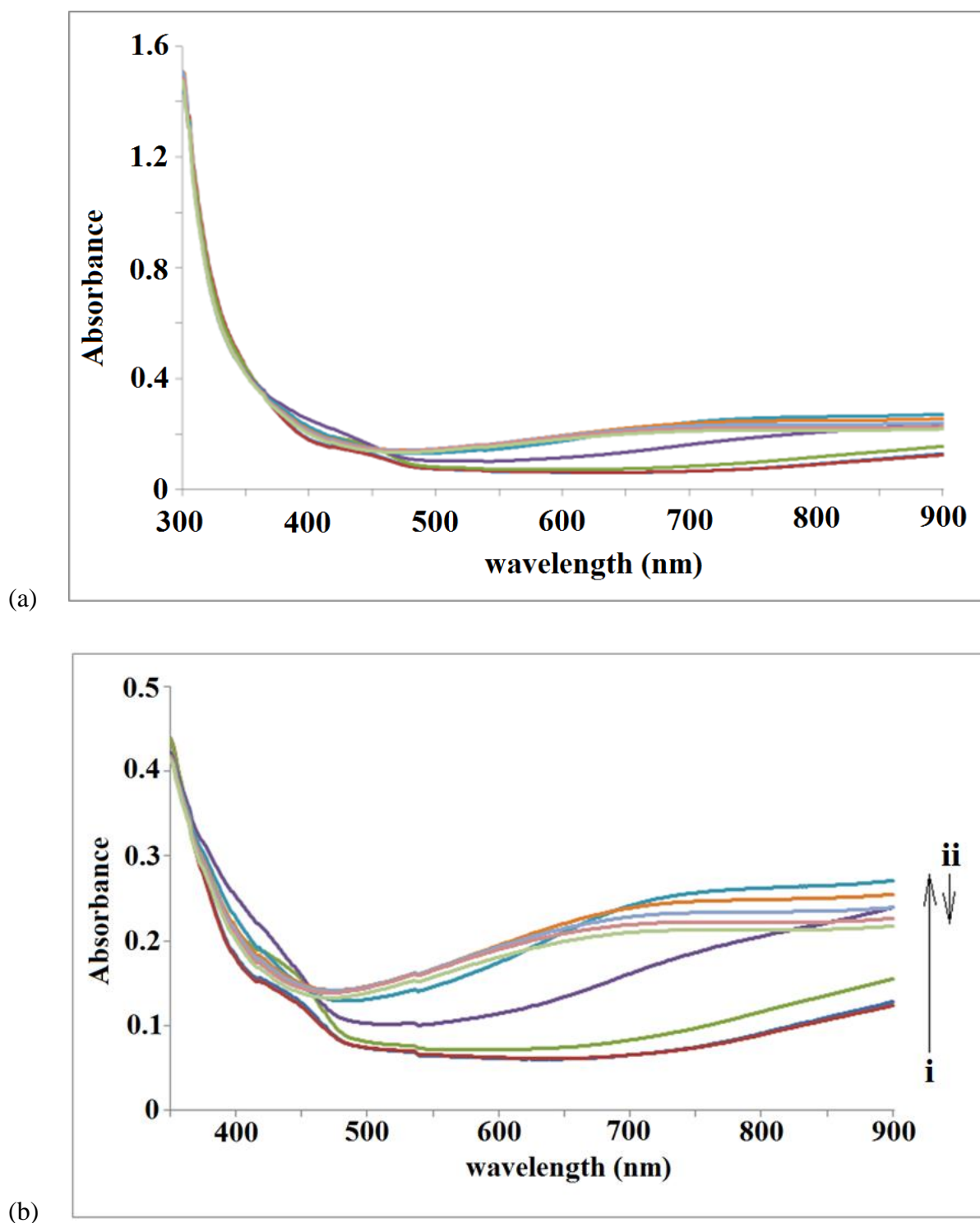
6.2.7. *in situ* UV-Vis spectroscopy of PANI film in 0.5 M oxalic acid solution

Figure 6.23. (a) Absorbance of polyaniline up to a value of 1.6, and (b) up to a value of 0.5, for 300 – 900 nm for *in-situ* UV-Vis in a 0.5 M oxalic acid electrolyte after running 10 cycles with 0.5 M oxalic acid in the presence of 0.1 M aniline monomer between -0.1 and 2.4 V at  $50 \text{ mV s}^{-1}$  with (i) -0.4 V to 0.4 V (max), and (ii) 0.4 V to 1.2 V.

At potential values of -0.4 V a weak band at 876 nm was observed, indicating that the reduction was not complete [284].

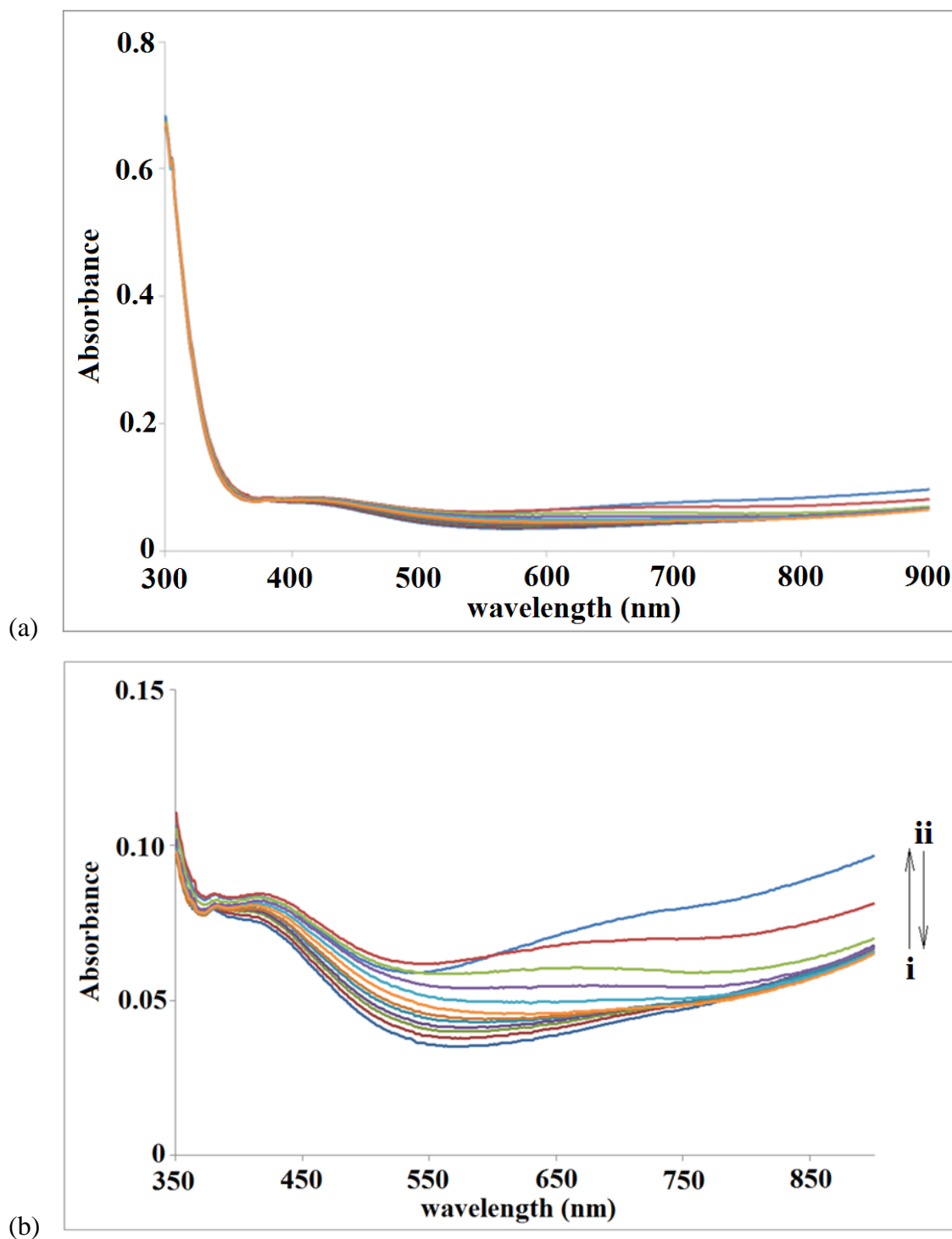


Figure 6.24. (a) Absorbance of polyaniline up to a value of 0.8, and (b) to 0.15, for 300 – 900 nm of *in-situ* UV-Vis in 0.5 M oxalic acid electrolyte after running 10 cycles in 0.5 M oxalic acid + 0.1 M aniline between -0.1 and 1 V at  $50 \text{ mV s}^{-1}$  (i) -0.1 V to 0.5 V (max), and (ii) 0.5 V to 1 V.

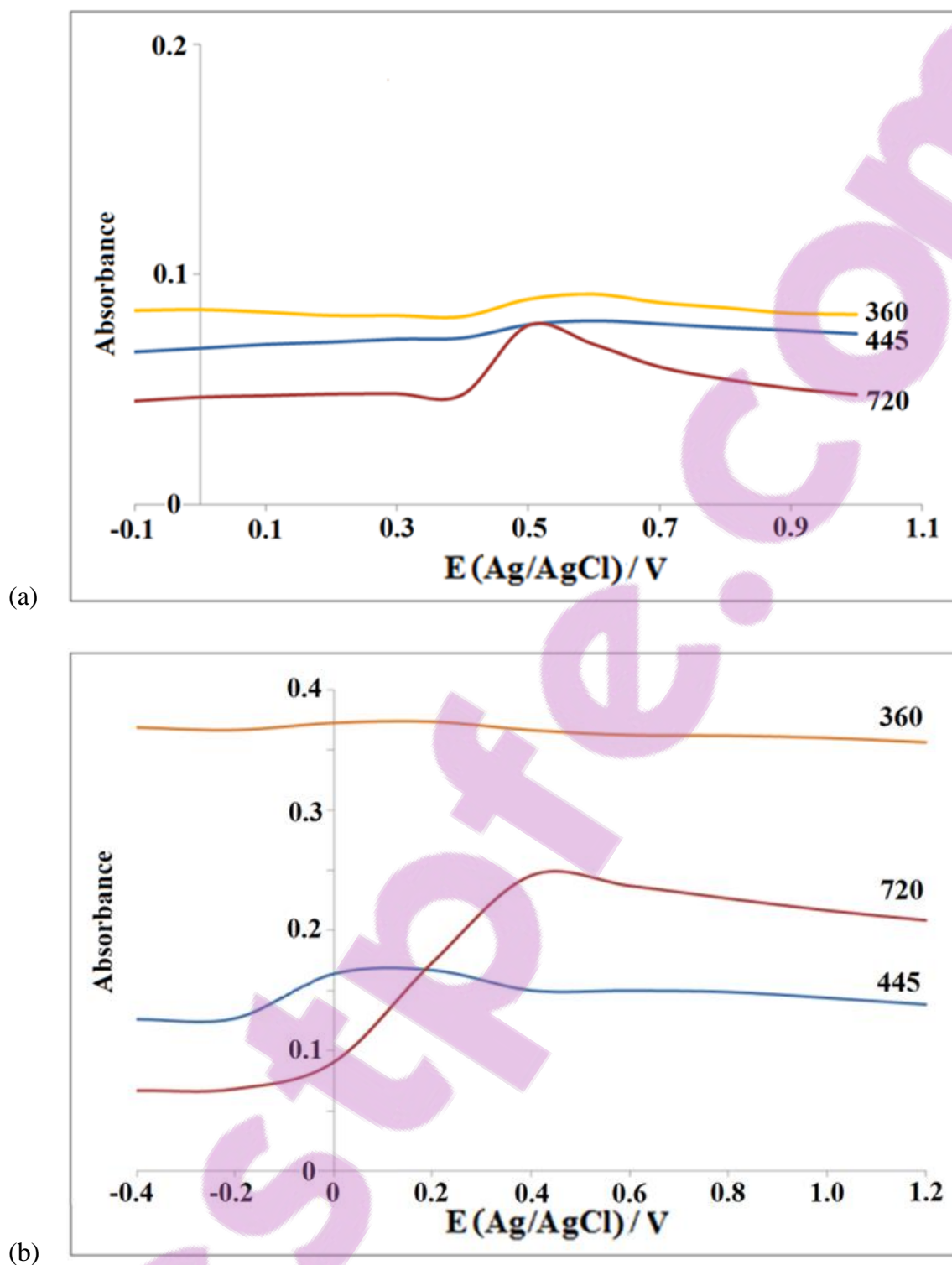


Figure 6.25. The absorption on electrode potential for the band at  $\lambda = 720$  nm in red,  $\lambda = 445$  nm in blue and at  $\lambda = 360$  nm in yellow with the PANI prepared in 0.5 M oxalic acid electrolyte in the presence of 0.1 M aniline monomer after running 10 cycles between (a) -0.1 and 1 V at  $50 \text{ mV s}^{-1}$ , and (b) -0.1 and 2.4 V at  $50 \text{ mV s}^{-1}$ , scan from -0.4 V to 1.2 V.

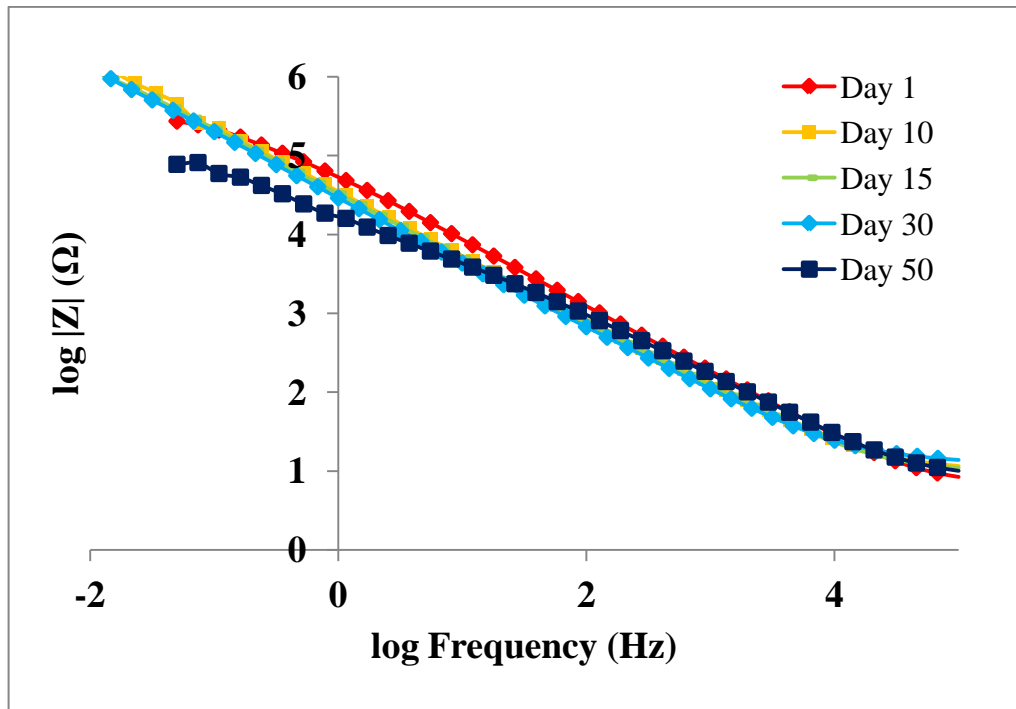
PANI films were grown under different conditions, -1 to 2.4 V and -0.1 to 1 V at  $50 \text{ mV s}^{-1}$  for 10 cycles, and these gave slightly different structural composition as can be seen from the UV-Vis spectra above, Figures 6.22 and 6.23. The peak at 360 nm is attributed to  $\pi \rightarrow \pi^*$  transition of the B rings and the broadening of this region suggested the presence of the LEB-type oligomer structures, whose peak is superimposed onto the peak from substituted quinones [280]. The peak at 415 nm is assigned to a polaron- $\pi$  transition, and the peak at 800 nm to a  $\pi$ -polaron transition [58]. As the potential was increased, the band at around 720 nm also increased, while the 445 nm band that corresponds to the presence of an intermediate state (polaron) formed during the electrooxidation of the LEB state of PANI. This peak maximises as a function of electrode potential at around  $E = 0.1 - 0.2 \text{ V}$  for the higher CV cycles. On the other hand, where the lower CV settings were used, the maximum is at ca. 0.5 V and would decrease back, with the  $\pi \rightarrow \pi^*$  electronic transition of neutral species at 362 nm, which is assigned to the aniline cation radical or oxidised benzidine dimer [58]. This band, as well as the decrease of its intensity with electrode potential shifted to higher values, has been reported at  $\lambda = 315 \text{ nm}$  [286]. A broad band at  $\lambda = 700 - 720 \text{ nm}$  was assigned to the *N*-phenyl-paraphenylenediamine (PPD) dimer and its dication [283]. The 720 nm band blue shifted to a higher value upon an increase in potential to 0.5 V, and then it would red shift back. For the absorption band at 420 nm, the maximum absorbance as a function of electrode potential was observed at around  $E = 0.6 \text{ V}$ . This band has been assigned to an intermediate state (polaron) formed during electrooxidation of the LEB state of PANI [286].

### 6.2.8. Corrosion resistance studies

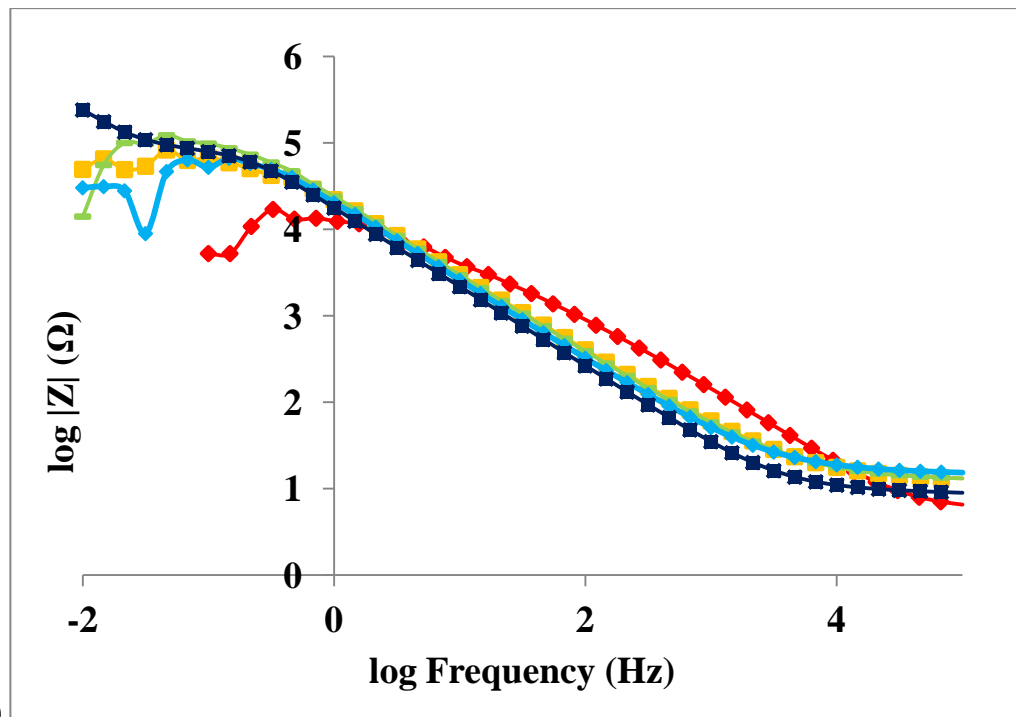
The corrosion protection afforded by a PANI coating systems on marine grade aluminium of different thickness was evaluated using impedance spectroscopy and compared at fixed immersion time. Polarisation experimental measurements revealed an ennobling of aluminium alloys to a higher potential in the presence of PANI coatings.

The corrosion protection mechanism provided to active metals by conducting polymers appears to involve a redox reaction, or formation of passivating metal oxide layer at the metal-polymer interface [79-80]. The anodisation process coupled with  $\text{O}_2$  reduction on the surface enables the film to remain stable [287]. Racicot et al reported that the corrosion rate of PANI-coated aluminium alloys was lowered by almost two orders of magnitude compared with that of a chromate conversion-coated sample with higher impedance values [288].

An electropolymerised PANI coating on three different grades of aluminium alloy was monitored by impedance measurements for periods of up to 50 days.



(a)



(b)

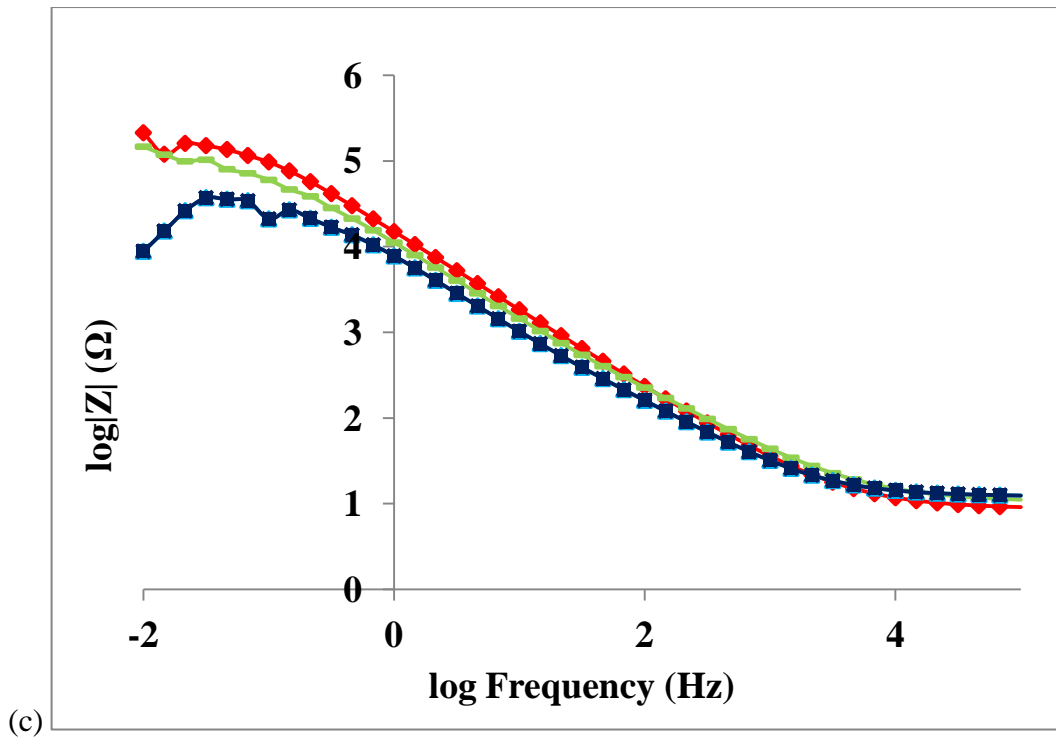
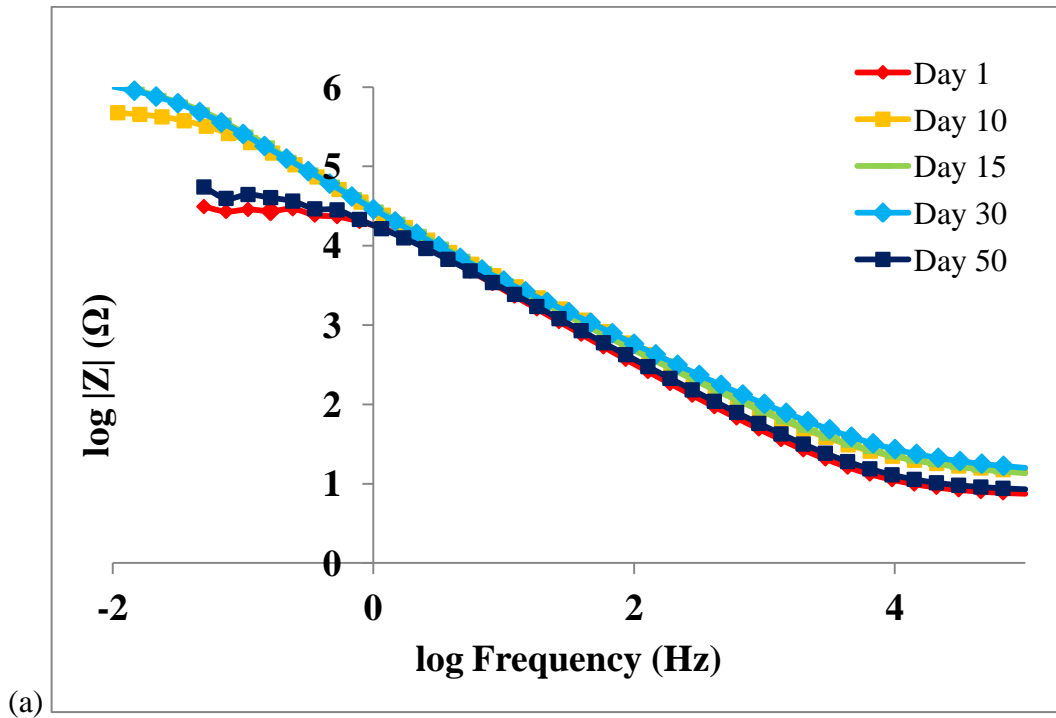


Figure 6.26. Bode plots of impedance modulus ( $|Z|$ ) vs frequency as a function of immersion time in 3.5 wt% NaCl solution for: (a) pure 1100, (b) pure 4043, and (c) pure 5083 alloys.





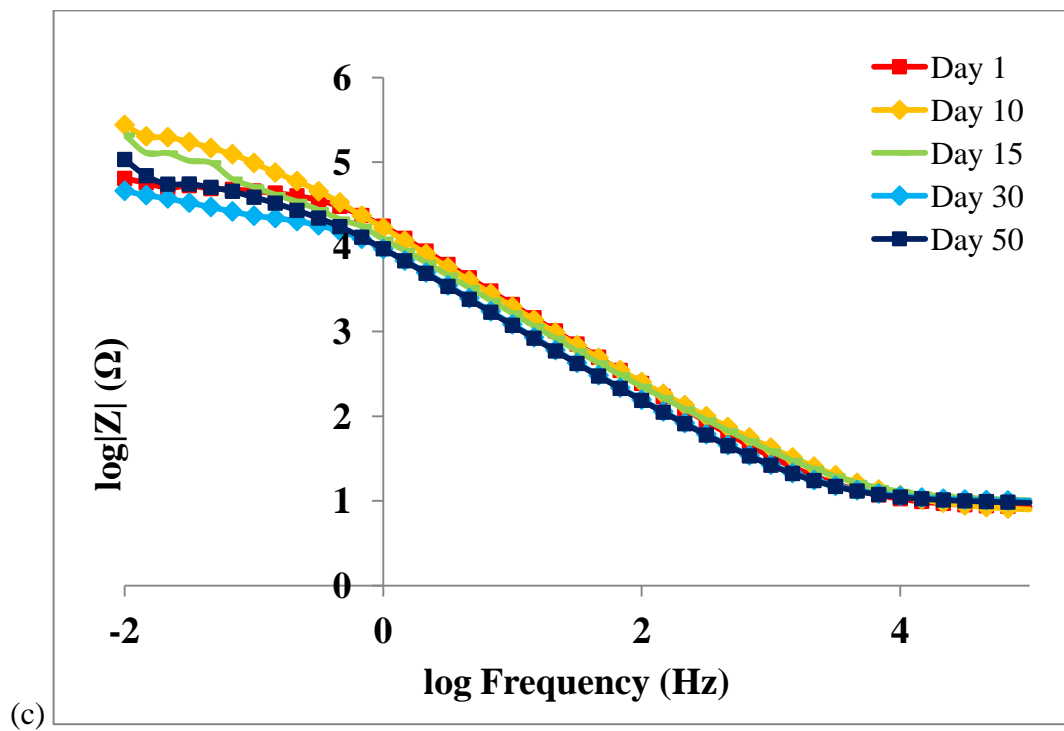
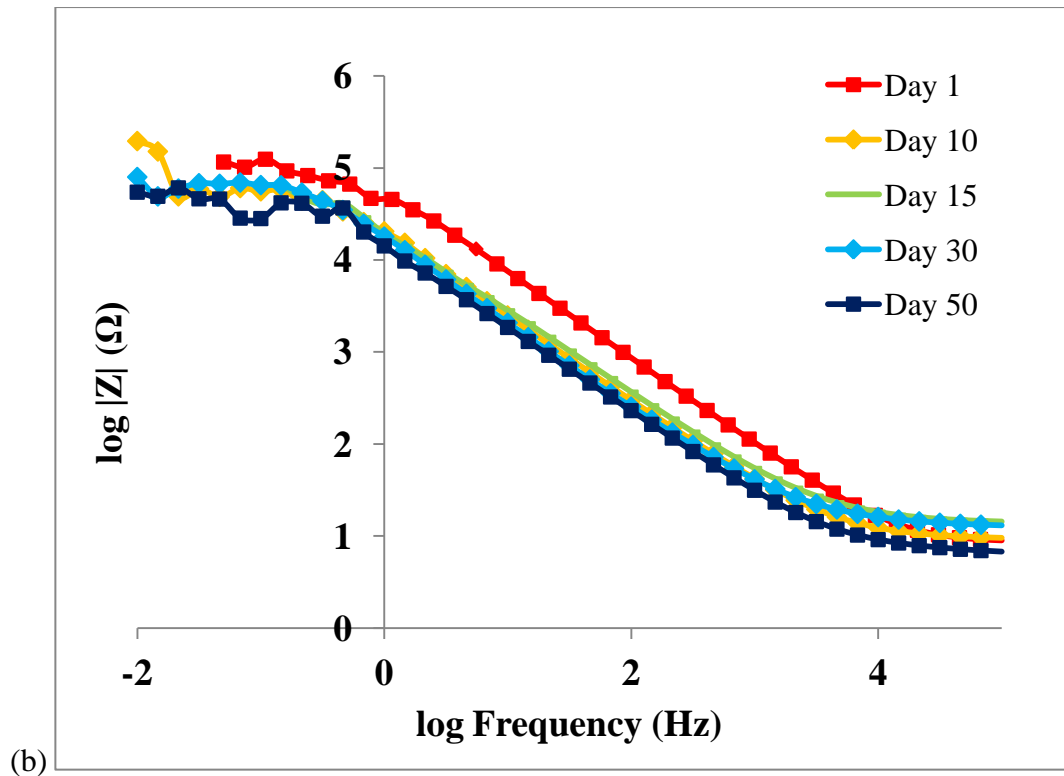
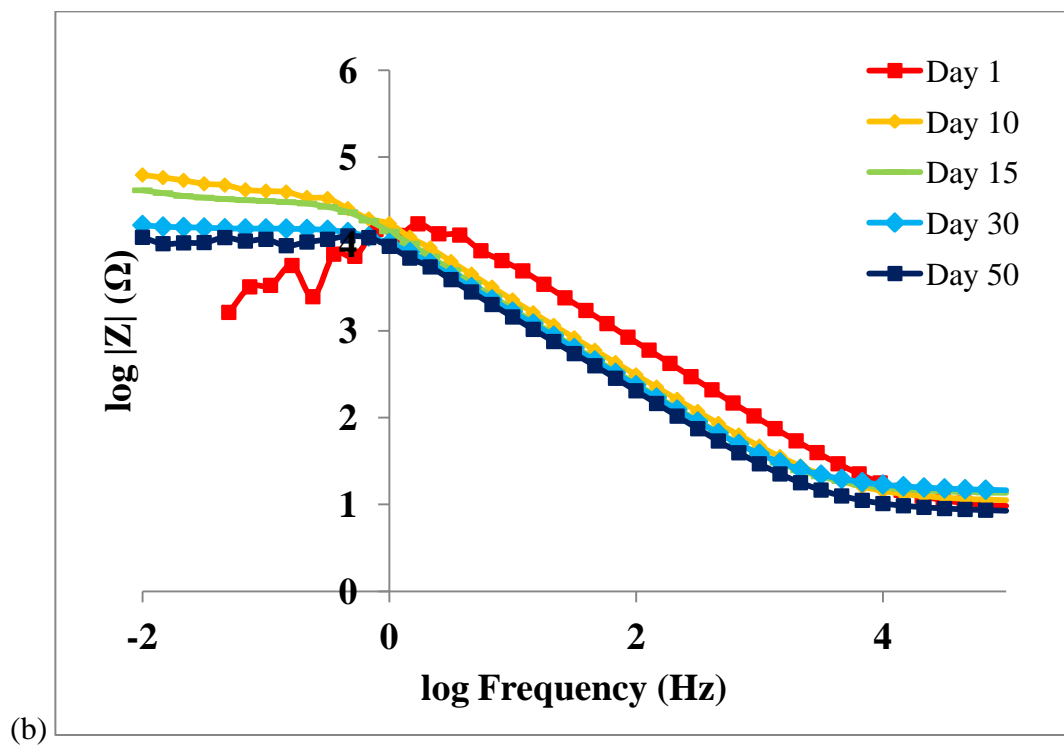
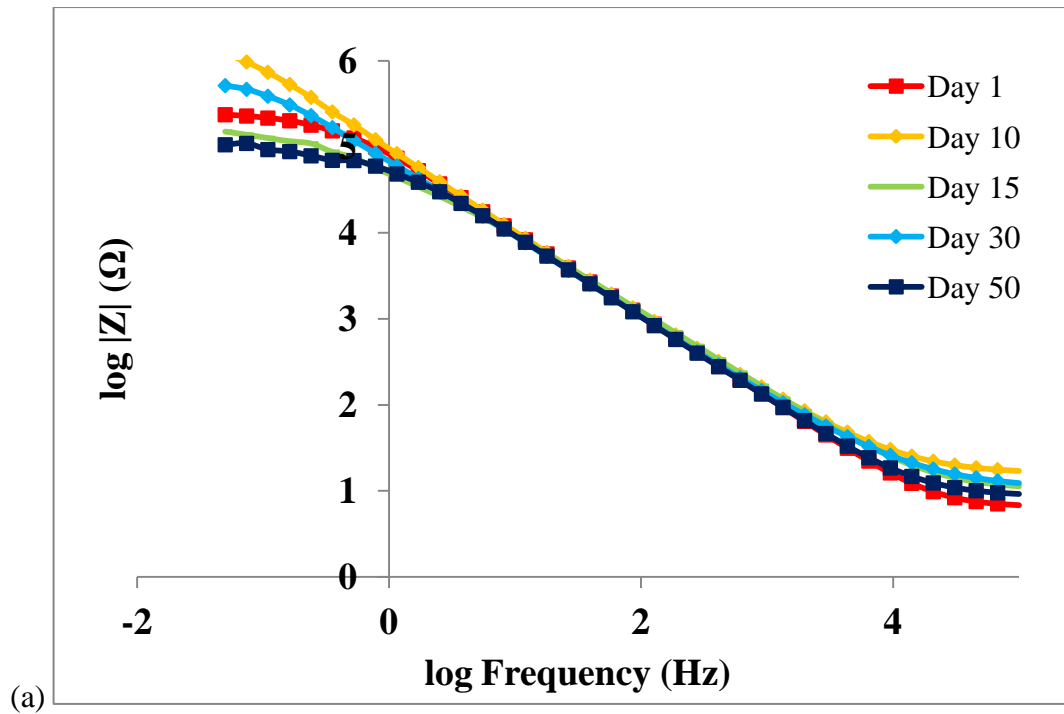


Figure 6.27. Bode plots of impedance modulus ( $|Z|$ ) vs frequency as a function of immersion time in 3.5 wt% NaCl solution for (a) PANI grown on 1100 at 1 V, (b) PANI grown on 4043 at 1 V, and (c) PANI grown on 5083 at 1 V.



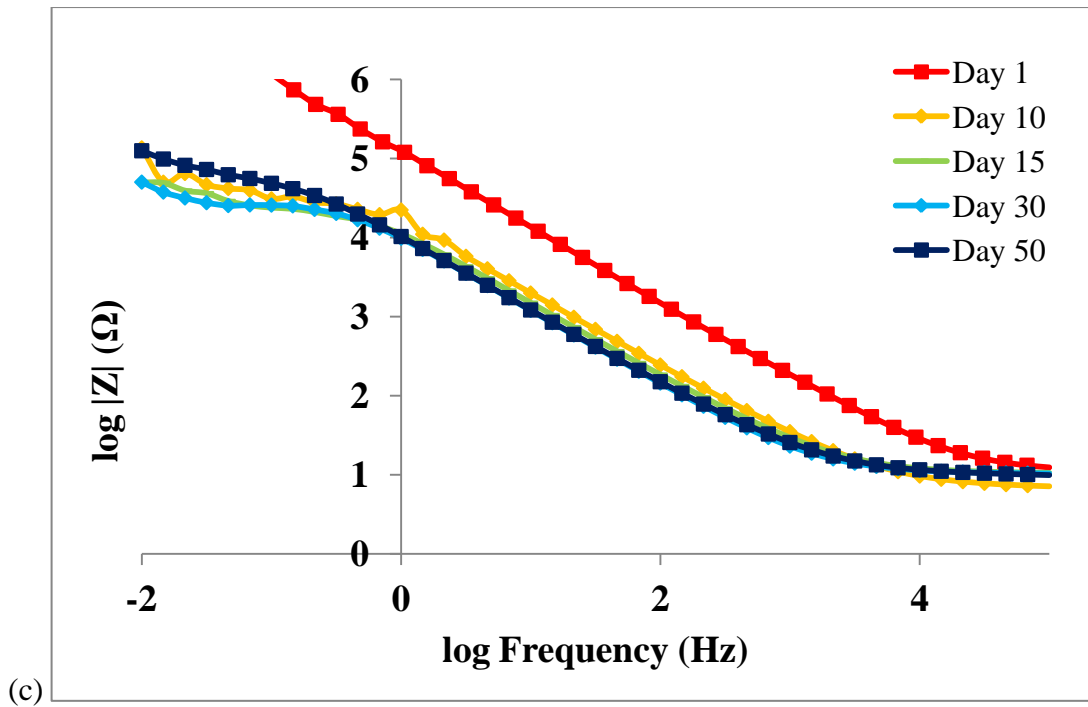
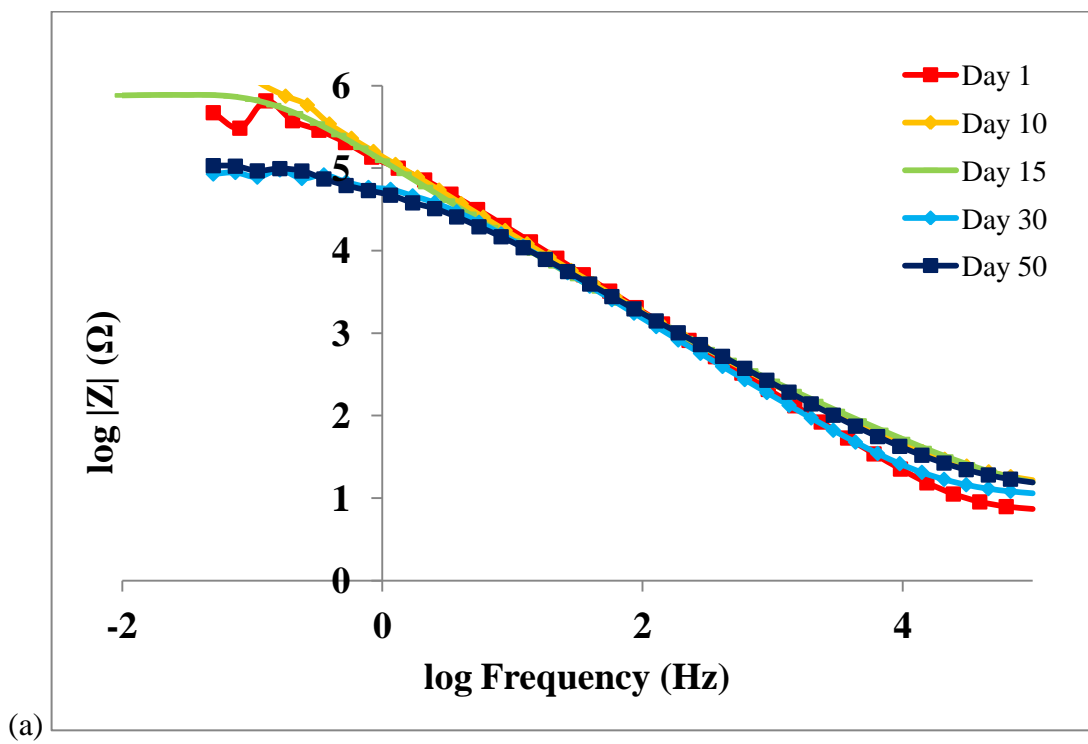


Figure 6.28. Bode plots of impedance modulus ( $|Z|$ ) vs frequency as a function of immersion time in 3.5 wt% NaCl solution for (a) PANI grown on 1100 at 2 V, (b) PANI grown on 4043 at 2 V, and (c) PANI grown on 5083 at 2 V.



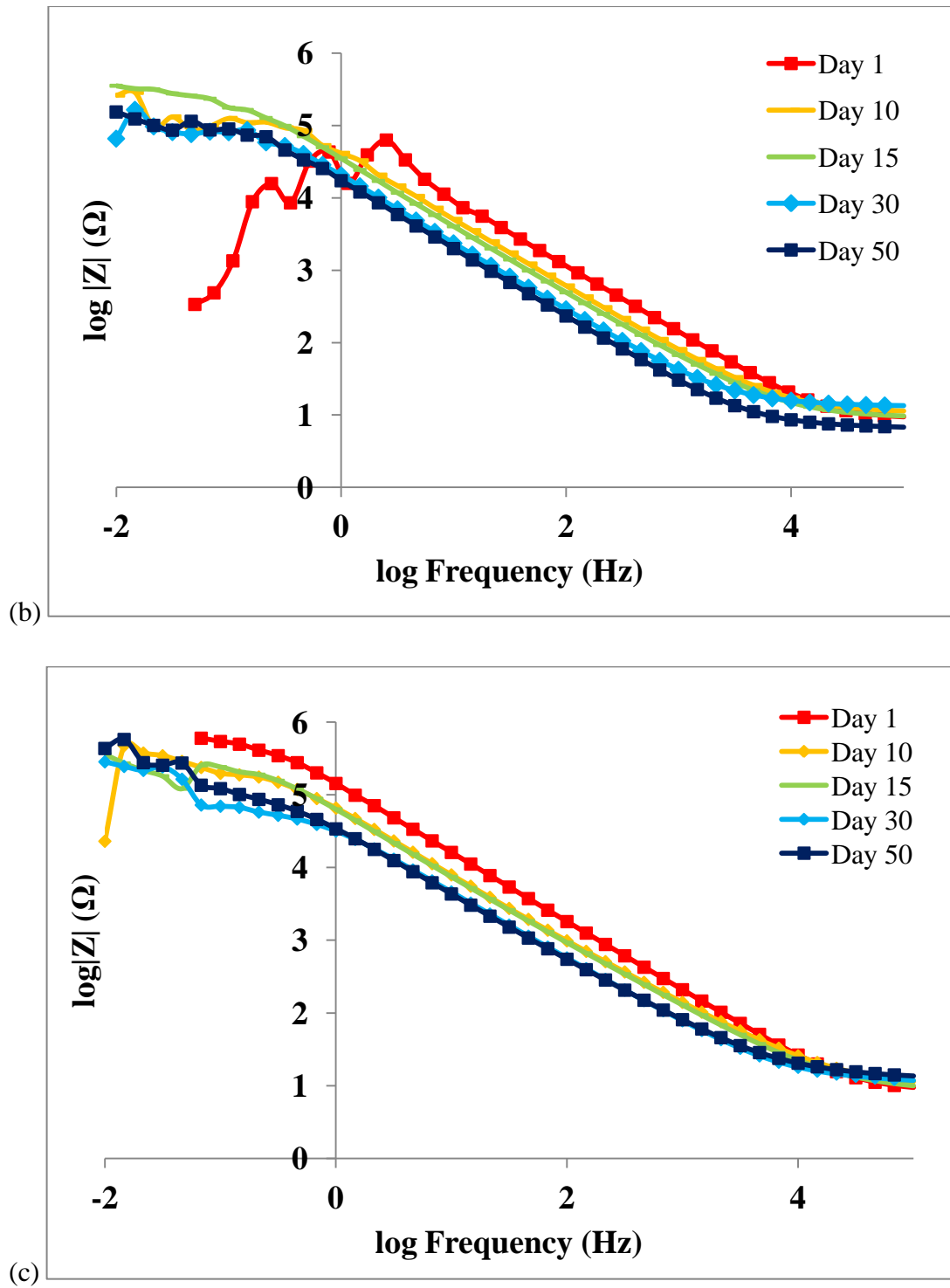
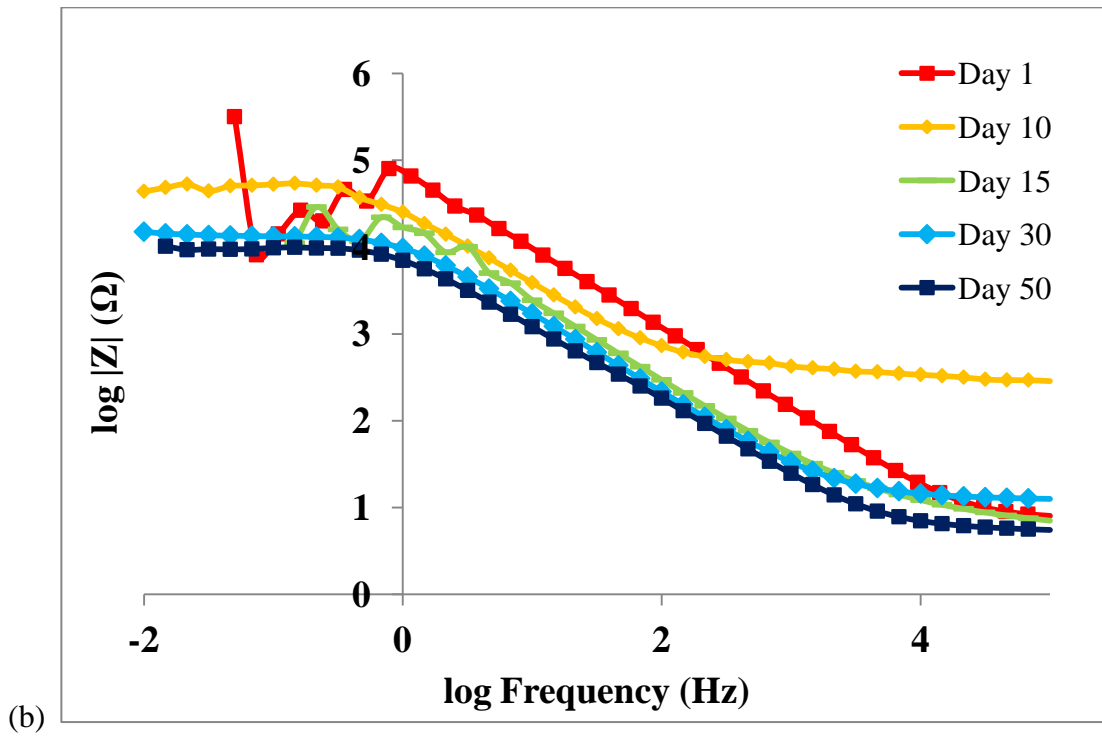
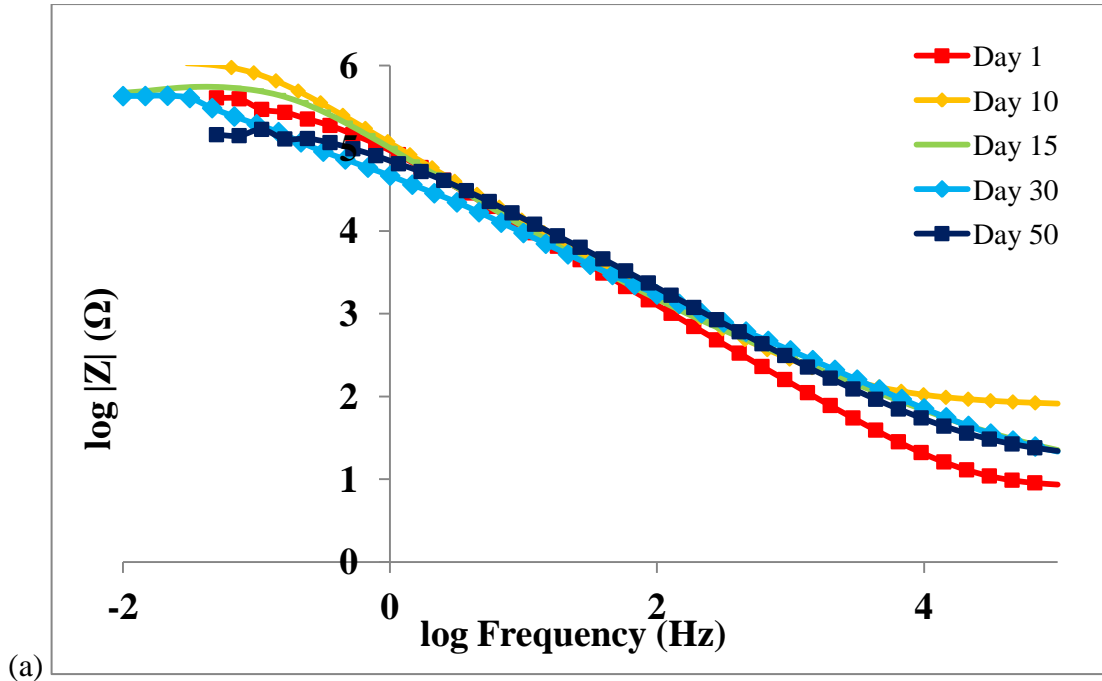


Figure 6.29. Bode plots of impedance modulus ( $|Z|$ ) vs frequency as a function of immersion time in 3.5 wt% NaCl solution for (a) PANI grown on 1100 at 3 V, (b) PANI grown on 4043 at 3 V, and (c) PANI grown on 5083 at 3 V.



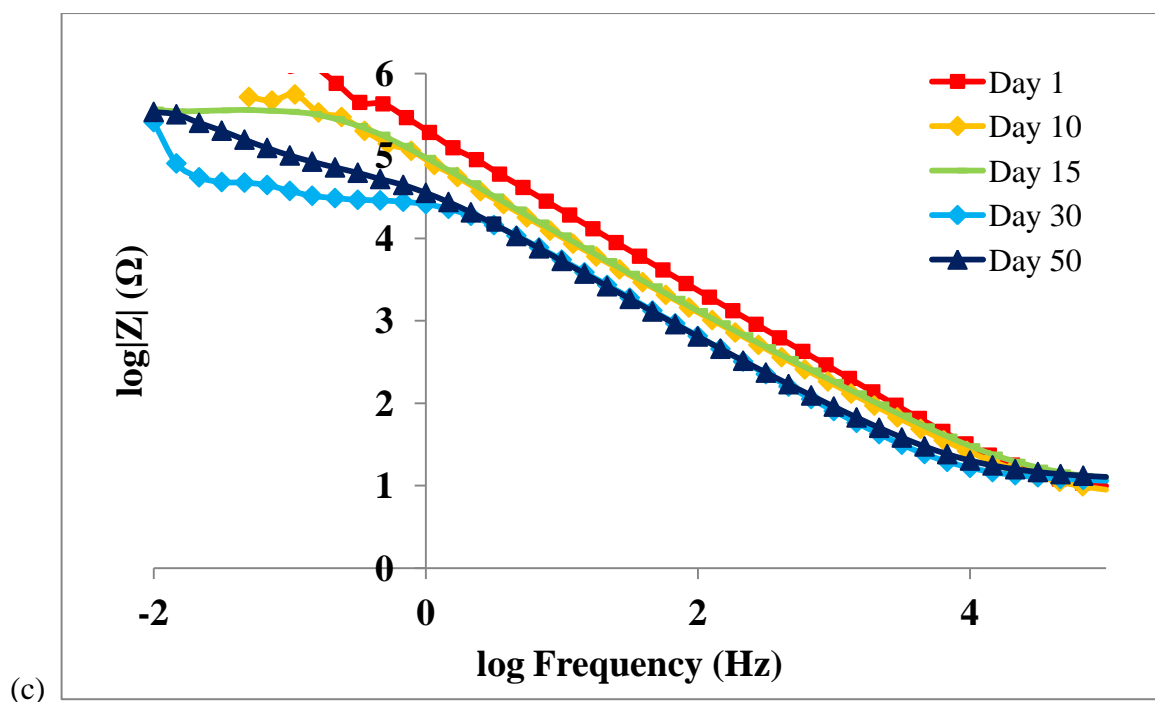


Figure 6.30. Bode plots of impedance modulus ( $|Z|$ ) vs frequency as a function of immersion time in 3.5 wt% NaCl solution for (a) PANI grown on 1100 at 4 V, (b) PANI grown on 4043 at 4 V, and (c) PANI grown on 5083 at 4 V.

The immersion behaviour of the aluminium alloys of the three different grades is presented above in Figures 6.26 – 6.30 in the absence (Figure 6.26) and presence of PANI coatings (Figures 6.27 – 6.30). Upon initial immersion, the coatings resistance was quite high and the behaviour could represent a capacitor. The coating took up water and ions rather rapidly, and the low-frequency impedance modulus decreased. The behaviour is quite similar with a decrease in impedance value upon time immersed in 3.5 wt% NaCl solution. Amongst the aluminium samples tested, the high purity aluminium, 1100 alloy, showed the best results. As PANI is grown at a higher applied potential, such as 2 V, it was possible to distinguish between the different alloys, with the high purity aluminium alloy 1100 always performing the best, while the other two alloys behaved similarly. As expected, the thicker PANI films performed the best (i.e. those prepared at 3 V and 4 V), with 1 V coated substrate being second best and 2 V being the worst, indicated by the large drop in impedance after one week. In other words, electrochemically synthesised PANI on marine grade aluminium at 3 V would be the ideal coating system for corrosion protection as it simplifies the preparation conditions and maximises performance. Hence the reason why 2 V applied potential PANI coated samples were used for testing the overall performance throughout this chapter and for

testing fouling protection in Chapter Seven. The theory behind it is that if the worst performing coated alloy is tested, the remaining samples should exceed the observed failure time.

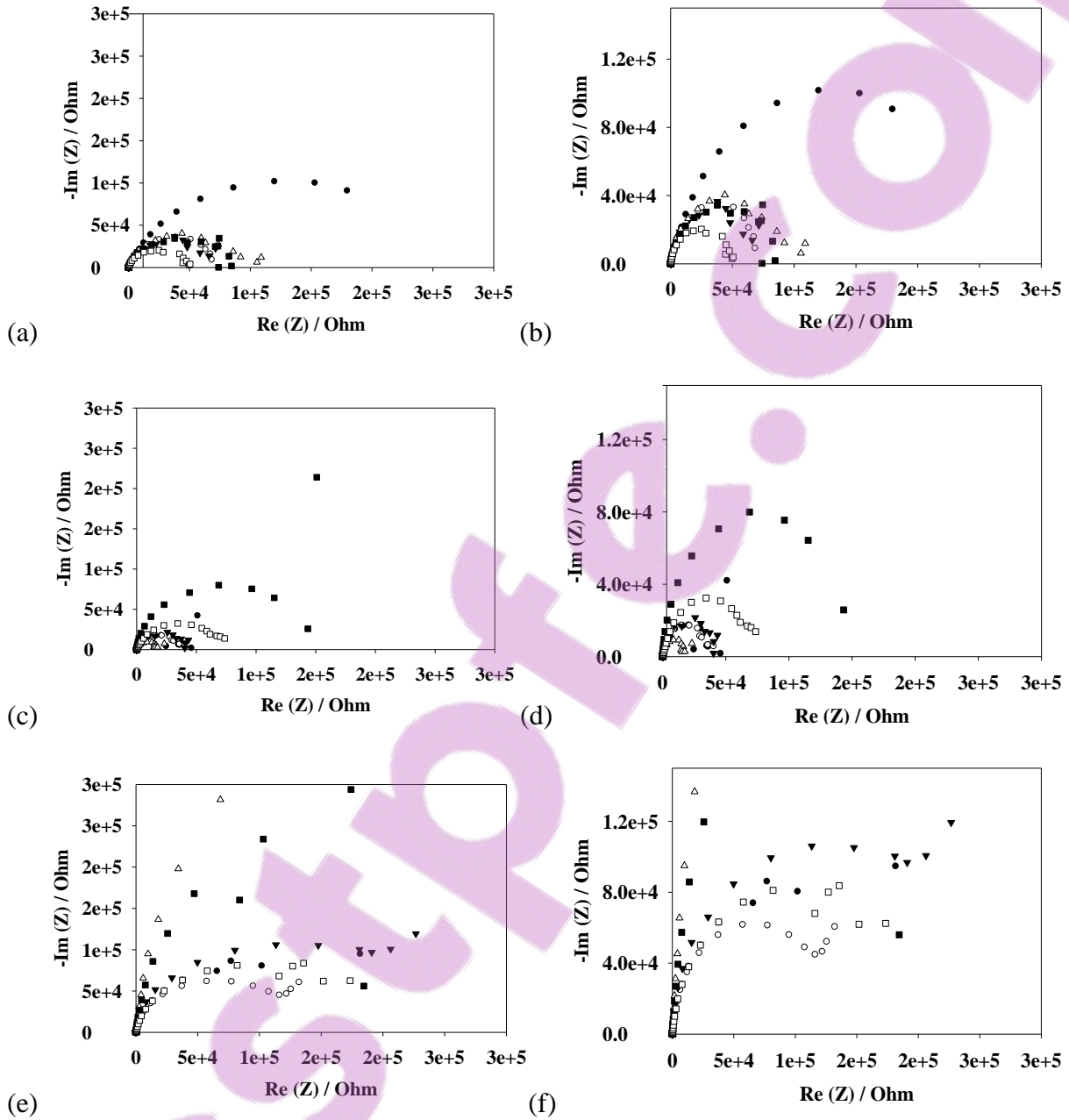


Figure 6.31. Nyquist plot of impedance data for coated and uncoated aluminium alloy at day 3 on (a) and (b) 1100 alloy, (c) and (d) 4043 alloy, and (e) and (f) 5083 marine grade alloy ● pure alloy ○ anodised 1 V ▼ PANI 1 V ▲ PANI 2 V ■ PANI 3 V □ PANI 4 V.

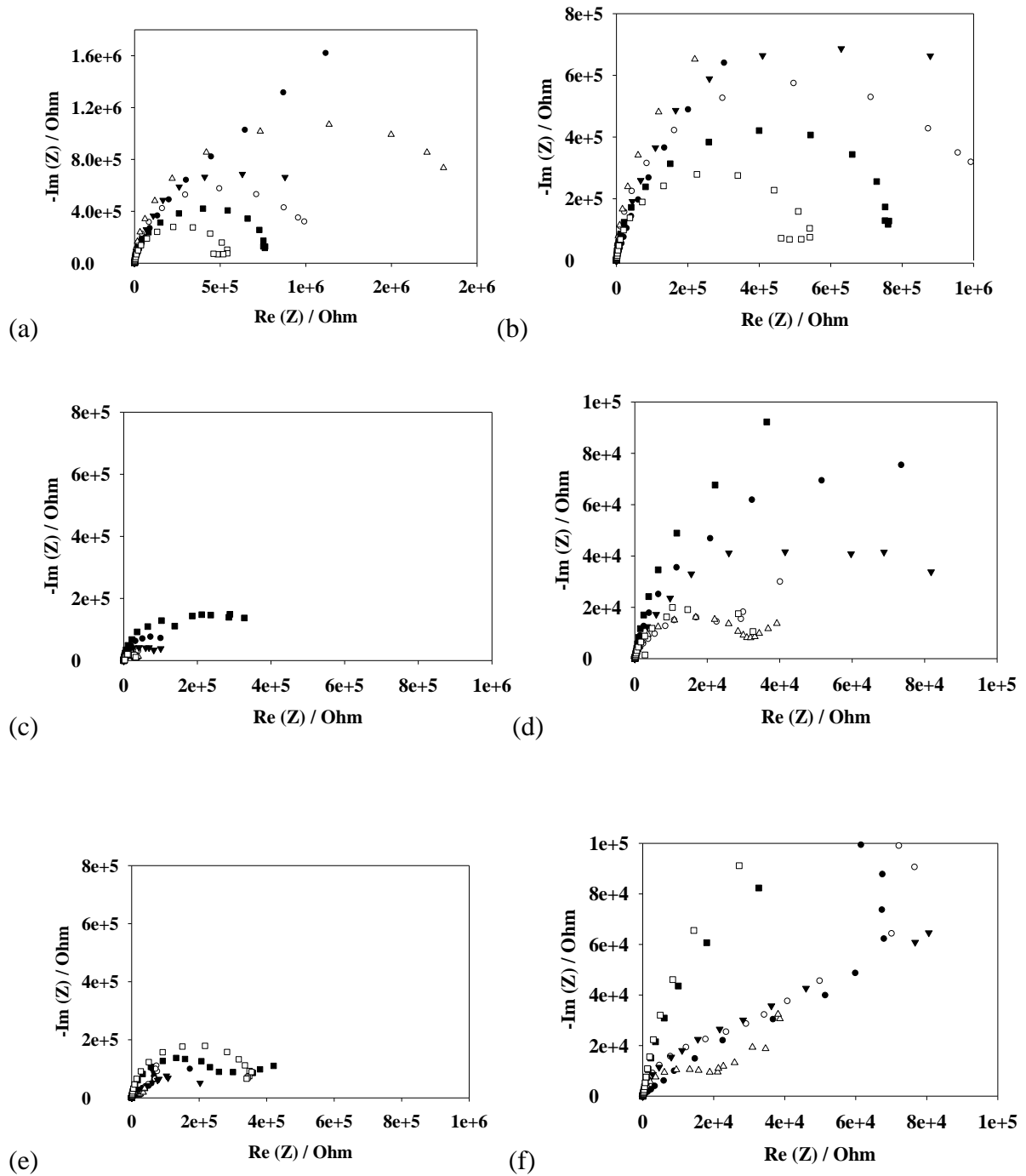


Figure 6.32. Nyquist plot of impedance data for coated and uncoated aluminium alloy at day 15 on (a) and (b) 1100 alloy, (c) (d) 4043 alloy, and (e) and (f) 5083 marine grade alloy  
 ● pure alloy ○ anodised 1 V ▼ PANI 1 V △ PANI 2 V ■ PANI 3 V □ PANI 4 V.



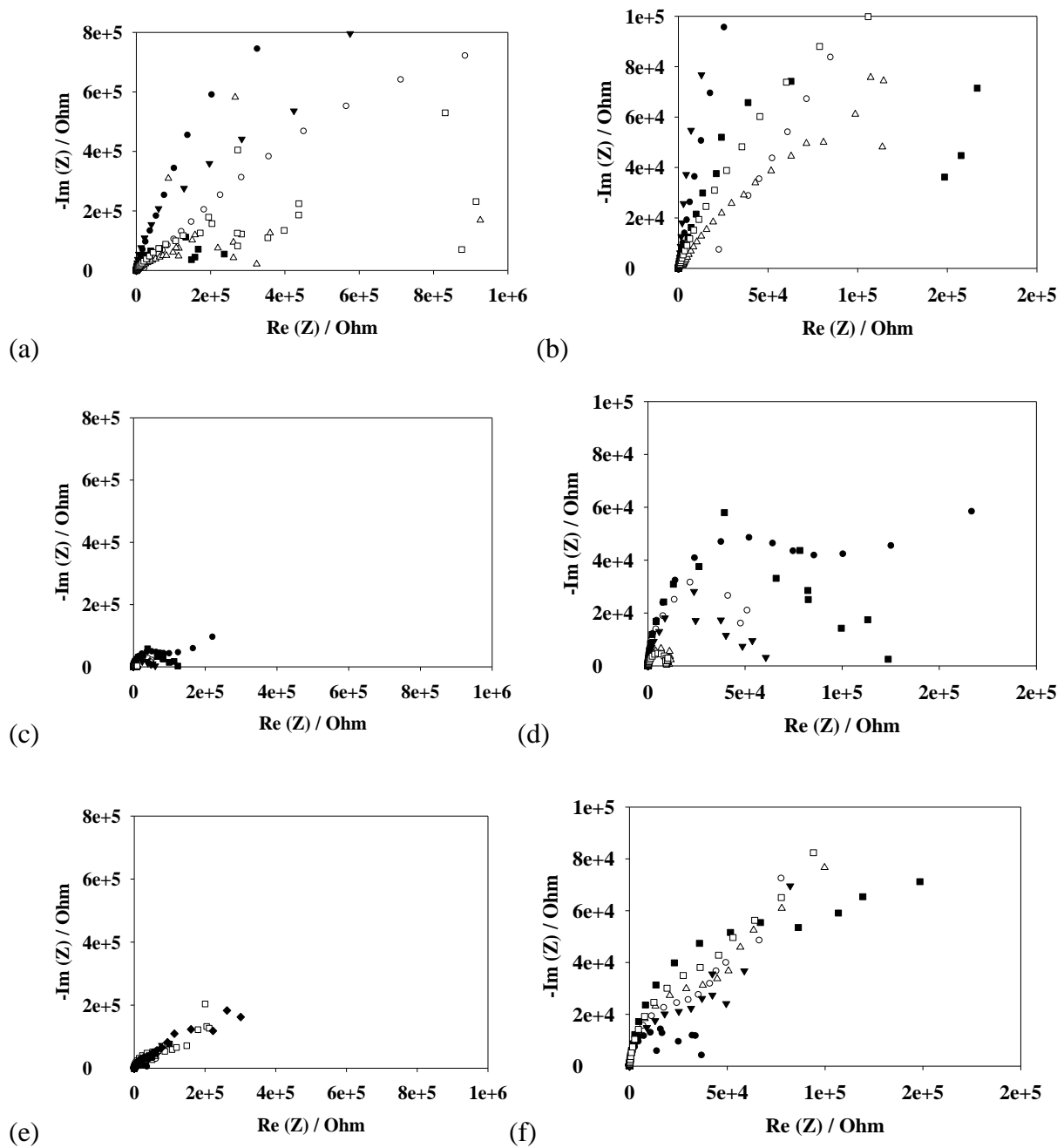


Figure 6.33. Nyquist plot of impedance data for coated and uncoated aluminium alloy at day 50 on (a) and (b) 1100 alloy, (c) and (d) 4043 alloy, and (e) and (f) 5083 marine grade alloy ● pure alloy ○ anodised 1 V ▼ PANI 1 V △ PANI 2 V ■ PANI 3 V □ PANI 4 V.

The  $R_{ct}$  is the charger transfer resistance of the area at the metal/coating interface at which corrosion occurs and  $C_{dl}$  is the corresponding capacitance.

The plot for the first day immersion revealed rather high impedance at low frequency ( $10^4 \Omega$ ) and reflected a largely capacitive behaviour. Such behaviour was indicative of the good barrier protection initially provided by the aluminium substrate. However, during the 10 day period, the impedance started to decrease for the marine grade aluminium, which was grown at 2 V, and it dropped by one order of magnitude to  $10^4 \Omega$ . This drop in impedance reflected a failure of the barrier property and the absorption of water through the coating in some cases [88]. The performance of PANI coated aluminium in general at 2 – 4 V improved, with 4 V performing the best, followed by 3 V > 2 V > 1 V > pure aluminium > pretreated aluminium.

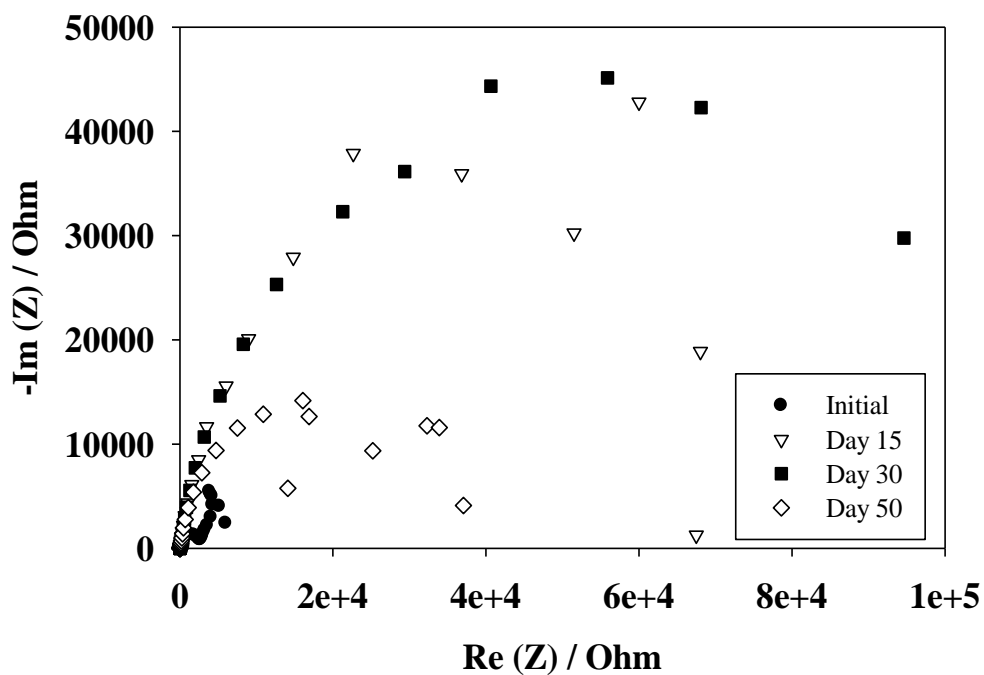
Marine grade aluminium alloy showed the greatest charge-transfer resistance values, while the other two alloys appeared similar in general on day 3, corresponding to the aluminium oxidation reaction. The corrosion resistance properties of PANI coating on 5083 alloy were not improved with an increase in electropolymerisation applied potential beyond 2 V. 4043 alloy showed the best corrosion performance in the next higher applied potential at 3 V. PANI 4 V and 2 V, 1 V, 3 V started off with a big semicircle, large  $R_{ct}$ , and then it decreased over time, with the decrease continuing after Day 50. A larger  $R_{ct}$  value attributed to a more effective barrier behavior of the coating. The impedance behaviour of bare 4043 shown above indicates that the corrosion resistance properties of the coating are not improved with extended electropolymerisation times. The  $R_{ct}$  decreased upon immersion time, unlike the other two grades of aluminium, indicating the least corrosion protection.

The lower values of  $C_c$  and  $C_{dl}$  for the coating provide further support for the protection of coating. Thus, the higher values of  $R_{ct}$  and  $R_{por}$  and lower values of  $C_c$  and  $C_{dl}$  indicate the excellent corrosion performance of the coating.

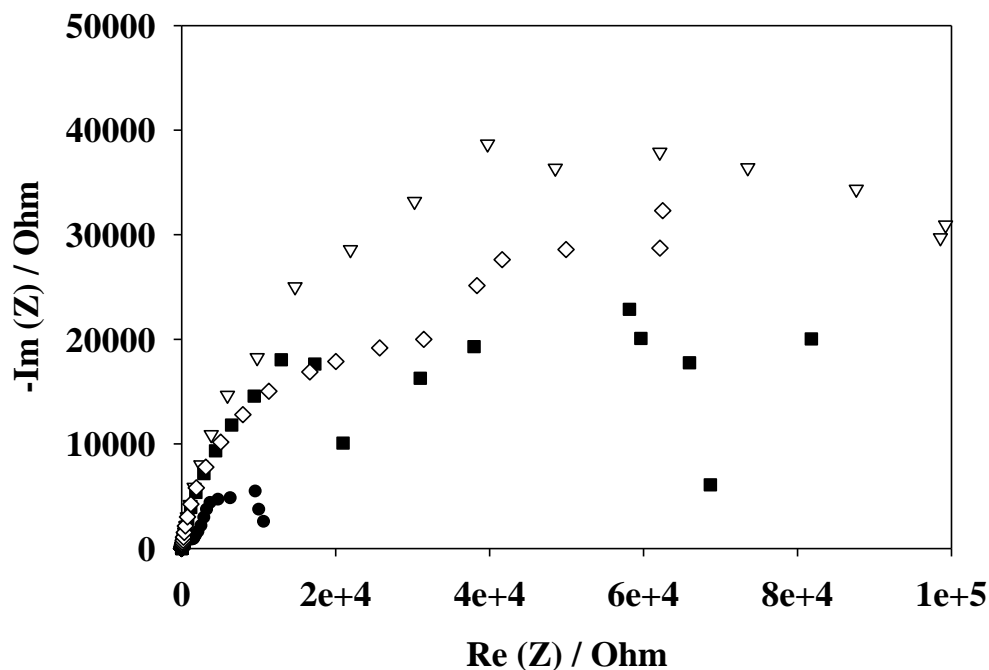
After Day 50 of alloy 1100 immersed in 3.5 wt% solution, oxidation occurs on the aluminium surface resulting in an increased oxide layer at the metal-conducting polymer interface and reduced PANI layer resulting in less conducting LEB form, as evidenced by an increase in the charge transfer resistance and a decrease in capacitance. The studies of EIS on the oxidation of aluminium take place on PANI-coated aluminium, while PANI redox reaction studies take place on PANI-coated platinum [193]. Therefore, the results are different to the earlier observed days, with pure aluminium (1100) only requiring an applied potential of 1 V to show the best performance, and the other two alloys requiring 3 V. The coating resistance degrades with time and the change is associated with ions and water penetrating into the coating and subsequent electrochemical reaction at the paint/metal interface. The decline of

impedance values can be interpreted as the delaminating of the coating, however, in general, coated outperformed uncoated aluminium and this remains a promising finding for a corrosive resistance coating.

From the measured charge-transfer resistance values, the protection efficiency of the coating was obtained from the relationship:  $\text{Protection efficiency (\%)} = \frac{R_{ct(C)} - R_{ct}}{R_{ct(C)}} \times 100$ , where  $R_{ct(C)}$  and  $R_{ct}$  are the charge-transfer resistance values in the presence and in the absence of a PANI coating, forcing on the marine grade aluminium alloys below.



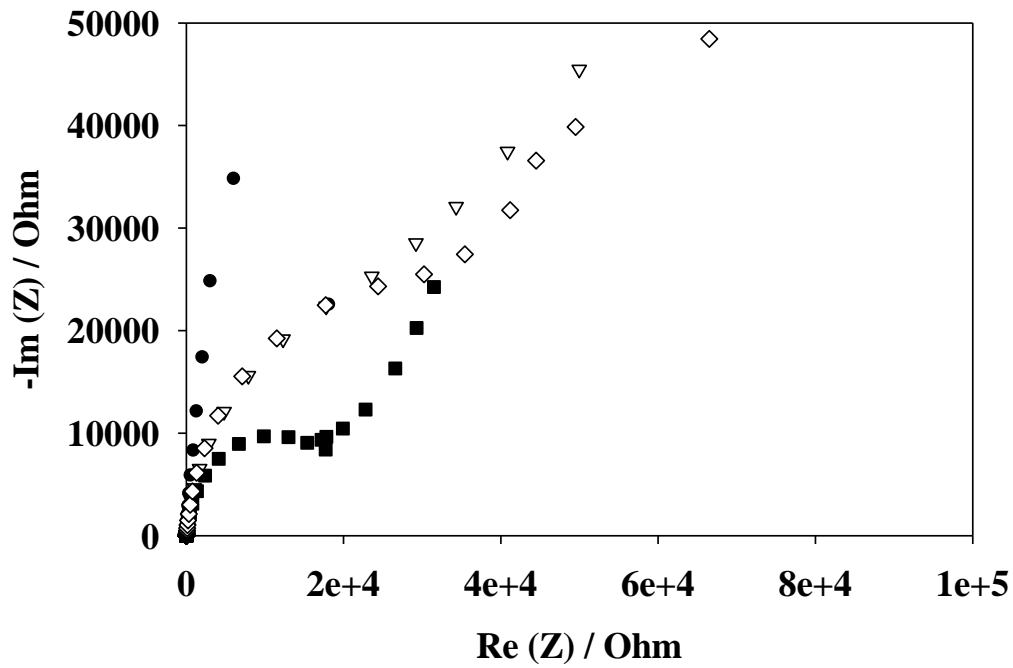
(a)



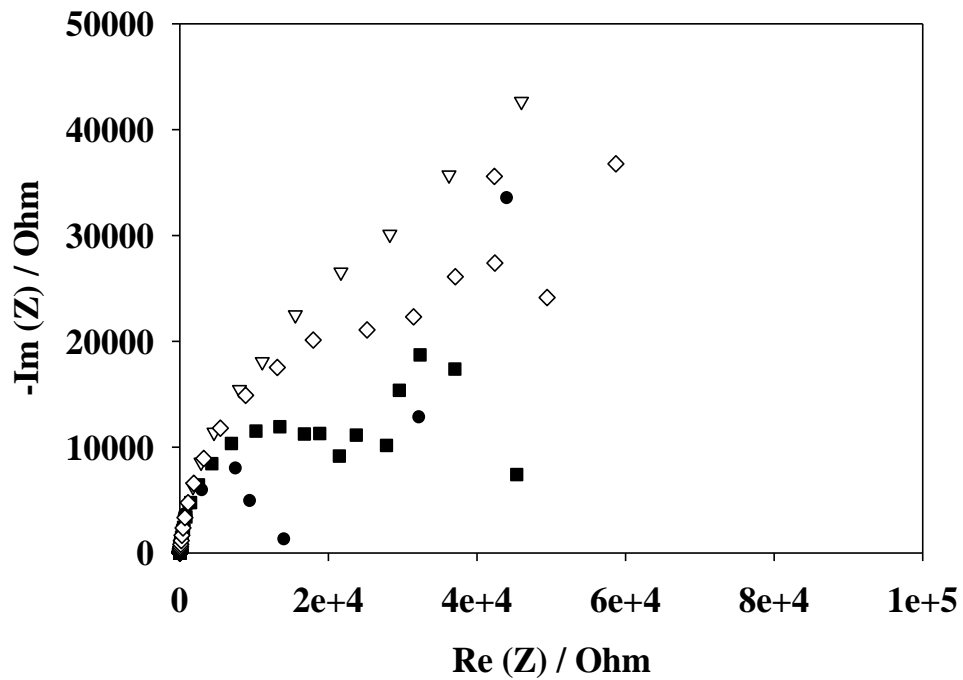
(b)

Figure 6.34. Nyquist plot of the imaginary component ( $Z_{\text{imag}}$ ) vs the real component ( $Z_{\text{real}}$ ) of the impedance for (a) pure marine grade aluminium alloy, (b) chemically pretreated pure marine grade aluminium alloy, • initial ▽ Day 15 ■ Day 30 ◇ Day 50.

The electrochemical impedance spectroscopy in 3.5 wt% NaCl solution indicates that pure 5083 provides poor corrosion protection after day 15. However, it improved after day 50, but never quite reached the original level of protection. Initially, a small capacitive arc was observed, reflecting a rather low impedance of an unhydrated oxide layer. Overtime, the arc increased and subsequently decreased after day 30 for pure and untreated 5083 alloy. Similar behaviour was observed with pretreated aluminium alloys, but the decrease of the arc occurred at an earlier stage (after day 15 rather than after day 30). The formation of an oxide layer on aluminium protects the aluminium surface and showed the best corrosion protection on day 30 and maintained it at similar level even after it been immersed for 50 days.



(a)



(b)

Figure 6.35. Nyquist plot of impedance data for (a) anodised marine grade aluminum alloy, (b) PANI coated 5083 at 1 V as a function of immersion time in 3.5 wt% NaCl solution  
 ● initial ▽ Day 15 ■ Day 30 ◇ Day 50.

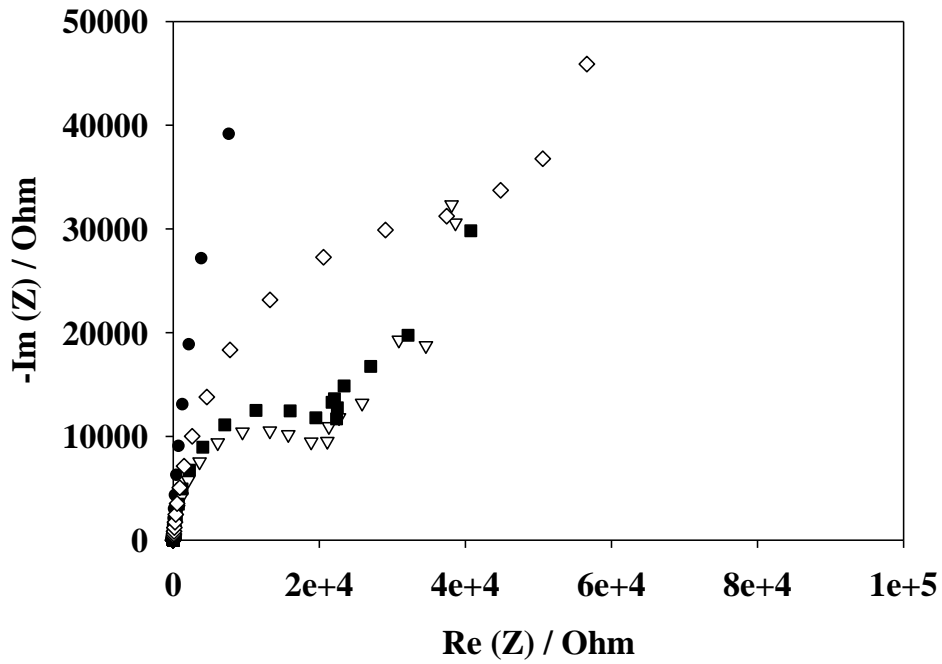
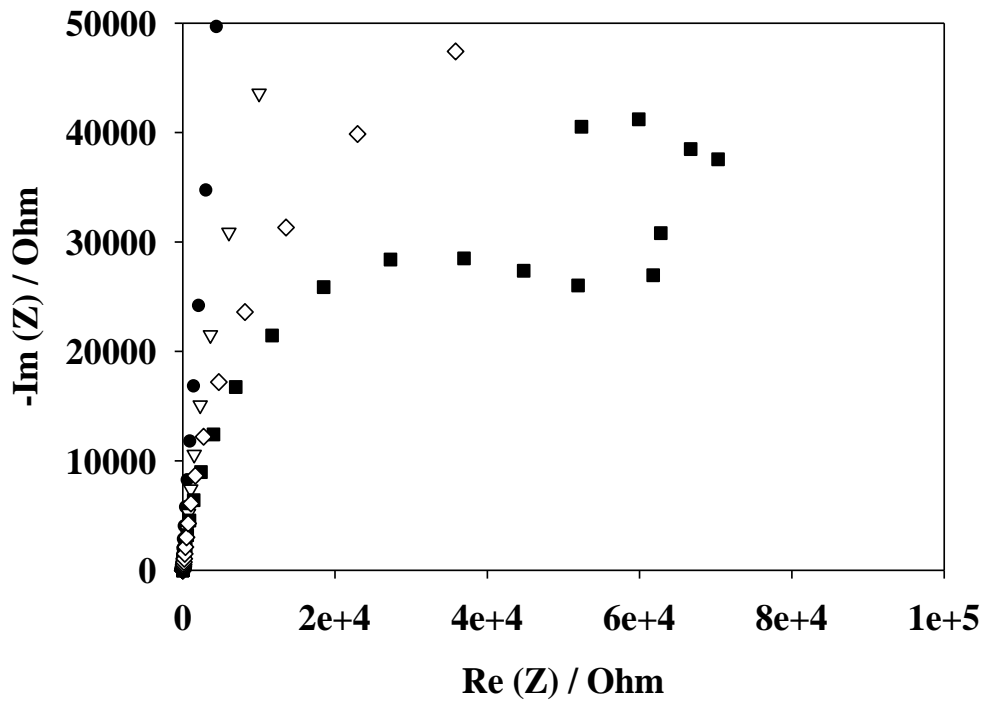
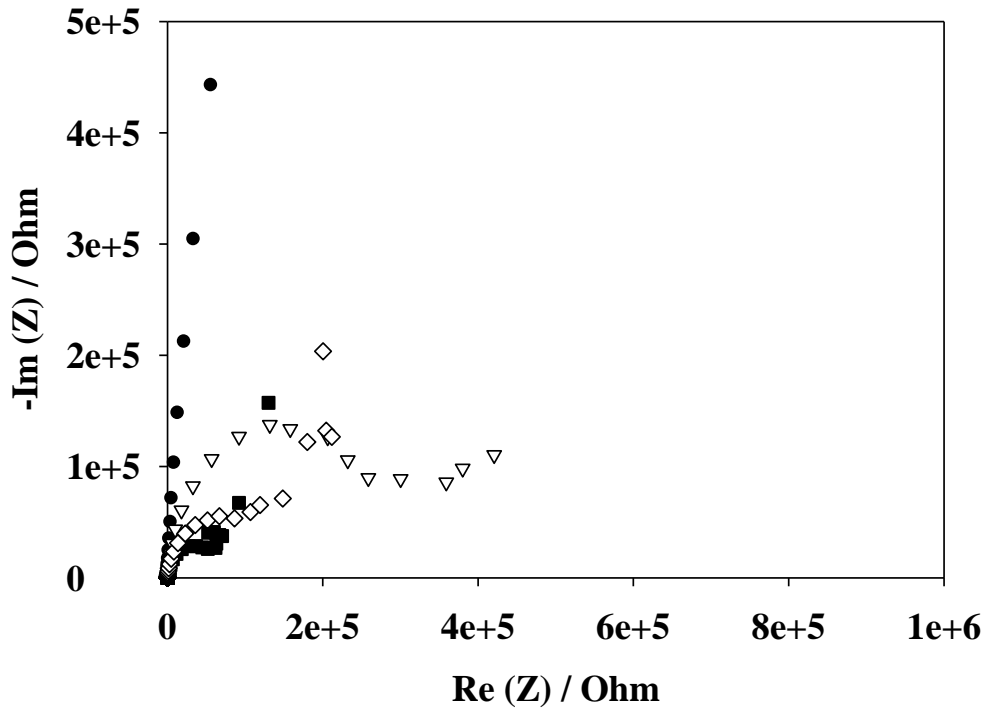


Figure 6.36. Nyquist plot of impedance data for PANI coated 5083 at 2 V as a function of immersion time in 3.5 wt% NaCl solution, ● initial ▽ Day 15 ■ Day 30 ◇ Day 50.

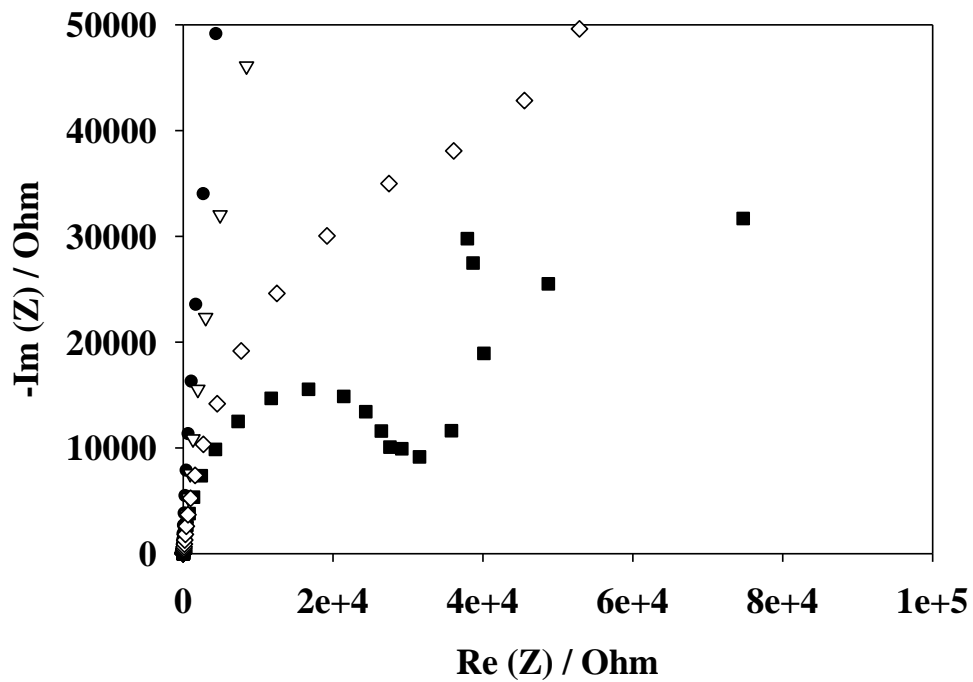


(a)



(b)

Figure 6.37. Nyquist plot of impedance data for PANI coated 5083 at 3 V as a function of immersion time in 3.5 wt% NaCl solution, ● initial ▽ Day 15 ■ Day 30 ◇ Day 50.



(a)

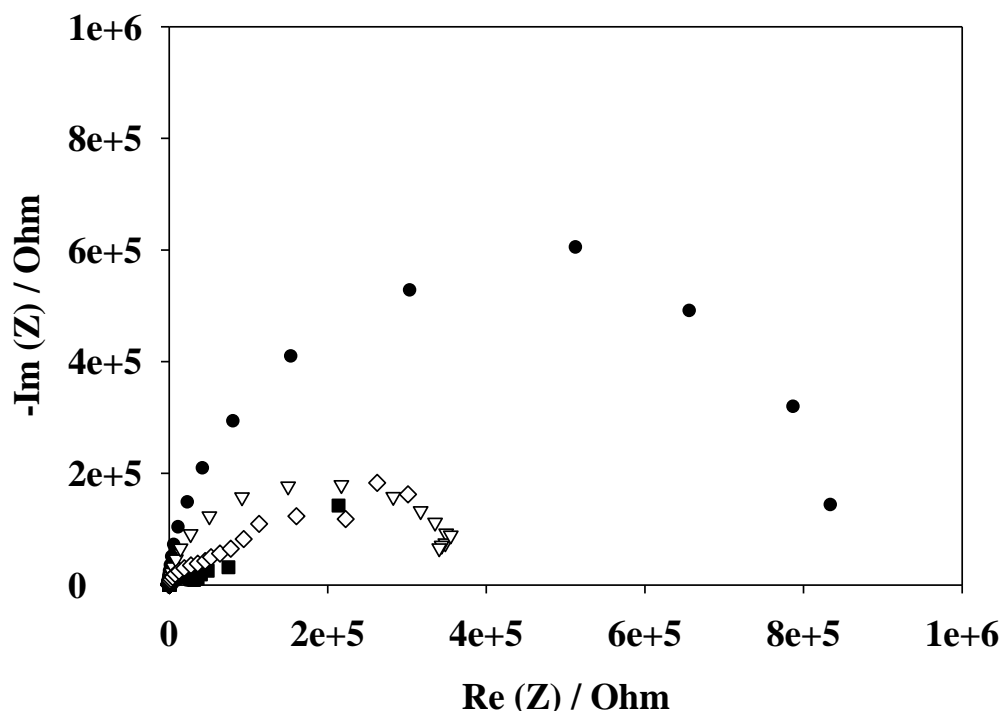


Figure 6.38. Nyquist plot of impedance data for PANI coated 5083 at 4 V as a function of immersion time in 3.5 wt% NaCl solution, ● initial ▽ Day 15 ■ Day 30 ◇ Day 50.

Two characteristic regions of distinct electrochemical response were observed, one at higher and the other at lower frequencies. At high frequencies, a partial arc was observed, characterised by a solution resistance ( $R_s$ ), a double-layer capacitance ( $C_{dl}$ ), and a charge transfer resistance ( $R_{ct}$ ). The kinetically controlled electrochemical reaction represents the  $R_{ct}$ , such as electron transfer between the metal alloy and the conducting polymer. At low frequencies, the response was controlled by a diffusion process, represented by a straight line with a  $45^\circ$  angle to the real axis that confirmed the presence of a redox process. The diameter of the arc decreased with immersion time, observed for PANI coated aluminium. This is in contrast to the behaviour typically observed with bare aluminium, which was characterised by a semicircle of increasing diameter with immersion time, caused by increasing the coating (pore) resistance, and the absence of a diffusion tail. The increase in diameter of the arc reflected an increase in the  $R_{ct}$ . Such an increase in  $R_{ct}$  is attributed to oxidation of the aluminium by the conducting polymer, resulting in an increasingly thicker layer of oxide at the metal/conducting polymer interface and also to the partial reduction of the PANI to its less conductive leuco form. A smaller arc, reducing  $R_{ct}$  was observed presumably because of



water ingress into the oxide layer, however, the low-frequency impedance of this small arc was still  $> 20^4 \Omega$ .

With PANI electrochemically grown for an hour at 1 V potential there was no corrosion protection, but by increasing it to 2 V, there was a marked improvement in corrosion protection, which could be seen even after day 15.

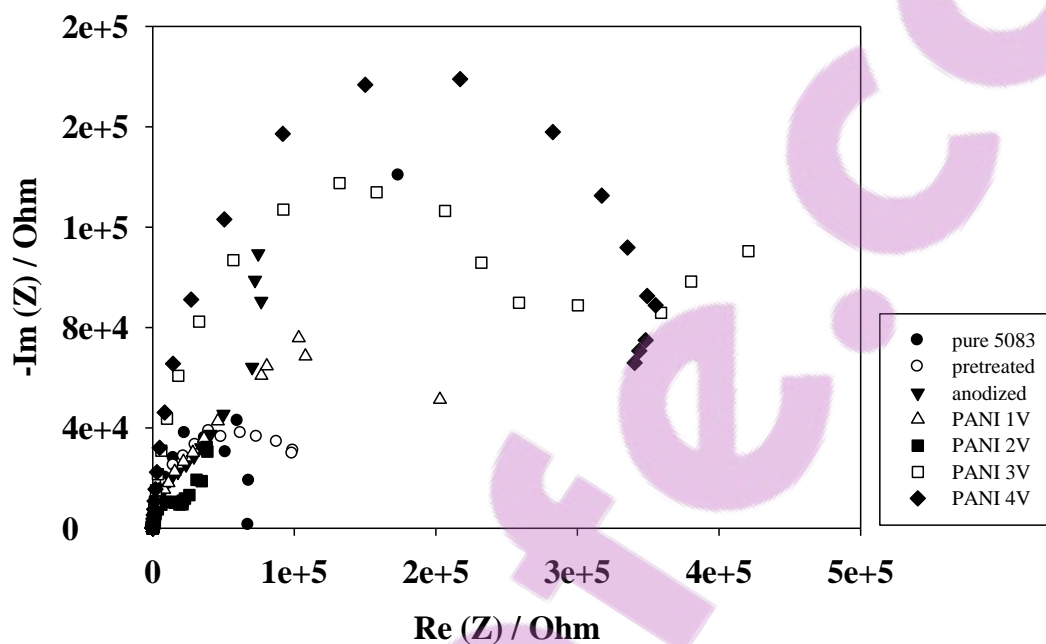


Figure 6.39. Nyquist plot of impedance data on day 15 for marine grade aluminium as a function of different surface in 3.5 wt% NaCl solutions.

Effective, nonconducting barrier coatings are typically characterised by a semicircle of decreasing diameter with immersion time, caused by decreasing coating (pore) resistance and the absence of a diffusion tail.

Day 15: 2 V > anodised > raw > pretreated > 1 V > 3 V > 4 V. On day 15 at low frequencies the response was limited by a diffusion process, represented by the straight line with a  $45^\circ$  angle with respect to the real axis. At higher frequencies, the kinetics of a charge-transfer process governed the response as manifested by the semicircle.  $R_{ct}$  arises from a kinetically controlled electrochemical reaction, such as electron transfer between the metal and CP.

Bode plots have been used in studying the corrosion protection with the bare marine grade aluminium after 50 days of immersion. In Figure 6.40(a) it can be seen that over a long

immersion time of 50 days, the uncoated aluminium decreased to a lower resistance value than the PANI coated aluminium, which remained above that of the bare aluminium. This decline was attributed to the influence of  $\text{Cl}^-$  ions incorporated at the surface of the aluminium oxide [25]. A more rapid decrease in coating resistance was observed with higher water permeability.

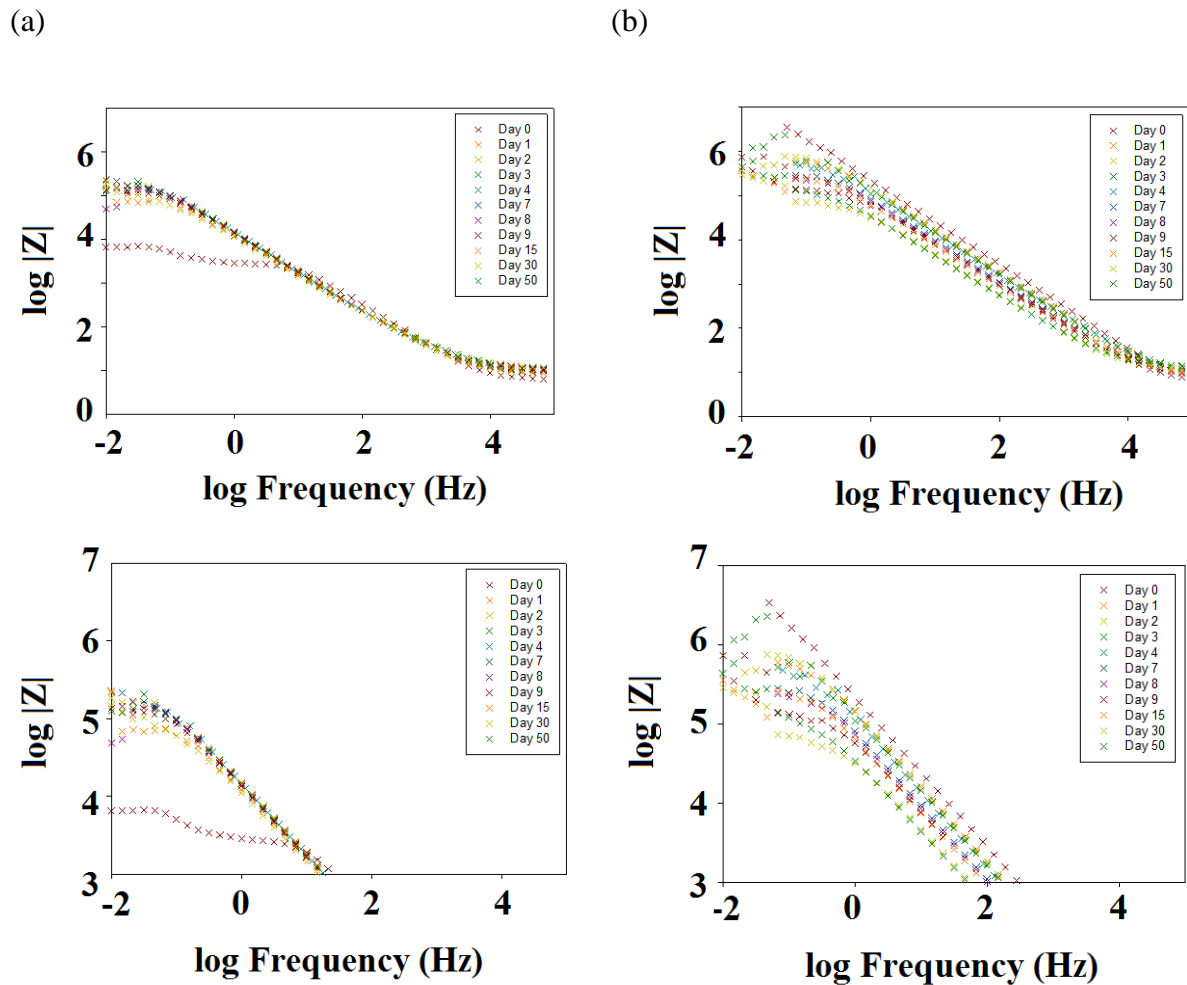


Figure 6.40. Bode plots ( $\log$  frequency vs.  $\log |Z|$ ) for impedance spectra at various immersion times for bare aluminium 5083, (a) PANI coated aluminium 5083 grown at 3 V, and (b) on anodised aluminium in 3.5 wt% saline solution at room temperature.

When PANI was coated on aluminium, higher resistance values were obtained (Figure 6.40(b), of the order of some thousands of  $\Omega \cdot \text{cm}^2$ ). Although after a long immersion time, the coating resistance decreased, and the effectiveness of the film would decrease due to the

ingress of chloride ions and water [25]. Conroy et al. have suggested that the ability of PANI to protect against corrosion is due to the barrier properties of the reduced polymer [86].

### 6.2.9. Free radical DPPH scavenging evaluation

The results for DPPH radical scavenging capacity, a widely used method to provide an estimate of antioxidant activity, are presented in Figure 6.36. The DPPH radical scavenging capacity of the PANI samples was in the following order: PANI 1 V > PANI 3 V > PANI 2 V > PANI 4 V.

The free radical scavenging activity in this study was evaluated at different hourly intervals after introducing the sample to the DPPH solution. The 32 hour time interval allowed the DPPH solution to access the entire polymer sample [289]. The initial rate of radical scavenging capacity of CPs is related to its surface area [23, 231]. As shown in Scheme 1.11, DPPH radicals oxidise the reduced (benzenoid) units of PANI, which involve the conversion of the benzenoid units of PANI to quinoid and quenching of the DPPH radical. PANI samples potentiostatically grown at 1 V had the lowest level of oxidation, characterised by a high proportion of benzenoid units, and were able to scavenge more DPPH• and exhibit superior antioxidant activity [230]. The electroactivity is not affected by the film thickness, which correlates with the voltage applied on the aluminium alloy, and there is no direct relationship between film thickness and CP performance in free radical scavenging tests.

To enable to understand the kinetics of PANI on aluminium surface, free radical DPPH scavenging solution was used.

DPPH radical scavenging capacity of electrosynthesised PANI was in the following orders: For the 1100 alloy: PANI on platinum > PANI at 4 V > bare 1100 > anodised at 1 V > PANI at 2 V and 3 V > PANI at 1 V.

For the 4043 alloy: PANI on Pt > PANI 3 V > PANI 4 V > anodised 1 V > 1 V > bare > 2 V.

For the 5083 alloy: PANI on Pt > bare > PANI 1 V > anodised 1 V > PANI 3 V > PANI 2 V > PANI 4 V.

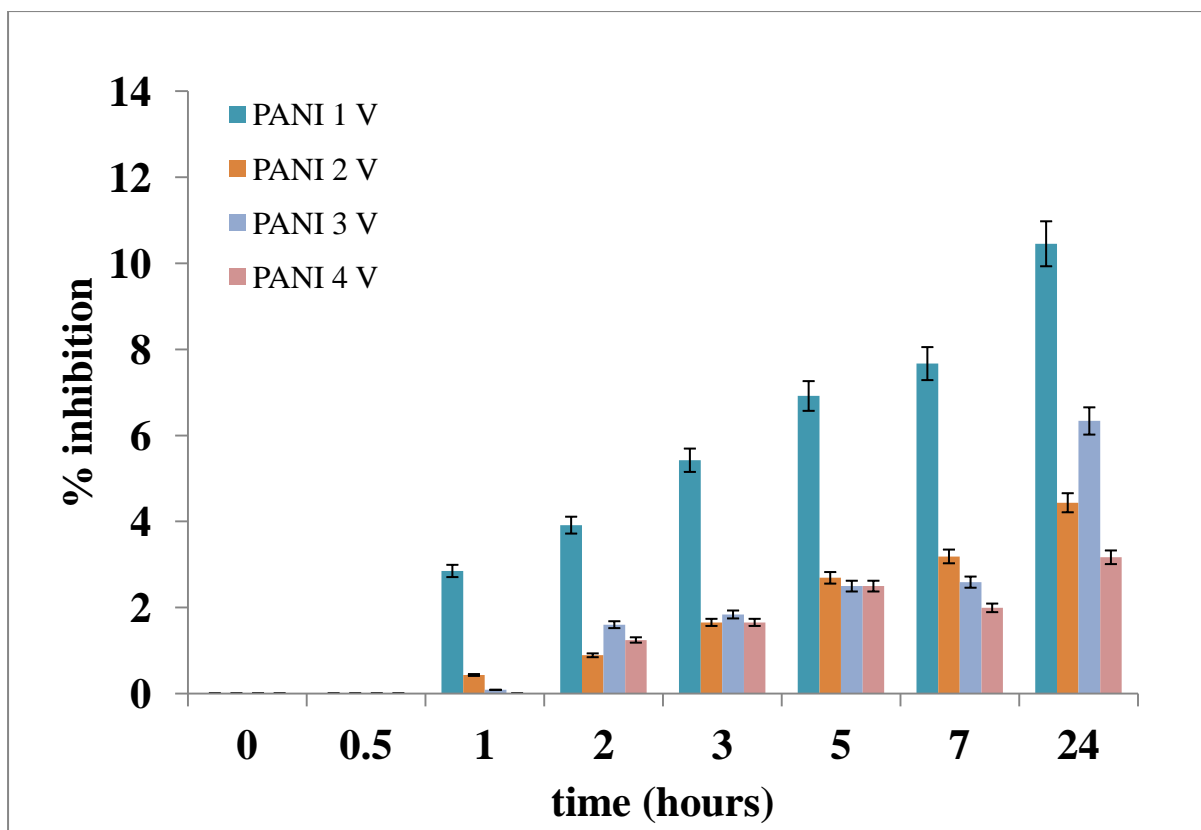


Figure 6.41. DPPH• scavenging capacity of electrochemically synthesised PANI samples on 5083 alloy; these were grown on alloy for 20 mins.

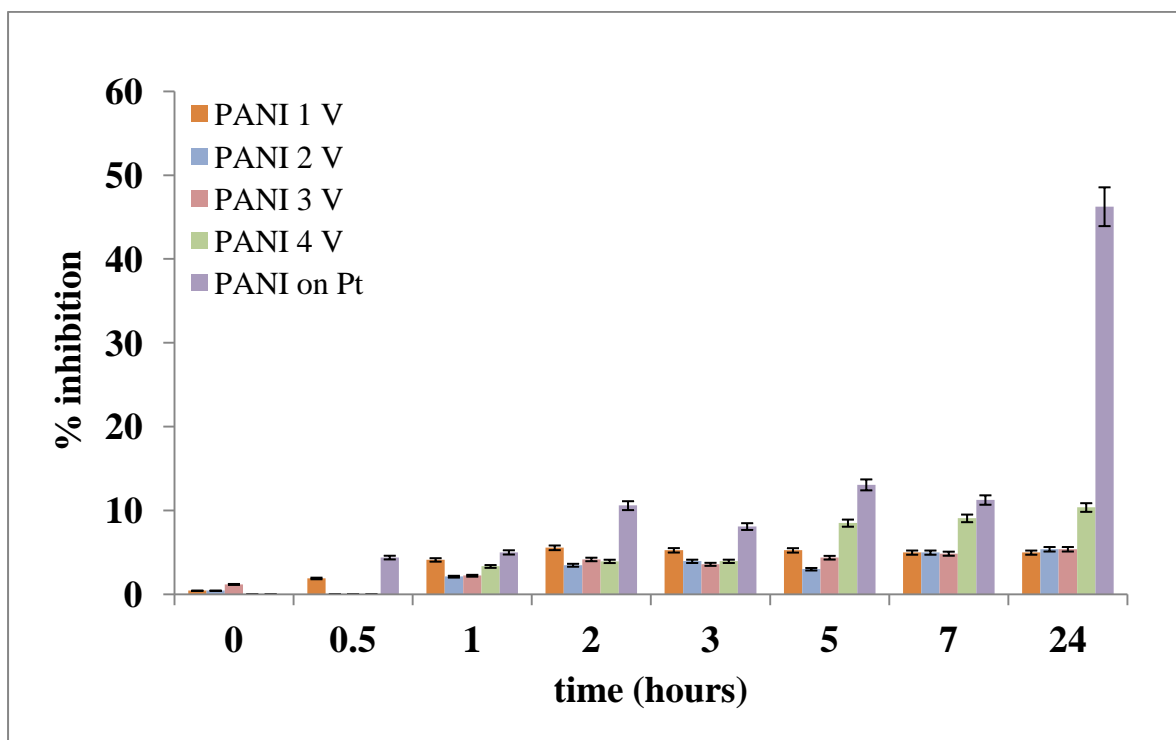


Figure 6.42. Complete set of % inhibition of 1100 alloy – 20 mins.

The free radical scavenging capacity of PANI has been reported by others [230-231] to be dependent on the surface area, meaning that higher surface area materials will have better scavenging activity. The radical scavenging activity is often tested for the duration of 30 minutes, especially in the food industry. However, tests were carried out at 30 mins intervals, then hourly, and then every 2 hours, ending after 24-hours. The extended 24-hour of exposure was found to be necessary to fully assess the radical scavenging capacity of CPs [279, 289]. Significant time must be allowed to enable the entire polymer sample to be accessed by the DPPH solution. At times, it is possible that the initial rate of radical scavenging is surface-related, therefore it needs to be considered. In general, the overall radical scavenging activity will be related to total redox capacity, given by the amount of conducting polymer, its initial oxidation state and its chemical nature.

DPPH radicals oxidise the reduced B units of PANI involving a process which converts the B units to Q in the PANI chain and quenches of the DPPH radical. Hence, PANI with lower level of oxidation, characterised by more B units, has a greater ability to scavenge more DPPH• and exhibits superior antioxidant activity [279].

PANI electrochemically grown on platinum showed the highest DPPH radical scavenging activity indicating the greatest ability to scavenge radicals as compared to being grown on aluminium alloys. PANI on Pt had a greater scavenging activity than PANI 4 V, followed by PANI 3 V, PANI 1 V and PANI 2 V.

The highest purity aluminium alloy, 1100, of low applied potential at 1 V showed the greatest radical scavenging activity, initially followed by the highest applied potential of 4 V, see Figure 6.42. However, this later was dominated by the highest applied potential, which showed the highest ability to scavenge the radicals. Apart from the highest applied potential samples, 4 V, the other samples prepared under different applied potential of the purest aluminium alloy showed the lowest % inhibition amongst the three grades of aluminium selected. In general, apart from free moving PANI grown on platinum, the highest radical scavenging activity was observed with the 4043 alloy, see Figure 6.43. Regardless of the type of surface coating applied, this finding suggests that the type of alloy also plays an important role. The marine grade aluminium, 5083, series showed the greatest relationship between the film formed and its performance, hence the % inhibition on surface of aluminium at different time intervals (see Figure 6.44).

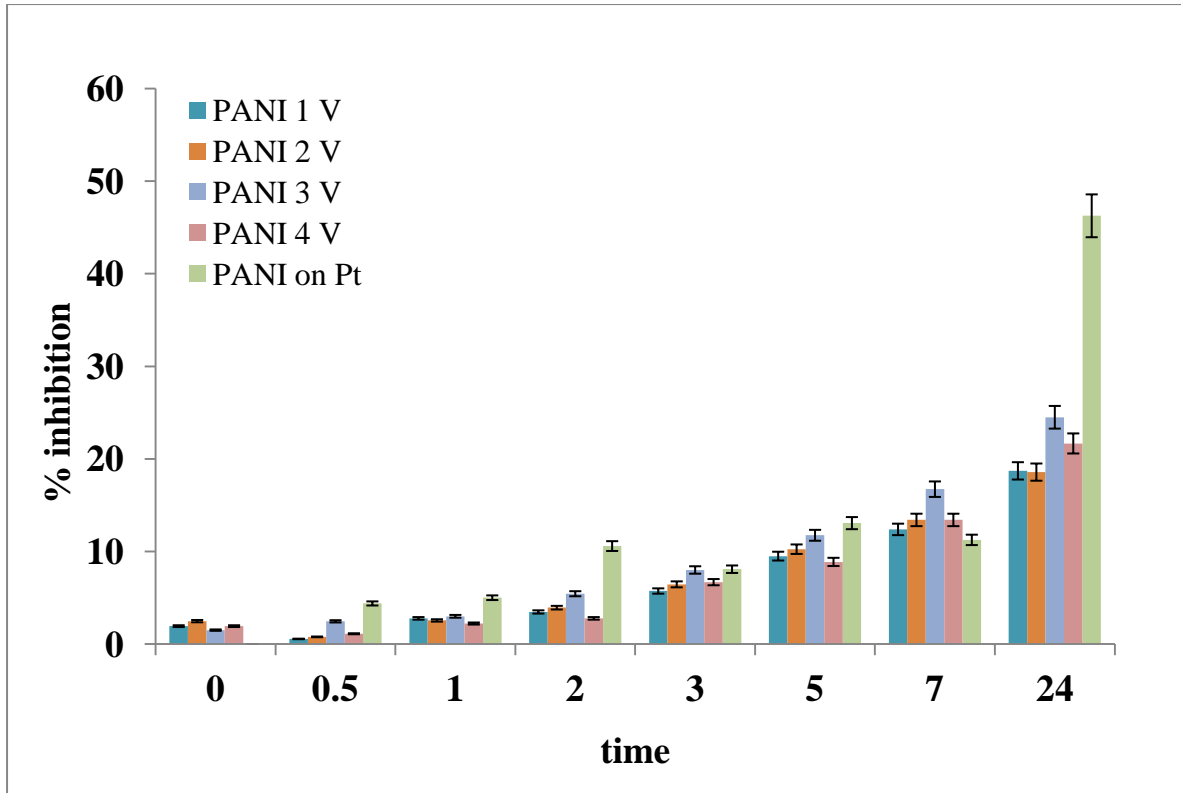


Figure 6.43. Complete set of % inhibition of 4043 alloy – 20 mins.

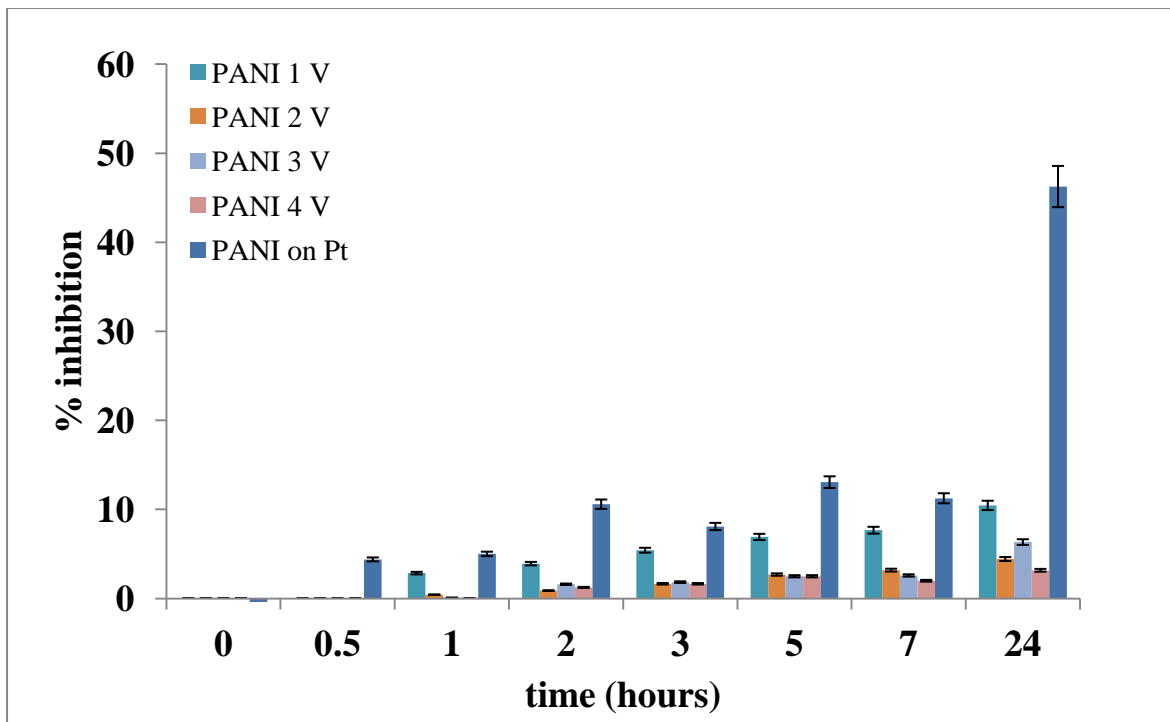


Figure 6.44. Complete set of % inhibition of 5083 alloy – 20 mins.

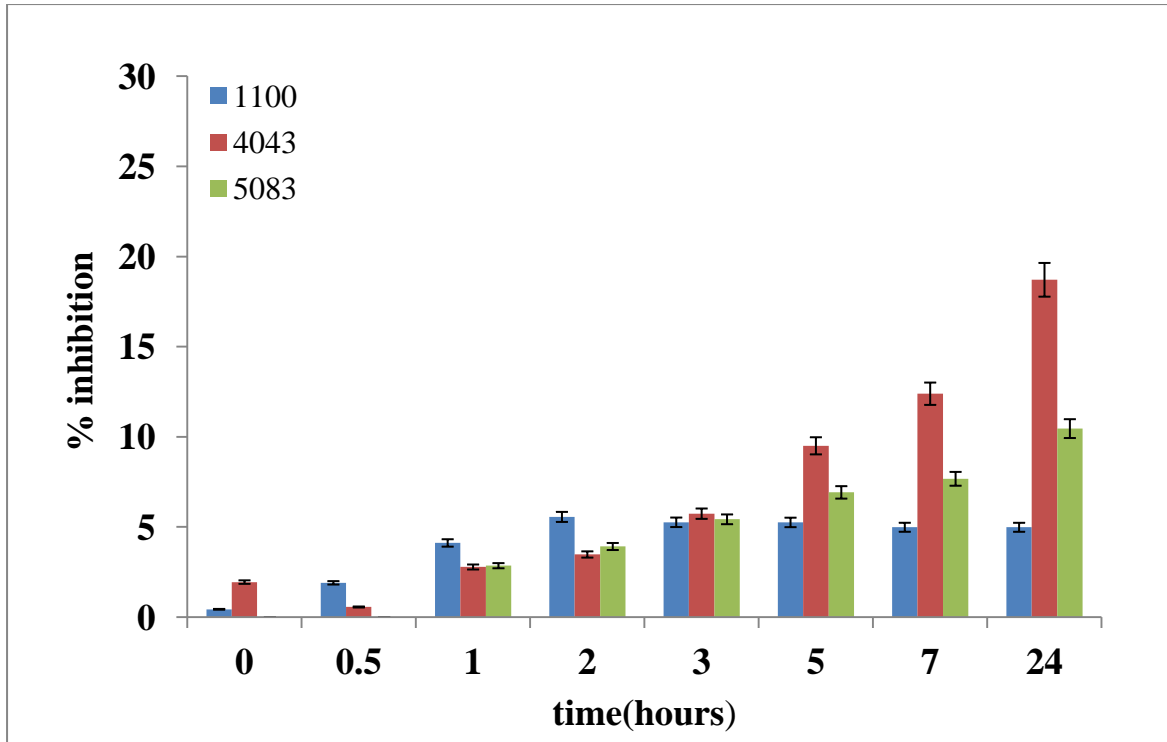


Figure 6.45. % inhibition of aluminium alloys electropolymerised at 1 V for 20 mins.

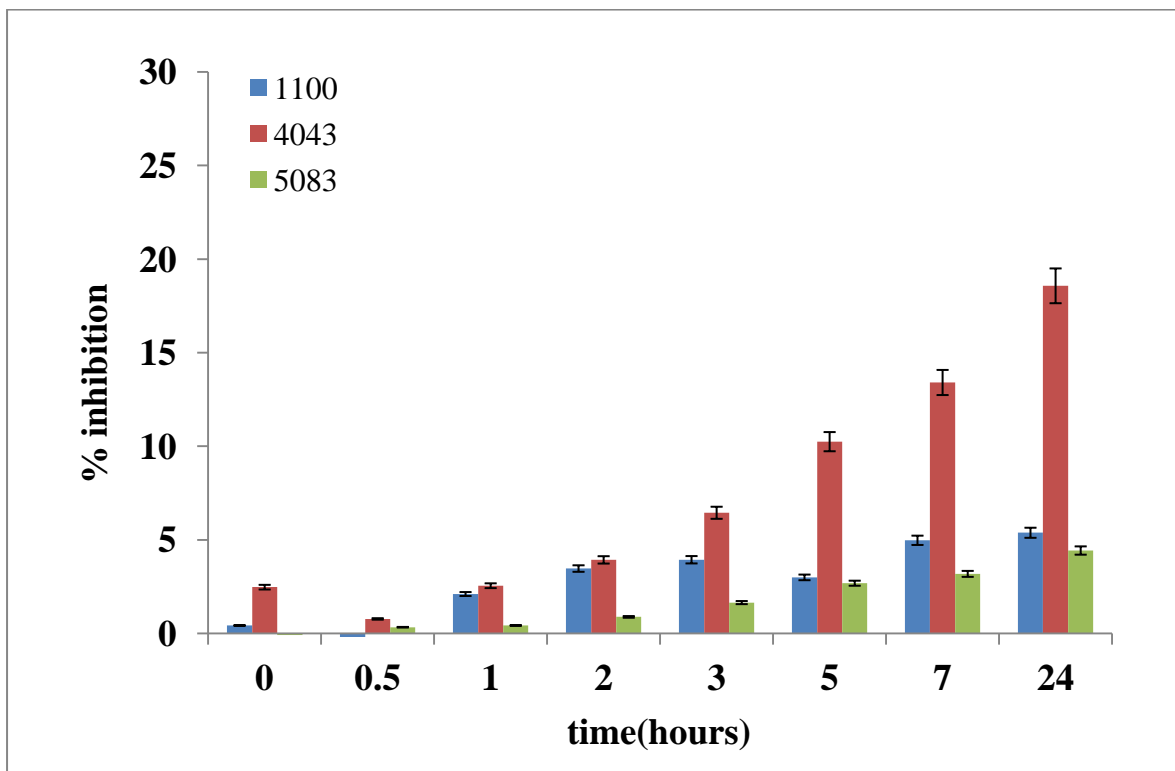


Figure 6.46. % inhibition of aluminium alloys electropolymerised at 2 V for 20 mins.

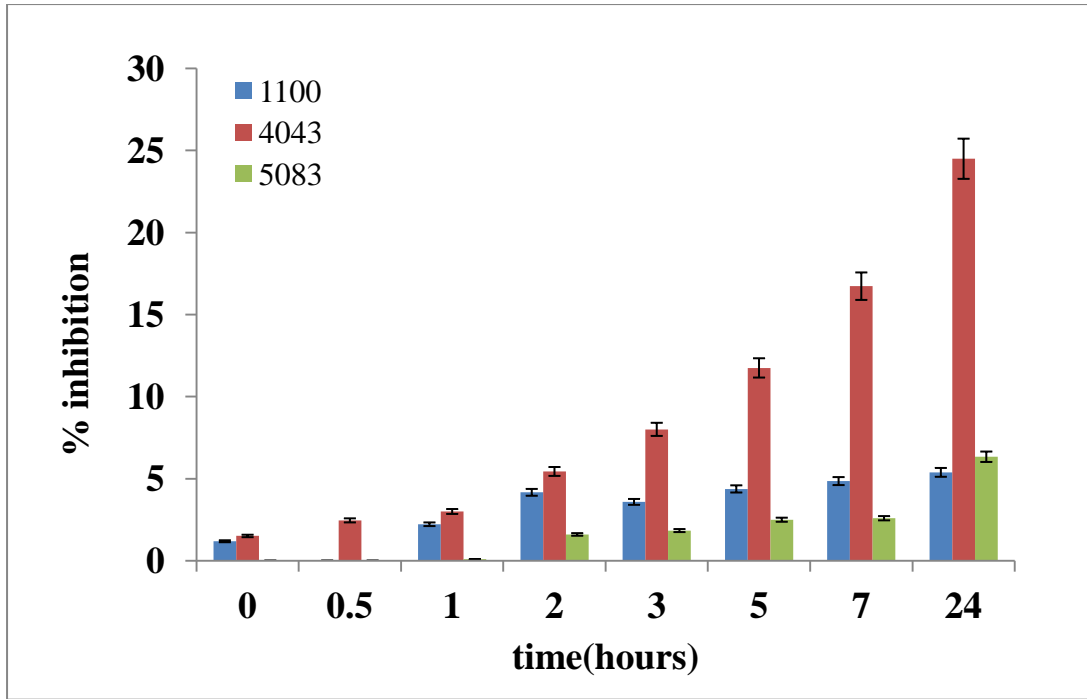


Figure 6.47. % inhibition of aluminium alloys electropolymerised at 3 V for 20 mins.

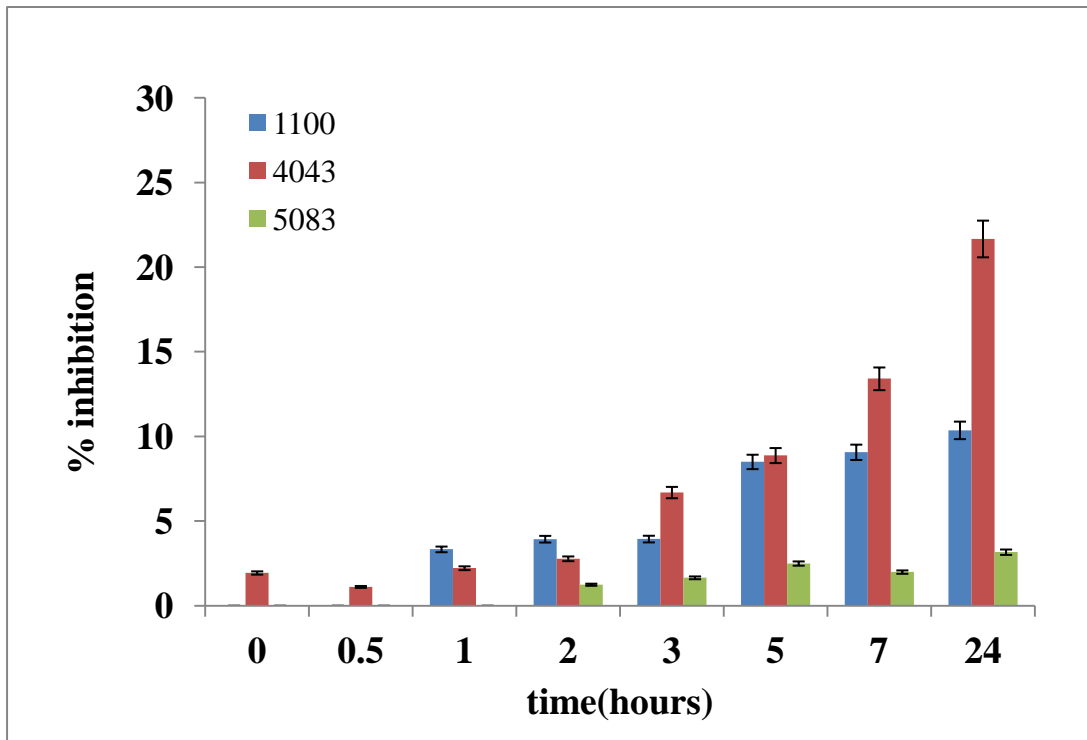


Figure 6.48. % inhibition of aluminium alloys electropolymerised at 4 V for 20 mins.



### **6.3. Conclusions**

PANI was successfully electropolymerised on three grades of aluminium using a one-step potentiostatic process holding it at a fixed potential over a period of time. In addition, studies were carried out on the marine grade aluminium under both one-step and two-step processes, which involved anodising the aluminium prior to electrosynthesis of PANI on the aluminium oxide layer.

Growing PANI on marine grade aluminium was achievable via either cycling or holding it at a fixed potential. Films grown under both methods were proven to show characteristic internal redox properties, which means they are electroactive as shown by the CV response. The composition of aluminium alloy does have an overall effect on the PANI growth. Pure aluminium with minimum impurities has proven to require less current to achieve the set voltage, the greatest radical scavenging activity and best corrosion resistance when compared with the other two aluminium alloys. The polymerisation of aniline occurs on the surface of aluminium alloy electrodes, as observed in voltammetric scans, SEM, and UV-Vis spectroscopy. The success of PANI grown on aluminium surfaces provides the opportunity for surfaces to be protected from antifouling, which will be discussed in Chapter Seven.

The alloy with the highest aluminium level showed the greatest radical scavenging activity

Also, in order to improve the anticorrosive and antioxidant properties, a thicker film or a film grown at a higher potential should be used as it would perform better. Moreover, pure aluminium with minimum impurities in the alloy would allow for greater protection.

## CHAPTER SEVEN: Fouling resistance studies

### 7.1. Abstract

This chapter focuses on a novel accelerated testing method that was developed for the evaluation of antifouling performance. This new testing procedure requires only weeks, as opposed to regular testing methods that require the samples to be immersed in the sea for several months at a time.

Antifouling coatings are generally defined as those that can prevent the settling of microorganisms on a surface through the controlled release of toxic agents. There is considerable interest in the development of coatings that are non-toxic to the environment, but also prevent unwanted microbial-based fouling. Many CPs have been studied for different applications, with PANI the first to show antifouling properties [12].

Four types of bacteria were used in fouling resistance tests described in this Chapter. All four types are *Gram-negative*, bioluminescent and rod-shaped bacteria. *E. coli* ATCC 25922 [226] and *E. coli* 536 [227] are commonly found in the lower intestine of warm-blooded organisms, while *Vibrio fischeri* ATCC 7744 [228] and *Vibrio harveyi* [229] can be found in the marine environment. They are found in a free living state in the aquatic environments and in a mutualistic association with certain squids and fishes. The bacteria belong to the *Vibrionaceae* family [228-229].

This chapter has been partially published as:

To T., Swift S., Kilmartin P. (2013) Evaluation of electrodeposited polyaniline on marine grade aluminium for antifouling properties, *International Conference on Marine Coatings*, Rina HQ, London, UK. In press.

## 7.2. Experimental Procedure

### 7.2.1. Materials

Aluminium samples, also referred to as coupons (10 mm x 20 mm x 3 mm), were used to test for biofouling. Three sets of controls (glass, aluminium oxide and pure marine aluminium) were tested alongside PANI-coated marine-grade aluminium. A commercial proprietary modified epoxy-amine coating system was also used for comparison purposes. For the marine grade alloy aluminium, only the bottom half was coated and the top half was masked with insulating tape to produce an effective working area of 1 cm<sup>2</sup>, acting as an internal control (see Figure 7.1). The tape was removed to form a pure aluminium control. Electropolymerisation of aniline was carried out using an EDAQ potentiostat with E-corder 410 holding the potential at 2 V in 0.5 M oxalic acid electrolyte and 0.1 M aniline monomer for 1 hour and 2 hour polymerisation time using a one-step process method. Aluminium oxide was prepared using the same preparation method as the PANI coated samples. However, only 0.5 M oxalic acid was used as the electrolyte with the absence of 0.1 M aniline monomer. Since the non-platinum metals are expected to undergo anodic oxidation during the polymerisation process, the reactivity of the electrodes themselves was studied using electrochemistry in oxalic acid electrolytes, in the absence of aniline monomer, both with bare aluminium and after PANI film formation [290]. Commercial samples were prepared by brush onto a primed and pretreated aluminium surface. The treatment and primer used in the system was one that was recommended by the supplier for such surface which was mentioned in Chapter Two.

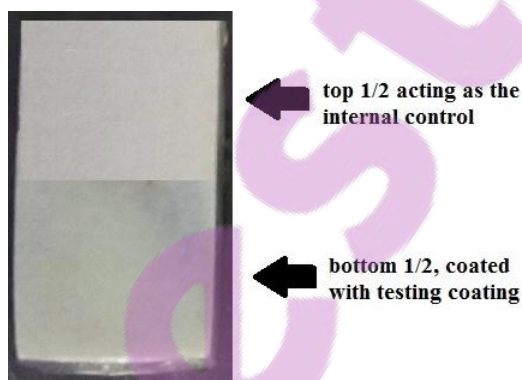


Figure 7.1. Image of coupon coated PANI by holding the potential at 2 V for 2 h on the bottom ½ while the bare aluminium top ½ act as an internal control.

L broth (Difco) and was used as the medium for the antifouling testing in the presence of *luxCDABE*-tagged strains of model bacteria, *E. coli* ATCC 25922 [226] or *E. coli* 536 [291] in the first test. Stable chromosomal inserts of the *luxCDABE* genes in *E. coli* were made using the p16Slux system so that they bioluminesce [292]. Marine broth was used as the medium for the antifouling testing in the presence of the two *Vibrio* strains of bacteria, *Vibrio fischeri* and *Vibrio harveyi*. All media were autoclaved prior to use for antifouling testing.

Cross sectional aluminium coupons of 0.5 cm<sup>2</sup> cubes scanning electron microscope (SEM) images were mounted in two-pack epoxy resin and allowed to set overnight to dry. The set epoxy block was then sanded and ground in perpendicular direction.

### **7.2.2. Testing procedure**

Four sets of controls and two sets of electrochemically deposited PANI on marine grade 5083 aluminium using potentiostatic method at two different polymerisation time was prepared, see potentiostatic preparation in Chapter Two, Section 2.5. The controls used were pure aluminium, anodised aluminium, a glass substrate and a commercially available epoxy-amine system coating with antifouling properties. Triplicates of each set were prepared for analysis.

#### **7.2.2.1. *Escherichia coli* strains**

The fouling tests were carried out in fresh L-broth inoculated with a 1 in 40 dilution of an overnight culture of the *E. coli* strains. Coupons, sterilised by dipping in ethanol and flamed to burn off the alcohol, were submerged in the inoculum in a petri dish and incubated at 37 °C with shaking at 80 r.p.m. After incubation coupons were rinsed in sterile saline, imaged and immersed in fresh inoculums and incubated again. This was repeated each day so that the coupons experienced a fresh and even population of bacteria throughout the duration of the testing.

Triplicate runs of each set were prepared for antifouling testing using two strains of bacteria, *E. coli* ATCC 25922 *lux* and *E. coli* 536 *lux* under controlled conditions to simulate the marine environment in an accelerated fashion. PANI coatings of two different thicknesses were tested. The PANI coated aluminium coupon itself has an internal standard, as only one half of the coupon was coated while the remaining half was uncoated.

This novel testing method allowed for a non-destructive evaluation of bacterial growth on surfaces over time, with bioluminescence from bacteria colonising the aluminium coupons imaged using an IVIS kinetic (Perkin Elmer) at 24-hour intervals over a two week period.

Only live bacteria are bioluminescent, and so bioluminescence indicates areas of the coupon that are colonised by bacteria. A single colony was placed in 10 mL of L-broth and incubated overnight with shaking at 37 °C and 200 r.p.m. A stock culture of 2.5 mL was diluted with 100 mL L broth and marine-grade aluminium coupons were then rinsed and immersed for continuous testing.

#### 7.2.2.2. *Vibrio* strains

The fouling testing with the *Vibrio* strains, *Vibrio fischeri* ATCC 7744 and *Vibrio harveyi* [228, 229], was carried out in marine broth (279110 – BD Difco™ Marine Broth 2216) over a period of 2 weeks with shaking at 28 °C and 80 r.p.m. In addition to the visual observation of bacteria growth on the surface, dilutions was made each day for plate counting and bioluminescent checks on the marine broth medium. Seven dilutions, ( $10^{-1}$ ,  $10^{-2}$ ,  $10^{-3}$ ,  $10^{-4}$ ,  $10^{-5}$ ,  $10^{-6}$ ,  $10^{-7}$ ) was carried out each day with each bacteria strain in sterile saline solution spread on marine agar plates.

### 7.3. Results and Discussions

#### 7.3.1. *Escherichia coli* fouling resistance studies

An accelerated testing method was developed to allow the evaluation of fouling properties on different surfaces over time. Coated and control marine grade aluminium were challenged by immersion in growing cultures of *E. coli* ATCC 25922 *lux* and *E. coli* 536 *lux* under controlled conditions to simulate the marine environment in an accelerated fashion. The two strains of bacteria are modified so that they bioluminesce. This novel testing method allows for a non-destructive evaluation of bacterial growth on different surfaces, using selected coatings, with bioluminescence from bacteria colonising the aluminium coupons imaged using an IVIS kinetic at 24-hour intervals over a 2 weeks period. See the images in Figure 7.3 taken after 4 days. Only live bacteria bioluminesce and so signal (seen as a pseudocolour image as the colour intensity index in Figure 7.3) reflects areas of the coupon colonised by bacteria. The coupons were initially seen as grayish in colour when there were no bacteria colonising the surface, then upon time the bacteria was detected in blue and green, as shown in Figure 7.2.

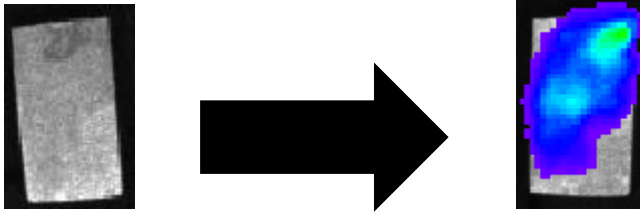


Figure 7.2. Observation of coupons upon time.

Three readings of each sample set with only the average radiance values were recorded at different time intervals and are plotted in Figures 7.5 and 7.6. An example of the quantified area is shown below in Figure 7.3. When measuring the radiance value, it is important to avoid quantifying the edges which are rough and may have incomplete coating that promotes colonisation. Statistical analysis was performed using one-way analysis of variance.

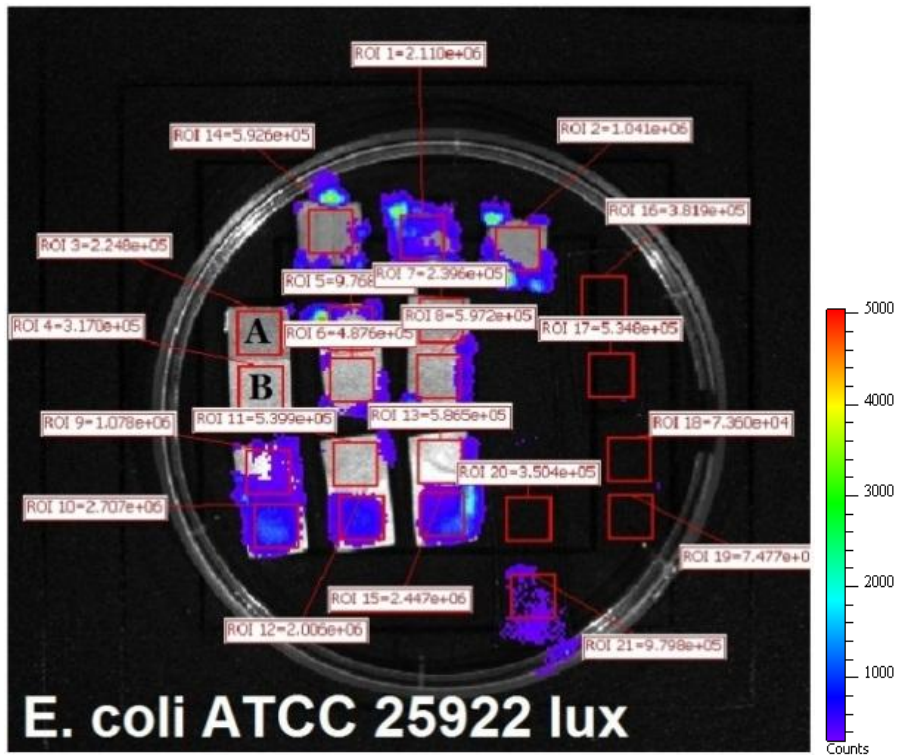


Figure 7.3. IVIS image surfaces with quantified area challenged with bioluminescent *E. coli* ATCC 25922 *lux* strains taken after 4 days of bacterial fouling, with the top half of each aluminium being the control labelled A; while the coated half is labelled B. The pseudocolour bar indicates bioluminescence intensity.

The antifouling performance was determined by IVIS bioluminescence measurements with evaluation of bacterial growth on selected substrates. The unit of measure was Avg (average) Radiance versus time recorded in days. A commercially available epoxy-amine antifouling coating system and electrochemically synthesised PANI on marine-grade aluminium of two thicknesses were compared with bare marine-grade aluminium and glass controls. Figure 7.4 shows a representative IVIS image of the various surfaces challenged with bioluminescent *E. coli* strains. Bacterial numbers colonising the surface are shown in the pseudocolour heat map and indicate the quantity and location of the bacteria on the coupons. These images were taken after 4 days of bacterial fouling.

One of the greatest challenges for this testing method is the fact that metal surfaces often exhibit some antimicrobial activity against shorter exposures to single inocula, making the effect of coated surfaces difficult to see. The PANI coated samples shown in Figure 7.4 in row two have less bioluminescence, indicating lower bacterial growth. The glass control samples showed the worst performance, with fouling covering almost the entire surface in the *E. coli* 536 lux medium. The performance of the aluminium controls were as effective as the commercial control due to self-inherent antibacterial effect, but superior results were obtained with PANI coated samples.

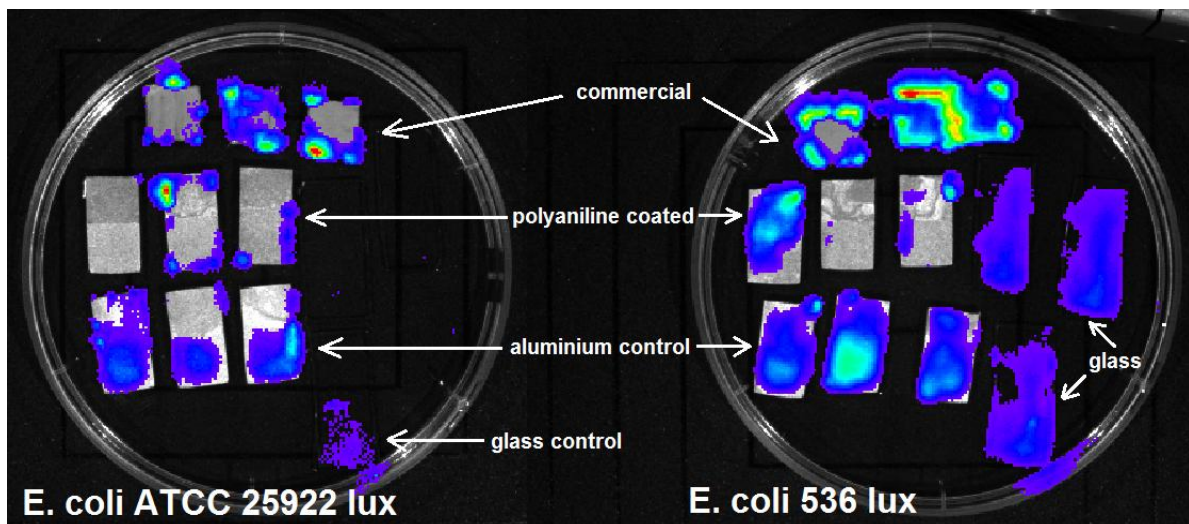


Figure 7.4. Bioluminescence images for coated and control samples. Both PANI and aluminium control samples have their own internal control, as only the bottom half of these were coated.



All four sets of controls behaved quite differently, with anodised aluminium and the commercial sample providing the best comparison, hence only these two along with the polyaniline coated aluminium were plotted in the next section. Bacteria did not adhere to the surface of glass as much as predicted, while the bare aluminium in the early stage of testing showed some antibacterial properties which might have led to false positive at the start of the experiment. Therefore it was concluded that anodised aluminium along with the commercial samples were the best controls to compare the PANI coatings against.

### 7.3.1.1. *Escherichia coli* ATCC 25922 lux

The hypothesis was that a PANI coating would inhibit or at least delay bacterial colonisation of the aluminium surface. It was further hypothesised that a thicker coating would have a stronger antifouling effect. The thinner layer of PANI (Figure 7.5) did not inhibit colonisation when compared to the uncoated control, and was significantly less effective than the commercially available product. A thicker coating (Figure 7.6) offered significant protection against fouling ( $p < 0.05$ ) indistinguishable from the commercially available product for 12 days. The result clearly illustrates the importance of film thickness for the overall performance. The antifouling ability improved with an increase in film thickness.

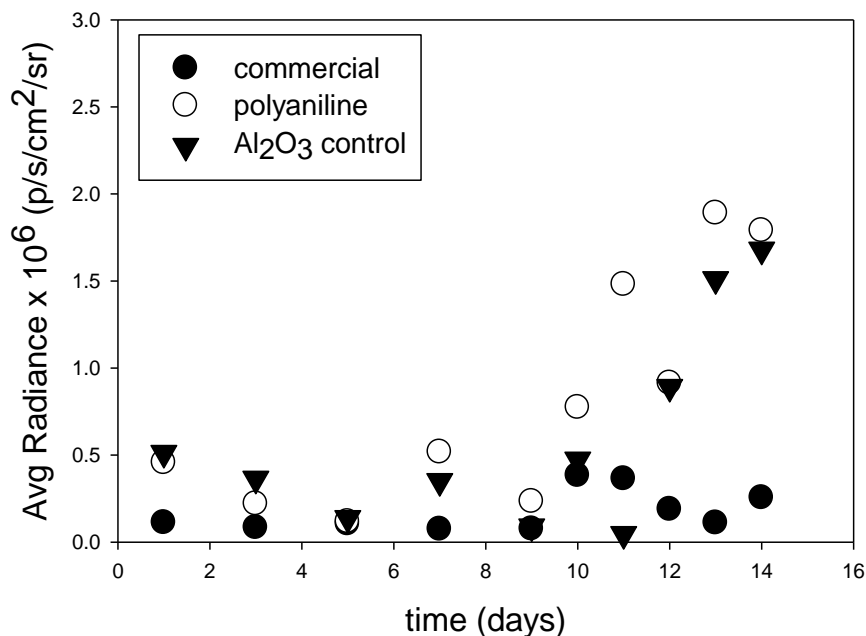


Figure 7.5. Mean average radiance values collected from three samples at different time intervals, showing the antifouling performance against *E. coli* ATCC 25922 lux bacteria. PANI films were grown electrochemically at a fixed potential of 2 V (Ag/AgCl) for 1 h.



During the first week the amount of bacteria that adhered to the surface was similar, but after one week the thicker film had half the amount of bacteria adhering to the surface of the coating. PANI electrochemically synthesised for 2 hours showed the least amount of bacteria on its surface indicating good antifouling performance, a result which was comparable to that of the “commercial” epoxy-amine sample. When PANI films were electrochemically synthesised on marine grade aluminium for an hour a 3.3  $\mu\text{m}$  PANI + aluminium oxide film was formed. However, if this period was extended for another hour, a total of 6.8  $\mu\text{m}$  was built. And two-fold increase of the film thickness dramatically increased the antifouling properties, with it performing even better than the control and commercial samples used for comparison. These results were more pronounced with the *E. coli* 536 *lux* bacterial strain, shown in Figure 7.7. The PANI coating of marine grade aluminium delayed colonisation, indicating a lower rate of fouling. Thicker PANI films appear to show greater antifouling performance (as shown in Figure 7.6).

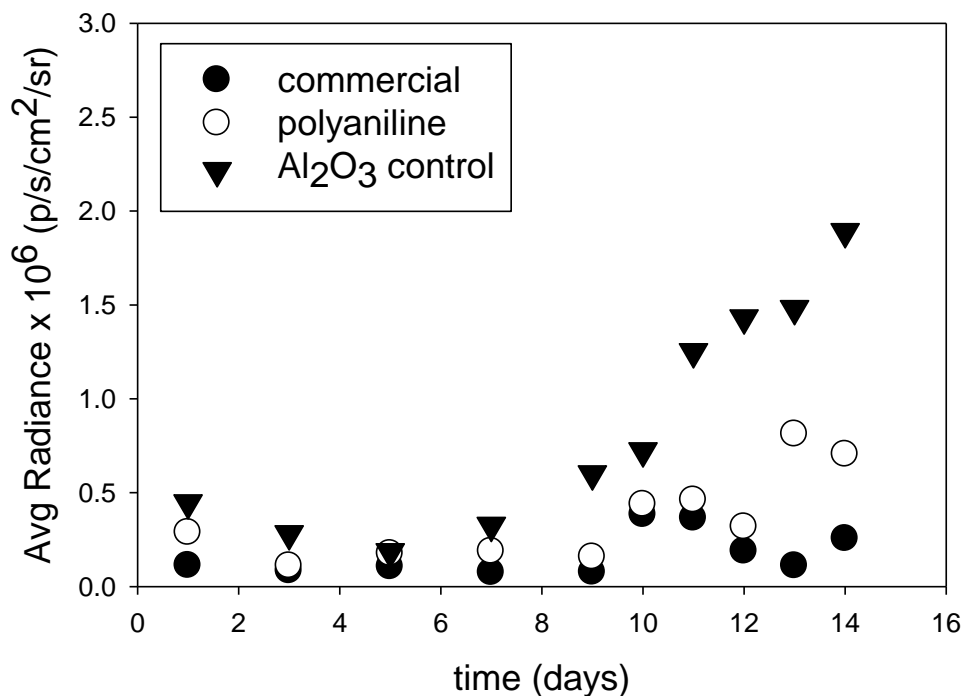


Figure 7.6. Mean average radiance values collected from three samples at different time intervals, showing the antifouling performance against *E. coli* ATCC 25922 *lux* bacteria. PANI films were grown electrochemically at a fixed potential of 2 V (Ag/AgCl) for 2 h.

### 7.3.1.2. *Escherichia coli* 536 lux

The different surfaces were then challenged using a different strain, *E. coli* 536 lux, that forms more extensive biofilms, i.e. it is a stickier version of *E. coli* ATCC 25922 lux. Only the thicker PANI coating, effective against ATCC 25922, was examined at this point (Figure 7.7).

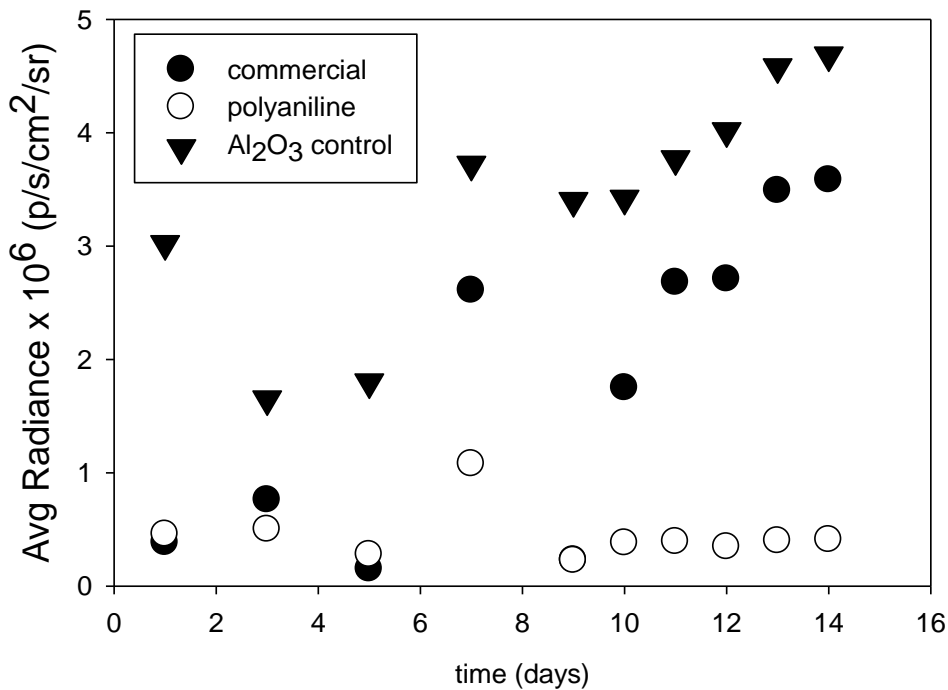


Figure 7.7. Mean average radiance values collected from three samples at different time intervals, showing the antifouling performance against *E. coli* 536 lux, a stickier version of *E. coli* ATCC 25922 lux.

The PANI surface showed significantly better inhibition of biofouling by *E. coli* 536 lux, when compared to both untreated ( $p < 0.05$ ) and epoxy-amine coated ( $p < 0.05$ ) marine grade aluminium.

### 7.3.2. *Vibrio fischeri* and *Vibrio harveyi* strains fouling resistance studies

Fouling resistance was tested for naturally bioluminescent marine micro-organisms *Vibrio fischeri* and *Vibrio harveyi*. Viable plate count and bioluminescence measurements were carried out each day on marine broth medium in addition to the visual observation of the substrate shown below in Figures 7.8 and 7.9. The testing method used with these two bacteria was different compared to the earlier *E. coli* strains; see Section 7.2 for the testing

procedure. Once again, only the thicker PANI electropolymerised for 2 hours was tested against the *Vibrio* strains. At the end of the two-week period there was clear evidence of more contaminant on the surface of the commercial samples for the *Vibrio fischeri* experiment, followed by the control sample and then the PANI coated sample. Whereas with *Vibrio Harveyi* there was clearly more contamination on the surface of the control substrate, followed by the commercial substrate and the least amount of bacteria could be found on the PANI coated aluminium coupon.

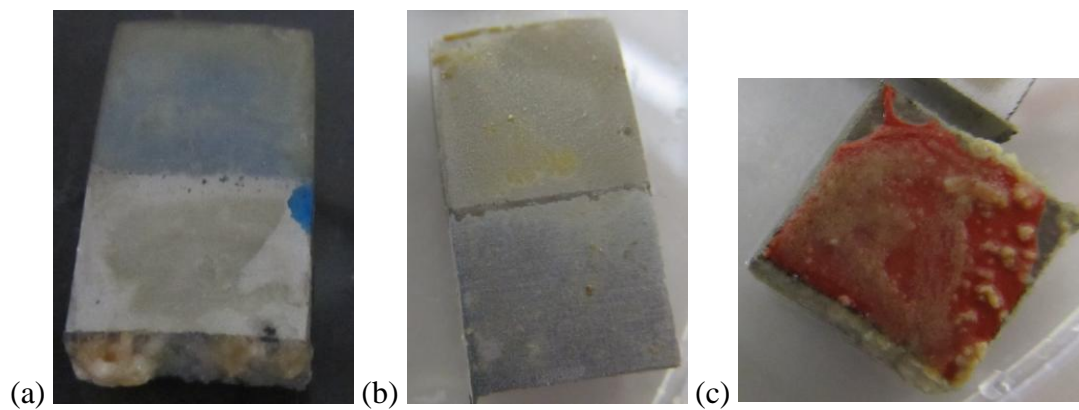


Figure 7.8. *Vibrio fischeri* for (a) PANI, (b) Control, and (c) commercial. Both PANI and aluminium control samples have their own internal control, as only the top half of these were coated while the bottom half was covered with masking tape in the preparation process and later removed before testing.

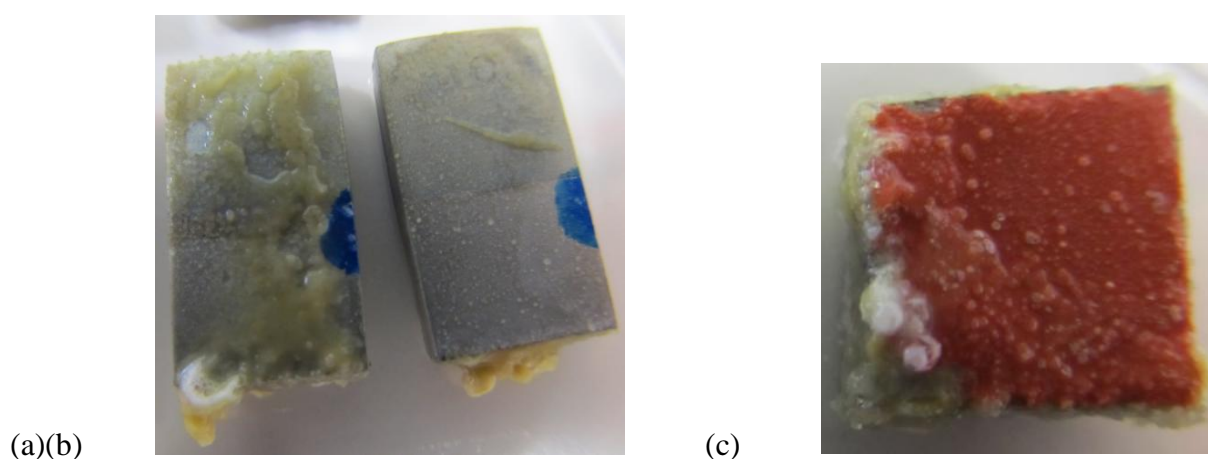


Figure 7.9. *Vibrio harveyi* for (a) control, (b) PANI, and (c) commercial. Both PANI and aluminium control samples have their own internal control, as only the top half of these were coated.

Although preliminary tests indicated that PANI-coated surface showed better and more promising antifouling properties, more tests are required using *Vibrio fischeri* and *harveyi* bacteria to confirm the results. Keeping *Vibrio fischeri* and *harveyi* alive throughout the duration of the test was challenging. These two strains of bacteria are extremely sensitive and do not like being disturbed, making the reproducibility of this test difficult.

## 7.4. Conclusions

In this study bioluminescence imaging testing method was used as an accelerated antifouling testing for novel coatings. Two *E. coli* strains were used for antifouling testing of metal samples. Common testing methods for antifouling properties are time-consuming and involve immersing samples of interest in the sea for a considerable period of time. The colour of the coating, the amount of fouling, adhesion of the coatings, and corrosion resistance could all be tested using the procedure adopted in this study, as a guide to the success or failure of a coating system. Over the years, there have been many studies on the different methods of simulating the marine environment, each with its advantages and disadvantages. There is no exact match between a lab test and a particular marine environment; nevertheless, the present testing method can enable better control and reproducibility than most current field tests. Furthermore, improvements can be made by evaluating these coatings under different culture conditions and other *lux* tagged bacterial species.

PANI is a well-known CP because of its ease of preparation, high conductivity, and its redox properties. Wang et al. [12] was the first to report the use of PANI as an antifouling agent for coatings. In their studies, PANI was used in conjunction with DDT or cuprous oxide and showed synergetic effects in antifouling behaviour. It is believed that electron transfer in the redox processes contributes to this effect. Therefore, the electrical conducting property plays an important role in providing antifouling behaviour. The electrical conductivity of doped PANI decreased with film thickness. The drop in film thickness is in direct relationship to the loss of antifouling effect. This suggests that the key to success in developing an antifouling coating is to ensure the conductivity is relatively stable, and as a result so is the antifouling behaviour. The optimal thickness of a PANI coating on marine grade aluminium alloy for an effective antifouling coating was determined. The film thickness of electrochemically deposited PANI plays an important role in antifouling performance and the use of a PANI coating on marine grade aluminium delays colonisation, indicating a lower rate of fouling in

*E. coli* 536 lux growing culture, is competitive with commercial coatings. This coating was proven to be non-toxic to the bacteria in the medium, as bacteria were seen to continue to grow throughout the duration of the test. The PANI coating acts in a manner similar to that of a shield: it inhibits the growth of bacteria and the micro-organisms on its surface, providing a useful antifouling property.

Bestpfe.com

## CHAPTER EIGHT: Conclusions

### 8.1. General Conclusions

The objectives of this PhD project were to develop novel antifouling systems to replace the organotin, copper-based compounds and other environmentally hazardous materials that are currently used. PANI, poly-ABAs and their copolymers are easily prepared either under chemical or electrochemical synthesis, with the polymer itself showing great signs of antimicrobial and anti-moulding properties. The oxidation state of these polymers can be controlled by the assistance of an external potential, the ability to have this control would enable the user to redope and activate the polymer when required. PANI could be electrochemically deposited on different grades of aluminium. The marine grade aluminium coated with PANI in particular showed a delay in fouling when challenged by the *E. coli* strain bacteria.

Firstly, PANI was synthesised via two different methods, chemically and electrochemically, doped with either H<sub>2</sub>SO<sub>4</sub> or oxalic acid at varying levels. Near-identical and characteristic bands were observed using FTIR and UV-Vis spectroscopy with the use of either dopant. However, an increase in the dopant level of H<sub>2</sub>SO<sub>4</sub> shifted the wavenumber of ~360 nm to a higher benzenoid ring value, suggesting that oxidant used to oxidise the polymer plays an important role in the oxidation state of the polymer formed. A higher benzenoid ring value indicate that a more reduced form of polymer was formed. Electrochemically synthesised PANI indicates that there are more intermediates, branching intermediate by-products formed when compared to chemical synthesis. Given the success of the electrochemical synthesis of PANI, this was further investigated in Chapter Six for electrodeposition of PANI on marine grade aluminium surfaces. Preliminary studies were carried out focusing on incorporating the chemically bound aniline base polymer, ABA, into an epoxy amine coatings system. The chemically synthesised PANI was dispersed into the epoxy component and used as a pigment for the system, as well as dissolved in the amine hardener in another attempt to achieve the ultimate goal of producing an antimould/antifouling surface. This has proven to be successful in the in-house lab test over a 2-year period in a heat and humidity chamber with 8-hour heating cycle at ~60 – 70°C.

Poly-2-ABA doped with either H<sub>2</sub>SO<sub>4</sub> or HCl and poly-3-ABA doped with 1 M HCl prepared chemically were successfully polymerised and tested. The use of different dopants in the

polymerisation of poly-2-ABA by chemical methods has no effect on the FTIR spectra and the overall morphology of the polymer formed. The sponge-like morphology was observed for poly-3-ABA. The appearance of the polymers formed did not affect their antimicrobial performance against the two strains of bacteria tested *S.aureus* 6838 and *E. coli* 25922. The CVs observed for the four polymers formed electrochemically differed in shape to that of PANI. In general, electrochemically synthesised polymers showed a greater proportion of intermediates and by-products. Out of the four poly-ABA formed (poly-2-ABA doped with either H<sub>2</sub>SO<sub>4</sub> or HCl and poly-3-ABA also doped with either H<sub>2</sub>SO<sub>4</sub> or HCl), in general, poly-2-ABA tended to provide a more promising polymerisation growth, hence this was further investigated in the thesis for better understanding of the structures formed using an *in situ* Raman spectroelectrochemistry study. Moreover, the polymerisation of aniline and ABA copolymers was also studied with the aim of improving the polymerisation rate as well as allowing the properties of the two individual polymers to merge into one effective polymer. The ability to control the oxidation state of polymers enabled better control and easier understanding of the mechanisms involved in the success or failure of fouling/corrosion performance. PANI along with its copolymer (aniline: 2-ABA) was studied using *in situ* Raman spectroscopy in order to provide useful information and controllability of the polymers. This ability could then be applied to the future evaluation tests.

The antifouling properties of PANI and its ability to be electrochemically synthesised on aluminium attract interest, as it add the conducting polymer properties in the the coating system as an added feature. There has been no report on the electrosynthesis of PANI on marine grade aluminium, possibly due to its high content of magnesium and high degree of impurities. However, this has been proven to be achievable. The composition of the alloy plays an important role in the performance. Pure aluminium, 1100, showed the best anticorrosive properties with the thicker PANI coating showing best performance. The morphology of the three selected aluminium alloys differed significantly even after chemical treatment. CVs showed that PANI grown on all three grades of aluminium have internal redox processes, and it was possible to obtain and collect these different oxidation states using reflectance UV-Vis and Raman spectroscopy. The corrosion protection was improved with the incorporation of PANI on the surface of the alloy compared to uncoated alloys. Free radical scavenging activity suggested that the presence of PANI on the surface allows for better antioxidant activity.

The last chapter of the thesis focused on the development of a new accelerated antifouling testing procedure, which has proven to have a great potential for the future and for ongoing testing on different surfaces. The ability to visually observe and identify the microorganism growth is a major breakthrough as it helps to better understand biofilm formation on surfaces. Instead of waiting for months for a preliminary indication of success or failure, the use of this novel testing method allows the researcher to identify the performance of their coating systems within weeks.

Although electrochemically synthesised PANI on marine grade aluminium showed greater antifouling properties, it may not be so practical for large objects. However, application for ocean-immersed objects, such as Buoys/ropes, is possibly a good starting point for field trials of this product. The lifetime of this product could potentially be extended with the incorporation of a top coat, a soluble matrix paint, to protect the electrochemical synthesised PANI layer. More testing is required with this novel PANI system before it could be introduced and scaled up for commercial use. The accelerated in-lab antifouling testing method also has a great potential for future accelerated testing for success or failure of the testing coating system.

Nevertheless, the aim of the project was met with promising future for this novel antifouling coating.

## **8.2. Future work**

Although the ultimate aims and objectives of the project in developing an antifouling coating for the marine environment on aluminium alloys have been met, there are potential future developments and extensions of this work to a broader range of surfaces where applicable. In addition, some areas within the thesis could further investigated, with future directions as suggested below.

Chemically synthesised PANI, poly-ABA and PANI-co-ABA could be further incorporated into more coating systems for anti-moulding, antifouling and anticorrosive studies. Accelerated testing would be ideal for evaluation, as a normal testing method requires long exposure. One option is to test these coatings with the developed antifouling evaluation system.



The novel preparation method of PANI on the three grades of aluminium could be further extended to the full range of aluminium grades. The current adhesion is good but it could be further improved with post-treatment, which requires in depth study for optimum efficiency. Electrodeposition of aniline substituted polymers, poly-ABA, or its copolymers on aluminium substrates could be further investigated, given the success of the polymers on Pt electrodes.

Apart from aluminium, other substrates could also be explored, e.g. steel, as there is considerable interest in antifouling protection of steel especially for the food industry. An on-going future project is to continue this work on steel substrates.

The potential accelerated antifouling evaluation method could be further investigated with cross reference to the sea test; this would allow a better understanding of the mechanisms of biofilm formation and its behaviour against the real and simulated environment. Furthermore, this work could be extended to different surfaces for broader study.

In addition there are also many more approaches for this project such as:

1. make a bioactive resin by chemically grafting epoxy with PANI or through in situ aniline polymerisation;
2. synthesise aniline directly onto polystyrene, or glycidal methacrylate monomer to generate a bioactive resin;
3. making a bioactive hardener, i.e. an isocyanate with aniline or bioactive substrates, could also be an alternative approach.

Although these ideas are beyond the scope of this thesis, they can be considered to be the ultimate goal and objective of this research.

## SIGMA-ALDRICH

## MATERIAL SAFETY DATA SHEET

Date Printed: 03/15/2007  
 Date Updated: 01/30/2006  
 Version 1.9

## Section 1 - Product and Company Information

Product Name POLYANILINE, EMERALDINE BASE, MW CA.  
 20,000  
 Product Number 556378  
 Brand ALDRICH  
 Company Sigma-Aldrich  
 Address 3050 Spruce Street  
 SAINT LOUIS MO 63103 US  
 Technical Phone: 800-325-5832  
 Fax: 800-325-5052  
 Emergency Phone: 314-776-6555

## Section 2 - Composition/Information on Ingredient

Substance Name	CAS #	SARA 313
POLYANILINE, EMERALDINE BASE	None	No

## Section 3 - Hazards Identification

## HMIS RATING

HEALTH: 0  
 FLAMMABILITY: 0  
 REACTIVITY: 1

## NFPA RATING

HEALTH: 0  
 FLAMMABILITY: 0  
 REACTIVITY: 1

For additional information on toxicity, please refer to Section 11.

## Section 4 - First Aid Measures

## ORAL EXPOSURE

If swallowed, wash out mouth with water provided person is conscious. Call a physician.

## INHALATION EXPOSURE

If inhaled, remove to fresh air. If breathing becomes difficult, call a physician.

## DERMAL EXPOSURE

In case of contact, immediately wash skin with soap and copious amounts of water.

## EYE EXPOSURE

In case of contact with eyes, flush with copious amounts of water for at least 15 minutes. Assure adequate flushing by separating the eyelids with fingers. Call a physician.

---

## Section 5 - Fire Fighting Measures

---

### FLASH POINT

N/A

### AUTOIGNITION TEMP

N/A

### FLAMMABILITY

N/A

### EXTINGUISHING MEDIA

Suitable: Water spray. Carbon dioxide, dry chemical powder, or appropriate foam.

### FIREFIGHTING

Protective Equipment: Wear self-contained breathing apparatus and protective clothing to prevent contact with skin and eyes.  
Specific Hazard(s): Emits toxic fumes under fire conditions.

---

## Section 6 - Accidental Release Measures

---

### PROCEDURE(S) OF PERSONAL PRECAUTION(S)

Exercise appropriate precautions to minimize direct contact with skin or eyes and prevent inhalation of dust.

### METHODS FOR CLEANING UP

Sweep up, place in a bag and hold for waste disposal. Avoid raising dust. Ventilate area and wash spill site after material pickup is complete.

---

## Section 7 - Handling and Storage

---

### HANDLING

User Exposure: Avoid inhalation. Avoid contact with eyes, skin, and clothing. Avoid prolonged or repeated exposure. Handle under nitrogen.

### STORAGE

Suitable: Keep tightly closed. Handle and store under nitrogen.

### SPECIAL REQUIREMENTS

Hygroscopic.

---

## Section 8 - Exposure Controls / PPE

---

### ENGINEERING CONTROLS

Safety shower and eye bath. Mechanical exhaust required.

### PERSONAL PROTECTIVE EQUIPMENT

Respiratory: Use respirators and components tested and approved under appropriate government standards such as NIOSH (US) or CEN (EU). Respiratory protection is not required. Where protection from nuisance levels of dusts are desired, use type N95 (US) or type P1 (EN 143) dust masks.

Hand: Protective gloves.

Eye: Chemical safety goggles.

### GENERAL HYGIENE MEASURES

Wash thoroughly after handling.

---

## Section 9 - Physical/Chemical Properties

---

Appearance	Physical State: Solid	
Property	Value	At Temperature or Pressure
pH	N/A	
BP/BP Range	N/A	
MP/MP Range	N/A	
Freezing Point	N/A	
Vapor Pressure	N/A	
Vapor Density	N/A	
Saturated Vapor Conc.	N/A	
SG/Density	N/A	
Bulk Density	N/A	
Odor Threshold	N/A	
Volatile%	N/A	
VOC Content	N/A	
Water Content	N/A	
Solvent Content	N/A	
Evaporation Rate	N/A	
Viscosity	N/A	
Surface Tension	N/A	
Partition Coefficient	N/A	
Decomposition Temp.	N/A	
Flash Point	N/A	
Explosion Limits	N/A	
Flammability	N/A	
Autoignition Temp	N/A	
Refractive Index	N/A	
Optical Rotation	N/A	
Miscellaneous Data	N/A	
Solubility	N/A	

N/A = not available

---

#### Section 10 - Stability and Reactivity

---

##### STABILITY

Stable: Stable.

Conditions to Avoid: Moisture.

Materials to Avoid: Strong oxidizing agents.

##### HAZARDOUS DECOMPOSITION PRODUCTS

Hazardous Decomposition Products: Carbon monoxide, Carbon dioxide, Nitrogen oxides.

##### HAZARDOUS POLYMERIZATION

Hazardous Polymerization: Will not occur

---

#### Section 11 - Toxicological Information

---

##### ROUTE OF EXPOSURE

Skin Contact: May cause skin irritation.

Skin Absorption: May be harmful if absorbed through the skin.

Eye Contact: May cause eye irritation.

Inhalation: Material may be irritating to mucous membranes and upper respiratory tract. May be harmful if inhaled.

Ingestion: May be harmful if swallowed.

##### SIGNS AND SYMPTOMS OF EXPOSURE

To the best of our knowledge, the chemical, physical, and toxicological properties have not been thoroughly investigated.

---

Section 12 - Ecological Information

---

No data available.

---

Section 13 - Disposal Considerations

---

APPROPRIATE METHOD OF DISPOSAL OF SUBSTANCE OR PREPARATION

Contact a licensed professional waste disposal service to dispose of this material. Dissolve or mix the material with a combustible solvent and burn in a chemical incinerator equipped with an afterburner and scrubber. Observe all federal, state, and local environmental regulations.

---

Section 14 - Transport Information

---

DOT

Proper Shipping Name: None  
Non-Hazardous for Transport: This substance is considered to be non-hazardous for transport.

IATA

Non-Hazardous for Air Transport: Non-hazardous for air transport.

---

Section 15 - Regulatory Information

---

UNITED STATES REGULATORY INFORMATION

SARA LISTED: No

CANADA REGULATORY INFORMATION

WHMIS Classification: This product has been classified in accordance with the hazard criteria of the CPR, and the MSDS contains all the information required by the CPR.

DSL: No  
NDSL: No

---

Section 16 - Other Information

---

DISCLAIMER

For R&D use only. Not for drug, household or other uses.

WARRANTY

The above information is believed to be correct but does not purport to be all inclusive and shall be used only as a guide. The information in this document is based on the present state of our knowledge and is applicable to the product with regard to appropriate safety precautions. It does not represent any guarantee of the properties of the product. Sigma-Aldrich Inc., shall not be held liable for any damage resulting from handling or from contact with the above product. See reverse side of invoice or packing slip for additional terms and conditions of sale. Copyright 2007 Sigma-Aldrich Co. License granted to make unlimited paper copies for internal use only.

## REFERENCES

- [1] Anderson C., Altar M., Callow M., Candris M., Milne A., Townsin R.L. (2003) The development of foul-release coatings for seagoing vessels. *Journal of Marine Design and Operations* B4: 11-23.
- [2] Smith M.J., Kerr A., Cowling M.J. (2007) Effects of marine biofouling on gas sensor membrane materials. *Journal of Environmental Monitoring* 9: 1378-1386.
- [3] Schultz M.P., Bendick J.A., Holm E.R., Hertel W.M. (2011) Economic impact of biofouling on a naval ship. *Biofouling* 27: 87-98.
- [4] Guardiola F.A., Cuesta A., Meseguer J., Esteban M.A. (2012) Risks of using antifouling biocides in aquaculture. *International Journal of Molecular Sciences* 13: 1541-1560.
- [5] Bressy C., Hugues C., Margailan A. (2009) Characterization of chemically active antifouling paints using electrochemical impedance spectrometry and erosion tests. *Progress in Organic Coatings* 64: 89-97.
- [6] Kim E.S., Hwang G., El-Din M.G., Liu Y. (2012) Development of nanosilver and multi-walled carbon nanotubes thin-film nanocomposite membrane for enhanced water treatment. *Journal of Membrane Science* 394-395: 37-38.
- [7] Yebra D.M., Kiil S., Dam-Johansen K. (2004) Antifouling technology-past, present and future steps towards efficient and environmentally friendly antifouling coatings. *Progress in Organic Coatings* 50: 75-104.
- [8] Evans S.M., Birchenough A.C., Brancato M.S. (2000) The TBT Ban: Out of the Frying Pan into the Fire? *Marine Pollution Bulletin* 40: 204-211.
- [9] Armstrong E., Boyd K.G., Burgess J.G. (2000) Prevention of marine biofouling using natural compounds from marine organisms. *Biotechnology Annual review* 6: 221-241.
- [10] Cowling M.J., Hodgkiss T., Parr A.C., Smith M.J., Marrs S.J. (2000) An alternative approach to antifouling based on analogues of natural processes. *The Science of the Total Environment* 258: 129-137.

- [11] Campbell S., Fletcher R., Powell C. (2004) Long-term exposure trials evaluating the biofouling and corrosion resistance of copper-nickel alloy sheathing materials. *The 12<sup>th</sup> International Congress on Marine Corrosion & Fouling 27-30 July 2004, University of Southampton, UK* 1-16.
- [12] Wang X.H., Li J., Zhang J.Y., Sun Z.C., Yu L., Jing X.B., Wang F.S., Sun Z.X., Ye Z.J. (1999) Polyaniline as marine antifouling and corrosion-prevention agent. *Synthetic Metals* 102: 1377-1380.
- [13] Langer J.J. (1990) A process leading to the domain structure of aniline black (polyaniline). *Synthetic Metals* 36: 35-40.
- [14] Abalyaeva V.V., Efimov O.N. (2010) Effect of electroactive anions on electrochemical behavior of polyaniline. *Russian Journal of Electrochemistry* 46: 571-580.
- [15] Kang E.T., Neoh K.G., Tan K.L. (1998) Polyaniline: A polymer with many interesting intrinsic redox states. *Progress in Polymer Science* 23: 277-324.
- [16] Schauer T., Joos A., Dulog L., Eisenbach C.D. (1998) Protection of iron against corrosion with polyaniline primers. *Progress in Organic Coatings* 33: 20-27.
- [17] Sathiyarayanan S., Karpakam V., Kamaraj K., Muthukrishnan S., Venkatachari G. (2010) Sulphonate doped polyaniline containing coatings for corrosion protection of iron. *Surface and Coatings Technology* 204: 1426-1431.
- [18] Sazou D., Georgolios C. (1997) Formation of conducting polyaniline coatings on iron surfaces by electropolymerization of aniline in aqueous solutions. *Journal of Electroanalytical Chemistry* 429: 81-93.
- [19] Tan K.L., Tan B.T.G., Khor S.H., Neoh K.G., Kang E.T. (1991) The effects of synthesis conditions on the characteristics and chemical structures of polyaniline: a comparative study. *Journal of Physics and Chemistry of Solids* 52: 673-680.
- [20] Campos T.L.A., Kersting D.F., Ferreira C.A. (1999) Chemical synthesis of polyaniline using sulphanic acid as dopant agent into the reactional medium. *Surface and Coatings Technology* 122: 3-5.

- [21] Saravanan K., Sathiyarayanan S., Muralidharan S., Syed A.S., Venkatachari G. (2007) Performance evaluation of polyaniline pigmented epoxy coating for corrosion protection of steel in concrete environment. *Progress in Organic Coatings* 59: 160-167.
- [22] Wang T., Tan Y.J. (2006) Electrodeposition of polyaniline on aluminium alloys for corrosion prevention-A study using the wire beam electrode (WBE). *Materials Science and Engineering: B* 132: 48-53.
- [23] Diniz F.B., De Andrade G.F., Martins C.R., De Azevedo W.M. (2013) A comparative study of epoxy and polyurethane based coatings containing polyaniline-DBSA pigments for corrosion protection on mild steel. *Progress in Organic Coatings* 76: 912-916.
- [24] Dispenza C., Leone M., Presti C.L., Librizzi F., Spadaro G., Vetri V. (2006) Optical properties of biocompatible polyaniline nano-composites. *Journal of Non-Crystalline Solids* 352: 3855-3840.
- [25] Hosseini M.G., Jafari M., Najjar R. (2011) Effect of polyaniline–montmorillonite nanocomposite powders addition on corrosion performance of epoxy coatings on Al 5000. *Surface and Coatings Technology* 206: 280-286.
- [26] Sathiyarayanan S., Muthukrishnan S., Venkatachari G., Trivedi D.C. (2005) Corrosion protection of steel by polyaniline (PANI) pigmented paint coating. *Progress in Organic Coatings* 53: 297-301.
- [27] Takeda S. (1999) A new type of CO<sub>2</sub> sensor built up with plasma polymerized polyaniline thin film. *Thin Solid Films* 343-344: 313-316.
- [28] De Barros R.A., de Azevedo W.M., de Aguiar F.M. (2003) Photo – induced polymerization of polyaniline. *Materials Characterization* 50: 131-134.
- [29] Gizdavic-Nikolaidis M.R., Stanisavljev D.R., Easteal A.J. Zujovic Z.D. (2010) Microwave assisted synthesis of functionalized polyaniline nanostructures with advanced antioxidant properties. *The Journal of Physical Chemistry C* 114: 18790-18796.
- [30] Dhand D., Das M., Datta M., Malhotra B.D. (2011) Recent advances in polyaniline based biosensors. *Biosensors and Bioelectronics* 26: 2811-2821.
- [31] Huh J.H., Oh E.J., Cho J.H. (2003) Investigation of corrosion protection of iron by polyaniline blend coatings. *Synthetic Metals* 137: 965-966.



- [32] Dominis A.J., Spinks G.M., Wallace G.G. (2003) Comparison of polyaniline primers prepared with different dopants for corrosion protection of steel. *Progress in Organic Coatings* 48: 43-49.
- [33] Chen C.H., Mao C.F., Su S.F., Fahn Y.Y. (2007) Preparation and characterization of conductive poly(vinyl alcohol)/polyaniline doped by dodecyl benzene sulfonic acid (PVA/PANDB) blends films. *Journal of Applied Polymer Science* 103: 3415-3422.
- [34] Zilberman M., Titelman G.I., Siegmann A., Haba Y., Narkis M., Alperstein D. (1997) Conductive blends of thermally dodecylbenzene sulfonic acid-doped polyaniline with thermoplastic polymers. *Journal of Applied Polymer Science* 66: 243-253.
- [35] Plesu N., Ilia G., Pascariu A., Vlase G. (2006) Preparation, degradation of polyaniline doped with organic phosphorus acids and corrosion essays of polyaniline-acrylic blends. *Synthetic Metals* 156: 230-238.
- [36] Ho K.S., Hsieh K.H., Huang S.K., Hsieh T.H. (1999) Polyurethane-based conducting polymer blends: I. Effect of chain extender. *Synthetic Metals* 107: 65-73.
- [37] Lakshmi K., John H., Mathew K.T., Joseph R., George K.E. (2009) Microwave absorption, reflection and EMI shielding of PU-PANI composite. *Acta Materialia* 57: 371-375.
- [38] Riaz U., Ahmad S.A., Ashraf S.M., Ahmad S. (2009) Effect of dopant on the corrosion protective performance of environmentally benign nanostructured conducting composite coatings. *Progress in Organic Coatings* 65: 405-409.
- [39] Lakshmi K., John H., Mathew K.T., Joseph R., George K.E. (2009) Microwave absorption, reflection and EMI shielding of PU-PANI composite. *Acta Materialia* 57: 371-375.
- [40] Riaz U., Ahmad S.A., Ashraf S.M., Ahmad S. (2009) Effect of dopant on the corrosion protective performance of environmentally benign nanostructured conducting composite coatings. *Progress in Organic Coatings* 65: 405-409.
- [41] Okamoto H., Okamoto M., Kotaka T. (1998) Structure development in polyaniline films during electrochemical polymerization. II: Structure and properties of polyaniline films prepared via electrochemical polymerization. *Polymer* 39: 4359-4367.

- [42] Tagowska M., Palys B., Jackowska K. (2004) Polyaniline nanotubules – anion effect on conformation and oxidation state of polyaniline studied by Raman spectroscopy. *Synthetic Metals* 142: 223-229.
- [43] Kang Y., Kim S.K., Lee C. (2004) Doping of polyaniline by thermal acid-base exchange reaction. *Materials Science and Engineering C24*: 39-41.
- [44] Salvagione H.J., Acevedo D.F., Miras M.C., Motheo A.J., Barbero C.A. (2004) Comparative study of 2-amino and 3-aminobenzoic acid copolymerization with aniline synthesis and copolymer properties. *Journal of Polymer Science Part A: Polymer Chemistry* 42: 5587-5599.
- [45] Rivas B.L., Sánchez C.O. (2003) Poly(2-) and (3-aminobenzoic acids) and their copolymers with aniline: Synthesis, characterization, and properties. *Journal of Applied Polymer Science* 89: 2641-2648.
- [46] Mav-Golež I., Pahovnik D., Bláha M., Žigon M., Vohlídal J. (2011) Copolymers of 2-methoxyaniline with 2- and 3-aminobenzenesulfonic and 2- and 3-aminobenzoic acids: Relationships between the polymerisation conditions, structure, spectroscopic characteristics and conductivity. *Synthetic Metals* 161: 1845-1855.
- [47] Euler W.B. (1986) Extended huckel calculations on the Pi system of polyaniline. *Solid State Communications* 57: 857-859.
- [48] Abdul Rahman N., Gizdavic-Nikolaidis M., Ray S., Easteal A.J., Travas-Sejdic J. (2010) Functional electrospun nanofibres of poly(lactic acid) blends with polyaniline or poly(aniline-co-benzoic acid). *Synthetic Metals* 160: 2015-2022.
- [49] Ahmed S.M. (2004) Mechanistic investigation of the oxidative polymerization of aniline hydrochloride in different media. *Polymer Degradation and Stability* 85: 605-614.
- [50] Yan H., Wang H.J., Adisasmito S., Toshima N. (1996) Novel syntheses of poly(o-aminobenzoic acid) and copolymers of o-aminobenzoic acid and aniline as potential candidates for precursor of polyaniline. *Bulletin of the Chemical Society of Japan* 69: 2395-2401.

- [51] Miras M.C., Acevedo D.F., Monge N., Frontera E., Rivarola C.R., Barbero C.A. (2008) Organic Chemistry of polyanilines: Tailoring properties to technological applications. *The Open Macromolecules Journal* 1: 58-73.
- [52] Singh A.K., Prakash R., Dwivedi A.D.D., Chakrabarti P. (2008) Electronic properties and junction behavior of polyanthranilic acid/metal contacts. *IEEE Electron device letters* 29: 571-574.
- [53] Chan H.S.O., Ng S.C., Sim W.S. (1992) Thermal analysis of conducting polymers. Part II. Thermal characterisation of electroactive copolymers from aniline and anthranilic acid *Thermochimica Acta* 197: 349-355.
- [54] Nateghi M.R., Fallahian M.H. (2007) Self-doped anthranilic acid-pyrrole copolymer/gold electrodes for selective preconcentration and determination of Cu(I) by differential pulse anodic stripping voltammetry. *Analytical sciences* 23: 563-567.
- [55] Samsonowicz M., Hrynaszkiewicz T., Swislocka R., Regulska E., Lewandowski W. (2005) Experimental and theoretical IR, Raman, NMR spectra of 2-, 3- and 4-aminobenzoic acids. *Journal of Molecular Structure* 744-747: 345-352.
- [56] Cheng W., Jin G., Zhang Y. (2005) Electrochemical characteristics of poly(*o*-aminobenzoic acid) modified glassy-carbon electrode and its electrocatalytic activity towards oxidation of epinephrine. *Russian Journal of Electrochemistry* 41: 940-945.
- [57] Sayyah S.M., Azooz R.E., El-Rehim S.S.A., El-Rabiey M.M. (2006) Electropolymerization of *o*-Aminobenzoic acid and characterization of the obtained polymer films. *International Journal of Polymeric Materials* 55: 37-63.
- [58] Albuquerque J.E., Mattoso L.H.C., Balogh D.T., Faria R.M., Masters J.G., MacDiarmid A.G. (2000) A simple method to estimate the oxidation state of polyaniline. *Synthetic Metals* 113: 19-22.
- [59] Volkov A., Tourillon G., Lacaze P.C., Dubois J.E. (1980) Electrochemical polymerization of aromatic amines IR, XPS and PMT study of thin film formation of a Pt electrode. *Journal of Electroanalytical Chemistry and Interfacial Electrochemistry* 115: 279-291.

- [60] Yue J., Wang Z.H., Cromack K.R., Epstein A.J., MacDiarmid A.G. (1991) Effect of sulfonic acid group on polyaniline backbone. *Journal of the American Chemical Society* 113: 2665-2671.
- [61] Chauhan N.P.S., Ameta R., Ameta R., Ameta S.C. (2010) Biological activity of emeraldine bases of polyaniline. *Journal of Indian Council of Chemists* 27: 128-133.
- [62] Molina J., Esteves M.F., Fernández J., Bonastre J., Cases F. (2011) Polyaniline coated conducting fabrics. Chemical and electrochemical characterization. *European Polymer Journal* 47: 2003-2015.
- [63] Samui A.B., Patankar A.S., Rangarajan J., Deb P.C. (2003) Study of polyaniline containing paint for corrosion prevention. *Progress in Organic Coatings* 47: 1-7.
- [64] Armelin E., Meneguzzi Á., Ferreira C.A., Alemán C. (2009) Polyaniline, polypyrrole and poly(3,4-ethylenedioxythiophene) as additives of organic coatings to prevent corrosion. *Surface and Coatings Technology* 203: 3763-3769.
- [65] Laco J.I.I., Mestres F.L., Villota F.C., Alter L.B. (2004) Urban and marine corrosion: comparative behaviour between field and laboratory conditions. *Materials and Corrosion* 55: 689-694.
- [66] Radhakrishnan S., Sonawane N., Siju C.R. (2009) Epoxy powder coatings containing polyaniline for enhanced corrosion protection. *Progress in Organic Coatings* 64: 383-386.
- [67] Li P., Tan T.C., Lee J.Y. (1997) Corrosion protection of mild steel by electroactive polyaniline coatings. *Synthetic Metals* 88: 237-242.
- [68] Chen C.H., Kan Y.T., Mao C.F., Liao W.T., Hsieh C.D. (2012) Fabrication and characterization of water-based polyurethane/polyaniline conducting blend films. *Surface and Coatings Technology* 231: 71-76.
- [69] Vikki T., Pietilä L.O., Österholm H., Ahjopalo L., Takala A., Toivo A., Levon K., Passiemi P., Ikkala, O. (1996) Molecular Recognition Solvents for Electrically Conductive Polyaniline. *Macromolecules* 29: 2945-2953.
- [70] Ikkala O.T., Pietilä L.O., Passiniemi P., Vikki T., Österholm H., Ahjopalo L., Österholm J.E. (1997) Processible polyaniline complexes due to molecular recognition: Supramolecular structures based on hydrogen bonding and phenyl stacking. *Synthetic Metals* 84: 55-58.

- [71] Epstein A.J., Smallfield J.A.O., Guan H., Fahlman M. (1999) Corrosion protection of aluminum and aluminum alloys by polyanilines: A potentiodynamic and photoelectron spectroscopy study. *Synthetic Metals* 102: 1374-1376.
- [72] Kamaraj K., Karpakam V., Sathiyarayanan S., Venkatachari G. (2010) Electrosynthesis of polyaniline film on AA 7075 alloy and its corrosion protection alloy. *Journal of the Electrochemical Society* 157: C102-C109.
- [73] Kinlen P.J., Menon V., Ding Y. (1991) A mechanical investigation of polyaniline corrosion protection using the scanning reference electrode technique. *Journal of the Electrochemical Society* 146: 3690-3695.
- [74] Wei Y., Wang J., Jia X., Yeh J.M., Spellane P. (1995) Polyaniline as corrosion protection coatings on cold rolled steel. *Polymer* 36: 4535-4537
- [75] Fahlman M., Jasty S., Epstein A.J. (1997) Corrosion protection of iron/steel by emeraldine base polyaniline: an X-ray photoelectron spectroscopy study. *Synthetic Metals* 85: 1323-1326.
- [76] Santos Jr J.R., Mattoso L.H.C., Motheo A.J. (1998) Investigation of corrosion protection of steel by polyaniline films. *Electrochimica Acta* 43: 309-313.
- [77] McAndrew T.P., Miller S.A., Gilicinski A.G., Robeson L.M. (1998) *ACS Symp. Ser* 689: 396-408.
- [78] Ahmad N., MacDiarmid A.G. (1996) Inhibition of corrosion of steels with the exploitation of conducting polymers. *Synthetic Metals* 78: 103-110.
- [79] Lu W.K., Elsenbaumer R.L., Wessling B. (1995) Corrosion protection of mild steel by coatings containing polyaniline. *Synthetic Metals* 71: 2163-2166.
- [80] Kinlen P.J., Silverman D.C., Jeffreys C.R. (1997) Corrosion protection using polyaniline coating formulations. *Synthetic Metals* 85: 1327-1332.
- [81] Sitaram S.P., Yu P., O'Keefe T., Stoffer J.O. (1996) Electrochemical evaluation of conducting polymers in corrosion protection. *Polymeric Materials: Science and Engineering* 75: 354-355.

- [82] Wang T., Tan Y.J. (2006) Understanding electrodeposition of polyaniline coatings for corrosion prevention applications using the wire beam electrode method. *Corrosion Science* 48: 2274-2290.
- [83] Cecchetto L., Ambat R., Davenport A.J., Delabouglise D., Petit J.P., Neel O. (2007) Emeraldine base as corrosion protective layer on aluminium alloy AA5182, effect of the surface microstructure. *Corrosion Science* 49: 818-829.
- [84] Kilmartin P.A., Trier L., Wright G.A. (2002) Corrosion inhibition of polyaniline and poly(o-methoxyaniline) on stainless steels. *Synthetic Metals* 131: 99-109.
- [85] Williams G., McMurray H.N. (2009) Polyaniline inhibition of filiform corrosion on organic coated AA2024-T3. *Electrochimica Acta* 54: 4245-4252.
- [86] Conroy K.G., Breslin C.B. (2003) The electrochemical deposition of polyaniline at pure aluminium: electrochemical activity and corrosion protection properties. *Electrochimica Acta* 48: 721-732.
- [87] Huerta-Vilca D., de Moraes S.R., de Jesus Motheo A. (2005) Aspects of polyaniline electrodeposition on aluminium. *Journal of Solid State Electrochemistry* 9: 416-420.
- [88] Cogan S.F., MGilbert M.D., Holleck G.L., Ehrlich J., Jillson M.H. (2000) Galvanic coupling of doped polyaniline and aluminium alloy 2024-T3. *Journal of the Electrochemical Society* 147: 2143-2147.
- [89] Shabani-Nooshabadi M., Ghoreishi S.M., Behpour M. (2009) Electropolymerized polyaniline coatings on aluminium alloy 3004 and their corrosion protection performance. *Electrochimica Acta* 54: 6989-6995.
- [90] Shah K.G., Akundy G.S., Iroh J.O. (2002) Polyaniline coated on aluminium (Al-2024-T3) characterization and electrochemical studies. *Journal of Applied Polymer Science* 85: 1669-1675.
- [91] Martins N.C.T., Moura e Silva T., Montemor M.F., Fenandes J.C.S., Ferreira M.G.S. (2008) Electrodeposition and characterization of pyrrole films on aluminium alloy 6061-T6. *Electrochimica Acta* 53: 4754-4763.

- [92] Martins N.C.T., Moura e Silva T., Montemor M.F., Fernandes J.C.S., Ferreira M.G.S. (2010) Polyaniline coatings on aluminium alloy 6061-T6: Electrosynthesis and characterization. *Electrochimica Acta* 55: 3580-3588.
- [93] Eftekhari A. (2001) Aluminium as a suitable substrate for the deposition of conducting polymers: application to polyaniline and enzyme-modified electrode. *Synthetic Metals* 125: 295-300.
- [94] Wessling B., Posdorfer J. (1999) Corrosion prevention with an organic metal (polyaniline): corrosion test results. *Electrochimica Acta* 44: 2139-2147.
- [95] DeBerry D.W. (1985) Modification of the Electrochemical and Corrosion Behavior of Stainless Steels with an Electroactive Coating. *Journal of the Electrochemical Society* 132: 1022-1026.
- [96] Camalet J.L., Lacroix J.C., Aeiyaich S., Chane-Ching K., Lacaze P.C. (1998) Electrosynthesis of adherent polyaniline films on iron and mild steel in aqueous oxalic acid medium. *Synthetic Metals* 93: 133-142.
- [97] Talo A., Forsén O., Yläsaari S. (1999) Corrosion protective polyaniline epoxy blend coatings on mild steel. *Synthetic Metals* 102: 1394-1395.
- [98] Zalewska T., Lisowska-Oleksiak L., Biallozor S., Jasulaitiene V. (2000) Polypyrrole films polymerised on a nickel substrate. *Electrochimica Acta* 45: 4031-4040.
- [99] Schrebler R., Gómez H., Córdova R., Gassa L.M., Vilche J.R. (1998) Study of the aniline oxidation process and characterization of Pani films by electrochemical impedance spectroscopy. *Synthetic Metals* 93: 187-192.
- [100] Liu C., Hayashi K., Toko K. (2009) A novel formation process of polyaniline micro-/nanofiber network on solid substrates. *Synthetic Metals* 159: 1077-1081.
- [101] Gomes E.C., Oliveira M.A.S. (2011) Corrosion protection by multilayer coating using layer-by-layer technique. *Surface and Coatings Technology* 205: 2857-2864.
- [102] Kilmartin P.A., Wright G.A. (1996) Photoeffects at a polyaniline film electrode. *Electrochimica Acta* 41: 1677-1687.

- [103] Kraljić M., Mandić Z., Duić L. (2003) Inhibition of steel corrosion by polyaniline coatings. *Corrosion Science* 45: 181-198.
- [104] Wessling B. (1994) Passivation of metals by coating with polyaniline: Corrosion potential shift and morphological changes. *Advanced Materials* 6: 226-228.
- [105] Jasty S., Epstein A.J. (1995) Corrosion prevention capability of polyaniline (emeraldine base and salt): An XPS study. *Polymeric Materials Science and Engineering* 72: 565-566.
- [106] Wei Y., Wang J., Jia X., Yeh J.M., Spelling P. (1995) Electrochemical studies of corrosion inhibiting effect of polyaniline coatings. *Polymeric Materials Science and Engineering* 72: 563-564.
- [107] Wessling B. (1996) Corrosion prevention with an organic metal (polyaniline): Surface ennobling, passivation, corrosion test results. *Materials and Corrosion* 47: 439-445.
- [108] Sazou D. (2001) Electrodeposition of ring-substituted polyanilines on Fe surfaces from aqueous oxalic acid solutions and corrosion protection of Fe. *Synthetic Metals* 118: 133-147.
- [109] Cruz G.J., Morales J., Castillo-Ortega M.M., Olayo R. (1997) Synthesis of polyaniline films by plasma polymerization. *Synthetic Metals* 88: 213-218.
- [110] Yin Y., Liu T., Chen S., Liu T., Cheng S. (2008) Structure stability and corrosion inhibition of super-hydrophobic film on aluminum in seawater. *Applied Surface Science* 255: 2978-2984.
- [111] Moon S.M., Pyun Su-Ii P.S. (1998) II, Growth mechanism of anodic oxide films on pure aluminium in aqueous acidic and alkaline solutions. *Journal of Solid State Electrochemistry* 2: 156-161.
- [112] Pyun S.I., Hong M.H. (1992) A model describing the growth kinetics of passivating oxide film prepared under potentiostatic conditions. *Electrochimica Acta* 37: 327-332.
- [113] Melendres C.A., Van Gils S., Terryn H. (2001) Toward a quantitative description of the anodic oxide films on aluminum. *Electrochemistry Communications* 3: 737-741.
- [114] Moon S.M., Pyun S.I. (1998) The mechanism of stress generation during the growth of anodic oxide films on pure aluminium in acidic solutions. *Electrochimica Acta* 43: 3117-3126.



- [115] Feliu S., Bartolomé M.J., González J.A., López V., Feliu S. (2008) Passivating oxide film and growing characteristics of anodic coatings on aluminium alloys. *Applied Surface Science* 254: 2755-2762.
- [116] Higo M., Fujita K., Mitsushio M., Yoshidome T., Kakoi T. (2007) Epitaxial growth and surface morphology of aluminium films deposited on mica studied by transmission electron microscopy and atomic force microscopy. *Thin Solid Films* 516: 17-24.
- [117] Bautista A., González J.A., López V. (2002) Influence of triethanolamine additions on the sealing mechanism of anodised aluminium. *Surface and Coatings Technology* 154: 49-54.
- [118] Snogan F., Blanc C., Mankowski G., Pébère N. (2002) Characterisation of sealed anodic films on 7050 T74 and 2214 T6 aluminium alloys. *Surface and Coatings Technology* 154: 94-103.
- [119] Bartolomé M.J., López V., Escudero E., Caruana G., González J.A. (2006) Changes in the specific surface area of porous aluminium oxide films during sealing. *Surface and Coatings Technology* 200: 4530-4537.
- [120] Zuo Y., Zhao P.H., Zhao J.M. (2003) The influences of sealing methods on corrosion behavior of anodized aluminum alloys in NaCl solutions. *Surface and Coatings Technology* 166: 237-242.
- [121] Moutarlier V., Gigandet M.P., Ricq L., Pagetti J. (2001) Electrochemical characterisation of anodic oxidation films formed in presence of corrosion inhibitors. *Applied Surface Science* 183: 1-9.
- [122] Moutarlier V., Gigandet M.P., Pagetti J. (2003) Characterisation of pitting corrosion in sealed anodic films formed in sulphuric, sulphuric/molybdate and chromic media. *Applied Surface Science* 206: 237-249.
- [123] Liu W., Zuo Y., Chen S., Zhao X., Zhao J. (2009) The effects of sealing on cracking tendency of anodic films on 2024 aluminum alloy after heating up to 300°C. *Surface and Coatings Technology* 203: 1244-1251.
- [124] Randall Jr J.J., Bernard W.J. (1975) A radiotracer study of the anodization of aluminum in aqueous phosphate solutions. *Electrochimica Acta* 20: 653-661.

- [125] Khalil N., Leach J.S.L. (1986) The anodic oxidation of valve metals—I. Determination of ionic transport numbers by  $\alpha$ -spectrometry. *Electrochimica Acta* 31: 1279-1285.
- [126] Kim J.D., Pyun S.I., Oriani R.A. (1995) Effects of applied current density and potential step on the stress generation during anodic oxidation of tungsten in 0.1 M H<sub>2</sub>SO<sub>4</sub> solution. *Electrochimica Acta* 40: 1171-1176.
- [127] Kim J.D., Pyun S.I., Oriani R.A. (1996) Effects of chloride ion and applied current density on the stress generation during anodic oxidation of tungsten in 0.1 M H<sub>2</sub>SO<sub>4</sub> solution. *Electrochimica Acta* 41: 57-62.
- [128] Genies E.M., Hany P., Santier C. (1988) A rechargeable battery of the type polyaniline/propylene carbonate-LiClO<sub>4</sub>/Li-Al. *Journal of Applied electrochemistry* 18:751-756.
- [129] Foot P.J.S., Simon R. (1989) Electrochromic properties of conducting polyanilines. *Journal of Physics D: Applied Physics* 22: 1598-1603.
- [130] Delichère P., Falaras P., Hugot-Le Goff A. (1989) WO<sub>3</sub> anodic films in organic medium for electrochromic display devices. *Solar Energy Materials* 19: 323-333.
- [131] Cushman R.J., McManus P.M., Yang S.C. (1986) Spectroelectrochemical study of polyaniline: The construction of a pH-potential phase diagram. *Journal of Electroanalytical Chemistry* 291: 335-346.
- [132] Huerta-Vilca D., de Moraes S.R., de Jesus Motheo A. (2004) Anodic treatment of aluminum in nitric acid containing aniline, previous to deposition of polyaniline and its role on corrosion. *Synthetic Metals* 140: 23-27.
- [133] Reddy C.M., Gaston R.S., Weikart C.M., Yasuda H.K. (1998) Influence of surface pretreatment and electrocoating parameters on the adhesion of cathodic electrocoat to the Al alloy surfaces. *Progress in Organic Coatings* 33: 225-231.
- [134] Critchlow G.W., Brewis D.M. (1996) Review of surface pretreatments for aluminium alloys. *Int. J. Adhesion and Adhesives* 16: 255-275.
- [135] Yaro A.S., AL-Asade A.M.A. (2009) Anodic polarization of anodized aluminium alloy 5052. *Journal of Chemical and Petroleum Engineering* 10: 35-42.

- [136] Li F., Zhang L., Metzger R.M. (1998) On the growth of highly ordered pores in anodized aluminium oxide. *Chemistry of Materials* 10: 2470-2480.
- [137] Anodising of Aluminium from the New Zealand Institute of Chemistry. <http://nzic.org.nz/ChemProcesses/metals/8E.pdf>, 1-7. (accessed July 04, 2013).
- [138] Patermarakis G., Masavetas K. (2006) Aluminium anodizing in oxalate and sulphate solutions. Comparison of chronopotentiometric and overall kinetic response of growth mechanism of porous anodic films. *Journal of Electroanalytical Chemistry* 588: 179-189.
- [139] McIntyre J.F., Hang L. (1994) Corrosion – January 1994; corrosion science. Effectiveness of Ion Vapor-deposited aluminium as a primer for epoxy and urethane topcoats.
- [140] Laco J.I.I., Villota F.C., Mestres F.L. (2005) Corrosion protection of carbon steel with thermoplastic coatings and alkyd resins containing polyaniline as conductive polymer. *Progress in Organic Coatings* 52: 151-160.
- [141] Park S.M., in: H.S.Nalwa (Ed.). (1997) Handbook of Organic Conductive Molecules and Polymers, Vol. 3, Wiley, New York, pp. 428.
- [142] Racicot R., Brown R., Yang S.C. (1997) Corrosion protection of aluminum alloys by double-strand polyaniline. *Synthetic Metals* 85: 1263-1264.
- [143] Kobayashi T., Yoneyama H., Tamura H. (1984) Polyaniline film-coated electrodes as electrochromic display devices. *Journal of Electroanalytical Chemistry and Interfacial Electrochemistry* 161: 419-423.
- [144] Smithells C.J. (2004) Smithells Metals Reference Book, 8th ed., Elsevier Butterworth-Heinemann, Amsterdam, Boston, pp. 1-25.
- [145] Zhou X., Sheasby P.G., Scott B.A. (2010) Coatings produced by anodic oxidation, *Shreir's Corrosion* 4: 2503-2518.
- [146] Brace A. (2002) Anodizing – its development, status, and future challenges. Elsevier Science B.V., Amsterdam, 100: 59-60, 62-63, 65-70.
- [147] Buchheit R.G., Kelly R.G., Missert N.A., Shaw B.A. (2003) Corrosion and protection of light metal alloys: proceedings of the International Symposium

[http://books.google.co.nz/books?id=8ymPiEi\\_E0cC&printsec=frontcover&source=gbs\\_ge\\_s  
ummary\\_r&cad=0#v=onepage&q&f=false](http://books.google.co.nz/books?id=8ymPiEi_E0cC&printsec=frontcover&source=gbs_ge_s<br/>ummary_r&cad=0#v=onepage&q&f=false)

[148] Chambers L.D., Stokes K.R., Walsh F.C., Wood R.J.K. (2006) Modern approaches to marine antifouling coatings *Surface and Coatings Technology* 201: 3642-3652.

[149] Pournaghi-Azar M.H., Habibi B. (2007) Electropolymerization of aniline in acid media on the bare and chemically pre-treated aluminum electrodes: A comparative characterization of the polyaniline deposited electrodes. *Electrochimica Acta* 52: 4222-4230.

[150] Geniès E.M., Boyle A., Lapkowski M., Tsintavis C. (1990) Polyaniline: A historical survey. *Synthetic Metals* 36: 139-182.

[151] Ogurtsov N.A., Pud A.A., Kamarchik P., Shapoval G.S. (2004) Corrosion inhibition of aluminum alloy in chloride mediums by undoped and doped forms of polyaniline. *Synthetic Metals* 143: 43-47.

[152] Cecchetto L., Delabouglise D., Petit J.P. (2007) On the mechanism of the anodic protection of aluminium alloy AA5182 by emeraldine base coatings: Evidences of a galvanic coupling. *Electrochimica Acta* 52: 3485-3492.

[153] Brand-Williams W., Cuvelier M.E., Berset C. (1995) Use of free radical method to evaluate antioxidant activity. *Food Science and Technology Research* 28: 25-30.

[154] Sánchez-Moreno C., Larrauri J.A., Saura-Calixto F. (1998) A procedure to measure the antiradical efficiency of polyphenols. *Journal of the Science of Food and Agriculture* 76: 270-276.

[155] Gizdavic-Nikolaidis M., Travas-Sejdic J., Bowmaker G.A., Cooney R.P., Thompson C., Kilmartin P.A. (2004) The antioxidant activity of conducting polymers in biomedical applications. *Current Applied Physics* 4: 347-350.

[156] Kilmartin P. (2010) Antioxidant Plastics based upon conducting polymers. *Chemistry in New Zealand*. 101-105.

[157] Gizdavic-Nikolaidis M., Travas-Sejdic J., Bowmaker G.A., Cooney R.P., Kilmartin P.A. (2004) Conducting polymers as free radical scavengers. *Synthetic Metals* 140: 225-232

- [158] Banerjee S., Saikia J.P., Kumar A., Kumar B.K. (2010) Antioxidant activity and haemolysis prevention efficiency of polyaniline nanofibers. *Nanotechnology* 21: 1-8.
- [159] Gizdavic-Nikolaidis M., Travas-Sejdic J., Kilmartin. P.A., Bowmaker G.A., Cooney R.P. (2004) Evaluation of antioxidant activity of aniline and polyaniline. (2004) *Current Applied Physics* 4: 343-346.
- [160] Boomi P., Prabu H.G., Mathiyarasu J. (2013) Synthesis and characterization of polyaniline/Ag-Pt nanocomposite for improved antibacterial activity. *Colloids and Surfaces B: Biointerfaces*. 103: 9-14.
- [161] Xuemei Guo. (2005) PhD. Thesis, Graduate school of Chinese Academy of Science, May, 88. (in Chinese).
- [162] Shi N., Guo X., Jing H., Gong J., Sun C., Yang K. (2006) Antibacterial effect of the conducting polyaniline. *Journal of Materials Science and Technology* 22: 289-290.
- [163] Kolbert A.C., Caldarelli S., Their K.F., Sacricifitci N.S., Cao Y., Heeger A.J. (1995) NMR evidence for the metallic nature of highly conducting polyaniline *Physical Review B, Condensed matter and materials physics* 51: 1541-1545.
- [164] Chapman J., Weir E., Regan F. (2010) Period four metal nanoparticles on the inhibition of biofouling. *Colloids and Surfaces B: Biointerfaces* 78: 208-216.
- [165] Boomi P., Prabu H. G. (2013) Synthesis, characterization and antibacterial analysis of polyaniline/Au-Pd nanocomposite. *Colloids and Surfaces A: Physicochemical and Engineering Aspects* 429: 51-59.
- [166] [http://en.wikipedia.org/wiki/File:Biofilm\\_Formation.jPNB](http://en.wikipedia.org/wiki/File:Biofilm_Formation.jPNB) (accessed March 06, 2012)
- [167] Chemistry of biofilm prevention.  
[http://en.wikipedia.org/wiki/Chemistry\\_of\\_biofilm\\_prevention#Composition\\_of\\_biofilm](http://en.wikipedia.org/wiki/Chemistry_of_biofilm_prevention#Composition_of_biofilm)  
(accessed March 06, 2012).
- [168] Petrone L. (2013) Molecular surface chemistry in marine bioadhesion. *Advances in Colloid and Interface Science* 195-196: 1-18.

- [169] Wang D.S., Zeng H., Masic A., Harrington M.J., Israelachvili J.N., Waite J.N. (2010) Protein- and metal-dependent interactions of a prominent protein in mussel adhesive plaques. *Journal of Biological Chemistry* 285: 25850-25858.
- [170] Champ M.A. (2000) A review of organotin regulatory strategies, pending actions, related costs and benefits. *Science of the Total Environment* 258: 21-71.
- [171] Townsin R.L. (2003) The ship hull fouling penalty. *Biofouling* 19S: 9-15.
- [172] Finnie A.A., Williams D.N. (2010) Paint and coatings technology for the control of marine fouling. In: Dürr S., Thomason J.C., editors. *Biofouling*. Oxford: Wiley-Blackwell: 185-206.
- [173] Wilke P., Bröner H.G. (2012) Mussel-glue derived peptide-polymer conjugates to realize enzymatically activated antifouling coatings. *ACS Macro Letter* 1: 871-875.
- [174] Pereira da Silva J.E., Córdoba de Torresi S.I., Torresi R.M. (2005) Polyaniline acrylic coatings for corrosion inhibition: the role played by counter-ions. *Corrosion Science* 47: 811-822.
- [175] Hudak E.M., Mortimer J.T., Martin H.B (2007) Platinum for neural stimulation: voltammetry considerations. *Journal of neural engineering* 7: 026005.
- [176] Avlyanov J.K., Josefowicz J.Y., MacDiarmid A.G. (1995) Atomic force microscopy surface morphology studies of 'in situ' deposited polyaniline thin films. *Synthetic Metals* 73: 205-208.
- [177] Passeri D., Biagioni A., Rossi M., Tamburri E., Terranova M.L. (2013) Characterization of polyaniline-detonation nanodiamond nanocomposite fibers by atomic force microscopy based techniques. *European Polymer Journal* 49: 991-998.
- [178] Porter T.L. (1994) Scanning tunnelling microscopy and atomic force microscopy studies of conducting polymer films *Atomic Force Microscopy/Scanning Tunneling Microscopy*, ed. Cohen S.H., Bray M. T., Lightbody M. L. New York, Plenum Press, 1994, pp. 229-36
- [179] Sutar D.S., Tewari R., Dey G.K., Gupta S.K., Yakhmi J.V. (2009) Morphology and structure of highly crystalline polyaniline films. *Synthetic Metals* 159: 1067-1071.

- [180] Kugler T., Rasusson J.R., Österholm J.E., Monkman A.P., Salaneck W.R. (1996) Atomic force microscopy investigations of morphologies in ultrathin polyaniline films. *Synthetic Metals* 76: 181-185.
- [181] Pereira-Da-Silva M.A., Balogh D.T., Eiras C., Kleinke M.U., Faria R.M. (2002) Analysis of polyaniline films using atomic force microscopy. *Molecular Crystals and Liquid Crystals* 374: 191-200.
- [182] Giz M.J., de Albuquerque Maranhão S.L., Torresi R.M. (2000) AFM morphological study of electropolymerised polyaniline films modified by surfactant and large anions. *Electrochemistry Communications* 2: 377-381.
- [183] Buron C.C., Lakard B., Monnin A.F., Moutarlier V., Lakard S. (2011) Elaboration and characterization of polyaniline films electrodeposited on tin oxides. *Synthetic Metals* 161: 2162-2169.
- [184] Venancio E.C., Costa C.A.R., Machado S.A.S., Motheo A.J. (2001) AFM study of the initial stages of polyaniline growth on ITO electrode. *Electrochemistry Communications* 3: 229-233.
- [185] Quillard S., Louran G., Lefrant S., Macdiarmid A.G. (1994) Vibrational analysis of polyaniline: A comparative study of leucoemeraldine, emeraldine and pernigraniline bases. *Physical Review B, Condensed matter and materials physics* 50: 12496-12508.
- [186] Mathew R., Mattas B.R., Espe M.P. (2002) A solid state NMR characterization of cross-linked polyaniline powder. *Synthetic Metals* 131: 141-147.
- [187] Lapkowski M., Berrada K., Quillard S., Louarn G., Lefrant S., Pron A. (1995) Electrochemical oxidation of polyaniline in nonaqueous electrolyte: "in situ" raman spectroscopic studies. *Macromolecules* 28: 1233-1238.
- [188] Yang D., Lu W., Goering R., Mattes B.R. (2009) Investigation of polyaniline processibility using GPC/UV-vis analysis. *Synthetic Metals* 159: 666-674.
- [189] Sariciftci N.S., Kuzmany H., Neubauer H., Neckel A. (1990) Structural and electronic transitions in polyaniline: A Fourier transform infrared spectroscopic study. *The Journal of Chemical Physics* 92: 4530-4539.

- [190] Bernard M.C., Goff A.H. (1997) Raman spectroscopy for the study of polyaniline. *Synthetic Metals* 85: 1145-1146.
- [191] Cochet M., Louarn G., Quillard S., Buisson J.P., Lefrant S. (2000) Theoretical and experimental vibrational study of polyaniline in base forms: non-planar analysis. Part I. *Journal of Raman Spectroscopy* 31: 1029-1039.
- [192] Louarn G., Lapkowski M., Quillard S., Pron A., Buisson J.P., Lefrant S. (1996) Vibrational properties of polyaniline-isotope effects. *Journal of Physical Chemistry* 100: 6998-7006.
- [193] Mažeikienė R., Statino A., Kuodis Z., Niaura G., Malinauskas A. (2006) In situ Raman spectroelectrochemical study of self-doped polyaniline degradation kinetics. *Electrochemistry Communications* 8:1082-1086.
- [194] Mažeikienė R., Niaura G., Malinauskas A. (2005) In situ raman spectroelectrochemical study of electrocatalytic processes at polyaniline modified electrodes: Redox vs. metal-like catalysis. *Electrochemistry Communications* 7: 1021-1026.
- [195] Furukawa Y., Ueda F., Hyodo Y., Harada I., Nakajima T., Kawagoe T. (1988) Vibrational spectra and structure of polyaniline. *Macromolecules* 21: 1297-1305.
- [196] Mažeikienė R., Tomkutė V., Kuodis Z., Niaura G., Malinauskas A. (2007) Raman spectroelectrochemical study of polyaniline and sulfonated polyaniline in solutions of different pH. *Vibrational Spectroscopy* 44: 201-208.
- [197] Efremova A., Regis A., Arsov L.J. (1994) Electrochemical formation and deposition of polyaniline on electrode surface; In situ Raman spectroscopical study. *Electrochimica Acta* 39: 839-845.
- [198] Bernard M.C., de Torresi S.C., Goff A.H. (1999) In situ Raman study of sulfonate-doped polyaniline. *Electrochimica Acta* 44: 1989-1997.
- [199] Sariciftci N.S., Kuzmany H. (1987) Optical spectroscopy and resonance Raman scattering of polyaniline during electrochemical oxidation and reduction. *Synthetic Metals* 21:157-162.
- [200] do Nascimento G.M., Kobata P.Y.G., Millen R.P., Temperini M.L.A. (2007) Raman dispersion in polyaniline base forms. *Synthetic Metals* 157: 247-251.



- [201] Furukawa Y., Hara T., Hyodo Y., Harada I. (1986) Vibrational spectra of polyaniline and its  $^{15}\text{N}$ - and  $^2\text{H}$ - substituted derivatives in as-polymerized, alkali-treated and reduced states. *Synthetic Metals* 16: 189-198.
- [202] Thiemann C., Brett C.M.A. (2001) Electrosynthesis and properties of conducting polymers derived from aminobenzoic acid and from aminobenzoic acids and aniline. *Synthetic Metals* 123: 1-9.
- [203] Han D., Song J., Ding X., Xu X., Niu L. (2007) Fabrication and characterization of self-doped poly(aniline-co-anthranilic acid) nanorods in bundles. *Materials Chemistry and Physics* 105: 380-384.
- [204] Lee J.Y., Cui C.Q. (1996) Electrochemical copolymerization of aniline and metanilic acid. *Journal of Electroanalytical chemistry* 403: 109-116.
- [205] Kilmartin P.A., Wright G.A. (1997) Photoelectrochemical and spectroscopic studies of sulfonated polyaniline. Part I. Copolymers of orthanilic acid and aniline. *Synthetic Metals* 88: 153-162.
- [206] Kilmartin P.A., Wright G.A. (1997) Photoelectrochemical and spectroscopic studies of sulfonated polyaniline. Part II. Copolymers of orthanilic acid and aniline. *Synthetic Metals* 88: 163-170.
- [207] Mandic Z., Duic L., Kovacicek F. (1997) The influence of counter-ions on nucleation and growth of electrochemically synthesized polyaniline films. *Electrochimica Acta* 42: 1389-1402.
- [208] Wei X., Epstein A.J. (1995) Synthesis of highly sulfonated polyaniline. *Synthetic Metals* 74: 123-125.
- [209] Guadalupe A.R., Abruna H.D. (1985) Electroanalysis with chemically modified electrodes. *Analytical Chemistry* 57: 142-149.
- [210] Benyoucef A., Boussalem S., Belbachir, M. (2009) Electrochemical synthesis of poly(o-aminobenzoic acid) and poly(o-aminobenzoic acid-co-aniline): Electrochemical and in-situ FTIRS characteriation. *World Journal of Chemistry* 4: 171-177.
- [211] Lu F.L., Wudl F., Nowak M., Heeger A.J. (1986) Phenyl-capped octaaniline (COA): An excellent model for polyaniline. *Journal of the American Chemical Society* 108: 8311.

- [212] Stafstorm S., Bredas J.L., Epstein A.J., Woo H.S., Tanner D.B., Huang W.S., MacDiarmid A.G. (1987) Polaron lattice in highly conducting polyaniline: theoretical and optical studies. *Physical Review Letters* 59: 1464-1467.
- [213] Habib M.A., Maheswari S.P. (1989) Electrochromism of polyaniline: An in situ FTIR study. *Journal of the Electrochemical Society* 136: 1050-1053.
- [214] Shreepathi S., Holze R. (2005) Spectroelectrochemical investigations of soluble polyaniline synthesized via new inverse emulsion pathway. *Chemistry of Materials* 17: 4078-4085.
- [215] Kaplan, S., Conwell E.M., Richter A.F., MacDiarmid A.G. (1988) Solid-state  $^{13}\text{C}$  NMR characterization of polyanilines. *Journal of the American Chemical Society* 110: 7647-7651.
- [216] Hjertberg T., Sandberg M., Wennerstrom O., Lagerstedt I. (1987) Polyaniline; Model studies. *Synthetic Metals* 21: 31-39.
- [217] Kababya S., Appel M., Haba Y., Titelman G.I., Schmidt A. (1999) Polyaniline – Dodecylbenzene sulfonic acid polymerized from aqueous medium: a solid state NMR characterization. *Macromolecules* 32: 5357-5364.
- [218] Zeng X.R., Ko T.M. (1998) Structures and properties of chemically reduced polyanilines. *Polymer* 39: 1187-1195.
- [219] Espe M.P., Mattes B.R., Schaefer J. (1997) Packing in amorphous regions of hydrofluoric-acid-doped polyaniline powder by  $^{15}\text{N}$ - $^{19}\text{F}$  REDOR NMR. *Macromolecules* 30: 6307-6312.
- [220] Raghunathan A., Rangarajan G., Trivedi D.C. (1996)  $^{13}\text{C}$  CPMAS NMR, XRD, d.c. and a.c. electrical conductivity of aromatic acids doped polyaniline. *Synthetic Metals* 81: 39-47.
- [221] Hjertberg T., Salaneck W.R., Lundstrom I., Somasiri N.L.D., MacDiarmid A.G. (1985) A  $^{13}\text{C}$  CP-MAS NMR Investigation of polyaniline. *Journal of Polymer Science: Polymer Letters Edition* 23: 503-508.
- [222] Goddard Y.A., Vold R.L., Hoatson G.L. (2003) Deuteron NMR study of polyaniline and polyaniline/clay nanocomposite. *Macromolecules* 36: 1162-1169.

- [223] Menardo C., Nechtschein M., Rousseau A., Travers J.P., Hany P. (1988) Investigation on the structure of polyaniline:  $^{13}\text{C}$  NMR and titration studies. *Synthetic Metals* 25: 311-322.
- [224] Hagiwara T., Yamaura M., Iwata K. (1988) Structural analysis of deprotonated polyaniline by solid-state  $^{13}\text{C}$  NMR. *Synthetic Metals* 26: 195-201.
- [225] Devreux F., Bidan G., Syed A., Tsintavis C. (1985) Solid state  $^{13}\text{C}$  NMR in conducting polymers. *Journal of Physics* 46: 1595-1601.
- [226] Jennings P.B., Crumrine M.H., Fischer G.W., Cunningham T.C. (1974) Small-sample blood culture method for identification of bacteria in central arterial and peripheral blood. *Journal of Applied Microbiology* 27: 297-299.
- [227] Brzuszkiewicz E., Brüggemann H., Liesegang H., Emmerth M., Olschläger T., Nagy G., Albermann K., Wagner C., Buchrieser C., Emody L., Gottschalk G., Hacker J., Dobrindt U. (2006) How to become a uropathogen: comparative genomic analysis of extraintestinal pathogenic *Escherichia coli* strains. *Proc Natl Acad Sci U S A*. 103:12879-12884.
- [228] Dunn A.K. (2012) Chapter Two – *Vibrio fischeri* Metabolism: Symbiosis and Beyond. *Advances in Microbial Physiology* 61: 37-68.
- [229] Cano-Gomez A., Bourne D.G., Hall M.R., Owens L., Høj L. (2009) Molecular identification, typing and tracking of *Vibrio harveyi* in aquaculture systems: Current methods and future prospects. *Aquaculture* 287: 1-10.
- [230] Zujovic Z.D., Gizdavic-Nikolaidis M.R., Kilmartin P.A., Idriss H., Senanayake, S.D., Bowmaker, G.A. (2006) Solid-state NMR study of  $^{15}\text{N}$  labeled polyaniline upon reaction with DPPH. *Polymer* 47: 1166-1171.
- [231] Hsu C.F., Zhang L., Peng H., Travas-Sejdic J., Kilmartin P.A. (2008) Scavenging of DPPH free radicals by polypyrrole powders of varying levels of overoxidation and/or reduction. *Synthetic Metals* 158: 946-952.
- [232] Barlett P.N., Astier Y. (2000) Microelectrochemical enzyme transistors. *Chemical Communication* 105-112.

- [233] Ivanov S., Mokreva P., Tsakova V., Terlemezyan L. (2003) Electrochemical and surface structural characterization of chemically and electrochemically synthesized polyaniline coatings. *Thin Solid Films* 441: 44-49.
- [234] Gao M., Zhang G., Zhang G., Wang X., Wang S., Yang Y. (2011) *Polymer Degradation and Stability* 96: 1799-1804.
- [235] Kobayashi T., Yoneyama H., Tamura H. (1984) Polyaniline film-coated electrodes as electrochromic display devices. *Journal of Electroanalytical Chemistry and Interfacial Electrochemistry* 161: 419-423.
- [236] Holze R. (1987) Raman spectroscopic investigation of aniline: adsorption and polymerization. *Journal of Electroanalytical Chemistry* 224: 253-260.
- [237] Šeděková I., Trchová M., Stejskal J. (2008) Thermal degradation of polyaniline films prepared in solutions of strong and weak acids and in water – FTIR and Raman spectroscopic studies. *Polymer Degradation and Stability* 93: 2147-2157.
- [238] Bernard M.C., Goff H.L. (2006) Quantitative characterization of polyaniline films using Raman spectroscopy II. Effects of self-doping in sulfonated polyaniline. *Electrochimica Acta* 52: 728-735.
- [239] Rehim M. A., Youssef A., Hassan E., Khatab N., Turkey G. (2010) Morphology and electrical properties of hybrid and sulphonated oxalic acid-doped polyaniline. *Synthetic Metals* 160: 1774-1779.
- [240] Li Yan., Peng H., Li G., Chen K. (2012) Synthesis and electrochemical performance of sandwich-like polyaniline/graphene composite nanosheets. *European Polymer Journal* 48: 1406-1412.
- [241] Gopalakrishnan K., Elango M., Thamilselvan M. (2012) Optical studies on nano-structured conducting polyaniline prepared by chemical oxidation method. *Archives of Physics Research* 3: 315-319.
- [242] Quillard S., Berrada K., Louarn G., Lefrant S., Lapkowski M., Pron A. (1995) In-situ Raman-spectroscopic studies of the electrochemical-behavior of polyaniline. *New Journal of Chemistry* 19: 365-374.

- [243] Zujovic Z.D., Gizdavic-Nikolaides M., Kilmartin P.A., Travas-Sejdic J., Cooney R.P., Bowmaker G.A. (2005) Solid-State Magnetic Resonance Studies of polyaniline as a radical scavenger. *Applied Magnetic Resonance* 28: 123-126.
- [244] Zujovic Z.D. Zhang L., Bowmaker G.A., Kilmartin P.A., Travas-Sejdic J. (2008) Self-Assembled, nanostructured aniline oxidation products: A structural investigation. *Macromolecules* 41: 3125-3135.
- [245] Shenglong W., Fosong W., Xiaohui G. (1988) Polymerization of substituted aniline and characterization of the polymers obtained. *Synthetic Metals* 16: 99-104.
- [246] Leclerc M., Guay J., Dao L.H. (1988) Synthesis and properties of electrochromic polymers from toluidines. *Journal of Electroanalytical Chemistry* 251: 21-29.
- [247] Wei Y., Focke W.W., Wnek G.E., Ray A., Macdiarmid A.G. (1989) Synthesis and electrochemistry of alkyl ring-substituted polyaniline. *Journal of Physical Chemistry* 95: 495-499.
- [248] Watanabe A., Mori K., Iwabuchi A., Iwasaki Y., Nakamura Y., Ito O. (1989) Electrochemical polymerization of aniline and N-alkylanilines. *Macromolecules* 22: 3521-3525.
- [249] Fujita I., Ishiguchi M., Shiota H., Danjo T., Kosai K. (1992) Spectroscopic study of polytoluidines in the UV-Visible and IR Regions. *Journal of Applied Polymer Science* 44: 987-992.
- [250] Macinnes D., Funt B.L. (1988) Poly-*o*-methoxyaniline: a new soluble conducting polymer. *Synthetic Metals* 25: 235-242.
- [251] Gazotti Jr W.A., Faez R., De Paoli M.A. (1996) Electrochemical, electrochromic and photoelectrochemical behavior of a highly soluble polyaniline derivative: poly(*o*-methoxyaniline) doped with functionalized organic acids. *Journal of Electroanalytical Chemistry* 415: 107 -113.
- [252] Ranger M., Leclerc M. (1997) Synthesis and characterization of polyanilines with electro-withdrawing substituents. *Synthetic Metals* 84: 85-86.
- [253] Masters J. G., Sun Y., MacDiarmid A.G., Epstein A.J. (1991) Polyaniline: allowed oxidation states. *Synthetic Metals* 41: 715-718.

- [254] Chan H.S.O., Ng S.C., Sim W.S., Tan K.L., Tan B.T.G. (1992) Preparation and characterization of electrically conducting copolymers of anilines and anthranilic acid: evidence for self-doping by X-ray photoelectron spectroscopy. *Macromolecules* 25: 6029-6034.
- [255] Ohsaka T., Ohnuki Y., Oyama N., Katagiri G., Kamisako K. (1984) IR absorption spectroscopic identification of electroactive and electroinactive polyaniline films prepared by the electrochemical polymerization of aniline. *Journal of Electroanalytical Chemistry* 161: 399-405.
- [256] Karyakin A.A., Strakhova A.K., Yatsimirsky A.K. (1994) Self-doped polyanilines electrochemically active in neutral and basic aqueous solutions. *Journal of Electroanalytical Chemistry* 371: 259-265.
- [257] Gizdavic-Nikolaidis M.R., Bennett J.R., Swift S., Easteal A.J., Ambrose M. (2011) Broad spectrum antimicrobial activity of functionalized polyanilines. *Acta Biomaterialia* 7: 4204-4209.
- [258] Ayad M.M., Salahuddin N.A., Abou-Seif A.K., Alghaysh M.O. (2008) Chemical synthesis and characterization of aniline and *o*-anthranilic acid copolymer *European Polymer Journal* 44: 426-435.
- [259] Cao Y., Li S., Xue Z., Guo D. (1986) Spectroscopic and electrical characterization of some aniline oligomers and polyaniline. *Synthetic Metals* 16: 305-315.
- [260] Ginder J.M., Epstein A.J. (1990) Role of ring torsion angle in polyaniline: Electronic structure and defect states. *Physical Review B* 41: 10674-10685.
- [261] Pasto D.J., Johnson D.R. (1996) In: *Organic Structure Determination*. Englewood Cliffs (NJ): Prentice-Hall, Inc., Englewood Cliffs, N.J., Prentice-Hall.
- [262] Cooper J.W. (1980) *Spectroscopic Techniques*. New York: Wiley.
- [263] Johnson B.J., Park S.M. (1996) Electrochemistry of conductive polymers. XX. Early stages of aniline polymerization studied by spectroelectrochemical and rotating ring disk electrode techniques. *Journal of the Electrochemical Society* 143: 1277-1282.
- [264] Asturias G.E., MacDiarmid A.G., McCall R.P., Epstein A.J. (1989) The oxidation state of "emeraldine" base. *Synthetic Metals* 29: E157-E162.

- [265] Wei Y., Haribaran R., Patel S.A. (1990) Chemical and electrochemical copolymerization of aniline with alkyl ring-substituted anilines. *Macromolecules* 23: 758-764.
- [266] Orata D., Buttry D.A. (1987) Determination of ion populations and solvent content as functions of redox state and pH in polyaniline. *Journal of American Chemical Society* 109: 3574-3581.
- [267] Shim Y.B., Won M.S., Park S.M. (1990) Electrochemistry of conductive polymers VIII. In situ spectroelectrochemical studies of polyaniline growth mechanisms *Journal of Electroanalytical Chemistry* 137: 538-544.
- [268] Lin H. K., Chen S. A. (2000) Synthesis of new water-soluble self-doped polyaniline. *Macromolecules* 33: 8117-8118.
- [269] Deore B.A., Yu I., Freund M.S. (2004) A switchable self-doped polyaniline: Interconversion between self-doped and non-self-doped forms. *Journal of American Chemical Society* 126: 52-53.
- [270] Wei X. L., Wang Y. Z., Long S.M., Bobeczko C., Epstein A. J. (1996) Synthesis and physical properties of highly sulfonated polyaniline. *Journal of American Chemical Society* 118: 2545-2555.
- [271] Duic L., Mandic Z., Kovac S. (1995) Polymer-dimer distribution in the electrochemical synthesis of polyaniline. *Electrochimica Acta* 40: 1681-1688.
- [272] Geniès E.M., Lapkowski M., Penneau J.F. (1988) Cyclic voltammetry of polyaniline: Interpretation of the middle peak mechanisms. *Journal of Electroanalytical Chemistry* 249: 97-107.
- [273] Hendra P., Jones C., Warnes G. (1991) Fourier transform raman spectroscopy: Instrumentation and chemical applications. New York, Ellis Horwood.

- [274] Dennany L., Innis P.C., McGovern S.T., Wallace G.G., Forster R.J. (2011) Electronic interactions within composites of polyanilines formed under acidic and alkaline conditions. Conductivity, ESR, Raman, UV-Vis and fluorescence studies. *Physical Chemistry Chemical Physics* 13: 3303-3310.
- [275] Reusch W. (2013)  
<http://www2.chemistry.msu.edu/faculty/reusch/VirtTxtJml/Spectrpy/InfraRed/infrared.htm>  
(accessed June 06, 2012).
- [276] Gizdavic-Nikolaidis M.R., Zujovic Z.D., Ray S., Eastal A.J., Bowmaker G.A. (2010) Chemical synthesis and characterization of poly(aniline-co-ethyl-3-aminobenzoate) copolymers. *Journal of Polymer Science: Part A: Polymer Chemistry* 48: 1339-1347.
- [277] Gazapo J., Gea J. (1994) Anodizing of Aluminium.  
<http://core.materials.ac.uk/repository/eaa/talat/5203.pdf> (accessed July 04, 2013)
- [278] Stejskal J., Sapurina I., Trchova M. (2010) Polyaniline nanostructures and the role of aniline oligomers in their formation. *Progress in Polymer Science* 35: 1420-1481.
- [279] C. F. Hsu, C. H. Peng, L. Zhang, J. Travas-Sejdic, P. A. Kilmartin. e-J. Surf., Sci. Nanotechnol. 7 (2009) 269.
- [280] Liu C., Zhang J., Shi G., Chen F. (2004) Doping level change of polyaniline film during its electrochemical growth process. *Journal of applied polymer science* 92: 171-177.
- [281] Mažeikienė R., Niaura G., Malinauskas A. (2010) A comparative Raman spectroelectrochemical study of selected polyaniline derivatives in a pH-neutral solution. *Synthetic Metals* 160: 1060-1064.
- [282] Rajendra Prasad K., Munichandraiah N. (2002) Electrochemically deposited crystalline thin film of polyaniline on nickel for redox reactions at positive potentials. *Synthetic Metals* 130: 17-26.
- [283] Shah A.H.A., Holze R. (2006) In situ UV-Vis spectroelectrochemical studies of the copolymerization of *o*-aminophenol and aniline. *Synthetic Metals* 156: 566-575.
- [284] Malinauskas A., Holze R. (1999) A UV-vis spectroelectrochemical study of redox reactions of solution species at a polyaniline electrode in the conducting and the reduced state. *Journal of Electroanalytical Chemistry* 461: 184-193.



- [285] Zujovic Z.D., Laslau C., Bowmaker G.A., Kilmartin P.A., Webber A.L., Brown S.P., Travas-Sejdic J. (2010) Role of aniline oligomeric nanosheets in the formation of polyaniline nanotubes. *Macromolecules* 43: 662-670.
- [286] Malinauskas A., Holze R. (1998) Organic electroluminescent devices using deposited poly(*p*-phenylene) film as hole transport layer. *Synthetic Metals* 87: 31-36.
- [287] Deng Z., Smyrl W.H., White H.S. (1989) Stabilization of metal-metal oxide surfaces using electroactive polymers films. . *Journal of the Electrochemical Society* 136: 2152-2158.
- [288] Racicot R.J., Clark R.L., Liu H.B., Yang S.C., Alias N.M., Brown R. (1995) Anti-corrosion studies of novel conductive polymeric coatings on aluminium alloys. *MRS Proceedings* 413-529.
- [289] Hsu C.F., Peng H., Basle C., Travas-Sejdic J., Kilmartin P.A. (2011) ABTS<sup>+</sup> scavenging activity of polypyrrole, polyaniline and poly(3,4-ethylenedioxythiophene). *Polymer International* 60: 69-77.
- [290] Prasad K.R., Munichandraiah N. (2001) Potentiodynamic deposition of polyaniline on non-platinum metals and characterization. *Synthetic Metals* 123: 459-468.
- [291] Brzuszkiewicz E., Brüggemann H., Liesegang H., Emmerth M., Olschläger T., Nagy G., Albermann K., Wagner C., Buchrieser C., Emody L., Gottschalk G., Hacker J., Dobrindt U. (2006) How to become a uropathogen: comparative genomic analysis of extraintestinal pathogenic *Escherichia coli* strains. *Proceedings of the National Academy of Sciences, U. S. A* 103:12879-12884.
- [292] Riedel C.U., Casey P.G., Mulcahy H., O’Gara F., Gahan C.G., Hill C. (2007) Constructure of p16Slux, a novel vector for improved bioluminescent labeling of gram-negative bacteria. *Applied and Environmental Microbiology* 73:7092-7095.